Structural and functional analysis of ZraP in *Salmonella* Typhimurium

Maria Elisabeth Johanna Zalm

100035163

A Thesis submitted to the University of East Anglia in accordance with the requirements of the degree of Doctor of Philosophy

School of Biological Science

September 2017

Abstract

The impact of *Salmonella* infections on global health is significant, and its treatment and prevention have proven to be a medical as well as a social-economical challenge. A major contributor to the pathogenicity of *Salmonella* is its ability to adapt to changing environments, and thrive despite exposure to environmental stresses. The Gram-negative cell envelope plays an important role in the natural resistance of *Salmonella* against various antimicrobial agents, providing a buffer that protects the *Salmonella* cytoplasm from immediate cellular stress. Periplasmic chaperones play a vital role in the biogenesis, maintenance and repair of the outer membrane. Although these chaperones are well studied in *Escherichia coli*, their functions are less well understood in other Gram-negative pathogens. This study investigates the involvement of *Salmonella* Typhimurium periplasmic proteins CpxP, FkpA, HtrA, PpiA/D, Skp, SurA, Spy, ZraP, and YncJ in the protection against a range of environmental stresses that challenge the cell envelope. The results obtained suggest that both Skp and SurA are of significant importance in the maintenance of the outer membrane, whereas the remaining chaperones appear to be involved in the protection against a narrower range of stresses.

Furthermore, this study presents new insights into the protein structure of the zinc-responsive, periplasmic chaperone ZraP. Data collected using X-ray crystallography analysis and small-angle X-ray scattering suggest that ZraP forms a globular protein of higher oligomeric state. The formation of higher oligomeric structures is not dependent on zinc interactions, nor does zinc affect the overall protein envelope. Although natural substrates of ZraP remain enigmatic, functional analysis of ZraP shows that protein interactions between ZraP and malate dehydrogenase or DNA gyrase may render these enzymes inactive. Suppression of enzymatic activity is reduced in ZraP constructs disrupted in the C-terminal ^{139}HRGGAH$^{144\ region}$, whereas the presence of excess zinc boosts interactions between ZraP and these enzymes.

This thesis is 332 pages, and approximately 94,500 words in length.

Table of Contents

List of figures

List of figures - continued   **Page**

List of tables   Page

List of abbreviations

(v/v)	Volume per volume
(w/v)	Weight per volume
Amp	Ampicillin
APS	Ammonium Persulphate
ATP	Adenosine triphosphate
AUC	Analytical ultracentrifugation
BAM	β-barrel assembly machinery
bEBP	Bacterial enhancer binding protein
Bp	Base pairs
BSA	Bovine serum albumin
CFU	Colony forming units
Cm	Chloramphenicol
CSIXR	Carbon-starvation induced stress response
DNaseI	Deoxy ribonuclease I
EDTA	Ethylenediaminetetraacetic acid
EHEC	Enterohaemorrhagic *Escherichia coli*
EPEC	Enteropathogenic *Escherichia coli*
ESR	Envelope stress response
FPLC	Fast protein liquid chromatography
FRT	Flippase recognition target
GnHCl	Guanidine hydrochloride
HEPES	4-(2-hydroxyethyl)-1-piperazineethanesulfonic acid
HiC	High concentration carbon
HRP	Horseradish peroxidase
HU	Hydroxyurea
IM	Inner membrane
IPTG	Isopropyl β-D-1-thiogalactopyranoside
Kan/km	Kanamycin
Kb	Kilobase(s)
kDa	Kilo Daltons
LoC	Low concentration carbon
LPS	Lipopolysaccharide
MALDI-TOF	matrix assisted laser desorption ionization-time of flight
MDH	Malate dehydrogenase
MDR	Multi-drug resistant
MOPS	3-(N-morpholino)propanesulfonic acid
MS	Mass spectrometry
NAD^+	Oxidised nicotinamide adenine dinucleotide
NADH	Reduced nicotinamide adenine dinucleotide
NTS	Non-typhoidal *Salmonella*
OM	Outer membrane
OMP	Outer membrane protein
PAGE	Polyacrylamide gel electrophoresis

PBS	Phosphate buffered saline
PCR	Polymerase chain reaction
PDB	Protein databank
PEG	Polyethylene glycol
PMB	Polymyxin B
ppGpp	Guanosine pentaphosphate
PPIase	Peptidyl-prolyl cis-trans isomerase
ROS	Reactive oxygen species
rpm	Revolutions per minute
RT	Room temperature
SANS	Small-angle neutron scattering
SAXS	Small-angle X-ray scattering
SCV	*Salmonella* containing vacuole
SDS	Sodium dodecyl sulphate
SEC-SAXS	Size-exclusion chromatography small-angle X-ray scattering
ser	serovar
SPI	*Salmonella* pathogenicity island
SSR	Starvation-stress response
STM	*Salmonella enterica* subsp. *enterica* ser. Typhimurium
subsp.	subspecies
Ta	Annealing temperature
TAE	Tris/Acetate/EDTA
TBE	Tris/Borate/EDTA
TBS	Tris buffer saline
TBST	Tris buffer saline Tween 20
TEMED	*N,N,N',N'*-Tetramethylethylenediamine
Tm	Melting temperature
TTSS	Type III secretion system
Van/Vm	Vancomycin
WHO	World Health Organisation
WT	Wild type

Acknowledgements

Firstly, I would like to thank my supervisory team, the BBSRC and Inspiralis for giving me the opportunity to conduct my PhD at the University of East Anglia. It goes without saying that without your support, I would not have been able to carry out the work presented here. I would like to extend this gratitude to the beamline scientists at the Diamond Light Source for their help and support.

I owe a great debt to Dr. Marcus Edwards, for his training, support and guidance throughout my PhD, as well as his aid in solving the crystal structures presented in this work. Marcus, you have taken me under your wing from the moment I started investigating ZraP. You were always there when I needed help with science and/or equipment, or when I just needed to have a little rant about scientific and not-so-scientific topics, and for all of this I owe you my eternal gratitude.

To the members of the Hutchings lab, thank you for branding me "honouree member of the lab" and making me feel included during times of isolation. In particular to Elaine Patrick, for being the best technician one could hope for, and for being a friend and listening ear when times were difficult. I fink u freeky and I like you a lot!

I would like to add a special thanks to my fellow students Dr. Hannah Wells, Dr John Munnoch, Dr. Janice Layhadi and Dr (to be) Rebecca Lo. Hannah, thank you for your help and guidance throughout my MSc project and the early years of my PhD. You have been a great teacher and a great inspiration. To Janice and Rebecca, thank you for the journey we embarked on together. It has been a bumpy ride, but you have been there at my side all along. I am exceedingly proud to have seen you both grow as scientists, and I am incredibly lucky to have had you as my friends. John, thank you for always being at my side and for helping me get through the darkest days of my PhD, for lifting my heart when I was feeling down, and for handing me tissues when they were needed. My dear friends, without you, my PhD would not have been. But as it was not all doom and gloom, thank you all for all the great times we have shared together too. You will hold a special place in my heart forevermore.

The greatest thanks goes to my fiancé Jordan Hill, my mum and dad, my sisters Lysanne and Merethe, any my family-in-law. Thank you all for putting up with me throughout the years. For cooking my dinners, for being my taxi service, for extending my bank account, for encouraging and inspiring me, but most of all for always believing in me, even when I could not do so myself. Your unwavering support has been the most precious gift I have ever received.

Finally, I dedicate this work to my grandad and my late grandparents, throughout the years you have encouraged me to reach beyond the stars. You taught me to pursue my dreams and to not give up in the face of adversity. You have been my inspiration from the start.

Chapter 1. Introduction

1.1 *Salmonella* taxonomy and nomenclature

Salmonellae are Gram-negative, rod-shaped, facultative anaerobic bacteria, predominantly found in host intestines and the environment. The genus belongs to the Enterobacteriaceae family that also includes the commonly known pathogens *Escherichia coli*, *Klebsiella, Shigella* and *Yersinia.* Although it is thought that *Salmonella* and its closest relative *E. coli* diverged from a common ancestor approximately 100 million years ago (Doolittle *et al.*, 1996), their genomes still share extensive regions of synteny, and genetic diversity has been driven primarily by horizontal gene transfer (McClelland *et al.*, 2000). Indeed, most genes unique to *Salmonella* serovars are located on discrete genomic islands, known as *Salmonella* pathogenicity islands (SPIs), which encode specialised loci and prophage elements as well many *Salmonella* specific virulence factors (McClelland *et al.*, 2001; Parkhill *et al.*, 2001).

Taxonomy of the genus *Salmonella* is complex, and prior to the determination of *Salmonella* nomenclature on a scientific basis, *Salmonella* serovars were treated as subspecies. In this thesis, *Salmonellae* will be referred to according to the Kauffmann-White method as agreed upon by the Taxonomic Subcommittee of Enterobacteriaceae of the International Committee on Systemic Bacteriology (Penner, 1988; Old, 1992; Grimont and Weill, 2007). Following DNA-DNA hybridisation experiments, the Kauffmann-White method separates *Salmonellae* into two species; *Salmonella bongori* and *Salmonella enterica* (Crosa *et al.*, 1973). The latter species is divided into six subspecies, *enterica, salamae, arizonae, diarizonae, houtenase* and *indica*, according to their biochemical properties and genomic relatedness. *Salmonella* is further divided into serovars which are defined by the antigenic variation found in the expressed lipopolysaccharide moieties (O-antigens), flagellar antigens (H-antigens) and capsular polysaccharides (Vi-antigens) (figure 1.1). Whereas *S. bongori* accommodates approximately two dozen serovars, *S. enterica* accommodates over 2500 different serovars, of which approximately 60% can be found among the subspecies *enterica*. The nomenclature of *S. enterica* subsp. *enterica* serovars differs from other serovars; whereas the serovars of *S. bongori* and other *S. enterica* subspecies are designated by their antigenic formulae only, *S. enterica* subsp. *enterica* serovars are denoted according to associated syndrome (e.g. *S. enterica* Typhi), associated host and syndrome (e.g. *S. enterica* Typhimurium), or origin of discovery of the first new serovar (e.g. *S. enterica* Dublin). These serovar names are maintained for ease of reference, particularly within the medical field, as >99.5% of serovars isolated from human and domesticated animal hosts belong to the

enterica subspecies. To emphasise reference to different serovars, and not distinct subspecies, serovars are not italicized and written with a capital letter (Brenner *et al.*, 2000; Grimont and Weill, 2007).
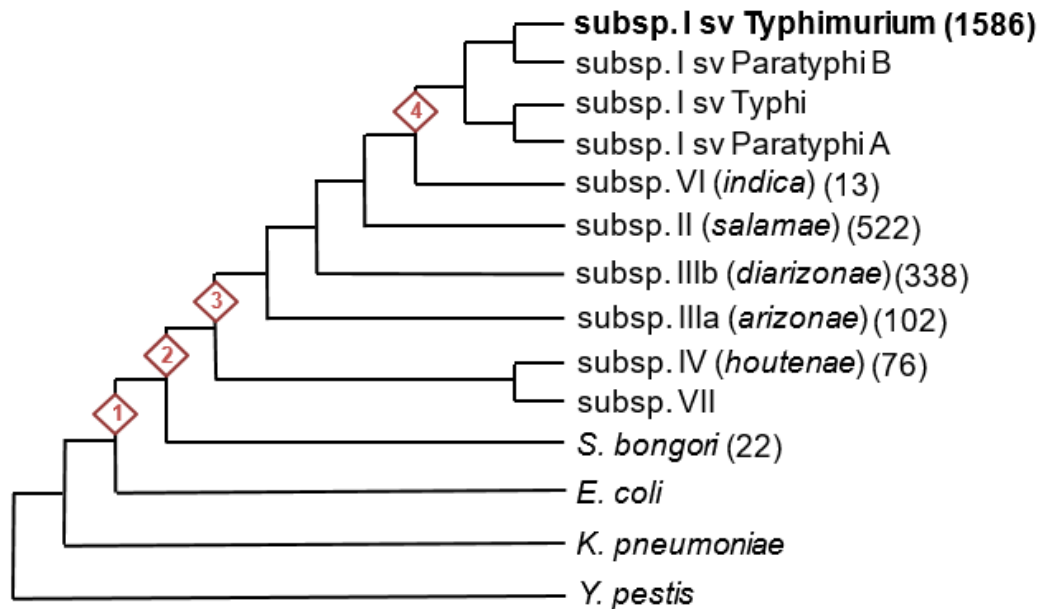
Figure 1.1 Phylogenetic representation of *Salmonella* subspecies and serovars in relationship to other Enterobacteriaceae. Critical evolutionary steps are marked in the order of occurrence, serovar numbers are recorded in parenthesis. **Step 1** represents the acquisition of SPI-1 by *Salmonella*'s common ancestor, creating a divergence between *Salmonella* and *Escherichia coli*. **Step 2** represents the acquisition of SPI-2 by the *Salmonella enterica* ancestor, separating the genus into the two species *S. enterica* and *S. bongori*. **Step 3** represents the acquisition of phase shifting of flagellin subunits, required to avoid the host's immune response. **Step 4** represents the ability of subspecies *enterica* (subsp. I) to colonise warm-blooded hosts. A result of serovar host adaptation, following the acquisition of *spv* (*Salmonella* plasmid virulence) genes. Adapted image (Ellermeier and Slauch, 2006) taken from Wells (2015).

1.2 *Salmonella* pathogenicity

Salmonella serovars are a major cause of global diarrhoeal disease, particularly in the developing world, where *Salmonella* infections play a significant role in morbidity and mortality of both humans and livestock (Rabsch, Tschape and Baumler, 2001; Crump and Mintz, 2010; Kirk *et al.*, 2015). Depending on the infecting serovar and the host, *Salmonella* infections can range from mild, self-limiting enterocolitis, to severe systemic infections and death. By mechanisms that remain poorly understood, some infected individuals progress into a chronic, asymptomatic carrier state, serving as a reservoir that allows for the shedding of *Salmonella* decades following initial infection (Gonzalez-Escobedo, Marshall and Gunn,

2011). Although *S. bongori* serovars usually infect cold-blooded animals, occasional cases of *S. bongori* induced enteritis are recorded in humans as well as warm-blooded mammal and avian hosts (Aleksic, Heinzerling and Bockemuhl, 1996; Woodward, Khakhria and Johnson, 1997; Giammanco *et al.*, 2002).

Despite their close genomic relatedness, *Salmonella* disease manifestation varies among the infecting serovars. Host-restricted serovars such as *S.* Typhi and *S.* Gallinarum, manifest as systemic disease in humans and fowl respectively, whereas host-adapted serovars such as *S.* Enteriditis and *S.* Typhimurium manifest as systemic infections in their primary host and as enterocolitis in other species (Uzzau *et al.*, 2000; Santos *et al.*, 2001; Suar *et al.*, 2006). As such, *Salmonella* enterica is a clear example of a species with a genomic signature that distinguishes between gastrointestinal and extra-intestinal serovars, whereby genes required for sustenance and growth in the intestinal lumen, have degraded in host-restricted, invasive serovars (Nuccio and Baumler, 2015).

1.2.1 Global impact

Despite global efforts to reduce morbidity and mortality, *Salmonella* remains a serious threat to global health. Although *S.* Typhi is all but eradicated from the developed world, in southeast Asia, Africa and Latin America, *S.* Typhi and *S.* Paratyphi infections are estimated at 25 million cases per year, resulting in 220.000 deaths annually (Crump, Luby and Mintz, 2004; Crump and Mintz, 2010; Buckle, Walker and Black, 2012; Mogasale *et al.*, 2014). Whereas typhoid fever is primarily restricted to the developing world, cases of *Salmonella* induced gastroenteritis are a global problem. The rate of non-Typhoidal *Salmonella* infections is estimated at approximately 93.8 million cases annually, of which approximately 155.000 result in death (Majowicz *et al.*, 2010) and the rate of invasive non-typhoidal *Salmonella* infections is estimated at approximately 3.4 million cases annually of which approximately 680.000 result in death (Ao *et al.*, 2015). Although *S.* Typhi infections are relatively uncommon in immunocompromised individuals, non-Typhoidal serovars, especially the invasive types, are of significant risk to patients suffering from HIV and AIDS (Chatterjee *et al.*, 2012; Feasey *et al.*, 2012, 2016; Ao *et al.*, 2015).

Studies carried out into two separate cases of *Salmonella* outbreaks in the past decade, demonstrate that the economic burden of *Salmonella* is significant. A *S.* Typhimurium outbreak of a municipal drinking water supply in Colorado, 2008, infected 434 people. The economic burden of this outbreak was estimated at $2.6 million (Ailes *et al.*, 2013). An outbreak of *S.* Thompson from smoked salmon in the Netherlands, 2012, resulted in 1149

cases and an estimated economic burden of €7.5 million (Suijkerbuijk *et al.*, 2016). Considering these two cases are but only specks on the global scale of *Salmonella* infections, the economic burden of Salmonellosis and Typhoid fever is considered a significant strain on the resources of developing countries.

1.2.2 Enteric fever

1.2.2.1 Organisms and origin

Enteric fever is an umbrella term for two diseases; typhoid fever and paratyphoid fever. Whereas the former is a result of infection with the host-restricted *S.* Typhi, the latter is the result of infection with the host-restricted *S.* Paratyphi A, or the host-adapted *S.* Paratyphi B, *S.* Paratyphi C and *S.* Sindai (Taylor and Eves, 1969; Tracz *et al.*, 2006; Zhou *et al.*, 2014). Despite belonging to different serogroups, *S.* Typhi and *S.* Paratyphi A are genomically more closely related than other *S. enterica* serovars, and are estimated to have adapted to the human host approximately 15.000 – 15.000 years ago (Kidgell *et al.*, 2002). Both serovars display similar genome degradation, including the accumulation of pseudogenes, mostly genes required for the colonisation and invasion of the gut (McClelland *et al.*, 2004) . *S.* Paratyphi B and *S.* Paratyphi C are genetically and antigenically distinct from the host-restricted serovars (Selander *et al.*, 1990; Porwollik *et al.*, 2004).

1.2.2.2 Incidence

Despite having been all but eliminated from Western countries, enteric fever remains a significant health burden in the developing world. Although rough estimations of incidence have been published, the real impact of *S.* Typhi and *S.* Paratyphi in endemic areas is difficult to determine due to various reasons (Crump, Luby and Mintz, 2004; Buckle, Walker and Black, 2012; Mogasale *et al.*, 2014). Enteric fever is most dominant in urban slums and rural areas with poor sanitation facilities. These areas often have limited or no access to health care, and only the most severe cases are hospitalised and documented. Therefore the registered number of cases reflects the hospitalisation rates, but not exposure rates among the whole community. Additionally, symptoms of enteric fever are very similar to other febrile diseases, and in areas with no access to pathological laboratories the incidence of *Salmonella* infections is often underestimated (World Health Organisation Department of Vaccines andBiologicals., 2003; Breiman *et al.*, 2012). The definitive diagnosis of typhoid fever requires the isolation of *S.* Typhi from stool samples, blood, bone marrow or anatomical lesions. However, this is a costly and specialised process, which is often not available or affordable in endemic regions (Vallenas *et al.*, 1985; Farooqui *et al.*, 1991; World Health

Organisation Department of Vaccines andBiologicals., 2003). Instead, diagnosis in these areas is often based on antibody responses using the Felix-Widal test. It measures agglutinating antibodies against *S.* Typhi O- and H-antigens over the course of 1-2 weeks. Although this test is suggestive of typhoid fever, the result is not definitive. Indeed, the Felix-Widal test demonstrates a negative result for up to 30% of confirmed *S.* Typhi infections (Bijapur *et al.*, 2014). New tests are in development to increase diagnostic speed and accuracy.
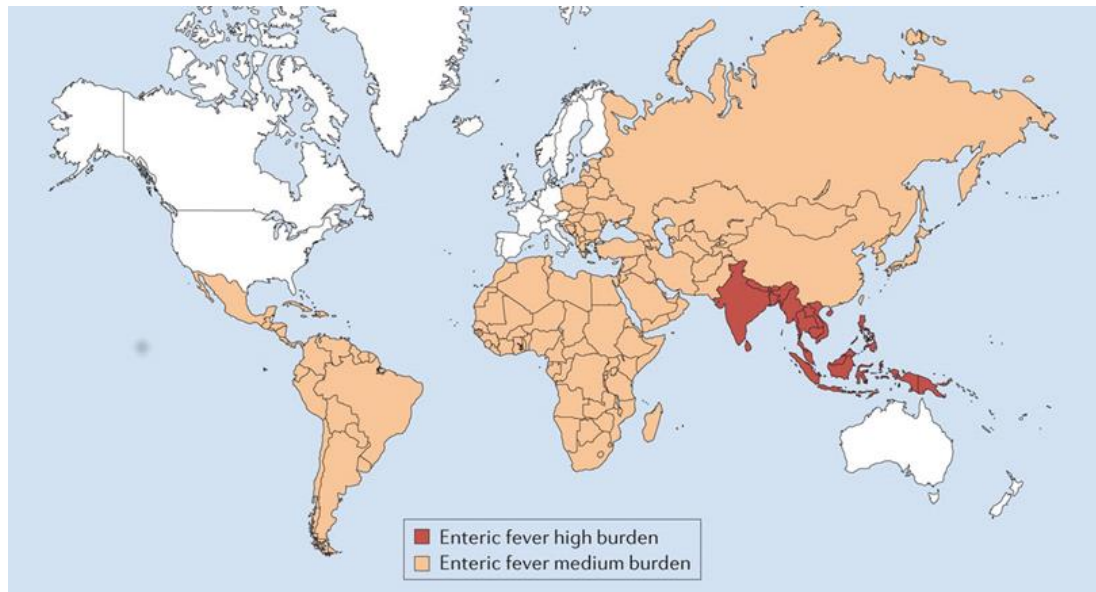
Figure 1.2 Global enteric fever burden. The geographic distribution of enteric fever demonstrates medium incidence (10-100 cases per 100,000 population per annum) occurs in Eastern Europe, Asia, Africa, Latin America and South America. High incidence (>100 cases per 100,000 population per annum) of *Salmonella* Typhi infections is recorded in South East Asia. Image taken from (Gilchrist, MacLennan and Hill, 2015)

Studies estimating the global burden of enteric fever enlist Southeast Asia and Sub-Saharan Africa as high-risk areas for enteric fever. Central Asia, the Middle-East, North Africa, and Latin and South America are reported as medium risk areas (figure 1.2). There has been an interesting shift in the risk classification for Sub-Saharan Africa; whereas earlier reports estimate a relatively low incidence of enteric fever, more recent studies clearly report this area as high risk. This shift is likely due to the increase in typhoid studies carried out in Africa. Another area of interest is the Guangxi province Southern China, where *S.* Paratyphi A has become the dominant cause of enteric fever (Yang *et al.*, 2004; Jin, 2008). This province has been subjected to an immunisation program against *S.* Typhi, using a locally produced Vi-polysaccharide vaccine; between 1995-2006 more than 4.2 million doses of the vaccine have been administered in the endemic region (Yang *et al.*, 2001; DeRoeck *et al.*, 2008). However,

the Vi-polysaccharide vaccine does not protect against *S.* Paratyphi A (DeRoeck *et al.*, 2008). The increased immunisation of the Guangxi community against *S.* Typhi has likely allowed for *S.* Paratyphi to become the dominant cause of enteric fever (Jin, 2008).

1.2.3 Salmonellosis

Salmonella enterica serovars are among the leading causes of foodborne diarrhoeal infections worldwide (Majowicz *et al.*, 2010; Havelaar *et al.*, 2015). However, not all *Salmonella* infections are created equal, and there are differences in disease prognoses between different infecting serovars. The fatality rate of *S.* Typhimurium infections is estimated at approximately 0.6%, the fatality rate of *S.* Newport is significantly lower at 0.3% and the fatality rate of *S.* Dublin is significantly higher at 3% (Jones *et al.*, 2008). At 6% and 7%, the chance of development into invasive disease is relatively low for *S.* Typhimurium and *S.* Enteritidis respectively, whereas rates of invasive disease are up to 57% for *S.* Choleraesuis and 64% for *S.* Dublin. Different age groups are also more susceptible to specific serovars; whereas *S.* Typhimurium is the most common infecting serovar in children, *S.* Dublin infections are more commonly found in the elderly (Jones *et al.*, 2008). Estimating local and global incidence of Salmonellosis is difficult. The non-typhoidal *Salmonella* serovars are broadly adapted to multiple hosts and infection generally results in self-limiting disease that does not require any treatment. Many cases of Salmonellosis therefore go unreported (Majowicz *et al.*, 2010). Although most cases of non-typhoidal *Salmonella* infections are restricted to localised inflammation of the intestinal epithelium, which is characterised by abdominal cramps, diarrhoea or constipation and vomiting, sometimes the infection progresses to invasive non-typhoidal disease, resulting in bacteraemia and/or focal infections. These patients require antibiotic treatment and hospitalisation for rehydration and treatment of complications (Chiu, Su and Chu, 2004; Haraga, Ohlson and Miller, 2008).

Researchers of *Salmonella* infections take particular interest in *Salmonella* serovar Typhimurium. When infecting mice, this serovar progresses into a systemic, typhoid-like disease. When infecting humans however, *S.* Typhimurium infections are restricted to enterocolitis and occasionally bacteraemia. This makes *S.* Typhimurium an invaluable model for the study into Typhoidal diseases and *Salmonella* induced enterocolitis alike (Baumler *et al.*, 1998).

1.2.4 Infection mechanisms

Salmonella infections typically occur after ingestion of contaminated food or water, or after close contact with an infected individual. The success rate of *Salmonella* infections is dependent on several parameters, including infecting serovar, ingested bacterial load, condition of the host's gut microbiota and the immunological state of the host (Darwin and Miller, 1999). Post ingestion, *Salmonella* must first overcome the stress posed by the low pH of gastric fluids. The acid tolerant responses include activation of several regulators, including the stress response regulators OmpR, PhoPQ and RpoS, the methyltransferase Ada, the ferric uptake regulator Fur, and more than 100 acid shock proteins (Foster, 1991; Bearson, Wilson and Foster, 1998; Bang *et al.*, 2002; Suar and Ryan, 2015). *Salmonella* passes from the stomach into the intestinal lumen, where it colonises the cecum and the ileum, attaching more tightly to the latter (Hohmann, Schmidt and Rowley, 1978). Once attached, *Salmonella* crosses the epithelium predominantly via the M-cells present in the Peyer's patches (Tam *et al.*, 2008). Upon crossing the epithelial layer separating the intestinal lumen from the host's tissues, *Salmonella* crosses the cells of the Peyer's patches and the mesenteric lymph nodes. Soon after initial *Salmonella* infection, the native immune system is activated and the intruding bacteria are contained by phagocytic cells. Virulence factors encoded on *Salmonella* pathogenicity islands (SPIs) allow *Salmonella* to survive within the phagocyte, resulting in transportation of *Salmonella* from its initial site of infection to other organs including the spleen, liver and gall bladder. Via the gall bladder, *Salmonella* re-enters the gastrointestinal tract, resulting in reinfection of the Peyer's patches which elicits a strong immunological response that leads to intestinal perforations, haemorrhage and necrosis (Jarvelainen, Galmiche and Zychlinsky, 2003; Tam *et al.*, 2008; Gonzalez-Escobedo, Marshall and Gunn, 2011).

1.2.5 *Salmonella* virulence factors

1.2.5.1 *Salmonella* pathogenicity islands

Many *Salmonella* virulence factors, including genes involved in adhesion, invasion and intracellular survival, are encoded on clustered genomic loci called *Salmonella* pathogenicity islands (SPIs). They are large, unstable elements of the *Salmonella* chromosome that are characterised by a low GC content and atypical codon usage, and are thought to be the result of horizontal transfer events (Kelly, Vespermann and Bolton, 2009). To date, 21 SPIs have been characterised, SPI-1-6, 9, 11, 12, 13 and 16 are found in both *S.* Typhimurium and *S.* Typhi, SPI-14 is unique to Typhimurium and SPI-7, 15, 17 and 18 are only found in Typhi,

other SPIs are absent in both Typhimurium and Typhi but are present in other serovars including Dublin, Enteritidis and Gallinorum (Shah *et al.*, 2005; Blondel *et al.*, 2009; Sabbagh *et al.*, 2010). Both SPI-1 and SPI-2 encode Type III Secretion Systems (TTSS). Interestingly, whereas SPI-1 is found both in *S. enterica* as well as in *S. bongori,* SPI-2, required for replication inside macrophages, is only found in *S. enterica* serovars. These observations suggest that SPI-1 was acquired by a common *Salmonella* ancestor after its divergence from the ancestor shared with *E. coli*, and SPI-2 was acquired by *Salmonella enterica* after its divergence from *S. bongori* (Fookes *et al.*, 2011). Furthermore, the lack of SPI-2 in *Salmonella bongori* may explain why this serovar predominantly infects cold-blooded animals, as the genes required for the successful invasion and infection of mammals are encoded on SPI-2 (Fookes *et al.*, 2011; Figueira and Holden, 2012).

1.2.5.2 Type III secretion systems and secreted effector proteins

Some SPIs encode proteins required for the formation of TTSS. These protein complexes form syringe-like macromolecular structures that deliver effector proteins to the host cell during infection. They consist of a motor, a needle complex and a translocon, through which effector proteins can be exported (Ghosh, 2004). TTSS encoded on SPIs are specific to the virulence genes encoded on that SPI, and *Salmonella* serovars can express several distinct TTSSs, depending on the SPIs they carry. The TTSS encoded on SPI-1 is required by *Salmonella* during the invasion of the host's intestinal epithelium and M-cells (Kaur and Jain, 2012). Expression of this system can be regulated by conditions that mimic the environment of the ileum, including high osmolarity, pH, oxygen tension, bile, Mg^{2+} concentration and short chain fatty acids (Altier, 2005). During invasion of the host's epithelium, the translocon proteins SipB and SipC, located at the tip of the TTSS needle-like structure, make contact with the M-cells found in the Peyer patches, and inject effector proteins directly into the cytosol. These excreted effector proteins, which include the *Salmonella* o̲uter p̲roteins SopB and SopE, as well as the *Salmonella* i̲nvasion p̲roteins SipA and SipB, induce M-cell membrane ruffling via reorganisation of actin filaments, leading to the uptake of *Salmonella* (Hansen-Wester and Hensel, 2001; McGhie, Hayward and Koronakis, 2001). Following uptake, *Salmonella* survives inside the *Salmonella* containing vacuole (SCV), and secretes effector proteins, including SptP, undo the actin filament reorganisation, allowing the M-cell to return to its native state, preventing activation of the host's inflammatory response (Fu and Galan, 1999).

The TTSS encoded on SPI-2 is required for survival and growth within the SCV during systemic infection. *Salmonella* requires a stable SCV to replicate within macrophages. The acidic

conditions inside macrophages activate the secretion of SPI-2 encoded effector proteins, including SifA, SseF, SseG, SopD2 and PipB2. These proteins are involved in the formation of *Salmonella*-induced filaments, required for stabilisation and growth of the SCV (Garcia-del Portillo *et al.*, 1993; Stein *et al.*, 1996; Jiang *et al.*, 2004; Knodler and Steele-Mortimer, 2005; Haraga, Ohlson and Miller, 2008; Figueira *et al.*, 2013). Other SPI-2 encoded effector proteins are involved in the inhibition of the MAP-kinase signalling pathways and limit the release of cytokines from infected macrophages, as well as regulated apoptosis of the infected macrophage, allowing *Salmonella* to escape the cell and infect tissues including liver, spleen and gall bladder (Hersh *et al.*, 1999; Monack, Bouley and Falkow, 2004; Figueira and Holden, 2012; Figueira *et al.*, 2013).

1.2.6 Treatment and prevention

1.2.6.1 Treatment of salmonellosis

Non-typhoidal *Salmonella* serovars are a major cause of food-borne disease worldwide. Although most infections result in self-limiting gastroenteritis that requires no further treatment, these serovars can cause serious morbidity and mortality in some individuals. Children with underdeveloped or compromised immune systems, including those very young of age, and those suffering from HIV infections, cancer, inflammatory bowel disease or immunosuppressive treatment are at risk of developing bacteraemia following non-typhoidal *Salmonella* infection. Adults with underlying conditions are at risk of developing focal infections following bacteraemia including meningitis, osteomyelitis and septic arthritis (Cohen, Bartlett and Corey, 1987; Chen *et al.*, 1999; Chiu, Lin and Ou, 1999, 2000; Chiu, Su and Chu, 2004). Uncomplicated non-typhoidal *Salmonella* infections are self-limiting and should not be treated with antimicrobial agents. However, when complications occur, or in patients at risk due to underlying conditions, treatment with broad-spectrum cephalosporins or fluoroquinolones is recommended until susceptibility patterns are known. The duration of the therapy averages between 2-6 weeks, depending on the site of infection (Chiu, Su and Chu, 2004). The rise of antimicrobial resistance is a significant threat, with 50-75% of reports from Sub-Saharan Africa mentioning multidrug resistant strains, including decreased susceptibility to fluoroquinolones and third generation cephalosporins (Kariuki *et al.*, 2015).

1.2.6.2 Treatment of typhoid fever

Typhoid fever infections can generally be managed at home, provided there are supportive measures in place, including the use of antipyretics, oral antibiotics, and medical follow-up. However, patients at risk of severe dehydration, patients with underlying condition, patients

suffering from complications, or those suffering from resistant *S.* Typhi infections may require hospitalisation (World Health Organisation. 2003). Considering most cases of typhoid fever occur in developing countries, efficacy, cost and availability are important factors in the choice of first line antibiotics. Due to its relative low cost and rapid and reliable efficacy, fluoroquinolones are generally regarded as the first choice of therapeutics. They are generally well tolerated, clear the symptoms within a week and display very low rates of carrier state development (Arnold et al. 1993; Cristiano et al. 1995; Chinh et al. 2000; World Health Organisation. 2003). However, in areas where *S.* Typhi is still sensitive to traditional first-line antibiotics, Chloramphenicol, Ampicillin, Amoxicillin and Trimethoprim-Sulfamethoxazole are also commonly used (World Health Organisation, 2011). The emergence of multidrug resistant strains has complicated the treatment of *S.* Typhi significantly. Resistance the traditional first-line of antibiotics mentioned above has been reported since the late 1980s. Additionally, an increasing number of studies report the emergence of partial and total resistance against fluoroquinolones, which can often be identified using nalidixic acid resistance as a marker. Nalidixic acid resistant strains are now endemic in the Indian subcontinent, Vietnam and Tajikistan (Das and Bhattacharya, 2000; Dutta *et al.*, 2001; Gupta, Swarnkar and Choudhary, 2001; Neopane *et al.*, 2008).

1.2.6.3 The chronic carrier state

The chronic carrier state is a condition in which patients have developed chronic *S.* Typhi infections of the gall bladder (Merselis et al. 1964; Levine et al. 1982). Untreated chronic carriers present a *Salmonella* Typhi reservoir, shedding large amounts of *S.* Typhi in their stool and urine, which can be a continuing source of infection for decades (Shpargel, Berardi and Lenz, 1985). Most chronic carriers suffered from typhoid fever prior to developing the chronic carrier state, however some individuals develop the chronic carrier state without previous symptoms of *S.* Typhi infection. The chronic carrier state is declared when *S.* Typhi can be isolated from stool samples a year post infection. Once identified, the WHO recommends treatment of the carrier with ciprofloxacin (World Health Organisation, 2011). Furthermore, to quench the spread of *S.* Typhi from chronic carriers, those affected and their close relatives are not to attend child care facilities, and not to participate in occupations involving handling of food, care for patients, and care for the very young and the elderly. However, identification of chronic carriers can be difficult, with 25% of cases presenting as asymptomatic infections. Tracking and treatment of chronic carriers is an important strategy in the prevention of the spread of *S.* Typhi (Sinnott & Teall 1987; World Health Organisation 2003; World Health Organisation 2011).

1.2.6.4 Vaccine development

Considering the rise in reports of MDR *Salmonella* infections and the emergence of resistance to fluoroquinolones and third generation cephalosporins, new treatment and prevention methods are urgently needed. Development of *Salmonella* vaccines has proven to be complicated. Unlike other enteric pathogens, *Salmonella* infections do not typically elicit long-term immunity and current *Salmonella* vaccines offer protection for a few years only (Galen *et al.*, 2016). Currently, three typhoid fever vaccines are licenced for human use: a live-attenuated vaccine, a capsular Vi polysaccharide preparation vaccine and a Vi polysaccharide-tetanus toxoid conjugate vaccine. The live attenuated vaccine, Ty21a (Vivotif®), is composed of a *S.* Typhi strain carrying several mutations in a pathway that allows the incorporation of galactose into its LPS. Successful immunisation requires three oral doses, and provides a 62%-78% protection over 5 years. The live-attenuated vaccine also provides some protection against *S.* Paratyphi B infections (MacLennan, Martin and Micoli, 2014). There are two brands of the capsular Vi polysaccharide preparation vaccine, Vi Typherix® (GSK) and Typhim Vi® (Sanofi Pasteur) and one brand of Vi polysaccharide-tetanus toxoid conjugate vaccine, Typbar TCV® (Pakkanen *et al.*, 2015; Tennant and Levine, 2015). *S.* Typhi Vi polysaccharides form a capsule that shield the LPS, preventing signalling between LPS and the Toll-like receptor 4 on the host's phagocytic cells (Wilson *et al.*, 2008). Because *S.* Paratyphi does not produce Vi polysaccharides, these engineered vaccines do not offer protection to serovars other than *S.* Typhi (DeRoeck *et al.*, 2008). Due to the relative short protection offered by the available *S.* Typhi vaccines, and the requirement for several doses, the licenced vaccinations are of little use to remote and impoverished endemic areas, and are primarily used by travellers (World Health Organisation 2003). Vaccine development for non-invasive Salmonella serovars is challenging considering number and variety of infecting serovars, as well as lack of funding. Although there are currently no human vaccines available for non-typhoidal *Salmonella* infections, monovalent and bivalent vaccines for *S.* Typhimurium and *S.* Enteritidis are currently under development (Tennant *et al.*, 2016).

1.3 Gram negative cell envelope

1.3.1 General composition of the Gram-negative cell envelope

Gram-negative bacteria have a complex cell envelope architecture, which plays a key role in their natural resistance against various environmental stresses and antimicrobial agents. The topography of the Gram-negative envelope displays two membranes, separated by an

aqueous compartment known as the periplasm. The cytoplasmic, inner membrane (IM) is a symmetrical bilayer of phospholipids, spanned by membrane proteins including the Sec- and Tat-translocation systems and two-component signal systems. The outer membrane (OM) is an asymmetrical bilayer, composed of phospholipids on the internal side, and lipopolysaccharide (LPS) on the external side. The OM is spanned by various porins that allow selective transport across the outer membrane. The IM and OM are separated by a gel-like periplasm, containing a thin layer of peptidoglycan for structural support and a range of chaperones involved in the biogenesis, maintenance and repair of the outer membrane (Gan, Chen and Jensen, 2008)

1.3.2 LPS

1.3.2.1 Structure and function of LPS

LPS is the major lipid component of the OM of many, but not all, Gram-negative bacteria. It covers approximately 75% of the cell surface, and is essential for the survival and pathogenicity of most Gram-negative bacteria (Sperandeo, Martorana and Polissi, 2016). LPS molecules typically consist of two or three components; a hydrophobic moiety known as lipid A that ensures the anchoring of LPS into the OM, a core oligosaccharide composed of repeating sugar residues that protrudes outwardly from the membrane and an *O*-antigen, attached to the core (see figure 1.3) (Raetz and Whitfield, 2002). The most conserved portion of LPS is lipid A, followed by the inner part of the core. The outer part of the core and the *O*-antigen can be highly variable, even within the same species, and some Gram-negative species lack an *O*-antigen altogether (Verma, Quigley and Reeves, 1988; Holst, 2007; Wang, Wang and Reeves, 2010). The combined negative charges of the LPS polysaccharide cores and *O*-antigens generate a significant repulsive force that risks compromising the integrity of the OM. The electrostatic force across the LPS layer is neutralised by interactions with divalent cations including Ca^{2+} and Mg^{2+}. The binding of these cations also allows for the formation of salt bridges, which strengthen the integrity of the LPS layer further (Clifton *et al.*, 2015). Indeed, the aliphatic nature of the fully saturated fatty acyl chains and cation interactions create a gel-like lipid layer with low fluidity, which contributes to the low permeability of hydrophobic solutes across the OM. It has long been known that the removal of LPS-bound divalent cations by chelating agents permeabilizes the OM, making the cell more susceptible to toxic agents and environmental stress (Leive, 1965; Vaara, 1992; Nikaido, 2003).

1.3.2.2 LPS biosynthesis and the Lpt machinery

Biosynthesis of lipid A and the first part of the core polysaccharide, Kdo, occurs at cytoplasmic side of IM, where the Lipid A-Kdo complex is formed. Lipid A is anchored in the IM via its hydrophobic moiety, with the hydrophilic moiety sticking out into the cytoplasm (Sperandeo, Martorana and Polissi, 2016). The Lipid A-Kdo complex is then flipped across the IM by the ATP-binding cassette (ABC) transporter MsbA, so that the hydrophilic moiety is exposed to the periplasm (Zhou *et al.*, 1998). In *O*-antigen producing strains, the residues that will form the repeat units are synthesised in the cytoplasm and transported to the periplasm, where extension of the core occurs (Greenfield and Whitfield, 2012). The extended *O*-antigen and the lipid A-core complex are ligated in the periplasm with the help of WaaL ligase, producing mature LPS (Han *et al.*, 2012). The transport of mature LPS across the periplasm and its insertion into the OM is aided by the Lpt molecular machine displayed as figure 1.4 (Sperandeo, Martorana and Polissi, 2016).
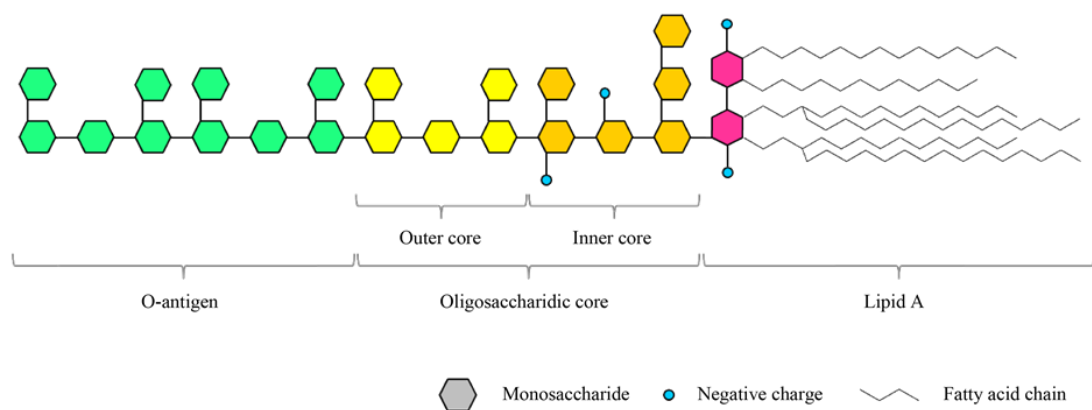
Figure 1.3 Schematic representation of lipopolysaccharide (LPS). LPS is a major component of the outer membrane of most Gram-negative bacteria, covering approximately 75% of the cell surface. The molecules typically of the membrane anchored moiety lipid A, a core oligosaccharide that protrudes outwardly from the membrane, and a highly variable *O*-antigen. Image taken from (Gemma, Molteni and Rossetti, 2016)

To allow for the transport of the partially hydrophobic, partially hydrophilic LPS molecules, a machinery that spans the periplasm is used. This multiprotein complex is named Lpt (Lipopolysaccharide transport) and is primarily studied in *Neisseria meningitidis* and *Escherichia coli* (Sperandeo, Martorana and Polissi, 2016). The Lpt complex is composed of seven essential proteins that interact with one another to form a bridge spanning the cell envelope (Ruiz *et al.*, 2008; Sperandeo *et al.*, 2008; Chng, Gronenberg and Kahne, 2010). Depletion of any of these components results in a block of *de novo* synthesised LPS in the

periplasm (Sperandeo, Martorana and Polissi, 2016). The seven proteins can be separated into two sub-complexes, the atypical ABC transporter LptBC$_2$FG at the inner membrane and LptDE translocon at the OM, connected by oligomeric structured periplasmic protein LptA (Sperandeo, Martorana and Polissi, 2016). The N-terminal domain of LptA interacts with the C-terminal domain of LptC at the IM site, and the C-terminal domain of LptA interacts with the N-terminal domain of LptD at the OM site (Freinkman *et al.*, 2012).
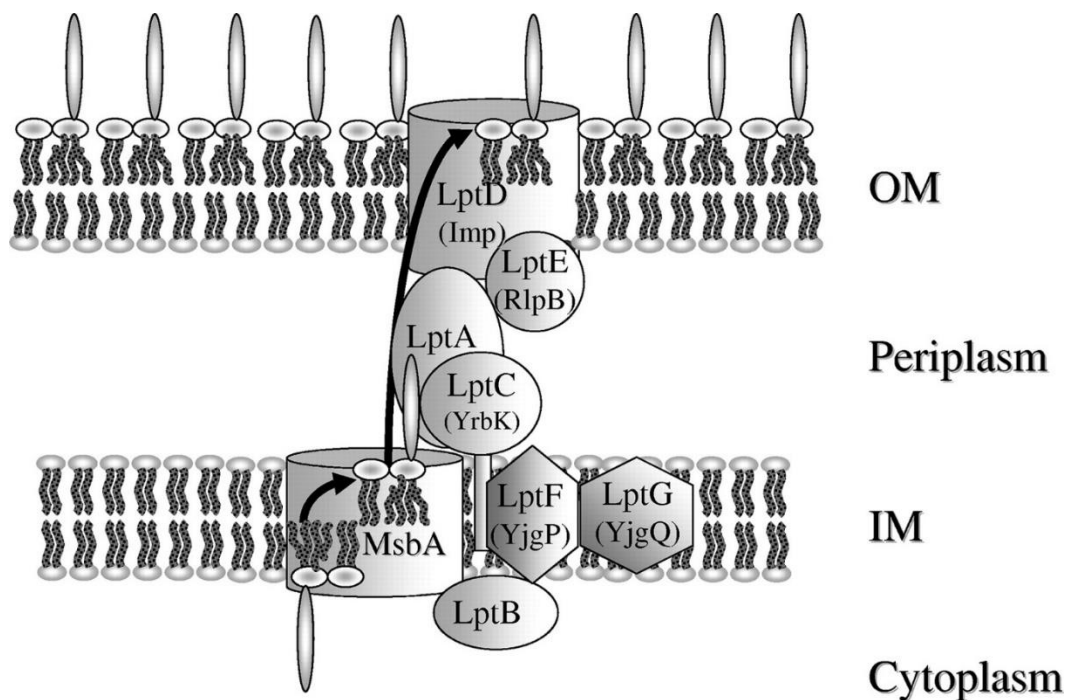
Figure 1.4 Model of the Lpt machinery. LPS is synthesised in the cytoplasm and subsequently transported to the outer membrane. The inner membrane (ABC) transporter MsbA the transports LPS across the inner membrane. LptA, LptB and LptC form a complex that aids in the transport of LPS across the periplasm to the OM, where it interacts with the LptD/LptE complex that is involved in the insertion of LPS into the OM. Image taken from (Sperandeo, Martorana and Polissi, 2016).

The transporter LptBC$_2$FG is not involved with the transport of LPS across the IM, but rather it couples energy gained by ATP hydrolysis in the cytoplasm with detachment of LPS from the IM. Once detached from the IM, LPS molecules are delivered to LptA at the expense of ATP hydrolysis (Sperandeo, Martorana and Polissi, 2016). The *in vivo* translocation of LPS requires at least two energy-dependent steps: to extract LPS from IM and to transfer LPS from LptC to LptA (Okuda, Freinkman and Kahne, 2012). Hydrophobic cavities shared by LptC, LptA and LptD supposedly create a hydrophobic groove that protects the lipid A portion of LPS, to allow safe transit in periplasm. The mechanism proposed by Kahne is a "PEZ candy dispenser" model in which energy released by ATP hydrolysis in the cytoplasm is used to push a

continuous stream of LPS through the LptA bridge towards the OM. Constitutive presence of LPS molecules is thought to stabilise interactions between proteins that form a bridge (Okuda, Freinkman and Kahne, 2012; Li *et al.*, 2015; Okuda *et al.*, 2016; Sperandeo, Martorana and Polissi, 2016). For the correct insertion of LPS, the Lpt machinery requires a translocon in the OM, composed of LptD and LptE. LptD is the largest monomeric β-barrel protein of which the structure is solved to date; composed of an N-terminal Lpt-fold and a C-terminal β-barrel domain consisting of 26 antiparallel strands. The barrel is plugged by LptE in a Plug-and-Barrel architecture (Chng *et al.*, 2010; Freinkman, Chng and Kahne, 2011; Dong *et al.*, 2014; Qiao *et al.*, 2014). The lipid A portion of LPS is transferred from LptA to the N-terminal of LptD, the saccharide portion of LPS enters a hydrophilic vestibule of the LptDE translocon. A hydrophobic intermembrane, formed by LptD could provide passage through which LPS-acyl chains can be inserted into the membrane. The core and O-antigen moieties are thought to pass laterally though a gate, created by weak β-strand hydrogen bonding in LptD. (Gu *et al.*, 2015; Li *et al.*, 2015). LptE is thought to be involved in interacting with the negatively charged units of LPS to affect the aggregation state during translocation. Bacteria producing less aggregation-prone LPS and bacteria missing O-antigens have a lesser need of LptE (Malojčić *et al.*, 2014; Sperandeo, Martorana and Polissi, 2016). In order to effectively interact with LptA, LptD requires reshuffling of intramolecular disulphide bonds, aided by LptE and the periplasmic chaperone BepA, to ensure correct coordination of the translocon assembly. (Ruiz *et al.*, 2010; Narita *et al.*, 2013; Botos *et al.*, 2016).

1.3.2.3 LPS induced envelope stress responses

LPS-damage induced envelope stress activates the Sigma E (σ^E) envelope stress response (Chapter 1.5.1) and the Rcs phosphorelay response (Chapter 1.5.3) (Sperandeo, Martorana and Polissi, 2016). Involved in the σ^E response are the regulatory proteins RseA and RseB, the cytoplasmic adaptor protein SspB, the proteases DegS and RseP and σ^E mediated transcription (Barchinger and Ades, 2013). The regulation of the σ^E response is described in detail in chapter 1.5.1.

The Rcs phosphorelay pathway is activated by alterations in LPS structure. Involved in this stress response are the two-component phosphorelay proteins RcsC and RcsD. These IM proteins act as sensor kinase and phosphotransferase to transduce membrane signal and activate the cytoplasmic response regulator RcsB (Sperandeo, Martorana and Polissi, 2016). RcsC can directly sense LPS stress in the periplasm, whereas envelope defects are sensed by the OM lipoprotein RcsF (Laubacher and Ades, 2008; Farris *et al.*, 2010). RcsF forms transmembrane complexes with OMPS and senses the status of the LPS layer. By an unknown

mechanism, RcsF activates the Rcs phosphorelay response, when lateral interactions between LPS molecules are altered or perturbed. (Cho *et al.*, 2014; Konovalova *et al.*, 2014; Konovalova, Mitchell and Silhavy, 2016; Sperandeo, Martorana and Polissi, 2016).

1.3.4 BAM-insertion complex

The OMPs of Gram-negative bacteria are essential to the function of the outer membrane (Kim, Aulakh and Paetzel, 2012). OMPs function as nonspecific porins, allowing passive diffusion of small hydrophilic molecules, or as substrate specific channels, allowing the diffusion of specific molecules (Nikaido, 1992, 2003). They can function as translocons involved in the export of proteins and drugs, or they can function as autotransporters, involved in the secretion of virulence factors (Jacob-Dubuisson, Locht and Antoine, 2001; Desvaux, Parham and Henderson, 2004; Zgurskaya *et al.*, 2011). Some OMPS have enzymatic properties, including proteases and phospholipases, whereas other OMPs are of a structural nature, involved in stabilising other OMPs and components of the outer membrane (Nikaido, 2003; Song *et al.*, 2008). Despite their varied roles, most OMPs share a β-barrel transmembrane architecture, which is unique to Gram-negative bacteria, mitochondria and chloroplasts. These β-barrel proteins contain between 8 and 26 transmembrane domains consisting of amphipathic β-strands arranged in an antiparallel fashion, with the first and the last strand interacting, to form a barrel-like shaped β-sheet (Walther, Rapaport and Tommassen, 2009; Misra, 2012). Although *in vitro* experiments demonstrated that OMPs are capable of spontaneous folding and insertion into synthetic phospholipid bilayer membranes, the rate of this spontaneous occurrence is too low to be considered biologically relevant (Tamm, Arora and Kleinschmidt, 2001; Burgess *et al.*, 2008). Indeed, the folding and insertion of OMPs into the outer membrane requires the aid of the β-barrel assembly mechanism complex, also known as the BAM-complex (Kim, Aulakh and Paetzel, 2012; Noinaj, Gumbart and Buchanan, 2017).

1.3.4.1 The BAM-Complex

The OMP BamA was the first discovered component of the BAM-complex, and homologues are found in all Gram negative species, mitochondria and chloroplasts (Voulhoux *et al.*, 2003; Schleiff and Soll, 2005). To form the assembly machinery, BamA interacts with various other proteins, which vary between species. In *E. coli* the BAM-complex consists of the essential core component BamA and four accessory lipoproteins BamB, BamC, BamD and BamE, as displayed in figure 1.5 (Onufryk *et al.*, 2005; Kim, Aulakh and Paetzel, 2012). The C-terminal membrane-spanning domain of BamA is formed of a 16-stranded β-barrel, and the N-

terminal domain of BamA extends into the periplasm and contains five polypeptide transport associated (POTRA) domains (Kim, Aulakh and Paetzel, 2012; Ni *et al.*, 2014; Noinaj, Gumbart and Buchanan, 2017). These POTRA domains are involved in protein-protein interactions; BamB, BamD and SurA all interact with at least one of the BamA POTRA domains (Bennion *et al.*, 2010; Jansen, Baker and Sousa, 2015; Bergal *et al.*, 2016; Chen *et al.*, 2016). BamB is a lipoprotein which adopts an eight-bladed β-propeller fold containing WD40-like motifs, suggesting it may act as a scaffold for the BAM-complex (Heuck, Schleiffer and Clausen, 2011; Kim and Paetzel, 2011). SurA is a periplasmic protein involved in the transport of nascent OMPs across the periplasm (Chapter 3.1.1.1). Although BamB is not an essential protein in *E. coli*, its absence results in a significant reduction in OMP assembly, demonstrating a phenotype that is nearly indistinguishable from *surA* null-mutants (Charlson, Werner and Misra, 2006; Ureta *et al.*, 2007). The absence of both BamB and SurA (Chapter 3.1.1.1) leads to synthetic lethality, suggesting that BamB may interact with SurA to deliver precursor OMPs to the BAM-complex (Onufryk *et al.*, 2005; Kim, Aulakh and Paetzel, 2012). BamC is a lipoprotein containing two surface-exposed helix-grip domains (Kim *et al.*, 2011; Webb *et al.*, 2012). Although BamC is not essential for cell viability, its absence results in membrane permeability defects. Despite the mutant phenotype, the role of BamC in the BAM-complex remains enigmatic (Kim, Aulakh and Paetzel, 2012; Noinaj, Gumbart and Buchanan, 2017). In *E. coli,* BamD is an essential lipoprotein consisting of five tetratricopeptide (TPR) domains, which form scaffolds to aid protein-protein interaction (Sandoval *et al.*, 2011; Dong *et al.*, 2012). It does not only interact with BamA, but BamD also interacts with BamC and BamE (Kim, Aulakh and Paetzel, 2011; Knowles *et al.*, 2011). The protein is thought to play a role in target signal recognition, substrate interaction and activation of BamA (Noinaj, Gumbart and Buchanan, 2017). The final *E. coli* BAM-complex associated lipoprotein is BamE, the smallest, non-essential accessory protein, containing an ααββ-fold which enhances the interactions between BamA and BamD. BamE is capable of recruiting phosphatidylglycerol, a ubiquitous lipid that enhances the insertion of OMPs into liposomes and membranes (Kim *et al.*, 2011; Knowles *et al.*, 2011).

The *Salmonella enterica* BAM-Complex is very similar to the well-studied *E. coli* BAM-complex, consisting of the OMP BamA and the lipoproteins BamB, BamC, BamD and BamE (Fardini *et al.*, 2009). In *Salmonella*, BamA is an essential protein but unlike the *E. coli* homolog, BamD is not essential in *Salmonella.* However, the deletion of BamD does result in several growth defects, including reduced growth in late exponential phase and early entry in stationary phase, as well as a reduction in viable cell count when exposed to nutrient

starvation. The phenotype of *S.* Enteriditis Δ*bamD* suggests that, although not essential, BamD plays an important role in cell growth. Whereas *Salmonella* BamE appears to play a minor role in the protection against toxic compound, the role of BamC remains enigmatic (Fardini *et al.*, 2007). Interestingly, *Salmonella* BamB is involved in pathogenesis. Suppression of this protein results in reduced transcription levels of at least three type three secretion systems essential for adhesion and invasion of epithelial cells and macrophages (Amy *et al.*, 2004; Fardini *et al.*, 2007).

1.3.4.2 BAM-complex mediated OMP biogenesis

The BAM-complex is essential to the insertion of new OMPs into the OM. Although recent studies have revealed new information regarding the crystal structure of and interaction between the components of the BAM-complex, the mechanism by which OMPs are inserted into the OM remains unclear. Two mechanistic models have been proposed for the role of the BAM-complex in OMP biogenesis (Noinaj, Gumbart and Buchanan, 2017). The first model works on the premise that OMPs fold intrinsically into the OM, but need a catalyst to lower the kinetic energy required for insertion into the membrane. In this model, OMPs are synthesised into the cytoplasm and guided towards the periplasm with an N-terminal signal sequence. Once emerging from the Sec-translocon, the precursors bind SurA or Skp and are delivered to the BAM-complex, where they interact with a C-terminal signal sequence. Upon target interaction, the BAM-complex destabilises the membrane bilayer and brings the nascent OMP into close proximity to the primed membrane, where they fold into their mature structure whilst they insert into the OM (Noinaj, Gumbart and Buchanan, 2017). The second model proposes a mechanism whereby the chaperone-stabilised precursor protein is delivered to the BAM-complex, where folding and insertion is initiated by the β-signal of the native OMP. The target enters the barrel of BamA, and is folded into its mature shape either strand by strand or by one β-hairpin at the time. The inserted, mature OMP eventually buds away from the BAM-complex (Noinaj, Gumbart and Buchanan, 2017).
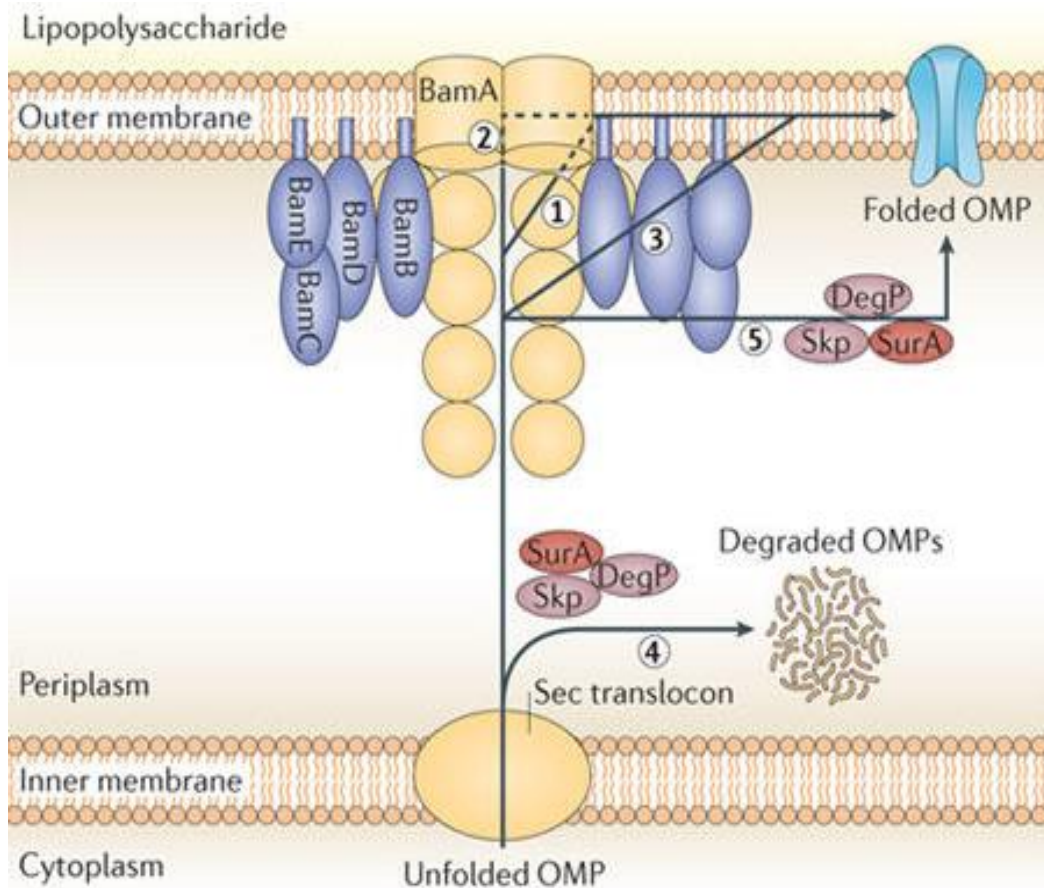
Figure 1.5 The BAM complex. For the insertion of β-barrel OMPs, Gram-negative bacteria employ the β-barrel assembly machinery (BAM). BamA is the essential core protein of the BAM complex, the rest of the complex is formed by BAM assessor proteins (B-E). Unfolded OMP precursor proteins emerging from the Sec translocon pathway interact with the periplasmic chaperones SurA, Skp and HtrA (DegP), which assist in the transport of OMPs across the periplasm, and their delivery to the BAM. The pore-forming model dictates that the nascent OMPs interact with BAM complex POTRA domains (1) and are threaded through the BamA pore (2). Depending on the substrate, this interaction is facilitated by various auxiliary proteins (3). An alternative model suggests that the BAM complex is only involved in the folding of OMPs (1 & 3) and interactions with SurA and Skp allow the insertion of the folded OMP (5). The degradation of OMPs is mediated by interactions with HtrA (DegP) following chaperoning by SurA and/or Skp (4) (Leyton, Rossiter and Henderson, 2012).

1.4 Bacterial stress responses

1.4.1 The general stress response RpoS

The global stress response sigma factor σ^S (RpoS) was initially identified as a sigma factor upregulated in response to entering the stationary phase. In the following years it became evident that RpoS is a global stress response sigma factor involved in the regulation of a wide range of stresses, including biofilm formation, changes in temperature, osmolarity or pH, virulence and nitrogen, phosphate, and carbon starvation (Battesti, Majdalani et al. 2011). As an RNA polymerase responding to a wide range of stresses, RpoS is involved in the transcriptional regulation of a wide range of genes. In *Escherichia coli*, approximately 10% of the genome is regulated, either directly or indirectly, by RpoS (Weber, Polen et al. 2005). To ensure steady expression of RpoS, ready to act instantaneously when encountering stress, whilst maintaining low cellular levels of RpoS during favourable conditions, RpoS is strictly regulated at all levels; transcriptional, translational and posttranslational (Hengge-Aronis 2002, Battesti, Majdalani et al. 2011).

1.4.4.1 Transcriptional regulation of *rpoS*

The transcription of *rpoS* is regulated by several proteins, allowing activation or repression of this stress response system in reaction to various stimulants. Positive regulators of *rpoS* include the histidine kinase BarA, involved in metabolism switches (Sahu *et al.*, 2003) and the alarmone guanosine pentaphosphate (ppGpp), which is involved in the response to amino-acid starvation (Hirsch and Elliott, 2002). Negative regulators of *rpoS* include the response regulator ArcA-P, which responds to change in respiratory conditions (Mika and Hengge, 2005), the DNA binding and bending protein Fis, which responds to changes in nutrient availability (Hirsch and Elliott, 2005), the response regulator UvrY, which responds to the switch between carbon sources (Pernestig *et al.*, 2003), and the global transcription factor cAMP-CRP, which is involved in catabolite repression (Lee *et al.*, 2008).

1.4.4.2 Translational regulation of *rpoS*

To ensure a rapid response to stress, *rpoS* transcription takes place even in the absence of stress, but translation of *rpoS* mRNA is inhibited during non-stress conditions. Post transcription, the long 5' untranslated region of *rpoS* mRNA folds into a stem-loop that occludes the ribosomal binding site, preventing translation (Brown and Elliott, 1997). Upon encountering stress, this structural inhibition can be overcome by *trans*-encoded small RNAs (sRNA) capable of binding their leader sequence within the hairpin region. The binding of

sRNA opens up the ribosomal binding site, allowing translation of the mRNA. At least three known sRNAs positively regulate *rpoS* mRNA translation; DsrA during growth at low temperatures, RprA in response to envelope stress and ArcZ during growth under aerobic-anaerobic stress (Majdalani *et al.*, 1998, 2001; Mandin and Gottesman, 2010). At least one sRNA is known to negatively regulate *rpoS* mRNA translation. OxyS, a sRNA expressed in response to oxidative stress, is thought to stimulate *rpoS* mRNA cleavage by the RNase E (Henderson *et al.*, 2013).

1.4.4.3 RpoS stability and turnover

The turnover of RpoS is aided by the adaptor protein RssB. During favourable growth conditions, RssB binds RpoS and targets it for degradation by the ClpXP pathway (Zhou *et al.*, 2001; Battesti, Majdalani and Gottesman, 2011). In response to stress, various Ira (Inhibitor of RssB Activity proteins) anti-adapter proteins are produced, which bind RssB and prevent the formation of an RssB-RpoS complex, resulting in rapidly increasing cellular levels of RpoS (Bougdour and Gottesman, 2007; Bougdour *et al.*, 2008; Hryckowian *et al.*, 2014).

1.4.4.5 RpoS and *Salmonella* virulence

During infection, *Salmonella* is exposed to various environmental stresses, including nutrient starvation, oxidative stress, and low pH. As the name suggests, the general stress response regulator RpoS is involved in the regulation of many genes involved in the defence against these stresses. However, RpoS is not only required for the regulation of stress defence. Various plasmid-borne virulence genes are positively upregulated during infection, including the transcriptional regulator *spvR,* the outer membrane protein *spvA*, the transferase *spvB*, the MAPK phosphothreonine lyase *spvC* and the cysteine hydrolase *spvD*. These virulence genes are required for intracellular growth as well as systemic infection in humans and mice (Fang *et al.*, 1992; Kowarz *et al.*, 1994), and mutant *rpoS* strains are impaired in their ability to colonise the spleen, liver and Peyer patches (Fang *et al.*, 1992; Nickerson and Curtiss, 1997).

1.5 Gram-negative envelope stress responses

1.5.1 RpoE stress response

The alternative sigma factor σ^E (RpoE) is involved in the response to envelope damage of many gram negative bacteria. Although RpoE is conserved among many Gram negative species, its role differs depending on the organism. In *E. coli,* RpoE is essential for growth at high temperatures, whereas in *Salmonella* RpoE is of great importance during the infection
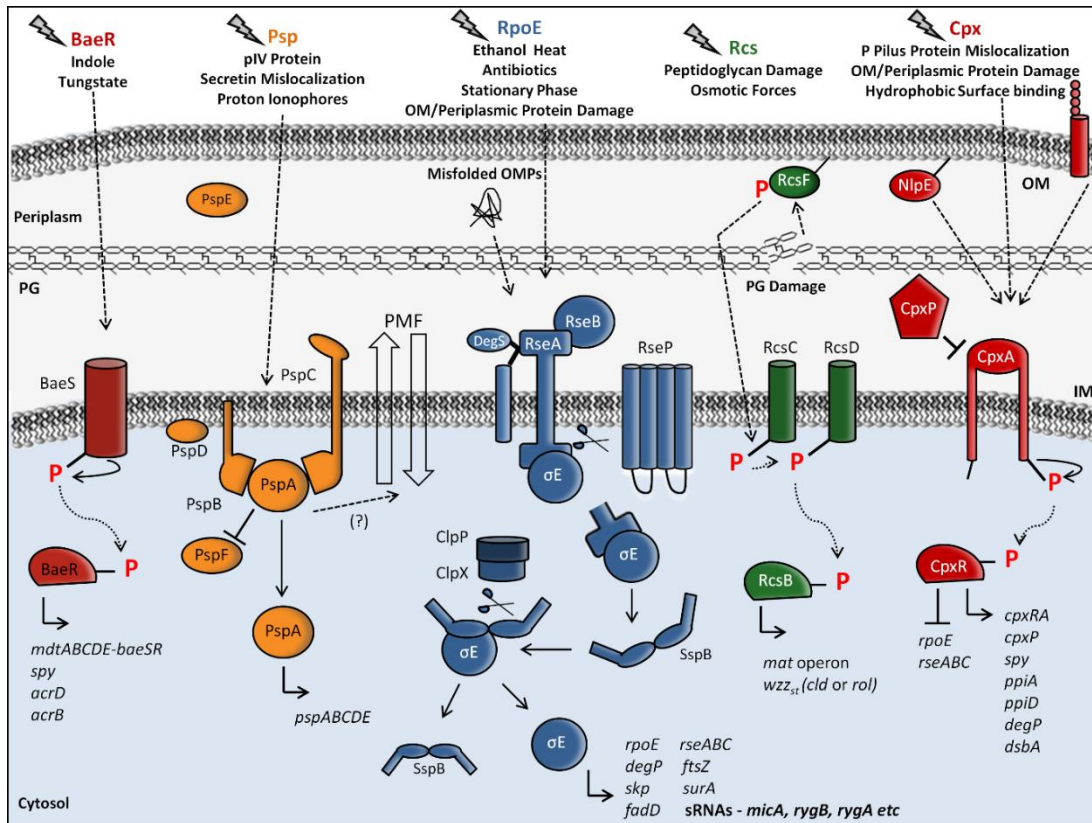
Figure 1.6 Schematic representation of envelope stress responses, inducing factors and genes regulated. Spaced lines represent inducing stress signals, whereas phosphate movement is represented with dotted lines. The movement and/or release of proteins is indicated by solid lines, and cleavage events are marked with scissor figures. A detailed description of each pathway can be found in relevant subchapter of chapter 1.5. Image taken from (Runkel, Wells and Rowley, 2013)

process (Hiratsu *et al.*, 1995; Humphreys *et al.*, 1999). Activation of RpoE results in the regulation of more than 100 genes involved in various cellular processes. Among these RpoE regulated genes are the stress response factors *rpoD, rpoE, rpoH* and *rpoN*, regulatory genes including *rseA, rseB* and *rseC*, periplasmic proteases and folding factors including *skp, surA, fkpA,* and *htrA*, genes involved in LPS and phospholipid biogenesis including *lpxA, lpxD, lpxP* and *psd*, the sensory proteins *cutC, mdoG* and *sixA,* and genes involved in primary metabolic functions including *fusA* (Rowley *et al.*, 2006) The periplasmic chaperones FkpA, HtrA, Skp and SurA are discussed in more detail in chapter 3.

1.5.1.1 Regulation of RpoE activation

To ensure a rapid response to envelope stress, RpoE is expressed at all times. In the absence of envelope damage, RpoE is kept inactive by the anti-sigma factor RseA (De Las Penas, Connolly and Gross, 1997; Missiakas *et al.*, 1997). This anti-sigma factor is an inner membrane protein that has a cytoplasmic N-terminal domain (RseA^cyto), a transmembrane segment, and a periplasmic C-terminal domain (RseA^peri). RpoE is tethered to the cytoplasmic

leaflet of the IM by interactions with RseA^{cyto}, preventing RpoE-regulated gene expression. For RpoE to be released, the transmembrane domain of RseA requires cleaving by DegS and RseP. During non-stressed conditions, this protease-mediated cleavage of RseA is prevented by RseB, a periplasmic protein that binds the RseA^{peri} domain (Campbell *et al.*, 2003; Kim *et al.*, 2007). During envelope stress, two events are required before RpoE can be released into the cell; the activation of DegS and the release of RseB. DegS is a trimeric periplasmic protein anchored to the IM. The protein has a protease domain, formed as a funnel, and a PDZ domain which holds DegS in an inactive state. Porins and OMPs have a conserved YxF domain at their C-terminal which is buried inaccessibly in mature proteins. When these proteins denature however, the domain becomes exposed and can bind to the PDZ domain of DegS. This interaction between DegS and misfolded proteins results in a conformational change that leaves the DegS protease domain active and accessibly (Walsh *et al.*, 2003; Wilken *et al.*, 2004). RseB is a periplasmic chaperone that binds RseA^{Peri} with both its C-terminal and N-terminal domain, preventing cleavage by DegS (Cezairliyan and Sauer, 2007; Kim *et al.*, 2007; Ahuja *et al.*, 2009). Upon interaction with LPS fragments, RseB dissociates from RseA, opening up the cleavage site for interaction with DegS (Lima *et al.*, 2013). DegS mediated removal of RseA^{peri}, opens up a cleavage site in the transmembrane region of RseA. This transmembrane region is cleaved by the protease RseP, releasing the RseA^{cyto}-RpoE complex into the cytoplasm (Alba *et al.*, 2002; Kanehara, Ito and Akiyama, 2002). The cytoplasmic adapter protein SspB binds the complex and delivers it to ClpXP. Here, the remaining RseA^{cyto} domain is removed from RpoE, activating RpoE (figure 1.6) (Flynn *et al.*, 2004).

Among the genes under σ^E regulation, are clusters involved in biogenesis, maintenance and repair of cell envelope, including genes *lptA, lptB* and *lptD* (Dartigalongue, Missiakas and Raina, 2001). Although modifications of LPS structure do not affect OMP composition, they do elicit a strong σ^E response (Tam and Missiakas, 2005; Martorana *et al.*, 2011). The specialised σ^E -dependent LPS stress signalling pathway involves LPS fragments containing lipid A, which can dissociate RseB from RseA, facilitating DegS mediated cleavage. This dissociation can be suppressed in presence of LptA, suggesting that periplasmic accumulation of LPS can activate RpoE response (Lima *et al.*, 2013; Sperandeo, Martorana and Polissi, 2016).

1.5.1.2 RpoE and sRNA

The maintenance of envelope homeostasis can be regulated by RpoE on both transcriptional and translational level. As a sigma-factor, RpoE is directly involved in the transcriptional activation and repression of genes required for membrane maintenance and repair.

However, some of the RpoE regulated transcripts encode sRNAs, allowing indirect regulation of gene expression by RpoE on a translational level (Klein and Raina, 2015). Expression of the sRNAs MicA, RybB and SlrA is positively regulated by RpoE (Papenfort *et al.*, 2006; Klein *et al.*, 2011). The sRNA MicA supresses translation of OmpA mRNA, an abundant OMP that plays a role in bacterial survival in various stress conditions, including SDS, cholate, low pH and high salt (Rasmussen *et al.*, 2005; Papenfort *et al.*, 2006). Although appears counterintuitive to downregulate OmpA during stress, reduced presence of OmpA in the OM renders bacteria more invisible to the host's immune system (Wang, 2002). In *E. coli*, the sRNA RybB suppresses WaaR mRNA translation. WaaR is a glucosyltransferase required for LPS glycoform formation (Klein and Raina, 2015). In *Salmonella*, the sRNA RybB inhibits the translation of multiple OMPs, including OmpA, OmpC, OmpD and OmpF (Papenfort *et al.*, 2006). Downregulation of OmpD increases *Salmonella*'s chances to survive and proliferate inside macrophages, as macrophages infected with Δ*ompD* strains produce lower levels of reactive oxygen species (Ipinza *et al.*, 2014). The third sRNA, SlrA, is thought to play a role in the RpoE feedback loop. SlrA transcription is positively regulated by RpoE, but the sRNA inhibits translation of RpoE mRNA and the mRNA of the major lipoprotein Lpp (Papenfort *et al.*, 2006; Guo *et al.*, 2014). A correct balance between LPS and phospholipids is important for OM integrity; when LipidA outcompetes phospholipids, the membrane destabilises. Lpp is an abundant protein that contains three fatty acid chains. The SlrA-mediated downregulation of Lpp production, results in an increased availability of fatty acids for phospholipid production, resulting in a restoration of the LPS::phospholipid balance (Guo *et al.*, 2014).

1.5.2 Two component envelope stress responses

Two component systems are common mechanisms used by bacteria to sense and respond to changes in their environment. They are fundamental to bacterial adaptability, virulence and antibiotic resistance, coupling changes in the environment to changes in cellular physiology (Capra and Laub, 2012). Two-component systems typically consist of a transmembrane histidine kinase and a cytoplasmic response regulator, and may be accompanied by auxiliary proteins. The histidine kinase acts as a sensory protein; upon sensing the particular signals the two-component system is attuned to, this protein catalyses an auto-phosphorylation reaction at a conserved histidine residue. This phosphoryl group is subsequently transferred to a conserved aspartate residue on the cognate response regulator, activating cellular responses to the perceived environmental changes (Capra and Laub, 2012). Analysis of bacterial genomes has shown a correlation between the number of

encoded two-component systems in an organism and its ecological and environmental niche; bacteria adapted to specific niches, including many pathogens, encode relatively few two-component systems, whereas bacteria surviving in rapidly changing environments encode significantly more two-component systems (Capra and Laub, 2012). Among the Gram negative Enterobacteriaceae, three two-component systems are associated with the envelope stress response: the Cpx response, the Bae response, and the Zra response.

1.5.2.1 The Cpx response

The Cpx response has been studied for several decades. Some of the first phenotypes associated with *cpx* mutations included alterations in conjugative plasmid expression, but the response has since been demonstrated to be involved in many cellular processes (McEwen and Silverman, 1980; Raivio, 2014). The Cpx response consists of the histidine kinase CpxA, the response regulator CpxR and the auxiliary proteins CpxP and NlpE (figure 1.6). Mutations of the CpxA sensing domain almost always result in activation of the Cpx response, suggesting that the regulation of the Cpx-response primarily focusses on inhibition of CpxA (Raivio, 2014). In *E. coli*, the periplasmic chaperone CpxP acts as a negative regulator of the Cpx system. A study investigating the interaction between CpxP and the signalling domain of CpxA suggests interaction between the positively charged surface of CpxP and negatively charged residues in the periplasmic sensing domain of CpxA. The model suggests that CpxP binds and inactivates CpxA, until CpxP is titrated away by misfolded proteins or degraded by the periplasmic protease HtrA (Zhou *et al.*, 2011). However, this model has been the topic of debate. In *Vibrio parahaemolyticus,* crystallisation studies of the CpxA sensing domain demonstrates a Per-Arndt-Sim (PAS) domain which consists of a central five-stranded β-sheet surrounded by several α-helices. Unlike in *E. coli*, no interaction could be observed between this purified CpxA domain and CpxP (Kwon *et al.*, 2012). In response to adhesion to abiotic surfaces, the OM lipoprotein NlpE (new lipoprotein E) activates the Cpx response by an as of yet unknown mechanism (Otto and Silhavy, 2002; Raivio, 2014). The list of Cpx activating signals is diverse and includes, but is not restricted to, elevated pH, high osmolarity, EDTA, ethanol, copper, indole, aminoglycosides, growth, adhesion, spheroplasting, misfolded pilus proteins, deletion of efflux pump components, YidC mutations, alterations in membrane phospholipid ratios, accumulation of antigen assembly intermediates and assembly of a type IV secretion system (Danese et al. 1998; Danese & Silhavy 1998; Raivio et al. 2000; Otto & Silhavy 2002; Raffa & Raivio 2002; Jubelin et al. 2005; Nevesinjac & Raivio 2005; Yamamoto & Ishihama 2006; Zahrl et al. 2006; Bury-Mone et al. 2009; Wang et al. 2010; Clarke & Voigt 2011; Kashyap et al. 2011; Rinker et al. 2011; Itou et

al. 2012). Although the number and broad range of signals complicates determining the molecular nature of inducing signals, a common theme among them is risk to IM integrity. Indeed, characterisation of the Cpx regulated transcriptome of various Gammaproteobacteria from different orders describe links between the Cpx response and functions of the IM, including energy generation and transport (Raivio, 2014). In *E. coli*, activation of the Cpx response leads to change of expression in 100s of genes. Gene set enrichment analysis identified Cpx-controlled genes were enriched for inner membrane proteins, as well as genes involved in electron transport, the TCA cycle, oxidative phosphorylation, transport and metal binding (Raivio, Leblanc and Price, 2013; Raivio, 2014). Analysis of Cpx-regulated gene expression in *Vibrio cholerae* also demonstrates enrichment of genes involved in transport and binding, energy metabolism and regulatory factors (Acosta, Pukatzki and Raivio, 2015). In *Haemophilus ducreyi,* the functional categories regulated by the Cpx response include cell surface structure and proteins, generation of precursor metabolites and energy and membrane transport and uptake (Labandeira-Rey, Brautigam and Hansen, 2010; Raivio, 2014). Interestingly, unlike *E. coli* and *Vibrio,* the *Haemophilus cpx* operon does not encode *cpxP* (Labandeira-Rey, Brautigam and Hansen, 2010). It is likely that the regulation and involvement of periplasmic proteases and chaperones may be a subset of the Cpx regulon that is only found in some organisms (Raivio, 2014).

Particular interest is taken into the Cpx response due to its involvement in pathogenicity, biofilm formation, and resistance to antibiotics and antimicrobials. The Cpx response has been linked to virulence in various pathogens; as a positive regulator in some pathogens and as a negative regulator in others (Humphreys *et al.*, 2004; Nevesinjac and Raivio, 2005; Carlsson *et al.*, 2007; Labandeira-Rey, Brautigam and Hansen, 2010; Debnath *et al.*, 2013; Acosta, Pukatzki and Raivio, 2015). It is clear that the Cpx response, although widely conserved, regulates various pathways in different ways, depending on the organism. Considering the interactions between the Cpx response and other cellular stress responses (see chapter 3 for further detail), it is not surprising that the Cpx response varies between different pathogens.

The involvement of the Cpx response in biofilm formation appears paradoxical. Activated CpxR negatively regulates the *motABcheAW* operon, encoding flagellar motor components, and indirectly represses the *flhDC* flagellar master regulator genes (Shin and Park, 1995; De Wulf *et al.*, 2002). In addition to repressing motility, the Cpx response positively regulates the production of DgcZ, which is involved in the production of polysaccharide adhesins

required for biofilm formation, and transcriptomic studies have demonstrated a positive correlation between biofilm gene expression profiles of *E. coli* and the Cpx regulon (Dorel, Lejeune and Rodrigue, 2006; Raivio, Leblanc and Price, 2013). However, the Cpx response inhibits transcription of the transcriptional activator CsgD, considered a key regulator of biofilm formation, and the CsgBAC and CsgEFG machineries required for curli production, both by binding to the *csgDEFG* and *csgBAC* operons, as well as by promoting expression of the sRNA RprA, which inhibits CsgD expression (Dorel *et al.*, 1999; Prigent-Combaret *et al.*, 2001; Raivio, Leblanc and Price, 2013). It is possible that the Cpx response is only beneficial for biofilms in later stages of its production, or that Cpx expression is required for discrete parts of the biofilm (Raivio, 2014).

Studies into various Gram-negative pathogens including *E. coli, S. enterica, Klebsiella pneumonia* and *H. ducreyi* have demonstrated the involvement of the Cpx response in resistance to antibiotics and antimicrobials. Resistance to aminoglycosides has been linked to the Cpx response since the 1970s (Thorbjarnardottir, Magnusdottir and Eggertsson, 1978). These antibiotics, which include gentamicin, kanamycin and amikacin, target the 30S ribosomal subunit and cause misfolding and malfunctioning of proteins by mismatching tRNA (Davis, 1987). The Cpx regulon is upregulated in the presence of gentamycin, and although the exact mechanism of Cpx-regulated stress relief is not known, one model proposes it involves Cpx-mediated upregulation *yccA*. YccA inhibits the activity of the protease FtsH, which in turn is responsible for degrading the SecY component of the Sec translocon apparatus. By overproducing YccA, FtsH-mediated degradation of SecY is inhibited, allowing secretion and clearance of aberrant proteins (Kihara, Akiyama and Ito, 1995, 1998; van Stelten *et al.*, 2009). The hypothesis of increased secretion of aberrant proteins is further supported by the increased sensitivity to aminoglycosides in a *Pseudomonas aeruginosa yccA* mutant, and the reported Cpx-mediated upregulation of SecA (De Wulf *et al.*, 2002; van Stelten *et al.*, 2009). Furthermore, the Cpx response has been implicated in the increased resistance against hydroxyurea, cationic antimicrobial peptides, chloramphenicol, β-lactams, deoxycholate, cefeprime, novobiocin and the small antibacterial molecule SM10 (Hirakawa, Nishino, Hirata, *et al.*, 2003; Hirakawa, Nishino, Yamada, *et al.*, 2003; Rinker *et al.*, 2011; Weatherspoon-Griffin *et al.*, 2011; Srinivasan *et al.*, 2012; Yitzhaki *et al.*, 2012; Mahoney and Silhavy, 2013). Interestingly, the Cpx-response has also been linked to an increased sensitivity to quinolones (Mahoney and Silhavy, 2013).

1.5.2.2 The BaeSR response

The BaeSR response is another two component envelope stress response which was first identified during a search for new two component systems (Raffa and Raivio, 2002). Although it was discovered in the early 2000s, the response lacks in depth characterisation, likely due to a lack of phenotypes associated with loss of the system. The BaeSR response consists of the BaeS sensory kinase and the BaeR response regulator (figure 1.6). Little is known about the BaeSR activating signals, which is most likely due to the overlap between activators of the BaeSR response and other envelope stress responses, including the Cpx response. This functional overlap extends to the genes regulated by BaeR, complicating the process of characterising the response (Raffa and Raivio, 2002; Appia-Ayme *et al.*, 2011; Leblanc, Oates and Raivio, 2011).

Activation of the BaeSR response is linked to various conditions, including stationary growth phase, and growth in the presence of indole, zinc, copper, iron and tungstate (Raffa and Raivio, 2002; Miticka *et al.*, 2003; Appia-Ayme *et al.*, 2011; Leblanc, Oates and Raivio, 2011). In *E. coli*, the core BaeSR regulon consists of *baeSR, spy, mdtA, acrB* and *acrD*. MtdA is a component of MdtABC influx pumps, for which sodium tungstate is a natural substrate. In *E. coli*, BaeR is involved in the regulation of *mtdABCD* expression (Baranova and Nikaido, 2002). In the presence of tungstate, BaeR expression is upregulated, and correspondingly deletion of *baeR* renders *E. coli* and *Salmonella* more susceptible to tungstate. Interestingly, although expression of *mtdA* and *acrD* is also regulated by CpxR, deletion of *cpxR* does not result in sensitivity to tungstate, marking it as a primary target of BaeR (Appia-Ayme *et al.*, 2011; Leblanc, Oates and Raivio, 2011). In *Salmonella*, the BaeSR response has been shown to be required for colonisation and systemic infection in serovar Dublin, but not in serovar Typhimurium (Pullinger *et al.*, 2010; Appia-Ayme *et al.*, 2011).

The BaeSR response is involved in the protection against antimicrobial agents. In *E. coli,* BaeR mutations have been linked to increased susceptibility to the antibiotic novobiocin, the secondary bile acid deoxycholate, condensed tannins and the essential oil allyl isothiocyanate (Baranova and Nikaido, 2002; Zoetendal *et al.*, 2008; Cordeiro *et al.*, 2014). In *Salmonella* Typhimurium, BaeR upregulates the expression of the superoxide dismutase SodA in response ciprofloxacin exposure (Guerrero *et al.*, 2013). In *Acinetobacter baumanni*, the BaeSR response induces expression of the pump genes *adeAB, adeIJK* and *macAB-tolC*, involved in the efflux of toxic molecules (Lin *et al.*, 2014; Lin, Lin and Lan, 2015). Deletion of BaeR resulted in increased susceptibility to the antibiotic tigecycline, as well as increased

susceptibility to tannic acid, a topical agent used to treat burn wounds (Akiyama *et al.*, 2001; Lin, Lin and Lan, 2015).

1.5.2.3 The ZraSR response

The ZraSR response is discussed in detail in chapter 5. Below is a brief introduction.

The ZraSR response is the most recently discovered two component envelope stress response (Appia-Ayme *et al.*, 2012). Before the discovery of the involvement of ZraSR in envelope stress, the system was studied as a two-component system responding to zinc levels. Formerly known as HydHG, the ZraSR response is significantly upregulated in the presence of Zn^{2+}, both in *E. coli* as well as in *Salmonella*, and was renamed as <u>z</u>inc <u>r</u>esponse <u>a</u>ssociated (Leonhartsberger *et al.*, 2001; Outten and O'Halloran, 2001; Appia-Ayme *et al.*, 2012). The ZraSR response consists of the histidine kinase ZraS, the response regulator ZraR, the periplasmic chaperone ZraP and the putative inner membrane protein YjaH. The structure and function of ZraP are discussed in detail in chapter 4 and chapter 5 respectively. Little is known about the activating conditions and mechanisms of the ZraSR response, and functional overlap between this response system and other envelope stress responses complicate research. Activating signals for the ZraSR response include the presence of Zinc, lead and tungstate (Appia-Ayme *et al.*, 2012). Activation of ZraR results in the expression of, among other genes, *zraP*. Deletion of *zraP* results in significant upregulation of *zraR* expression, suggesting a similar negative feedback loop as is found between CpxP and the Cpx response (Raivio, Popkin and Silhavy, 1999; Appia-Ayme *et al.*, 2012).

1.5.3 Rcs Phosphorelay stress response

The Rcs Phosphorelay stress response is a complex signal transduction system that was first identified as a <u>r</u>egulatory <u>s</u>ystem of <u>c</u>apsule synthesis in *E. coli* (Gottesman, Trisler and Torres-Cabassa, 1985). It has since been shown to be conserved among Enterobacteriacea, playing a regulatory role in many cellular processes including biofilm formation, pathogenesis, motility and general stress responses (Majdalani and Gottesman, 2005; Guo *et al.*, 2015). Although the activating signals of the Rcs phosphorelay response remain enigmatic, the activating conditions are diverse and include growth at low temperature, growth on solid surfaces, growth in the presence of 1mM external zinc, copper stress, damage to the peptidoglycan layer, osmotic shock, exposure to Polymyxin B, overexpression of *djlA*, and *tolB* or *prmA* mutations (Clarke, Holland and Jacq, 1997; Bader *et al.*, 2003; Ferrieres and Clarke, 2003; Francez-Charlot *et al.*, 2003, 2005; Hagiwara *et al.*, 2003; Mouslim and Groisman, 2003; El-Kazzaz *et al.*, 2004; Laubacher and Ades, 2008; Pontel, Pezza and

Soncini, 2010; Oropeza, Salgado-Bravo and Calva, 2015). The system consists of the transmembrane sensor kinase RcsC, the response regulator RcsB, the phosphoryl transferase RcsD, and various auxiliary proteins (figure 1.6). Upon receiving activating signals, RcsC hydrolyses ATP and autophosphorylates. The phosphoryl group is transferred from a conserved histidine residue to a conserved aspartate residue in the RcsC receiver domain. This domain then functions as a phosphoryl donor to the histidine phosphotransferase RcsD, which in turn donates the phosphoryl group to RcsB. Once phosphorylated RcsB regulates gene expression (Takeda *et al.*, 2001; Majdalani and Gottesman, 2005). However, studies into the Rcs Phosphorelay response have demonstrated that the system is more complex than this phosphorylation cascade; RcsB is able to interact with different auxiliary proteins, both dependently and independently of RcsB phosphorylation. The interactions, or lack thereof, between RcsB and the auxiliary proteins determine the targets of RcsB regulated transcription. RcsB-interacting auxiliary proteins include, but are not restricted to, RcsA, BglJ, GadE and MatA (Majdalani and Gottesman, 2005; Pannen *et al.*, 2016). Interaction between RcsB and RcsA requires phosphorylated RcsB. The RcsBA complex activates transcription of loci involved in exopolysaccharide production, required for biofilm formation, and represses the transcription of the *flhDC* flagellar master regulator genes (Stout *et al.*, 1991; Majdalani and Gottesman, 2005). In *Yersinia pseudotuberculosis,* the RcsBC complex suppresses expression of the biofilm formation related genes *hmsCDE*, whereas RcsB alone upregulates expression of these genes instead (Guo *et al.*, 2015). The interaction between RcsB and BglJ does not require phosphorylation of RcsB. The RcsB-BglJ complex regulates the transcription of more than 10 separate loci, including expression of transcriptional regulator *leuO*, which is involved in the regulation of virulence determinants (Venkatesh *et al.*, 2010; Stratmann *et al.*, 2012; Salscheider, Jahn and Schnetz, 2014). The interaction between RcsB and GadE is also independent of RcsB phosphorylation. Whereas the RcsB-GadE complex activates transcription of *gadA*, a glutamate decarboxylase involved in the acid stress response, phosphorylated RcsB unpaired to any auxiliary proteins represses *gadA* transcription (Castanie-Cornet *et al.*, 2010). The interaction between RcsB and MatA occurs independently of RcsB phosphorylation and the RcsB-MatA complex represses motility and activates transcription of the *mat* operon, which encodes a fimbrial adhesin in *E. coli* (Pannen *et al.*, 2016). RcsB is also involved in the downregulation of the Rcs Phosphorelay response. The expression of *rcsB* is regulated by two promoters: P_{rcsDB} and P_{rcsB} resulting in high levels of RcsB transcription. When the cellular concentration of RcsB reaches a threshold, RcsB binds the P_{rcsCB} promoter and negatively regulates Rcs expression. As a result, RcsB is only

transcribed from the P_{rcsB} promoter, and the protein concentration returns to basal levels (Pescaretti *et al.*, 2010).

1.5.4 Phage Shock Protein stress response

Studies into the *Escherichia coli* filamentous phage f1 initially discovered upregulation of an *E. coli* protein in response to the production of phage secretin protein pIV. This upregulated protein was named phage shock protein and is now known as PspA of the Psp stress response (Brissette *et al.*, 1990, 1991). The Psp response is widely conserved, with Psp-like proteins found in both Gram positive and Gram negative bacteria, as well as in archaea and chloroplasts (Flores-Kim and Darwin, 2016). In *Salmonella,* the Psp response is essential for virulence and survival inside macrophages (Karlinsey *et al.*, 2010; Wallrodt *et al.*, 2014). Despite more than 25 years of study, the exact nature of the Psp stress response, its inducing signals, protein interactions, and mechanisms of envelope protection remain poorly understood (Flores-Kim and Darwin, 2016). Unlike other envelope stress responses, the Psp response acts relatively autonomously, with little evidence for interaction with other stress response systems (Seo *et al.*, 2007). The stress response is thought to be activated upon reduction of the proton motive force (PMF) across the IM, or in response to increased IM permeability (Flores-Kim and Darwin, 2016). Conditions that lead to the induction of the *pspA* operon include mislocalization of secretins, extremes in temperature or osmolarity, disruption of fatty acid biosynthesis, ethanol shock and proton ionophores (Brissette *et al.*, 1990; Bergler *et al.*, 1994; Weiner and Model, 1994; Kobayashi, Yamamoto and Aono, 1998).

Four core proteins of the Psp stress response are PspA, PspB, PspC and PspF (figure 1.6) (Flores-Kim and Darwin, 2016). Of these proteins, *pspA, pspB* and *pspC* are encoded in the *pspABCDE* operon, the regulatory protein PspF is encoded upstream of *pspA* (Jovanovic, Weiner and Model, 1996; Lloyd *et al.*, 2004). During stress, PspF negatively regulates *pspF* expression and positively regulates the *psp* operon by binding to the *pspA* promoter (Lloyd *et al.*, 2004). The activation of PspF is dependent on two protein binding partner-switching events (Flores-Kim and Darwin, 2016). In the absence of an inducing signal, PspA binds and inactivates the ATPase activity of PspF, rendering the regulatory protein inactive (Osadnik *et al.*, 2015). Meanwhile, the IM protein PspB interacts with a C-terminal domain of PspC (PspC^{CTERM}) that is also capable of binding PspA (Gueguen, Savitzky and Darwin, 2009; Jovanovic *et al.*, 2010; Flores-Kim and Darwin, 2012, 2015). During IM stress, PspB dissociates from PspC, allowing interaction between PspC^{CTERM} and PspA (Flores-Kim and Darwin, 2015). This interaction interrupts the bond between PspA and PspF, allowing for activation of the

response regulator (Flores-Kim and Darwin, 2016). This model is incomplete however, for the N-terminal domain of PspC (PspC^{NTERM}) has proven to be required for the interaction between PspB and PspC, and removal of this domain results in constitutive PspA-PspC interaction and activation of the Psp stress response (Gueguen, Savitzky and Darwin, 2009; Yamaguchi *et al.*, 2013). However, the mechanism by which the PspC^{NTERM} ensures PspB-PspC^{CTERM} interaction in the absence of stress remains enigmatic (Flores-Kim and Darwin, 2016).

Knowledge of the physiological role of the Psp response and its individual components remains incomplete (Flores-Kim and Darwin, 2016). Although some studies suggest PspB and/or PspC act as signal sensor, activation of the *E. coli* Psp response in response to pIV secretins, heat-shock or stored curvature elastic stress all happen independently of PspB and PspC, and genome analysis has demonstrated that organisms encoding *pspA* and *pspF* do not always carry genes for *pspB* and *pspC* (Weiner, Brissette and Model, 1991; Jovanovic, Engl and Buck, 2009; Huvet *et al.*, 2011; McDonald *et al.*, 2015). It has been suggested that PspB and PspC do not act as sensors, but are instead involved in the protection against cell collapse following increased IM permeability. However, the mechanism by which this stress relief would function remains enigmatic (Flores-Kim and Darwin, 2016). *E. coli pspA* mutant strains display phenotypes that could be assigned to reduction in PMF and in *S.* Typhimurium PspA is thought to be required for the maintenance of PMF during survival within macrophages (Karlinsey *et al.*, 2010; Flores-Kim and Darwin, 2016). Upon induction of the Psp response, PspA transitions from a hexamer to oligomers of 36 units and more. It has been proposed that these large oligomers might coat the IM to prevent proton leakage (Kobayashi, Suzuki and Yoshida, 2007; Standar *et al.*, 2008; Engl *et al.*, 2009). However, fluorescence assays of PspA in live *E. coli* and *Yersinia enterocolitica* cells do not support this notion (Engl *et al.*, 2009; Yamaguchi *et al.*, 2013). More complex mechanisms have been proposed, suggesting PspA function relates to the organisation of the cell envelope and the biogenesis of peptidoglycan and phospholipid biogenesis (Engl *et al.*, 2009; Wallrodt *et al.*, 2014). These mechanisms however remain unclear and also do not explain the prevention of proton leakage by PspA from membrane vehicles *in vitro* (Flores-Kim and Darwin, 2016).

1.6 Thesis overview

1.6.1 Research gap

The Gram-negative cell envelope plays an important role in the natural immunity of pathogens against environmental stresses. The periplasmic chaperones involved in the biogenesis, maintenance and repair of the outer membrane are of great importance to its integrity, and therefore they are indirectly involved in the cellular resistance against environmental threats. The persistent increase and spread of multi-drug resistant pathogens is an urgent threat to global health. An improved understanding of the targets of periplasmic chaperones, as well as the mechanisms by which they operate, would further our understanding of bacterial adaptability to hostile environments, and could contribute towards the development of novel vaccines and antibiotic treatments.

1.6.2 Aims

The intention of this thesis is to expand on the current knowledge base regarding the involvement of several periplasmic chaperones in the protection against environmental threats. A particular interest was taken in the ZraSR-associated, zinc-responsive periplasmic chaperone ZraP. Although this chaperone and its associated envelope stress response is highly conserved among Gram-negative Enterobacteriaceae, little is known about its chaperoning mechanisms or protective function in the cell. This thesis specifically aims to:

- Investigate the involvement of a selection of periplasmic chaperones in the protection against environmental stresses (Chapter 3).

- Analyse the structure of ZraP, and investigate the involvement of the cysteine residues in protein oligomerisation (Chapter 4)

- Determine if the ZraP protein structure is influenced by the absence and/or presence of zinc (Chapter 4)

- Characterise substrate chaperoning by ZraP (Chapter 5).

Chapter 2. Materials and Methods

2.1 Materials

All chemicals, reagents and tools used in this study are of standard laboratory grade or higher. Unless stated otherwise, purchases were made from Thermo Fisher Scientific (UK) or Sigma Aldrich (UK). The solutions and media were prepared in reverse osmosis water (dH$_2$O), except for those buffers involved in metal assays, where Sigma W4502 0.1 µM filtered, molecular grade water (not treated with DEPC, nuclease and protease free) was used (further referred to as Sigma water).

2.2 Bacterial strains and plasmids

During this study, *Salmonella* Typhimurium SL1344 WT and mutant strains have been used to analyse the involvement of selected periplasmic chaperones on outer membrane integrity. *E. coli* strains have been involved in the mutagenesis process. Furthermore, STM SL1344 Δ*zraP* and *E. coli* stains have been utilised for protein overexpression. A comprehensive list of strains and plasmids used in this study can be found in paragraph 2.2.1 and 2.2.2 respectively.

2.2.1 Bacterial strains

The bacterial strains used in this study are *Salmonella enterica* subspecies, *Salmonella bongori* and *Escherichia coli* K-12 derivatives. The isogenic parent strain of the *S. enterica* subspecies is *Salmonella enterica* subspecies *enterica* serovar Typhimurium strain SL1344 (referred to as SL1344), and the 'wild-type' strain (WT) used in this study refers to SL1344. Table 2.1 summarises the strains used in this study.

The majority of strains used in this study were inherited from previous lab members. Prior to use, the validity of the mutant strains was tested using the external verification primers summarised in table 2.4. Verification of the mutants was conducted as described in chapter 2.5.2.7. New mutant strains were created by lambda red mutagenesis as described in chapter 2.5.2.

2.2.2 Plasmids

The plasmids used in this study include pKD plasmids involved in mutagenesis and pBAD plasmids used for overexpression constructs. The S*trepII*-tagged pBAD constructs were created from previously constructed pBAD/*Myc*-His overexpression constructs by whole plasmid PCR, as described in chapter 2.5.4.1.

Table 2.1 Strains used in this study

Strain	Description	Reference
***Escherichia coli* Strains**		
MG1655	Prototroph; K-12 derivative; F-, lambda-, rph-1	(Guyer et al., 1981), (Lacey et al., 2010)
Top10	*mcrA, Δ(mrr-hsdRMS-mcrBC), Phi80lacZ(del)M15, ΔlacX74, deoR, recA1, araD139, Δ(ara-leu)7697, galU, galK, rpsL(SmR), endA1, nupG*	Invitrogen™
DE3 BL21	*fhuA2 [lon] ompT gal (λ DE3) [dcm] ΔhsdS λ DE3 = λ sBamHIo ΔEcoRI-B int::(lacI::PlacUV5::T7 gene1) i21 Δnin5*	NEB
***Salmonella* Strains**		
SL1344	*Salmonella enterica enterica* serovar Typhimurium 4/74, *hisG, rpsL*	(Hoiseth and Stocker, 1981), (McClelland et al., 2001)
DT104	*Salmonella enterica enterica* serovar Typhimurium DT104 NCTC 13348	(Sanger Institute)
bongori	*Salmonella bongori* 12419 ATCC 43975.	(Sanger Institute)
***Salmonella* mutant strains**		
Δ*baeR*	SL1344 Δ*baeR* ::pCP20	(Appia-Ayme et al., 2011)
Δ*baeR* Δ*cpxR* Δ*zraSR*	SL1344 Δ*baeR* ::pCP20 Δ*cpxR* ::cm Δ*zraSR* ::kan	(Appia-Ayme et al., 2011)
Δ*cpxP*	SL1344 Δ*cpxP* ::cm	(Appia-Ayme et al., 2011)
Δ*cpxP* Δ*spy*	SL1344 Δ*cpxP* ::cm Δ*spy* ::kan	(Appia-Ayme et al., 2011)
Δ*cpxP* Δ*spy* Δ*zraP*	SL1344 Δ*cpxP* ::pCP20 Δ*spy* ::kan Δ*zraP* ::cm	(Appia-Ayme et al., 2011)
Δ*cpxP* Δ*yncJ*	SL1344 Δ*cpxP* ::cm Δ*yncJ* ::kan	(Williams, 2013)
Δ*cpxP* Δ*zraP*	SL1344 Δ*cpxP* ::cm Δ*zraP* ::kan	(Appia-Ayme et al., 2012)
Δ*cpxR*	SL1344 Δ*cpxR* ::kan	(Humphreys et al., 1999)
Δ*fkpA*	SL1344 Δ*fkpA* ::kan	(Williams, 2013)
Δ*fkpA* Δ*ppiA*	SL1344 Δ*fkpA* ::kan Δ*ppiA* ::cm	(Williams, 2013)
Δ*fkpA* Δ*ppiD*	SL1344 Δ*fkpA* ::kan Δ*ppiD* ::cm	(Williams, 2013)
Δ*fkpA* Δ*ppiAD*	SL1344 Δ*fkpA* ::kan Δ*ppiA/D* ::cm	(Williams, 2013)
Δ*fkpA* Δ*ppiAD* Δ*surA*	SL1344 Δ*fkpA* ::kan Δ*ppiA/D* ::cm Δ*surA* ::kan	(Williams, 2013)
Δ*htrA*	SL1344 Δ*htrA* ::kan	(Williams, 2013)
Δ*htrA* Δ*skp*	SL1344 Δ*htrA/Δskp* ::kan	(Williams, 2013)
Δ*htrA* Δ*zraP*	SL1344 Δ*htrA* ::kan Δ*zraP* ::cm	(Williams, 2013)
Δ*ppiAD*	SL1344 Δ*ppiA/D* ::cm	(Williams, 2013)
Δ*rpoE*	SL1344 Δ*rpoE* ::kan	(Humphreys et al., 1999)
Δ*skp*	SL1344 Δ*skp* ::kan	(Williams, 2013)
Δ*skp* Δ*surA*	SL1344 Δ*skp* ::kan Δ*surA* ::cm	This study
Δ*skp* Δ*zraP*	SL1344 Δ*skp* ::kan Δ*zraP* ::cm	(Williams, 2013)
Δ*spy*	SL1344 Δ*spy* ::kan	(Williams, 2013)
Δ*spy* Δ*surA*	SL1344 Δ*spy* ::kam ΔsurA::cm	(Williams, 2013)
Δ*spy* Δ*yncJ*	SL1344 Δ*spy/yncJ* ::kan	(Williams, 2013)
Δ*spy* Δ*zraP*	SL1344 Δ*spy* ::kan Δ*zraP* ::cm	(Williams, 2013)
Δ*surA*	SL1344 Δ*surA* ::cm	(Williams, 2013)
Δ*surA* Δ*ppiAD*	SL1344 Δ*surA/ppiA/ppiD* ::cm	(Williams, 2013)
Δ*surA* Δ*yncJ*	SL1344 Δ*surA* ::cm Δ*yncJ* ::kan	This study
Δ*surA* Δ*zraP*	SL1344 Δ*surA* ::cm Δ*zraP* ::kan	(Williams, 2013)
Δ*yncJ*	SL1344 Δ*yncJ* ::kan	This study
Δ*zraP*	SL1344 Δ*zraP* ::cm	(Appia-Ayme et al., 2012)
Δ*zraSR*	SL1344 Δ*zraSR* ::cm	(Appia-Ayme et al., 2011)

Table 2.2 Plasmids used in this study

Plasmid	Description	Reference
pBAD/*Myc*-His A	pBR322 origin, *araBAD* promoter(pBAD) C-terminal *Myc* epitope tag, C-terminal 6xHis tag, *rrnB* transcription termination region, *araC*; AmpR	Invitrogen™
pKD3	pANT-Sγ derivative; containing a FRT-flanked CmR AmpR;	(Datsenko and Wanner, 2000)
pKD4	pANT-Sγ derivative containing a FRT-flanked KanR; AmpR	(Datsenko and Wanner, 2000)
pKD46	pINT-ts derivative containing *araC*-P*araB* and *γ, β, exo* genes; AmpR	(Datsenko and Wanner, 2000)
***Myc*- His-tagged protein overexpression constructs**		
p*zraP* 6xHIS	*zraP* gene in pBAD *Myc*/His A expression plasmid in phase with C-terminal 6xHis epitope; AmpR	(Wells, 2015)
p*zraP* AAAAA	*zraP* gene, with L44A; T45A; T46A; E47A; Q48A mutations, in pBAD *Myc*/His A expression plasmid in phase with C-terminal 6xHis epitope; AmpR	(Wells, 2015)
p*zraP* HRGGAH	*zraP* gene, with G134A mutation, in pBAD *Myc*/His A expression plasmid in phase with C-terminal 6xHis epitope, AmpR	(Wells, 2015)
p*zraP* LTxxQ	*zraP* gene, with Q48A mutation, in pBAD *Myc*/His A expression plasmid in phase with C-terminal 6xHis epitope; AmpR	(Wells, 2015)
p*zraP* SDM	*zraP* gene, with G120A; G121A; C122A; G123A;G124A; Y125A mutations, in pBAD *Myc*/His A expression plasmid in phase with C-terminal 6xHis epitope, AmpR	(Wells, 2015)
p*zraP* ZA	*zraP* gene, with H130A; R131A; G132A; G133A; G134A; H135 mutations, in pBAD *Myc*/His A expression plasmid in phase with C-terminal 6xHis epitope, AmpR	(Wells, 2015)
***StrepII*-tagged protein overexpression constructs**		
pzraP-S	*zraP* gene in pBAD expression plasmid in phase with C-terminal *strepII* epitope; AmpR	This study
pzraPAAAAA-S	*zraP* gene, with L44A; T45A; T46A; E47A; Q48A mutations, in pBAD expression plasmid in phase with C-terminal *strepII* epitope; AmpR	This study
pzraPHRGGAH-S	*zraP* gene, with G134A mutation, in pBAD expression plasmid in phase with C-terminal *strepII* epitope; AmpR	This study
pzraPLTxxQ-S	*zraP* gene, with Q48A mutation, in pBAD expression plasmid in phase with C-terminal *strepII* epitope; AmpR	This study
pzraPSDM-S	*zraP* gene, with G120A; G121A; C122A; G123A;G124A; Y125A mutations, in pBAD expression plasmid in phase with C-terminal *strepII* epitope; AmpR	This study
pzraPZA-S	*zraP* gene, with H130A; R131A; G132A; G133A; G134A; H135 mutations, in pBAD expression plasmid in phase with C-terminal *strepII* epitope; AmpR	This study

2.3 Culture conditions

2.3.1 Media

The media and antibiotics used in this study were prepared according to appendix A. The STM SL1344 WT strain and its mutant derivatives are histidine auxotrophs. To allow STM SL1344 growth in minimal media, supplements of 40mg/ml histidine were added. Where applicable, antibiotics were added to final concentrations of 100µg/ml for ampicillin (amp), 10µg/ml for chloramphenicol (cm), and 50µg/ml for kanamycin (kan).

2.3.2 Overnight cultures

Stationary phase overnight cultures were produced by inoculating 10ml LB with a single colony from a short-term storage streak plate (2.3.3). Cultures were incubated at 37°C, 200 rpm for a minimum of 12 hours. When required, overnight cultures were normalised to an optical density (OD) of 1.000. A SpectraMax™ M5 spectrophotometer (Molecular Devices) was used at λ = 600, room temperature, to analyse the optical density of cultures in reference to a blank prepared from fresh media. For normalisation of overnight cultures, the OD at λ = 600nm (OD_{600}) was taken and the culture was diluted down to a final OD_{600} of 1.000 using the following calculations:

Amount of overnight culture per ml: $1/_{OD_{600}\ reading}$

Amount of fresh LB culture per ml: $1 - amount\ of\ added\ overnight\ culture$

2.3.3 Short and long term storage

For long-term storage at -80°C, Microbank™ stocks were prepared according to manufacturer's instructions (Prolab Diagnostics). For short-term storage, spread plates were prepared from a single Microbank™ bead, grown overnight at 37°C and stored at 4°C for a maximum of two weeks.

2.3.4 Aerobic growth

Aerobic batch culture for growth curves was carried out using 50ml of media in 250ml conical flasks. Flasks were supplemented with appropriate antimicrobials and inoculated with 1:100 (v/v) dilution of normalised overnight culture (2.3.2). Unless otherwise stated, cultures were grown at 37°C, 200 rpm for 24 hours. To determine cell density, the OD_{600} of 1ml samples was measured at hourly intervals. When the OD_{600} was larger than 1.000, a 1/10 dilution of

the sample and all subsequent samples was prepared and the final OD_{600} was calculated using the dilution factor for correction.

Chapter 2.4 Electrophoresis

Electrophoresis is a technique that involves the movement of charged particles through a matrix. It separates molecules based on their size and/or charge, and it is frequently used to analyse biological macromolecules such as DNA and proteins.

2.4.1 DNA electrophoresis

DNA electrophoresis was used to separate and analyse PCR products by size. Analysis was carried out using a 1% (w/v) agarose gel, prepared using 1 x TBE buffer (appendix B) and supplemented with 2μg/ml ethidium bromide. Prior to loading, 5x DNA loading buffer (BIOLINE) was added to the samples. Hyperladder™ (BIOLINE) was used as size marker. Gel electrophoresis was carried out for an hour (unless otherwise stated) in 1 x TBE buffer at 110 V, using a Sub-Cell GT electrophoresis system (BIOLINE). DNA was visualised by UV light, using a Molecular Imager® Gel Doc™ System (BIORAD).

2.4.2 Protein separation by PAGE

Polyacrylamide gel electrophoresis (PAGE) is a technique used to separate proteins according to their electrophoretic mobility. SDS-PAGE can be used to separate proteins based on their charge-to-mass ratio when in denatured state following treatment with the denaturing agent sodium dodecyl sulphate (SDS). Alternatively, the process known as native-PAGE can be used to analyse the oligomeric state of proteins, by running them on a gel in their native form after treatment with a cross-linking agent such as formaldehyde.

2.4.2.1 SDS-PAGE

SDS-PAGE was used to separate denatured proteins according to their size. SDS is a detergent that disrupts the tertiary structure of proteins and coats them in a negative charge, resulting in the denaturation of folded proteins into linear strings of amino acids. The negatively charged SDS also masks intrinsically charged R-groups, ensuring the protein's negative charge is proportional to its molecular weight. To avoid smeared protein gels as a result of protein entering the resolving gel at separate times, the SDS-PAGE gels were prepared with a stacking gel (top quarter of gel) and a resolving gel (bottom three quarters of gel). Using ProtoGel™ acrylamide/methylene bisacrylamide solution (ratio 37.5:1) (National Diagnostics), the resolving gels (15% (w/v)) and the stacking gels (5% (w/v)) were prepared as described in table 2.3 and cast in Mini-PROTEAN® Tetra hand-cast systems (BIO-RAD).

Wells were created using 0.75mm and 1.0mm combs between integrated spacer plates, prior to the setting of the gel by polymerisation at room temperature for a minimum of one hour. Samples analysed using SDS-PAGE were dissolved in SDS loading buffer (appendix B) containing 5% (v/v) β-mercapthoethanol (Sigma-Aldrich) at a ratio of 1:9. The solutions were boiled at 100°C for 10 minutes and centrifuged at 17000 x g (13500rpm) for 2 minutes prior to gel loading. Protein samples were loaded in volumes of 5-10µl alongside the protein size marker PageRuler™ Prestained Protein Ladder (Thermo Scientific). Gel electrophoresis was carried out at 200 V in 1 x TGS buffer (appendix B) for approximately one hour using Mini-PROTEAN® Tetra Cell systems (BIO-RAD).

2.4.2.2 Native-PAGE

Native-page was used to analyse potential differences in oligomeric states between the wild-type protein and mutated proteins. During Native-PAGE proteins are separated by the differences in their intrinsic charge and hydrodynamic size. Native-PAGE gels were cast as a single entity using 6% (w/v) acrylamide containing native gel table 2.3, according to the protocol described for SDS-PAGE gels (2.4.2.1). Prior to casting the gels, equipment was thoroughly washed in soapy water and rinsed with ethanol to remove any residual SDS contamination. Protein samples (1mg/mL) were aliquoted in volumes of 20µL and exposed to 1% (v/v) formaldehyde (pH 8.0) for 1 minute to chemically cross-link oligomers. The reaction was terminated by the addition of 2 M glycine, prior to addition of 10µL SDS-loading buffer (appendix B). Native-PAGE gels were pre-run in 1 x TBE buffer (appendix B) at 120 V for 15 minutes at 4°C to remove any unpolymerised acrylamide and excessive ammonia and persulfate ions. Samples were loaded onto the native gel in volumes of 10µL and electrophoresed at 120 V for approximately one hour at 4°C using Mini-PROTEAN® Tetra Cell systems (BIO-RAD). Gels were stained and imaged according to PAGE-staining protocol described in chapter 2.7.2.1.

2.5 Manipulation of genetic material

During this study, DNA manipulation has been carried out to delete genes of interest, and to create overexpression plasmids. The production of knock-out strains was accomplished using the lambda red method, followed by transduction using the P22 bacteriophage. The alteration of pre-existing over-expression plasmids was carried out by whole-plasmid PCR, and the resulting plasmids were formed into both an *E. coli* and a *Salmonella* background.

Table 2.3 Components and compositions of PAGE gels

Component	Stock Solution	Volume	Final Concentration
SDS-PAGE resolving gel			
Acrylamide/Bis-acrylamide	30% (w/v)	10mL	15%
*Tris-HCl pH 8.8	1.5 M	5mL	375mM
*SDS	10% (w/v)	100µL	0.05%
dH2O		4.795mL	
TEMED	>99%	5µL	0.5%
°APS	20% (w/v)	100µL	0.1%
SDS-PAGE stacking gel			
Acrylamide/Bis-acrylamide	30% (w/v)	1.66mL	5%
*Tris-HCl pH 8.8	1.5 M	1.26mL	63mM
*SDS	10% (w/v)	50µL	0.05%
dH2O		6.975mL	
°TEMED	>99%	5µL	1%
°APS	20% (w/v)	50µL	0.1%
Native PAGE gel			
Acrylamide/Bis-acrylamide	30% (w/v)	3.96mL	6%
*TBE buffer	10X	2mL	1X
dH2O		13.93mL	
°TEMED	>99%	10µL	0.5%
°APS	20% (w/v)	100µL	0.1%

* buffers/solutions prepared with dH2O. ° reagents added directly before casting of gel

2.5.1 Primer list

Table 2.4 summarises the primers used during this study. All primers used throughout this work were synthesised by Integrated DNA Technologies (IDT).

2.5.2 *De novo* mutagenesis using the lambda (λ) red method

Deletion mutants were produced using a homologous recombination method derived from the lambda (λ) red bacteriophage. During this process, the gene of interest is replaced with a linear, FRT-flanked (flippase recognition target) resistance gene construct (Datsenko and Wanner, 2000), derived from pKD3 (chloramphenicol) or pKD4 (kanamycin) (2.5.2.3). Cassettes were transformed into freshly prepared, electrocompetent *Salmonella* Typhimurium 12023 donor strains carrying the helper plasmid pKD46, which encodes the λ-red bacteriophage recombinase genes *exo, bet,* and *gam,* under the control of an L-arabinose inducible promoter (2.5.2.5). Due to the temperature sensitive pKD46 origin of replication, electroporation was the chosen method of transformation (2.5.2.6). Following verification of

gene deletion (2.5.2.7), the resistance cassette was transfected to a clean background by P22 transduction (2.5.3). Non-lysogenic colonies were selected and used for the production of long-term storage stocks.

Table 2.4 Primers used in the experiments described in this thesis.

External verification primers for knock-out confirmation

Gene	Forward primer (5' - 3')	Reverse primer (5' - 3')
cpxP	GAAATTACGTCATCAGGCGT	TATCTTCTGCCGGTAGTATA
fkpA	AGAAGTGATAATAGGCGTG	CTATTTCAGACTACGTGTGC
htrA	TACGCATGGGATGAATATCG	ACAGGTCTCGACATTGTGCA
ppiA	GAATACGGCGTTGCGTCGTA	ATATGCCTGTGCTTGACCAC
ppiD	CGATGCGCGTGAAGTCTCTA	AACAGTGCAGCCACGATAGC
skp	CCGAGCAGTTCCAGTTTAAC	CGGTACTTAGGATTCACCAT
spy	CCGTTGTTATGACTAATTGA	TGTCAGGTCAATATGAGATC
surA	TGAGCTCTAACTACGGCCTC	TTCAATCGGCCACGCGCGTT
yncJ	CTATGGAACGAATTGGCTCG	CGAAATGCATGTCATTGGCA
zraP	CTTTCGGATACGGATGGGTA	TGCTGGTGGCGAATTCAGAT

Sequencing primers for pBAD constructs

Gene	Forward primer (5' - 3')	Reverse primer (5' - 3')
pBAD	TTATCGCAACTCTCTACTG	TGATTTAATCTGTATCAGGC

Whole plasmid primers encoding *strepII* tag

Gene	Forward primer (5' - 3')	Reverse primer (5' - 3')
His-to-*strepII*	CAATTTGAAAAATGAGTTTAAACGGTCTCCAG	TGGATGGCTCCACCAGTTTCCCATACCCATGT

Mutagenesis primers for the production of FRT-flanked chloramphenicol and kanamycin cassettes

Gene	Forward primer (5' - 3')	Reverse primer (5' - 3')
skp	GTGAAAAAGTGGTTATTAGCTGCAGGTCTCGGT TTAGCACGTGTAGGCTGGAGCTGCTTC	TTATTTAACCTGTTTCAGTACGTCGGCAGTGAT GTCTTTTCATATGAATATCCTCCTTAG
surA	CAACGTAATCCGCATTGCGGTTAATTGAAATGG AAAAAGTGTGTAGGCTGGAGCTGCTTC	GGTTCGCCGGGAGTGATAACAACGCGTTGCGC ACTGCTCACATATGAATATCCTCCTTAG

2.5.2.1 Polymerase chain reaction

Polymerase chain reactions (PCR) were carried out using ultra-stable Taq DNA polymerase (NEB) and Phusion™ high-fidelity DNA polymerase (NEB) (table 2.5). Template DNA used in this study includes chromosomal DNA, plasmid DNA and synthesised constructs. The primers used in this study are summarised in table 2.4. The melting temperatures (Tm) and annealing temperatures (Ta) were chosen according to primer specifications and enzyme used. The elongation time allowed for one minute per kilo base (kb) of double stranded product. The PRC programs (table 2.6) were conducted using a Techne Prime Elite Satellite Thermal Cycler (Cole-Parmer®).

Table 2.5 PCR reaction components

Reagent	Volume (µL)	
Ultra-stable *Taq* DNA polumerase		
	verification	*construction*
2X BioMix (Bioline)	12.5	25
Forward primer (5'-3') [20µM]	0.5	1
Reverse primer (3'-5') [20µM]	0.5	1
Template DNA	variable	variable
Nuclease-free dH2O	Σ 25	Σ 50
Phusion ® High fidelity (HF) DNA Polymerase		
	His-to-Strep	
Phusion® buffer HF	10	
dNTP mixture (2.5mM)	4	
template DNA (0.2µg/µL)	5	
Forward primer (5'-3') [20µM]	1	
Reverse primer (3'-5') [20µM]	1	
Phusion® HP polymerase	1	
Nuclease-free dH2O	28	

Table 2.6. Thermocycling steps for PCR.

PCR Stages	Mutagenesis		Verification		Whole Plasmid	
	Temp (ºC)	Time min	Temp (ºC)	Time min	Temp (ºC)	Time min
1) Initial denaturation	96	3	98	2	98	3
2) Denaturation	95	0.3	98	0.5	98	0.5
3) Annealing	52-60*	0.5	60	0.5	70	0.5
4) Elongation	72	2	72	2.5	72	5
5) Repeat stages 2-4		(35x)		(29x)		(29X)
6) Final elongation	72	10	72	5	72	20

*Annealing temperature dependent on primer specific melting temperatures

2.5.2.2 Plasmid DNA extraction and purification

To extract and purify plasmid DNA, QIAprep^{TM} Spin Miniprep Kits (QIAGEN) and QIAprep^{TM} Spin Midiprep Kits (QIAGEN) were used. The maximum volume of culture advised by the manufacture was adopted (10mL and 100mL respectively) due to the low-copy number nature of the plasmids used in this study. To compensate for the increased volumes of cultures subjected to the minipreps, the recommended volume of buffers was adapted accordingly. The QIAprep^{TM} Spin Miniprep Kit buffers P1, P2 and N3 volumes were doubled, whereas the QIAprep^{TM} Spin Midiprep Kit buffers remained unchanged from the manufacturer's guidelines. Plasmid DNA was eluted from the QIAprep^{TM} Spin columns using 50μL of nuclease free dH$_2$O, preheated to 60°C (for increased yield). The same volume of nuclease free dH$_2$O was used for the resuspension of air-dried DNA pellets obtained from the Midiprep kit. Analysis of plasmid DNA concentration and purity was carried out using a NanoDrop 2000c UV-Vis spectrophotometer (Thermo Scientific) with NanoDrop 2000 software (Thermo Scientific). Purified plasmid DNA was stored at -20°C until further use.

2.5.2.3 Generation of FRT-flanked resistance cassette constructs

FRT-flanked resistance cassettes were produced using the primers summarised in table 2.4. All gene-specific primer pairs used for the cassette constructs contained 40bp long extensions that are homologous to the flanking region of the genes of interest, and 20bp extensions that are complementary to the 5' and 3' ends of the antibiotic resistance cassettes encoded on the plasmids pKD3 (chloramphenicol) and pKD4 (kanamycin). The cassettes were produced using purified pKD3/pKD4 DNA (2.5.2.2) as template following the set-up described in table 2.5.

2.5.2.4 PCR product purification

Prior to use, PCR products were purified using a QIAquick™ PCR purification kit (QIAGEN) as per manufacturer's instructions. Elution of the product was carried out using 50μL of nuclease free dH$_2$O, preheated to 60°C for increased yield, and stored at -20°C until further use.

2.5.2.5 Preparation of electro-competent cells

Electro-competent cells were freshly produced on the day they were required. Prior to their production, overnight cultures (2.3.2) were prepared of pKD46 harbouring STM SL1344 and pKD46 harbouring *E. coli* MG1655. Due to the temperature sensitive nature of the λ-red gene (*exo, bet, gam)* encoding pKD46 plasmid, the overnight cultures and subsequent inoculated cultures were grown at 30°C. Inoculation of 50mL Lennox broth (appendix A) was carried out

using 1% (v/v) overnight culture. Cultures were incubated at 30°C, 200 rpm until an OD_{600} of 0.5-0.6 was reached. Cultures were cooled on ice and cells were harvested by centrifugation at 3450 x g (4000 rpm), 4°C. After removal of the supernatant, the pellet was resuspended in 25mL ice-cold glycerol (10% (v/v)). The harvesting and resuspending of the cells was thrice repeated. During the final harvest, cells were resuspended in 2mL glycerol and aliquoted into 100μL volumes. The aliquots were stored on ice until further use.

2.5.2.6 Transformation by electroporation

Electroporation was carried out using MicroPulser™ Electroporation Cuvettes (BIO-RAD), precooled at -20°C for a minimum of one hour before use. Exogenous DNA (5μL) was added to aliquots of freshly prepared electro competent cells (2.5.2.5) before the cells were transferred to the electroporation cuvettes. Negative controls were produced by replacing the exogenous DNA added to aliquoted electro competent cells with sterile dH_2O. Using a MicroPulser™ Electroporation Apparatus (BIO-RAD), the cells were subjugated to a single electrical pulse at 2.5kV (programme EC2). Following the pulse, 1mL of LB broth was added to the transformed cells and mixed by gentle pipetting. The culture was subsequently transferred to a 1.5mL micro centrifuge tube, and incubated at 37°C, 200 rpm for one hour to recover. Recovered cultures were spread aseptically on antibiotic selective LB agar (1.5% (w/v)) plates, and incubated at 37°C for a minimum of 12 hours. Colonies were selected to be carried forward for knock-out verification (2.5.2.7).

2.5.2.7 Verification of gene knock-out using colony PCR

To verify the knock-out of genes of interest by PCR, genomic DNA of bacterial colonies of interest were used to extract template DNA. Genomic DNA was obtained by resuspending a colony in 50μL dH_2O, boiling at 100°C for 10 minutes and centrifuging at 17000 x g (13500 rpm) for two minutes. During knock-out verification, the PCR product of the strain of interest was compared to the PCR product of the isogenic parent strain. The samples for PCR verification were prepared according to table 2.5, using primers summarised in table 2.4, and subjected to the knock-out verification PCR program described in table 2.6. The 20 bp long external verification primers were designed from the region 50-200 bp up- and down-stream from the gene of interest, allowing for the amplification of either the gene of interest (in the WT and unsuccessful knock-outs) or the antibiotic cassette (in successful knock-outs). Analysis of the PCR products by agarose gel electrophoresis (2.4.1) was carried out by size comparison between the PCR fragments generated from the WT SL1344 gene and the antibiotic cassette of known size (1300 bp for chloramphenicol, 1700 bp for kanamycin).

2.5.3 P22 transduction

To prevent any undesired additional recombination events, the desired mutation was transduced into a clean background strain using the *Salmonella* specific P22 bacteriophage (Kwoh and Kemper, 1978). The recognition sites used by the λ *bet* and *exo* genes encoded on pKD46 used during *de novo* mutagenesis, can also be utilised by the recombination system encoded by P22 bacteriophage, allowing for transduction of the newly inserted antibiotic cassette into a clean background strain (Poteete and Fenton, 1984; Murphy, 1998). The transduction is a three-part process starting by production of donor strain lysate, followed by transduction of a recipient strain and finished by selection for stable, non-lysogenic colonies.

2.5.3.1 Lysate production from donor strain

The donor lysates were produced from verified knock-out strains carrying antibiotic cassettes (2.5.2). LB broth (10mL) was inoculated (1% (v/v)) from an overnight culture containing the appropriate selective antibiotic. After one hour incubation at 37°C, 200rpm, bacteriophage P22 lysate (20µL) was added and the incubation was continued for a further six hours. The cultures were transferred to sterile, chloroform resistant tubes (Falcon™ 15mL conical centrifugation tubes) prior to the addition of 1mL chloroform. The samples were incubated overnight at 4°C with gentle agitation. Supernatant, cell debris and chloroform were separated by centrifugation at 3450 x g (4000 rpm) for 15 minutes before the lysate (supernatant) was transferred to a fresh Falcon™ tube and stored at 4°C until further use.

2.5.3.2 Transduction of recipient strain

Overnight cultures of the recipient strain were prepared (2.3.2) and aliquoted into volumes of 100µL. Prior to incubation at 37°C, 200 rpm, 10µL P22 lysate was added to the aliquots. After 45 minutes incubation, cultures were spread onto LB agar (1.5% (w/v) plates supplemented with the appropriate selective antibiotics, and incubated at 37°C for a minimum of 12 hours. Negative control plates were produced by spreading a non-transduced recipient aliquot and by spreading pure lysate.

2.5.3.3 Selection of non-lysogenic colonies

Colonies produced during transduction assays (2.5.3.2) were streaked onto UCB indicator plates (Bochner, 1984), further referred to as green plates. These plates contain pH indicators which turn the plates green at neutral pH, and non-lysogenic strains grow as light coloured colonies. However, when cells undergo lysis, the pH of the medium drops, resulting in a dark colouration of the colonies. After overnight incubation at 37°C, light-coloured non-

lysogenic colonies were selected and spread on a fresh green plate and incubated overnight at 37°C, to confirm their non-lysogenic state. When subsequent green plate analysis confirmed non-lysogenic state, colonies were spread onto a fresh LB agar (1.5% (w/v)) and the gene knock-out was verified as described in chapter 2.5.2.7.

2.5.4 Preparation of overexpression strains

The *E. coli* BL21 DE3 strains carrying N-terminal *myc*-His-tagged overexpression plasmids used in this study were prepared by Dr. Wells, a former PhD candidate from the Rowley lab (Wells, 2015). Due to concerns of potential interference of the *myc*-His tags during zinc assays, the tags were replaced with the *Strep*-tag™ II (henceforth referred to as *StrepII*-tags) derived from *Streptomyces avidinii* (Skerra and Schmidt, 2000). The tag-replacement consisted of several steps. First, a linear *StrepII*-tagged plasmid was prepared from *myc*-His-tagged ZraP overexpression constructs using whole plasmid PCR (2.5.4.1). To ensure only *StrepII*-tagged plasmid remained prior to transformation into recipient strains, the template *myc*-His-tagged plasmids were digested using the methylated-DNA targeting enzyme *Dpn*I. The newly constructed plasmids were transformed into recipient strains by heat-shock (2.5.4.5). To verify the whole-plasmid PCR, the plasmids were purified from their recipient strains using Qiaquick PCR Purification Kits (Qiagen), and sequenced using pBAD sequencing primers (table 2.4) (2.5.4.6).

2.5.4.1 PCR-mediated substitution of *myc*-His-tag with a *StrepII*-tag

To replace the *myc*-His-tag with a *StrepII*-tag, whole plasmid PCR was carried out using purified plasmid DNA (2.5.2.2) as template. The polymerase used for the reaction was Phusion™ high-fidelity DNA polymerase (NEB). The PCR reaction was set-up as described in table 2.5, and subjugated to the whole plasmid PCR program described in table 2.6, using a Techne Prime Elite Satellite Thermal Cycler (Cole-Parmer®). The whole-plasmid PCR products were verified using agarose gel electrophoresis (2.4.1).

2.5.4.2 Removal of methylated template DNA

After verification of the whole plasmid PCR products, the *StrepII*-tagged PRC products were separated from the *myc*-His tagged template DNA using digestion by *Dpn*I (NEB). This restriction enzyme targets methylated DNA. The methylation of DNA is an epigenetic modification which is involved in the regulation of gene expression, and in bacteria DNA methylation also serves as a method to target and destroy bacteriophage DNA. Unlike the plasmid DNA template, the PCR product had not been introduced to bacterial cells yet, meaning *Dpn*I would only target template DNA. The set-up of the reaction for the *Dpn*I

mediated digestion of template DNA is summarised in table 2.7. The digestion was carried out by incubation in a water bath at 37°C for 2 hours. After the digestion was completed, the whole-plasmid PCR products were purified using a QIAquick™ PCR purification kit (QIAGEN) as described in chapter 2.5.2.4, and quantified and analysed for quality using a NanoDrop 2000c UV-Vis spectrophotometer (Thermo Scientific; software NanoDrop 2000, Thermo Scientific).

2.5.4.3 Ligation of linear plasmid

Phosphorylation using T4 DNA Ligase (NEB) was used to create circular plasmids from the linear whole-plasmid PCR products. Prior to the ligation, the 5' end of the linear whole-plasmid PCR products was phosphorylated using T4 Polynucleotide Kinase (NEB). The phosphorylation reactions were set-up as described in table 2.7. The reaction was incubated in a water bath at 37°C for 5 minutes. The ligation reaction was carried out sequentially, by adding 1μL T4 DNA ligase (NEB) directly to the incubated sample. The ligation was carried out overnight at 16°C. Following the ligation, a QIAprep™ Spin Miniprep Kit (QIAGEN) was used to purify the ligated, circular plasmid DNA. During the purification of the plasmid from the ligase reaction, the first four steps of the miniprep kit, involving the isolation of the cell lysate, were skipped, and the ligase reaction was directly loaded onto the QIAprep spin columns. From this point onwards the protocol was followed as per manufacturer's instructions. Elution was carried out using 50μL sterile dH2O, preheated to 60°C to increase yield. Purified product was quantified and analysed for quality using a NanoDrop 2000c UV-Vis spectrophotometer (Thermo Scientific; software NanoDrop 2000, Thermo Scientific), and stored at -20°C until further use.

Table 2.7 Isolation, phosphorylation and ligation of linear plasmids.

Reagent	Volume (µL)
***Dpn* I mediated digestion of template DNA**	
PCR product	10
DpnI enzyme (NEB)	1
10X DpnI reaction buffer	5
dH2O	34
Phosphorylation and ligation of plasmids	
T4 polynucleotide kinase (NEB)	1
DNA lygase reaction buffer	2
Pure PCR product (150ng/µL)	12.5
dH2O	4.5
*T4 DNA ligase (NEB)	1

*T4 DNA ligase added after initial 5 minute incubation at 37°C

2.5.4.4 Preparation of chemically competent cells

Chemically competent cells were freshly produced on the day they were required. Prior to their production, overnight cultures (2.3.2) were prepared of recipient STM SL1344 and *E. coli* BL21 DE3. Inoculation of 50mL Lennox broth (appendix A) was carried out using 1% (v/v) overnight culture. Cultures were incubated at 37°C, 200 rpm until an OD_{600} of 0.5-0.6 was reached. Cultures were cooled on ice and cells were harvested by centrifugation at 3450 x g (4000 rpm), 4°C. After removal of the supernatant, the pellet was resuspended in 10mL pre-cooled 0.1 M $CaCl_2$, and rested on ice for 15 minutes, prior to a second cell harvest by centrifugation at 3450 x g (4000 rpm), 4°C. The harvested cells were resuspended in 1mL pre-cooled 0.1 M $CaCl_2$, and aliquoted into 100µL volumes. The aliquots were stored on ice until further use.

2.5.4.5 Transformation by heat shock

Heat shock transformation was carried out using freshly prepared chemically competent cells (2.4.5.4). After addition of 50ng of pure plasmid DNA (2.5.2.2) to each aliquot, cells were incubated on ice for 10 minutes. Using a water bath at 42°C, cells were shocked for 45 seconds and put back on ice to recover for two minutes. Following recovery, 1mL LB broth was added to each aliquot and the cells were incubated at 37°C, 200rpm for one hour, before being spread onto LB agar plates (1.5% (w/v)) containing 100µg/ml ampicillin. The plates were incubated overnight at 37°C before colonies were selected for verification of transformation.

2.5.4.6 Verification of transformation

To confirm successful transformation, overnight cultures were prepared from selected colonies (chapter 2.3.2) in LB broth supplemented with 100µg/mL ampicillin. The overnight cultures were used for plasmid extraction using QIAprep^{TM} Spin Miniprep Kits (QIAGEN) as described in chapter 2.5.2.2. The quality and quantity of the purified plasmids was analysed using a NanoDrop 2000c UV-Vis spectrophotometer (Thermo Scientific; software NanoDrop 2000, Thermo Scientific). Aliquots of the purified plasmid were taken and sequenced by Eurofins MWG Operon Value Read, using the external pBAD sequencing primers listed in 2.4.

2.6 Susceptibility assays

To investigate the role of various periplasmic chaperones, several assays were conducted to assess the susceptibility of chaperone mutant strains to a range of environmental stresses, including antimicrobial stresses and temperature stress. These susceptibility assays were carried out comparing the phenotype of knock-out strains to a wild-type control. To ascertain the involvement of gene products in the protection against a range of antimicrobial agents, growth curves, carbon-starvation induced cross-resistance assays, spot plate assays and disc diffusion assays were conducted.

2.6.1 Growth curves carried out in aerobic batch culture

Growth curves were carried out to estimate minimal inhibitory concentrations for the antimicrobial agents used in this study. Overnight cultures of STM SL1344 WT were prepared and normalised to an OD_{600} of approximately 1.000 (2.3.2). The normalised overnight cultures were used to inoculate 50mL of fresh LB broth (1% (v/v)) supplemented with antimicrobial agents of interest. Prior to incubation at 37°C, 200 rpm, 1mL samples were taken to establish the OD_{600} at time point $t_{(0)}$. Optical density measurements were taken hourly for a minimum of 8 hours using a SpectraMax™ M5 spectrophotometer (Molecular Devices), and final $t_{(1440)}$ readings were taken 24 hours post incubation. Due to reduced spectrophotometer sensitivity at values above 1.0, samples exceeding this limit were subjected to a $^1/_{10}$ dilution for the measurements of optical density, and the obtained results were corrected by multiplication by 10. The growth curves testing susceptibility to antimicrobial stresses have been carried out in singular samples, as these curves were only used to estimate concentrations to be tested in further assays. Growth curves testing susceptibility to metal stress have been carried out with a minimum of three triplicates, to allow for statistical analysis.

2.6.2 Carbon-starvation induced cross-resistance assays

The method described by Kenyon *et al.*, (2002) was used to analyse the involvement of periplasmic chaperones in the carbon-starvation induced cross-resistance (CSIXR) against heat and polymyxin B (PMB) exposure. Prior to mutant testing, trial assays were carried out to ascertain optimal testing conditions including exposure time and concentration.

2.6.2.1 Generation of carbon-starved cells and exponential control cells for CSIXR assays

To conduct the CSIXR assays, 24 hour carbon starved cells were required to be tested, using exponential phase cells as control. For the production of 24-hour starved cells, overnight cultures were produced of STM SL1344 WT and mutant strains of interest, and normalised to an OD_{600} of 1.0 (2.3.2). The normalised cultures were used to inoculate (1% (v/v)) 10mL of low carbon MOPS media (LoC MOPS) (appendix A). Inoculated cultures were incubated at 37°C, 200rpm for 29 hours to generate carbon starved cells; five hours to allow for depletion of the available carbon in the LoC MOPS media, and a further 24 hours to generate the starved cells. Particular note was taken of the incubation time. Exponential-phase control cells were incubated 24 hours after the incubation of their LoC MOPS counterpart cultures. The exponential growth control samples were prepared by inoculating 10mL of high carbon MOPS media (HiC MOPS) (appendix A) with normalised STM SL1344 WT or mutant strain overnight culture (1% (v/v)). The HiC MOPS exponential-phase control samples were incubated at 37°C, 200 rpm for 5 hours.

2.6.2.2 CSIXR trial assays

The CSIXR trial assays carried out in regards to heat stress tested carbon-stressed STM SL1344 WT resistance against 55°C during exposure times ranging from 4 minutes to 16 minutes. The CSIXR trial assays carried out in regards to PMB exposure tested carbon-stressed STM SL1344 WT resistance against one hour exposure to PMB concentrations ranging between 1μg/mL - 100μg/mL. To conduct the trial assays, CSIXR samples were prepared as described in chapter 2.6.3.1. Prior to exposure, samples were normalised to $OD_{600} = 0.35$ using M9 minimal salts buffer (appendix B) and 100μL of each samples was streaked onto LB agar plates (1.5% (w/v)) to allow determination of colony forming units (CFU mL^{-1}) . The determination of CFU mL^{-1} was carried out by multiplying the counted colony numbers with the appropriate dilution rate.

To test for heat resistance, the normalised samples were incubated in preheated tubes, in a water bath at 55°C. The first 100μL sample was taken after 4 minutes exposure and streaked onto LB agar plates (1.5% (w/v)), the next samples were taken every 4 minutes thereafter

and streaked onto separate LB agar plates (1.5% (w/v)). Plates were incubated at 37°C for a minimum of 12 hours before determination of CFU mL^{-1}.

To test for polymyxin B resistance, the normalised samples were incubated in separate tubes and supplemented with various concentrations of PMB. The PMB exposed cultures were incubated at 37°C, 200rpm for one hour prior to sampling. Post incubation, samples of 100µL were spread onto separate LB agar plates (1.5% (w/v)) and incubated at 37°C for a minimum of 12 hours before determination of CFU mL^{-1}.

2.6.2.3 CSIXR assays

The CSIXR assays carried out in this study tested carbon-starved stress resistance of investigative strains and compared them to the phenotype of the control strain STM SL1344 WT. Carbon-starved and exponential cells were prepared (2.6.3.1), normalised (2.6.3.2) and exposed to 55°C for 16 minutes, or to 100µg/mL PMB for one hour at 37°C. After stress exposure, the samples were serial diluted to 10^{-5} in M9 minimal salts buffer (appendix B). The serial dilutions were spread onto LB agar plates (1.5 w/v) in triplicate, and incubated at 37°C for a minimum of 12 hours before determination of final CFU mL^{-1} (2.6.3.2). Experiments were repeated a minimum of three times to allow for statistical analysis of the samples. To normalise data collected across a lengthy period of time, survival has been calculated and expressed as percentage survival compared to the WT strain.

2.6.3 Sensitivity spot plate assays

Sensitivity spot plate assays were carried out to determine the sensitivity of *Salmonella* deletion mutants to heat and antimicrobial stress. The assays were conducted using overnight cultures (2.3.2) of the investigative strains and the comparative control strain STM SL1344 WT. LB agar plates (1.5% w/v) prepared were supplemented with compounds of interest (indole 2mM, nalidixic acid 1µg/ml, phosphomycin 50ng/ml, spermidine 6mM, polymyxin B 100ng/ml, vancomycin 65µg/ml). Plain LB agar plates (1.5% w/v) were used for the preparation of control plates. For the heat-sensitivity tests, extra thick LB agar plates (1.5% w/v) were poured to prevent dehydration of the growth media. Overnight cultures were normalised to OD$_{600}$ = 1.000 (2.3.2) prior to 10-fold serial dilution series in 1 x PBS to a final dilution of 10^{-7}. The compound containing LB agar plates and the plain control LB agar plates were consecutively spotted with 10 µL of the appropriate dilutions (typically 10^{-2} – 10^{-7}) and dried at room temperature in a laminar flow cabinet. The antimicrobial plates and the control plates were incubated at 37°C for a minimum of 12 hours until single colonies could easily be detected. The plates used to test for heat sensitivity were incubated at 42°C for a

minimum of 18 hours, and at 46°C for a minimum of 36 hours. The CFU mL^{-1} was calculated by multiplying the counted colony numbers with the appropriate dilution rate. To allow for comparison to the STM SL1344 WT control strain, as well as to allow comparison of data collected over a prolonged time period, survival rates were calculated using the CFU mL^{1}. To allow for statistical analysis, all spot plates were conducted in biological triplicate as a minimum.

2.6.4 Antimicrobial disc diffusion assays

Disc diffusion assays were carried out to analyse the sensitivity of *Salmonella* deletion mutants to a range of antimicrobial agents. The assays were conducted using individual top agar plates for investigative strains and for the comparative control strain STM SL1344 WT. Normalised overnight cultures (2.3.2) were used to inoculate 10mL fresh LB broth (10% v/v) and the newly inoculated cultures were incubated at 37°C for one hour, 200 rpm. Fresh, thin 1.5% (w/v) LB agar plates were prepared and set at room temperature, meanwhile fresh top agar was prepared by adding agarose (0.75% w/v) to LB broth. The solution was boiled for 5 minutes to allow the agarose to dissolve. Once cooled to 60°C, the top agar was aliquoted into pre-heated sterile 5mL Bijou tubes in 4mL volumes. The top agar was maintained in liquid form in a water bath at 45°C. Once the one hour incubation period was over, 100µL of the 10% subculture of interest was aliquotted to the molten top agar, and poured immediately over the pre-set, thin LB agar plates. The newly-poured top agar plates were left to set at room temperature for 30 minutes.

To disperse the antimicrobial agents of interest in an equal, concentration dependent manner, Sterile Whatman® antibiotic assay discs (6mm) were used. Once the top-agar had solidified, discs were placed aseptically on the top agar plates and impregnated with 10µL of the compound of interest (see chapter 3.4.4 for the concentrations used). Plates were incubated at 37°C overnight, for a minimum of 12 hours, before diameter of inhibition (mm) was recorded. The zone of inhibition (A in mm^2) was calculated using the following calculation: $A = \pi r^2$ (r being the radius of the zone of inhibition). To allow for statistical analysis, all assays were carried out in biological and technical triplicate as a minimum.

2.6.5 Statistical analysis of sensitivity assays

The statistical analysis of the sensitivity spot plate assays, the disk diffusion assays, and the CSIXR assays was carried out using R Statistical Software and Excel (R Core Team, 2013). One-way ANOVA tests were carried out to test if the means of the WT and deletion mutants were equal under studied circumstances. If the ANOVA test indicated significantly unequal means

(P ≤ 0.05), F-tests were performed on each sample to determine whether their variance was equal or unequal. Subsequently two-sample t-tests were carried out between the wild type and each mutant strain, assuming equal or unequal variance depending on results acquired by the F-tests. In figures statistically significant difference between samples at P ≤ 0.05 and P ≤ 0.01 is indicated using * and ** respectively.

2.7 Protein overexpression and purification

All purified proteins were either tagged with a *myc*-His C-terminal epitope or a S*trepII* C-terminal epitope. The purified proteins were expressed from pBAD overexpression vectors under the control of *L*-arabinose inducible promotors. Overexpression trials were carried out for all described *myc*-His-tagged and *StrepII*-tagged plasmid constructs overexpressed in *E. coli* and *Salmonella* backgrounds, testing arabinose concentrations ranging from 0.2% to 0.00002% (v/v), and over-expression inducing times of 4 hours and 5 hours. Proteins with a *myc*-His tag were isolated using a 1ml capacity HisTrap™ HP column (GE Healthcare Life Sciences) on an ÄKTAprime plus FPLC (GE Healthcare Life Sciences) at room temperature. Proteins with a *StrepII*-tag were isolated using 5ml capacity StrepTrap™ HP column (GE Healthcare Life Sciences) on an ÄKTAFPLC (GE Healthcare Life Sciences) at 4°C.

2.7.1 Protein overexpression trials

Prior to large scale purification, ZraP overexpression was tested in small-scale expression assays both to confirm successful overexpression and to ascertain optimal overexpression conditions regarding time, temperature and L-arabinose concentration. Ampicillin (100µg/ml) containing overnight cultures of zraP-overexpressing *E. coli* and *Salmonella* were used to inoculate 10mL ampicillin (100µg/ml) supplemented LB broth (1% (v/v)). Cultures were incubated at either 30°C or 37°C, 200rpm for three hours prior to induction of overexpression. To induce overexpression, L-arabinose was added to the cultures to create final concentrations of 0.2%, 0.02%, 002%, 0.0002% and 0.00002%. A negative control was prepared by not adding any L-arabinose during the induction stage. The cultures were subsequently incubated for a further four or five hours. Cells were harvested by centrifugation at 17000 x g (13500 rpm) for 2 minutes and the pellets were snap frozen and stored at -20°C to promote cell lysis.

To confirm protein overexpression, the protein profile of the cell pellets was analysed using SDS-PAGE (2.4.2.1). The pellets were defrosted on ice and resuspended in 90µl SDS loading buffer (appendix B) containing β-mercapthoethanol (5% (v/v)). The samples were boiled at 100°C for 10 minutes and the cell debris was separated from the supernatant by

centrifugation at 17000 x g (13500 rpm) for 2 minutes. For analysis of the soluble protein profile, samples were loaded onto SDS-PAGE gels (15% acrylamide (v/v)), using PageRuler™ Prestained Protein Ladder (Thermo Scientific) as marker. Using Mini-PROTEAN® Tetra Cell systems (BIO-RAD), samples were electrophoresed in 1x TGS running buffer (appendix B) at 200 V until the PageRuler™ marker dye had run of the gel (approximately one hour). Gels were washed trice in dH$_2$O (approximately 10 minutes per wash) and subsequently stained using InstantBlue™ Ultrafast Protein Stain (Sigma) overnight at room temperature with gentle agitation. Protein gels were washed in dH$_2$O prior to imaging using a Molecular Imager® Gel Doc™ System (BIO-RAD) at white light settings.

2.7.2 PAGE analysis

PAGE analysis was carried out either to analyse the presence or quality of all proteins loaded onto the gel, or to confirm the presence of a *myc*-His or *StrepII* tag. The former analysis was carried out by a staining technique using protein-binding Coomassie Brilliant Blue dye. The latter analysis was carried out by Western blotting.

2.7.2.1 PAGE straining using Coomassie Brilliant Blue

Following electrophoresis the gels were washed trice in dH$_2$O (approx. 10 minutes) prior to staining using InstantBlue™ Ultrafast Protein Stain (Sigma) overnight at room temperature with gentle agitation. After staining the gels were washed in dH$_2$O until excess dye had cleared away and contrast had been improved. Gels were imaged using white light on a Molecular Imager® Gel Doc™ system (BIO-RAD).

2.7.2.2 Analysis of tagged protein using Western blotting

Prior to Western blotting, protein samples of interest were electrophoresed on an SDS-PAGE gel (2.4.2.1). These gels were used for membrane transfer using a Trans-Blot® SD Semi-Dry Transfer Cell (BIO-RAD). Prior to Western blotting, six layers of blotting paper equal in size to the PAGE membrane were soaked in 1 x transfer buffer (appendix B), nitrocellulose membrane equal in size to the PAGE membrane was soaked in 100% methanol for one minute followed by a transfer buffer wash of 5 minutes. Once soaked in buffer, three layers of blotting paper were stacked on the anode plate of the transfer cell. The nitrocellulose membrane was placed on top of the blotting paper, followed by the PAGE gel and topped by three more layers of blotting paper. After attachment of the transfer cell cathode lid, the proteins were transferred from the PAGE gel to the nitrocellulose membrane at a current of 10 V for one hour. To confirm protein transfer, the nitrocellulose gel was washed in 1 x TBS buffer and stained using Ponceau stain (appendix B). After confirmation of transfer, the

membranes were destained in dH$_2$O until clear. The nitrocellulose membrane was subsequently soaked in blocking buffer overnight at 4°C with gentle agitation to prevent unspecific binding of antibodies to the nitrocellulose membrane.

To visualise *myc*-His-tagged proteins Anti-His antibody conjugated to horseradish peroxidase (HRP) (QIAGEN) was diluted 1:20,000 in blocking buffer. To visualise S*trep*II-tagged proteins the monoclonal Strep•Tag® II antibody HRP conjugate (MERCK) was used. The membranes were soaked in 25mL antibody-containing blocking buffer and incubated for one hour at room temperature with gentle agitation. To remove excess, unbound antibodies the membranes were thrice washed in 1 x TBST (appendix B) for 10 minutes with gentle agitation. The proteins were visualised using a chemiluminescent staining protocol. Western blot development Buffers A and B (appendix B) were prepared separately and stored in darkness until used. The visualisation of the Western blots was carried out in a dark development room. With the aid of red light only, the Western blot development Buffers A and B were mixed, and ample amounts of the liquid mixture were poured over the nitrocellulose membranes, so that the top of the membrane was covered in developing liquid. To record the luminescence, photosensitive CL-XPosure™ Films (Thermo Scientific) were exposed to the chemiluminescent membranes for various time intervals between 30 seconds and 10 minutes. The CL-XPosure™ Films were developed using a SRX-101A tabletop processing Xograph (Konica Minolta).

2.7.3 Large scale overexpression and cell harvest

For large-scale protein harvest, overexpressing *Salmonella* and *E. coli* was grown in litre volumes. Both *myc*-His tagged and *StrepII*-tagged ZraP overexpression plasmids have been subjected to large scale overexpression, with varying degrees of success. To maximise protein yield, large scale over-expression assays were conducted using optimal expression conditions determined by overexpression trials (2.7.1). Litre bottles containing LB broth supplemented with ampicillin (100µg/ml) were inoculated (1% (v/v)) using ampicillin supplemented overnight cultures (2.3.2) and incubated at 37°C and 200 rpm for three hours prior to induction of overexpression. ZraP overexpression in *E. coli* (WT and mutants, both *myc*-His and *StrepII* tagged) was induced by addition of arabinose to a final concentration of 0.2% (v/v), and ZraP overexpression in STM SL1344 Δ*zraP* (WT and mutants, both *myc*-His and *StrepII* tagged) was induced by the addition of arabinose to a final concentration of 0.02% (v/v). Cells were incubated for another 5 hours post induction. Prior to cell harvest, 1mL samples were collected and analysed on SDS-PAGE as described in 2.4.2.1 to confirm

protein overexpression. For cell harvest, the remaining cultures were transferred to 95 x 191mm, 1 L volume polycarbonate centrifugation bottles (Beckman Coulter) and centrifuged 3450 x g (6000 rpm) using a JLA-8.1000 rotor (Beckman Coulter) in a Beckman Coulter Avanti® J-20 high performance centrifuge. Cell pellets were transferred to 50ml Falcon™ conical centrifugation tubes, snap frozen and stored at -20°C for a minimum of 12 hours to promote cell lysis.

2.7.4 Collection of cell lysate

To collect the cell lysate containing soluble overexpressed protein, cell pellets collected during large scale cell harvest (2.7.3) were defrosted on ice and resuspended in 20ml 1 x PBS. To aid cell lysis, 50mg lysozyme from chicken egg white (Sigma Aldrich) was added. Furthermore, 40µg DNase I from bovine pancreas (Sigma Aldrich) was added to promote DNA degradation, and one cOmplete mini EDTA-free® protease inhibitor cocktail tablet (Roche) was added to prevent protein degradation. Cells were lysed by two passes through an IEC French® Press Cell Disrupter (Thermo Scientific) with treatment at 1000 psi (6.9MPa). To separate the soluble protein from the cell debris, the cell lysate was centrifuged using a Ti45 rotor (Beckman) in an Optima XL100K ultracentrifuge (Beckman) at 205,000 x g (42,000 rpm) for 2 hours. The supernatant was carefully separated from the pellet and stored on ice.

2.7.5 Purification of tagged proteins from cell lysate

2.7.5.1 Purification of *myc*-His-tagged protein from cell lysate

The *myc*-His-tagged proteins were isolated from the supernatant using interactions with the HisTrap™ HP Column (GE Healthcare Life Sciences) on an ÄKTAFPLC (GE Healthcare) at room temperature. The soluble cell fraction (2.7.4) was applied to the HisTrap™ cartridge after pre-equilibration with HEPES storage buffer (appendix B). The column was washed with HEPES storage buffer prior to one-step protein elution using HEPES elution buffer containing 300mM imidazole. The purity and quality of the protein was analysed by SDS-PAGE (2.4.2.1).

2.7.5.2 Purification of *Strep*II-tagged protein from cell lysate

The *Strep*II-tagged proteins were isolated from the supernatant using interactions with the StrepTrap™ HP column (GE Healthcare Life Sciences) on an ÄKTAFPLC (GE Healthcare) at 4°C. Prior to use, the StrepTrap™ cartridge was recharged using 0.5 M NaOH at a flow rate of 2ml/min for 15 minutes. The column was subsequently equilibrated with StrepII storage buffer (appendix B) at a flowrate of 2mL/min for 30 minutes before the loading of the soluble fraction. Once the soluble fraction was loaded onto the column, a wash step was performed

using StrepII storage buffer at a flow rate of 2mL/min until the fluorescence readings read clear (approximately 1 hour). The protein was eluted by one-step elution using StrepII storage buffer supplemented with 2.5mM desthiobiotin (Sigma). The purity and quality of the protein was analysed by SDS-PAGE (2.4.2.1).

2.7.6 Combining, buffer exchange, and concentrating of eluted protein fractions

Eluted protein fractions (2.7.5) of sufficient purity (2.4.2.1) were combined, concentrated and exchanged into fresh buffer without eluting agent, using Amicon® Ultra-15 Centrifugal Filter units (10.000 NWML). To combine the selected eluted fractions, samples were centrifuged at 3450 x g (4000 rpm) at 5 minute intervals, resuspending the pellet prior to adding more liquid between each spin, until all selected fractions had been reduced to a 4mL final sample. To exchange eluting buffer for fresh buffer, this process was repeated adding fresh buffer between each spin, until the sample was washed with a minimum of 25mL of the final storage buffer. To concentrate the sample, the buffer exchanged, combined protein sample was centrifuged down until a final volume of 500-1000μL remained with a protein concentration ranging between 15mg/ml - 20mg/ml. The quality of the final protein sample was analysed by SDS-PAGE analysis, and the quantity was determined quickly analysed by nanodrop (2.7.7.1) and verified by Bradford assay (2.7.7.2). Considering ZraP is a stable protein, samples used soon after purification were stored at 4°C to prevent freeze-thawing induced protein damage. Protein samples stored over a longer period of time were snap-frozen and stored at -80°C.

2.7.7 Determination of protein concentration

Protein concentrations were analysed using two methods. Firstly, proteins were subjected to analysis by nanodrop to obtain a quick, but inaccurate protein concentration. Once the protein was deemed sufficiently concentrated, the exact protein concentration was determined using the Bradford assay.

2.7.7.1 Estimation of protein concentration by nanodrop

To obtain a rough estimation of protein concentration, protein samples were analysed using a NanoDrop 2000c UV-Vis spectrophotometer (Thermo Scientific) according to manufacturer's instructions. The machine was blanked using the fresh storage buffer matching the buffer of the sample to be analysed. The absorbance of 1μL of protein solution was measured at $\lambda = 280$nm, and the estimated protein solution was recorded.

2.7.7.2 Determination of protein concentration using the Bradford assay

The Bradford assay was used to obtain an accurate estimation of protein concentrations. This colourimetric assay uses the colour shift of Coomassie Brilliant Blue G-250 from a brown liquid to a blue liquid upon protein binding to accurately measure protein concentration. Samples for the Bradford assay were set up as described in table 2.8. Absorbance was measured at $\lambda = 595$nm. A standard curve was created by measuring the A_{595} of bovine serum albumin (BSA) standards and plotting this against their concentration, and the function of the plot was determined with a line-of-best-fit (equation 2.1).

$$\text{Equation 2.1} \quad y = ax + b$$

Equation 2.1 demonstrates the function of the Bradford plot, in which **y** represents the A_{595} reading, **x** represents the protein concentration, **a** determines the slope of the plot, and **b** describes the intercept with the y-axis.

The protein concentration of the purified samples was deduced from their absorbance readings using the function of the plot. To prevent equipment derived inaccuracies, samples with absorbance readings exceeding 1.0 were diluted and reanalysed. The final protein concentration of diluted samples was corrected by multiplication with the dilution factor.

Table 2.8 Composition of Bradford assay reaction. Standard curve produced from BSA samples with known concentration, used for the testing of unknown samples.

Sample	Protein sample (µg/µL)	dH$_2$O	Bradford reagent (mL)
	BSA standards		
Blank	0	0.800	0.2
1	1	0.799	0.2
2	2	0.798	0.2
3	5	0.795	0.2
4	10	0.790	0.2
5	15	0.785	0.2
6	20	0.780	0.2
	Unknown samples		
*n	2	0.798	0.2

*As many samples tested as required. Samples with high concentrations were diluted prior to the Bradford assay for better accuracy.

2.8 Functional analysis of purified protein

Functional protein analysis studying chaperone function consisted of malate dehydrogenase assays and DNA gyrase assays. Pull-down assays were carried out to identify biologically relevant substrates.

2.8.1 MDH assays

Malate dehydrogenase activity assays were carried out to assess the chaperone activity of ZraP. Whereas previous studies have demonstrated the ability of ZraP to prevent protein aggregation in response to heat stress, this study aims to analyse if ZraP is also capable of protecting and/or restoring protein function (Appia-Ayme *et al.*, 2012; Petit-Hartlein *et al.*, 2015; Wells, 2015). Malate dehydrogenase (MDH) is an enzyme that utilises $NADH^+$/NAD to reversibly catalyse the conversion between malate and oxaloacetate. Prior to experiments comparing the activity of the ZraP mutants to the ZraP-WT activity, trial assays were carried out for buffer determination, determination of zinc concentration and incubation time (2.8.1.1). During the experiments conducted in this study, MDH activity was measured by recording the shift in absorbance, resulting from the MDH induced oxidation of $NADH^+$ to NAD. Chaperone activity was assessed by exposing MDH to the denaturing agent guanidine hydrochloride (GnHCl) in the presence and absence of ZraP, prior to measuring MDH activity. All MDH assays were conducted using a Hitachi U-3310 UV-visible spectrophotometer at λ = 340nm (A_{340}) (2.8.1.2). Due to the sensitive nature of the assay, graphs comparing data collected at different dates are presented as percentage activity compared to an MDH control, as opposed to relative MDH activity.

2.8.1.1 Optimisation of malate dehydrogenase assays

Malate dehydrogenase assays were conducted by incubating MDH (70µM) for 40 minutes at room temperature in specified conditions, prior to assessing its activity. In this study, the incubation conditions differed in buffer used, presence or absence of ZraP WT and mutant proteins at a concentration of 70µM, zinc chloride concentrations, and the absence or presence of the denaturing agent guanidine hydrochloride (GnHCl) at various concentrations see table 2.9. During Standard MDH trials A_{340} measurements were taken every 0.5 seconds over a period of 3 minutes ($t_0 - t_{180}$). The timed measurement was started once the machine was blanked, using a cuvette (brand and size) filled with 2mL buffer. At t_{10}, 4µL of the cofactor $NADH^+$ (0.1M) was added to the cuvette, resulting in increased absorbance. At t_{25}, 40µL of the incubated protein sample was added to the cuvette. At t_{40}, 10µL of the substrate oxaloacetate (200mM) was added, resulting in an immediate reaction and drop in

absorbance. The relative MDH activity was determined by measuring the slope of the first 5 seconds following substrate addition. All samples were repeated as technical and biological replicates.

MDH assays were optimised for the buffer used for incubation and assay conduction. The buffers tested included 50mM HEPES buffer pH 7.5, PBS, and StrepII storage buffer with and without EDTA (also referred to as Tris buffer) (appendix B). Further MDH optimisation included the testing $ZnCl_2$ concentrations ranging from 2mM to 100µM, as well as varied EDTA exposure times (ranging between 10 seconds and 3 minutes). Finally, the GnHCl concentrations were tested ranging from 0.2 M to 1.6 M).

Table 2.9 Schematic overview of the preparation of MDH assay protein samples.

Sample	MDH (70µM) (µL)	ZraP (70µM) (µL)	°Zinc chloride (µL)	GnHCl (6 M) (µL)	ᵝbuffer (µL)
MDH only	1.3	-	-	-	Σ 130
MDH + GnCHl	1.3	-	-	*n x 2.167	Σ 130
MDH + ZraP	1.3	1.3	-	-	Σ 130
MDH + ZraP + GnHCl	1.3	1.3	-	*n x 2.167	Σ 130
MDH + Zinc	1.3	-	13	-	Σ 130
MDH + zinc + GnHCl	1.3	-	13	*n x 2.167	Σ 130
MDH + Zinc + ZraP	1.3	1.3	13	-	Σ 130
MDH + Zinc + ZraP + GnHCl	1.3	1.3	13	*n x 2.167	Σ 130

°Stock concentration of zinc chloride differered depending on the assay conducted. *Guanidine hydrochloride was testeda ta range of concentrations. Added in volumes equated to 2.167µL per 0.1 M in final solution. ᵝMDH activity has been tested in various buffers.

2.8.1.2 Testing chaperone activity using malate dehydrogenase assays

To test ZraP-WT and ZraP-mutant chaperone activity standard MDH assays were conducted as described in chapter 2.8.1.1. To avoid potential interference of the *myc*-His-tag with zinc trials, all ZraP protein samples used in this assay were *Strep*II-tagged. As determined by the optimisation trials, the chaperone activity assessing MDH assays were carried out in Tris buffer. ZraP was added to the incubation sample at a 1:1 ratio to MDH (70µM). Samples containing zinc were supplemented with 100µM $ZnCl_2$, as opposed to higher concentrations, to minimise zinc-induced inhibition of MDH. Samples testing for MDH activity following denaturation were supplemented with GnHCl concentrations ranging between 0.2 M and 0.6 M. The incubation conditions are summarised in table 2.9.

2.8.2 DNA gyrase supercoiling assays

Periplasmic proteins have been suggested as a potential tool to be used in the protection of vulnerable enzymes used in the biotechnological and biomedical industry. The use of ATP-independent chaperones could potentially increase shelf-life, or remove the need to store

enzymes at sub-zero temperatures, thereby reducing freeze-thaw induced damage to enzymes. In collaboration with Inspiralis Ltd., the ability of ZraP to protect the activity of commercially available enzymes during non-optimal storage conditions was investigated. Using protein supplied by Inspiralis Ltd., DNA gyrase activities were conducted comparing the activity of DNA gyrase stored at -80°C *versus* DNA gyrase stored at -20°C in the presence and absence of zinc and ZraP-WT, and the DNA gyrase activity was visualised using DNA gel electrophoresis (2.4.1).

DNA gyrase is a type II topoisomerase that catalyses the ATP-dependent negative supercoiling for double stranded, closed-circular DNA. Purified DNA gyrase is relatively unstable and quickly loses activity when stored under suboptimal conditions. The chaperoning activity of S*trep*II-tagged ZraP-WT was analysed by storing DNA gyrase together with ZraP at various temperatures, by comparing DNA gyrase super-coiling activity of samples stored in different conditions. Samples containing DNA gyrase and ZraP (ratio of 1:1), both in the presence and in the absence of excess zinc chloride (100µM) were stored overnight -80°C and -20°C. Assays were carried out using DNA gyrase assay buffer (appendix B) (Inspiralis) and DNA gyrase dilution buffer (appendix B) (Inspiralis). The substrate used was the plasmid pBR322 (1µg/µL). Samples were set-up as described in table 2.10. Firstly the sample mix was prepared, containing assay buffer, relaxed pBR322 and water. The mix was aliquoted into separate tubes, and subsequently the solvent and test compound were added to the aliquots. Once dilution buffer had been added to the control tubes, the incubated sample was added to the remaining dilution buffer, the mixture was then serial diluted and added to the remaining tubes as indicated in table 2.10. The samples were mixed and incubated in a water bath at 37°C for 30 minutes. Following incubation the reaction was terminated by the addition of 30µL STEB (appendix B) and 30µL chloroform/isoamyl alcohol (24:1 (v/v)). To analyse the super-coiling of pBR322, the sample was centrifuged at 17000 x g (13500 rpm) for one minute, before 20µL of the aqueous phase was loaded onto an ethidium-bromide free agarose gel (1% (w/v)) made using TAE buffer (appendix B). The samples were electrophoresed at 85 V for 2 hours and stained in a 1µg/mL ethidium bromide solution (dH$_2$O). After destaining in dH$_2$O the gel was visualised by UV-light, using a Molecular Imager® Gel Doc™ System (BIO-RAD).

Table 2.10 Preparation of DNA gyrase supercoiling assays.

Sample	MIX (μL)	serial diluted enzyme (μL)	Final enzyme dilution
1	27	0	0
2	27	3	1/600
3	27	3	1/300
4	27	3	1/200
5	27	3	1/150
6	27	3	1/120
7	27	3	1/100
8	27	3	1/60
9	27	3	1/30
10	27	3	1/20
11	27	3	1/15
12	27	3	1/12
13	27	3	1/10
14	27	3	1/6

2.8.3 Pull-down assays

To identify potential natural substrates of ZraP, a ProFound™ Pull-Down PolyHis Protein:Protein Interaction kit (Thermo Scientific) was used for pull-down assays carried out on *myc*-His tagged ZraP-WT as per manufacturer's instruction. The bait protein used was pure *myc*-His-tagged ZraP-WT, and whole-cell lysate of stressed *Salmonella* was used to isolate potential prey protein. Following reports of upregulated ZraPSR activity in response to heat and sodium tungstate (Appia-Ayme *et al.*, 2011; Wells, 2015), stressed *Salmonella* whole-cell lysate was obtained either by subjecting STM SL1344 WT to 55°C for 15 minutes, or by subjecting STM SL1344 Δ*baeR* to 20mM Sodium tungstate for 1 hour (37°C, 200 rpm). During the assay, purified bait ZraP was bound to the column resin and then exposed to the lysate of stressed cells in order to bait ZraP- target proteins. After several washes, ZraP and any bound target protein is eluted using imidazole. Eluted fractions were analysed using SDS-PAGE (2.4.2.1).

2.9 Protein structural analysis

To increase current knowledge of the structure of ZraP, X-ray crystallography and small angle X-ray scattering (SAXS) assays were conducted. To investigate potential influences of zinc on the tertiary and quaternary structure of ZraP, analysis was carried out using analytical ultracentrifugation (AUC), inductively coupled plasma mass spectrometry (ICP-MS), and native PAGE.

2.9.1 Analysis of oligomeric state using analytical ultracentrifugation

To investigate potential differences in oligomeric state between ZraP-WT and ZraP-mutants, sedimentation velocity experiments by analytical ultracentrifugation were conducted. *myc*-His-tagged ZraP-WT and ZraP-mutants (70µM) were prepared in StrepII storage buffer and EDTA-free StrepII buffer with additional zinc chloride (70µM), and centrifuged at 8050 x g (10000 rpm), at 20°C using an An50-Ti rotor. Absorbance was monitored at λ = 280nm. Scans were recorded every 5 hours until an equilibrium was achieved. Once the equilibrium was reached, five final scans were recorded of each sample, and using Ultrascan II software (Demelar 2005), a single species model was used to fit the sample scans. To calculate the weight average molecular mass of the samples, the partial specific volume (v) of ZraP had to be estimated. Using the software SEDNTERP (version 1.05), the value (v) was estimated at 0.712mL/g based on the amino acid sequence of ZraP.

$$\text{Equation 2.2} \quad \overline{M}_{W,app} = \frac{dln(c)}{dr^2}\frac{2RT}{\omega^2(1-\bar{v}\rho)}$$

Equation 2 describes the calculation used to determine the apparent weight average molecular mass, where M represents weight average, c is the protein concentration, r describes the radius, ω represents the angular velocity (in radians/sec), v is the partial specific volume and ρ describes solvent density. To determine the standard deviation, individual scans were fitted separately.

2.9.2 Analysis of bound metal by inductively coupled plasma mass spectrometry

Following reports of ZraP interacting with zinc (Appia-Ayme *et al.*, 2012) and binding copper (Petit-Hartlein *et al.*, 2015), inductively coupled plasma mass spectrometry (ICP-MS) was carried out to investigate the metals bound to ZraP following protein purification. To ensure only tightly bound metals were analysed, protein samples were purified in the presence of 1mM EDTA, a chelating agent. Furthermore, to prevent metal contamination from glass ware and dH$_2$O, all reagents were prepared using Sigma water, and all glassware used in the

preparation of the samples was acid washed with 50% nitric acid and rinsed with Sigma water prior to use.

Samples prepared for analysis include *myc*-His-tagged ZraP-WT and ZraP-SDM, purified from both STM SL1344 Δ*zraP* and *E. coli* BL21 DE3, and were submitted at a concentration of 600μM in StrepII storage buffer (appendix B). Samples to be analysed by ICP-MS were submitted to the analytical chemistry department of the University of East Anglia, where they were tested By Graham Chilvers for the presence of cadmium (λ = 228.802nm), magnesium (λ = 285.213nm), zinc (λ = 213.857nm), cobalt (λ = 228.615nm), copper (λ = 327.395nm), iron (λ = 259.940nm), and manganese (λ = 259.372nm). Due to malfunctioning of the equipment, these experiments have only been carried out twice (from separately prepared samples), and insufficient data has been collected for statistical analysis.

2.9.3 X-ray crystallography

To investigate the crystal structure of ZraP-WT and ZraP-SDM, *StrepII*-tagged ZraP-WT and ZraP-SDM was used at concentrations between 15mg/mL – 30mg/mL (approximately 0.9mM – 1.8mM) (Chapter 2.7). Crystallisation conditions were identified by sparse matrix screening conducting sitting drop assays using the screening matrices described in chapter 2.9.3.1. Following successful crystal screens, an optimisation tray was prepared for the harvest of high quality protein crystals (appendix C) (2.9.3.2). Proteins harvested for X-ray crystallography analysis were coated in optimised mother liquor containing either glycerol or ethylene glycol for cryoprotection and snap-frozen using liquid nitrogen (2.9.3.3). X-ray diffraction data were collected at the Diamond Light Source beamline I24 MX and beamline I04 using a gaseous nitrogen streamline to preserve the crystals (2.9.3.4). The data reduction, refinement and model-building was carried out by Dr. Marcus Edwards.

2.9.3.1 Protein crystallisation trials

Protein crystallisation trials were carried out using the sitting drop vapour diffusion method. Pure protein samples were prepared to a final concentration between 15mg/mL and 20mg/mL. With the aid of an OryxNano robot (Douglas Instruments), sparse matrix screens were set-up in 96-well 2-drop MRC crystallography plates (Molecular Dimensions), using two drops per condition at 1:1 and 2:1 ratios of mother liquor to protein samples. Crystallization trials were carried out using mother liquor from the readily supplied sparse matrix screening kits Classics I (QIAGEN), Classics II (QIAGEN), MB Class (QIAGEN), MB Class II (QIAGEN), JCSG+ suite (QIAGEN), ProComplex Suite (QIAGEN), MemPlus™ (Molecular Dimensions), and PACT *premier*™ HT-96 (Molecular Dimensions). Following dispersion of the protein solutions and

the mother liquor, crystallisation trays were sealed using ClearVue sheets (Molecular dimensions), and incubated at 4°C and 16°C for at least 1 month prior to crystal harvest. Several successful crystallisation conditions were selected after analysis by microscope, and used for the preparation of a mother liquor tray optimised for the production of ZraP protein crystals (appendix C).

2.9.3.2 Optimisation of ZraP crystallisation

Following crystallisation trials, the conditions chosen to optimise the crystallization of zraP included QIAGEN's Classics II suite condition 77 (0.2 M Lithium sulphate , 0.1 M Tris pH 8.5, 25% (w/v) PEG 3350), QIAGEN's MB Class II suite condition 89 (0.1 M Tris pH 8.5 – 1.5 M potassium phosphate), Molecular Dimension's PACT suite condition 6 (0.1 M SPG buffer pH 8 (appendix B), 25% (w/v) PEG 1500), and Molecular Dimension's PACT suite condition 14 (0.1 M MIB buffer pH 4 (appendix B), 25% (w/v) Peg 1500). Optimising QIAGEN's Classics II suite condition 77 included changing the concentration lithium sulphate by increments of 0.1M, covering total concentrations of 0.1 M to 0.4 M, and by changing the percentage PEG 3350 used by increments of 2.5%, covering total concentrations of 20% - 32.5% PEG 3350. Optimising QIAGEN's MB Class II suite condition 89 included changing the buffer pH by 0.5 increments, covering pH ranging from pH 7.5 to pH 9, and by changing the concentration potassium phosphate used by increments of 0.25 M, covering total concentrations of 1 M to 2.25 M. Optimising Molecular Dimension's PACT suite condition 6 included the change of pH by 0.5 increments, screening SPG buffers ranging between pH 7.5 and pH 9, and by changing the percentage PEG 1500 by increments of 2.5%, screening final concentrations ranging from 17.5% to 30% PEG 1500. Optimising Molecular Dimension's PACT suite condition 14 included the change of pH by 0.5 increments, screening MIB buffers ranging between pH 4.5 and pH 6, and by changing the percentage PEG 1500 by increments of 2.5%, screening final concentrations ranging from 17.5% to 30% PEG 1500. The finalised tray as described in appendix C is further referred to in this study as the Optimisation Tray. ZraP protein crystals grown under optimised conditions were prepared in 96-well 2-drop plates using Oryx robotics (Douglas Instruments), sealed using ClearVue sheets (Molecular Dimensions) and incubated at 16°C for a minimum of one month prior to crystal harvest.

2.9.3.3 Harvesting and transport of protein crystals

The use of ClearVue sealing sheets allowed for the analysis of crystal growth without disruption of the wells. Once protein crystals had grown to a suitable size for harvesting, cryogenic solutions were prepared from the mother liquor. The cryoprotectants used in this

study were glycerol and ethylene glycol. The cryogenic solutions were created by incrementally decreasing the concentration of mother liquor by adding increasing levels of cryoprotectant, until liquid nitrogen exposed solutions no longer showed signs of freezing. Depending on the type and volume of PEG used in the mother liquor, the cryogenic solutions used to store harvested crystals contained between 0% and 15% glycerol or ethylene glycol. Using 0.1-0.2mm Mounted LithoLoops (Molecular Dimensions), ZraP crystals were harvested at 16°C, doused in cryogenic solution, and vitrified using liquid nitrogen at 77 K. After harvest, crystals were stored in liquid nitrogen-filled cryogenic Dewars shipped to the Diamond Light Source UK.

2.9.3.4 X-ray crystallography data collection and processing

X-ray diffraction data of the harvested crystals were collected using the I04 macromolecular crystallography beamline at the Diamond Light Source UK, which supplies X-rays at wavelengths ranging between 0.69Å and 2.066Å (corresponding energy: 6.0KeV to 18KeV). The wavelength used to collect native X-ray diffraction data during this study was set at 1.27Å (corresponding energy: 9.76KeV), as this is close to the theoretical absorption peak for anomalous scattering by zinc. During the process of data-collection crystals were preserved at 100 K using a nitrogen cryostream. A full diffraction data-set was collected for a *StrepII*-tagged ZraP-WT crystal grown in mother liquor containing 0.1 M magnesium chloride, 0.1 M sodium chloride, 10% PEG 1500 and 5% ethanol. This data-set consisted of 241 images, taken at 100% transmission with an oscillation of $\omega = 1.5°$ and an exposure time of 0.2 seconds to a beam sized 32μm by 20μm.

The datasets obtained were processed using the CCP4 suite of software for macromolecular X-ray crystallography (CCP4, 1994). MOSFILM was used for the integration and indexing of the datasets (Battye *et al.*, 2011), followed by data scaling and merging using AIMLESS (Evans and Murshudov, 2013). Phasing of the data was performed by molecular replacement using PHASER (McCoy *et al.*, 2007). For the molecular replacement, ten ZraP monomers were isolated form the 3LAY PDB (ZraP). Refinement was of the data was carried out using REFMAC (Murshudov *et al.*, 2011), and the model maps were finalised using COOT (Emsley and Cowtan, 2004).

2.9.4 SAXS

Small angle X-ray scattering (SAXS) experiments were carried out to analyse the oligomeric state of ZraP in solution, to analyse the effect of presence and absence of zinc on ZraP structure, and improve our understanding of the ZraP protein structure by investigating the

disordered terminal regions that remain unsolved following X-ray crystallography experiments. Furthermore, SAXS analysis was carried out to investigate the role of increased zinc concentrations on the oligomeric state WT zraP and the ZraP-SDM mutant.

Samples were analysed using the EMBL Arinax sample handling robot of the Diamond Light Source bioSAXS beamline B21 (2.9.4.2). The sample handling robot was used to analyse the structure and oligomeric state of *Strep*-tagged ZraP-WT and ZraP-SDM samples at various concentrations (1, 5, and 10μg/mL) in the presence of either EDTA or at zinc chloride concentrations ranging between 100ng/mL - 10μg/mL (2.9.4.3). Data analysis and model building was carried out using the ATSAS 2.6.1 suite, the ATSAS online servers and PyMol (2.9.4.4).

2.9.4.1 Analysis of polydispersity by gel-filtration analysis

For effective SAXS analysis, tested samples should be monodispersed in solution. Furthermore, the gel filtration column was used to exchange proteins into the correct buffers to be used during SAXS analysis. To rule out polydispersity, protein samples were subjected to gel-filtration using a Superdex 75 10/300 GL column (GE Healthcare Life Sciences). The column was pre-equilibrated using EDTA-free StrepII storage buffer (appendix B), supplemented with additional zinc where required. The protein concentrate was applied at a flow-rate of 0.5mL/min and fractions were analysed on SDS-PAGE gels.

2.9.4.2 Setting up SAXS manual robot samples

SAXS analysis was carried out using the B21 solution state SAXS beamline at Diamond Light Source UK. SAXS data collection was carried out in batch mode. Prior to SAXS data collection, protein samples, dissolved in EDTA-free StrepII buffer supplemented with 100nM, 500nM, 1μM, 10μM or 100μM $ZnCl_2$, were prepared into monodisperse solutions with a protein concentrations of 1mg/mL, 5mg/mL, and 10mg/mL. Aliquots of 30μL were dispersed into PCR tubes and inserted in the manual BioSAXS™ beamline robot (EMBL Arinax). Buffer samples were aliquoted into micro centrifuge tubes and transferred to the manual beamline robot. During data collection, samples were automatically loaded into the BioSAXS™ quartz cell capillary.

2.9.4.3 SAXS data collection

The Diamond Light Source B21 beamline is dedicated to solution state SAXS experiments which utilises bending magnets to generate 10^{11} photons directly to the sample. To minimise radiation damage whilst enhancing particle signals, the photons are distributed over the cross section of the beamline capillary (1mm by 5mm). The detector measures scattering

vectors (q) ranging between 0.0022 Å^{-1} to 0.42 Å^{-1}. The camera length configuration at B21 is fixed at 4.014 m, and the generated energy is fixed at 12.4KeV (corresponding wavelength: 1.0 Å). Data collection was carried out at 10°C, in medium viscosity. Exposure time was set at 10 seconds per frame and 18 frames per sample. Prior to sample analysis, the capillary was flushed with the appropriate buffer and background buffer sample readings were taken and recorded.

2.9.4.4 SAXS data analysis

Analysis of the collected SAXS data was carried out using the ATSAS 2.6.1 software suite. PRIMUS was used for buffer subtraction and for averaging of the collected frames. Guinier plots were carried out using PRIMUS QT. These plots allowed for the analysis of data quality, including investigation into potential radiation damage, aggregation and protein-protein interactions. Furthermore, the Guinier plots (log(I) *versus* s^2) were used to make an initial estimation of the radius of gyration (R_g) and the extrapolated intensity at zero scattering angle I_0 (forward scattering). Porod plots (I*s^4 *versus* s) were used to estimate the Porod volume of the particles. The Porod volumes allow for rough estimations of molecular weight, by dividing the obtained Porod volume by 1.7. Kratky plots (I*s^2 *versus* s) were used to investigate the overall folding of the protein samples. Different samples were plotted and scaled on the Kratky plot, to gain insight in the difference in folding between the various samples. The program GNOM was used to carry out indirect Fourier transforms on the data collected, to produce a real-space electron pair-distance distribution plot P_r. *Ab initio* model building was carried out using the DAMMIF program available in the ATSAS online suite. Samples were analysed in "slow" mode, with imposed symmetry constrains of P1 (no symmetry), P5 (pentamer), and P52 (decamer). Each sample was run 20 times, and Clustering and Resolution Assessment Algorithms were carried out to automatically analyse and average the results of these 20 runs. The obtained DAMAVER file, containing the averaged data of the discrete models, was used to run the DAMMIN program to further refine and filter the models obtained. Simultaneously, samples were analysed using the *ab initio* protein reconstruction software GASBOR, which creates models using chain-like assemblies of dummy residues. GASBOR samples were subjected to the reciprocal space fit (fitting I_s) with P5 and P52 symmetry constrains. The number of dummy residues in the asymmetric part was set at 160, to accommodate for the *strep*II-tag.

2.9.5 Native PAGE

Native page was used to analyse the oligomeric state of *StrepII*-tagged ZraP in purified samples. Native polyacrylamide gels (6% acrylamide (w/v)) and native samples were prepared as described in chapter 2.4.2.2. *Strep*II-tagged protein samples were diluted to a final concentration of 1mg/mL and chemically fixed prior to analysis on native PAGE. Gels were stained using Coomassie Brilliant Blue as described in chapter 2.7.2.1.

Chapter 3.
Investigation into the contribution of periplasmic
proteins to the protection against environmental stresses

3.1 Introduction

The understanding of the molecular mechanisms of periplasmic chaperones poses a great challenge to scientists. Prior to being inserted into the outer membrane, OMPs, lipoproteins and other OM-associated proteins synthesised in the cytoplasm have to be transported across the inner membrane and the periplasm. Chaperone-assisted transport and folding in the cytoplasm is usually an ATP-driven process, but the periplasm lacks energy sources such as ATP. Therefore, an alternate source of chemical energy or auxiliary factors are required to drive the transport, chaperoning and folding of nascent proteins in the periplasm. To date, little is known about the nature of these auxiliary factors or the mechanical principles that underlie the functioning of periplasmic chaperones. In addition, the exact function of periplasmic chaperones is not always clear. Despite their conserved nature across Gram-negative bacterial species, many chaperone-deletion mutants lack clear phenotypes due to the overlapping nature of the pathways involved. This chapter will discuss a selection of periplasmic proteins and corresponding response pathways found in *Salmonella.* The current knowledge regarding the periplasmic chaperoning, transport, folding and degradation of outer membrane associated proteins stems primarily from *E. coli* research, and the pathways described in the introduction will refer to this organism unless stated otherwise.

3.1.1 The transporting three

Outer membrane associated proteins are initially synthesised in the cytoplasm prior to their transport and insertion into the outer membrane. After synthesis, nascent OMPs are transported across the inner membrane via either the Sec or Tat secretion systems. Upon emerging from the inner membrane translocases, the nascent OMPs require the aid of the periplasmic chaperones SurA, Skp and FkpA to be safely transported to the BAM machinery and to correctly fold into their mature structure. In *E. coli* emerging OMPs primarily interact with SurA for their transport across the periplasm, and observed interactions between SurA and BamA suggest that SurA is primarily responsible for the delivery of the nascent protein to the BAM insertion complex (Sklar *et al.*, 2007). Although *surA* is not an essential gene, the OM of *E. coli* Δ*surA* mutant strains displays significantly reduced levels of OmpA, OmpF and LamB, rendering it more susceptible to environmental stresses (Lazar and Kolter, 1996). Functional overlap between SurA, Skp and FkpA, means that any single deletion results in stress-susceptible but viable cells (Ge, Lyu, *et al.*, 2014). However, once the chaperones are deleted in tandem, viability is not always guaranteed. *E. coli* strains with a double Δ*surA* Δ*skp* deletion are not viable at 37°C, but are viable at 44°C, and strains with a double Δ*surA* Δ*fkpA*

deletion are viable at 37°C but not viable at 44°C. This demonstrates that FkpA is capable of rescuing ΔsurA Δskp cells during heat-shock only, whereas Skp is capable of rescuing ΔsurA ΔfkpA cells at 37°C but not during heat-stress (Ge, Lyu, *et al.*, 2014). For the correct assembly of some OMPs the chaperones work together to ensure correct insertion of the substrate into the OM. An example of this multi-chaperone coordinated effort is the insertion of LptD. In *E. coli* defects in LptD assembly arise both in ΔsurA and Δskp ΔfkpA double mutants. Overexpression of either Skp or FkpA does not restore LptD levels in a ΔsurA mutant, nor does overexpression of SurA restore LptD levels in a Δskp ΔfkpA double mutant. This suggests that SurA acts in concert with Skp when transporting LptD across the periplasm (Schwalm *et al.*, 2013).

3.1.1.1 SurA

SurA was initially identified as a protein required for stationary phase survival (sur) in *Escherichia coli* in the absence of RpoS (Tormo, Almiron and Kolter, 1990; Lazar *et al.*, 1998). Subsequent studies presented SurA as a peptidyl-prolyl isomerase (PPIase) that facilitates the conversion between *cis-* and *trans-* isomers in peptide bonds containing a proline, and so facilitates the folding and assembly of major β-barrel OMPs (Missiakas, Betton and Raina, 1996; Rouviere and Gross, 1996; Lazar *et al.*, 1998). Behrens *et al* later demonstrated that

although SurA exhibits some PPIase activity, it primarily functions as a periplasmic chaperone (Behrens *et al.*, 2001).

SurA plays a role in the virulence of several Gram-negative pathogens. Although the details of the involvement are not clearly understood, *surA* mutant *S.* Typhimurium strains are defective in their ability to bind and invade eukaryotic host cells, and they display a reduced oral virulence in mice (Sydenham *et al.*, 2000). *Shigella flexneri* strains defective in *surA* can no longer spread from host-cell to host-cell (Purdy, Fisher and Payne, 2007). The reduction in

Figure 3.1 SurA dimer interacting with peptide substrate. Ribbon schematic of SurA dimer (reds) forming complex with a peptide substrate (blue). Image prepared using 2pv2.pdb in PyMol.

virulence of *surA* mutant strains in UPEC has been attributed to a series of defects, including but not restricted to the decreased biogenesis of type 1-fimbriae and the decreased ability to take up iron (Justice *et al.*, 2005, 2006; Vertommen *et al.*, 2009).

The amino acid sequence of SurA dictates an N-terminal region followed by two parvulin-like domains (PPIase I and II), of which only domain II exhibits significant PPIase activity, and a C-terminal tail. Removal of the parvulin-like domains does not result in significant loss of SurA activity, suggesting SurA acts primarily as a chaperone (Rouviere and Gross, 1996; Behrens *et al.*, 2001). The SurA crystal structure forms an asymmetrical dumbbell shape, with a core module consisting of the N-terminal region, C-terminal region and PPIase I, displaying an extended crevice that functions as a peptide-binding site. The PPIase II domain is a satellite fragment tethered at approximately 30 Å from the core module. Interestingly, it was noted that the SurA homologue of *Haemophilus influenzae* and *Pasteurella multocida* have only one PPIase domain, which more closely resembles the extended PPIase II domain of *E. coli* (Bitto and McKay, 2002). Further crystallographic analysis has shown that SurA can bind to peptides in different conformations by changing its tertiary and quaternary structure. It has a preference for binding aromatic residues and the PPIase I domain located in the core is adapted to fit the side-chains of these aromatic residues. SurA can bind peptides of both extended and helical formations, with binding of helical substrates inducing SurA dimerization as visualised in figure 3.1 (Xu *et al.*, 2007). The relationship between the chaperone core and the PPIase II domain remains unclear. Current knowledge suggests that SurA exhibits two separate functions which may or may not be adapted to polypeptide substrates to improve fitness under certain conditions, but further studies are required to clarify the role of the second parvulin-domain and its catalytic folding abilities (Behrens-Kneip, 2010).

3.1.1.2 Skp

The seventeen kilo Dalton protein Skp (also referred to as OmpH and HlpA in the literature) is a periplasmic chaperone that interacts with unfolded β-barrel OMPs in the periplasm after they have been translocated by the Sec translocase pathway, and helps them release from the inner membrane (Schafer, Beck and Muller, 1999). The binding of Skp prevents aggregation of the nascent β-barrel OMPs during their transport across the periplasm. Upon interaction with LPS, Skp undergoes a conformational change, which is thought to be required for the delivery of the substrate to the outer membrane (Bulieris *et al.*, 2003). Although in *E. coli* SurA is considered the primary chaperone involved in the periplasmic transport of nascent OMPs, *skp* deletion mutants demonstrate diminished levels of OmpA and several OM porins, suggesting that Skp is involved in the transport of these proteins (Chen and Henning, 1996). Interestingly, the outer membrane of *Neisseria meningitidis* is not majorly affected by the deletion of *surA*, but shows a significant reduction in major OMPs

and porins in the absence of *skp*, suggesting that in this organism Skp, rather than surA, is the primary transporting chaperone (Volokhina *et al.*, 2011).

Skp forms a homotrimer that bears similarity to the hexameric Prefoldin found in archaea and eukarya in both structure and function (Vainberg *et al.*, 1998; Walton and Sousa, 2004). The quaternary structure is jellyfish-like in shape, with a triangular body and tentacle-like protrusions sticking out at one side (figure 3.2). The body is a 12-stranded β-barrel formed of four β-strands from the C-terminal of each monomer, providing strength and stability. The core of the basket-like shaped body is hydrophobic, allowing for binding and protection of the hydrophobic OMP substrates. Each monomer provides one 65 Å long α-helical "tentacle" that protrudes from

Figure 3.2 Predicted interaction of Skp homotrimer with spherical substrates. The jellyfish-like Skp is a flexible protein that folds around its substrate upon interaction. Image adapted from (Burmann, Wang and Hiller, 2013)

the core. The tentacles are rich in positively charged residues and very flexible, and together with the body they define a central cavity for substrates to bind. Putative LPS binding sites have been identified on the external surface of the Skp tentacles (Walton and Sousa, 2004). Interestingly, in the 1970's Skp was initially purified from *Salmonella* Minnesota as an LPS-binding protein (Geyer *et al.*, 1979). It is thought that the conformational change of Skp, induced by LPS, aids docking and delivery of the substrates to the outer membrane (De Cock *et al.*, 1999). It should be noted that Skp is smaller than some of its targeted substrates. Current models based on the OmpA substrate suggest that the β-barrel domain of nascent OMPS binds the hydrophobic core of Skp, whereas the soluble parts of the nascent OMP stick out, allowing for the substrate's periplasmic domain to be folded into its native state, whilst the membrane domain remains protected by Skp (Walton *et al.*, 2009).

3.1.1.3 FkpA

FkpA is a heat-shock PPIase that belongs to the FK506-binding protein family. It was initially discovered as an RpoE regulated PPIase that was upregulated in response to moderate heat stress (Dartigalongue, Missiakas and Raina, 2001). However, aggregation assays have

demonstrated that FkpA can prevent substrate aggregation in a stoichiometric matter as opposed to a catalytic manner, suggesting that similarly to SurA, FkpA is a bifunctional protein that exhibits both chaperone and PPIase activity (Arie, Sassoon and Betton, 2001).

FkpA is formed of a homodimer, with each monomer consisting of two domains, the N-terminal domain thought to be involved in chaperone activity, and the C-terminal domain responsible for the PPIase activity (figure 3.3). The N-terminal domain of the FkpA monomer consists of three helices that interlace with the three corresponding helices from a second subunit, forming a symmetric dimer. The C-terminal domains extend outwards from the dual N-terminal core in opposing directions,

Figure 3.3 The FkpA dimer adopts different conformations. Crystallographic analysis of FkpA indicates that the protein can adopt different conformations, which is thought to aid in protein folding. Image taken from Saul, *et al*. (2004).

and with the FK506-binding sites facing inwards. Little is known about either the chaperone or the PPIase activities of FkpA, but published crystal structures show there is some flexibility in the relative position and orientation of the C-termini. The flexibility in the C-termini would allow for two independent folding mechanisms in the bifunctional protein (Saul *et al.*, 2004).

3.1.2 The emergency response team

Bacteria need to be able to sense and adapt to their environments in order to thrive and survive. In Gram-negative bacteria, environmental stresses are primarily encountered by the outer membrane, and any stress signals have to pass the periplasm before they can be sensed by inner membrane-bound response regulators. The denaturation, misfolding and accumulation of proteins in the periplasm is a cellular indication of envelope stress. Periplasmic stress response chaperones of the CpxP-family respond to the accumulation of mis- and unfolded proteins in the periplasm and allow for the activation of associated two component stress response systems.

3.1.2.1 CpxP

The periplasmic chaperone CpxP was first identified during a screen looking for products upregulated by the Cpx envelope stress response (Danese and Silhavy, 1998). The protein has a dual function as it acts both as a repressor of the Cpx stress response and as a chaperone that facilitates the proteolysis of misfolded proteins found in the periplasm. The Silhavy group demonstrated that CpxP binds misfolded PapE and PapG pili subunits that accumulate in the periplasm of uropathogenic *E. coli* during infection. Whereas cytoplasmic chaperones are usually recycled after substrate delivery, CpxP is degraded by HtrA together with the bound substrates. It has been suggested that the degradation of periplasmic chaperones is a result of the lack of energy sources required for recycling (Isaac *et al.*, 2005; Zhou *et al.*, 2011). The Cpx-pathway can be activated in different ways, depending on the inducing stresses. HtrA-mediated degradation of CpxP is one proposed mechanism for the release of CpxP induced inhibition of this pathway. The partial inactivation of the Cpx response in an *E. coli* Δ*htrA* mutant suggests that the proteolysis of CpxP by HtrA plays an important role in regulating the Cpx response (Buelow and Raivio, 2005).

CpxP belongs to the CpxP-family of molecular chaperones, which also includes Spy and ZraP (Appia-Ayme *et al.*, 2012). Although the sequence identity of these proteins is low, 29% identity between CpxP and Spy, and 12% identity between CpxP and ZraP, all three proteins share at least one LTxxQ motif of unknown function, and all three proteins form α-helical hairpin structures (figure 4.1) (Raivio, Popkin and Silhavy, 1999; Appia-Ayme *et al.*, 2012). The CpxP crystal structure (figure 4.2) displays an antiparallel homodimer of intertwined α-helices, which forms a basket-like shape with a highly basic concave surface and an acidic convex surface. The *E. coli cpxP* encodes two LTxxQ motifs, which can be found at one end of the diverging turns of the long, hooked hairpin folds that form the monomer (Thede *et al.*, 2011). In the absence of a stress signal, CpxP interacts with the sensor domain of CpxA and renders the Cpx signalling system inactive. This bond is broken by envelope stresses such as increased salinity or the build-up of misfolded pilus subunits in the periplasm (Raivio *et al.*, 2000; Zhou *et al.*, 2011; Tschauner *et al.*, 2014). The saline-induced dissociation of CpxP from CpxA is not a gradual process, but rather an instant release once a threshold concentration has been reached, suggesting that the interaction between these two proteins is electrostatic in nature (Tschauner *et al.*, 2014).

3.1.2.2 Spy

The periplasmic chaperone Spy was first identified as an abundantly produced protein in spheroplasts, and was named spheroplast protein Y accordingly (Hagenmaier, Stierhof and Henning, 1997). Although it is barely detectable under favourable growth conditions, when *E. coli* is challenged by stimuli that activate the BaeSR, CpxAR or Rsc phosphorelay systems, expression of *spy* can increase up to 700-fold, raising Spy levels to up to 48% of the total periplasmic content (Raffa and Raivio, 2002; Bury-Mone *et al.*, 2009; Quan *et al.*, 2011). The upregulation of σ^E-regulated genes in Δspy mutants is another indication that Spy plays a role in the envelope stress response of *E. coli* (Raivio *et al.*, 2000). The physiological function of Spy has been demonstrated by Quan *et al.* (2011) in a series of malate dehydrogenase (MDH) assays. Spy prevents the aggregation of denatured MDH at sub-stoichiometric concentrations, suggesting it is a highly effective, ATP-independent chaperone. The extent of the Spy chaperone activity was demonstrated at a range of denaturing agents including heat, ethanol, tannic acid and urea, and the chaperone activity was further demonstrated across a range of substrates including lactate dehydrogenase, aldolase, alkaline phosphatase and glyceraldehyde 3-phosphate dehydrogenase, indicating that Spy is capable of protecting a wide range of substrates against various environmental stresses (Quan *et al.*, 2011). The discovery that Spy is capable of preventing periplasmic polymerisation and aggregation of the curli subunit CsgA is further proof of the Spy chaperone activity *in vivo*. CsgA monomers are self-polymerising subunits that need to pass the periplasm prior to the extracellular formation of amyloid curli fibres. The ability of Spy to prevent amyloid formation in the periplasm underlines the importance of Spy as an periplasmic stress-response chaperone (Evans *et al.*, 2011). Spy does not appear to regulate the activity of two-component envelope stress response sensors, nor does its deletion or overexpression affect the expression levels of σ^E-, Bae-, Cpx-, Rsc-, or Psp-regulated genes, suggesting that unlike CpxP, Spy exhibits chaperone function only (Quan *et al.*, 2011).

The crystal structure of Spy (figure 4.2) shows a tightly bound homodimer that is very similar in shape to CpxP. The monomers consist of four α-helices, the first three of which fold into a hairpin structure. The hairpins of the two dimers interact in an anti-parallel coiled-coil manner, with extensive contact between the monomers. The two conserved LTxxQ motifs can be found at the horizontal end of the dimers, thought to be involved in the stabilisation of the structure. Similarly to CpxP, the dimer forms a cradle-like shape with a highly concave surface and a highly convex surface. The concave surface has an overall positive charge, but it is lined with conserved, a-polar side chains that cluster to form two exposed hydrophobic

patches. The lack of a significant globular core allows for high flexibility in the protein that is required to bind a wide range of substrates (Quan *et al.*, 2011; Kwon *et al.*, 2012).

Recent studies have shed more light on the chaperoning mechanism of Spy. In a series of studies using stopped flow fluorescence, X-ray crystallography and NMR spectroscopy the Bardwell group has demonstrated that Spy binds Immunity protein 7 (Im7) in unfolded, intermediate and native conformations, and allows the non-native Im7 to fold into its native state whilst bound to Spy, proving that Spy is not a holdase, but instead it is a foldase in its own right (Horowitz *et al.*, 2016; Stull *et al.*, 2016). The model they propose for Spy chaperone activity resolves around the hydrophobic and electrostatic properties of the Spy surface. The high density of positive charged residues on the substrate binding surface of Spy allows for rapid and directed binding of unfolded, negatively charged substrates (Koldewey *et al.*, 2016). Most periplasmic proteins are negatively charged, allowing for chaperoning by Spy (Heidary *et al.*, 2014). After initial binding, hydrophobic interactions between Spy and its substrate entropically stabilise the complex, and the hydrophobic surface of the substrate is shielded from the aqueous periplasm by Spy. The mixture of hydrophobic and electrostatic residues on the concave surface of Spy allow for a favourable folding landscape for the substrate, where electrostatic interactions help the substrate fold itself. Folding of the substrate drives its release. As the substrate is folding into its native shape, the hydrophobic residues are buried into the interior of the substrate, which reduces the hydrophobic component of the Spy-substrate complex. The reduction of hydrophobic interactions destabilises the complex and the folded substrate is released (Koldewey *et al.*, 2016).

3.1.2.3 ZraP

A detailed description of ZraP can be found in chapter 4 and chapter 5, this paragraph will only provide a brief overview.

The periplasmic chaperone ZraP is an auxiliary protein to the ZraSR two-component envelope stress response. It was first identified as a putative zinc-dependent transcriptional activator in *Proteus mirabilis* (Noll, Petrukhin and Lutsenko, 1998), but despite its upregulation in response to elevated zinc levels, studies have failed to prove a link between ZraP and zinc-tolerance (Noll, Petrukhin and Lutsenko, 1998; Appia-Ayme *et al.*, 2012; Petit-Hartlein *et al.*, 2015). The first functional characterisation of ZraP carried out by Appia-Ayme (2012) in *Salmonella* Typhimurium, demonstrated that ZraP regulates the activity of ZraSR in a manner that appears to be similar to the CpxP-mediated regulation of CpxAR. Furthermore the study demonstrated that ZraP is capable of preventing MDH aggregation even more effectively

than Spy. This chaperone activity was shown to increase in the presence of zinc, demonstrating that ZraP is a bifunctional protein that acts as regulator of the ZraSR two-component envelope stress response and as a zinc-dependent periplasmic chaperone (Appia-Ayme *et al.*, 2012).

ZraP belongs to the CpxP family of molecular chaperones and similarly to CpxP and Spy its monomer consists of α-helices. Unlike CpxP and Spy, ZraP only has one LTxxQ motif, and the structural analysis carried out to date suggests that ZraP does not form a dimer, but instead takes on a larger oligomeric structure (see chapter 5). Despite the increased chaperone activity in the presence of zinc, and the zinc-dependent upregulation of the ZraSRP system, the function of zinc in relation to this system, as well as any potential zinc-binding domains remain enigmatic.

3.1.3 HtrA

HtrA, also referred to as DegP in the literature, was the first identified σ^E-regulated gene involved in bacterial virulence (Humphreys *et al.*, 1999). Initially identified as an essential protein for *E. coli* growth at elevated temperatures, HtrA (<u>h</u>igh <u>t</u>emperature <u>r</u>equirement A) is a heat-shock protein with protease activity (Lipinska *et al.*, 1989; Strauch, Johnson and Beckwith, 1989; Kim *et al.*, 1999). Although HtrA is not essential for *Salmonella* growth at
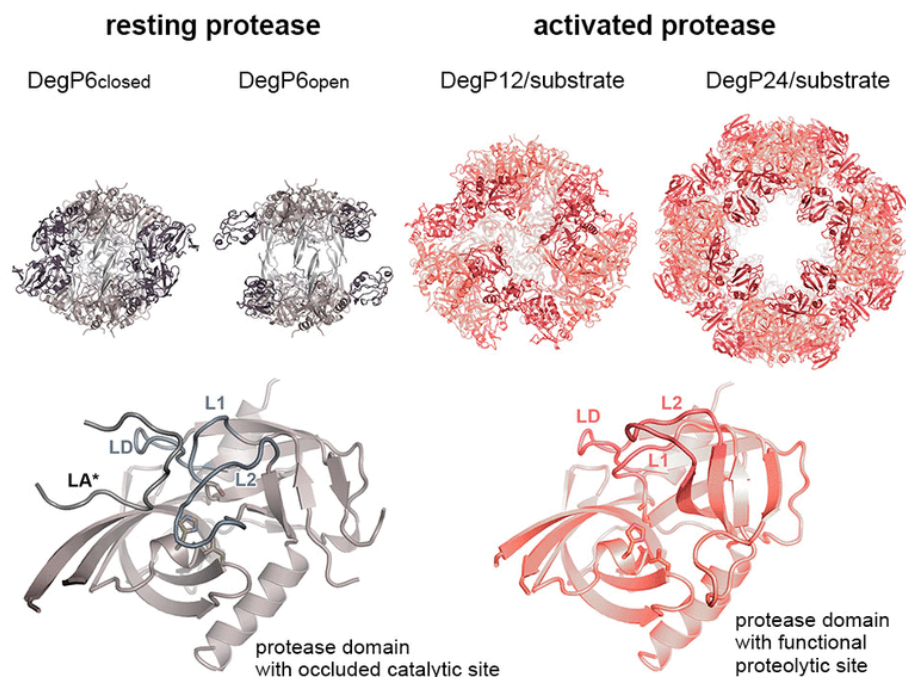
Figure 3.4 Schematic overview of the activation and oligomerisation of HtrA (DegP). The periplasmic protease HtrA adopts a closed hexameric conformation when inactive, but opens up into a large oligomer when activated. Image taken from (Krojer *et al.*, 2008)

mildly elevated temperatures (42°C), *htrA*-defective *Salmonella* strains are more susceptible to heat compared to their wild-type counterparts. At significantly elevated temperatures (46°C), HtrA is also required for survival in *Salmonella* (Lewis *et al.*, 2009). HtrA is not only required for survival at elevated temperatures, but also for replication and survival within macrophages in adherent and invasive *E. coli, Legionella pneumophila* and *Salmonella* Typhimurium (Bäumler *et al.*, 1994; Pedersen *et al.*, 2001; Bringer *et al.*, 2005). Furthermore, *htrA*-defective strains of *Klebsiella pneumoniae, Salmonella* Typhimurium and *Yersinia pestis* display attenuated virulence in animal models (Williams *et al.*, 2000; Cortes *et al.*, 2002).

HtrA belongs to the HtrA-like family of oligomeric serine proteases, and contains an N-terminal chymotrypsin-like serine protease domain and two C-terminal PDZ-domains. The chymotrypsin-like serine protease has a S1 pocket that is more hydrophobic than that of the average serine proteases, resulting in a specificity for hydrophobic substrates which allows for greater affinity to misfolded OMPs. The catalytic triad of the protease domain consists of a histidine, a serine and an aspartic acid, and mutations in these amino-acids render the protease inactive (Hedstrom, 2002). The PDZ domains allow for interaction between HtrA and protein substrates (Krojer *et al.*, 2002).

In 1999, an electron microscopy study of HtrA gave the first indication that HtrA may be capable of self-compartmenting (Kim *et al.*, 1999), but due to the low resolution of the images this was not confirmed until crystal structures of multiple HtrA oligomeric states were first published in 2008 and confirmed in 2013 (Jiang *et al.*, 2008; Hansen and Hilgenfeld, 2013). The first crystal structures of HtrA were published in 2002, and they presented HtrA as a hexamer formed of two interlocked trimers in a face-to-face arrangement. The monomers interact via hydrophobic bonds to form stable trimers. The protease domains of each stable trimer displays extensive contact, and the hexamer is stabilised by three pairs of intertwined loops from opposing monomers forming a pillar-like arrangement. The structure of the crystallised hexamer suggests an inactive resting state; the protease domains are located on the inside of the hexamer with the access blocked off by the intertwined loops of opposing monomers. The hexameric structure was solved in two different conformations, suggesting that, unlike the locked-in protease domain, the PDZ domains are flexible in the hexameric orientation (Krojer *et al.*, 2002; Hansen and Hilgenfeld, 2013). In 2008, HtrA crystal structures of dodecamers and 24-mers provided a better understanding of the potential protease mechanism of HtrA. The large oligomers appear to be formed of self-compartmenting HtrA trimers that form hollow spheres with diameters of approximately 160Å for the dodecamer and 195Å for the 24-mer (figure 3.4). Unlike in the hexamer, in these

higher oligomeric states the PDZ domains are inflexible and integral to the protein shell, and the protease-active sites on the inner wall of the protein are no longer blocked by loops (Jiang *et al.*, 2008; Krojer *et al.*, 2008; Hansen and Hilgenfeld, 2013). Although there is no *in vivo* evidence for the existence of these large HtrA oligomers, the interactions and stability of the HtrA dodecamer with lysozyme fragments have been confirmed *in vitro* by fluorescence anisotropy assays (Kim, Grant and Sauer, 2011).

HtrA chaperone activity at low temperatures was first reported following refolding assays using MalS. It was suggested that HtrA was a bifunctional protein, acting as a protease at higher temperatures and functioning as a chaperone at lower temperatures (Spiess, Beil and Ehrmann, 1999). Reports of HtrA chaperone activity in *Salmonella* Typhimurium followed (Lewis *et al.*, 2009). However, recent studies have challenged this concept. Firstly, it should be noted that Gram-negative periplasmic proteins are highly resistant to aggregation and have a strong refolding capacity (Liu *et al.*, 2004), and the substrate MalS used in the refolding assays is a periplasmic protein that could be capable of self-folding under oxidative conditions or in favourable pH (Spiess, Beil and Ehrmann, 1999; Chang, 2016). Furthermore, the concept that HtrA may act as a chaperone at lower temperatures and as a protease at higher temperatures is inconsistent with observations of Kim, *et al.* who reported a consistent rate of degradation of an oxidised insulin β-chain by HtrA across temperatures ranging from 35°C to 55°C, and observations by Ge *et al.* (2014), who reported HtrA protease activity of β-barrel substrates across temperatures ranging from 28°C to 44°C (Kim *et al.*, 1999; Ge, Wang, *et al.*, 2014; Chang, 2016). The temperature-dependent protease activity of HtrA has since been linked to the increased rate of substrate unfolding at high temperatures (Ge, Wang, *et al.*, 2014). Furthermore, substrates with disulphide bonds, such as MalS, are unable to enter the HtrA catalytic centre efficiently, which would interfere with the protease activity of HtrA, suggesting chaperone-like function instead (Kim *et al.*, 1999; Chang, 2016). Another observation that challenges the concept of HtrA acting as a chaperone, is the notion that the protease defective HtrA(S210A) is capable of capturing substrate proteins but cannot release its substrates (Misra, CastilloKeller and Deng, 2000; CastilloKeller and Misra, 2003). Although overexpression of HtrA(S210A) allowed for the rescue of heat-shocked cells, replacing *htrA* with *htrA(S210A)* no longer resulted in rescue. This demonstrates that the protease-inactive HtrA(S210A) can only rescue heat-shocked cells when present in great abundance, suggesting that it can capture toxic protein aggregates, but it cannot truly chaperone them (Ge, Wang, *et al.*, 2014). The study suggesting HtrA chaperone activity in *Salmonella*, studied the survivability of strains expressing WT HtrA in the mouse liver and

spleen, and compared it to strains that expressed HtrA mutated in the protease domain strains mutated in the PDZ domains (Lewis *et al.*, 2009). These experiments showed that mutations in the protease domain affect survivability less than mutations of the PDZ domains. However, studies supporting the theory that HtrA can act as a chaperone have demonstrated that potential chaperone-activity is largely independent of the PDZ domains, whereas protease activity is significantly reduced when at least one PDZ domain is missing (Spiess, Beil and Ehrmann, 1999). Furthermore, the study by Lewis *et al.* (2009) lacks biochemical analysis of potential chaperone activity by HtrA. It is possible that protease-inactive, *Salmonella* HtrA can still bind misfolded proteins, but can no longer process or release them. This theory would also explain why *Salmonella ΔhtrA* mutants becomes increasingly more sensitive at higher temperatures; whereas HtrA is still capable of binding denatured proteins irreversibly when exposed to mild heat, higher temperatures increase the amount of misfolded proteins present in the periplasm, oversaturating the protease-inactive HtrA. True chaperone activity requires both binding and the subsequent release of substrates to promote folding and assembly of native or misfolded proteins. The chaperone-like activity observed by HtrA(S210A) is an intrinsic property of protease-defective proteases, for they are still capable of binding their substrates, but they are unable to release them (Ellis and van der Vies, 1991). A final observation challenging the concept of HtrA acting as chaperone refers to the thermodynamic properties of HtrA. Unlike effective chaperones which bind substrates quickly but loosely, HtrA binds its substrate slowly but strongly, which is a thermodynamic attribute assigned to proteases (Ellis and van der Vies, 1991; Wu *et al.*, 2011). Although some studies consider a HtrA as a bifunctional protease-chaperone protein, the evidence is accumulating in favour of the concept of HtrA acting solely as a protease, with no true chaperone activity (Chang, 2016).

3.1.4 PpiAD

Little is known about the periplasmic protein PpiA, sometimes referred to as rotamase A. It was discovered as a cyclosporin A-resistant periplasmic homologue of the human protein cyclophilin A, and it has peptidyl-prolyl isomerase activity (Liu and Walsh, 1990). PpiA is capable of refolding thermally denatured proteins, but it is not an essential protein and little is known about its associated pathways or its function in the periplasm (Schonbrunner *et al.*, 1991; Compton *et al.*, 1992; Kleerebezem, Heutink and Tommassen, 1995).

PpiD was initially identified as a periplasmic chaperone with a parvulin-like peptidyl-prolyl isomerase domain. The protein is anchored in the inner membrane by an N-terminal

transmembrane segment, and its C-terminal catalytic domain faces the periplasm. Initial studies reported synthetic lethality in *E. coli* Δ*ppiD* Δ*surA* double mutants (Dartigalongue and Raina, 1998), but has since been disproven (Justice *et al.*, 2005). Expression of *ppiD* is regulated by σ^H and the Cpx pathway, suggesting it may play a role in the response to envelope stress (Dartigalongue and Raina, 1998). The parvulin domain has been reported to be devoid of catalytic activity *in vitro* and resembles the inactive parvulin-like domain found in SurA (Matern, Barion and Behrens-Kneip, 2010; Weininger *et al.*, 2010). The chaperone activity of PpiD is independent of its parvulin domain, as Parvulin domain-lacking PpiD can fully complement the growth defects resulting from a Δ*fkpA* Δ*ppiD* Δ*surA* triple mutant, and is capable of protecting citrate synthase from thermal aggregation even more effectively than the wild-type protein (Matern, Barion and Behrens-Kneip, 2010). The chaperone domain of PpiD shows sequence similarity with the conserved SurA chaperone module, but shows less substrate specificity than SurA (Matern, Barion and Behrens-Kneip, 2010). PpiD is anchored in the inner membrane close to the Sec translocase machinery, and it has been suggested that this periplasmic chaperone may act as a gatekeeper responsible for newly translocated OMPs. The chaperone activity of PpiD may capture newly secreted envelope proteins as they emerge from the inner membrane, and mediate their initial folding (Antonoaea *et al.*, 2008; Matern, Barion and Behrens-Kneip, 2010).

3.1.5 YncJ

YncJ is a putative periplasmic protein of unknown function. Several studies, including unpublished work from the Rowley lab, have shown that *yncJ* is upregulated by NlpE (Raivio, Leblanc and Price, 2013). The latter is an outer membrane lipoprotein that is involved in the activation of the Cpx-pathway in response to adhesion to hydrophobic surfaces (Otto and Silhavy, 2002). The upregulation of this putative periplasmic chaperone by a regulator of the Cpx-pathway, suggests that the protein may be involved in an envelope stress response pathway.

3.2 Aim

The aim of this chapter is to further characterise a selection of periplasmic proteins found in *Salmonella* Typhimurium, to broaden our understanding of their involvement in the protection against different envelope stresses that this pathogen may be subjected to. Furthermore, in this chapter the investigated function of these chaperones is compared with the literature describing the function of the chaperones' homologs in in *E. coli* and other pathogenic species of the Enterobacteriaceae family.

The proteins selected for this study include the periplasmic chaperones FkpA, Skp, and SurA involved in outer membrane biogenesis, the periplasmic chaperones CpxP, Spy, and ZraP involved in the envelope stress response, the periplasmic protease HtrA, and the periplasmic chaperones PpiA, PpiD and YncJ whose chaperone functions remain unclear.

In order to investigate the involvement of these proteins in the protection of the outer membrane against external stress, antimicrobial sensitivity assays were carried out in the form of sensitivity spot plate assays, disc diffusion assays and carbon-starvation induced cross resistance assays. The data obtained in this study was investigated alongside published literature in order to obtain a better understanding of the involvement of periplasmic chaperones in the protection against environmental stress experienced by Enterobacteriaceae.

3.3 Results

3.3.1 Preparation and verification of knock-out strains

Most of the *Salmonella* deletion strains used for the antimicrobial sensitivity assays were prepared prior to the start of this PhD by former lab members including Dr. Corrine Appia-Ayme, Dr. Hannah Wells and Thomas Williams. External verification primes (table 2.4) were designed to confirm the validity of these deletion mutants. Gel electrophoresis was used to compare the band sizes obtained from the presumed deletion mutants to the STM SL1344 WT control bands. Whereas the band size of a successful mutant would either match the approximate size of the antibiotic cassettes (1300bp for chloramphenicol, 1700bp for kanamycin) or present as a very short band indicating removal of the antibiotic cassette post gene deletion, the band size of an unsuccessful mutant would match the band size obtained from the STM SL1344 WT control. The expected band sizes for the STM SL1344 WT control when using the designed external verification primers are shown in table 3.1 below.

Table 3.1 Expected band size obtained from WT SL1344 using verification primers

Gene	Band size	Gene	Band size
cpxP	765 bp	*skp*	792 bp
fkpA	1086 bp	*spy*	716 bp
htrA	1714 bp	*surA*	1512 bp
ppiA	799 bp	*yncJ*	530 bp
ppiD	2137 bp	*zraP*	719 bp

PCR analysis verified the indicated gene deletion in 25 of the 27 tested strains (figure 3.5 – figure 3.8). However, the band sizes observed for *surA* in the Δ*htrA* Δ*surA* and Δ*fkpA* Δ*surA* strains indicate that *surA* was not successfully removed from these strains. Although attempts have been made to create these double knock-out strains using both existing p22 phage stocks and freshly prepared p22 phage stocks, all colonies obtained proved to be false positives. The strains have therefore been removed from the list for further susceptibility analysis. To ensure that *ppiA* was still present in the Δ*fkpA* Δ*ppiD* mutant, and *ppiD* was still present in the Δ*cpxP* Δ*fkpA* Δ*ppiA* mutant, both strains were included in the verification of *ppiA* and *ppiD* deletion respectively (figure 3.5, figure 3.7). To extend the library of double and triple chaperone knock-out mutants, *de novo* mutagenesis was carried out using the lambda (λ) red method as described in chapter 2.5.1. The *Salmonella* Typhimurium knock-out strains that were successfully created in this study include Δ*yncJ*, Δ*surA* Δ*yncJ*, and Δ*skp* Δ*surA*. The gene knock-outs of these strains were confirmed using external verification primers comparing the deletion strains to STM SL1344 WT (figure 3.9)
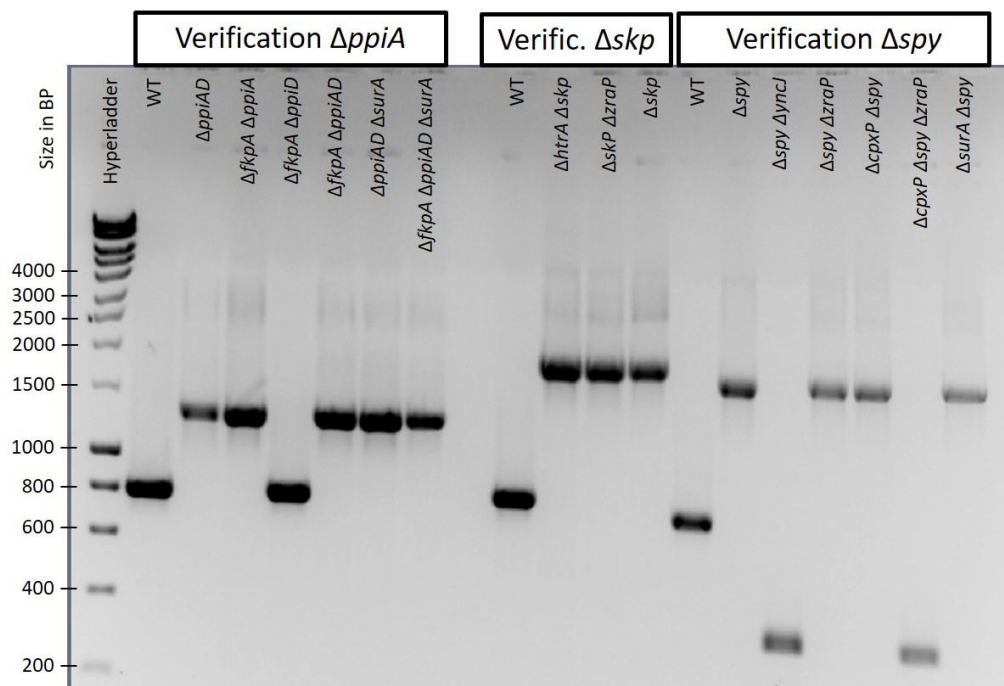
Figure 3.5 Verification of deletion of *ppiA*, *skp*, and *spy* from the indicated STM SL1344 deletion strains. PCR analysis was carried out using primers listed in table 2.4. The expected band size for WT ***ppiA*** is 799 bp, which is matched by the bands found in the WT lane and the Δ*fkpA* Δ*ppiD* lane, indicating presence of the *ppiA* gene in these strains. The bands found in the lanes for Δ*ppiAD*, Δ*fkpA* Δ*ppiA*, Δ*fkpA* Δ*ppiAD*, Δ*ppiAD* Δ*surA*, and Δ*fkpA* Δ*ppiAD* Δ*surA* are of approximately 1300 bp in size, matching the expected size for the chloramphenicol cassette. These bands indicate successful deletion of *ppiA* by replacement of the gene with a chloramphenicol cassette. The expected band size for WT ***skp*** is 792 bp, which is matched by the band found in the WT lane. The bands found in the lanes for Δ*htra* Δ*skp*, Δ*skp* Δ*zraP*, and Δ*skp* are of approximately 1700 bp in size, matching the expected size for the kanamycin cassette. These bands indicate successful deletion of *skp* by replacement of the gene with a kanamycin cassette. The expected band size for WT ***spy*** is 716 bp, which is matched by the band found in the WT lane. The bands found in the lanes for Δ*spy*, Δ*spy* Δ*zraP*, Δ*cpxP* Δ*spy*, and Δ*surA* Δ*spy* are of approximately 1700 bp in size, matching the expected size for the kanamycin cassette. These bands indicate successful deletion of *spy* by replacement of the gene with a kanamycin cassette. The bands found in Δ*spy* Δ*yncJ* and Δ*cpxP* Δ*spy* Δ*zraP* are of approximately 300bp in size, indicating successful deletion of *spy* and subsequent removal of the antibiotic cassette. The DNA ladder used as size marker was 1 kb Hyperladder (BIOLINE).

.
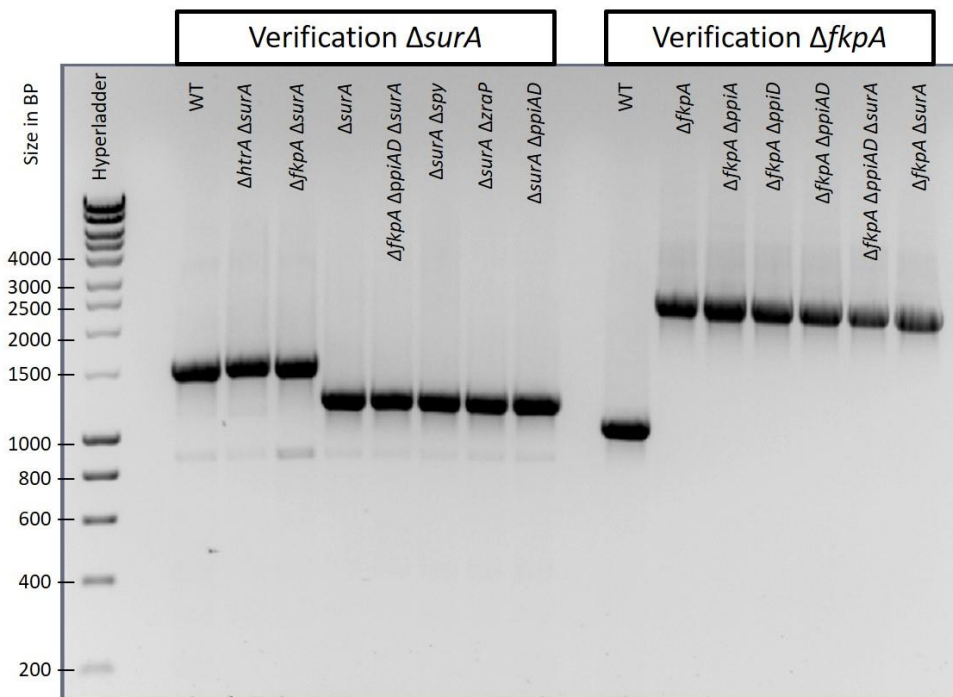
Figure 3.6 Verification of deletion of *surA* and *fkpA* from the indicated STM SL1344 deletion strains. PCR analysis was carried out using primers listed in table 2.4. The expected band size for WT **surA** is 1512 bp, which is matched by the bands found in the lanes for WT, Δ*htrA* Δ*surA*, and Δ*fkpA* Δ*surA*, indicating presence of the *surA* gene in these strains. This suggests that the deletion of *surA* was unsuccessful in Δ*htrA* Δ*surA*, and Δ*fkpA* Δ*surA*. The bands found in the lanes for Δ*surA*, Δ*fkpA* Δ*ppiAD* Δ*surA,* Δ*surA* Δ*spy*, Δ*surA* Δ*zraP*, and Δ*ppiAD* Δ*surA* are of approximately 1300 bp in size, matching the expected size for the chloramphenicol cassette. These bands indicate successful deletion of *surA* by replacement of the gene with a chloramphenicol cassette. The expected band size for WT **fkpA** is 1086 bp, which is matched by the band found in the WT lane. The bands found in the lanes for Δ*fkpA*, Δ*fkpA* Δ*ppiA*, Δ*fkpA* Δ*ppiD*, Δ*fkpA* Δ*ppiAD* Δ*surA*, and Δ*fkpA* Δ*surA* are of approximately 1700 bp in size, matching the expected size for the kanamycin cassette. These bands indicate successful deletion of *fkpA* by replacement of the gene with a kanamycin cassette. The DNA ladder used as size marker was 1 kb Hyperladder (BIOLINE)
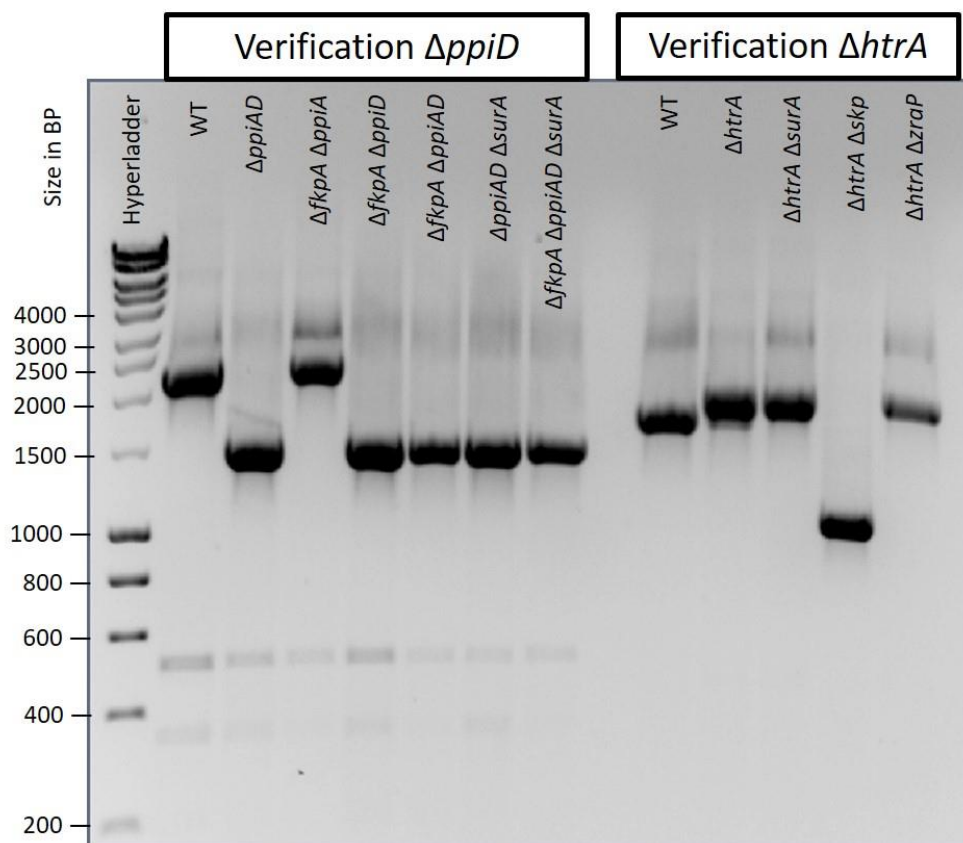
Figure 3.7 Verification of deletion of *ppiD* and *htrA* from the indicated STM SL1344 deletion strains. PCR analysis was carried out using primers listed in table 2.4. The expected band size for WT ***ppiD*** is 2137 bp, which is matched by the bands found in the lanes for WT and *ΔfkpA ΔppiA*, indicating presence of the *ppiD* gene in these strains. The bands found in the lanes for *ΔppiAD*, *ΔfkpA ΔppiD*, *ΔfpkA ΔppiAD*, *ΔppiAD ΔsurA,* and *ΔfkpA ΔppiAD ΔsurA* are of approximately 1500 bp in size, matching neither the expected size for the chloramphenicol or the kanamycin cassette. Although these bands do not match the expected cassette sizes, they are clearly shorter than the band found for the WT. These bands indicate successful deletion of *ppiD*, potentially by replacement of the gene with a gentamicin cassette, used by the lab who donated this strain. The expected band size for WT ***htrA*** is 1714 bp, which is matched by the band found in the WT lane. The bands found in the lanes for *ΔhtrA*, *ΔhtrA ΔsurA*, and *ΔhtrA ΔzraP* are of approximately 1700 bp in size, matching the expected size for a kanamycin cassette. These bands indicate successful deletion of *htrA* by replacement of the gene with a kanamycin cassette. The band found in the lane for *ΔhtrA ΔsurA* is of approximately 1300 bp in size, matching the expected size for a chloramphenicol cassette. This band indicates successful deletion of *htrA* by replacement of the gene with a chloramphenicol cassette. The DNA ladder used as size marker was 1 kb Hyperladder (BIOLINE)
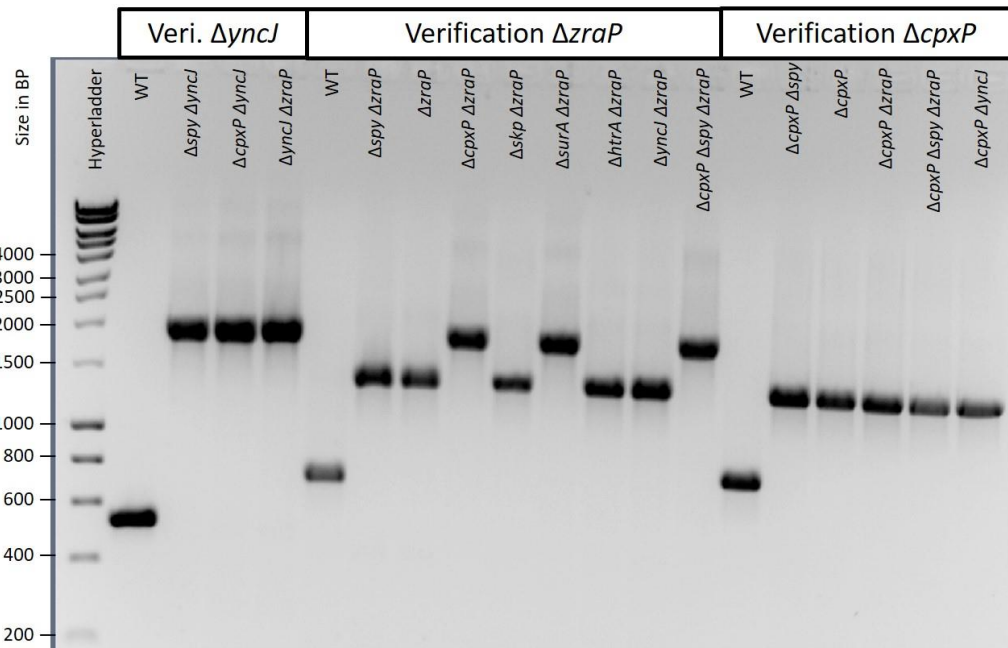
Figure 3.8 Verification of deletion of *yncJ*, *zraP*, and *cpxP* from the indicated STM SL1344 deletion strains. PCR analysis was carried out using primers listed in table 2.4. The expected band size for WT **yncJ** is 530 bp, which is matched by the band found in the WT lane. The bands found in the lanes for Δ*spy* Δ*yncJ*, Δ*cpxP* Δ*yncJ*, and Δ*yncJ* Δ*zraP* are of approximately 1700 bp in size, matching the expected size for the kanamycin cassette. These bands indicate successful deletion of *yncJ* by replacement of the gene with a kanamycin cassette. The expected band size for WT **zraP** is 719 bp, which is matched by the band found in the WT lane. The bands found in the lanes for Δ*spy* Δ*zraP*, Δ*zraP*, Δ*skp* Δ*zraP*, Δ*htrA* Δ*zraP*, and Δ*yncJ* Δ*zraP* are of approximately 1300 bp in size, matching the expected size for the chloramphenicol cassette. These bands indicate successful deletion of *zraP* by replacement of the gene with a chloramphenicol cassette. The bands found in the lanes for Δ*cpxP* Δ*zraP*, Δ*surA*Δ*zraP*, and Δ*cpxP* Δ*spy* Δ*zraP*, are of approximately 1700 bp in size, matching the expected size for the kanamycin cassette. These bands indicate successful deletion of *zraP* by replacement of the gene with a kanamycin cassette. The expected band size for WT **cpxP** is 765 bp, which is matched by the band found in the WT lane. The bands found in the lanes for Δ*cpxP* Δ*spy*, Δ*cpxP*, Δ*cpxP* Δ*zraP*, Δ*cpxP* Δ*spy* Δ*zraP*, and Δ*cpxP* Δ*yncJ* are of approximately 1300 bp in size, matching the expected size for the chloramphenicol cassette. These bands indicate successful deletion of *cpxP* by replacement of the gene with a chloramphenicol cassette. The DNA ladder used as size marker was 1 kb Hyperladder (BIOLINE).
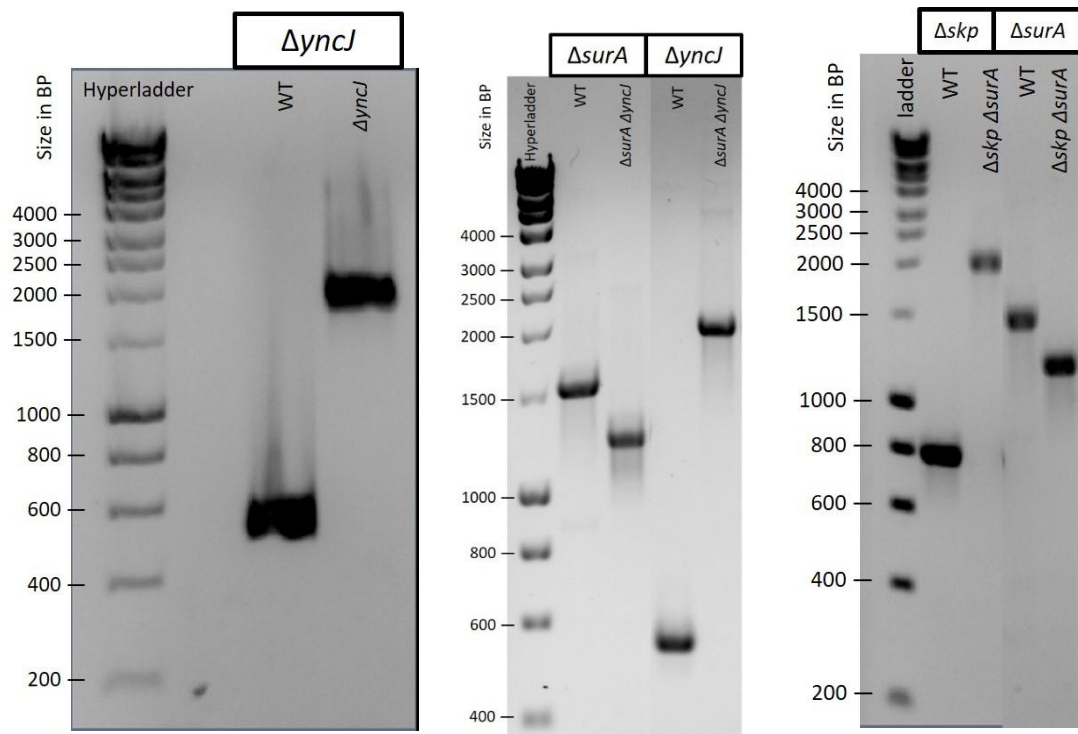
Figure 3.9 Verification of deletion of *yncJ*, *surA*, and *skp* from the indicated STM SL1344 deletion strains. PCR analysis was carried out using primers listed in table 2.4. The expected band size for WT ***yncJ*** is 530 bp, which is matched by the band found in the WT lane. The bands found in the lanes for Δ*yncJ*, and Δ*surA* Δ*yncJ* are of approximately 2000 bp in size, matching the expected size for the kanamycin cassette including external regions. These bands indicate successful deletion of *yncJ* by replacement of the gene with a kanamycin cassette. The expected band size for WT ***surA*** is 1512 bp, which is matched by the band found in the WT lane. The bands found in the lanes for Δ*surA* Δ*yncJ*, and Δ*skp* Δ*surA* are of approximately 1300 bp in size, matching the expected size for the chloramphenicol cassette. These bands indicate successful deletion of *surA* by replacement of the gene with a chloramphenicol cassette. The expected band size for WT ***skp*** is 792 bp, which is matched by the band found in the WT lane. The band found in the lane for Δ*skp* Δ*surA* is of approximately 2000 bp in size, matching the expected size for the kanamycin cassette including external regions These bands indicate successful deletion of *skp* by replacement of the gene with a kanamycin cassette. The DNA ladder used as size marker was 1 kb Hyperladder (BIOLINE).

3.3.2 Determination of inhibiting concentrations

Using growth curves, the susceptibility of STM SL1344 WT to a range of antimicrobial agents was analysed. A literature search was conducted to estimate the minimal inhibitory concentrations of antimicrobial agents of interest. The concentrations described in the papers studied were used as a starting point around which a range of concentrations was prepared to be tested in growth curves.

The antimicrobial agent bacitracin is a mixture of cyclic polipeptides derived from *Bacillus subtilis* var Tracy, which interfere with the formation of peptidoglycan (Molenkamp and Veerkamp, 1976). A study into the susceptibility of *Escherichia coli* to bacitracin reported that disruptions of the *E. coli bcrC$_{EC}$* gene, a homologue to the BcrC subunit of the bacitracin permease from *Bacillus licheniformis*, results in increased susceptibility to bacitracin. The study examined susceptibility of *E. coli* on solid LB agar plates containing bacitracin concentrations ranging between 30 - 220 U/mL (Harel, Bailone and Bibi, 1999). To analyse the susceptibility of STM SL1344 to bacitracin, growth curves were conducted in LB broth with bacitracin concentrations ranging between 50μg/mL – 1500μg/mL (approx. 3.7 IU – 110 IU). At 1500μg/mL a slight reduction in growth rate was observed compared to growth in plain LB (figure 3.10).

In *Salmonella* Typhimurium, the presence of hydroxyurea activates the expression of *nrd* operons encoding Class I ribonuclease reductases. Ribonuclease reductases are involved in the reduction of ribonucleotides into deoxyribonucleotides required for DNA replication and repair. Addition of 10mM hydroxyurea to LB broth increased expression of *nrd* operons but did not impair *Salmonella* Typhimurium growth (Panosa, Roca and Gibert, 2010). To analyse the susceptibility of STM SL1344 to hydroxyurea, growth curves were conducted in LB broth with hydroxyurea concentrations ranging between 5mM – 15mM. No significant growth reduction could be detected for STM SL1344 in the presence of hydroxyurea at the tested concentrations (figure 3.10).

Indole is an intracellular signalling molecule produced by *E. coli*, but not by *Salmonella.* Environmental indole encountered by *Salmonella* results in an increased production of multidrug efflux pumps, but it also leads to a down regulation of SPI-1 encoded virulence genes required for host cell invasion, as well as genes involved in flagellar production and anaerobic respiration. Assays have been carried out studying gene expression in *Salmonella* in response to indole exposure. These assays were carried out in LB broth supplemented with 1-4mM indole (Nikaido *et al.*, 2012). To analyse the susceptibility of STM SL1344 to indole,

growth curves were conducted in LB broth with indole concentrations ranging between 0.5mM – 4mM. The growth of STM SL1344 was affected at tested concentrations upwards of 2mM (figure 3.10).

Recent reports suggest that fluoroquinolone-resistant *Salmonella* Typhi strains are becoming increasingly more common. Clinicians require early detection of fluoroquinolone resistance in *S.* Typhi, however current interpretive guidelines for fluoroquinolone disk susceptibility testing would categorise these *Salmonella* strains as susceptible. The synthetic quinolone nalidixic acid is frequently used to screen for fluoroquinolone resistance instead. The concentration of nalidixic acid in the discs for susceptibility screens is 16µg/mL. To analyse the susceptibility of STM SL1344 to nalidixic acid, growth curves were conducted in LB broth with nalidixic acid concentrations ranging between 1µg/mL – 50µg/mL. Although 16µg/ml nalidixic acid appeared to inhibit all STM SL1344 growth, 24-hour screens demonstrated restoration of growth with a final cell density comparable to growth in plain LB after 24 hours of incubation. At higher concentrations, STM SL1344 growth appeared to be restricted indefinitely (figure 3.10).

The phosphonic acid derivative phosphomycin in an antibiotic substance that interferes with the cell wall formation of both Gram positive and Gram negative bacteria. It inhibits the synthesis of peptidoglycan by inactivating the transferase MurA. Antimicrobial sensitivity assays were conducted on *E. coli* and *Klebsiella pneumoniae* on LB agar using discs containing 200µg phosphomycin (Michalopoulos, Livaditis and Gougoutas, 2011). To analyse the susceptibility of STM SL1344 to phosphomycin disodium salt, growth curves were conducted in LB broth with phosphomycin concentrations ranging between 200ng/mL – 130µg/mL. In liquid culture, STM SL1344 recovers growth to a cell density comparable to growth in LB only during an incubation period of 24 hours. No growth was observed at any phosphomycin concentration above 500ng/mL (figure 3.10).

Spermidine is a natural polyamine found in living tissues. Cationic polyamines are involved in a wide range of biological processes as they enhance the expression of regulatory genes of hundreds of genes involved in cell growth and viability. In *E. coli,* polyamines are also involved in control of membrane permeability and the protection against certain external stresses including oxidative stress, radiation and high acidity. However, in *Pseudomonas aeruginosa,* exogenous natural polyamines can enhance susceptibility to multiple antibiotic compounds including β-lactams, chloramphenicol, trimethoprim and nalidixic acid. Although *P. aeruginosa* was able to survive in the presence of 20mM spermidine, growth in 1mM

spermidine significantly increased susceptibility to antibiotics (Kwon and Lu, 2006). To analyse the susceptibility of STM SL1344 to spermidine, growth curves were conducted in LB broth with spermidine concentrations ranging between 0.25mM – 10mM. At 10mM spermidine the growth of STM SL1344 was significantly slower than growth in plain LB (figure 3.10).

The results of the growth curves, displayed in figure 3.10 were used as a starting point for the susceptibility testing of chaperone mutant strains by spot plate assays and disc diffusion assays. The growth curve assays testing bacitracin susceptibility demonstrated that STM SL1344 WT was not sensitive to high concentrations of bacitracin (1.5mg/mL). Higher concentrations were not tested in growth curves due to solubility limitations of bacitracin. The disc diffusion assays testing bacitracin susceptibility of the STM mutant strains were conducted at a final concentration of 10mM. The growth curves testing susceptibility to hydroxyurea demonstrate that STM SL1344 WT is not sensitive to the maximum tested concentration. Instead of testing further concentrations using growth curves, disc diffusion assays testing STM SL1344 WT and mutant sensitivity to this compound was carried out using the concentration of the stock, 1 M hydroxyurea. In accordance with Wells (2015), STM SL1344 WT demonstrates susceptibility to 2mM Indole. This concentration was used for further susceptibility checks. Following the growth curve assays, initial spot plate assays testing STM SL1344 WT and mutant susceptibilities against nalidixic acid were carried out at a concentration of 15µg/mL. However, the strains proved more sensitive to nalidixic acid on solid agar plates compared to liquid batch culture. Following spot plate tests at a wide range of concentrations, the final testing concentration for spot plates was set at 1µg/mL. The disc diffusion assays were tested using the stock concentration, 10mM. The growth curve assays demonstrate that STM SL1344 WT suffers an extended lag phase when grown in the presence of 500ng/mL Phosphomycin, but does eventually growth to a final OD comparable to WT grown in plain LB. For the spot plate assays, $^1/_{10}$ dilution of this concentration was chosen (50ng/mL), and for the disc diffusion assays, the stock concentration of 10mM was tested. During the growth curve assays, STM SL1344 WT started to show susceptibility to spermidine at a concentration of 10mM. However, on spot plate assays, growth of the WT appeared to be strongly inhibited at a concentration of 7mM. Therefore, the tested concentrations for spermidine were 6mM for spot plate assays, and 10mM for disc diffusion assays.
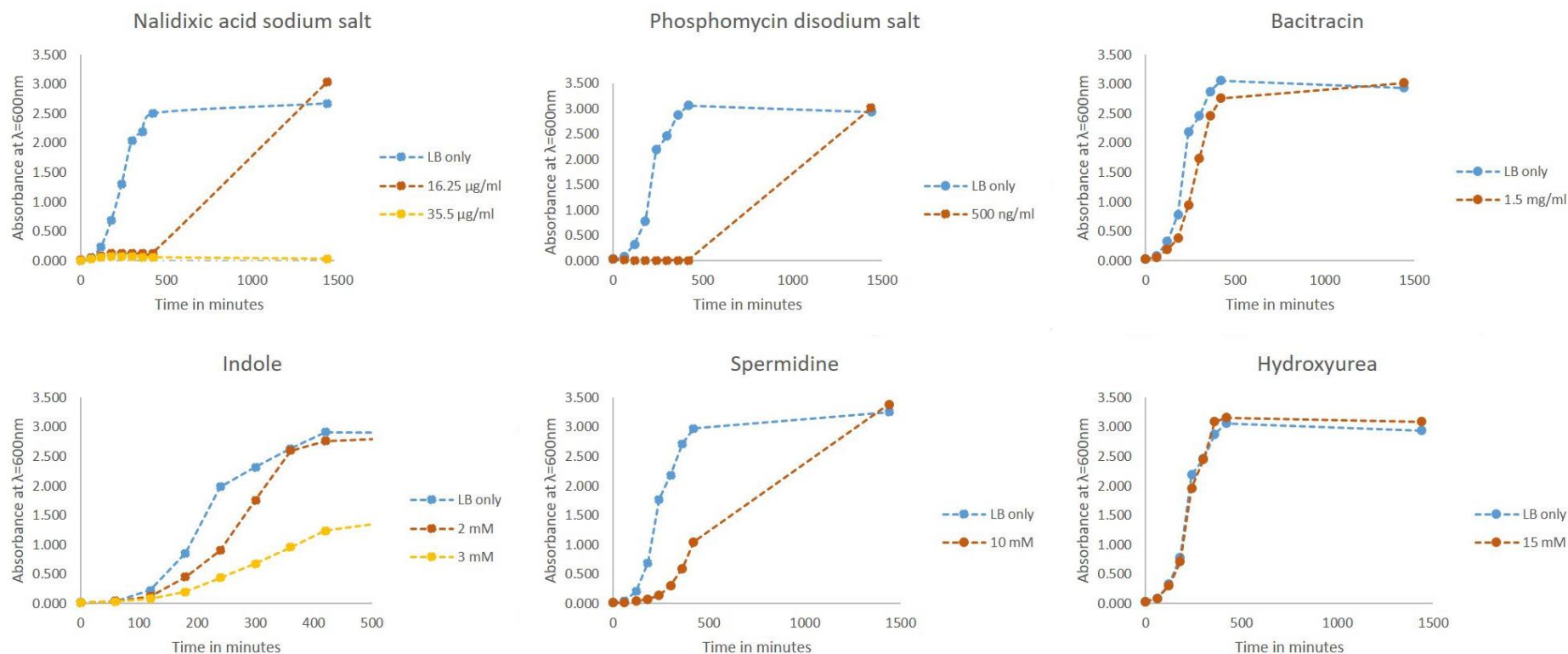
Figure 3.10 Estimation of antimicrobial concentrations required during susceptibility assays. Growth curves of STM SL1344 WT were carried out aerobically using LB broth supplemented with antimicrobials at various concentrations. All cultures were grown at 37°C, 200rpm for 24 hours, and the OD_{600} was recorded at regular intervals. In the presence of **bacitracin**, a slight reduction in growth rate was observed at 1500µg/mL. No significant growth reduction could be detected in the presence of **hydroxyurea**. STM SL1344 WT growth was negatively affected by **indole** at 2mM. In the presence of 16.5µg/mL **Nalidixic acid** and 500 ng/mL **phosphomycin** STM SL1344 growth is significantly affected during the first 8 hours of incubation, but after 24 hours of growth at 37°C, their OD_{600} has recovered to the density observed for growth in plain LB broth. The presence of 10mM **spermidine** significantly slows the initial growth of STM SL1344, but after 24 hours incubation, optical density has been restored to the level of the control.

3.3.3 Susceptibility assays

To analyse the involvement of the *S.* Typhimurium periplasmic chaperones and proteins CpxP, FkpA, HtrA, PpiAD, Skp, Spy, SurA, YncJ and ZraP in the protection against environmental stresses, disc diffusion assays and sensitivity spot assays were carried out. An overview of the strains and conditions tested can be found in tables 3.2 − 3.7, a graphic overview of all strains tested for antimicrobial and heat susceptibility can be found in appendix E.

3.3.3.1 Skp contributes to *S.* Typhimurium survival during exposure to bacitracin.

Disc diffusion assays carried out using 10mM bacitracin (figure 3.11) demonstrated that the removal of *skp* renders STM SL1344 more sensitive (P < 0.01). In agreement with this, the other two tested mutants carrying a *skp* deletion, Δ*htrA* Δ*skp*, Δ*skp* Δ*zraP*, are both significantly more affected by bacitracin compared to the WT. However, neither strain is affected significantly more than Δ*skp*, suggesting that the increased sensitivity is the result of the removal of *skp* alone. Although the deletion of *surA* or *ppiAD* does not affect susceptibility to bacitracin, the combined mutation of Δ*ppiAD* Δ*surA* does result in greater susceptibility to bacitracin (P < 0.01). Furthermore, the deletion of *fkpA* alone does not affect susceptibility to bacitracin, nor does the combined mutation of Δ*fkpA* Δ*ppiAD*. However, the quadruple mutant Δ*fkpA* Δ*ppiAD* Δ*surA* is more susceptible than both the WT and the Δ*ppiAD* Δ*surA* mutant (P < 0.01), suggesting that removal of all four genes has a serious impact on the survivability of STM SL1344 in the presence of bacitracin. For a full overview of all strains tested for bacitracin susceptibility, see figure E7.

3.3.3.2 HtrA contributes to *S.* Typhimurium survival during heat stress.

Sensitivity spot plate assays were carried out to determine the sensitivity of STM SL1344 mutants to heat exposure at 42°C and 46°C (figure 3.12). The data collected for the exposure to 42°C are inconclusive. At 42°C, Δ*skp* and Δ*cpxP* Δ*spy* appear to be significantly less susceptible than the WT (P < 0.05), but this does not hold for exposure to 46°C. Also, although Δ*fkpA* Δ*ppiA* appears to be significantly more affected than the WT at 42°C, this does not appear to be the case for Δ*fkpA* Δ*ppiAD*, or Δ*fkpA* Δ*ppiAD* Δ*surA*. However, the data collected for the exposure to 46°C are more consistent. The percentage survival of Δ*htrA* is reduced by 63.6% compared to the WT survival (45.7% survival *versus* 71.86% survival respectively), the large deviation between the data collected for Δ*htrA* (50.5%) means that the two strains are not considered statistically different. The data collected for Δ*htrA* Δ*skp*, and Δ*htrA* Δ*zraP* however, show significant reduction in survival compared to the wild type (P < 0.01).

Considering the percentage survival for both Δ*skp* and Δ*zraP* are similar to the WT percentage survival, it is probable that the sensitivity is the result of the deletion of *htrA*. For a full overview of all strains tested for susceptibility to heat, see figures E1 and E2.

Figure 3.11 Susceptibility of STM SL1344 WT and mutant strains to bacitracin. SL1344 WT and mutant strains were screened for sensitivity to bacitracin using disc diffusion assays. The zones of inhibition of WT and nineteen mutant strains have been calculated in mm^2 (table 3.2), and those strains demonstrating significantly increased sensitivity to the tested compounds have been included in the figure, the level of WT inhibition included for comparison. Significant differences to STM SL1344 WT are indicated by * ($P < 0.05$) and ** ($P < 0.01$), Student's t-test assuming equal variance, n = 3. Error bars indicate standard deviation.
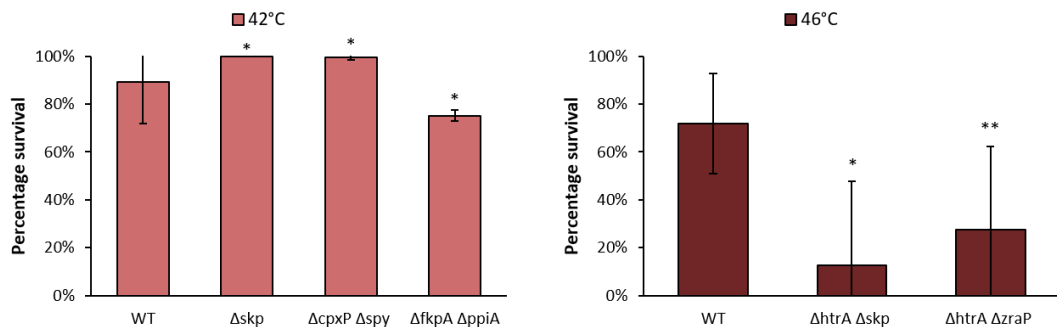
Figure 3.12 Susceptibility of STM SL1344 WT and mutant strains to 42°C and 46°C. STM SL1344 WT and mutant strains were tested for their sensitivity to heat using spot plate assays. Percentage survival was calculated by comparing the viable count of strains exposed to stress, to the viable count of strains grown at 37°C. Of all strains tested, only mutant strains displaying significantly increased sensitivity are included in the figure. Significant differences to STM SL1344 WT are indicated by * ($P < 0.05$) and ** ($P < 0.01$), Student's t-test, minimum n = 3. Error bars indicate standard deviation.

3.3.3.3 FkpA, SurA and ZraP contribute to *S.* Typhimurium persistence against hydrogen peroxide.

Disc diffusion assays carried out using 30% hydrogen peroxide (figure 3.13) demonstrated that FkpA, SurA and ZraP play a role in the protection of STM SL1344 against hydrogen peroxide. Both Δ*fkpA* and Δ*fkpA* Δ*ppiAD,* as well as the quadruple mutant Δ*fkpA* Δ*ppiAD* Δ*surA* are significantly more susceptible to hydrogen peroxide compared to the WT (P < 0.05). All tested strains with a *surA* deletion, including Δ*surA*, Δ*spy* Δ*surA*, Δ*surA* Δ*zraP*, and Δ*ppiAD* Δ*surA*, demonstrate significantly increased sensitivity to hydrogen peroxide compared to the WT (P < 0.05-0.01). All tested strains with a *zraP* deletion, including Δ*zraP*, Δ*htrA* Δ*zraP*, Δ*skp* Δ*zraP*, Δ*surA* Δ*zraP*, and Δ*cpxP* Δ*spy* Δ*zraP*, demonstrate significantly increased sensitivity to hydrogen peroxide compared to the WT (P < 0.05-0.01). Of all the tested double, triple and quadruple mutants that displayed increased sensitivity to hydrogen peroxide, none were significantly more sensitive to the Δ*fkpA*, Δ*surA*, or Δ*zraP* mutants, suggesting that their sensitivity is the result of the deletion of one or more of these three chaperones. For a full overview of all strains tested for susceptibility to hydrogen peroxide, see figure E8.

Figure 3.13 Susceptibility of STM SL1344 WT and mutant strains to hydrogen peroxide. SL1344 WT and mutant strains were screened for sensitivity to hydrogen peroxide using disc diffusion assays. The zones of inhibition of WT and nineteen mutant strains have been calculated in mm^2 (table 3.2), and those strains demonstrating significantly increased sensitivity to the tested compounds have been included in the figure, the level of WT inhibition included for comparison. Significant differences to STM SL1344 WT are indicated by * (P < 0.05) and ** (P < 0.01), Student's t-test assuming equal variance, n = 3. Error bars indicate standard deviation.

3.3.3.4 Periplasmic chaperones do not appear to be involved in the protection against hydroxyurea.

To determine the involvement of periplasmic chaperones in the protection against hydroxyurea, disc diffusion assays carried out using 1 M hydroxyurea (figure 3.14). The data collected from these assays are inconclusive. Although increased sensitivity to hydroxyurea was recorded for the single mutant Δ*htrA* (P < 0.01), none of the tested double mutants carrying an *htrA* deletion displayed an increased sensitivity. The single mutant Δ*zraP*, and the double mutant Δ*surA* Δ*zraP* appeared more sensitive compared to the WT (P < 0.05), but other double and triple mutants carrying a *zraP* deletion did not confirm this phenotype. The

Figure 3.14 Susceptibility of STM SL1344 WT and mutant strains to hydroxyurea. SL1344 WT and mutant strains were screened for sensitivity to hydroxyurea using disc diffusion assays. The zones of inhibition of WT and nineteen mutant strains have been calculated in mm^2 (table 3.2), and those strains demonstrating significantly increased sensitivity to the tested compounds have been included in the figure, the level of WT inhibition included for comparison. Significant differences to STM SL1344 WT are indicated by * (P < 0.05) and ** (P < 0.01), Student's t-test assuming equal variance, n = 3. Error bars indicate standard deviation.

quadruple mutant Δ*fkpA* Δ*ppiAD* Δ*surA* may be significantly more sensitive to hydroxyurea than the WT (P < 0.05), but as the deletion of the individual genes do not appear to affect its sensitivity, further experiments are required to confirm this phenotype. For a full overview of all strains tested for susceptibility to hydroxyurea see figure E9.

3.3.3.5 Skp and SurA contribute to the survival of *S.* Typhimurium when exposed to nalidixic acid.

To determine the involvement of periplasmic chaperones in the protection against nalidixic acid, disc diffusion assays were carried out using 10mM nalidixic acid, and sensitivity spot plate assays were carried out using 1µg/mL nalidixic acid (approximately 4-5µM)(figure 3.15).

The disc diffusion assays demonstrated an increased sensitivity to nalidixic acid for the single mutants Δ*skp* and Δ*surA* compared to the WT (P < 0.01), and all subsequently tested double, triple and quadruple mutants carrying either a *skp* or *surA* also showed significantly increased susceptibility to nalidixic acid compared to the WT (P < 0.01), suggesting that both Skp and SurA are involved in the protection of STM SL1344 against nalidixic acid. These phenotypes were confirmed by sensitivity spot plate assays, which demonstrated a significant reduction in percentage survival for Δ*skp* and Δ*surA* when grown in the presence of nalidixic acid compared to the WT (P < 0.01). The disc diffusion assays also suggested an increased sensitivity to nalidixic acid for the triple mutant Δ*cpxP* Δ*spy* Δ*zraP* compared to the WT (P < 0.05), however this phenotype was not confirmed by sensitivity spot plate assays, where the percentage survival of the triple mutant was reduced by only 0.1% compared to the WT (94.2% survival *versus* 94.3% survival respectively). Furthermore, in addition to the quadruple mutant Δ*fkpA* Δ*ppiAD* Δ*surA*, the triple mutant Δ*fkpA* Δ*ppiAD* appears to be significantly affected by nalidixic acid when tested on disc diffusion plates (P < 0.01), whereas the individual deletions do not affect sensitivity. Sensitivity spot plate assays have not been carried out for these strains, so further analysis is required to confirm this phenotype. For a full overview of all strains tested for susceptibility to nalidixic acid see figures E5 and E10.
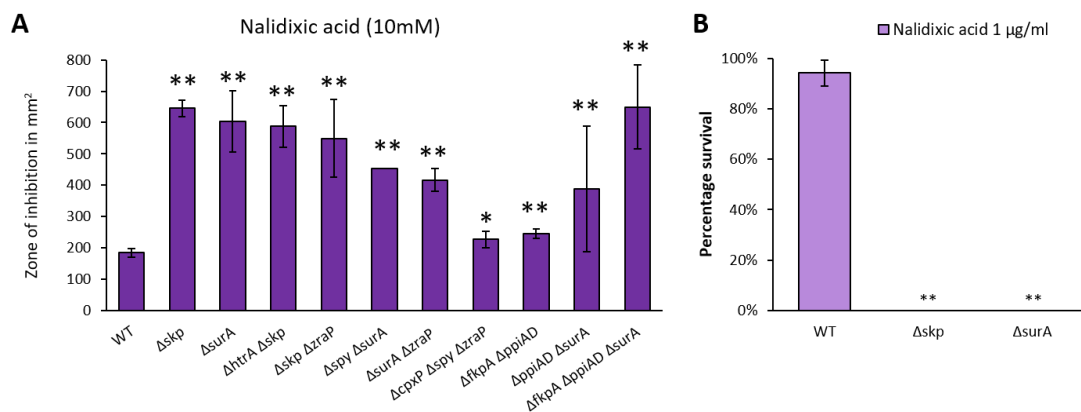
Figure 3.15 Susceptibility of STM SL1344 WT and mutant strains to nalidixic acid. SL1344 WT and mutant strains were screened for sensitivity to nalidixic acid using disc diffusion assays **(A)** and spot plate assays **(B)**. The zones of inhibition of WT and nineteen mutant strains have been calculated in mm^2 (table 3.2). Percentage survival was calculated by comparing the viable count of strains exposed to stress, to the viable count of strains grown on plain LB agar. Those strains demonstrating significantly increased sensitivity to the tested compounds have been included in the figure, the level of WT inhibition included for comparison. Significant differences to STM SL1344 WT are indicated by * (P < 0.05) and ** (P < 0.01), Student's t-test assuming equal variance, n = 3. Error bars indicate standard deviation.

3.3.3.6 FkpA, PpiAD, SurA, Skp and ZraP contribute to the survival of *S.* Typhimurium during exposure to penicillin G.

Disc diffusion assays carried out using 10mM penicillin G (figure 3.16) suggest that FkpA, PpiAD, Skp, SurA and ZraP play a role in the protection of STM SL1344 against penicillin G. The single mutants Δ*fkpA* and Δ*surA*, and the double mutant Δ*ppiAD* are more susceptible to penicillin G than the WT (P < 0.01), and so are the single mutants Δ*skp* and Δ*zraP* (P < 0.01). All tested double, triple and quadruple mutant strains carrying a deletion of *fkpA, PpiAD* and/or *surA* are significantly more affected by penicillin G than the WT strain (P < 0.01). All tested double mutant strains carrying a deletion of either *skp* or *zraP* are also significantly more susceptible to penicillin G than the WT strain (P < 0.05 – 0.01), but they are not significantly more susceptible than the single deletion strain, suggesting that the increased sensitivity to penicillin G is the result of the deletion of either *skp* or *zraP*. For a full overview of all strains tested for susceptibility to penicillin G see figure E11.
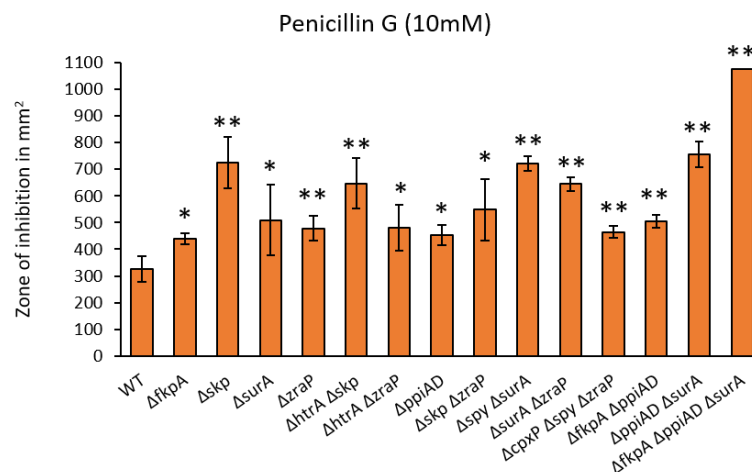
Figure 3.16 Susceptibility of STM SL1344 WT and mutant strains to penicillin G. SL1344 WT and mutant strains were screened for sensitivity to penicillin using disc diffusion assays. The zones of inhibition of WT and nineteen mutant strains have been calculated in mm^2 (table 3.2), and those strains demonstrating significantly increased sensitivity to the tested compounds have been included in the figure, the level of WT inhibition included for comparison. Significant differences to STM SL1344 WT are indicated by * (P < 0.05) and ** (P < 0.01), Student's t-test assuming equal variance, n = 3. Error bars indicate standard deviation.

3.3.3.7 SurA contributes to the survival of *S.* Typhimurium during phosphomycin exposure; ZraP may also be involved.

To determine the involvement of periplasmic chaperones in the protection against phosphomycin, disc diffusion assays were carried out using 10mM phosphomycin, and sensitivity spot plate assays were carried out using 50ng/mL phosphomycin (approximately

0.3 μM)(figure 3.17). The disc diffusion assay suggests that the single mutant Δ*surA* is significantly more susceptible to phosphomycin than the WT strain ($P < 0.01$), and this phenotype is confirmed by the sensitivity spot plate assay ($P < 0.05$). All tested double, triple and quadruple deletion mutants carrying a *surA* deletion are also significantly more sensitive to phosphomycin compared to the WT ($P < 0.01$). The tested double and triple deletion mutants are not significantly more susceptible than the Δ*surA* strain, but the quadruple Δ*fkpA* Δ*ppiAD* Δ*surA* strain is significantly more affected ($P < 0.01$), suggesting that FkpA and PpiAD may play a minor role in the protection of the outer membrane in the presence of phosphomycin. Another chaperone that may be involved in the protection against phosphomycin is ZraP. Disc diffusion assays suggest that the Δ*zraP* strain is more susceptible to phosphomycin than the WT ($P < 0.05$), and this increased susceptibility was also demonstrated using disc diffusion assays for the double deletion strains Δ*htrA* Δ*zraP*, Δ*skp* Δ*zraP*, and Δ*surA* Δ*zraP* ($P < 0.05 - 0.01$). However, both the disc diffusion assays and susceptibility spot plate assays show that the triple deletion mutant Δ*cpxP* Δ*spy* Δ*zraP* is not more susceptible than the WT, raising suspicion regarding the involvement of ZraP in the protection against phosphomycin. Further investigation is required to clarify the role of ZraP. The disc diffusion assay results for both Δ*htrA* Δ*skp*, and Δ*fkpA* Δ*ppiAD* require further investigation. Both strains demonstrate an increased sensitivity to phosphomycin compared to the WT ($P < 0.05$), but none of the individual genes appear to be essential. To determine their exact role in the protection against phosphomycin, further studies are required. For a full overview of all strains tested for susceptibility to phosphomycin see figures E5 and E12.
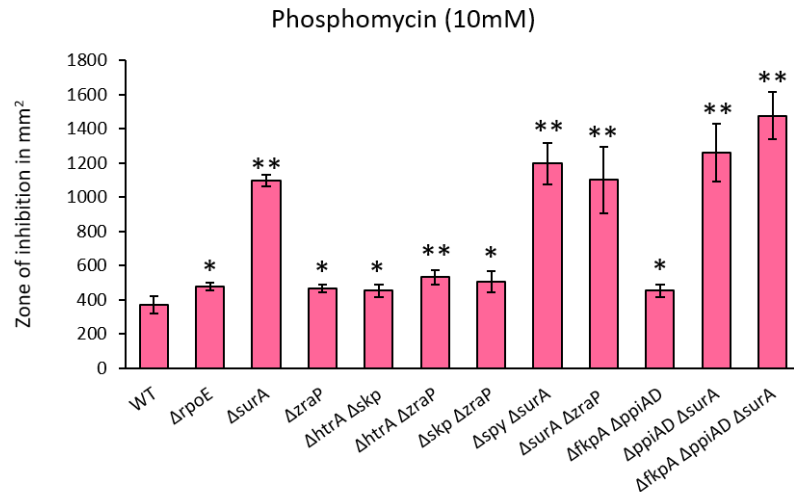
Figure 3.17 Susceptibility of STM SL1344 WT and mutant strains to phosphomycin. SL1344 WT and mutant strains were screened for sensitivity to phosphomycin using disc diffusion assays. The zones of inhibition of WT and nineteen mutant strains have been calculated in mm^2 (table 3.2), and those strains demonstrating significantly increased sensitivity to the tested compounds have been included in the figure, the level of WT inhibition included for comparison. Significant differences to STM SL1344 WT are indicated by * ($P < 0.05$) and ** ($P < 0.01$), Student's t-test assuming equal variance, n = 3. Error bars indicate standard deviation.

3.3.3.8 Skp and SurA are involved in the protection of *S.* Typhimurium against polymyxin B exposure; ZraP may contribute.

To determine the involvement of periplasmic chaperones in the protection against polymyxin B, disc diffusion assays were carried out using 1mM polymyxin B, sensitivity spot plate assays were carried out using 100ng/mL polymyxin B (approximately 0.75 µM)(figure 3.18). The disc diffusion assay suggests that the single mutants Δ*skp* and Δ*surA* are significantly more susceptible to phosphomycin than the WT strain ($P < 0.01$ and $P < 0.05$ respectively). All tested double, triple and quadruple deletion strains lacking either *skp* or *surA* also demonstrate increased sensitivity to polymyxin B ($P < 0.01$). These phenotypes are confirmed by the sensitivity spot assays, which demonstrate an increased sensitivity for mutant strains carrying a Δ*skp* or Δ*surA* ($P < 0.01$). The disc diffusion assays also suggest a role for ZraP in the protection against polymyxin B, as both the single deletion strain Δ*zraP* and all tested double and triple deletion strains demonstrate increased sensitivity to polymyxin B compared to the WT ($P < 0.05$ -0.01).

However, the susceptibility spot assays do not confirm this phenotype for any of the *zraP* deletion strains, but rather suggest there is no significant difference. To clarify the contribution of ZraP to the protection of STM SL1344 against polymyxin B, further

investigation is required. ZraP is not the only protein that shows inconsistency between the susceptibility screens; whereas the disc diffusion assays suggest significant susceptibility to polymyxin B for Δ*cpxP* and Δ*fkpA* Δ*ppiAD* (P < 0.01 and P < 0.05 respectively), these phenotypes are not confirmed by the susceptibility spot plate assays. Furthermore, whereas the susceptibility spot plate assays suggest a reduced percentage survival for the single mutant strain Δ*htrA* (P < 0.05), this phenotype is not confirmed by the disc diffusion assays. For a full overview of all strains tested for susceptibility to polymyxin B, see figures E3 and E13.
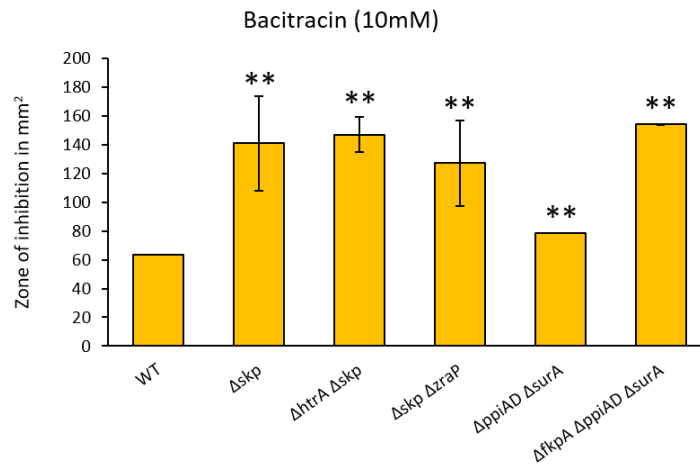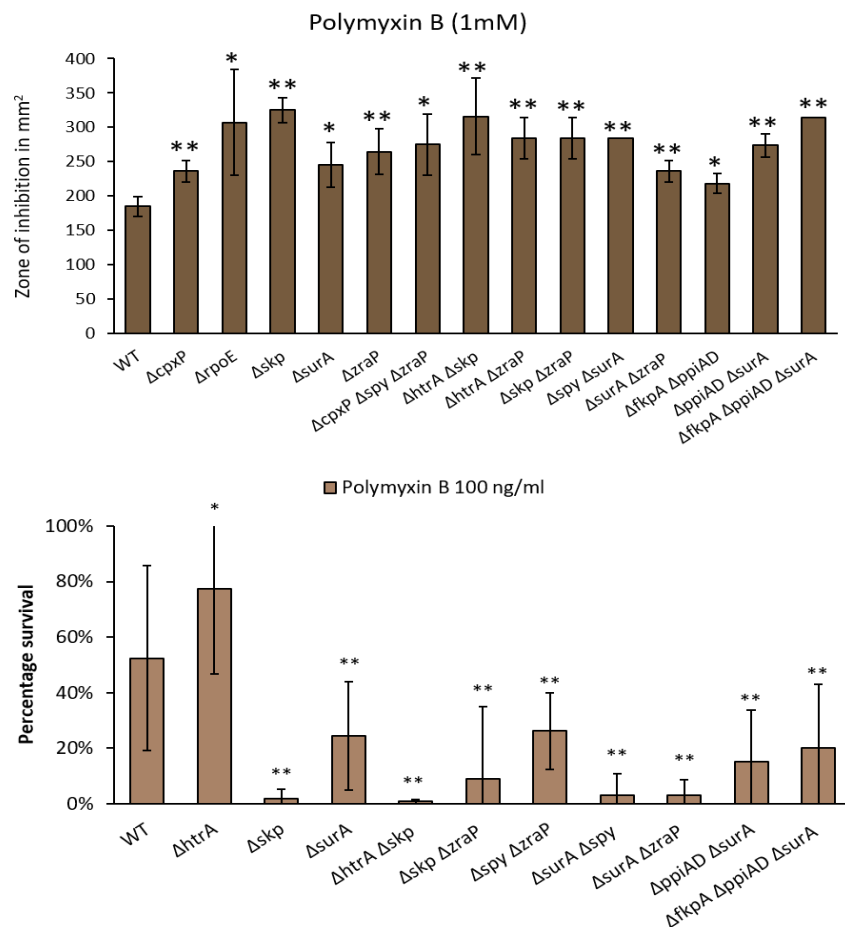

Figure 3.18 Susceptibility of STM SL1344 WT and mutant strains to polymyxin B. SL1344 WT and mutant strains were screened for sensitivity to polymyxin B using disc diffusion assays **(A)** and spot plate assays **(B)**. The zones of inhibition of WT and nineteen mutant strains have been calculated in mm^2 (table 3.2). Percentage survival was calculated by comparing the viable count of strains exposed to stress, to the viable count of strains grown on plain LB agar. Those strains demonstrating significantly increased sensitivity to the tested compounds have been included in the figure, the level of WT inhibition included for comparison. Significant differences to STM SL1344 WT are indicated by * (P < 0.05) and ** (P < 0.01), Student's t-test assuming equal variance, n = 3. Error bars indicate standard deviation.

3.3.3.9 Periplasmic chaperones do not appear to be involved in the protection against spermidine.

To determine the involvement of periplasmic chaperones in the protection against phosphomycin, disc diffusion assays were carried out using 10mM spermidine, and sensitivity spot plate assays were carried out using 6mM spermidine (figure 3.19). Although the sensitivity spot plate assays suggested a significantly reduced percentage survival for Δ*spy* and Δ*zraP* compared to the WT when exposed to 6mM spermidine, these phenotypes were not confirmed by the disc diffusion assays. The latter assays suggested that none of the tested strains were more susceptible to 10mM spermidine than the WT, indicating that the periplasmic chaperones of interest to this study may not be involved in the protection against spermidine. For a full overview of all strains tested for susceptibility to spermidine see figures E6 and E14.
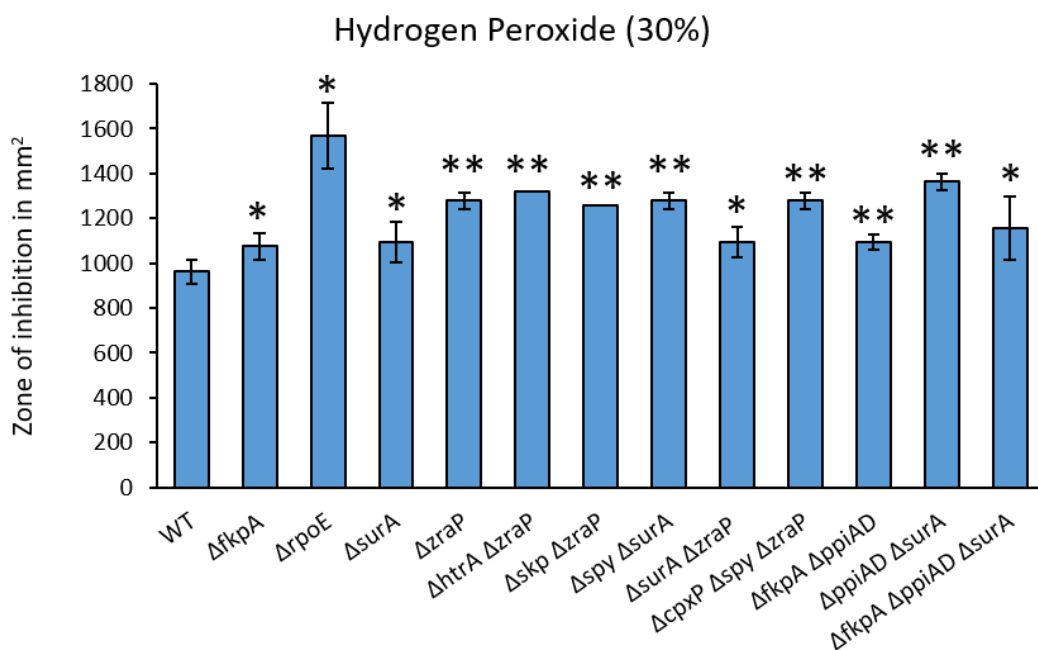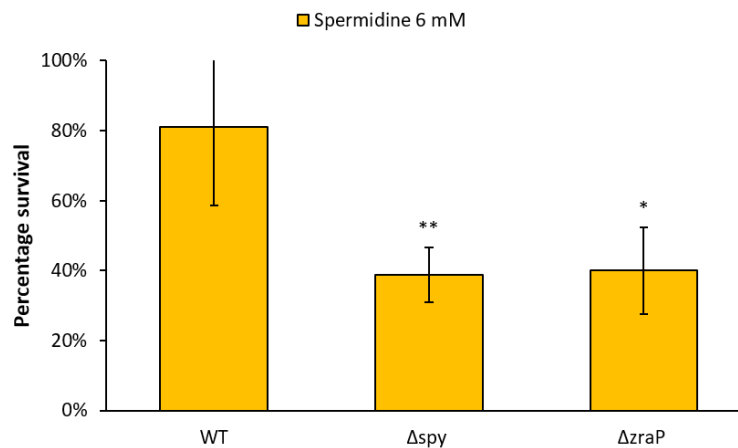

Figure 3.19 Susceptibility of STM SL1344 WT and mutant strains to spermidine. SL1344 WT and mutant strains were screened for sensitivity to spermidine using disc diffusion assays. The zones of inhibition of WT and nineteen mutant strains have been calculated in mm^2 (table 3.2), and those strains demonstrating significantly increased sensitivity to the tested compounds have been included in the figure, the level of WT inhibition included for comparison. Significant differences to STM SL1344 WT are indicated by * ($P < 0.05$) and ** ($P < 0.01$), Student's t-test assuming equal variance, n = 3. Error bars indicate standard deviation.

3.3.3.10 Skp and SurA contribute to *S.* Typhimurium survival during exposure to vancomycin.

To determine the involvement of periplasmic chaperones in the protection against phosphomycin, disc diffusion assays were carried out using 65mg/ml vancomycin, and sensitivity spot plate assays were carried out using 65μg/ml vancomycin (figure 3.20). The disc diffusion assays demonstrated that the single deletion mutant strains Δ*skp* and Δ*surA*

are significantly more susceptible to vancomycin than the WT (P < 0.01), and all the tested double, triple and quadruple deletion mutants lacking either *skp* or *surA* were also significantly affected (P < 0.01). These phenotypes were confirmed by the sensitivity spot plate assays, which also demonstrated a significantly reduced percentage survival for all the strains carrying either Δ*skp* or Δ*surA* (P < 0.01). Furthermore, the sensitivity spot plate assays suggested a reduced percentage survival in the presence of vancomycin for Δ*fkpA*, Δ*htrA*, Δ*fkpA* Δ*ppiAD*, and Δ*htrA* Δ*zraP* at P < 0.05 and for Δ*zraP* at P < 0.01. However, these phenotypes have not been confirmed by the disc diffusion assays, and they require further investigation to determine their involvement in the protection of STM SL1344 against vancomycin. For a full overview of all strains tested for susceptibility to vancomycin see figures E4 and E15.
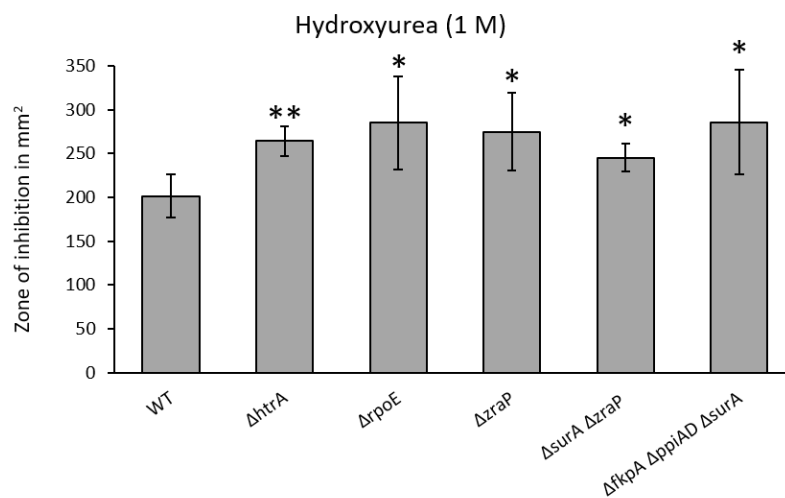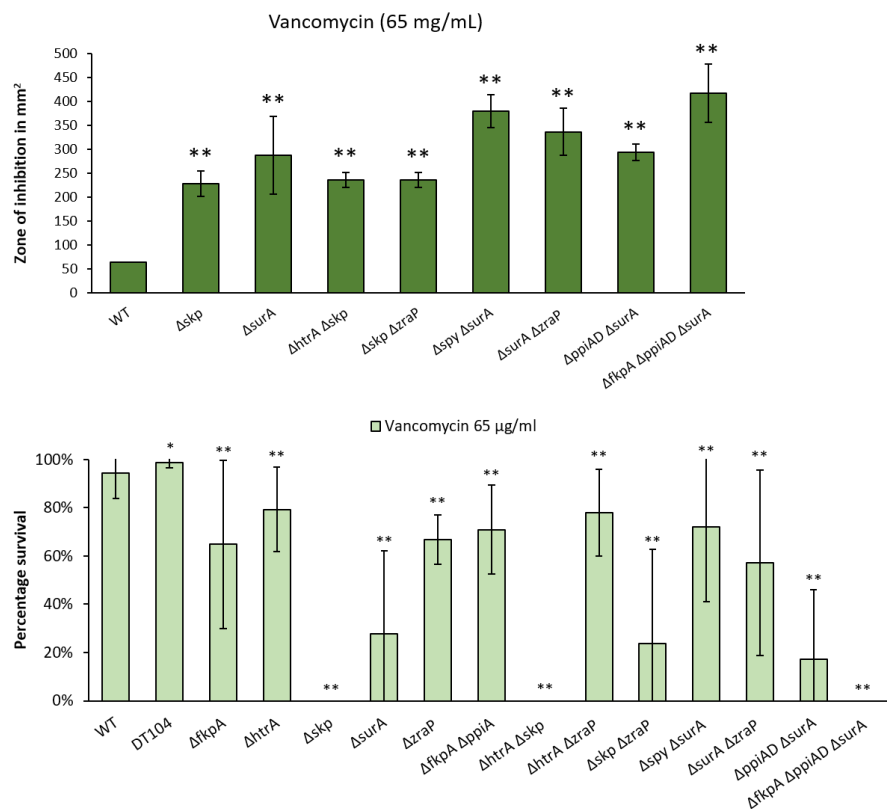

Figure 3.20 Susceptibility of STM SL1344 WT and mutant strains to vancomycin B. SL1344 WT and mutant strains were screened for sensitivity to vancomycin using disc diffusion assays **(A)** and spot plate assays **(B)**. The zones of inhibition of WT and nineteen mutant strains have been calculated in mm^2 (table 3.2). Percentage survival was calculated by comparing the viable count of strains exposed to stress, to the viable count of strains grown on plain LB agar. Those strains demonstrating significantly increased sensitivity to the tested compounds have been included in the figure, the level of WT inhibition included for comparison. Significant differences to STM SL1344 WT are indicated by * (P < 0.05) and ** (P < 0.01), Student's t-test assuming equal variance, n = 3. Error bars indicate standard deviation.

Table 3.2 Overview results of susceptibility spot plate assays – heat, polymyxin B, and vancomycin.

Strain	42ºC			46ºC			Polymyxin B (100ng/mL)			Vancomycin (65µg/mL)		
	Average	stdev	T-test	Average	stdev	T-test	Average	stdev	T-test	Average	stdev	T-test
WT	89.3%	17.4%		71.9%	20.9%		52.4%	33.2%		94.4%	10.7%	
DT104	86.6%	15.5%	0.395	88.0%	13.7%	0.121	40.0%	22.2%	0.242	98.8%	2.4%	**0.044**
bongori	89.7%	9.3%	0.484	79.4%	31.4%	0.358	54.1%	27.8%	0.462	76.9%	34.2%	0.192
ΔcpxP	98.9%	2.2%	0.059	83.9%	11.7%	0.178	43.2%	28.3%	0.229	81.4%	28.8%	0.110
ΔfkpA	98.0%	4.0%	0.083	77.1%	15.8%	0.352	34.2%	25.4%	0.068	64.8%	34.9%	**0.017**
ΔhtrA	88.8%	11.7%	0.364	45.7%	50.5%	0.181	77.3%	30.5%	**0.046**	79.3%	17.4%	**0.018**
Δskp	100.0%	0.0%	**0.042**	89.7%	19.1%	0.084	1.9%	3.3%	**0.000**	0.0%	0.0%	**0.000**
Δspy	79.3%	16.4%	0.171	77.8%	13.0%	0.322	43.2%	33.1%	0.308	91.9%	7.4%	0.327
ΔsurA	88.3%	13.3%	0.337	71.4%	19.1%	0.487	24.4%	19.6%	**0.023**	27.6%	34.4%	**0.001**
ΔzraP	92.5%	4.3%	0.301	81.8%	10.9%	0.216	38.4%	28.7%	0.220	66.8%	10.2%	**0.000**
ΔcpxPΔyncJ	98.0%	4.0%	0.084	89.5%	7.4%	0.114	39.7%	41.4%	0.252	90.3%	12.1%	0.246
ΔcpxPΔspy	99.5%	1.0%	**0.050**	90.1%	9.2%	0.080	45.0%	24.0%	0.339	100.0%	0.0%	0.155
ΔcpxPΔzraP	94.3%	8.4%	0.299	89.4%	18.3%	0.150	41.3%	37.1%	0.172	87.9%	25.1%	0.177
ΔfkpAΔppiA	75.2%	2.3%	**0.015**	80.5%	11.6%	0.276	63.1%	33.4%	0.281	70.9%	18.5%	**0.020**
ΔfkpAΔppiD	84.7%	14.8%	0.323	82.5%	5.8%	0.200	59.7%	31.8%	0.345	97.2%	3.8%	0.160
ΔhtrAΔskp	94.4%	9.6%	0.052	12.5%	35.4%	**0.006**	0.8%	0.8%	**0.000**	0.0%	0.0%	**0.000**
ΔhtrAΔzraP	90.1%	13.6%	0.484	27.4%	34.7%	**0.023**	33.5%	30.6%	0.098	77.9%	18.1%	**0.027**
ΔppiAD	83.8%	8.0%	0.279	86.6%	18.1%	0.163	57.3%	37.5%	0.397	72.0%	34.1%	0.110
ΔskpΔzraP	86.2%	15.5%	0.381	84.0%	19.1%	0.212	8.9%	26.2%	**0.000**	23.6%	39.1%	**0.000**
ΔspyΔyncJ	92.9%	14.3%	0.363	86.4%	19.3%	0.230	29.9%	21.2%	0.104	89.8%	12.0%	0.219
ΔspyΔzraP	76.0%	12.0%	0.095	81.6%	14.6%	0.238	26.1%	13.7%	**0.001**	88.6%	23.9%	0.196
ΔsurAΔspy	94.7%	9.0%	0.288	73.4%	5.3%	0.446	3.0%	7.7%	**0.000**	71.9%	30.9%	**0.008**
ΔsurAΔzraP	91.6%	15.1%	0.412	85.8%	14.7%	0.159	3.1%	5.4%	**0.000**	57.2%	38.3%	**0.003**
ΔyncJΔzraP	90.1%	4.8%	0.451	91.9%	14.0%	0.107	58.7%	39.4%	0.369	92.1%	9.9%	0.348
ΔcpxPΔzraPΔspy	83.0%	13.5%	0.267	80.4%	14.5%	0.263	31.9%	38.2%	0.140	84.4%	28.1%	0.265
ΔfkpAΔppiAD	92.1%	9.5%	0.385	80.0%	7.3%	0.245	54.5%	32.1%	0.456	72.4%	37.7%	0.108
ΔsurAΔppiAD	92.3%	13.5%	0.304	79.5%	34.3%	0.354	15.1%	18.8%	**0.000**	17.1%	28.9%	**0.000**
ΔsurAΔfkpAΔppiAD	95.4%	9.2%	0.264	68.5%	36.1%	0.435	20.2%	22.7%	**0.039**	0.0%	0.0%	**0.000**

Table 3.2 Overview results of susceptibility spot plate assays – heat, polymyxin B, and vancomycin.

Strain	Nalidixic acid			Spermidine			Phosphomycin			Indole		
	Average	stdev	T-test	Average	stdev	T-test	Average	stdev	T-test	Average	stdev	T-test
WT	94.3%	5.05%		81.0%	22.4%		92.31%	13.32%		82.39%	16.33%	
ΔcpxP		no data		82.0%	20.4%	0.4733		no data		87.89%	20.97%	0.3376
Δskp	0.0%	0.00%	**0.0000**	87.2%	12.7%	0.2817	82.02%	15.57%	0.2168	99.66%	0.83%	**0.0136**
Δspy		no data		38.9%	7.8%	**0.0090**		no data		45.80%	11.97%	**0.0057**
ΔsurA	0.0%	0.00%	**0.0000**	66.1%	33.6%	0.1937	50.49%	16.79%	**0.0139**	44.80%	41.83%	**0.0337**
ΔzraP		no data		40.0%	12.3%	**0.0117**		no data		41.79%	9.42%	**0.0029**
ΔcpxPΔzraPΔspy	94.2%	10.04%	0.1125	74.3%	24.7%	0.3167	84.41%	9.41%	0.2244	80.75%	9.75%	0.4185

Table 3.4 Overview results of disc diffusion assays - bacitracin, hydrogen peroxide, and hydroxyurea.

Strain	Bacitracin (10mM)			Hydrogen Peroxide (30%)			Hydroxyurea (30%)		
	Average	stdev	T-test	Average	stdev	T-test	Average	stdev	T-test
WT	63.6	0.0		962.6	55.0		201.6	25.1	
ΔcpxP	63.6	0.0	0.5000	1037.0	33.1	0.0580	156.0	44.0	0.0981
ΔfkpA	63.6	0.0	0.5000	1075.7	58.1	**0.0352**	185.4	27.2	0.2459
ΔhtrA	63.6	0.0	0.5000	856.9	91.1	0.0792	264.2	16.8	**0.0043**
ΔrpoE	63.6	0.0	0.5000	1569.2	147.5	**0.0010**	285.1	53.1	**0.0301**
Δskp	140.8	32.6	**0.0040**	890.4	30.4	0.0581	119.6	11.3	**0.0027**
Δspy	63.6	0.0	0.5000	890.9	61.7	0.1026	155.2	90.1	0.1933
ΔsurA	63.6	0.0	0.5000	1095.9	90.2	**0.0456**	246.4	41.8	0.0945
ΔyncJ	63.6	0.0	0.5000	908.4	53.4	0.1439	193.5	29.0	0.3623
ΔzraP	63.6	0.0	0.5000	1277.8	36.7	**0.0007**	274.9	44.2	**0.0323**
ΔhtrAΔskp	146.9	12.2	**0.0001**	1056.6	67.1	0.0659	154.2	87.3	0.1802
ΔhtrAΔzraP	63.6	0.0	0.5000	1320.3	0.0	**0.0002**	157.6	60.9	0.1439
ΔppiAD	63.6	0.0	0.5000	890.9	61.7	0.1026	237.2	42.2	0.1373
ΔskpΔzraP	127.2	29.8	**0.0071**	1256.6	0.0	**0.0005**	153.9	0.0	**0.0129**
ΔspyΔsurA	68.6	8.6	0.1870	1277.8	36.7	**0.0007**	209.7	15.0	0.3217
ΔsurAΔzraP	73.6	8.6	0.0581	1095.4	67.1	**0.0286**	245.3	15.9	**0.0334**
ΔcpxPΔspyΔzraP	63.6	0.0	0.5000	1277.8	36.7	**0.0007**	230.6	68.0	0.2867
ΔfkpAΔppiAD	63.6	0.0	0.5000	1094.8	34.0	**0.0124**	229.1	53.4	0.2409
ΔppiADΔsurA	78.6	0.1	**0.0000**	1363.7	37.6	**0.0003**	236.7	30.8	0.1026
ΔfkpAΔppiADΔsurA	154.0	0.1	**0.0000**	1156.9	141.5	**0.0417**	285.6	59.7	**0.0404**

Table 3.5 Overview results of disc diffusion assays - nalidixic acid, Penicillin G, and phosphomycin.

Strain	Nalidixic Acid (10mM)			Penicillin G (10mM)			Phosphomycin (10mM)		
	Average	stdev	T-test	Average	stdev	T-test	Average	stdev	T-test
WT	184.8	14.1		325.9	49.4		369.9	51.4	
ΔcpxP	228.6	44.9	0.0945	440.1	21.3	**0.0121**	358.1	38.1	0.3890
ΔfkpA	219.4	39.4	0.1151	440.1	21.3	**0.0121**	404.2	41.7	0.2084
ΔhtrA	228.6	47.6	0.0945	391.9	20.4	0.0506	284.1	29.8	**0.0323**
ΔrpoE	209.7	15.0	0.0506		No data		478.0	22.2	**0.0167**
Δskp	645.6	25.8	**0.0000**	724.9	97.7	**0.0002**	427.8	21.3	0.0759
Δspy	209.7	15.0	0.0506	357.6	19.5	0.1743	293.7	17.7	**0.0343**
ΔsurA	604.0	97.9	**0.0004**	509.5	132.1	0.1295	1094.8	34.0	**0.0000**
ΔyncJ	163.6	45.4	0.2338	371.0	72.3	0.2108	293.7	17.7	**0.0343**
ΔzraP	209.7	15.0	0.0506	478.6	45.3	**0.0086**	465.2	22.2	**0.0237**
ΔhtrAΔskp	588.0	66.2	**0.0001**	647.7	95.2	**0.0025**	452.9	37.7	**0.0456**
ΔhtrAΔzraP	201.6	25.1	0.1870	480.7	87.1	**0.0267**	531.5	40.8	**0.0074**
ΔppiAD	273.1	125.9	0.1420	452.9	37.7	**0.0127**	314.7	31.4	0.0945
ΔskpΔzraP	549.5	124.1	**0.0018**	549.0	115.6	**0.0167**	505.3	61.4	**0.0212**
ΔspyΔsurA	452.5	0.2	**0.0000**	722.8	27.7	**0.0000**	1196.7	122.5	**0.0001**
ΔsurAΔzraP	416.0	36.1	**0.0002**	645.6	25.8	**0.0005**	1100.1	192.7	**0.0008**
ΔcpxPΔspyΔzraP	227.5	26.7	**0.0334**	465.2	22.2	**0.0066**	403.7	20.4	0.1743
ΔfkpAΔppiAD	245.3	15.9	**0.0039**	504.2	23.1	**0.0030**	452.9	37.7	**0.0456**
ΔppiADΔsurA	388.2	199.3	**0.0042**	755.3	48.7	**0.0003**	1260.3	168.9	**0.0002**
ΔfkpAΔppiADΔsurA	649.8	133.8	**0.0007**	1075.2	0.0	**0.0000**	1477.1	140.2	**0.0043**

Table 3.6 Overview results of disc diffusion assays - polymyxin B, spermidine, and vancomycin.

Strain	Polymyxin B (1mM)			Spermidine (6mM)			Vancomycin 65μgmL		
	Average	stdev	T-test	Average	stdev	T-test	Average	stdev	T-test
WT	184.8	14.1		63.6	0.0		63.6	0.0	
ΔcpxP	236.1	15.9	**0.0066**	63.6	0.0	0.5000	63.6	0.0	0.5000
ΔfkpA	185.9	37.4	0.5000	63.6	0.0	0.5000	68.6	8.6	0.1870
ΔhtrA	184.8	14.1	0.5000	63.6	0.0	0.5000	63.6	0.0	0.5000
ΔrpoE	307.1	76.8	**0.0219**	78.5	0.0	**0.0000**	90.1	20.0	**0.0334**
Δskp	324.9	18.6	**0.0002**	63.6	0.0	0.5000	227.5	26.7	**0.0001**
Δspy	177.2	23.6	0.3217	63.6	0.0	0.5000	63.6	0.0	0.5000
ΔsurA	245.8	32.6	**0.0176**	63.6	0.0	0.5000	287.2	81.7	**0.0014**
ΔyncJ	210.7	39.8	0.1743	63.6	0.0	0.5000	63.6	0.0	0.5000
ΔzraP	264.7	32.6	**0.0079**	63.6	0.0	0.5000	63.6	0.0	0.5000
ΔhtrAΔskp	315.7	55.8	**0.0057**	63.6	0.0	0.5000	236.1	15.9	**0.0000**
ΔhtrAΔzraP	284.1	29.8	**0.0027**	73.6	8.6	0.0581	63.6	0.0	0.5000
ΔppiAD	201.6	25.1	0.1870	63.6	0.0	0.5000	63.6	0.0	0.5000
ΔskpΔzraP	284.1	29.8	**0.0027**	68.6	8.6	0.1870	236.1	15.9	**0.0000**
ΔspyΔsurA	283.5	0.0	**0.0002**	73.6	8.6	0.0581	380.7	34.6	**0.0000**
ΔsurAΔzraP	236.1	15.9	**0.0066**	78.5	0.0	**0.0081**	336.7	49.0	**0.0001**
ΔcpxPΔspyΔzraP	274.9	44.2	**0.0121**	73.6	8.6	0.0581	63.6	0.0	0.5000
ΔfkpAΔppiAD	218.3	15.0	**0.0237**	63.6	0.0	0.5000	63.6	0.0	0.5000
ΔppiADΔsurA	273.8	16.8	**0.0011**	68.6	8.6	0.1870	293.7	17.7	**0.0000**
ΔfkpAΔppiADΔsurA	314.2	0.0	**0.0001**	63.6	0.0	0.5000	417.0	61.2	**0.0001**

Table 3.7 Sensitivity screens by disc diffusion assays of *S.* Typhimurium SL1344 WT and nineteen deletion mutants. Susceptibility of STM SL1344 WT and mutant strains were analysed by determining the zone of inhibition (mm^2) after approximately 18 hours growth at 37°C. Mutant strain phenotypes were compared to the WT and summarised as no increased sensitivity (-) or increased sensitivity (+). Statistical analysis carried out using Student's t-test assuming equal variance (p<0.05), n = 3.

Compound - concentration	ΔcpxP	ΔfkpA	ΔhtrA	ΔrpoE	Δskp	Δspy	ΔsurA	ΔyncJ	ΔzraP	ΔhtrA Δskp	ΔhtrA ΔzraP	ΔppiAD	Δskp ΔzraP	Δspy ΔsurA	ΔsurA ΔzraP	ΔcpxP Δspy ΔzraP	ΔfkpA ΔppiAD	ΔppiAD ΔsurA	ΔfkpA ΔppiAD ΔsurA
Bacitracin - 10 mM	-	-	-	-	+	-	-	-	-	+	-	-	+	-	-	-	-	+	+
Hydrogen peroxide - 30%	-	+	-	+	-	-	+	-	+	-	+	-	+	+	+	+	+	+	+
hydroxyurea - 1 M	-	-	+	+	-	-	-	-	+	-	-	-	-	-	+	-	-	-	+
Nalidixic acid - 10 mM	-	-	-	-	+	-	+	-	-	+	-	-	+	+	+	+	+	+	+
Penicillin G - 10 mM	-	+	-	-	+	-	-	-	+	+	-	+	+	+	+	+	+	+	+
Phosphomycin - 10 mM	-	-	-	+	-	-	+	-	+	+	+	-	+	+	+	-	+	+	+
Polymyxin B - 1 mM	+	-	-	+	+	-	+	-	+	+	+	-	+	+	+	+	+	+	+
Spermidine - 10 mM	-	-	-	-	-	-	-	-	-	-	-	-	-	-	-	-	-	-	-
Vancomycin - 65 mg/mL	-	-	-	-	+	-	+	-	-	+	-	-	+	+	+	-	-	+	+

STM SL1344 Strains

Table 3.8 Sensitivity screens by spot plate assays of STM SL1344 deletion mutants. Susceptibility of *Salmonella* WT and mutant strains were analysed by determining the percentage survival after approximately 18 hours growth at 37°C. Mutant strain phenotypes were compared to the WT and summarised as no increased sensitivity (-) or increased sensitivity (+). Absence of marker indicates no data were collected. Statistical analysis carried out using Student's t-test assuming equal variance (P < 0.05), minimum n = 3. Abbreviations of compounds tested: nalidixic acid (NDA), phosphomycin (PPM), polymyxin B (PMB), vancomycin (VCM).

Compound - Concentration	ΔcpxP	ΔfkpA	ΔhtrA	Δskp	Δspy	ΔsurA	ΔzraP	ΔcpxP ΔyncJ	ΔcpxP Δspy	ΔcpxP ΔzraP	ΔfkpA ΔppiA	ΔfkpA ΔppiD	ΔhtrA Δskp	ΔhtrA ΔzraP	ΔppiAD	Δskp ΔzraP	Δspy ΔsurA	Δspy ΔyncJ	Δspy ΔzraP	ΔsurA ΔzraP	ΔyncJ ΔzraP	ΔcpxP ΔzraP Δspy	ΔfkpA ΔppiAD	ΔsurA ΔppiAD	ΔfkpA ΔppiAD ΔsurA
42°C - NA	-	-	-	+	-	-	-	-	+	-	+	-	-	-	-	-	-	-	-	-	-	-	-	-	-
46°C - NA	-	-	-	-	-	-	-	-	-	-	-	-	+	+	-	-	-	-	-	-	-	-	-	-	-
Indole - 2 mM	-			+	+	+	+															-			
Nalidixic acid - 1 µg/ml				+		+																-			
Phosphomycin - 50 ng/ml				-		+																-			
Polymyxin B - 100 ng/ml	-	-	+	+	-	+	-	-	-	-	-	-	+	-	-	+	+	-	+	+	-	-	-	+	+
Spermidine - 6 mM	-			-	+	-	+															-			
Vancomycin - 65 µg/ml	-	+	+	+	-	+	+	-	-	-	+	-	+	+	-	+	-	-	+	+	-	-	-	+	+

3.3.4 Carbon starvation assays

Starvation of carbon energy sources is the one of the most common stresses encountered by bacteria in their natural habitat (Spector, 1998). During prolonged periods of carbon starvation, many non-spore-forming bacteria rely on their starvation-stress response (SSR) for survival. The SSR induces major alterations in gene expression, resulting in cells that are not only morphologically and physiologically different, but that are also more resistant to general stress. Unlike the stationary-phase response, the SSR is activated in response to carbon starvation only, and the densities of SSR cells are significantly lower than the densities of typical stationary-phase cells (Spector and Cubitt, 1992; Spector, 1998; Kenyon *et al.*, 2002; Fung *et al.*, 2010). The function of the SSR is both to allow for long-term carbon starvation survival (LTCSS) and to generate carbon-starvation induced cross resistance (CSIXR) to other environmental stresses including pH, oxidative agents, temperature, and antimicrobial agents. In *Salmonella* Typhimurium, the general stress response sigma factor σ^S (chapter 1.4.1) and the envelope stress response sigma factor σ^E (chapter 1.5.1) regulate the expression of several loci activated during the SSR (O'Neal *et al.*, 1994; Seymour *et al.*, 1996; Spector, 1998; Spector *et al.*, 1999; Kenyon *et al.*, 2002). Functional overlap between σ^E and the two-component envelope stress response systems raises the question if these systems are also involved in the SSR. The *Salmonella* σ^E regulon is involved in the SSR-induced cross resistance against heat stress, acidity, and the cationic antimicrobial peptide polymyxin B (Spector *et al.*, 1999; Spector and Kenyon, 2012). In *E. coli*, constitutive activity of σ^E and the Cpx regulon increases resistance of phosphate- and nitrogen-starved cells against the aminoglycoside gentamycin (Moreau, 2014). Also in *E. coli,* the two-component response sensor ZraS is capable of phosphorylating the adaptor protein RssB (chapter 1.4.4.3) *in vitro*, suggesting that the two component system ZraSR may directly interact with σ^S (Yamamoto *et al.*, 2005). Furthermore, in *E. coli* genes expressed under the control of σ^E include the periplasmic chaperones *surA, fkpA* and *skp* (Dartigalongue, Missiakas and Raina, 2001)*.* Considering the importance of these chaperones to general membrane homeostasis and the involvement of σ^E in the SSR, investigation into the contribution of these periplasmic chaperones to the SSR is of interest.
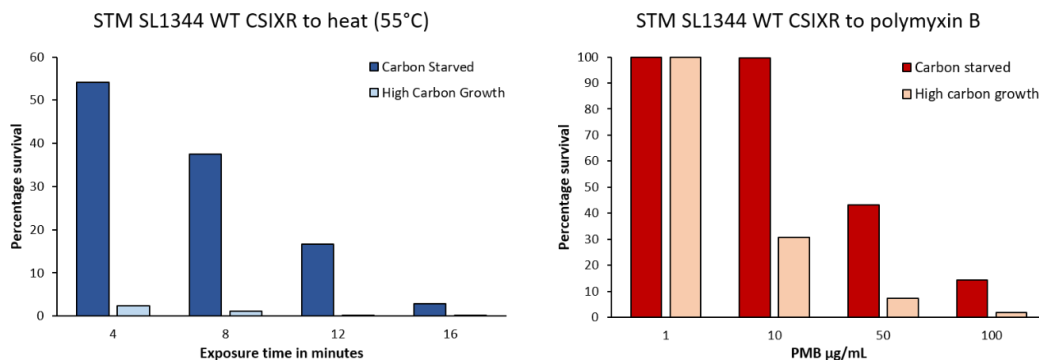
Figure 3.21 Carbon-starved STM SL1344 WT is more resistant to heat-stress and polymyxin B exposure than exponential cells grown in high carbon. Carbon-starvation significantly increases resistance of STM SL1344 WT to heat-stress **(55°)** compared to non-starved cells. As the heat-exposure time interval increases, the percentage survival of both carbon-starved and high-carbon grown cells decreases rapidly. Comparing carbon-starved STM SL1344 WT to cells grown in excess carbon, there is no difference in susceptibility to **polymyxin B** at low concentrations. As the concentration of PMB increases however, the susceptibility of carbon-starved cells is significantly lower than that of high carbon grown cells. The percentage survival of both carbon-starved and high-carbon grown cells decreases significantly as the PMB concentration goes up.

To investigate the involvement of two-component envelope stress responses as well as periplasmic chaperones in the carbon-starvation induced cross-resistance against heat and polymyxin B, CSIXR experiments were carried out according to the protocol described by Kenyon *et al.* (2002). Following their report of significant RpoE involvement in the CSIXR against both stresses, STM SL1344 Δ*rpoE* was used as a benchmark to measure susceptibility against. Prior to CSIXR testing, a series of experiments was carried out to determine the parameters to be tested. For heat resistance, percentage survival of carbon-starved STM SL1344 was tested at a range of exposure times, and for polymyxin B resistance, carbon-starved STM SL1344 was tested at a range of concentrations. The CSIXR to heat graph shown in figure 3.21 demonstrates that carbon starved STM SL1344 cells are significantly more resistant to heat-stress, and that the percentage survival declines rapidly when exposed to 55°C for longer periods of time. Furthermore, the CSIXR to polymyxin B demonstrates that at all tested concentrations above 1μg/mL, carbon starved cells are significantly more resistant than the exponential cells grown in high carbon, and the percentage survival declines as the PMB concentration goes up.

The involvement of periplasmic chaperones and two-component envelope stress response systems in CSIXR against heat (55°C for 16 minutes) and polymyxin B (100μg/mL) was tested by subjecting STM SL1344 mutant strains to CSIXR experiments. In agreement with previously published data by Kenyon *et al.* (2002), figure 3.22 shows that the percentage

survival of Δ*rpoE* (4.5%) is significantly reduced (P=0.01) when exposed to heat compared to the WT (24%). Periplasmic proteins that appear to influence the CSIXR against heat include HtrA and SurA. The percentage survival of both Δ*htrA* and Δ*surA* (0.03% and 2.5% respectively) is significantly reduced compared to the WT when exposed to heat (P=0.01), but there is no significant difference between either Δ*htrA* or Δ*surA* and Δ*rpoE* (student t-test assuming unequal variance). Whereas expression of *htrA* and *surA* is RpoE regulated in *E. coli* (Hiratsu *et al.*, 1995), the expression of *htrA* and *surA* in *Salmonella* Typhimurium is not dependent on RpoE (Kenyon *et al.*, 2002; Lewis *et al.*, 2009), suggesting that the Δ*rpoE* reduction in survival during heat-stress occurs independently of HtrA or SurA levels.

Although the two-component system ZraSR does not appear to be involved in the CSIXR against heat, the percentage survival (6.8%) of the quadruple mutant *baeR*Δ*cpxR*Δ*zraSR* is significantly reduced compared to the WT strain (P=0.05). The observation that carbon-starved Δ*baeR* is significantly more affected (3.7%) by heat than the WT (P=0.01), suggest that the response regulator BaeR may be involved in the CSIXR against heat (figure 3.22).
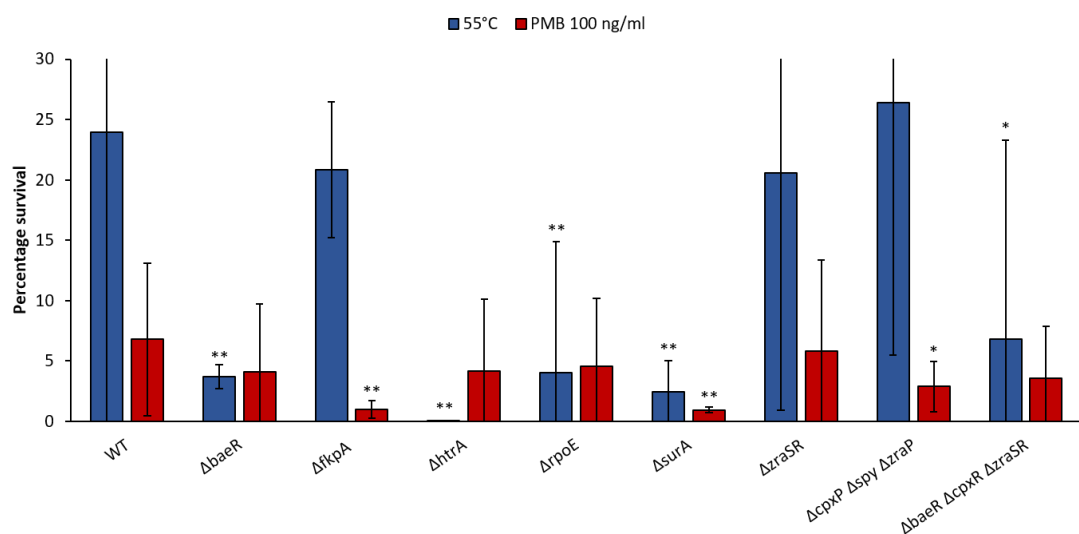
Figure 3.22 CSIXR against heat involves expression of *baeR*, *htrA,* and *surA*; CSIXR against polymyxin B involves expression of *fkpA, surA,* and *cpxPspyzraP*. Survival of 24-hour carbon starved cells following exposure to polymyxin B (100µg/mL) or heat-stress (16 minutes at 55°C). Statistical analysis carried out using Student t-tests, * signifies difference at P=0.05 compared to WT, ** signifies difference at P=0.01 compared to WT.

Unlike previously published data by Kenyon *et al.* (2002), the percentage survival (4.5%) of Δ*rpoE* does not appear to be significantly reduced compared to the WT (6.8%) when exposed to polymyxin B (figure 3.22). Percentage survival of Δ*fkpA* (1%) and Δ*surA* (0.9%) after exposure to polymyxin B are significantly reduced compared to the WT (P=0.01). Furthermore, the percentage survival of the triple knockout strain Δ*cpxP*Δ*spy*Δ*zraP* (2.9%)

also appears to be significantly reduced compared to the WT (P=0.05). These data suggest that that the periplasmic chaperones FkpA, SurA, CpxP, Spy and ZraP may be involved in the CSIXR against polymyxin B.

3.4 Discussion and future work

In this study a physiological approach was used to investigate the contribution of various periplasmic proteins to environmental stresses encountered by *Salmonella* Typhimurium, with the aim to better understand cross-talk among proteins involved in envelope stress response systems and proteins involved in outer membrane biogenesis.

3.4.1 Contribution of periplasmic proteins in the protection against environmental stresses

The antibiotics bacitracin, penicillin and vancomycin interfere with peptidoglycan biogenesis. However, due to the impenetrability of the outer membrane, most Gram negative species are naturally resistant against these agents (Munita and Arias, 2016). Mutation of periplasmic proteins can result in a compromised outer membrane, which in turn can lead to increased susceptibility to antimicrobial agents harmless to the WT strain. Of the nineteen STM SL1344 deletion mutants screened for increased susceptibility to bacitracin, only those carrying a *skp* deletion and the quadruple knock-out strain Δ*fkpA* Δ*ppiAD* Δ*surA* demonstrated increased susceptibility compared to the WT. Bacitracin is a cyclic polypeptide that binds and inactivates C_{55}-isopropenyl pyrophosphate, a membrane carrier molecule required for the transport of peptidoglycan subunits. Compared to Gram positive species, Gram negative species including *Salmonella* and *E. coli* are naturally more resistant against bacitracin, as these molecules struggle to penetrate the outer membrane. In *E. coli*, deletion of *surA* leads to an increased susceptibility to bacitracin, which has been attributed to increased outer membrane permeability due to the decreased levels of the outer membrane proteins LamB, OmpA, OmpC and OmpF (Lazar and Kolter, 1996; Justice *et al.*, 2005). Although *surA* deletion also reduces the level of OmpA, OmpC and OmpF in *Salmonella* (Fardini *et al.*, 2009)*,* the STM SL1344 Δ*surA* mutant is not more sensitive to bacitracin than the WT strain. Interestingly, mutations of the maltoporin LamB result in an increased susceptibility to antibiotics of larger molecular weight (Klebba, Hofnung and Charbit, 1994; Charbit *et al.*, 1998). *Salmonella* Skp has been shown to interact with LamB (Grabowicz, Koren and Silhavy, 2016) whereas Δ*skp* mutants are more susceptible to bacitracin, and in *E. coli*, Δ*surA* mutants both demonstrate reduced levels of LamB and display an increased sensitivity to bacitracin. It is possible that the increased sensitivity to bacitracin reported in

the *Salmonella* Δ*skp* mutants and the *E. coli* Δ*surA* mutants are the result of disruption in the biogenesis of the outer membrane protein LamB.

An increased susceptibility to vancomycin was detected in all tested strains carrying either a Δ*skp* or a Δ*surA* mutation. The glycopeptide vancomycin inhibits the biogenesis of peptidoglycans by binding to the D-ala residue of peptidoglycan subunits, preventing peptidoglycan polymerisation (Barna and Williams, 1984; Healy *et al.*, 2000). In *E. coli,* Δ*skp* and Δ*surA* mutants are more susceptible to vancomycin compared to the wild-type, which has been contributed to the changes in the composition of the outer membrane in these mutant strains (Lazar and Kolter, 1996; Schafer, Beck and Muller, 1999; Schwalm *et al.*, 2013). The data presented in this study suggest that the *Salmonella* Δ*skp* and Δ*surA* mutants are affected by vancomycin similarly to *E. coli*. Interestingly, the data collected for STM SL1344 Δ*skp* suggest that *Salmonella* lacking *skp* is more strongly affected by vancomycin than the *E. coli* Δ*skp* reported by Schwalm *et al*. (2013). Most of the current knowledge regarding the contribution of Skp and SurA to outer membrane biogenesis stems from research carried out using *E. coli* (chapter 3.1.1). Considering that *Salmonella* Δ*skp* appears to be more strongly affected by vancomycin than *E. coli* Δ*skp,* and considering the *Salmonella* Δ*skp* is also more strongly susceptible to bacitracin than the *Salmonella* Δ*surA* mutant, despite the *E. coli* Δ*surA* mutant being more strongly affected than the Δ*skp* mutant, the contributions of Skp and SurA to outer membrane biogenesis may differ between *E. coli* and *Salmonella.* It would be interesting to compare the outer membrane defects of *Salmonella* Δ*skp* and Δ*surA* mutants to those recorded for *E. coli*, to gain a better understanding of the contribution of these two genes to the outer membrane biogenesis of *Salmonella*.

Penicillins interfere with peptidoglycan cell wall formation by binding to DD-transpeptidase, an enzyme involved in the cross-linking of peptidoglycan subunits (Yocum, Rasmussen and Strominger, 1980). The data collected in this study indicate that periplasmic chaperones of *Salmonella* Typhimurium play a significant role in the protection against Penicillin G. Significantly increased susceptibility was detected for Δ*fkpA*, Δ*ppiAD*, Δ*skp*, Δ*surA*, and Δ*zraP* mutants. In the literature, no other reports are found linking any of these chaperones specifically to penicillin G resistance. However, as the natural resistance of Gram negative bacteria against penicillins is the result of an impenetrable outer membrane, it is likely that increased outer membrane permeability is responsible for these phenotypes. Interestingly, whereas increased vancomycin and bacitracin susceptibility phenotypes were only seen in the significantly disrupted membranes of the STM SL1344 Δ*skp* and Δ*surA* mutants, penicillin G is able to cross the outer membrane following mutations in chaperones assigned minor

tasks in outer membrane biogenesis. Considering penicillin G molecules are significantly smaller than either vancomycin or bacitracin, it is possible that penicillin G requires much smaller disruptions in the outer membrane in order to cross.

Heat-stress affects most bacterial cellular processes and structures, including the outer membrane. Exposure to high temperatures leads to an increased fluidity of the bacterial membranes, which in turn results in an increased permeability of the outer membrane and a greater susceptibility to antimicrobial agents. Furthermore, prolonged exposure to high temperatures results in the denaturation of outer membrane proteins, resulting in an instable cell wall and a build-up of misfolded proteins in the periplasm (Willey, Sherwood and Woolverton, 2008). Of the nineteen STM SL1344 deletion mutants screened for increased susceptibility to heat (46°C), only the *htrA* deletion mutants demonstrated increased susceptibility. The periplasmic protease HtrA is essential for heat-shock survival in *E. coli* (Lipinska *et al.*, 1989; Lipinska, Zylicz and Georgopoulos, 1990), and although not essential in *Salmonella*, Δ*htrA* mutants are significantly more susceptible to heat than the WT strain (Mo *et al.*, 2006). Our results are in agreement with the published literature.

Hydrogen peroxide is commonly used as a biocide, antiseptic and disinfectant, but despite its common use both in and outside of the lab, little is known about the exact mechanism of cytotoxicity. Capable of producing highly reactive hydroxyl radicals, hydrogen peroxide acts as an oxidizing agent damaging lipids, proteins and nucleic acids (Linley *et al.*, 2012). Exposure to hydrogen peroxide results in a large decrease of cell volume and significant damage to the cell membrane in *E. coli* (Brandi *et al.*, 1991). The average zones of inhibition obtained in the disc diffusion assays testing 30% hydrogen peroxide demonstrate that the WT and all tested strains are clearly susceptible to high levels of hydrogen peroxide. However, the deletion of either *fkpA, surA* or *zraP* appear to result in a greater susceptibility to hydrogen peroxide compared to the WT strain. As far as we are aware, these chaperones have not been linked directly to hydrogen peroxide sensitivity before, and it would be worth to investigate these strains further.

Of the nineteen STM SL1344 deletion mutants screened for increased susceptibility to hydroxyurea, none appeared to be more susceptible than the WT strain. The toxic small molecule hydroxyurea is converted into a free radical nitoxide that inhibits the activity of class I ribonucleotide reductase, which is responsible for the formation of deoxyribonucleotides (dNTPs) from ribonucleotides. Depletion of the cellular dNTP pool leads to replication fork arrest and genome instability (Sinha and Snustad, 1972).

Furthermore, replication fork arrest promotes the production of hydroxyl radicals, which mediates in the hydroxyurea induced cell death of *E. coli* (Davies *et al.*, 2009). In *E. coli*, Δ*cpxA* and Δ*cpxR* mutations result in an increased susceptibility to hydroxyurea, whereas constitutive expression of CpxA increases tolerance to hydroxyurea in both *E. coli* and *Salmonella* (Thorbjarnardottir, Magnusdottir and Eggertsson, 1978; Humphreys *et al.*, 2004; Mahoney and Silhavy, 2013). The mechanism by which the Cpx two-component system confers resistance against hydroxyurea is not clear, but the data presented in this study suggest that the resistance is independent of periplasmic chaperone levels.

Nalidixic acid is a first generation quinolone antibiotic that irreversibly binds DNA and prevents RNA synthesis. Of the nineteen STM SL1344 deletion mutants screened for increased susceptibility to nalidixic acid in this study, all the mutants carrying either a Δ*skp* or a Δ*surA* mutation display increased sensitivity compared to the WT. A common mechanism of quinolone resistance exhibited by Gram negative bacteria resolves round changes in porin expression. By either downregulating drug influx or upregulating drug efflux, low level resistance to quinolones is acquired (Aldred, Kerns and Osheroff, 2014). In the case of nalidixic acid, increased resistance has been demonstrated for *Acinetobacter baumannii* and *Stenotrophomonas maltophilia* when exposed to efflux pumps inhibitors (Ribera *et al.*, 2002). It is possible that the increased susceptibility of *Salmonella* Δ*skp* and Δ*surA* mutants to nalidixic acid is the result of misregulated porin formation in the outer membrane, resulting in increased cellular nalidixic acid concentrations compared to the WT strain.

 Of the nineteen STM SL1344 deletion mutants screened for increased susceptibility to phosphomycin, those carrying mutations in either Δ*surA* or Δ*zraP* demonstrated increased susceptibility compared to the WT. Phosphomycin is a small phosphonic acid derivative that binds to phosphoenolpyruvate synthetase, a cytoplasmic protein that is involved in the production of peptidoglycan precursors (Michalopoulos, Livaditis and Gougoutas, 2011). An *E. coli* strain with increased tolerance to phosphomycin demonstrated alterations of the GlpT and Uhp transport systems, thought to be involved in the efflux of phosphomycin. Considering the involvement of SurA in the biogenesis of many outer membrane porins, the It is possible that the increased phosphomycin sensitivity of STM SL1344 Δ*surA* strains is linked to these transport systems. However, further investigation is required into the potential interaction of SurA with these proteins to determine if this is the case.

The cationic antimicrobial lipopeptide polymyxin B targets the LPS layer of the outer membrane and Gram negative *Acinetobacter baumannii* strains lacking LPS are highly resistant against PMB (Moffatt *et al.*, 2010; Velkov *et al.*, 2010). Polymyxin B contains two hydrophobic domains and is amphipathic in nature, allowing it to both be soluble and interact with lipophilic membranes. It displaces the divalent cations Ca^{2+} and Mg^{2+} required for LPS stability and then inserts its N-terminal fatty acid chain into the outer membrane, weakening the packaging of LipidA and increasing membrane permeability (Velkov *et al.*, 2010, 2013; Yu *et al.*, 2015). The exact mechanisms of polymyxin induced cell death are unclear but it has been suggested that osmotic imbalance due to cell leakage (Cajal *et al.*, 1996; Clausell *et al.*, 2006, 2007; Yu *et al.*, 2015), and polymyxin B induced hydroxyl radical cell damage are involved (Sampson *et al.*, 2012; Yu *et al.*, 2015). Resistance against polymyxin toxicity involves the upregulation of the LPS modulation inducing genes *pmrA-B* by the PhoPQ system, which results in an increased length of the O-antigen chains, shielding LPS from interaction with polymyxin B (Delgado, Mouslim and Groisman, 2006; Barrow and Kwon, 2009; Pescaretti *et al.*, 2011; Yu *et al.*, 2015). The upregulation of efflux pumps appears to play a role in the resistance against polymyxin B for *Burkholderia vietnamien, E. coli, Klebsiella pneumoniae,* and *Pseudomonas aeruginosa* (Fehlner-Gardiner and Valvano, 2002; Pamp *et al.*, 2008; Padilla *et al.*, 2010; Warner and Levy, 2010; Munita and Arias, 2016). An increased susceptibility to polymyxin B was detected in those strains carrying mutations in Δ*skp,* Δ*surA*, and Δ*zraP*. The results recorded in this study for Δ*surA* and Δ*zraP* are in agreement with the current literature. SurA has previously been demonstrated to be involved in the protection of *Salmonella* against polymyxin B (Tamayo *et al.*, 2002), and ZraP has been shown to be required for the resistance against polymyxin B in *Salmonella* (Appia-Ayme *et al.*, 2012). However, the data recorded for the Δ*skp* mutant are not in agreement with the current literature, as *Salmonella* Typhimurium Δ*skp* has previously been recorded as unaffected by polymyxin B (Rowley *et al.*, 2011). The investigation into the role of Skp in the protection of *Salmonella* Typhimurium against polymyxin B requires further investigation.

3.4.2 Periplasmic chaperones are involved in the carbon starvation induced cross resistance against heat and polymyxin B.

A common stress encountered by *Salmonella* is starvation of carbon energy sources. The cellular response to carbon starvation includes a large shift in gene expression that results in cells that are both morphologically and phenotypically different from stationary phase cells. The carbon-starved cells are not only equipped for long-term survival in the absence of

carbon sources, but also exhibit cross-resistance to various other environmental stresses that may be encountered during the carbon starvation ordeal (Spector, 1998; Kenyon *et al.*, 2010). The general envelope stress response RpoE has previously been demonstrated to contribute to the carbon starvation response in *Salmonella*, whereas the Cpx two-component envelope stress response did not appear to contribute to the CSIXR against heat or polymyxin B (Kenyon *et al.*, 2002). The data collected in this study confirm the involvement of RpoE in the CSIXR during heat exposure, and suggest further roles for the periplasmic chaperone SurA, the periplasmic protease HtrA and the two component envelope stress response regulator BaeR. Unlike the study reported by Wells (2015), the data collected in this study do not confirm a role for the ZraSRP envelope stress response system in the CSIXR against heat stress, but they do suggest a role for the BaeSR two-component envelope stress response. In *E. coli*, periplasmic proteins upregulated by RpoE in response to heat include SurA and FkpA. Kenyon *et al.* (2010) previously demonstrated that the upregulation of SurA and FkpA in response to heat is not dependent on RpoE regulation in *Salmonella*. They also demonstrated the involvement of SurA and FkpA in the *Salmonella* CSIXR against heat stress. The data reported in this study do confirm the involvement of SurA in the CSIXS against stress, but they fail to confirm the FkpA phenotype reported by Kenyon. Investigation into the CSIXR against polymyxin B, has demonstrated a role for the periplasmic chaperones CpxP, FkpA, Spy, SurA, and ZraP. The role for SurA in the CSIXR response is in agreement with the data published by Kenyon (2010), whereas the phenotype found for FkpA is not confirmed in the literature. The involvement of the CpxP family of bacterial chaperones in the *Salmonella* Typhimurium response against polymyxin B has also been reported by Appia-Ayme (2012), whereas our data failed to confirm the ZraSR CSIXR phenotype in response to polymyxin B as reported by Wells (2015). The discrepancies between the data collected in this study and those published in the literature ask for further investigation into the contribution of periplasmic proteins to the CSIXR response. It should be noted that the standard deviations of the data recorded in this study are very large, which may have influenced the statistical analysis.

To conclude, the screens conducted to investigate the contribution of various periplasmic proteins in response to environmental stresses have expanded upon the current literature. For various conditions there appears to be a difference in the involvement of the periplasmic proteins of *Salmonella* recorded in this study, compared to the involvement of their homologues in *E. coli* recorded in the literature. Considering the current knowledge of the biogenesis and repair of outer membranes is largely dependent on studies carried out in *E.*

coli, this work contributes to highlight variation in periplasmic chaperone function between different Gram negative species. Furthermore, the data reported in this study broaden the knowledge of their involvement in the protection against various antimicrobial agents including phosphomycin and penicillin G.

Chapter 4.
Structural analysis of the periplasmic chaperone ZraP
from *Salmonella* Typhimurium.

4.1 Introduction

4.1.1 Structure of ZraP

ZraP belongs to the same family of bacterial proteins as CpxP and Spy and, arguably, CnrX (Thede *et al.*, 2011). CpxP, Spy and ZraP are periplasmic proteins associated with envelope stress response systems, whereas CnrX is a membrane-bound periplasmic sensor protein associated with the nickel and copper sensing CnrYXH transmembrane signal transduction pathway (Kim *et al.*, 2008; Thede *et al.*, 2011; Trepreau *et al.*, 2014). Despite poor sequence identity between the CpxP family of chaperones, 29% identity between CpxP and Spy, 13% identity between CpxP and ZraP, and 12% identity between Spy and ZraP, all proteins of this family share structural similarities (figure 4.1). They are exclusively composed of α-helices, share a similar hairpin-core formed of the two longest antiparallel helices, and the three chaperones all encode an LTxxQ domain of unknown function (Raivio, Popkin and Silhavy, 1999; Kim *et al.*, 2008; Appia-Ayme *et al.*, 2012). The N-terminal LTxxQ domains are conserved among CpxP ([51]LTEHQ[55]), Spy ([57]LTDAQ[61]), and ZraP ([44]LTEEQ[48]). However, whereas ZraP only has one LTxxQ motif, CpxP and Spy both encode a second LTxxQ domain located at the C-terminal end of the central helix. It is thought that this second LTxxQ motif is required for protein stability of CpxP and Spy (Kwon *et al.*, 2010; Quan *et al.*, 2011).
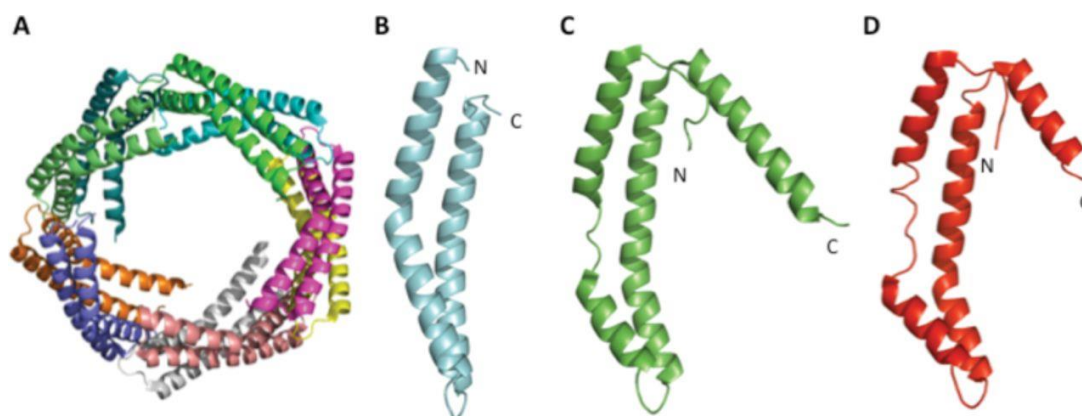
Figure 4.1 Cartoon representation of the crystal structures of the CpxP family members. A. representation of the incomplete, decameric ZraP protein (PDB file 3LAY). **B.** Structure of the ZraP monomer covering residues [44]Leu-Glu[122]. **C.** Structure of the CpxP monomer covering residues [44]His-Lys[151] (PDB file 3QZC). **D.** Structure of the Spy monomer covering residues [29]Phe-Thr[124] (PDB file 3O39). Image taken from Appia-Ayme *et al.* (2012).

The crystal structures of CpxP (PDB ID: 3QZC) and Spy (PDB ID: 3O39) show monomers that form two antiparallel α-helices and a third α-helix pointing further outwards. The crystal structures further suggest that both chaperones form homodimers with a high level of surface contact between the α-helices of the monomers (figure 4.2), which includes both the

helices found in the antiparallel core and the third extending α-helix (Kwon *et al.*, 2010; Quan *et al.*, 2011; Thede *et al.*, 2011). In contrast to this, the crystal structure of ZraP (PDB ID: 3LAY), deposited by the Centre for Structural Genomics of Infectious Disease, demonstrates a monomer that also forms the core antiparallel α-helical structure, but lacks the third extending α-helix (figure 4.1B). Furthermore, unlike the dimers presented for CpxP and Spy, the crystal structure of ZraP is solved as a ring-shaped decamer (figure 4.1A). This decameric shape can only be formed because of the lack of the third α-helix found in the other members of the CpxP family of proteins. It should be noted that the crystal structure of ZraP is only a partially solved structure, with residues 20-44 and 123-151 appearing to be of a disordered nature. In addition to the disordered C-terminal region and the apparent oligomeric states, another significant structural difference between ZraP and the other two chaperones of this family is found midway through the N-terminal α-helix. In CpxP and Spy this is a disordered region, attributed to the Pro[71] and Pro[72] found in CpxP, and the Pro[56] found in Spy (*E. coli* Spy contains two prolines Pro[56] and Pro[57] in this region, similarly to CpxP) (Schrödinger, 2015). These prolines may contribute to the flexibility of the CpxP and Spy dimers, allowing them to better shape around their targets. ZraP does not share this disordered region. Instead, a kink can be found in the helix, which arises from a broken hydrogen bond between the carbonyl group of Thr[61] and the amine group of Ser[64]. This feature makes the α-helical pair of ZraP more stable than the helices of CpxP and Spy, but as a result the ZraP core antiparallel α-helical structure is likely to be less flexible. Interestingly, despite numerous reports of interaction between ZraP and zinc (Noll, Petrukhin and Lutsenko, 1998; Lee, Barrett and Poole, 2005; Sevcenco *et al.*, 2011; Appia-Ayme *et al.*, 2012), no bound zinc was detected in the crystal structure. It is therefore assumed that the ZraP zinc-binding site is located in the disordered C-terminal region (Appia-Ayme *et al.*, 2012; Wells, 2015).
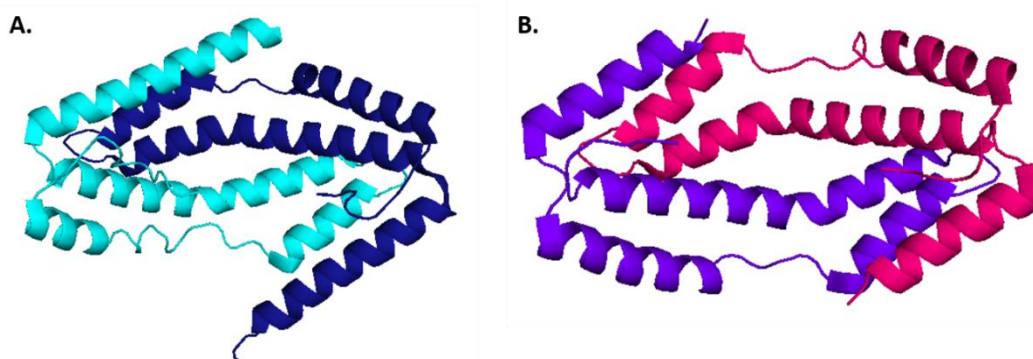
Figure 4.2 Cartoon representation of the CpxP and Spy dimers. Cartoon representation of the CpxP (**A**) and Spy (**B**) homodimers. Image produced in PyMol using PDB 3QZC (CpxP) and PDB (Spy)

A common theme in studies resolving around ZraP and its associated two component system ZraSR is its responsiveness to and interaction with zinc. Although the ZraSR system has repeatedly been shown to be upregulated in the presence of zinc, no phenotype has been detected for Δ*zraSR* strains in the presence of excess zinc as of yet (Noll, Petrukhin and Lutsenko, 1998; Leonhartsberger *et al.*, 2001; Appia-Ayme *et al.*, 2012; Petit-Hartlein *et al.*, 2015; Wells, 2015). It has been theorised that ZraP and ZraSR use zinc as an indicator to mark specific changes in environment, as opposed to the system being involved in the protection against toxic zinc concentrations (Appia-Ayme *et al.*, 2012; Wells, 2015). Sedimentation assays demonstrated that zinc is involved in the stabilisation of large ZraP oligomers. These experiments suggest that ZraP molecules incubated with zinc chloride in a 1:2 ratio form either homologous pentadecamers, or a heterogeneous mixture of ZraP decamers and eicosamers (Appia-Ayme *et al.*, 2012). The binding of zinc to form large oligomeric structures may explain the observed scavenging of zinc molecules by ZraP whilst also explaining the lack of a sensitive phenotype in high zinc conditions *in vitro* (Lee, Barrett and Poole, 2005).

Although ZraP is classified as a zinc binding protein, and its chaperone activity appears to be more effective in the presence of zinc, there is no physical evidence for the binding of Zn^{2+} to ZraP. As mentioned before, the solved crystal structure of ZraP does not demonstrate any bound zinc ions, despite the crystallisation experiments having been conducted in the presence of 0.2mM zinc acetate (PDB 3LAY). Prediction of zinc-binding sites using TEMPS software (3D <u>Te</u>mplate based <u>M</u>etal <u>S</u>ite <u>P</u>rediction) failed to identify any zinc-binding sites for *Salmonella* ZraP (Zhao *et al.*, 2011; Appia-Ayme *et al.*, 2012). Although Noll *et al.,* (1998) described two zinc-binding domains in *Proteus mirabilis* ZraP, these HMGMGH and HGGHGM sites are not present in *Salmonella* ZraP. However, the similar domain [130]HRGGGH[135] is found in *Salmonella* ZraP, and Appia-Ayme, *et al*. (2012) proposed this to be the potential binding site for zinc. Note that the amino acids 130-135 are part of the disordered region that remains unsolved in the published crystal structure. In known zinc-binding proteins, Zn^{2+} ions predominantly bind complexes to form tetra-, penta- or hexahedral geometries with amino acid side chains (Alberts, Nadassy and Wodak, 1998), and a single monomer does not appear to be able to fulfil these conditions. The type of ligand that forms the binding site of Zn^{2+} influences function and dynamics. Zinc sites are classified according to the pattern of the coordinated amino acids, based on their type and position (Daniel and Farrell, 2014). Although some reports regard histidine (His, H) as the most common Zn^{2+} ligand, followed by glutamine (Glu, Q), aspartic acid (Asp, D) and cysteine (Cys, C) (Vallee and Auld, 1993), analysis of X-ray and NMR structures has demonstrated that zinc ions have a higher

disposition towards cysteine than histidine (Patel, Kumar and Durani, 2007). Furthermore, cysteine-Zn^{2+} complexes have been shown to contribute to structural integrity of proteins, as well as their regulatory and catalytic functions (Tainer, Roberts and Getzoff, 1991; Giles *et al.*, 2003). Analysis of the *Salmonella* ZraP structure demonstrates the presence of four histidine residues: His^{28}, His^{29}, His^{140}, and His^{145}. All four amino acids are part of the disordered region of ZraP and are not visible in the published crystal structure. Interestingly, the *E. coli* ZraP sequence reveals five histidine residues, His^{27}, His^{30}, His^{52}, His^{135}, and His^{140}, that are located in a similar location (two at the N-terminal end, two at the C-terminal end), but their spacing within the protein sequence is not equal to that of the histidines found in *Salmonella*. If these histidines are indeed involved in zinc binding, the variation in their motif may explain the inconsistencies reported in their metal affinity (Leonhartsberger *et al.*, 2001; Appia-Ayme *et al.*, 2012; Petit-Hartlein *et al.*, 2015). The sequences for both *Salmonella* ZraP and *E. coli* ZraP also reveal the presence of a cysteine in a GYGGCGGxG motif that appears more conserved among the two species than the aforementioned histidine motif (figure 4.3). Although this cysteine is a potential candidate for zinc binding, this amino acid has also been proposed to be involved in the dimerization of ZraP monomers by forming sulphur-bridges (Petit-Hartlein *et al.*, 2015). Considering the binding Zn^{2+} ions requires several coordinated amino acids (Daniel and Farrell, 2014), it is possible that the binding of zinc involves zinc-oriented sites of several monomers. As such, it has been suggested that the function of metal interactions between ZraP and zinc is structural rather than functional in nature.

```
Yersinia     MNLNKTAIVTLLSLATLIGFGGSAIAQNAMGTHMNGDGTDMSHSQGKHSGKNSMANLTTE
Klebsiella   MKRNRNLPLTLVTLAAL-TFGSNA----AWANHHWGDNNRM--------GAQGYSQLTQE
Eschericia   MKRNTKIALVMMALSAM-AMGSTS----AFA--HGGH--GM--------WQQNAAPLTSE
Shigella     MKRNTKIALVMMALSAM-AMGSTS----AFA--HGGH--GM-------WQQNAAPLTSE
Salmonella   MKRNNKSAIALIALSLL-ALSSGA----AFAGHHWGNNDGM-------WQQGGSPLTTE
             *: *  .  :.:::*: :  :..:     * .   *    *           :. : ** *

Yersinia     QQAIRQQVLNEFQASTADMRQQLTSKNYEYKALLTSKPVDEQKVLAVSKEIQTLRDSLYQ
Klebsiella   QQATAQKLHNDYAAQTSALRQQLQSKRYEYNALLTTQKPDSGKIEAVAQEMEGLRQKLDQ
Eschericia   QQTAWQKIHNDFYAQSSALQQQLVTKRYEYNALLAANPPDSSKINAVAKEMENLRQSLDE
Shigella     QQTAWQKIHNDFYAQSSALQQQLVTKRYEYNALLAANPPDSSKINAVAKEMENLRQSLDE
Salmonella   QQATAQKIYDDYYTQTSALRQQLISKRYEYNALLTASSPDTAKINAVAKEMESLGQKLDE
             **:   *:: ::: :.:: :.*** :*.***:***::.   *   *: **::*:: * :.* :

Yersinia     RRVSMDTQLAKAGIAMT-----GNHGSR--------GGNHMGMAGGRGCR
Klebsiella   QRVKFDVALAEAGVPRGAGM--GYNGCRG------NGGGHRGM----NHW
Eschericia   LRVKRDIAMAEAGIPRGAGMGMGYGGCG--------GGGHMGM----GHW
Shigella     LRVKRDIAMAEAGIPRGAGMGMGYGGCG--------GGGHMGM----GHW
Salmonella   QRVKRDVAMAQAGIPRGAGM--GYGGCGGYGGGYHRGGGHMGM----GNW
             **. *  :*:**:.       *  *.        **.* **    . .|
```

Figure 4.3 Alignment of the ZraP protein sequence of different members of the Enterobacteriaceae family, including *Yersinia pestis*, *Klebsiella pneumoniae, Escherichia coli, Shigella flexneri*, and *Salmonella enterica* serovar Typhimurium.

4.1.2 Basic theory behind sedimentation velocity and equilibrium

Sedimentation velocity is an analytical ultracentrifugation method (AUC) that analyses macromolecules by measuring the rate at which they move in response to a centrifugal force. The sedimentation rate recorded in these experiments provides information regarding the shape and molecular mass of molecules. AUC is a powerful tool that is commonly used in the characterisation of proteins and the analysis of protein complexes (Cole *et al.*, 2008).

The basic theory of AUC analysis dictates that mass, such as proteins, will continuously redistribute in a gravitational field, until the gravitational potential energy exactly balances the chemical potential energy at each radical position. A sedimentation velocity experiment monitors the rate at which the boundaries of molecules move throughout the redistribution (Cole *et al.*, 2008). Several forces act upon the protein during the experiment. Firstly, there is the force of the gravitational field (F_s) which is defined by the mass of the particle (M_p), the rotation speed in radians per second ($\omega = 2\pi*rpm/60$) and the distance of the sample from the centre of the rotor (r).

$$\text{Equation 4.1:} \qquad F_s = M_p\omega^2 r$$

Secondly, as the protein sediments, gravitational force is opposed by a buoyancy counterforce (F_b) produced by the mass of the buffer solution (M_s).

$$\text{Equation 4.2:} \qquad F_s = M_s\omega^2 r$$

The value for the mass of the displaced buffer (M_s) is obtained by multiplying the particle mass by the partial specific volume (v in cm^3/g) and the solvent density (p in g/cm^3).

$$\text{Equation 4.3:} \qquad M_s = M_p vp$$

The third force acting upon the protein is the frictional force (F_f) which is defined by the frictional coefficient of the protein (f) and the velocity (u), which increases as the distance to the axis of rotation decreases.

$$\text{Equation 4.4:} \qquad F_f = -fu$$

Combining all the individual forces together allows for the determination of the frictional coefficient and the sedimentation coefficient (s) which is recorded in Svedberg units ($S = 10^{-13}$ sec). The Svedberg equation is defined as follows:

$$\text{Equation 4.5:} \qquad S = \frac{v}{\omega^2 r} = \frac{m_p(1-vp)}{f} = \frac{M_b}{f}$$

The obtained sedimentation coefficient and the frictional coefficient contain valuable information regarding the size and shape of the proteins subjected to the assay, and can be used to provide an accurate measurement of the molecular weight, size and shape of the proteins in solution (Cole *et al.*, 2008).

When the sedimentation flux is exactly balanced by the diffusion flux, an equilibrium concentration distribution is obtained. The equilibrium radial concentration gradient c(r) can be determined using equation 4.6 (Cole *et al.*, 2008).

$$\text{Equation 4.6:} \qquad c(r) = c_0 \exp\left[\frac{M_b\omega^2}{RT}\left(\frac{r^2-r^0}{2}\right)\right] = c_0\exp\left[\sigma\left(\frac{r^2-r^0}{2}\right)\right]$$

In this equation C_0 represents the concentration at an arbitrary reference distance (r_0), and σ is referred to as the reduced molecular weight (represented by $M_b\omega^2/RT$). This calculation allows for a very precise determination of the molecular weight of the sample, which in turn can be used to determine the oligomeric state of a sample, provided the weight of the monomeric protein is known (Cole *et al.*, 2008).

4.1.3 Introduction into macromolecular X-ray crystallography

4.1.3.1 Production and harvest of protein crystals

Macromolecular X-ray crystallography is a technique that allows for the structural analysis of macromolecules such as proteins in crystal formation. High quality protein crystals are required to successfully perform X-ray crystallography experiments. The production of these crystals is a challenging task. For proteins to crystallise, the molecules must separate from their buffer and assemble into periodic crystal lattices. In these crystal lattices, proteins form an orderly, repetitive structure via interactions with neighbouring molecules, using weak surface interactions such as electrostatic interactions, hydrophobic interactions and hydrogen bonds. Crystals formed from polydispersed or impure protein sample are seldom of high enough quality for X-ray analysis. The process of crystal formation occurs when the protein concentration exceeds its solubility limit, which can be induced using vapour diffusion assays. The solution becomes supersaturated and metastable, allowing for the formation of nucleation sites from which crystals can grow (figure 4.4). The preparation of crystals can be a tedious process, for there is currently no accurate method of predicting what conditions will allow protein crystals to grow. Furthermore, previous success does not guarantee a protein crystal will form again under the same conditions.
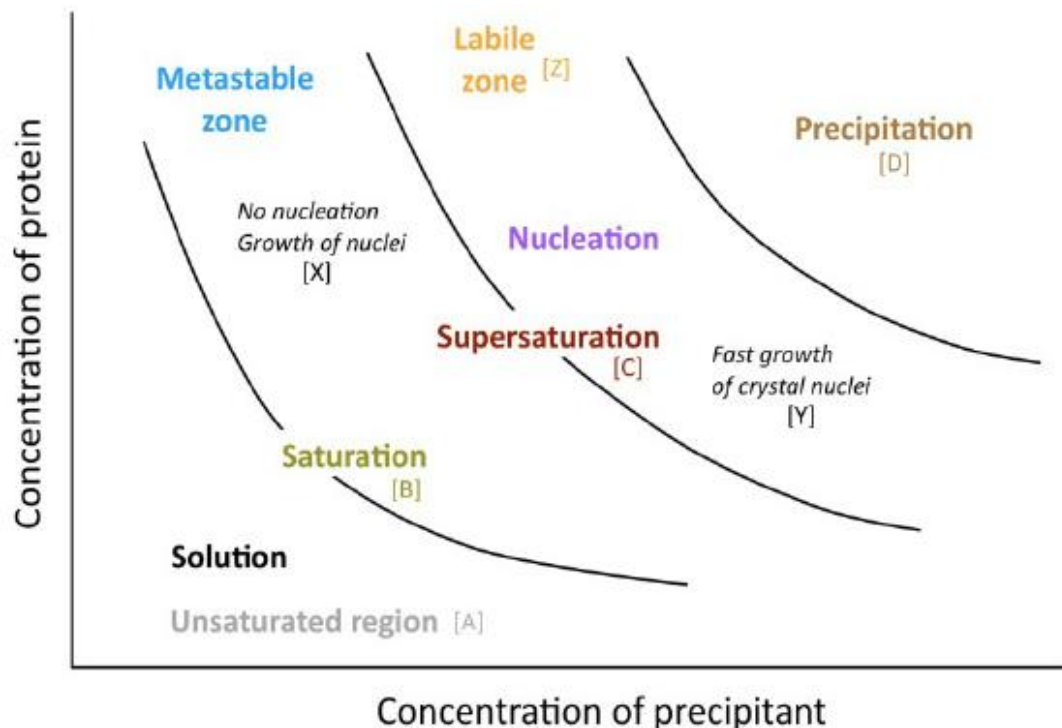
Figure 4.4 Typical schematic solubility curve of protein samples as a function of their buffer conditions. To form protein crystals, protein solutions need to reach a stage of supersaturation that is saturated enough for crystal nuclei to form, but not over-saturated, lest the protein precipitates and drops out of solution. Image taken from (Nemčovičová and Kutá-Smatanova, 2012)

Crystallisation trials are often carried out across a wide range of conditions, including changes in buffer, pH and temperature. Crystals obtained from these general screens are often of low quality, and optimisation trays are designed for conditions that have proven to be favourable for crystal growth, in an attempt to harvest crystals of high quality for X-ray crystallography experiments. Harvestable crystals are coated in a cryoprotectant solution and snap-frozen in liquid nitrogen in an attempt to minimise the damaging effects of X-ray exposure and ice contamination. Formation on ice-crystals on the protein sample affect the crystallography process in two ways. Firstly, the formation of ice forces expansion of the crystal solvent, which in turn can damage the crystal packaging. In best case scenario this lowers the quality of the harvested crystal, in the worst case scenario it destroys the crystal altogether. Secondly, ice crystals exhibit intense diffraction patterns, which interfere with the signals from the protein crystal collected during X-ray crystallography experiments (Rupp, 2009).

4.1.3.2 Collection of X-ray diffraction data

The Diamond Light Source is a UK science facility that generates Synchrotron radiation using particle accelerators. The polygonal storage ring utilises magnets to channel particles around

a booster ring and into an outer storage ring at energy of 3GeV and a maximum current of 300mA. Undulators are used to accelerate and direct X-rays from the storage ring towards individual beamlines, where monochromators, mirrors, and slits are used to generate the correct X-rays required for the crystallography experiments. Protein crystals are rotated in the monochromatic beamline and the diffracting X-ray radiation is recorded by a detector (Rupp, 2009; Diamond Light Source, 2017). During X-ray crystallography experiments, atoms in a crystal will scatter incident X-rays in all directions. The only X-rays that contribute to the recorded scattering pattern are the reflected X-rays that remain in phase, as out-of-phase X-rays cancel one another by destructive interference. X-rays which are reflected in any given direction by the same plane remain in phase. These "in phase" reflected X-rays form the Bragg spots seen on X-ray diffraction patterns, and contain information about protein structure (Rupp, 2009).

4.1.3.3 Insight into the assignment of space groups

Macromolecular X-ray crystallography can be used to analyse proteins packed in crystal structures. These crystals grow within tight symmetry constrains, which can be categorised and reported by their space group. Space groups are mathematical groups of symmetry operations that represent a description of symmetry in a crystal. They give rise to 65 unique chiral arrangements of motifs in a 3-dimentional periodic crystal structure (Rupp, 2009). Space groups are commonly reported in a XY_z manner according to the Hermann-Manguin convention. The X is indicated with a letter (A, B, C, F, I, P or R) to refer to the Bravais lattice type, Y denotes a gyration point which can be replaced by a screw axis. It is indicated by a number which refers to the angle of rotation. The degree of translation is added as the z superscript to indicate how far along the axis the translation can be found. For example, the commonly occurring lattice $P2_12_12_1$ indicates a primitive lattice (indicated by P) which contains three separate symmetry components ($2_12_12_1$), each with two-fold screw axes where the cell is rotated 180° around the screw axis ($\frac{360°}{2}$) and translated ½ of the repeat distance to complete a translation. The lattice $I4_1$ indicates a body centred lattice (I for Innenzentriert) which contains one symmetry component of a four-fold screw axis where the cell is rotated 90°C ($\frac{360°}{4}$) around the screw axis and translated ¼ of the repeat distance to complete a translation (Rupp, 2009).

4.1.3.4 Computational programs involved in X-ray diffraction data refinement

Various programs are available to aid in the analysis of collected X-ray crystallography data. Crystallography programs such as XDS, POINTLESS and MOSFILM are able to determine the

space group of a crystal based on the 2-dimentional diffraction pattern (Evans, 2006; Battye *et al.*, 2011). The crystal's space group needs to be established before X-ray crystallography diffraction data can be reduced and processed (Rupp, 2009). XIA2 and AIMLESS are data-reduction packages that assess the completeness and quality of collected X-ray crystallography data. They combine symmetry-related measurements and uses these data to determine correction factors associated with radiation damage, X-ray absorption effects and detector imperfections. The R-factor and correlation coefficients associated with the scaled and merged output of reduced data provide information about the data quality (Winter and Waterman, 2012; Evans and Murshudov, 2013). The next step, after reducing and scaling the collected data, is phasing. Because (incomplete) crystal structures of the chaperones of the CpxP family are already available, phasing can be carried out using molecular replacement. This method of phasing requires the rigid-body positioning of a molecular body of similar structure (CpxP, Spy or ZraP) to use as a scaffold for solving protein substructures. Model search pipelines such as MrBUMP and PHASER are available to aid in the process of molecular replacement (Keegan and Winn, 2007; McCoy *et al.*, 2007). The substructure phases and amplitudes calculated by molecular replacement analysis provide initial density maps that can be used to build protein models. For data collected at low resolutions (upwards of 3Å) additional experimental data is usually required to provide phase improvements, whereas data collected at high resolutions (below 3Å) can usually be improved using the refining software such as PHENIX, RESOLVE, REFMAC and COOT. The final model is scored and evaluated using a final residual factor (R-factor). This value gives an indication of the quality of the solved structure, as it represents a measure of how well the solved crystallographic model agrees with the collected X-ray diffraction data, by describing the difference between the experimental observations and the ideal calculated values (Terwilliger, 2000; Emsley and Cowtan, 2004; Terwilliger *et al.*, 2008; Rupp, 2009; Murshudov *et al.*, 2011).

4.1.3 Introduction into small angle X-ray scattering (SAXS)

Although macromolecular X-ray crystallography is a very powerful tool that aids in the discovery and investigation of protein structures to great detail, it also has its drawbacks. The formation of protein crystals is a process that takes place under extreme conditions that are not at all representative of the natural environment of these proteins. Although the structures obtained from X-ray crystallography can provide detailed information of the general shape and lay-out of a protein, as well as information on how a protein may interact with cofactors or substrates, the data collected may not be fully representative of the protein

structure *in vivo*. Furthermore, due to the absolute requirement of a symmetrical crystal lattice, X-ray crystallography analysis is of limited use in the investigation of highly flexible proteins, highly flexible regions within proteins, or heterogenic samples. For the investigation of proteins that are difficult to analyse using macromolecular X-ray crystallography, small angle X-ray scattering (SAXS) may be a suitable alternative. The use of SAXS as a technique to study particles in solution dates back to the 1950s, but the development of biological SAXS applications have only recently gained popularity. Although the data produced by SAXS are of low-resolution, the strength of SAXS lies in its ability to study proteins in a biologically relevant solution. This allows for the study of proteins that are resistant to crystallisation, as well as protein properties that are difficult to analyse using macromolecular X-ray crystallography, such as flexile regions, differences in oligomeric state, and real-time fibre/oligomer formations and protein interactions. Furthermore, SAXS can be used as a tool to verify crystal structures obtained using macromolecular X-ray crystallography (BioSAXS, 2017).

4.1.3.1 Basic principles of SAXS

SAXS resolve around the elastic scattering of incident X-rays. These X-rays can be recorded to obtain a 2-dimentional scattering (interference) pattern, which represents the averaged electronic distribution of molecules interfering with the X-ray beam. This technique stems from two basic principles. Firstly, all atoms inside a sample will scatter incident X-rays in all directions, which allows for an almost constant background radiation at small angles. Secondly, particles such as proteins are different in density and/or composition compared to their buffer solution. Due to these differences, atoms that are part of particles produce additional scattering, known as excess scattering. By measuring the detected intensities of the excess scatter profiles (angle-dependent distribution of scattered radiation), conclusions can be drawn about particle structure and size (Schnablegger and Singh, 2013).

4.1.3.2 Analysis of SAXS data.

Distance is normally measured relative to the wavelength (λ) of the applied radiation (r). Therefore, an identical interference pattern would be produced every time the ratio r/λ is identical. To ensure the measurements of intensity are independent of the wavelength used for the incident beam, the intensities of the diffracted X-rays are measured as a function of their momentum transfer (q in nm^{-1}). This value can be derived from the wavelength of the applied radiation (λ) and azimuth angle (φ).

$$\text{Equation 4.6:} \qquad q = \frac{4\pi}{\lambda} sin\varphi$$

SAXS analysis requires the measurement of background samples as well as the measurement of the samples of interest. That way, the signal intensities resulting from biological samples of interest can be revealed by subtracting the data recorded on the sample holder alone, and the sample holder intensities (I), once they have been normalised against the flux density of the incident beam and the exposed sample volume. To produce a 1-dimentional plot of the absolute intensity as a function of momentum transfer (Log(I) *versus* q), primary data is reduced by averaging the recorded intensities as a function of momentum transfer as displayed in figure 4.5 (Schnablegger and Singh, 2013).

The structure factor $q_{(r)}$ can be used to determine if the attraction or repulsion between particles affects the data of samples with differing particle concentrations. To do so, the shape of the shattering curve at low q values is compared. If particle-particle interactions appear to affect the results, the data obtained at high and low concentrations can be merged so that the high-concentration scattering curves can be used without significant interference of inter-particle effects (Schnablegger and Singh, 2013). The radius of gyration (R_g) provides model-independent information about the size of the scattering particles. The intensity at zero angle (I_0) and Rg can be estimated from the extrapolated line fit to a linear Guinier region on Guinier plots (ln(I) *versus* q) (Mertens and Svergun, 2010; Schnablegger and Singh, 2013). Kratky plots (q^2I *versus* q) are used for the determination of tertiary structure features. In this plot, flexible proteins and flexible structural protein units will produce a gradually increasing q^2I as the value of q increases, whereas rigid, globular proteins produce a prominent peak at low q values (Mertens and Svergun, 2010). The structure factor $p_{(r)}$ provides further information about the shape and internal density distribution of the scattering particle. The $p_{(r)}$ can be calculated by the computational software GNOM, which performs a Fourier transform of the scattering intensities as a function of their momentum. This produces the reciprocal-space intensity profile $I_{(q)}$ that closely matches the experimentally observed intensity profile (Svergun, 1992; Liu and Zwart, 2012). The plot of a pair-distance distribution (P(r) *versus* r) can be used to observe structural properties of the particle (figure 4.5). The shape of the curve provides information about the rough shape of the protein. For example, a bel-shaped curve indicates a globular protein, whereas ring-shaped proteins have a $p_{(r)}$ that increases as the value of r(Å) increases, until a sudden sharp drop at high values of r(Å) (Svergun and Koch, 2003; Mertens and Svergun, 2010).
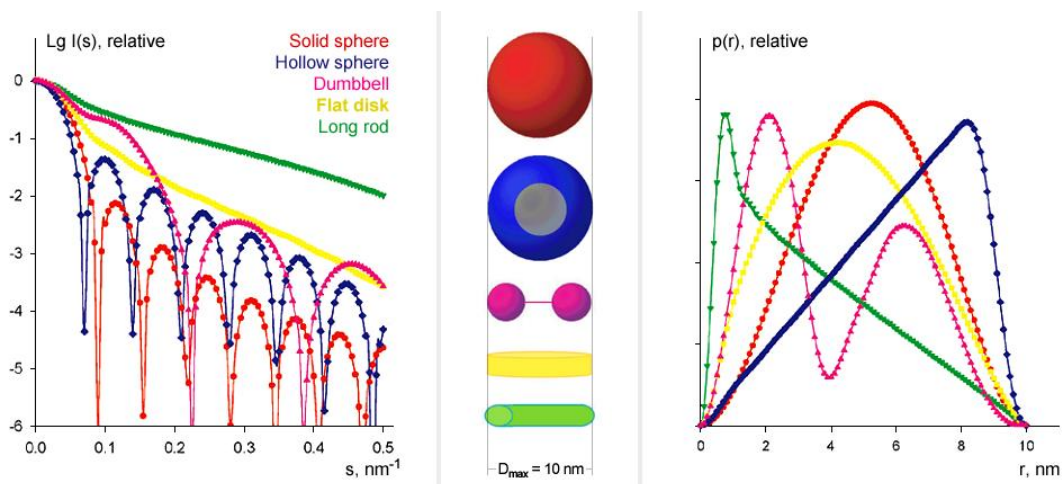
Figure 4.5 Scattering profile and pair-distance distribution of various geometrical bodies. A schematic overview of how the scattering intensity profiles (**left**) collected during SAXS data-collection and the derived pair-distance distribution (**right**) are representative of various geometrical bodies (**middle**). Image taken from (Svergun and Koch, 2003).

Using computational ATSAS software, the $p_{(r)}$ distribution can be used to create a bead model of the particle structure with maximum diameter *ab initio*. The DAMMIN and DAMMIF features of the ATSAS software allow for shape determination by simulated annealing from a single phase dummy atom model. The software produces bead models of the particle using the refined experimental data. The hypothetical scattering of the model is calculated and the model is further refined until the hypothetical scattering closely matches the refined data. The independently produced bead models are then averaged and filtered to produce a final bead model structure that represents the most probable distribution of atoms within the particle (Svergun, 1999; Franke and Svergun, 2009). Another program available in the ATSAS suite is GASBOR. This computational program reconstructs *ab initio* protein structures using a chain-like ensemble of dummy residues, which are representative of amino acid chains. The length of the dummy chains represent the number of amino acids of the protein of interest. GASBOR aims to centre the residues in approximate positions of the α-carbon atoms in protein structures.

This study used SAXS analysis in an attempt to investigate the role of zinc in the formation of higher oligomeric structures. Furthermore, SAXS analysis was carried out to create a better understanding of the structural properties of the unresolved N- and C-terminal regions of *Salmonella* ZraP.

4.2 Aims

The aim of this chapter was to use macromolecular X-ray crystallography and small angle X-ray scattering experiments in an attempt to 1. improve and expand on the currently published *Salmonella* ZraP crystal structure, and 2. investigate the potential contribution of zinc to structural features of ZraP.

In order to investigate the contribution of zinc on the structural features of ZraP, structural analysis was carried out comparing the structure of wild type ZraP with the structure of ZraP mutated in a predicted zinc-binding region (ZraP-SDM). The mutation of the ZraP-SDM mutant involves replacement of ZraP's only encoded cysteine and its neighbouring amino acids with alanines. Previous investigations into the oligomeric state of this mutated protein suggested that the loss of a cysteine results in the inability of higher oligomeric structures (Wells, 2015). In this study, crystallography and small-angle X-ray scattering assays were carried out to further investigate and compare the structural characteristics of ZraP-WT and the ZraP-SDM mutant.

Further ZraP mutants investigated in this study include proteins mutated in the predicted zinc-binding site ^{130}HRGGGH^{134}, and the proteins mutated in the conserved domain of unknown function ^{44}LTxxQ^{48}. Because previous structural analysis by Wells (2015) suggested that the oligomeric structure of ZraP is not affected in these mutants, crystallography and SAXS analysis has been restricted to ZraP-WT and ZraP-SDM.

4.3 Results

4.3.1 Construction of S*trepII*-tagged ZraP-overexpression plasmids

4.3.1.1 Construction and verification of *StrepII*-tagged *zraP* overexpression plasmids

The pBAD constructions overexpressing WT and mutant *myc*-His-tagged ZraP were constructed prior to this study (Wells, 2015). Due to concerns of the size and charge of this tag and its metal-binding propensity, primers (table 2.4) were designed to replace the C-terminal *myc*-His tag with the smaller *StrepII* tag. *StrepII*-tags bind to the truncated core of the *Streptomyces avidinii* derived protein streptavidin. This protein has a strong affinity for biotin, allowing for the purification of proteins using biotin as a competitor for streptavidin binding (Dundas, Demonte and Park, 2013). During the purification of S*trepII*-tagged proteins, the *strep*-tag interacts with the matrix-bound streptavidin, allowing for the isolation of tagged proteins from lysate solutions. The *StrepII*-tagged proteins are then eluted from the matrix by the addition of desthiobiotin. The highly-specific interaction between streptavidin and the *StrepII*-tag resulted in very pure elution fractions, which can be observed in section D of figures 4.7-4.12. To verify successful tag-replacement of the pBAD constructs, newly constructed plasmids were purified from *E. coli* Top 10 and the plasmid insertion site was sequenced by Eurofins Genomics. The sequencing results summarised in appendix D, verify successful replacement of the *myc*-His-tags with S*trepII*-tags for the WT and mutant constructs. Furthermore, the sequencing results in appendix D confirmed the amino-acid substitutions of the mutant strains described in Wells (2015).

4.3.1.2 Transformation and verification of *zraP*-overexpressing pBAD into STM SL1344 Δ*zraP*

Although there are differences between the protein sequence of *Salmonella* ZraP and its homolog in *E. coli*, the LTxxQ motif and the YGGCGGG are conserved among the two species. These two regions are both of interest in the study into ZraP oligomerisation, and concerns were raised about the potential interaction between overexpressed *Salmonella* ZraP monomers and native *E. coli* ZraP produced by the overexpression strain. To avoid the potential interaction between native *E. coli* ZraP and overexpressed *Salmonella* ZraP, the pBAD plasmids encoding *zraP* were purified from the *E. coli* Top10 strain and transformed into a STM SL1344 Δ*zraP* background by heat shock. PCR analysis was carried out to confirm successful transformation. External *zraP* verification primers were used to confirm the Δ*zraP* background of the host strains, whereas pBAD sequencing primers were used to confirm the presence of the *zraP* gene insert in the plasmids, by sequencing the pBad insertion site. Figure 4.5 demonstrates the PCR analysis carried out to confirm the transformation. The

Δ*zraP* background was confirmed for all plasmid strains, demonstrating a band representing the chloramphenicol cassette used to knock-out *zraP*, the *zraP* insert was confirmed in all tested plasmids. Interestingly, the band for *StrepII*-tagged ZraP-ZA was slightly larger than the bands for the other *StrepII*-tagged plasmids, but it was of the same size as the *myc*-His-tagged ZraP-WT plasmid used as a control. Further analysis by purification demonstrated that the *StrepII*-tagged ZraP-ZA does purify from a StrepTrap™ column and does not purify from a HisTrap™ column, confirming the presence of a *StrepII* tag (figure 4.11).
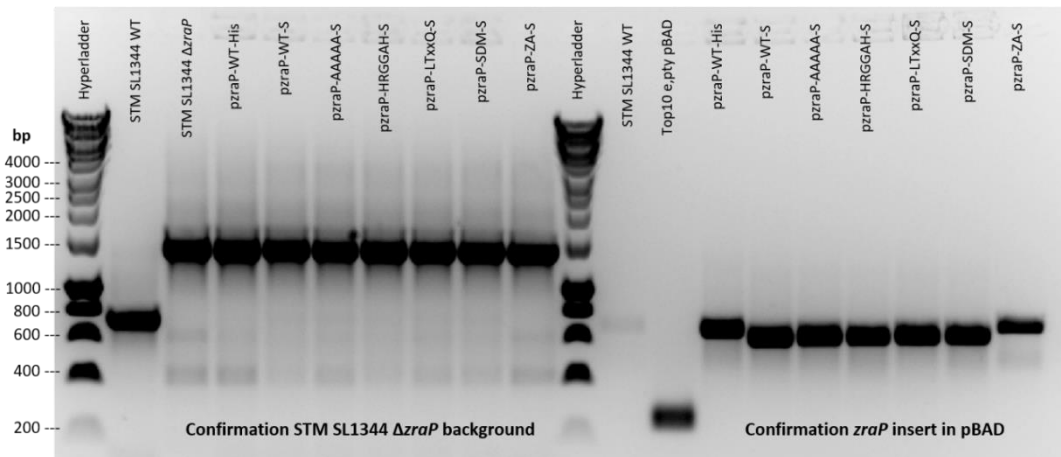
Figure 4.6 Confirmation of successful transformation of pBAD plasmids into STM SL1344 Δ*zraP* background. Band 2-10 demonstrate the PCR products of *zraP* verification primers used on genomic DNA, comparing the background of the strains carrying the indicated pBAD primers (lane 4-10) to STM SL1344 (lane 2) and STM SL1344 Δ*zraP* (lane 3). The image shows that bands for the strains carrying a plasmid match the bands found in the STM SL1344 Δ*zraP* strain, as opposed to the lane found in the WT strain, indicating the presence of a chloramphenicol cassette, as opposed to a *zraP* gene in the background strain. Bands 12-20 demonstrate the PCR products of pBAD insert verification produced using pBAD sequencing primers. Lane 11 demonstrates the absence of a band in the background strain lacking pBAD. Lane 12 demonstrates a small band found when using the sequencing primers on an empty pBAD vector. Lane 13 is a positive control using *myc*-His-tagged ZraP-WT encoded on pBAD. Lane 14-20 demonstrate a band of similar size to the positive control, confirming the presence of *zraP* on the pBAD vectors.

4.3.2 Overexpression trials of newly constructed overexpression plasmids

Prior to protein purification, overexpression trials were carried out to confirm successful overexpression from the newly constructed plasmids, followed by investigation into optimal overexpression conditions. Initial overexpression trial assays were conducted in the *E. coli* Top10 background, which demonstrated successful overexpression of the *StrepII*-tagged ZraP-WT and all mutant constructs. Overexpression trials were carried out testing ZraP overexpression at 30°C and 37°C, testing induction of 4 hours and 5 hours, and testing *L*-arabinose concentrations ranging from 0.2% to 0.00002%. Figures 4.7-4.12 demonstrate the

process of overexpression and purification of the *StrepII*-tagged proteins from *E. coli* Top10, grown at 37°C and induced for 5 hours. Panels A demonstrate presence of overexpressed proteins when stained with Instant*Blue*™ protein stain, and panels B confirm the presence of overexpression by Western blotting. Whereas optimal overexpression of ZraP from an *E. coli* Top10 background required addition of 0.2% *L*-arabinose, 0.02% *L*-arabinose was enough to suffice overexpression of ZraP-WT from the STM SL1344 background. Although *StrepII*-tagged ZraP-WT and mutants were all easily overexpressed and purified from the *E. coli* background, this was not the case for the proteins overexpressed in the STM SL1344 background. Despite using the sample plasmids for ZraP overexpression in STM SL1344 as were used for overexpression in *E. coli* Top10, ZraP-AAAAA, ZraP-SDM, and ZraP-ZA did not appear to overexpress in the *Salmonella* background under any of the tested circumstances. Because of the lack of overexpression of these mutant proteins in the STM SL1344 background, all assays comparing ZraP-WT with ZraP-mutant structure or function have been carried out using proteins purified from an *E. coli* Top10 background. The successful purification of these proteins is visible in figures 4.6-6.11 (panels C demonstrate *StrepII*-trap elution profile, panels D show eluted fractions analysed by SDS-PAGE), and is further described in chapter 4.4.3.
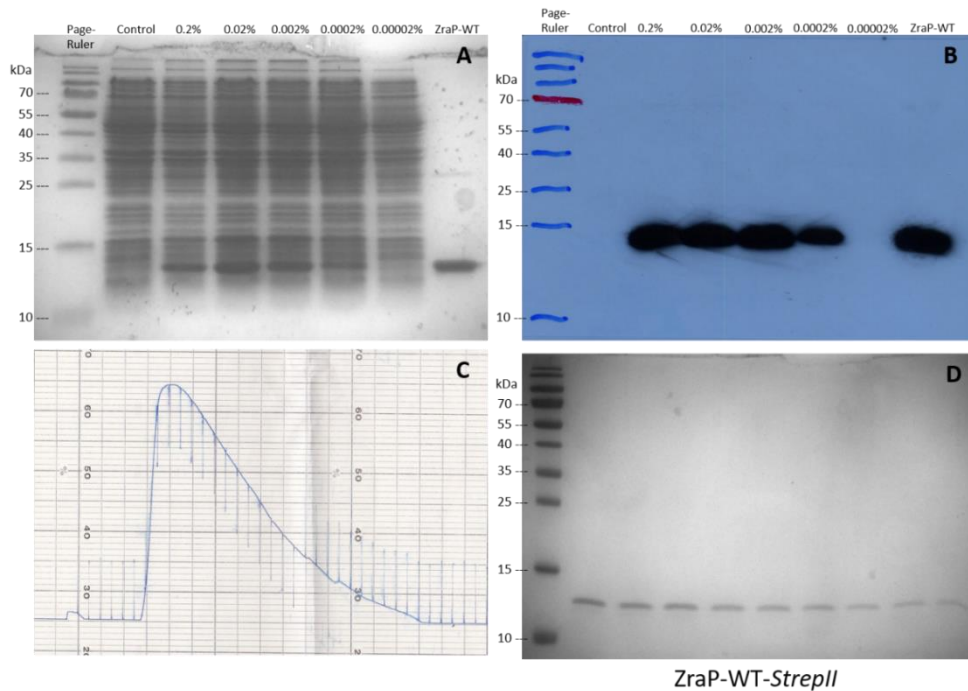
Figure 4.7 Overview of overexpression and purification process of *strepII*-tagged ZraP-WT. A. overexpression trials investigating ZraP-WT overexpression 5 hours post induction when grown at 37°C, 200 rpm, testing different *L*-arabinose concentrations. **B.** Western blot confirmation of protein overexpression. **C.** Elution profile of one-step protein purification from a StrepTrap™ column on an ÄKTAprime plus FPLC. **D.** SDS-PAGE analysis of eluted protein samples.
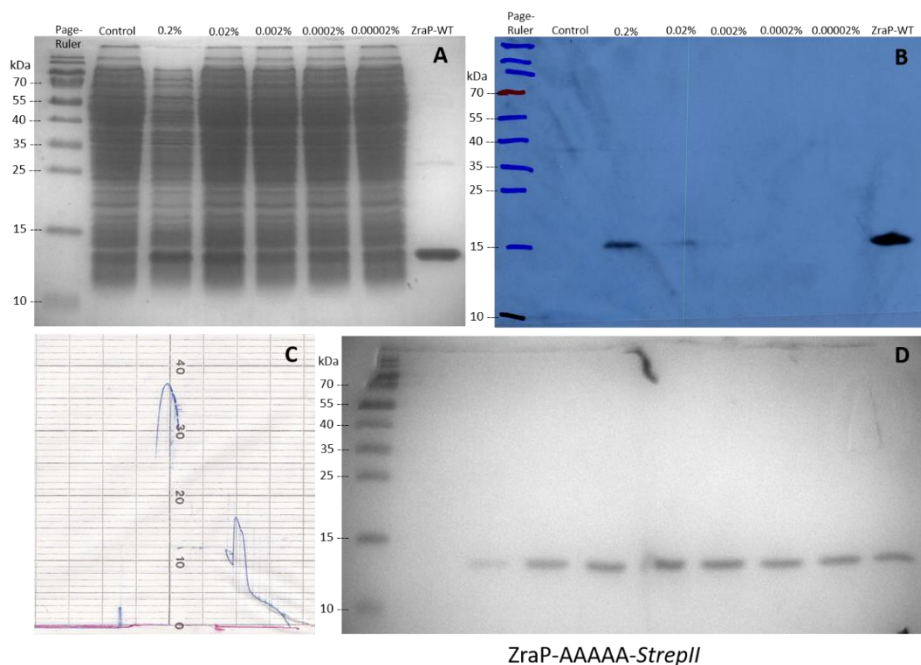
Figure 4.8 Overview of overexpression and purification process of *strepII*-tagged ZraP-AAAAA. A. overexpression trials investigating ZraP-WT overexpression 5 hours post induction when grown at 37°C, 200 rpm, testing different *L*-arabinose concentrations. **B.** Western blot confirmation of protein overexpression. **C.** Elution profile of one-step protein purification from a StrepTrap™ column on an ÄKTAprime plus FPLC. **D.** SDS-PAGE analysis of eluted protein samples.

ZraP-HRGGAH-*StrepII*
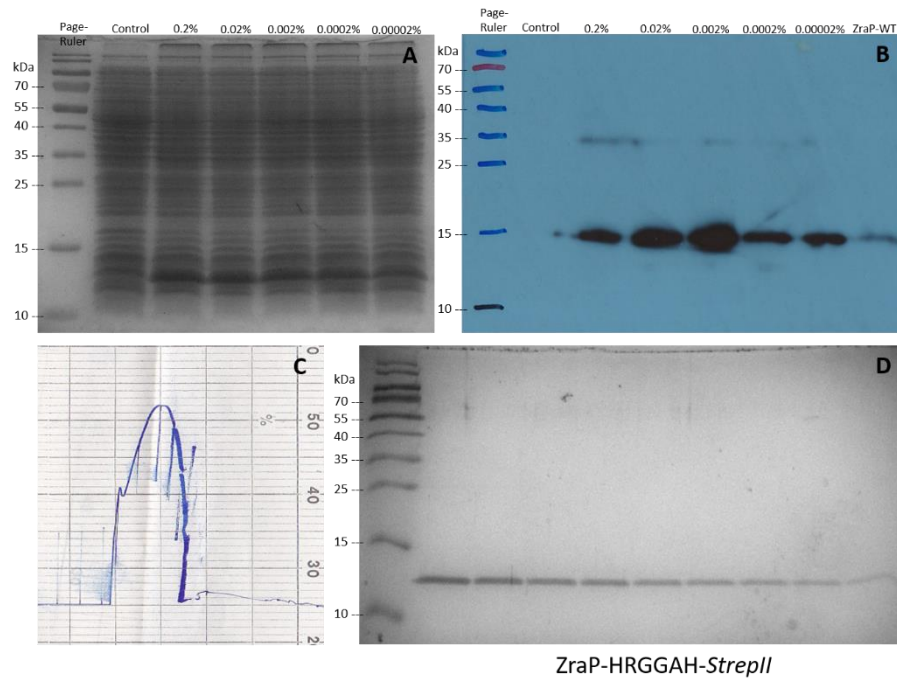
Figure 4.9 Overview of overexpression and purification process of *strepII*-tagged ZraP-HRGGAH. A. overexpression trials investigating ZraP-WT overexpression 5 hours post induction when grown at 37°C, 200 rpm, testing different *L*-arabinose concentrations. **B.** Western blot confirmation of protein overexpression. **C.** Elution profile of one-step protein purification from a StrepTrap™ column on an ÄKTAprime plus FPLC. **D.** SDS-PAGE analysis of eluted protein samples.
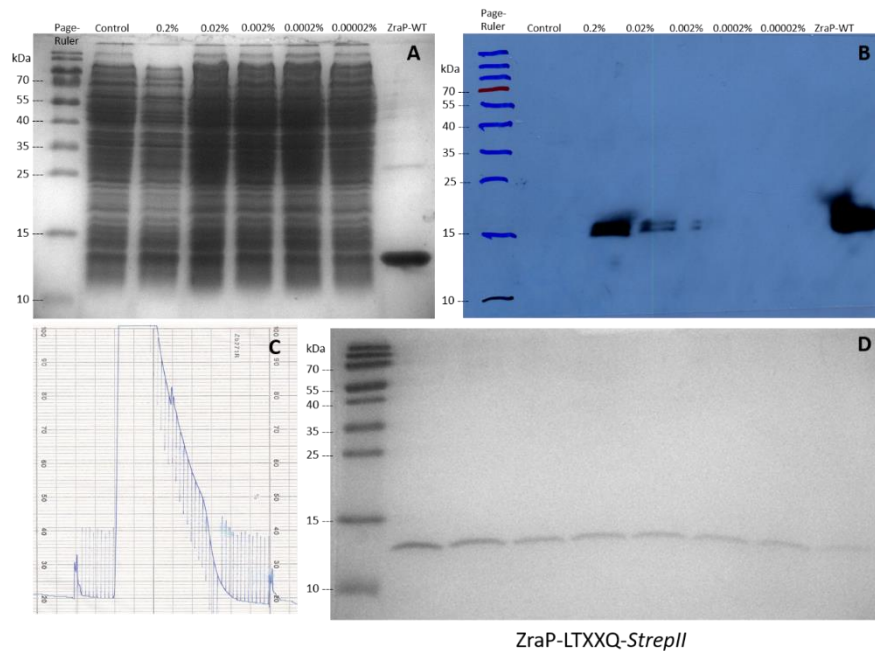
ZraP-LTXXQ-*StrepII*

Figure 4.10 Overview of overexpression and purification process of *strepII*-tagged ZraP-LTXXQ. A. overexpression trials investigating ZraP-WT overexpression 5 hours post induction when grown at 37°C, 200 rpm, testing different *L*-arabinose concentrations. **B.** Western blot confirmation of protein overexpression. **C.** Elution profile of one-step protein purification from a StrepTrap™ column on an ÄKTAprime plus FPLC. **D.** SDS-PAGE analysis of eluted protein samples.

159
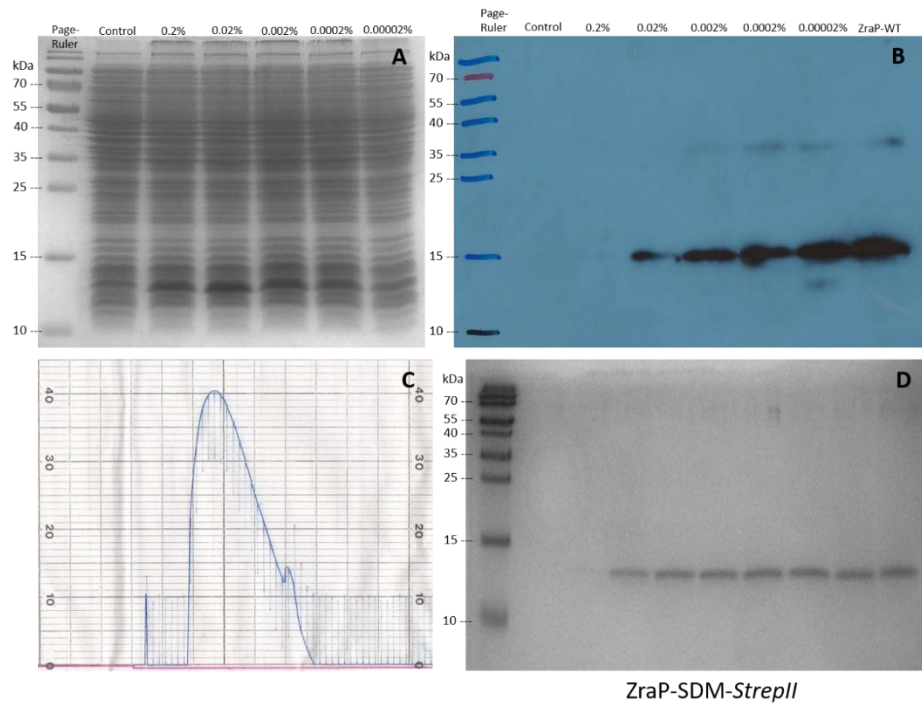
ZraP-SDM-*StrepII*

Figure 4.11 Overview of overexpression and purification process of *strepII*-tagged ZraP-SDM. A. overexpression trials investigating ZraP-WT overexpression 5 hours post induction when grown at 37°C, 200 rpm, testing different *L*-arabinose concentrations. **B.** Western blot confirmation of protein overexpression. **C.** Elution profile of one-step protein purification from a StrepTrap™ column on an ÄKTAprime plus FPLC. **D.** SDS-PAGE analysis of eluted protein samples.
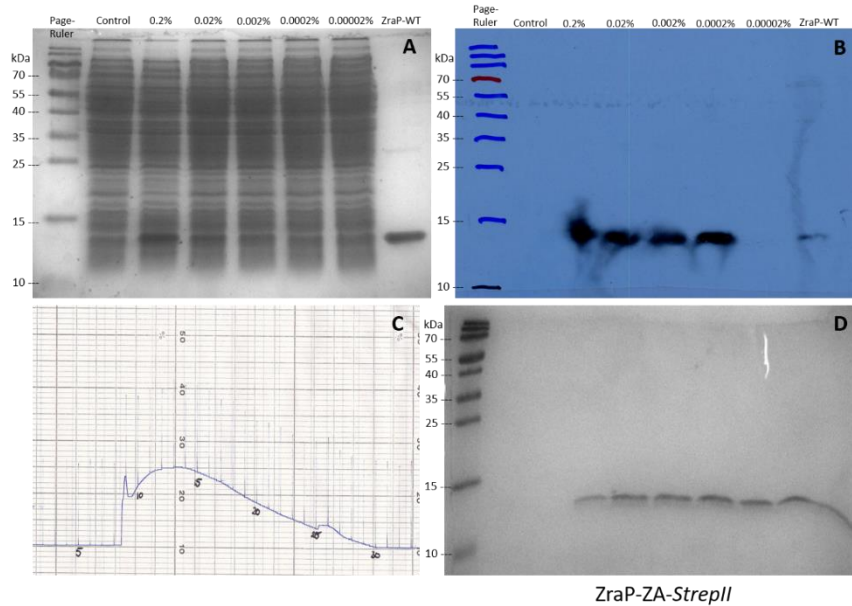
ZraP-ZA-*StrepII*

Figure 4.12 Overview of overexpression and purification process of *StrepII*-tagged ZraP-ZA. A. overexpression trials investigating ZraP-WT overexpression 5 hours post induction when grown at 37°C, 200 rpm, testing different *L*-arabinose concentrations. **B.** Western blot confirmation of protein overexpression. **C.** Elution profile of one-step protein purification from a StrepTrap™ column on an ÄKTAprime plus FPLC. **D.** SDS-PAGE analysis of eluted protein samples.

4.3.3 Purification of ZraP constructs carrying *myc*-His and S*trepII* epitopes

Following overexpression trials, large scale protein purification was initially conducted using constructs encoding a *myc*-His epitope. Although purification of ZraP from these constructs were successful, figure 4.13 demonstrates that eluted fractions contained significant unspecific protein contamination. At the expense of protein yield, the contamination was removed by size-exclusion chromatography (SEC).

Whereas the elution profile of ZraP proteins carrying a *myc*-His epitope demonstrate significant contamination, the elution profiles of *strepII*-tagged ZraP demonstrate very pure protein samples. Verification of the protein purity by SEC resulted in a single peak, representative of pure, monodispersed protein solutions (figure 4.14).
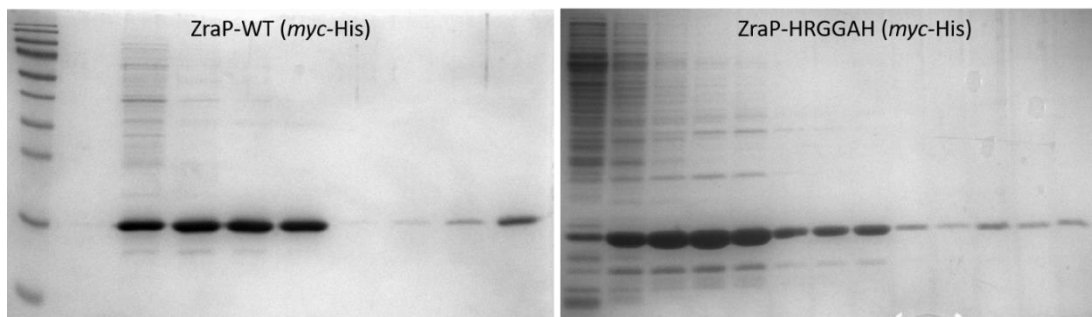
Figure 4.13 Elution profile of *myc*-His-tagged ZraP-WT and ZraP-HRGGAH. The purification of proteins constructed with a C-terminal *myc*-His epitope using a HisTrap™ column was successful, but also demonstrated significant contamination of the eluted samples. The contamination is particularly strong at the early eluted samples, which also contain the highest concentration of protein of interest.
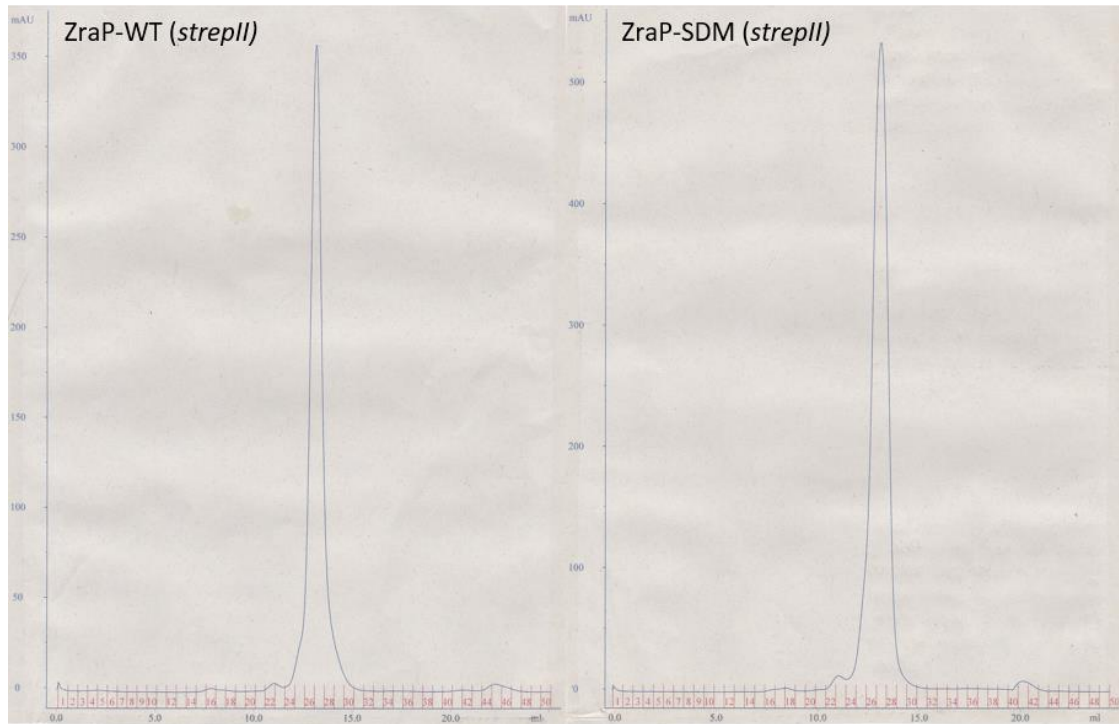
Figure 4.14 SEC elution profile of S*trepII*-tagged ZraP-WT and ZraP-SDM. Following purification using a StrepTrap™ column, protein samples were subjected to gel-filtration using a Superdex 75 10/300 GL column (GE Healthcare Life Sciences). The chromatograph produced plots absorbance at 280 (mAU) against volume flowing through the column (mL). The clear, single peaks suggests the protein samples are pure and monodispersed.

4.3.4 Analysis of *myc*-His-tagged ZraP-LTxxQ and ZraP-ZA oligomeric state by Analytical Ultracentrifugation

Following up from experiments previously started by Dr. Wells (2015), analysis by ultracentrifugation was carried out to test the oligomeric state of ZraP mutants. Sedimentation equilibrium experiments were carried out on *myc*-His-tagged ZraP-WT, LTXXQ, and ZA, in the presence of EDTA. Scans were collected for rotation at 10.000 rpm, and the recorded absorbance was plotted *versus* the radius^2-radius$_{referece)}$^{2} (figure 4.15 panel B). To analyse the molecular mass of the tested proteins, the natural log (ln) of the absorbance was plotted against the radius^2-radius$_{referece)}$^{2} (figure 4.15 panel C). This produced a linear plot the gradient of which is proportional to the molecular mass of the protein tested. To demonstrate the estimated match of the simulated best-fit to the data obtained, the residual absorbance, calculated by subtracting the experimental data from the simulated fit, is displayed in figure 4.14 panel A. Using Ultrascan II (Demelar, 2005), the average molecular mass was calculated and fitted to the absorbance profile of the protein sample. The calculated molecular mass equated to approximately 175kDa for ZraP-LTXXQ, 128kDa for ZraP-ZA, and 138kDa for ZraP-WT. The estimated molecular weight of a *myc*-His-tagged ZraP

monomer is approximately 18.6kDa (ExPASy pI/Mw tool), which suggests that the ZraP-WT, ZraP-LTXXQ, and ZraP-ZA protein samples are not uniformly decamers nor monomers. However, further investigation is required to determine if the sample contains a mixture of monomers and decamers, or if further oligomeric forms are also present.
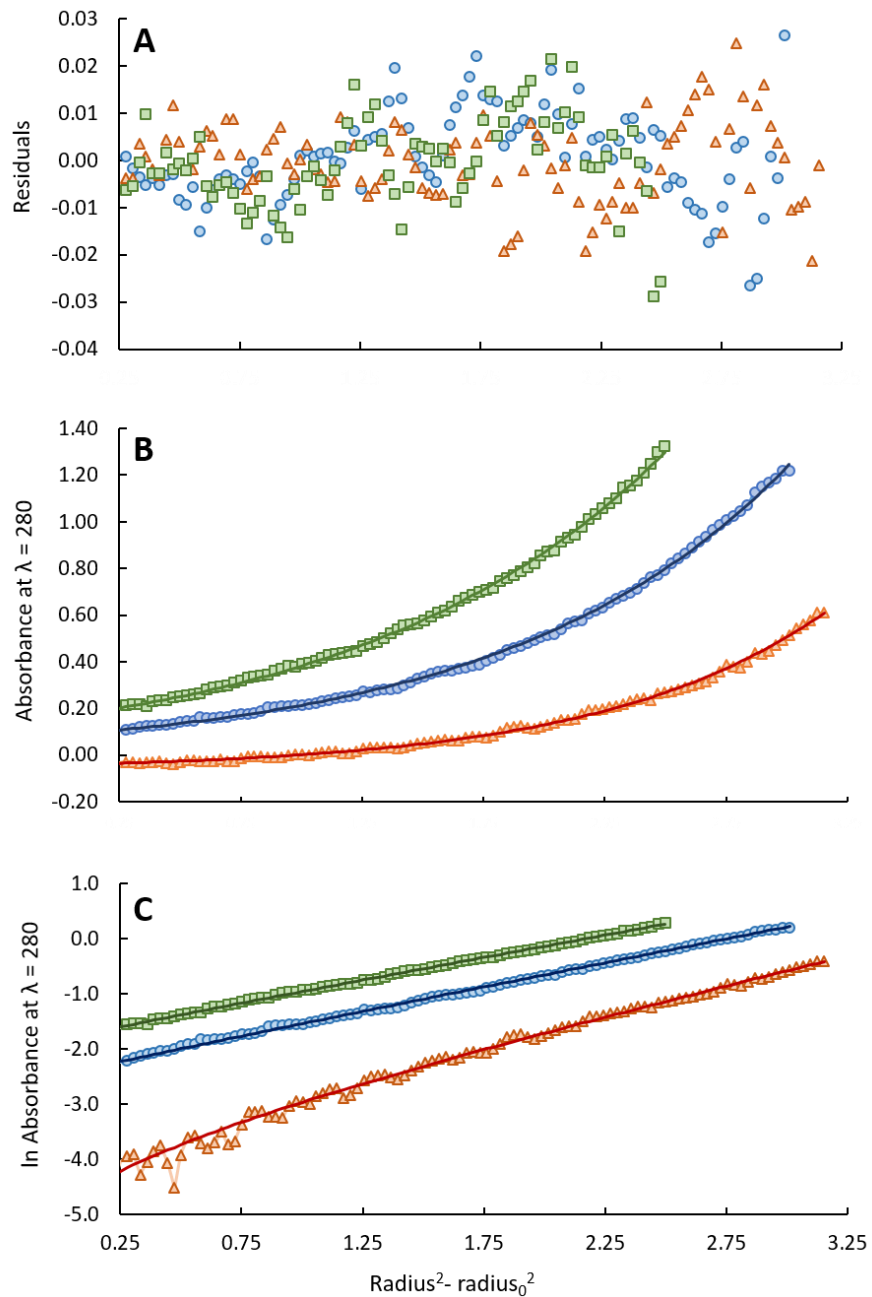
Figure 4.15 Sedimentation equilibrium analysis of *myc*-His tagged ZraP-WT, ZraP-LTxxQ, and ZraP-ZA at 10,000 rpm. A. residual differences between the collected experimental data and the fitted curve. B. Measured absorbance at λ = 280nm in the presence of 1mM EDTA. C. Investigation of the proportional molecular mass using the natural log of the measured absorbance.

4.3.5 Analysis and quantification of bound metal in *StrepII*-tagged ZraP-WT and ZraP-SDM constructs by inductively coupled plasma mass spectrometry

ZraP has previously been reported to bind metals, including zinc, copper and iron (Appia-Ayme *et al.*, 2012; Petit-Hartlein *et al.*, 2015; Wells, 2015). To investigate the role of the [128]GGCGGY[133] region in metal binding of *Salmonella* ZraP, inductively coupled plasma mass spectrometry (ICP-MS) was carried out on *strepII*-tagged ZraP. Due to the lack of ZraP-SDM overexpression in a *Salmonella* background, analysis was carried out comparing *strepII*-tagged ZraP-WT purified from an *E. coli* Top10 background to ZraP-SDM purified from the same background, as well as comparing *strepII*-tagged ZraP-WT purified from an *E. coli* Top10 background to *strepII*-tagged ZraP-WT purified from a STM SL1344 Δ*zraP* background. Table 4.1 demonstrates the concentration of different metals detected in the samples described. The ICP-MS results suggest there are differences in magnesium and zinc concentrations between the tested samples. The amount of magnesium found in the ZraP-WT sample purified from an *E. coli* background is increased 2.3 fold compared to the magnesium concentration found in the buffer, and for the ZraP-WT sample purified from a *Salmonella* background the magnesium concentration has increased 3.5 fold compared to the buffer. The ZraP-SDM mutant displays a significantly higher concentration of magnesium, with a 13.2 fold increase in magnesium concentration compared to the buffer, and a 5.6 fold increase in magnesium concentration compared to the WT protein overexpressed in the same background. The substitution of the [128]GGCGGY[133] region with alanines may result in an increased binding capacity for magnesium. The analysis of zinc suggests that the fold increase of zinc concentration for ZraP-WT and ZraP-SDM purified from an *E. coli* background compared to the buffer are 13.9 and 11.7 respectively. In contrast, the concentration of zinc detected in the ZraP-WT purified from a *Salmonella* background was almost equal to the amount of zinc detected in the buffer (fold increase <1.01). These results may suggest that the environment in which ZraP is expressed plays a more significant role in the binding of zinc than the presence of an intact [128]GGCGGY[133] region.

Table 4.1 ICP-MS analysis of metals found in ZraP samples. Analysis of *StrepII*- tagged ZraP purified from *E. coli* and *Salmonella* , stored in EDTA-free StrepII buffer.

	Cd 228.802 ug/kg	Mg 285.213 ug/kg	Zn 213.857 ug/kg	Co 228.615 ug/kg	Cu 327.395 ug/kg	Cu 324.754 ug/kg	Fe 259.940 ug/kg	Mn 259.372 ug/kg
Zrap-WT purified from *E. coli*	111.1	916.3	7876.7	-190.9	58.9	-23.1	-1377.4	-41.1
Zrap-WT purified from *Salmonella*	348.7	1358.6	571.9	-139.1	377.0	137.9	-1658.1	-37.1
ZraP-SDM purified from *E. coli*	231.9	5169.9	6611.3	-2.8	-77.8	39.9	-132.4	-73.1
Tris BUFFER	81.7	392.5	567.0	-271.4	-26.6	5.6	-949.3	-10.8

Figures in red are below the limit of detection.

It should be noted that there are limitations to the ICP-MS data presented in this study. Firstly, the ICP-MS experiments have not been carried out in a sufficient number of repeats for statistical analysis, and it cannot be ruled out that the data presented are a one-time observation. Furthermore, the background knowledge of the overexpression conditions are too limited to determine whether they have had an influence on the amounts of metal present in the protein. Overexpression has been carried out in rich media, and therefore it is not possible to determine if there have been variations in the metal concentrations available during overexpression. The data presented here should be considered as a starting point for further investigation only.

4.3.6 Investigation into the protein structure of ZraP using X-ray crystallography

X-ray crystallography analysis was carried out on *strepII*-tagged ZraP-WT in an attempt to improve on the incomplete ZraP structure deposited to the protein databank (3LAY), and analysis was carried out on *StrepII*-tagged ZraP-SDM to determine if the mutated protein was capable of oligomerisation. Protein samples were prepared at final concentration between 15mg/mL and 30mg/mL, as quantified by Bradford assay, and subjected to drop vapour diffusion crystallisation using various sparse matrix screens (2.9.3.1). Crystal formation was observed after 1-2 months incubation at 16°C among various conditions (figure 4.16). After 2 months incubation, crystals were harvested for X-ray crystallography analysis (2.9.3.3), and an optimisation tray was made using four selected conditions. Across all screened conditions, the best diffraction data for ZraP-WT were collected from crystals grown in 0.1 M potassium chloride, 0.1 M Tris pH 8.0, 15% (w/v) PEG 2000. The best diffraction data for ZraP-SDM were collected from crystals grown in 0.1M Tris pH 8.5, 0.3 M lithium sulphate, 25% PEG 3350.
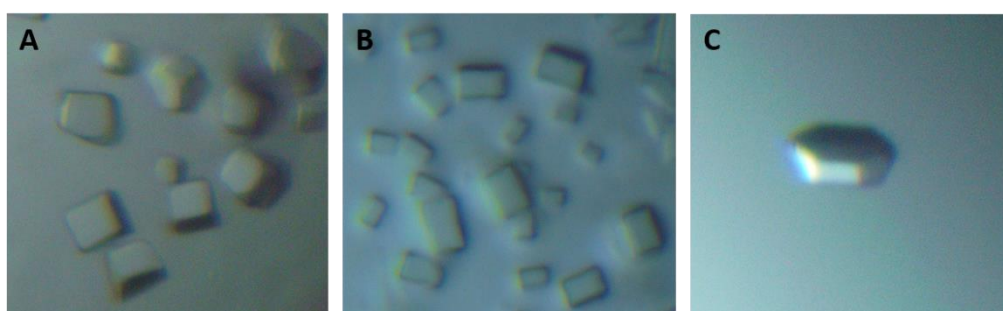
Figure 4.16 Crystals of S*trepII*-tagged ZraP-WT and ZraP SDM grown at 16°C for 2 months in sparse matrix screens. All crystals were grown using the sitting drop vapour diffusion method. Crystallisation conditions represented by these images were carried forward to create a ZraP crystallography optimisation tray. **A.** ZraP-SDM crystals grown in 0.1 M Tris pH 8.5, 1.5 M potassium phosphate. **B.** ZraP-WT crystals grown in 0.2 M lithium sulphate, 0.1 M phosphate-citrate pH 4.2, 25% PEG 1000. **C.** ZraP-WT crystal grown in 0.1 M SPG buffer pH 8.5, 25% PEG 1500.

X-ray diffraction data were collected using the I03 and the I24 MX beamlines at the Diamond Light Source UK. Analysis of the observed Bragg spots on the test images demonstrated the highest resolution of diffraction data, with a resolution of 3.5 Å, for ZraP-WT from crystals grown in 0.1 M potassium chloride, 0.1 M Tris pH 8.0, 15% (w/v) PEG 2000. Using Bragg spot analysis, the highest resolution of diffraction data for ZraP-SDM, with a resolution of 3.15 Å, was detected from crystals grown in 0.1M Tris pH 8.5, 0.3 M lithium sulphate, 25% PEG 3350. Full data-sets were collected from crystals demonstrating the highest resolution diffraction in the test rounds.
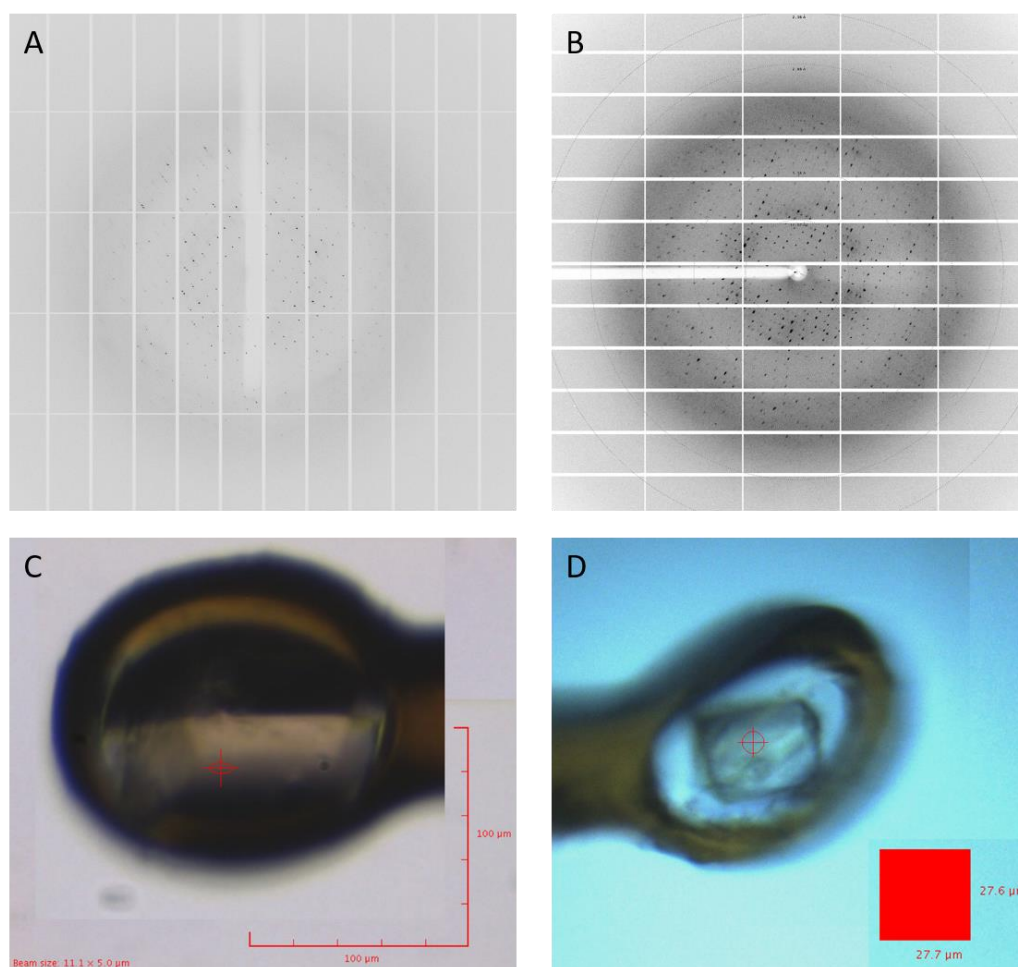
Figure 4.17 Bragg spot diffractions obtained from ZraP-WT and ZraP-SDM protein crystals using X-ray diffraction experiments. X-ray diffraction experiments carried out for ZraP-WT were conducted on the Diamond Light Source beamline I03, X-ray diffraction experiments carried out for ZraP-SDM were conducted on the Diamond Light Source beamline I24 MX. **A.** Bragg spot diffractions (resolution: 3.5 Å) collected for ZraP-WT crystal grown in 0.1 M potassium chloride, 0.1 M Tris pH 8.0, 15% (w/v) PEG 2000. **B.** Bragg spot diffractions (resolution: 3.15 Å) collected for ZraP-SDM crystal grown in 0.1M Tris pH 8.5, 0.3 M lithium sulphate, 25% PEG 3350. **C.** Representative image of ZraP-WT crystal used for the collection of the Bragg spot diffraction data presented in panel A (displayed crystal harvested from same solution). **D.** Image of ZraP-SDM crystal used to collect of the Bragg spot diffraction data presented in panel B.

Data-analysis of the collected datasets was carried out by Dr. Marcus Edwards using the CCP4 suite of software for macromolecular X-ray crystallography (CCP4, 1994). The data collection and refinement statistics are summarised in table 4.2. Initial integration and indexing of the datasets was carried out using MOSFILM (Battye *et al.*, 2011), followed by scaling and merging of the data using AIMLESS (Evans and Murshudov, 2013). The space group assigned to ZraP-WT was C2, 2, 21, with average unit cell dimensions of a = 104.613, b = 113.966, and c = 184.15. The space group assigned to ZraP-SDM was P21, 2, 21, with average unit cell dimensions of a = 147.63, b = 72.81, and c = 97.45. The availability of the previously solved ZraP crystal structure allowed for phasing of the data by molecular replacement using PHASER (McCoy *et al.*, 2007). A single monomer of the 3LAY PDB file was isolated and used as the asymmetric unit building block during molecular replacement. There is a recorded bias in the statistics data, which is the result of using a building block model that is resolved at a higher resolution than the data collected in the current study. Refinement of the data was performed using REFMAC (Murshudov *et al.*, 2011), and the crystal model maps were finalised using COOT (Emsley and Cowtan, 2004).

Table 4.2 Data collection and refinement statistics of ZraP-WT and ZraP-SDM crystals.

Data collection	ZraP-WT	ZraP-SDM
Resolution range	56.98 - 3.5 (3.625 - 3.5)	58.33 - 3.15 (3.263 - 3.15)
Space group	C 2 2 21	P 21 2 21
Unit cell dimensions		
a, b, c (Å)	104.613, 113.966, 184.15	147.63, 72.81, 97.45
A,B,Γ (°)	90, 90, 90	90, 90, 90
Refinement		
Unique reflections	14217 (1380)	18122 (1789)
Completeness (%)	99.96 (100.00)	96.37 (97.92)
Wilson B-factor	119.03	88.31
Reflections used in refinement	14216 (1380)	18119 (1789)
Reflections used for R-free	730 (56)	911 (94)
R-work	0.2563 (0.2979)	0.2430 (0.3026)
R-free	0.2959 (0.3068)	0.2951 (0.4227)
Number of non-hydrogen atoms	5940	5830
macromolecules	5940	5830
Protein residues	780	790
RMS(bonds)	0.002	0.003
RMS(angles)	0.5	0.72
Ramachandran favored (%)	97.24	96.75
Ramachandran allowed (%)	2.24	2.99
Ramachandran outliers (%)	0.53	0.26
Rotamer outliers (%)	1.05	0
Clashscore	2.51	3.88
Average B-factor	112.4	86.61
macromolecules	112.4	86.61

Statistics for the highest-resolution shell are shown in parentheses.

The X-ray crystallography data collected of the ZraP-SDM crystals suggest that ZraP-SDM is not restricted to its monomeric shape, but instead forms decameric structures which are similar in shape as the structures collected from the ZraP-WT crystals, which in turn are almost identical to the ZraP structure published as 3LAY (figure 4.17). The data suggest that, in contrast to reports by Wells (2015), ZraP-SDM does form higher oligomeric structures, as a decameric crystal structure is observed. The observed decameric shape may have been enforced by the extreme conditions under which protein crystals are being formed, and the decameric arrangement may be the most favourable alignment for crystal formation. To rule out the enforced oligomerisation of ZraP-SDM during crystal formation, SAXS analysis was used to study this protein in a biologically relevant buffer solution (4.4.7).
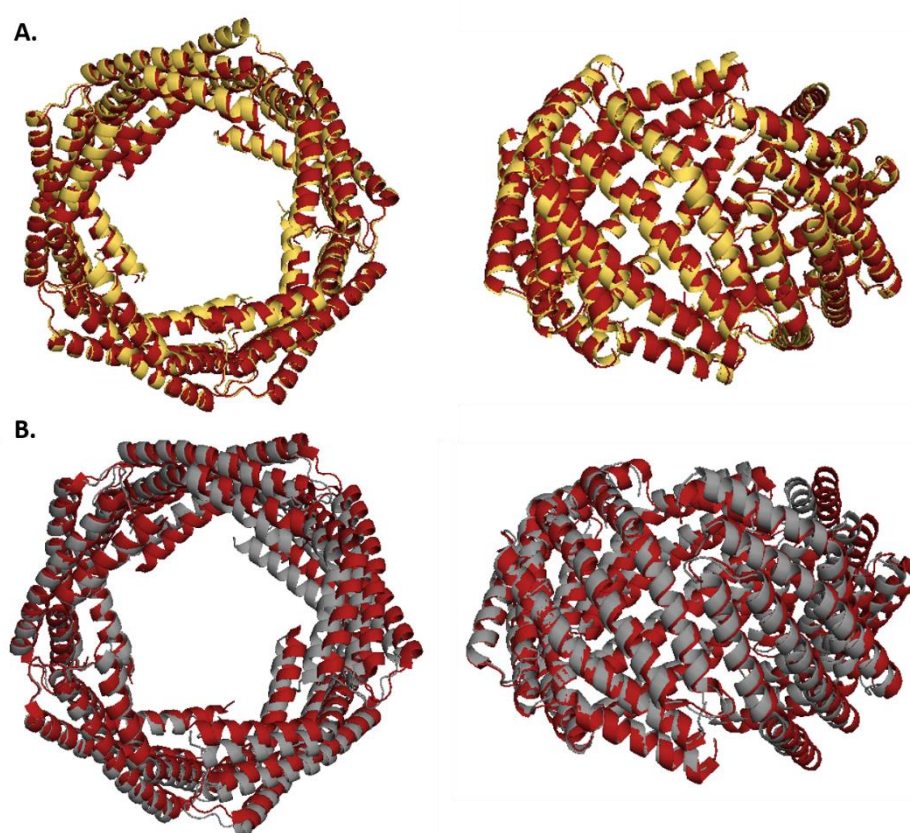
Figure 4.18 Solved ZraP crystal structures superimposed to the published ZraP crystal structure. An overlay was created of the solved ZraP-WT and ZraP-SDM crystal structures, with the published ZraP structure as obtained from the PDB file 3LAY. **A.** Overlay of ZraP-WT (in yellow) with 3LAY (in red). **B.** Overlay of ZraP-SDM (in grey) with 3LAY (in red). The figure shows that both ZraP-WT and ZraP-SDM form decameric structures under crystallising conditions. The overlay of the ZraP-WT structure with the 3LAY PDB structure is a very close match. The overlay of the ZraP-SDM structure with the 3LAY PDB structure demonstrates slight differences. These differences may be structural in nature, or they may have been the result of the differences in crystallisation conditions and subsequent differences in crystal lattice.

The X-ray crystallography data collected in this study did not improve on the previously published ZraP crystal structure. This result was expected as the refraction data collected were of lower resolution than the resolution of the published structure. Subsequent X-ray crystallography assays failed to improve on the ZraP diffraction resolution. The lack of high resolution diffraction data is possibly a result of flexible regions within the protein. In order to collect good resolution data, the difference in formation and orientation between the proteins within the protein lattice must be smaller than 1 Å. Flexible regions do not conform to the crystal lattice, and the diffraction data of these regions is of low quality. To investigate the protein structure in more detail, ZraP was further studied using SAXS experiments. Although SAXS is a low-resolution technique, it is a powerful tool in the investigation of flexible proteins and protein domains.

4.3.7 Small-angle X-ray scattering (SAXS) mediated analysis of ZraP envelope structure, size, oligomeric state, and zinc interactions

To further investigate ZraP protein structure and oligomerisation, and overcome the restrictions imposed by X-ray crystallography, ZraP-WT and ZraP-SDM samples were analysed using small angle X-ray scattering (SAXS). In order to solve protein structures at high resolution using X-ray crystallography analysis, proteins must conform to tight symmetry restrictions within a crystal lattice. Flexible proteins, or proteins with highly flexible domains can only be solved at low resolution, or they can be partially solved at a higher resolution provided the flexible domains are removed. Furthermore, the extreme conditions may result in the forced formation of a protein structure that does not truly represent its biological shape. The published structure of ZraP was solved at 2.7 Å, but the resolved structure only represented approximately 58% of the total protein sequence (excluding N-terminal signal sequence). Although SAXS analysis does not allow investigation of protein structures at high resolution, the technique can be used to obtain accurate information about the shape, size, oligomeric state and overall fold of protein samples in solution. The SAXS experiments conducted in this study were designed to obtain information regarding the overall shape of ZraP-WT, to determine if there are differences in overall shape between *myc*-His-tagged proteins and *strepII*-tagged proteins, to investigate if the alanine substitution of the C-terminal [128]GGCGGY[133] region affects overall protein shape and/or size, and finally to determine if the presence of excess zinc affects the protein shape and/or oligomeric state in solution. The SAXS experiments recorded in this study were carried out using the manual BioSAXS™ beamline robot (EMBL Arinax), testing each protein sample at concentrations of 1mg/mL, 5mg/mL, and 10mg/mL. Eighteen frames were collected of each sample, with an

exposure time of 10 seconds per frame. Before and after each sample, buffer readings were taken to allow subtraction of background scattering. Collected SAXS data are presented as scatter curves, which plot the (log) detected intensities against the scattering angle (q). Prior to any further data analysis, the ATSAS suite software PRIMUS was used to merge the scatter curves of all 18 frames into one combined curve, and to normalise the curve by subtracting the data collected for the buffer reading. These merged and buffer subtracted data files were used for further SAXS analysis.

4.3.7.1 Investigation of sample quality and concentration dependent protein interaction.

The first step of the data analysis of each tested condition was to test the SAXS samples for concentration dependent protein-protein interaction, as well as to determine if any aggregation, repulsion, or radiation damage affected the collected datasets. The data collected by the detector during SAXS experiments can be reduced down to the simple equation $I_{(q)} = F_{(q)} * S_{(q)}$, where I refers to the experimental intensity, F refers to the form factor of the particle (intra-particle interactions, atomic distances within envelope, size and shape), and S refers to the structure factor of the solution (inter-particle interactions). Inter-particle interactions such as repulsion and attraction contribute to the scattering intensity. When the value of S is different from 1 (which refers to no interactions), it becomes difficult to separate S from F, which greatly complicates the investigation into the size and shape of the protein of interest (Svergun and Koch, 2003; Grant, 2014). To investigate the quality and usability of the collected data, Guinier plots (ln(I) *versus* q^2) were drawn using the data collected at the lowest scattering angles. In monodispersed samples, this plot results in a straight line that can be extrapolated in order to estimate the radius of gyration (R_g) and the scattering at the zero angle $I_{(0)}$. If the investigated samples are affected by radiation damage or aggregation, the radius of gyration and the zero angle intensity $I_{(0)}$ increase over time, which results in either a "smiling" or a "frowning" Guinier plot, as opposed to the usual linear plot (Svergun and Koch, 2003). Guinier analysis was carried out on each sample tested in this study, and both radiation damage and aggregation were ruled out for each sample. Panel A in figures 4.21-4.22 demonstrate Guinier analysis carried out on *strepII*-tagged ZraP-WT and ZraP-SDM tested in the presence of 1µM excess zinc respectively. The Guinier plot can also be used to investigate potential inter-particle interactions, which would become evident by an incline of the Guinier plots at the lowest scattering angles. Figure 4.19 demonstrates the Guinier plot comparing the ln absorbance at low scattering angles of *strepII*-tagged ZraP-WT 5mg/mL and 10mg/mL in the presence of EDTA. The straight line observed for both samples

suggests there is no interference in the data from concentration dependent inter-particle interactions.

Using the collected scattering data, a Kratky curve can be constructed by plotting $I_{(q)}q^2$ *versus* q (intensity times scattered angle squared *versus* the scattering angle). The resulting Kratky plot can be used to monitor the degree of compactness of the investigated protein sample. Particles that are globular in shape will form a Gaussian bell-shaped curve at the lower q-values whereas Gaussian chains, such as unfolded or flexible protein domains, peak and plateau at the higher q-values. Proteins with multiple domains form a curve with multiple peaks, and proteins with partial flexible regions present themselves as a combination of the previously described plots (Svergun and Koch, 2003). For each tested condition, the Kratky plots of the 5mg/mL and the 10mg/mL samples were compared to determine concentration dependent protein folding. The Kratky plot demonstrated in figure 4.19 demonstrates that at 10mg/mL the protein samples appear to be more compact, whereas at the 5mg/mL protein samples are still globular, but with a little more flexibility than the samples tested at higher protein concentration. This observed concentration-dependent difference in overall protein fold was recorded in all ZraP-WT samples, but did not seem to occur in the ZraP-SDM samples tested.

Although the Guinier plots demonstrated the absence of concentration-dependent inter-particle interactions, the Kratky plots have demonstrated a concentration-dependent change in overall protein fold for the tested ZraP-WT samples. Due to the observed differences within the same tested condition, the data for the different concentrations were analysed independently, as opposed to merged into one, condition dependent dataset.

4.3.7.2 Analysis of S*trepII*-tagged ZraP-WT and ZraP-SDM data sets demonstrates differences in overall shape, size and flexibility between the WT and the SDM constructs.

General analysis of the obtained scatter data demonstrated little difference between samples exposed to different zinc concentrations, therefore only one full set of analysed *strepII*-tagged ZraP-WT data and one set of analysed *strepII*-tagged ZraP-SDM have been included in this thesis. The overall numerical results of all analysed samples have been summarised in table 4.3. Untreated SAXS data are presented as scatter curves. Scatter curves represent three dimensional, vectorial intensity distributions on a one-dimensional, scalar plane. In SAXS analysis, the law of reciprocity dictates that the scattering of larger dimensions such as overall protein shape (r) is represented by the data collected at the smaller scattering angles (q), whereas the scattering of smaller dimensions such is intramolecular features are

represented at the higher scattering angles (Svergun and Koch, 2003; Mertens and Svergun, 2010). Panels A of figures 4.21-4.22 demonstrate merged and buffer-subtracted scatter curves obtained during data collections.
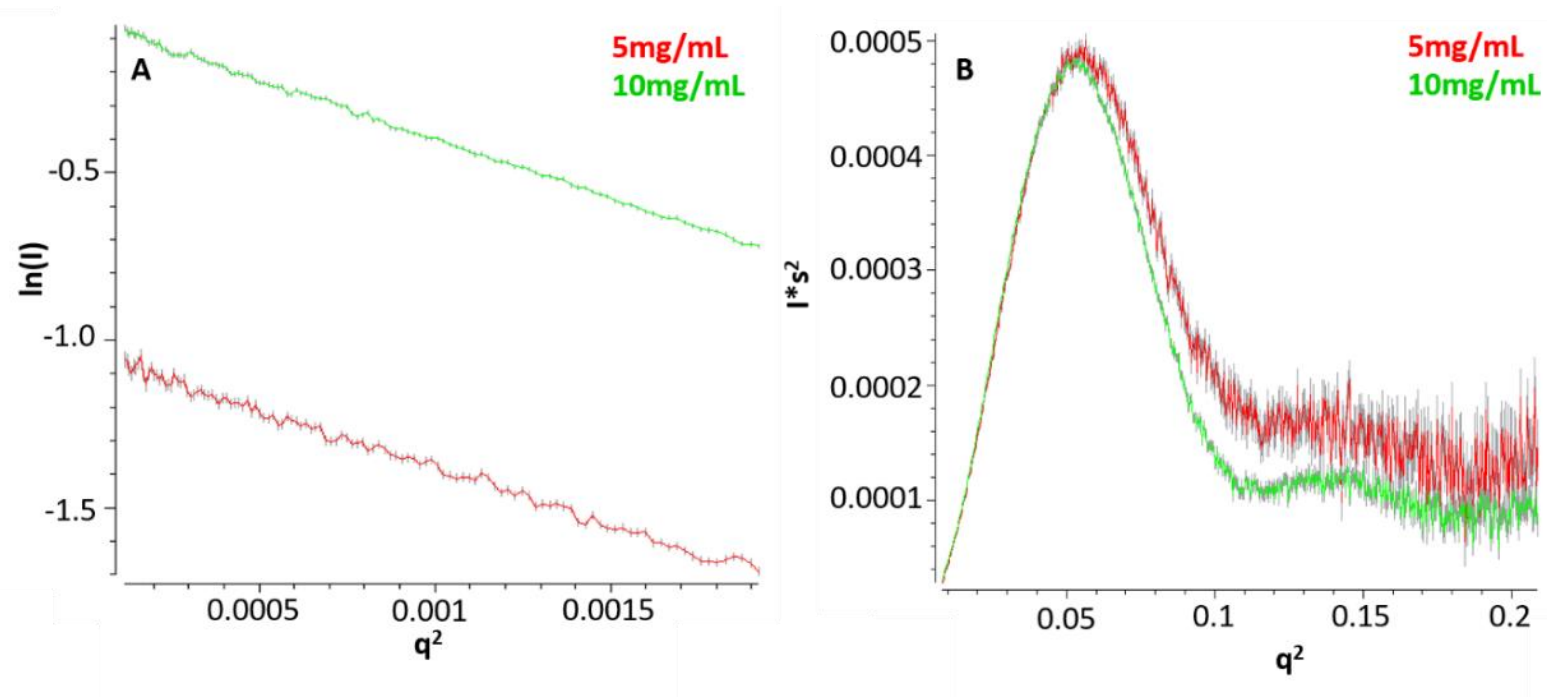
Figure 4.19 Analysis of concentration-dependent protein interactions in *strepII*-tagged ZraP-WT exposed to 1µM ZnCl$_2$. The scatter data was analysed to determine if the protein data sets collected for different protein concentrations could be merged, or if they had to be analysed independently. **A.** Guinier plot comparing the inter-particle interactions between the samples tested at 5mg/mL and 10mg/mL. The straight lines obtained for each concentrations suggest there are no inter-particle interactions at either concentration. The graph displayed here represents data collected for the *strepII*-ZraP-WT exposed to 1µM ZnCl$_2$, but similar results were obtained for all tested samples (data not shown). **B.** Kratky plot comparing the compactness of the tested protein samples. The plot shows differences in the tightness of the globular fold between samples tested at 5mg/mL and samples tested at 10mg/mL, suggesting that the protein is more flexible at 5mg/mL than at 10mg/mL. The graph displayed here represents data collected for the *strepII*-ZraP-WT exposed to 1µM ZnCl$_2$, but similar results were obtained for all tested ZraP-WT samples (data not shown). The concentration dependent difference in the flexibility of the globular protein was not demonstrated in the tested ZraP-SDM samples (data not shown).

As described in chapter 4.4.7.1, the quality of the data can be analysed by plotting the natural log of the intensities at the smallest scattering angles. Protein denaturation, aggregation and radiation damage would demonstrate a non-linear line in the Guinier plot. Panels B of figures 4.21-4.22 demonstrate that neither the ZraP-WT nor the ZraP-SDM samples displayed any sign of aggregation, denaturation, or radiation damage. Using the program PRIMUSQT of the ATSAS 2.6.1 suite, the Guinier plot was also used to estimate the Radius of gyration (R_g) and the intensity at zero scattering angle ($I_{(0)}$) value of each sample. These results are summarised in table 4.3. The radius of gyration refers to the distribution of mass around the centre of an object, and is measured by calculating the root mean square of object distances to its centre of mass. Differences in the obtained R_g value between samples is indicative to differences in protein shape and/or mass. As a rule of thumb, the q-range of data used to calculate the R_g is restricted by $q_{min} < \pi/D_{max}$ and $q_{max} < 1.3/R_g$. The $I_{(0)}$ can be used to calculate the molecular mass of a protein provided that the sample concentration, the partial specific volume, the number of incident photons and the intensity on an absolute scale are known. Instead of using the $I_{(0)}$ to calculate molecular weight, normally the value is used to estimate molecular mass and check for monodispersity among protein samples (Svergun and Koch, 2003; Mertens and Svergun, 2010). The overview of all obtained R_g values demonstrates that all tested samples demonstrate a relatively similar R_g value, apart from the *myc*-His-tagged ZraP-SDM sample at 5mg/mL, suggesting that this sample is different in shape and/or size from the other tested samples. Further data collection confirm that the *myc*-His-tagged ZraP-SDM protein samples behave differently from the other strains screened (4.4.7.4).

Comparison of the scatter plot and the Kratky plot of the *strepII*-tagged ZraP-WT and ZraP-SDM samples, demonstrates a clear difference in overall shape and fold between the two species (figure 4.20). The SDM protein samples demonstrate scatter plots that suggest round, globular proteins, whereas the scatter plot for the WT protein samples suggest slightly more elongated globular proteins. The Kratky plots of the two proteins suggest there are differences in flexibility between the two species.
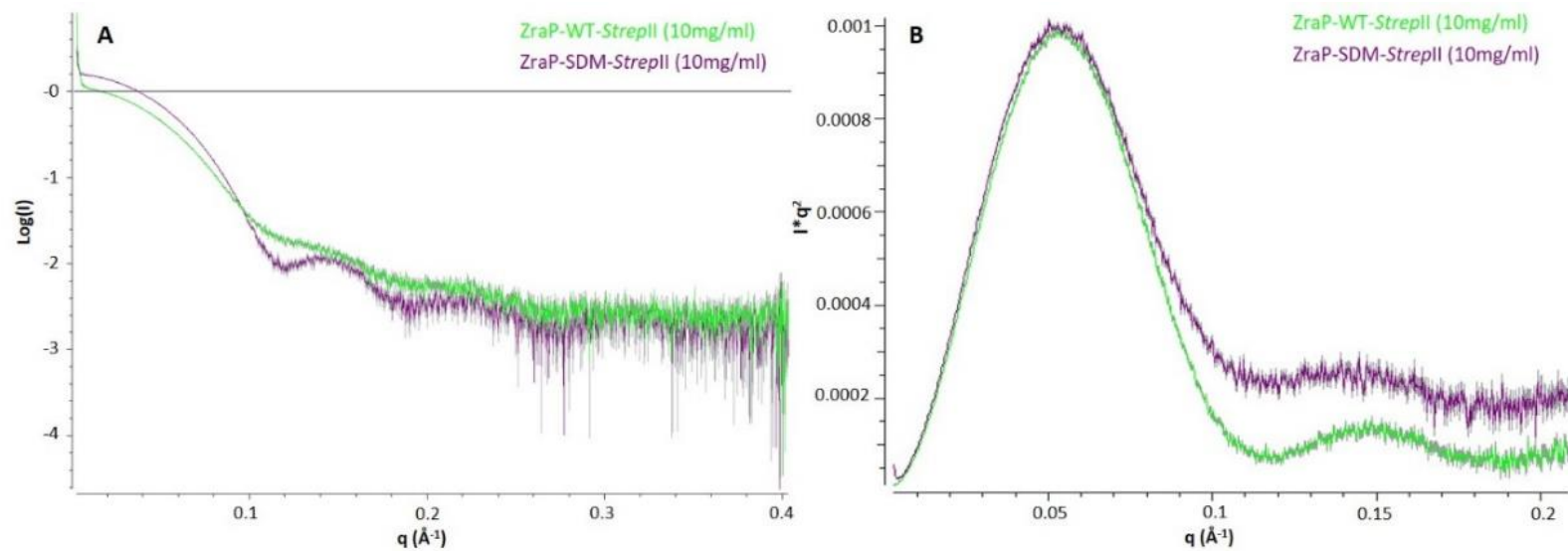
Figure 4.20 The scatter profile and Kratky plot obtained from *strepII*-tagged ZraP-WT and ZraP-SDM suggest there is a difference in overall shape, fold and flexibility between the two species. A. Overlay of the scatter profile of ZraP-WT in green and ZraP-SDM in purple. The scatter curves suggest that ZraP-WT is a globular protein that is slightly elongated in shape, whereas ZraP-SDM is a very round, globular protein. **B.** Overlay of Kratky curves of ZraP-WT and ZraP-SDM demonstrates that although the proteins are likely to share similar core folds, there are differences in overall flexibility between the two species.

175

The Porod plot is used to extract information regarding the fractal dimension and excluded volume of the scattering objects. Using the Porod's invariant and the Porod asymptotic, the volume of a hydrated particle can be derived. The Porod invariant is proportional to the integrated intensity weighted with q^2, and the asymptotic behaviour of the scattering curve at larger angles indicates that the measured intensity is proportional to q^{-4} and the product of the surface area (Kachala, Valentini and Svergun, 2015). Using PRIMUSQT from the ATSAS 2.6.1 suite, Porod plots (I_q*q^4 *versus* q) were created (panels C in figures 4.21-4.22) and the estimated R_g, $I_{(0)}$, and Porod volume were recorded in table 4.3. SAXS is a low-resolution technique, and as a result, record Porod volumes should be considered with an approximate error margin of approximately 10%. This means that minor changes in protein volume might go undetected, but significant changes in particle volume can successfully be derived using Porod plots. As a rule of thumb, the molecular weight of a particle can be estimated by dividing the Porod volume by 1.7 (Svergun and Koch, 2003; Kachala, Valentini and Svergun, 2015). The estimated molecular weight was calculated for all samples following this rule of thumb, the associated oligomeric state was estimated by dividing the obtained molecular weight estimate by the approximate weight of a *strepII*-tagged ZraP monomer (16kDa). The data collected from the Porod plot, as well as the estimated molecular weights and oligomeric states summarised in table 4.3, demonstrate that the Porod volumes for all *strepII*-tagged proteins are similar, and the 10mg/mL data present a slightly increased Porod volume compared to the 5mg/mL data. However, the *myc*-His-tagged ZraP-SDM samples demonstrate a significantly reduced Porod volume compared to both the *myc*-His-tagged ZraP-WT sample, and to its *strepII*-tagged ZraP-SDM counterpart. These data suggest that the *myc*-His epitope interferes with the ability of the ZraP-SDM mutant to form larger oligomers.

To determine the protein radius (D_{max}), the distance distribution function (P(r) curve) of the protein samples was plotted using PRIMUSQT. This curve is a radial Patterson function which describes the probably frequency of interatomic vector lengths (r) within a particle. To obtain the P(r) curve of the scattered protein samples, an indirect Fourier transformation is applied to the scattering profile. The distance distribution function that is produced by this transformation plots a histogram of the probability (P) of finding vector length r within the particle. The P(r) curve is sensitive to symmetry and domain structure, and the shape of the P(r) curve yields information regarding the shape and volume of the scattered particle. A P(r) curve with a Gaussian bell-shape indicates a globular protein, whereas a left-skewed curve is representative of an elongated particle, and a right-skewed curve with a sudden drop

indicates a hollow ring-shaped particle. The P(r) curve is used to obtain a more accurate estimation of the R_g and $I_{(0)}$ values, which can be compared to previously obtained data. Furthermore, the P(r) curve allows for the determination of the D_{max} value of the particle, which represents the maximum size of the particle (Svergun and Koch, 2003; Mertens and Svergun, 2010; Kachala, Valentini and Svergun, 2015). All the P(r) curves obtained in this study formed a Gaussian bell-shape indicative of a dense, globular proteins. Panels F in figures 4.21-4.22 demonstrate P(r) curves obtained for *strepII*-tagged ZraP-WT and ZraP-SDM respectively, the E panels compare the fit of the calculated curve to the collected scatter data. Following analysis of the P(r) curve, it is clear that ZraP does not form a hollow, doughnut shaped protein, but instead forms a dense, globular protein. The obtained D_{max} values for each sample are summarised in table 4.3. The summarised results demonstrate that the D_{max} values of the SDM constructs are consistently lower than the recorded D_{max} values for the WT constructs. The Kratky curves for the mutant constructs suggest a tighter fold, and the scatter data suggest a rounder particle. The Porod volume recorded for the mutant constructs is consistently higher than the recorded Porod volume of the WT constructs. These obtained data suggest that *strepII*-tagged ZraP-SDM construct forms a more tightly folded protein that is more globular in shape, whereas the *strepII*-tagged ZraP-WT protein is also a globular protein, but likely flatter in shape, and with slightly more flexibility.

4.3.7.3 Overall protein shape is not affected by changes in zinc concentrations

One of the aims of the SAXS analysis was to investigate the influence of the absence and presence of zinc on protein oligomerisation. In order to do so, *strepII*-tagged ZraP-WT and ZraP-SDM samples were dissolved in StrepII buffer (appendix B) containing either 1mM EDTA, or zinc concentrations of 100nM, 500nM, 1μM, 10μM, or 100μM, and analysed by SAXS to determine if changes in zinc concentration affected the oligomeric state or overall fold of ZraP. The data summarised in table 4.3 demonstrate that neither the presence nor the absence of zinc effects protein oligomerisation. The Porod volume is not significantly affected by zinc concentration either. To determine if there was any difference in overall protein shape or fold, a scaled overlay of the scatter curves and the Kratky curves was produced for both the ZraP-WT construct (figure 4.23) and the ZraP-SDM construct (figure 4.24) at different zinc concentrations. The figures show that the zinc concentration in the buffer does not affect the overall shape or fold of either ZraP-WT or ZraP-SDM.
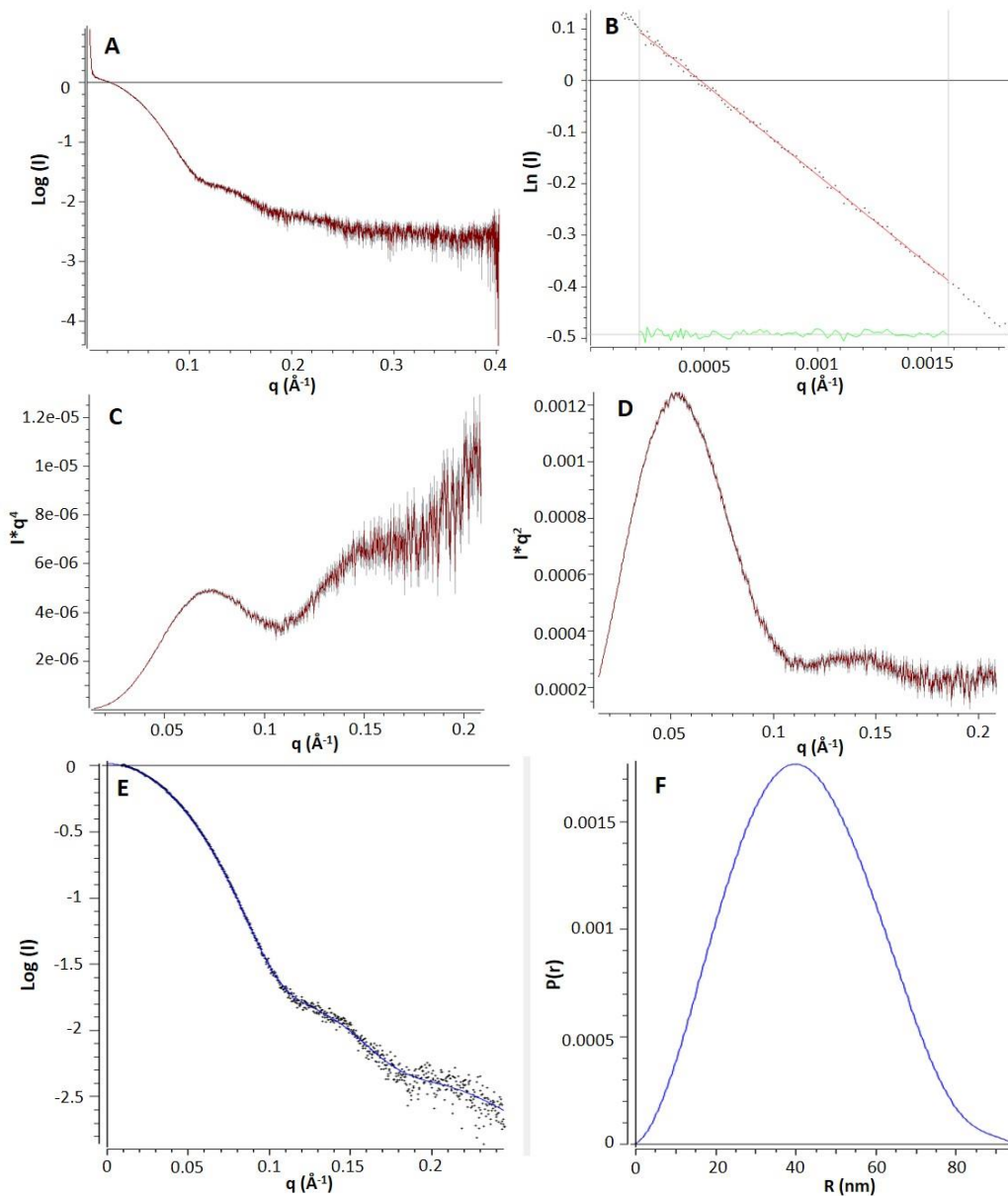
Figure 4.21 Analysis of SAXS derived data for 10mg/mL *strepII*-tagged ZraP-WT suggest the protein is a tightly folded, dense, globular oligomer. A. Scatter curve representing the merged, buffer-subtracted data collected for the sample, and used for further analysis. **B.** Guinier plot of low q intensity vs the momentum transfer (q) demonstrates good quality data. No aggregation, repulsion or radiation damage is detected in the sample. **C.** Porod plot used to estimate the Porod volume, molecular weight and oligomeric state of the protein sample. **D.** Kratky plot of *strepII*-tagged ZraP-WT is typical of a globular protein with minor flexibility. **E.** Comparison of the fit of the calculated P(r) curve to the collected scatter data. **F.** distance distribution function (P(r)) of *strepII*-tagged ZraP-WT using a D_{max} of 94.2.
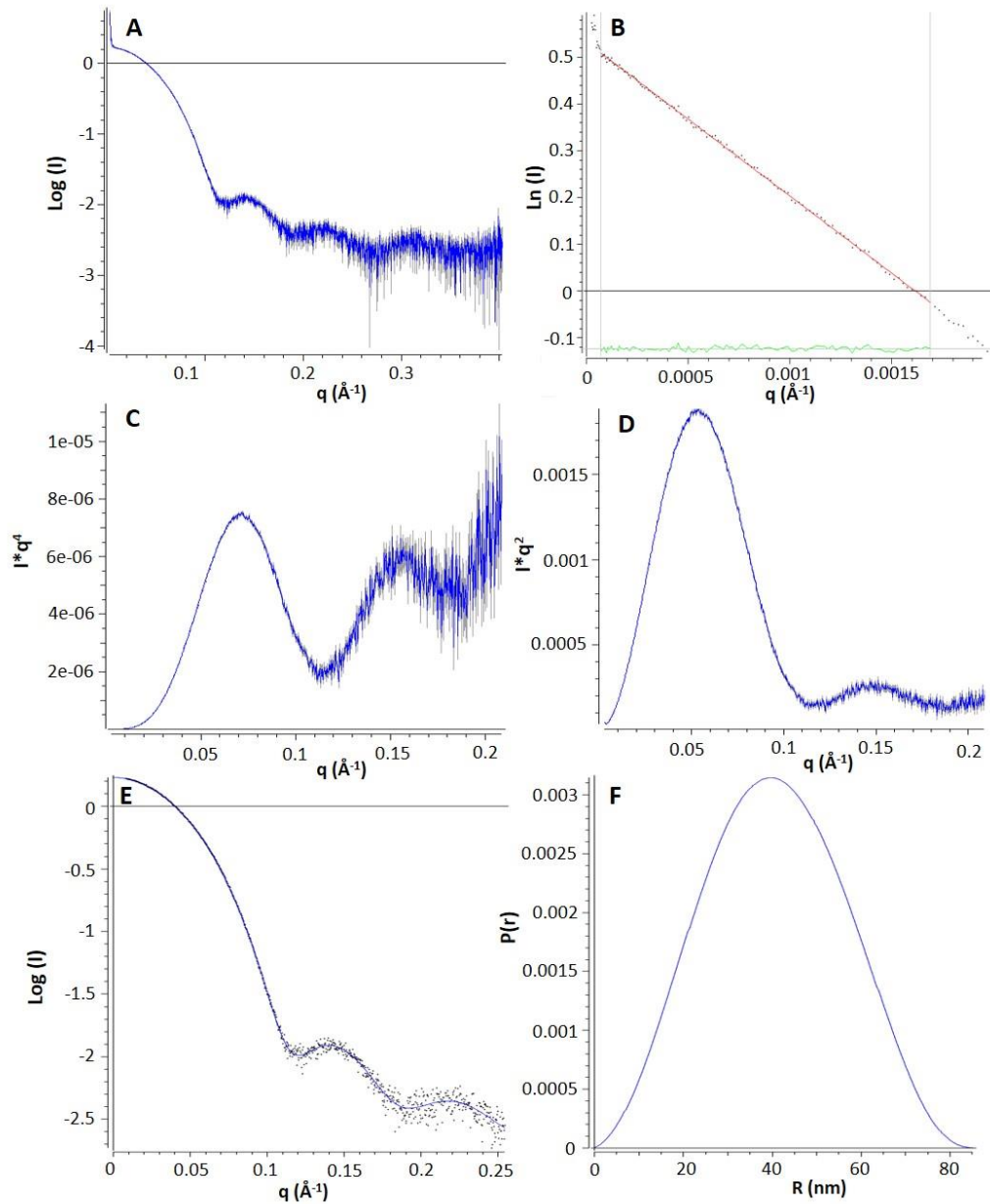
Figure 4.22 Analysis of SAXS derived data for 10mg/mL *strepII*-tagged ZraP-SDM suggest the protein is a tightly folded, dense, globular oligomer. A. Scatter curve representing the merged, buffer-subtracted data collected for the sample, and used for further analysis. **B.** Guinier plot of low q intensity vs the momentum transfer (q) demonstrates good quality data. No aggregation, repulsion or radiation damage is detected in the sample. **C.** Porod plot used to estimate the Porod volume, molecular weight and oligomeric state of the protein sample. **D.** Kratky plot of *strepII*-tagged ZraP-SDM is typical of a globular protein with little flexibility. **E.** Comparison of the fit of the calculated P(r) curve to the collected scatter data. **F.** distance distribution function (P(r)) of *strepII*-tagged ZraP-SDM using a D_{max} of 85.12.
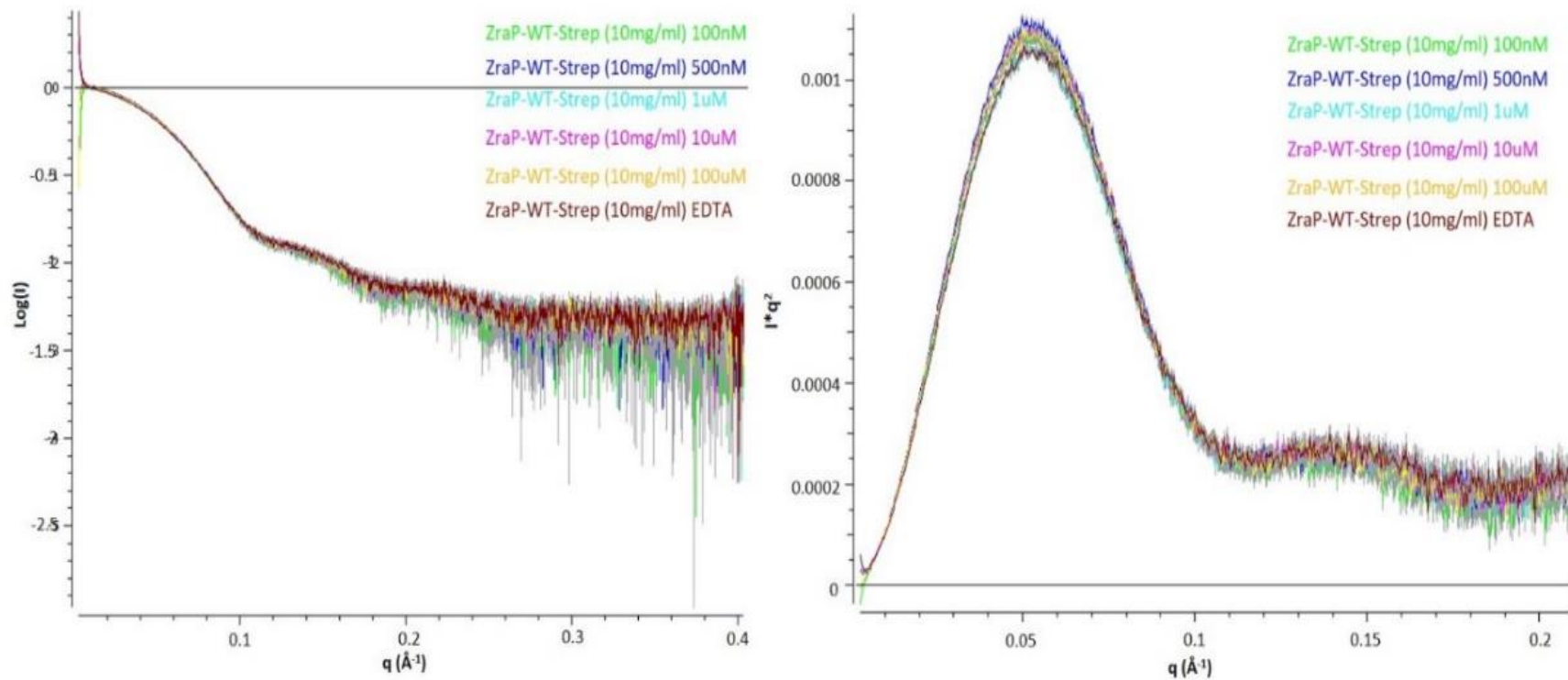
Figure 4.23 Zinc concentration in SAXS buffer does not affect *strepII*-tagged ZraP-WT shape or fold. A. Overlay of ZraP-WT scatter curves demonstrates lack of difference in overall protein shape in the presence or absence of $ZnCl_2$. **B.** Overlay of ZraP-WT Kratky curves demonstrates that the absence or presence of $ZnCl_2$ does not affect the overall fold and compactness of the protein.
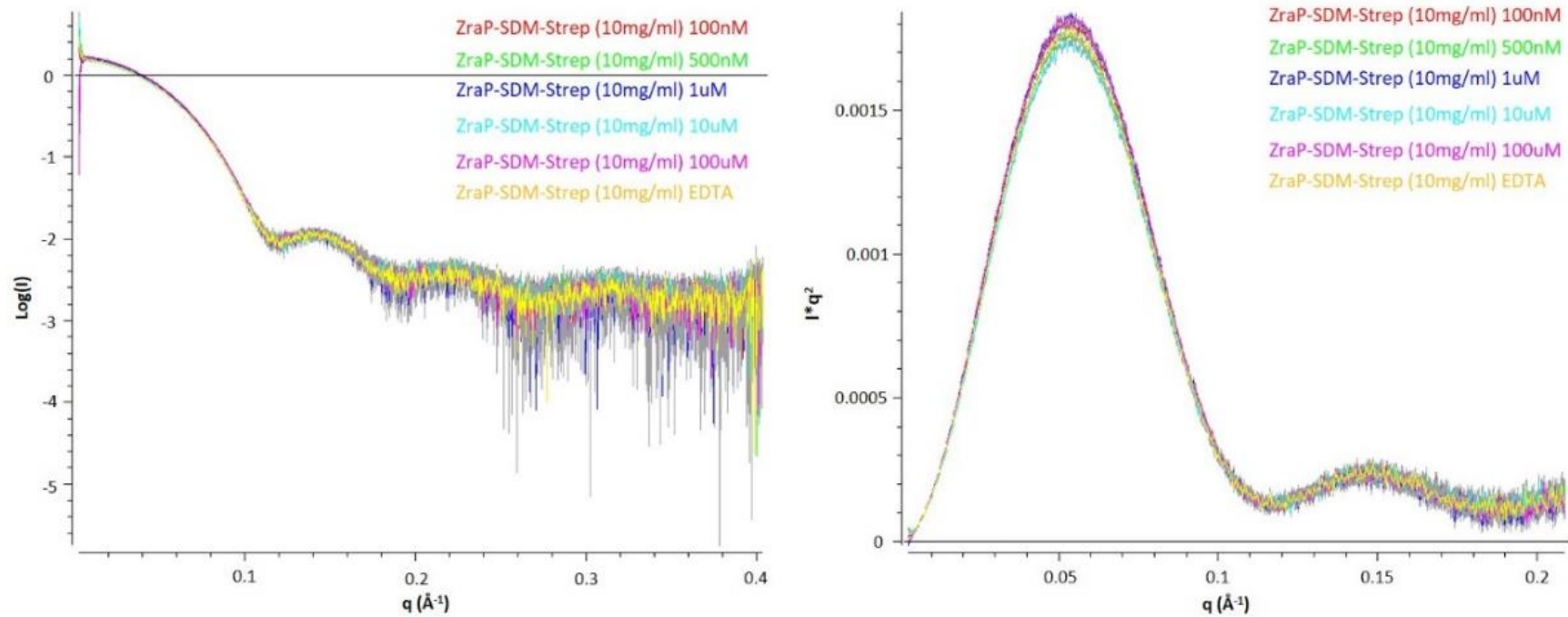
Figure 4.24 Zinc concentration in SAXS buffer does not affect *strepII*-tagged ZraP-SDM shape or fold. A. Overlay of ZraP-SDM scatter curves demonstrates lack of difference in overall protein shape in the presence or absence of $ZnCl_2$. **B.** Overlay of ZraP-SDM Kratky curves demonstrates that the absence or presence of $ZnCl_2$ does not affect the overall fold and compactness of the protein.

4.3.7.4 The *myc*-His-tag interferes with the oligomerisation of ZraP-SDM

Comparison of the SAXS scatter data collected of the ZraP-WT and ZraP-SDM constructs with either *myc*-His epitopes or *strepII* epitopes demonstrated that the *myc*-His epitope interferes with the oligomerisation of the ZraP-SDM construct, but not with the oligomerisation of the ZraP-WT construct. This interference was not detected for the *strepII*-tagged constructs. Figure 4.25 demonstrates the overlay of the scatter curves and the Kratky plots of *myc*-His-tagged and *strepII*-tagged ZraP-WT and ZraP-SDM constructs (comparing data collected at 10mg/mL). Whereas there is only a small observable difference between the two different epitopes on the WT construct, there is a very clear difference in the two SDM constructs. The plots of the *strepII*-tagged SDM construct suggests a tightly folded, round shape, whereas the scatter curve of the *myc*-His-tagged construct suggests a less tightly folded, flexible, elongated shape. The data summarised in table 4.3 also display significant differences between the *myc*-His-tagged and the *strepII*-tagged SDM constructs in regards to Porod volume and radius of gyration.
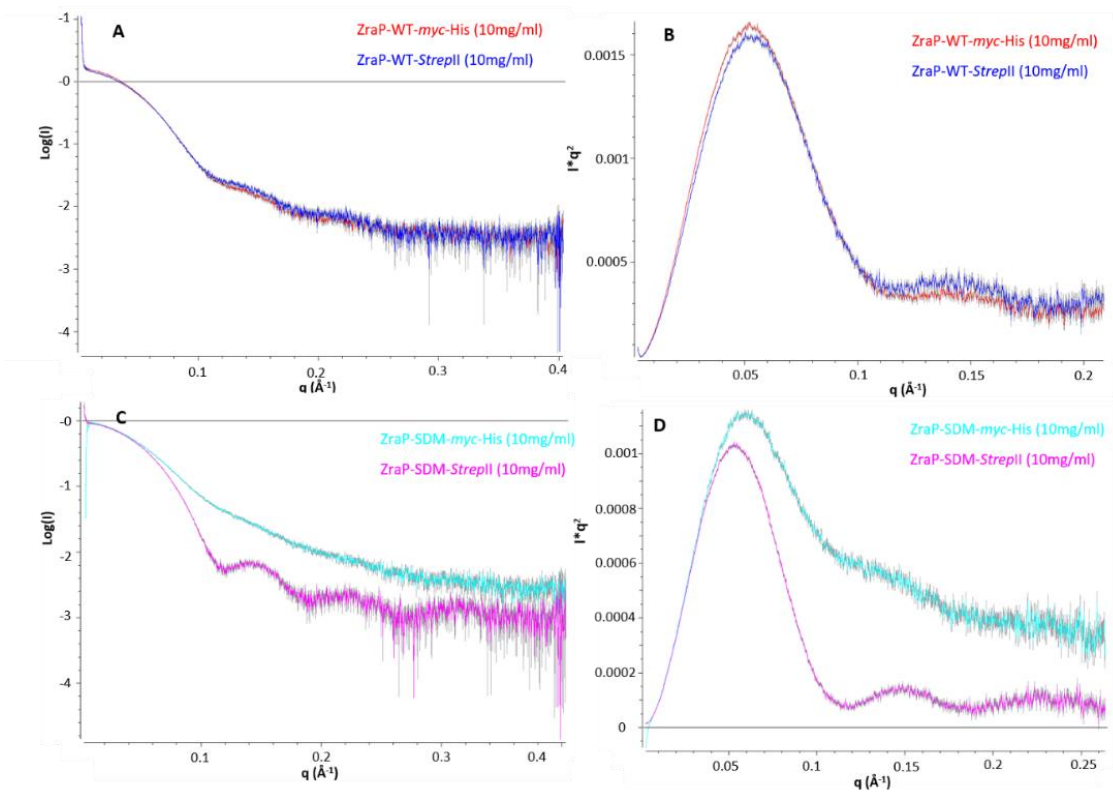
Figure 4.25 The *myc*-His epitope affects the overall shape and fold of ZraP-SDM, but not of ZraP-WT. A. Overlay of scatter profile obtained for ZraP-WT constructs with either a *myc*-His epitope (in red), or a *strepII* epitope (in blue). **B.** Overlay of the Kratky plots ZraP-WT constructs with either a *myc*-His epitope or a *strepII* epitope. Some minor differences are visible between the two species, but overall shape, fold, and flexibility appears to be similar. **C.** Overlay of scatter profile obtained for ZraP-SDM constructs with either a *myc*-His epitope (in cyan), or a *strepII* epitope (in magenta). The scatter plots display significant differences in overall shape, size and fold between the two species. **D.** Overlay of the Kratky plots ZraP-WT constructs with either a *myc*-His epitope or a *strepII* epitope. The plots demonstrate a clear difference in overall fold and flexibility between ZraP-SDM constructs carrying either a *myc*-His epitope or a *strepII* epitope.

4.3.7.5 The predicted scatter profile of the published ZraP crystal structure does not fit the scatter profiles collected during SAXS analysis of soluble ZraP samples.

To predict the theoretical SAXS scattering of a protein crystal structures, protein databank files can be submitted to CRYSOL, part of the ATSAS 2.6.1 program suite (Svergun, Barberato and Koch, 1995). The predicted scattering curve is fitted to experimentally collected SAXS data to allow for comparison. The PDB file of the deposited ZraP structure (3LAY) was used to create a predicted scattering curve and compared with the scattering curve of *myc*-His-tagged ZraP-WT. The CRYSOL settings for obtaining the predicted scattering curve were selected as follows: order of harmonics = 50, order of Fibonacci grid =18, maximum S value = 0.5, number of points = 250, solvent density = 0.334. The overlay of the predicted scattering for 3LAY and the collected scattering for *myc*-His-tagged ZraP-WT is displayed in figure 4.26. The overlay demonstrates that there are clear differences between the predicted scatterings of the 3LAY PDB derived ZraP protein crystal and the experimentally collected ZraP scattering profile.
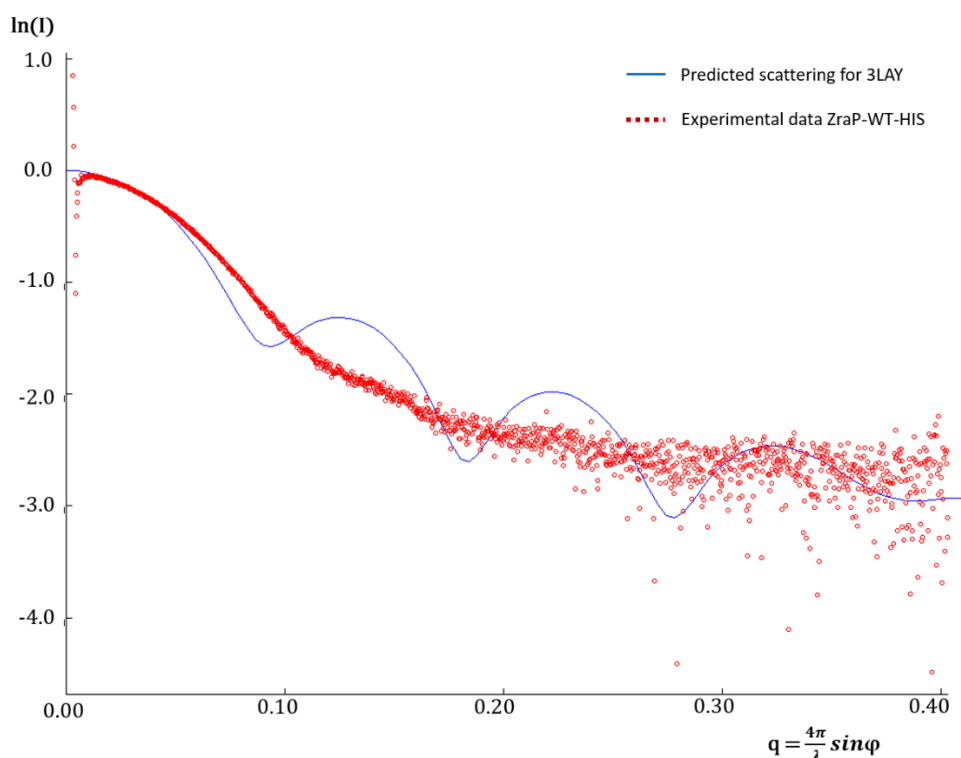
Figure 4.26 Overlay of theoretical 3LAY (ZraP) scatter profile with experimentally collected ZraP scatter profile. The comparison between the theoretical scatter profile predicted from the 3LAY PDB file (ZraP) and the experimentally collected scatter profile for *myc*-His-tagged ZraP-WT demonstrates that the published doughnut shaped ZraP protein structure is not representative of the ZraP protein structure in solution.

4.3.7.6 Suggested protein envelopes

The data collected during the indirect Fourier transform performed on the scattering data to produce distance distribution plots is saved in a .GNOM file output. GNOM is a program that is part of the ATSAS suite, and is able to read one-dimensional scattering curves and evaluates their P(r) distribution. The .GNOM files that are created during the evaluation of the P(r) curve are required as input files for the analysis of the protein envelope using bead models (Svergun, 1992). Several programs can be used to carry out *ab initio* bead modelling based on the P(r) function determined by GNOM. Using GASBOR on the ATSAS online server, *ab initio* reconstruction was carried out by a chain-like ensemble of dummy residues (Svergun, Petoukhov and Koch, 2001). Models were created from all tested samples, enforcing different symmetry arrangements, including no symmetry, P10 (decamer) and P52 (decamer). The number of dummy residues in asymmetric part was set at 160. Models were created both in the slower reciprocal space mode (fits $I_{(q)}$) and in the faster real space mode (fits P(r)). The best-fitted GASBOR models for *strepII*-tagged ZraP-WT and *strepII*-tagged ZraP-SDM were selected, based on the predicted fit *versus* collected experimental data output. Both models were created by GASBOR run at a reciprocal space fit, with a P52 symmetry. The WT envelope was created from the GNOM file created from the P(r) curve of ZraP-WT 10mg/mL exposed to 500nM $ZnCl_2$, whereas the SDM envelope was created from the GNOM file created from the P(r) curve of ZraP-SDM 10mg/mL ex5posed to 100nM $ZnCl_2$. PyMOL was used to create the protein envelope and overlay the 3LAY PDB crystal structure. Figures 4.27-4.28 demonstrate the overlay between the GASBOR predicted envelope structures and the deposited ZraP crystal structure. The images show that ZraP is a globular protein. The envelope of the WT protein appears to be slightly elongated, whereas the SDM envelope appears to form a particle more spherical in shape. The GASBOR theoretical fits with the collected data demonstrate that the envelopes are a rough estimation, and that they should be treated with caution.
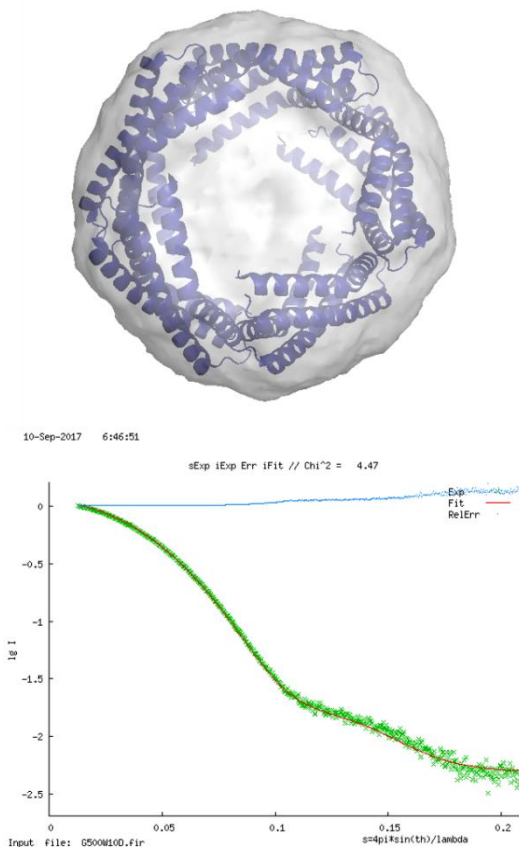
Figure 4.27 GASBOR predicted envelope structure of ZraP-WT 10mg/mL exposed to 500nM ZnCl₂. The envelope structure of ZraP-WT suggests a slightly cylindrical, globular protein that protrudes outwards. The theoretical fit of the GASBOR produced envelope is not a perfect match with the experimental data, which suggests the envelope structure might not be accurately represented by the model.
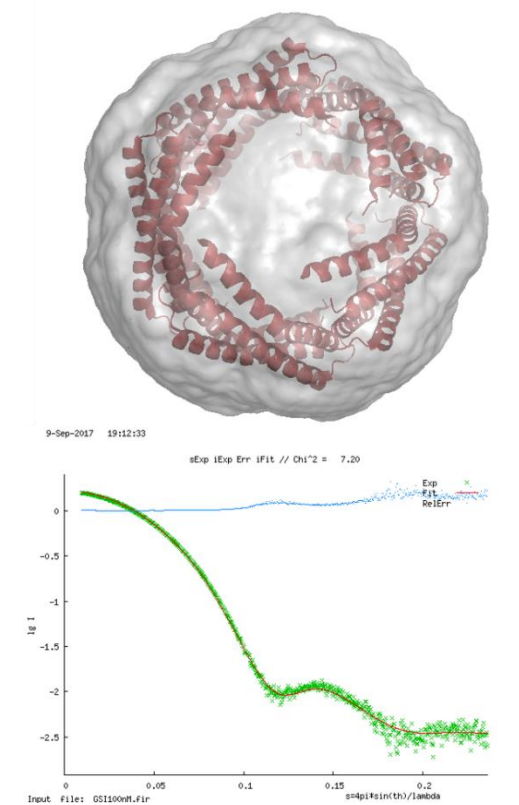
Figure 4.28 GASBOR predicted envelope structure of ZraP-SDM 10mg/mL exposed to 100nM ZnCl₂. The envelope structure of ZraP-SDM suggests a spherical protein that appears slightly flattened at the ends. The theoretical fit of the GASBOR produced envelope is not a perfect match with the experimental data, which suggests the envelope structure might not be accurately represented by the model.

Table 4.3 Overview of SAXS derived ZraP envelope parameters.

Strain	tag	$ZnCl_2$	concentration	Rg	Rg±	I(0)	I(0)±	Fidelity	Porod	Dmax	*TQE	Mw kDa	oligomer
WT	his	-	5mgmL	32.67	0.17	0.71	0.0011	0.93	160000	110.73	0.77	94.12	5.9
			10mgmL	32.91	0.64	1.62	0.0014	0.95	183000	111.03	0.79	107.65	6.7
WT	StrepII	-	5mgmL	32.04	2.40	0.35	0.0008	0.96	169000	101.95	0.73	99.41	6.2
			10mgmL	32.63	4.37	0.96	0.0011	0.97	169000	100.95	0.73	99.41	6.2
WT	StrepII	100nM	5mgmL	32.05	0.50	0.40	0.00098	0.91	138000	99.99	0.73	81.18	5.1
			10mgmL	32.62	0.30	1.04	0.0011	0.96	173000	94.56	0.73	101.76	6.4
WT	StrepII	500nM	5mgmL	32.72	4.13	0.49	0.0012	0.95	130000	100.86	0.72	76.47	4.8
			10mgmL	32.69	0.18	1.07	0.0011	0.97	174000	96.31	0.80	102.35	6.4
WT	StrepII	1uM	5mgmL	32.35	1.24	0.45	0.00098	0.94	137000	98.09	0.77	80.59	5.0
			10mgmL	32.63	2.84	1.19	0.0015	0.93	174000	94.21	0.74	102.35	6.4
WT	StrepII	10uM	5mgmL	32.31	1.73	0.43	0.00093	0.95	135000	99.80	0.70	79.41	5.0
			10mgmL	32.66	3.86	1.13	0.0014	0.95	173000	31.94	0.74	101.76	6.4
WT	StrepII	100uM	5mgmL	32.72	4.13	0.49	0.0012	0.95	156000	102.51	0.72	91.76	5.7
			10mgmL	32.65	0.30	1.16	0.0013	0.94	173000	98.18	0.73	101.76	6.4
SDM	his	-	5mgmL	29.55	0.40	0.36	0.00075	0.97	72200	99.53	0.67	42.47	2.7
			10mgmL	31.09	0.24	0.95	0.0012	0.97	99100	95.03	0.68	58.29	3.6
SDM	StrepII	-	5mgmL	31.08	2.74	0.80	0.00091	0.96	184000	90.66	0.75	108.24	6.8
			10mgmL	31.5	5.19	1.58	0.0012	0.98	197000	84.31	0.80	115.88	7.2
SDM	StrepII	100nM	5mgmL	31.59	0.17	0.78	0.001	0.83	183000	87.17	0.79	107.65	6.7
			10mgmL	31.38	0.04	1.63	0.0013	0.97	197000	85.84	0.77	115.88	7.2
SDM	StrepII	500nM	5mgmL	31.63	0.40	0.78	0.00097	0.92	183000	89.26	0.77	107.65	6.7
			10mgmL	31.46	2.35	1.62	0.0014	0.96	192000	87.02	0.79	112.94	7.1
SDM	StrepII	1uM	5mgmL	31.67	1.01	0.74	0.00098	0.89	176000	88.10	0.80	103.53	6.5
			10mgmL	31.5	0.59	1.60	0.0012	0.96	197000	85.81	0.77	115.88	7.2
SDM	StrepII	10uM	5mgmL	31.61	0.07	0.83	0.0012	0.76	178000	87.74	0.80	104.71	6.5
			10mgmL	31.43	0.69	1.70	0.0012	0.98	198000	85.12	0.77	116.47	7.3
SDM	StrepII	100uM	5mgmL	31.62	0.19	0.87	0.0012	0.92	184000	88.64	0.77	108.24	6.8
			10mgmL	31.45	0.16	1.72	0.0015	0.97	197000	85.74	0.77	115.88	7.2

*TQE = total quality estimate

4.3.8 Analysis of ZraP oligomeric state by Native PAGE

Following the discovery of the interference of the *myc*-His epitope with ZraP-SDM oligomerisation, analysis of *strepII*-tagged ZraP-WT and ZraP-mutant constructs was carried out comparing cross linked protein after storage in 1mM EDTA and storage in 10µM $ZnCl_2$. Previous Native PAGE examination of *myc*-His-tagged ZraP constructs by Wells (2015) indicated that, in the presence of EDTA, the ZraP-SDM mutant was incapable of forming higher oligomeric structures, whereas the ZraP-WT control and all other mutants tested were able to form higher order structures following exposure to EDTA. The results obtained in the current study (figure 4.29) suggest that the *strepII*-tagged ZraP-SDM construct does not suffer from restricted oligomerisation following exposure to EDTA. These results are in agreement with the difference in oligomeric state (volume) between the *myc*-His-tagged and *strepII*-tagged ZraP construct as observed during SAXS analysis (4.4.7.4).
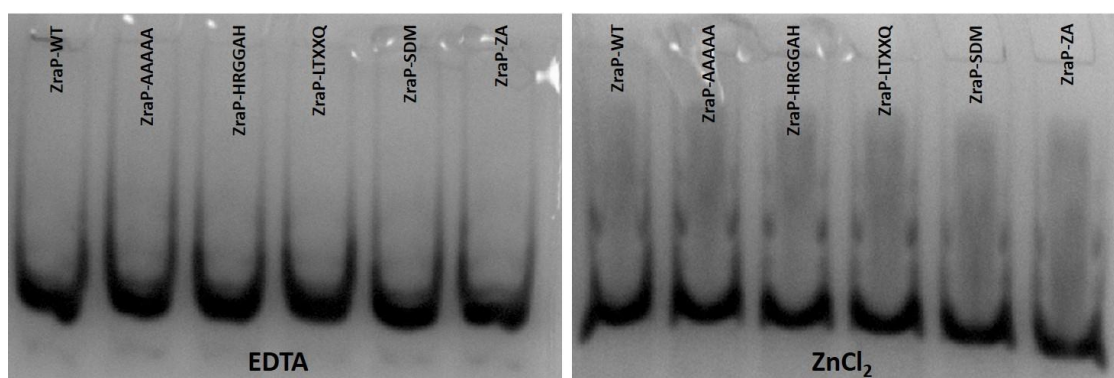
Figure 4.29 Native PAGE analysis of *strepII*-tagged ZraP-constructs following chemical cross-linking exposed to 1mM EDTA and 10µM $ZnCl_2$. The figure demonstrates that the oligomerisation of the ZraP-mutant strains is not affected by either the presence of the metal chelator EDTA (left) or the presence of excess zinc (right) compared to the ZraP-WT construct.

4.4 Discussion and future work

4.4.1 Considerations for future overexpression-plasmid construction

The ZraP proteins used in this study have been overexpressed and purified using C-terminal tags that cannot be removed by restriction enzyme-mediated digestion. Over-expression of ZraP in plasmids encoding cleavable N-terminal tags has been investigated, but following trial assays it became clear that overexpression attempts from these plasmids were unsuccessful. Initial replacement of the previously constructed *zraP* overexpressing pBAD vectors encoding *myc*-His epitopes with *strepII* epitopes, was driven by the aim to prevent potential interference of the additional C-terminal histidines with the zinc assays carried out during SAXS analysis and the zinc-involving chaperone assays described in chapter 5. Furthermore, the presence of histidines in proteins other than the *myc*-His-tagged protein results in background binding of other proteins to the purification column (figure 4.13). Although the one-strep chromatography of His-tagged proteins are relatively pure (>80% according to the purification column manufacturer's guide), the yield of His-tagged proteins is reduced by the need to exclude the earliest elution fractions due to contamination with non-specifically bound proteins, or the requirement of an additional purification step by gel filtration. PAGE analysis of eluted *strepII*-tagged protein samples showed no signs of contamination, and gel filtration analysis demonstrated a clear, single peak, suggesting pure, monodispersed protein samples. The specificity and size of the *strepII* epitope was a clear improvement on the previous *myc*-His epitope.

The presented inconsistencies in the behaviour of *myc*-His-tagged ZraP-SDM reported by Dr. Wells (2015) and the behaviour of *strepII*-tagged ZraP-SDM observed in this study, suggest that the *myc*-His-tag may interfere with the oligomerisation of this particular mutant protein. The significant difference in protein folding and Porod volumes observed using SAXS experiments (figure 4.25) further suggest interference of the *myc*-His-tag in oligomerisation of ZraP-SDM. The *strepII*-tag ($^{N'}$WSHPQFEK'^{C}) used in this study is significantly smaller than the *myc*-His-epitope ($^{N'}$EQKLISEEDLNSAVDHHHHHH'^{C}) previously used for the analysis of ZraP, and is unlikely to interfere with protein folding or secretion (Kimple, Brill and Pasker, 2013). However, the addition of eight unfolded amino acids at the end of each ZraP monomer may interfere in the collection of crystallography data at high resolution. All things considered, it would be greatly beneficial for future studies into ZraP structure and functionality if plasmids were constructed that allowed for the purification of ZraP with a cleavable tag. In the early stages of this study, attempts have been made to produce a *zraP*

encoding overexpression vector with cleavable N-terminal tag using pET-16B (data not shown). This plasmid encodes a polyhistidine tag (10 histidine residues), followed by a restriction site for the restriction protease Factor Xa. Although the plasmid was successfully created, the overexpression trials demonstrated the construct was not being overexpressed. The design for a cleavable tag for a Gram-negative protein targeted to the periplasm or the outer membrane is a challenging task. These proteins, including ZraP, contain an N-terminal signal sequence that allows them to be transported across the inner membrane by the Sec-translocase pathway or the tat-translocase pathway (chapter 1.3). A construct with a cleavable N-terminal epitope could be constructed so that the tag is located before the signal sequence. However, this would likely affect the transport of the protein to the periplasm. Not only would this interfere with the folding of these proteins into their active formation, which happens in the periplasm after their transport across the inner membrane, these proteins would still contain their N-terminal signal sequence after purification and cleavage, which in turn is also likely to interfere with the folding of the protein. Alternatively, a construct could be made lacking the N-terminal sequence. This requires exact knowledge of the end of the signal sequence and the start of the protein. In this study, investigations into the N-terminal of the purified ZraP constructs have been attempted using Maldi-TOF mediated mass fingerprinting analysis following protein digestion with trypsin, a service provided by the John Innis Centre. Unfortunately, attempts to identify the N-terminal sequence of submitted protein samples were unsuccessful, complicating the design for an N-terminal epitope present in between the signal peptide and the protein sequence. An alternative method to create an N-terminal cleavable tag on ZraP would be to truncate the N-terminal sequence to the approximate start of the protein (Petit-Hartlein *et al.*, 2015). Using N-terminal signal peptide prediction software such as SignalP (Nielsen, 2017), the N-terminal signal sequence can be estimated and the overexpression vector can be created using the approximate beginning of the protein of interest. However, the lack of a signal peptide would likely result in accumulation of these overexpressed constructs in their native state in the cytoplasm. Considering this study attempted to ascertain structural properties of ZraP, the lack of exposure to the periplasm could compromise any structural assays conducted. The ideal solution would be the construction of a vector with a cleavable C-terminal epitope. Plasmids have been designed with a TEV (tobacco etch virus) restriction site at the C-terminus. The TEV restriction protease usually targets the N-terminal, cleaving the protein at the C' end of its recognition site. Transferring the TEV restriction site to the C-terminal of a protein results in an overhang of this recognition site (6 amino acids in length)

at the end of the C-terminal after TEV mediated cleavage of the tag. Derivatives of the pMCSG7 vector could be considered for potential future use to create overexpression vectors with a cleavable C-terminal epitope (Eschenfeldt *et al.*, 2010). However, considering the overhang remaining after cleaving is only two amino acids shorter than the current *strepII*-epitopes, it is questionable if changing to a C-terminal cleavable epitope will provide an improvement on the constructed vectors used in this study.

4.4.2 Complications involving protein overexpression in an STM SL1344 background

The overexpression trials of ZraP-WT and mutants in the STM SL1344 Δ*zraP* background, demonstrated the apparent lack of overexpression of *strepII*-tagged ZraP-AAAAA, ZraP-SDM, and ZraP-ZA, despite their successful overexpression and purification from an *E. coli* top10 background. The original *myc*-His tagged constructs were created by Dr. Wells (2015) as mutant from the ZraP-WT overexpression plasmid. Although both ZraP-WT and all mutants are easily overexpressed and purified in *E. coli* Top10, not all mutants could be purified from the *Salmonella* background. The overexpression vectors transformed into *Salmonella* were purified from *E. coli* Top10, and the vectors only differ in the mutated amino acids encoded by *zraP.* The transformation was repeated several times, and despite verification of transformation, including re-sequencing of ZraP-mutant encoding plasmids purified from the *Salmonella* background, attempts to overexpress these ZraP-mutants in *Salmonella* remained unsuccessful. These observations suggest that significant alterations in the N-terminal ^{44}LTxxQ^{48} region, the C-terminal ^{128}GGCGGY^{133} region, or the C-terminal ^{139}HRGGGH^{144} region results in early denaturation or digestion of the overexpressed ZraP-mutant by *Salmonella*. Due to the inability to purify mutant proteins from the STM SL1344 background, any assays comparing ZraP-WT to ZraP-mutants, has been carried out using protein purified from an *E. coli* Top10 background. To ensure purity of the ZraP samples, protein samples used for crystallography and SAXS analysis were analysed for their purity using gel filtration. The clear, single peaks produced by these assays demonstrated the protein samples were pure and monodispersed, which suggests there has not been any interaction between overexpressed *Salmonella* ZraP and native *E. coli* ZraP. To rule out any interaction between the two homologs, the plasmids could be transformed into an *E. coli* Top10 Δ*zraP* background.

4.4.3 Restriction in ZraP-SDM oligomerisation appear to be an artefact of the *myc*-His epitope

The sedimentation equilibrium experiments carried out by AUC reported in this study were a follow-up from previously reported analysis of recombinant ZraP constructs. The experiments carried out in this study analysed ZraP sedimentation at a single speed (10,000 rpm) and a single condition (1mM EDTA) only. To determine potential zinc involvement in oligomerisation, future experiments should include analysis of ZraP at different rotational speeds, as well as include samples exposed to excess zinc. Previous experiments conducted by Dr Wells (2015), demonstrated a significant difference in oligomeric state between the (*myc*-HIS-tagged) ZraP-SDM construct and the other ZraP constructs when exposed to EDTA. This observed difference was confirmed by native PAGE analysis of protein samples chemically cross-linked after exposure to 10mM EDTA. When the native PAGE analysis was repeated using *strepII*-tagged protein constructs instead, the previously observed difference in oligomeric state between ZraP-SDM and the other ZraP constructs, was not observed. Data collected during SAXS analysis demonstrated a significant difference in scattering, fold and size between *myc*-HIS-tagged ZraP-SDM and *strepII*-tagged ZraP-SDM. This difference was not observed between the two corresponding ZraP-WT constructs, suggesting that the observed lack of oligomerisation of the ZraP-SDM mutant may have been an artefact of the *myc*-His epitope. Following up on the SAXS derived observations of differences in molecular weight between *myc*-His-tagged and *strepII*-tagged ZraP-SDM, as well as the inconsistencies between native PAGE analysis of *myc*-His-tagged constructs and *strepII*-tagged constructs, it would be of interest to collect a new set of data for all recombinant ZraP constructs tagged with a *strepII* epitope. This set of data should include analysis at different rotational speeds, as well as analysis of samples as purified, samples in the presence of EDTA, and samples exposed to excess levels of zinc.

4.4.4 Overexpression background may influence ZraP-metal interaction

The ICP-MS data obtained in this study raise some interesting questions regarding ZraP and metal binding. Interactions between zinc and ZraP have previously been recorded (Appia-Ayme *et al.*, 2012; Petit-Hartlein *et al.*, 2015; Wells, 2015), and the metal-binding properties of the *E. coli* ZraP homolog have previously been described by Petit-Härtlein (2015). As a result of lacking ZraP-SDM overexpression in a *Salmonella* background, this study aimed to investigate the metal binding properties of this mutant protein when purified from *E. coli*, and compare it to the metal binding properties of the WT protein purified from *E. coli*, using the ZraP-WT purified from *Salmonella* as a positive control sample. Contrary to the expected

results (similar zinc concentrations for the ZraP-WT proteins purified from different backgrounds, and either similar or different zinc concentrations for ZraP-SDM), the zinc concentration detected for both the WT and the SDM-mutant purified from an *E. coli* background was significantly higher than the zinc concentration recorded for the buffer and the ZraP-WT sample purified from *Salmonella*. The difference in zinc concentration between the ZraP-WT sample purified from *Salmonella* and the buffer was minimal. One possible explanation for the difference in observed zinc concentrations is a difference in the strength of zinc-binding between the proteins purified from *E. coli* compared to the protein purified from *Salmonella*. Although all protein samples were stored in EDTA-free strep buffer, purification of the protein samples was carried out in buffer containing 1mM EDTA, and any loosely bound zinc may have been stripped from the proteins during the purification step. However, considering the ZraP-WT proteins were expressed from the same plasmid in different background strains, it is unlikely that the recorded difference in zinc concentrations is the result of the strength of zinc binding, unless the protein has undergone different post-translational modifications in *E. coli* compared to *Salmonella.* Another explanation of the recorded difference in zinc concentration would be potential difference in zinc availability between *E. coli* and *Salmonella*. Despite being considered a trace element, the apparent zinc availability of *E. coli* is approximately 10^{-4} M, with most of the available zinc being bound to proteins (Outten and O'Halloran, 2001). It is possible that the bioavailability of zinc is lower in *Salmonella* compared to *E. coli*. Zinc is an important cofactor for many bacterial proteins (5.1.3). Nutritional immunity is a process in which the host starves pathogens from essential metals in an attempt to fight infection (Gammoh and Rink, 2017). Zinc is essential to *Salmonella* virulence (Campoy *et al.*, 2002; Ammendola *et al.*, 2007; Karlinsey *et al.*, 2010; Liu *et al.*, 2012; Cerasi *et al.*, 2014), and it is possible that the cellular zinc is primarily bound to other proteins in *Salmonella*. Although Sevcenco *et al*. (2011) reported that the vast majority (>70%) of cellular zinc levels is bound to ZraP, it should be considered this study was conducted in *E. coli*. The results obtained in this study confirm high levels of bound zinc by ZraP when purified from an *E. coli* background, but they also suggest that ZraP may not be the primary zinc-binding protein in *Salmonella*. Although the ZraP-SDM mutant could not be purified from a *Salmonella* background, it would be interesting to repeat the ICP-MS experiments comparing ZraP-mutants that can be purified from a *Salmonella* background, with the corresponding mutants from an *E. coli* background to confirm the observations made during this study. The difference in detected zinc levels between an *E. coli* and a *Salmonella* background may suggest that ZraP may play a more significant role in the

scavenging of excess zinc in *E. coli* than it does in *Salmonella.* However, a report by Petit-Härtlein *et al.* (2015) confirms that, similarly to *Salmonella*, deletion of *zraP* does not result in increased zinc susceptibility in *E. coli.*

A study by Petit-Härtlein *et al.* (2015) on the *E. coli* homolog of ZraP confirmed binding of ZraP to zinc, but claimed ZraP has a higher affinity for copper than for zinc. The data presented in the current study demonstrate that the copper levels detected in the analysed samples are below the minimum detection level. Considering the significant levels of zinc detected in this study, it is unlikely that *Salmonella* ZraP shares the high affinity for copper that has been reported for its homolog in *E. coli.*

4.4.5 SAXS analysis suggests ZraP is a globular protein with a rigid, ring-shaped core.

The structural characterisation of ZraP-WT and ZraP-SDM following X-ray analysis indicates that ZraP forms a globular protein with a rigid ring-shaped core and a more flexible centre. The SAXS data collected from the ZraP-WT constructs suggest that the protein regions unsolved by X-ray crystallography, fill the centre of the protein and may form outward protrusions, giving the protein a more cylindrical shape. However, it should be noted that the predicted scattering of the *ab initio* bead models created by GASBOR, as well as those created by DAMMIF and DAMMIN (data not included) were not a perfect match with the collected scattering data, and should be treated with due care. Due to the lack of clear publishing standards for biomolecular SAXS analysis, analysis and reporting of experimentally collected SAXS data must be carefully considered. In order to correctly analyse SAXS samples, experimentally collected data need to be cut at the right angles to obtain the appropriate information for the questions asked. Whereas X-ray crystallography focuses on the scattering data collected at large angles, which provide information about the atomic structure of a molecule, SAXS is a low-resolution technique that focusses on the data collected from the low angles, which provide information about the shape and size of a particle. Small changes in the angles included in the data-analysis can have significant effects on the overall analysis of the molecule. The SAXS analysis presented in this study was carried out to investigate three separate hypotheses. The first hypothesis stated would be no significant change in protein structure between the ZraP constructs with a C-terminal *myc*-His epitope and those with a *strepII* epitope in the absence of zinc. The second hypothesis stated that loss of the cysteine in the [128]GGCGGY[133] region, would affect the fold and/or oligomeric state of ZraP. The third hypothesis stated that the absence or presence of zinc

affects ZraP shape and/or oligomeric state. Furthermore, SAXS analysis was carried out in an attempt to either confirm or reject the ZraP structure presented by the crystallographic data deposited in the PDB by the centre for structural genomics of infectious disease, as well as the crystallographic data collected in this study.

Comparison of the SAXS data collected for ZraP (wild type and mutant) in the presence of the chelating agent EDTA, demonstrated that whereas there is no major difference in the size and fold of the WT when tagged with either an *myc*-His epitope or a *strepII* epitope, the size and fold of the SDM mutant is significantly affected by the *myc*-His epitope. This tag-induced interference of ZraP-SDM oligomerisation in the absence of zinc, may explain the differences analysis of ZraP-SDM obtained in this study, which suggests there is no inhibition of oligomerisation, and the native gel analysis and AUC data previously recorded by Wells (2015), which indicate ZraP-SDM is incapable of forming higher oligomeric structures in the absence of zinc. Whereas the latter study investigated WT and mutant oligomeric states of constructs carrying a *myc*-His epitope, the current study only analysed constructs carrying a *strepII*-epitope. To confirm this suspicion, the native gels could be repeated analysing *myc*-His-tagged and *strepII*-tagged constructs simultaneously. Furthermore, it would be worth to collect full AUC data sets of *strepII*-tagged ZraP constructs, and compare the collected data to previously recorded experimental data sets.

Comparison of the SAXS data collected from the *strepII*-tagged ZraP-WT and ZraP-SDM demonstrated that disruption of the ^{128}GGCGGY^{133} region does affect the overall protein shape and size. Whereas the X-ray crystallography data collected for the *strepII*-tagged ZraP-WT and ZraP-SDM proteins demonstrated that both proteins form a decameric protein with a ring-shaped core, analysis of the SAXS data presented in this study suggest that the ZraP-SDM construct is more spherical in shape and has a higher Porod volume, but a lower D_{max} than the ZraP-WT construct. The scatter curve collected for ZraP-SDM, as well as the envelope model produced by GASBOR, suggest that the spherical structure of ZraP-SDM is slightly flattened or possibly slightly hollow at the top and bottom end of the protein. In contrast to this, The ZraP-WT protein envelope appears to be more cylindrical in shape, with unresolved parts of the protein filling the hollow centre of the ring-shaped X-ray crystal structure, and parts of the unresolved protein protruding slightly outwards. Although the Porod volume of the ZraP-WT protein in smaller than the volume obtained for ZraP-SDM, the D_{max} is larger, which may be a result of the slightly narrower but more elongated shape of the wild type protein. Although there is a difference in overall shape and size between ZraP-WT and ZraP-SDM, the SAXS data collected suggest that there is no difference in oligomeric

state between the two species once the 10% error in the Porod volume values has been taken into consideration. Experiments carried out on an *E. coli* ZraP homolog with a C104A substitution, suggested that the cysteine was required for the formation of ZraP dimers (Petit-Hartlein *et al.*, 2015). The data presented in this study suggest that the single cysteine residue of *Salmonella* ZraP is not critically required for the formation of higher oligomeric structures in either the presence or absence of zinc.

The SAXS data collected of the *strepII*-tagged ZraP-WT and ZraP-SDM constructs comparing samples stored in either EDTA or in a range of zinc concentrations indicate that exposure to zinc does not affect ZraP oligomerisation for either ZraP-WT or ZraP-SDM. The data collected for the ZraP-WT sample suggest there may be a slight reduction in total volume in the presence of EDTA, but this reduction is negligible once the error in Porod volume values (10%) has been taken into account. There is no significant difference in Porod volume between any of the tested ZraP-SDM samples. The Kratky plots collected for ZraP-WT and ZraP-SDM suggest that zinc does not affect the overall compactness or protein folding of ZraP. Although ZraP-mediated protection against protein aggregation is reported to be significantly more effective in the presence of zinc (Appia-Ayme *et al.*, 2012; Petit-Hartlein *et al.*, 2015; Wells, 2015), the SAXS data collected in this study indicate that it is unlikely that this increased chaperone activity is a result of conformational changes or changes in oligomeric state.

Overall, the SAXS data reported in this study clearly demonstrate that the hollow, ring-shaped crystal structure of ZraP is but only a partial representation of the whole protein. The scattering data collected for the protein envelope suggest ZraP is a globular protein that is potentially cylindrical or spherical in shape. The unresolved regions missing in the X-ray crystal structure fill the hollow space and may protrude outwards from the centre of the protein ring. Although the exact protein structure remains enigmatic, the data presented in this study indicate that ZraP is a globular protein, capable of forming higher order oligomeric structures independent of zinc concentrations. Furthermore, in *Salmonella*, the [128]GGCGGY[133] C-terminal region does not appear to be critically required for the oligomerisation of ZraP.

Chapter 5.
Functional analysis of the periplasmic chaperone ZraP
from *Salmonella* Typhimurium

5.1 Introduction

Periplasmic chaperones play an important role in the biogenesis, maintenance and repair of the Gram-negative outer membrane. Due to their involvement in the protection against many environmental hazards, the cellular functions of periplasmic chaperones frequently overlap with those of other periplasmic proteins. The overlapping nature of periplasmic chaperones and their associated envelope stress responses, complicates the study into the functions of individual members. ZraP is a periplasmic protein and an auxiliary member of the most recently discovered zinc-responding two-component envelope stress response ZraSR. This chapter investigates the role of zinc in the chaperoning function of *Salmonella* ZraP.

5.1.1 Current knowledge of the function of the ZraSR two component system

Initial identification of the *E. coli* ZraSR two-component system classed it as a homologue of the nitrogen-responding NtrBC two-component system of *Klebsiella pneumoniae* based on sequence similarity, and named it HydGH for its regulation of the *hyd* genes associated with the production of hydrogenase 3 in *E. coli* (Stoker *et al.*, 1989). It was later revealed that the regulation of the *hyd* genes by ZraR (then called HydG) was the result of non-specific cross talk, and that expression of the system was actually responsive to elevated zinc levels. The two-component system was renamed to <u>z</u>inc <u>r</u>esistance <u>a</u>ssociated, ZraSR. Furthermore, the study reported that phosphorylated ZraR binds to the intergenic region of ZraS and ZraP, regulating their expression, and implicating involvement of ZraP in the workings of the ZraSR two component system (Leonhartsberger *et al.*, 2001).

The function of the ZraSRP envelope stress response system remains unclear. Expression of the *zraSR* operon is induced in the presence of lead, tungstate and zinc, and the periplasmic chaperone ZraP appears to be zinc responsive (Leonhartsberger *et al.*, 2001; Appia-Ayme *et al.*, 2011, 2012). *In vitro* functional characterisation of *E. coli* two component systems demonstrated that the response regulator ZraR is not only phosphorylated by ZraS, but can also be phosphorylated by UhpB, a sensor protein of the UhpABC phosphorelay system involved in the regulation of the sugar phosphate transporter UhpT (Island, Wei and Kadner, 1992; Yamamoto *et al.*, 2005). Cross-talk between ZraS and the RpoS-regulating anti-sigma factor RssB, as well as cross-talk between ZraS and the putative polyketide synthase YjhK in a synthetic environment has been suggested (Zhang *et al.*, 2008; Wells, 2015). Furthermore, ZraR has been demonstrated to act as a bacterial enhancer binding protein (bEBP) for the

nitrogen-utilisation sigma factor RpoN (Samuels *et al.*, 2013), and an RpoN binding site is found within the *zraP-zraSR* intergenic region (figure 5.1). It has been suggested that the binding of RpoN to this site is facilitated by ZraR (as bEBP). Expression of this promoter is switched off in the absence of transcriptional activators (Noll, Petrukhin and Lutsenko, 1998), however a weak constitutive promoter of *zraSR* allows for basal expression levels (Noll, Petrukhin and Lutsenko, 1998; Leonhartsberger *et al.*, 2001; Ravikumar *et al.*, 2011).
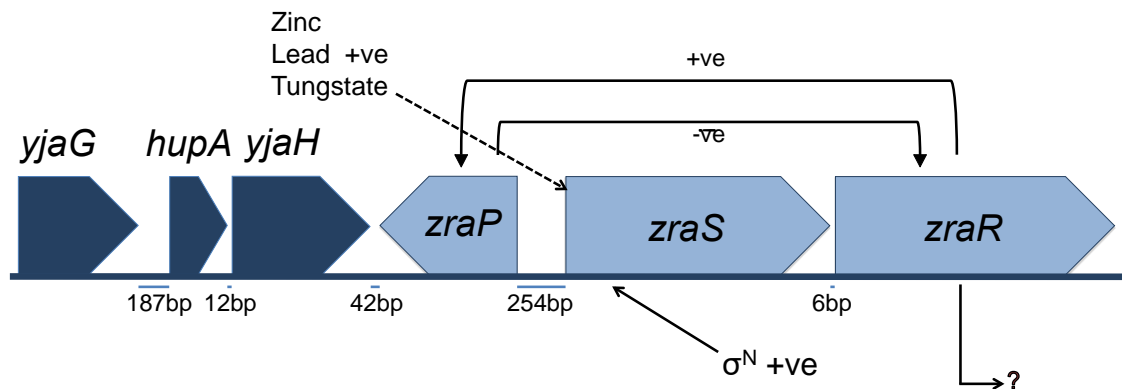
Gene Summary
hupA = transcriptional regulator
yjaH = inner membrane protein
zraP = zinc responsive periplasmic chaperone
zraS = sensor kinase
zraR = response regulator and enhancer binding protein

Figure 5.1 Schematic representation of the ZraPSR operon. The RpoN regulated two component system ZraSR positively regulates the transcription of its inversely oriented auxiliary protein ZraP. In turn, the expression of ZraR is negatively regulated by ZraP. Although evidence suggests expression of the ZraSR two-component system is induced in the presence of zinc, lead and tungstate, little is known about the precise function of this envelope stress response system. Image taken from Wells (2015).

Considering ZraSR activity is responsive to zinc, an important cofactor for many cellular process, and ZraSR activity is linked to multiple cellular functions, including the regulation of two major stress response sigma factors, sugar metabolism and glucose-6-phosphate uptake, it is surprising that Δ*zraSR* strains do not appear to have a particularly significant phenotype in *Salmonella*. To further investigate the role of this two-component system, transcriptomic analysis has been carried out by a previous member of the Rowley lab (Wells, 2015). Their analysis demonstrated differential expression for 186 genes, including the *zraSRP* operon and 89 genes that belong to the RpoN regulon. The regulation of the latter genes are attributed to the bEBP activity of ZraR, as opposed to genes being directly regulated by the ZraSR system. Among the 97 genes not belonging to the RpoN regulon is only one known metal trafficking protein: the divalent metal cation transporter MntH,

involved in the uptake of manganese and iron (Golynskiy *et al.*, 2006; Wells, 2015). The upregulation of a manganese transporter in response to high zinc may seem out of place, but it has been suggested that this phenomenon plays a role in *Salmonella* virulence (Wells, 2015). MntH has been implicated in the virulence of *Salmonella*, *Shigella flexneri* and *Yersinia pestis* (Zaharik *et al.*, 2004; Runyen-Janecky *et al.*, 2006; Perry *et al.*, 2012). There is evidence to suggest that immune cells protect themselves against infection in a process named nutrient immunity, which involves increasing intracellular levels of copper and zinc, and that this sudden increase can be damaging for intracellular pathogens (Hood and Skaar, 2012; Stafford *et al.*, 2013). MntH could contribute to the prevention of extreme nutrient limitation, by increasing cellular concentrations of Mg^{2+} and Fe^{2+} (Jabado *et al.*, 2000; Porcheron *et al.*, 2013). This way, the ZraSR system may not directly protect against the increase of extracellular zinc, but instead it could be acting as a sensory system to detect environmental conditions. Other genes of interest that are regulated by ZraR include the heat-shock responsive chaperones ClpB, DnaK, GroEL, GroSL, and GrpE. These cytoplasmic chaperones are all involved in the protection against the formation of protein aggregates, as well as the unfolding and refolding of heat-damaged proteins (Horwich *et al.*, 1993; Schroder *et al.*, 1993; Rosen and Ron, 2002). The regulation of these chaperones by ZraR suggest involvement of ZraSR in the heat-shock response. Previously a role for ZraSR was implicated in the CSIXR response to heat (Wells, 2015), but data presented in this study suggest otherwise (3.4.3) . The exact role of ZraSRP in response to heat requires further investigation. Another group of genes that are shown to be transcriptionally regulated by ZraR include genes associated with survival inside the *Salmonella* containing vacuole (SCV). Expression of *fadL*, a fatty acid transporter, is upregulated by ZraR. Fatty acids are used as the primary source of carbon by *Salmonella* surviving in the phagosomes of macrophages (Fang *et al.*, 2005; Wells, 2015). Genes involved in anaerobic growth are also targeted by ZraR. These include the operons *dcuAB, frdABCD,* and *hypABC,* as well as the cytochrome o oxidase *cyoA,* the nitroreductase *hypO,* and the transcriptional regulator *slyA*. Although there is no evidence for the requirement of the ZraSRP response system for survival inside the SCV specifically, the evidence presented in the literature so far suggests ZraSR is a regulator of protein homeostasis in response to external stress (Wells, 2015).

5.1.2 Current knowledge of the function of the periplasmic chaperone ZraP

Little is known about the role of ZraP in response to envelope stress. Appia-Ayme *et al.* (2012) demonstrated that this periplasmic chaperone is involved in the negative regulation of the ZraSR two-component envelope stress response system. Upregulation of gene expression in the presence of zinc has been recorded for all three periplasmic chaperones of the CpxP family. However, the upregulation of ZraP is more profound than that of CpxP and Spy (Graham *et al.*, 2009). A 12-fold upregulation of *zraR* is reported in the absence of *zraP*, whereas overexpression of *zraP* results in *zraR* downregulation (Leonhartsberger *et al.*, 2001; Lee, Barrett and Poole, 2005; Appia-Ayme *et al.*, 2012). It is thought that the regulatory function of ZraP acts as part of a negative feedback loop (figure 5.1), similar to the one observed for CpxP and CpxR. There is no evidence for a similar feedback loop between Spy and the two component envelope stress response system BaeSR (Quan *et al.*, 2011; Appia-Ayme *et al.*, 2012). Furthermore, in the presence of zinc, ZraP exhibits more potent chaperone activity than Spy *in vitro*, whereas the presence of zinc chelating agents significantly reduces ZraP chaperone activity. (Quan *et al.*, 2011; Appia-Ayme *et al.*, 2012). In *E. coli*, zinc binding assays carried out on 30 soluble, zinc-associated proteins, identified ZraP as the primary zinc binding protein *in vitro,* binding over 70% of the total zinc available (Sevcenco *et al.*, 2011). Despite the extensive evidence on the upregulation of ZraSRP and the increased chaperone activity of ZraP, the biological relevance of the interactions between zinc and this two-component envelope stress response remain enigmatic.

The overlapping interactions between different two-component systems and periplasmic chaperones complicates the investigation into the function of ZraP. The identification of ZraSRP as a two-component envelope stress response system was first reported by Appia-Ayme *et al.* (2011), after overexpression of the response regulator BaeR resulted in *zraP* repression. In Salmonella, the deletion of *baeR* results in an upregulation of the *zraSRP* operon in the presence of tungsten (Appia-Ayme *et al.*, 2011). In *E. coli,* the repression of *baeSR* in the presence of zinc has been attributed to *zraSRP* upregulation (Graham *et al.*, 2012). Phenotypical analysis of ZraP suggests potential involvement of ZraP in the protection against oxidative stress. Assays carried out in this study have demonstrated an increased sensitivity of the *Salmonella ΔzraP* strain in the presence of hydrogen peroxide, hydroxyurea and polymyxin B. The involvement of ZraP in polymyxin B induced envelope stress has also been recorded by Appia-Ayme *et al*. (2012) and Wells (2015). Furthermore, results presented in chapter 3.4 suggest a role for ZraP in the protection of outer membrane integrity.

Salmonella Δ*zraP* mutants appear more sensitive to penicillin G and phosphomycin compared to the WT control. Penicillin G and phosphomycin are antibiotics that act upon the formation of the peptidoglycan layer. The natural immunity of Gram negative species to these compounds is a result of the impenetrability of the outer membrane. The increased sensitivity of *Salmonella* Δ*zraP* mutants to these compounds suggest outer membrane defects. Interestingly, the *Salmonella* Δ*zraP* mutants did not show increased sensitivity to either vancomycin or bacitracin, two antibiotics also involved in the prevention of peptidoglycan formation. Considering both penicillin G and phosphomycin are small molecules, whereas vancomycin and bacitracin are significantly larger, it is possible that Δ*zraP* only results in minor membrane defects and a slight increase in permeability.

It has been suggested that the ZraSRP system is involved in the regulation of envelope stress during survival in the SCV. Upon infection, immune cells are known to sequester trace minerals including zinc so as to reduce their availability to pathogens and induce nutritional immunity (Gammoh and Rink, 2017). However, this increase in intracellular levels of zinc in macrophages could act as an inducing signal for intracellular pathogens such as *Salmonella*, who would be exposed to increased levels of zinc due to the increased cellular concentration of Zn^{2+} in the host cell. Interestingly, a study into the investigation of the structure and function of *E. coli* ZraP reported a contradiction in the apparent metal interactions between *E. coli* ZraP and *Salmonella* ZraP (Petit-Hartlein *et al.*, 2015). Whereas studies into *Salmonella* ZraP have demonstrated interactions of ZraP and zinc (Appia-Ayme *et al.*, 2012; Wells, 2015) and studies into *E. coli* ZraP have reported a strong preference of ZraP for zinc (Leonhartsberger *et al.*, 2001; Lee, Barrett and Poole, 2005), the study of Petit-Hartlein *et al.* (2015) claims that *E. coli* ZraP binds copper more strongly than zinc. These discrepancies may further support the theory of a role for ZraP in the protection of the cell during infection. The sequestering of zinc by macrophages would act as an indicator for the intracellular pathogen *Salmonella*. However, most pathogenic *E. coli* strains act as extracellular organisms and they lack the genes required for survival inside the macrophage phagosomes. Among other biocidal components, macrophages recruit copper to the phagosome (Djoko *et al.*, 2015), and mutations of the *cusFCBA* operon in *E. coli*, encoding a secondary copper efflux system, significantly affects colonisation and survival (Subashchandrabose *et al.*, 2014). If the binding of zinc to *Salmonella* ZraP functions as a signal for gene regulation required for survival inside the SCV, it is possible that the binding of zinc as well as the binding of copper to *E. coli* ZraP is linked to survival inside the phagosome. The potential involvement of the ZraSRP system in survival inside the SVC or phagosomes is purely hypothetical, based on observations

regarding the ZraR regulon members reported by Wells (2015), and further research is required to confirm this hypothesis.

5.1.3 Bacterial regulation of zinc availability

Zinc is an abundant metal in the environment and plays an important role in many cellular processes of both prokaryotic and eukaryotic organisms. Zinc is incorporated in approximately 10% of the eukaryotic proteome, and binds between 5-6% of prokaryotic proteins (Andreini *et al.*, 2006). Cellular zinc levels are tightly controlled; zinc starvation is a major stress to bacteria due to its involvement in a wide range of cellular processes. However, high zinc levels are toxic due to the highly competitive nature of zinc, which is able to displace less tightly-bound transition metals in active sites of metalloenzymes (Capdevila, Wang and Giedroc, 2016). Homeostasis of cellular zinc levels is maintained by the transcriptional regulation of metalloregulatory proteins, the regulation of zinc influx and efflux, and by reallocating zinc among dependent proteins (Capdevila, Wang and Giedroc, 2016). Genes involved in the transcriptional regulation of zinc levels include the zinc uptake repressor Zur and the transcriptional regulator ZntR. During periods of excess zinc, Zur-Zn^{2+} complexes inhibit the expression of high-affinity zinc uptake systems such as the ABC-transporter ZnuABC, and the zinc-bound ZntR allosterically activates transcription of the ATPase efflux transporter ZntA. During periods of zinc starvation, the apo-form of ZntR represses the expression of zinc efflux systems instead (Ma, Jacobsen and Giedroc, 2009; Gilston *et al.*, 2014; Capdevila, Wang and Giedroc, 2016). These ZntR regulated transporters include the efflux transporter ZntA, the cation diffusion facilitator ZitB and the periplasm-spanning efflux guns CzcD and CzcBCA (Blindauer, 2015; Capdevila, Wang and Giedroc, 2016). Other proteins thought to be involved in the regulation of cellular zinc levels, include the outer membrane porin CbpA, the zinc/cadmium transporter YiiP and the zinc binding protein ZinT (Grass *et al.*, 2005; Wei and Fu, 2006; Petrarca *et al.*, 2010; Stork *et al.*, 2013). Furthermore, zinc can be reallocated among proteins during zinc starvation conditions. During this process zinc-containing protein subunits are replaced with non-zinc-containing subunits, so that the zinc ions can be used for key zinc-dependent metabolic functions instead (Panina, Mironov and Gelfand, 2003; Capdevila, Wang and Giedroc, 2016). Although ZraP and ZraSR are strongly zinc-responsive, there is currently no evidence for their involvement in cellular zinc homeostasis.

5.2 Aims

The chapter aims to expand on the current understanding of the chaperoning role of ZraP, by further investigating the contribution of zinc, as well as by analysing how the LTxxQ domain of unknown function, and two potential zinc-binding sites, affect overall chaperone activity of ZraP.

Previous studies have indicated that ZraP chaperone activity is capable of protecting malate dehydrogenase against thermal aggregation. These studies have also demonstrated that the chaperone activity is positively affected by zinc (Appia-Ayme *et al.*, 2012; Petit-Hartlein *et al.*, 2015; Wells, 2015). To investigate if, in addition to protection against aggregation, ZraP is capable of protecting substrate activity in denaturing conditions, MDH activity assays were conducted. Furthermore, to investigate if the predicted zinc-binding regions [120]GGCGGY[125] and [130]HRGGGH[134], as well as the conserved region of unknown function [44]LTxxQ[48] are involved in chaperone activity, assays were conducted comparing the chaperone activity of these mutant proteins with ZraP-WT.

In addition to general chaperone activity, the ability of ZraP to protect the protein activity of commercially available DNA gyrases has been investigated using DNA Gyrase provided by Inspiralis Ltd. Furthermore, this study aimed to improve our current understanding of the involvement of ZraP in the protection against envelope stress, by identifying natural ZraP substrates during protein pull-down assays.

5.3 Results

5.3.1 Optimisation of malate dehydrogenase activity assays

Malate dehydrogenase (MDH) is a ubiquitous enzyme that is found in eukaryotes, prokaryotes and archaea. Utilising NAD^+/NADH as cofactors, MDH reversibly catalyses the conversion between malate and oxaloacetate, a reaction required in various metabolic pathways (Minárik *et al.*, 2002). The oxidation of NADH to NAD^+ results in a colour shift from the orange coloured NADH to the colourless NAD^+. This colour shift allows for colourimetric assays that analyse the activity of MDH by measuring the colour change that represents conversion of NADH into NAD^+. The MDH activity assays were carried out to analyse the effect of zinc on the chaperoning activities of ZraP, as well as to investigate the importance of the two proposed zinc binding regions, and the LTxxQ region in chaperone activity. To analyse general ZraP chaperone activity, MDH was exposed to the denaturing agent guanidine hydrochloride (GnHCl) either in the presence or in the absence of ZraP. These experiments were carried out in a range of zinc concentrations to determine the effect of zinc on ZraP chaperone activity. Furthermore, the chaperone activity of the ZraP mutant proteins was assessed both in the presence and in the absence of zinc.

5.3.1.1 HEPES buffer is unsuitable for MDH activity assays

Initial MDH activity experiments were carried out following the protocol as described by Wells (2015). This protocol dictated the incubation of MDH and the execution of the assay in 50mM HEPES buffer pH 7.4. However, when conducting the assays in HEPES buffer, only very limited MDH activity could be detected (data not shown). Further method investigation of published work involving MDH activity assays suggested the use of PBS buffer pH 7.4 instead (Han *et al.*, 2014; Worthington Biochemical Corporation., 2015; Karuppanan *et al.*, 2017). The activity of MDH in PBS buffer was significantly improved compared to the activity of MDH in HEPES buffer and PBS buffer was initially adopted to investigate ZraP chaperone activity.

5.3.1.2 PBS buffer is unsuitable for MDH activity assays

Although MDH activity was significantly increased using PBS buffer, repeatability and consistency of the assay became a significant issue in PBS (figure 5.2). To set a standard for MDH activity, experiments were carried out incubating MDH only in the absence of zinc and chaperone first. MDH activity was then assessed after incubation with 100 µM zinc chloride to assess the effect of zinc on MDH activity to ensure any observed changes in MDH activity in chaperone experiments were correctly attributed to the chaperone. However, the MDH-zinc control experiments were inconsistent in their repeatability. Sometimes zinc

significantly affected MDH activity either positively or negatively, other times significant differences could not be observed. The data collected for MDH incubated with ZraP-WT, either in the presence or absence of excess zinc, were slightly more consistent in their repeatability, but the data demonstrated conflicting evidence for the chaperoning of MDH by ZraP and the effect of zinc on ZraP chaperone activity (figure 5.2). In the absence of a denaturing agent, ZraP appears to inhibit MDH activity in the absence of zinc, but boost its activity in the presence of zinc. The data collected for MDH-zinc samples suggested that this boost was the result of the presence of zinc boosting MDH activity. At lower denaturant concentrations, the presence of ZraP and the presence of zinc appeared to increase MDH activity. At a GnHCl concentration of 0.6 M, the presence of zinc suddenly affected MDH activity negatively, whereas the presence of ZraP (no excess zinc) still boosted MDH activity. At high denaturant concentrations, the presence of both zinc and ZraP negatively impacted MDH activity.
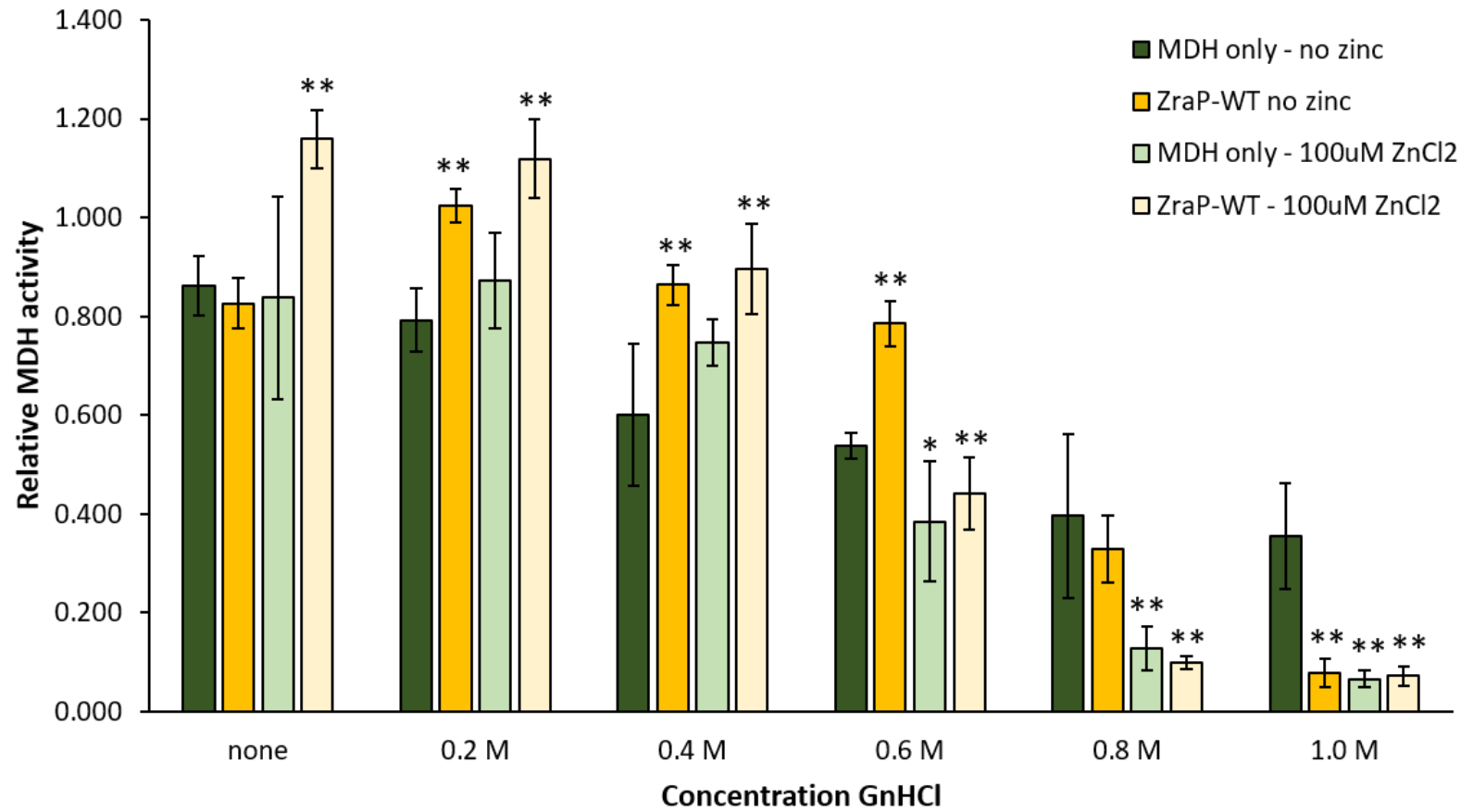
Figure 5.2 MDH activity assays carried out in PBS buffer pH 7.4. PBS-buffer derived data collected for the activity of MDH in the absence and presence of chaperone and/or zinc were inconsistent. Whereas MDH activity appeared to be protected by ZraP at some concentrations GnHCl, this protection was lost at higher concentrations. The presence of zinc both activates and represses MDH activity in an inconsistent manner.

5.3.1.3 Tris buffer is suitable for MDH activity assays

Following an accidental mix-up of buffers, MDH activity was tested in the Tris buffer used for purification of *Strep*-tagged proteins. It was immediately apparent that MDH is significantly more active in Tris buffer than it was in either PBS or HEPES buffer. Furthermore, the data collected for MDH assays carried out in Tris buffer were more consistent and more repeatable than the data collected in PBS. Further experiments were conducted in Tris buffer.

5.3.1.4 Zinc negatively affects MDH activity

Using Tris buffer for MDH activity assays revealed an additional complication to the chaperone assays; the rate at which MDH converts oxaloacetate into L-malate is significantly reduced in the presence of zinc (figure 5.3). At 100µM zinc, MDH activity is reduced by approximately 17%, whereas 2mM zinc reduced MDH activity by approximately 70%. In an attempt to curb the zinc-induced inhibition of MDH, MDH activity assays were carried out in Tris buffer containing 1mM EDTA. The rationale behind these tests was that the zinc bound to MDH during the incubation period, may be chelated when exposed to EDTA post incubation. Although significant differences were detected between the activity of MDH in buffers with and without EDTA at the higher zinc concentrations, the difference between the two conditions was only about 2%. Furthermore, for the conditions in which significant differences were detected, the samples exposed to EDTA showed lower MDH activity than those not exposed to a chelator (figure 5.3).

A similar effect was observed for samples comparing MDH incubated in the presence of ZraP-WT and various zinc concentrations. Execution of these assays in the presence of EDTA did not restore MDH activity to zinc-free level, and if significant differences were detected between the EDTA-containing conditions and the EDTA-free conditions, the presence of EDTA appeared to reduce MDH activity further (figure 5.4). Furthermore, incubation with ZraP-WT, regardless of zinc or chelator, also reduces MDH activity, compared to MDH activity alone. This inhibiting effect of ZraP-WT on MDH activity is observed across all tested zinc concentrations (figure 5.5).

The zinc chelation experiments were repeated testing the effect of prolonged EDTA exposure. These experiments tested MDH incubated in Tris buffer, either in the absence of zinc or with 500µM and 2mM zinc chloride (figure 5.6), and MDH incubated with ZraP-WT under the same conditions (figure 5.7). The activity assays were then conducted in EDTA-containing Tris buffer. Considering MDH will only oxidise NADH in the presence of

oxaloacetate, the EDTA exposure time of the incubated samples could be increased by holding off the addition of oxaloacetate and thus postponing the onset of the reaction. The data presented in Figure 5.5 and figure 5.6 demonstrate that regardless of ZraP-WT presence, increased exposure to EDTA does not restore MDH activity levels to the activity of unexposed MDH samples. Considering the negative effect of zinc on MDH activity cannot be avoided, further MDH activity assays screening the chaperone effect of different ZraP mutants were carried out in the presence of 100µM zinc.
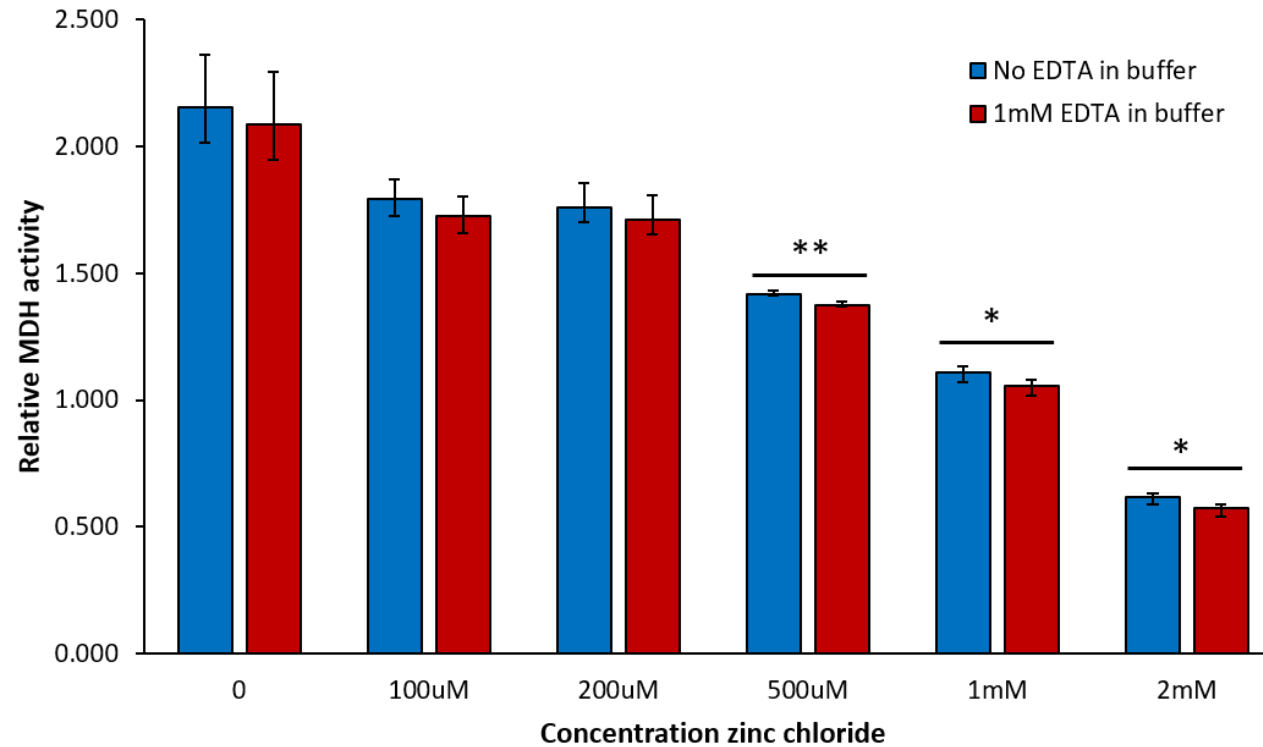
Figure 5.3 Zinc negatively regulates the ability of MDH to convert oxaloacetate into *L*-malate. MDH activity assays carried out in Tris buffer demonstrated that MDH activity is reduced in the presence of zinc. To test if the chelator EDTA was capable of reversing this inhibition, MDH activity was assessed in Tris buffer with EDTA and Tris buffer without EDTA. At lower zinc concentrations there was no significant difference in MDH activity between samples tested with and without EDTA in the buffer. Presence of EDTA in the buffer demonstrated a significant difference in MDH activity at 500µM, 1mM and 2mM zinc. Interestingly, instead of boosting MDH activity, the presence of EDTA appeared to reduce MDH activity even further. Significant differences between the samples tested in Tris buffer with and without EDTA are indicated by * ($P < 0.05$) and ** ($P < 0.01$), Student's t-test assuming equal variance, n = 3. Error bars indicate standard deviation.
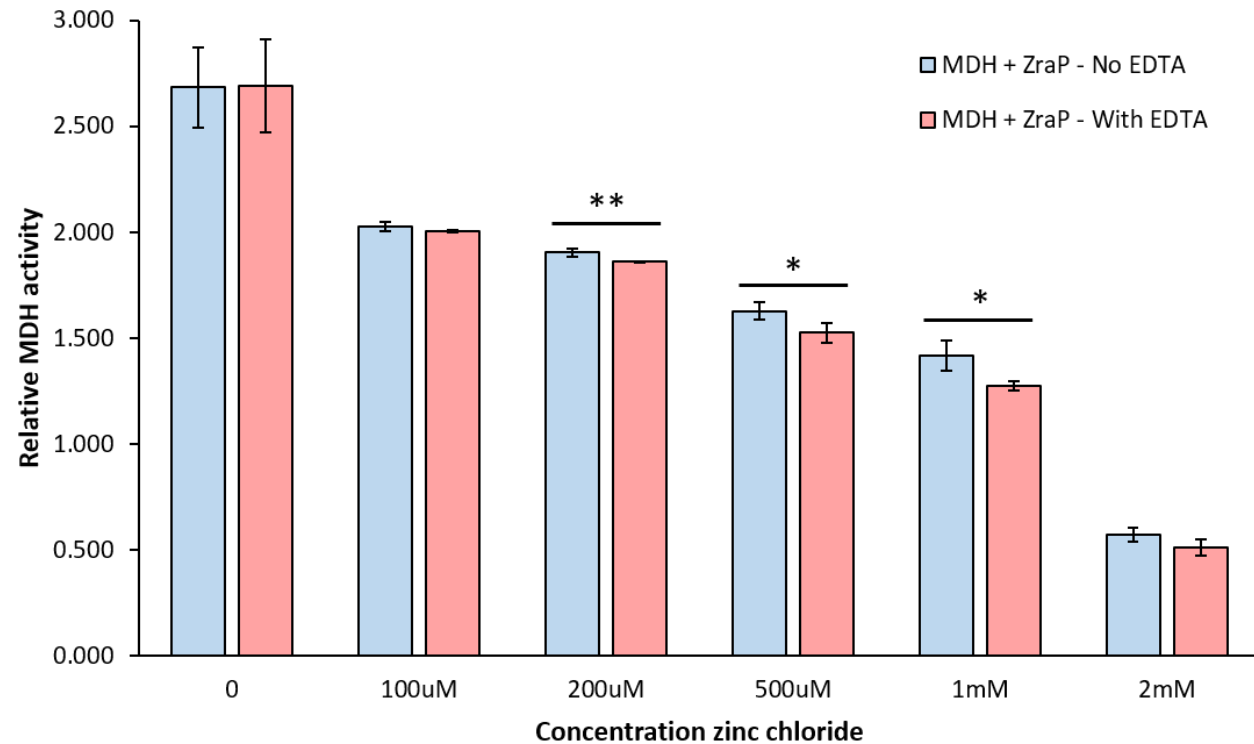
Figure 5.4 The presence EDTA does not negate the zinc-induced inhibition of MDH activity in the presence of ZraP-WT. MDH activity assays carried out in Tris buffer demonstrated that MDH activity is reduced in the presence of zinc. To test if the chelator negatively affects MDH activity in the presence of ZraP, MDH assays were conducted at different zinc concentrations, comparing activity of samples in Tris buffer with and without EDTA. Significant difference in MDH activity between samples tested with and without EDTA in the buffer was detected at 200µM, 500µM and 1mM zinc chloride. Similarly to the results obtained in the assays testing MDH without chaperone, the presence of EDTA appears to reduce MDH activity even further. Significant differences between the samples tested in Tris buffer with and without EDTA are indicated by * (P < 0.05) and ** (P < 0.01), Student's t-test assuming equal variance, n = 3. Error bars indicate standard deviation.
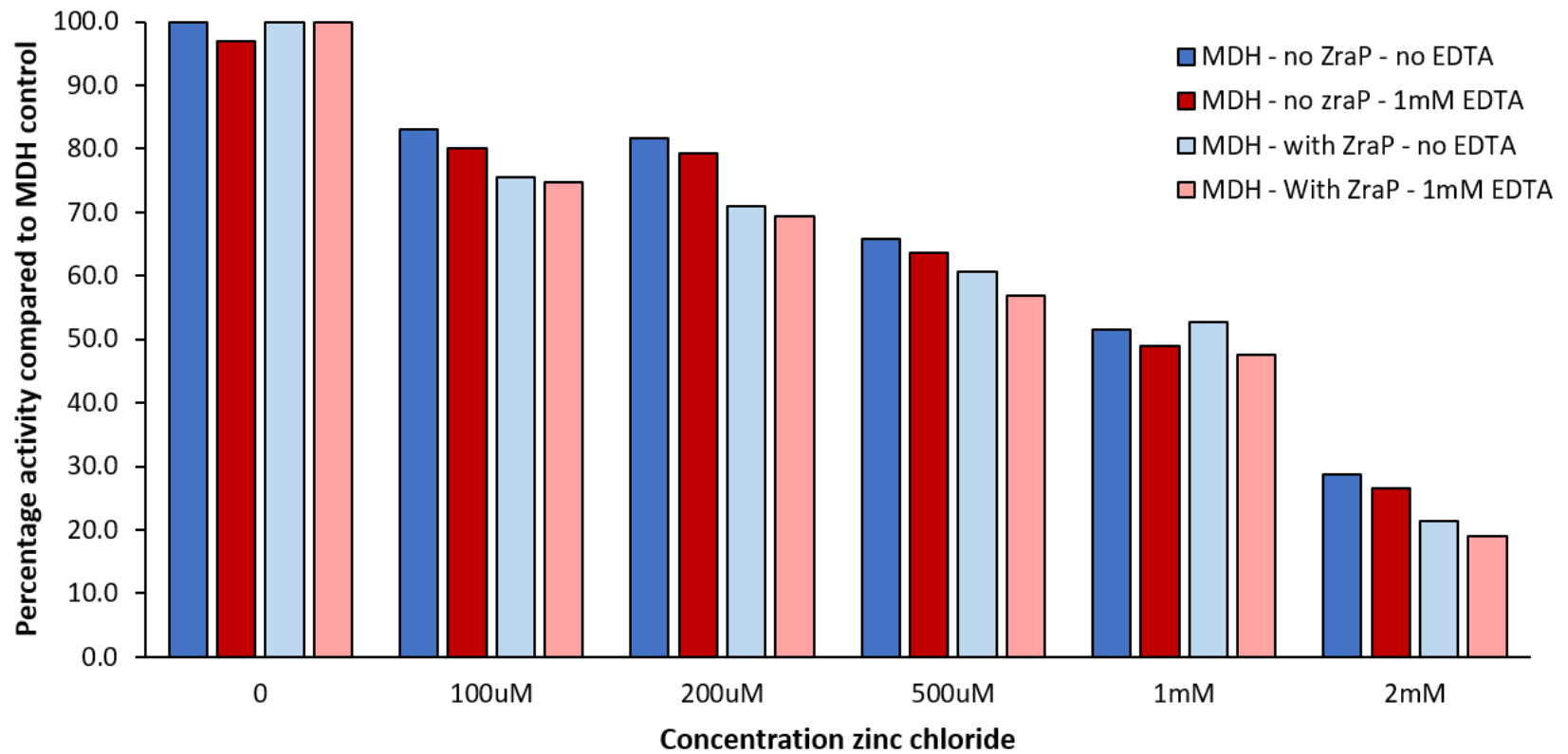
Figure 5.5 The presence of ZraP-WT further reduces MDH activity in the presence of zinc. MDH activity assays carried out in Tris buffer represented as percentage activity compared to the MDH-only (no zinc) condition. This figure shows that incubation of MDH with ZraP-WT and excess zinc reduces MDH activity significantly. Execution of the MDH assays in the presence of EDTA cannot reverse this inhibition.
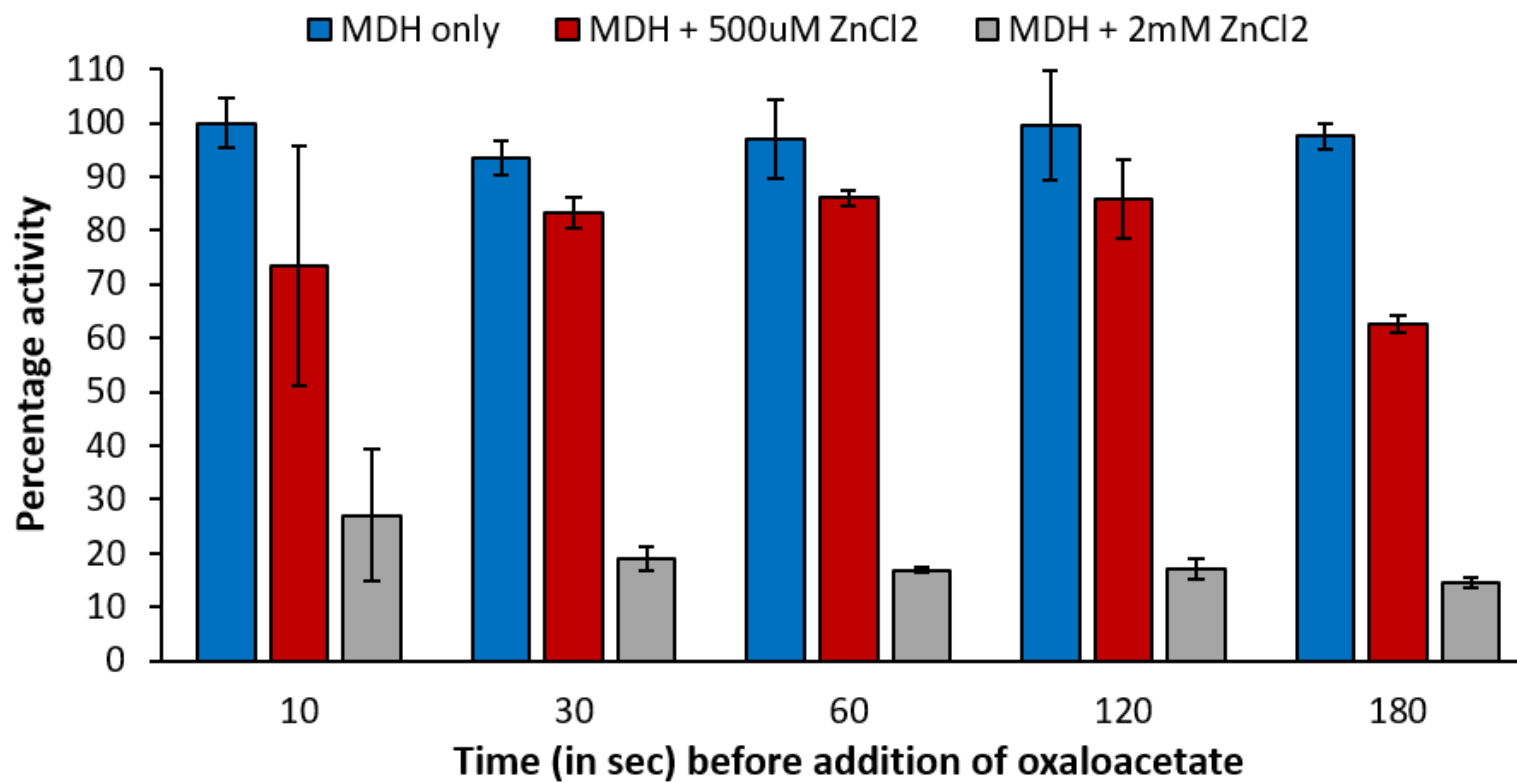
Figure 5.6 Prolonged exposure to EDTA does not restore MDH activity in the presence of zinc. MDH activity assays carried out in Tris buffer represented as percentage activity compared to the MDH-only (no zinc) condition. Comparing the MDH activity of MDH only samples to samples incubated with either 500μM ZnCl$_2$ or 2mM ZnCl$_2$, the figure shows that prolonged exposure to EDTA prior to substrate addition does not reverse the zinc-induced inhibition of MDH activity.
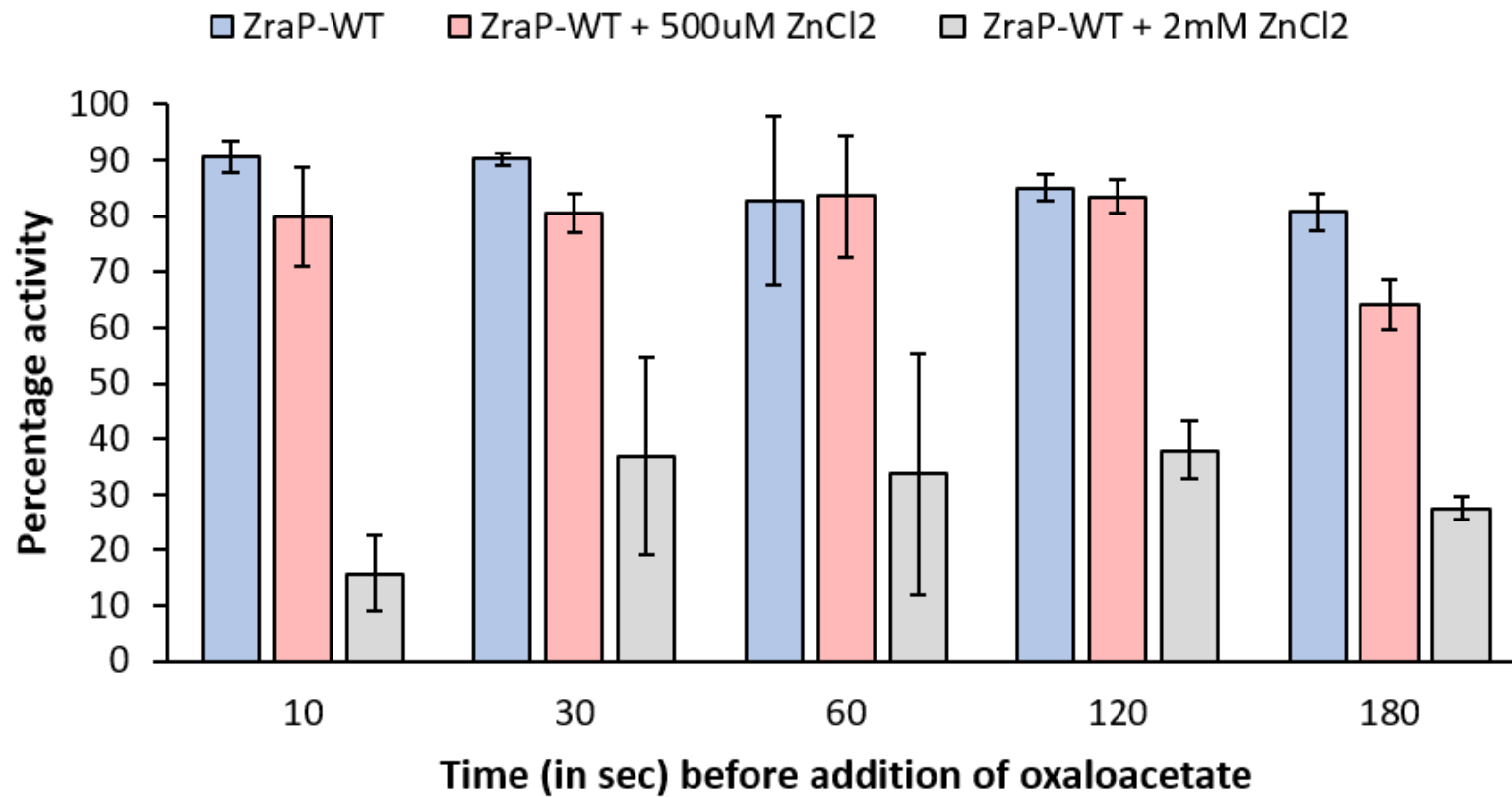
Figure 5.7 Prolonged exposure to EDTA does not restore MDH activity after incubation with ZraP-WT and excess zinc. MDH activity assays carried out in Tris buffer represented as percentage activity compared to the MDH-only (no zinc) condition. Comparing the MDH activity of ZraP-WT chaperoned MDH samples with no excess zinc, to samples incubated with either 500µM ZnCl$_2$ or 2mM ZnCl$_2$, the figure shows that prolonged exposure to EDTA prior to substrate addition does not reverse the zinc-induced inhibition of MDH activity. The figure also shows that even in the absence of zinc, the presence of ZraP reduces MDH activity by approximately 10-15% compared to the MDH only (no zinc, no chaperone) condition.

5.3.2 Malate dehydrogenase activity assays analysing ZraP chaperoning

The ability of ZraP-WT and ZraP mutants to protect MDH activity against chemical denaturation was assessed using MDH activity assays carried out in Tris buffer. Chaperone assays investigating the ability of ZraP to protect MDH against thermal denaturation have indicated that ZraP chaperone activity is enhanced in the presence of excess zinc (Appia-Ayme *et al.*, 2012; Petit-Hartlein *et al.*, 2015; Wells, 2015). Experiments carried out during the optimisation of the MDH activity assay have demonstrated that zinc negatively affects MDH-assisted conversion of oxaloacetate to L-malate. The analysis of ZraP chaperoning has therefore been compared to MDH "only" (no chaperone) samples incubated with and without zinc. An overview of the chaperoning abilities by ZraP-WT and mutants in the presence of zinc is presented in figure 5.8, whereas analysis of the individual ZraP proteins has been visualised in figures 5.9 – 5.14. The overview in figure 5.8 demonstrates that ZraP-WT and the ZraP proteins mutated in either the ^{44}LTxxQ^{48} region or the ^{128}GGCGGY^{133} region affect MDH activity negatively, both in the absence and the presence of denaturing agents. However, ZraP proteins mutated in the ^{139}HRGGGH^{144} region do not negatively affect MDH activity, and may even protect protein function.

Of all the tested proteins, ZraP-ZA is the only mutant that does not significantly reduce MDH activity in the absence of a denaturing agent. In the presence of 0.4 M and 0.6 M GnHCl, ZraP-HRGGAH is the only protein that does not significantly reduce MDH activity, but instead appears to boost its activity. Although ZraP-ZA does negatively affect MDH activity at these concentrations, the negative effect of the chaperone is significantly lower than that of the other proteins that negatively affect MDH activity. At 0.8 M GnHCl MDH is severely affected, and no ZraP protein was able to protect MDH activity. With the exception of ZraP-HRGGAH at 0.6 M GnHCl, all conditions tested demonstrated significantly reduced MDH activity in the presence of zinc (figure 5.9-5.14). Although ZraP is capable of protecting MDH against thermal aggregation, the evidence presented in this study demonstrate that ZraP is not able to protect MDH activity during chemical denaturation. Interestingly, proteins mutated in the ^{139}HRGGAH^{144} region do not appear to affect MDH activity as badly as the WT protein, or the other tested mutants
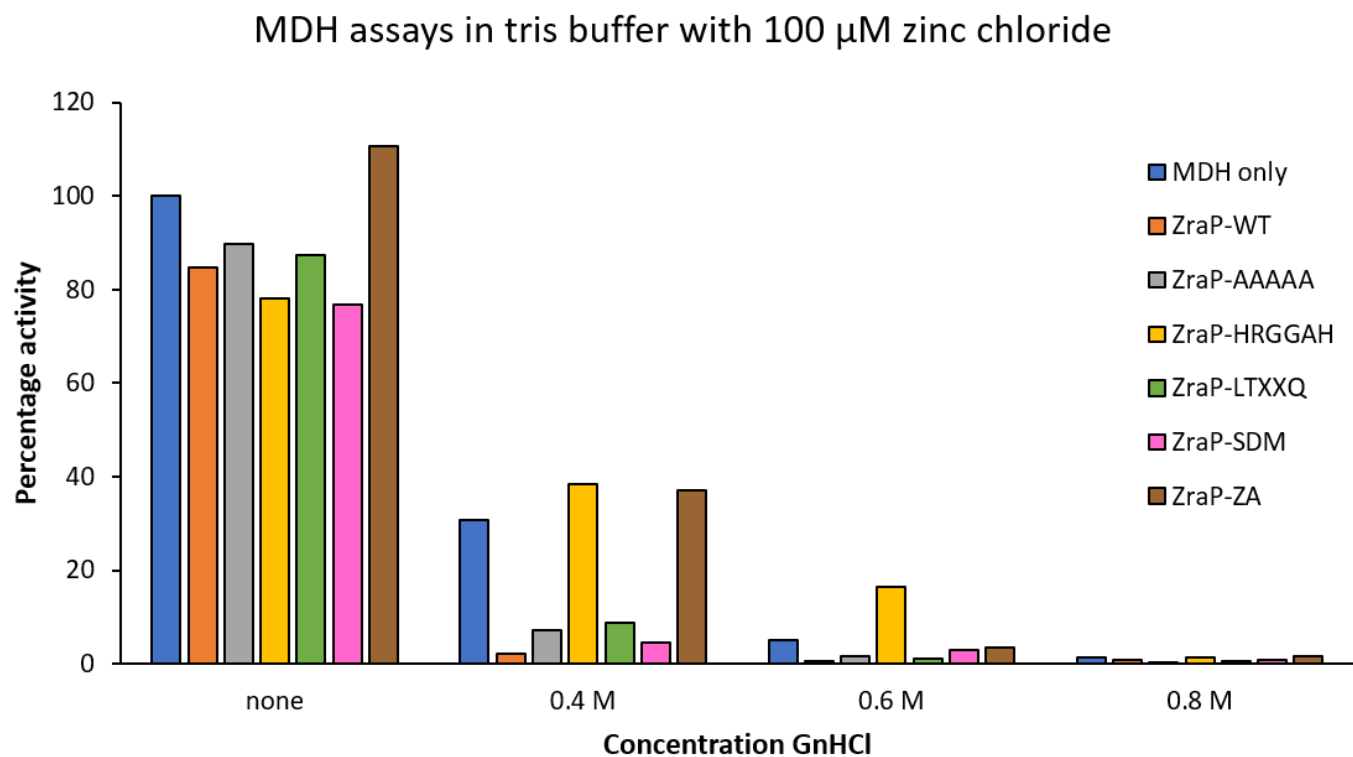
Figure 5.8 Mutations in the [139]HRGGGH[144] region of ZraP negate the ZraP-induced inhibition of MDH activity. MDH activity assays carried out in Tris buffer represented as percentage activity compared to the MDH-only (100µM ZnCl$_2$) condition. In the absence of denaturant, MDH activity is reduced when incubated with all tested chaperones except for ZraP-ZA ([139]AAAAAA[144]). When exposed to 0.4 M GnHCl, the chaperones mutated in the [139]HRGGGH[144] region do not exhibit any additional inhibition of MDH activity, and when exposed to 0.6 M GnHCl, the ZraP-HRGGAH mutant does not restrict MDH activity.
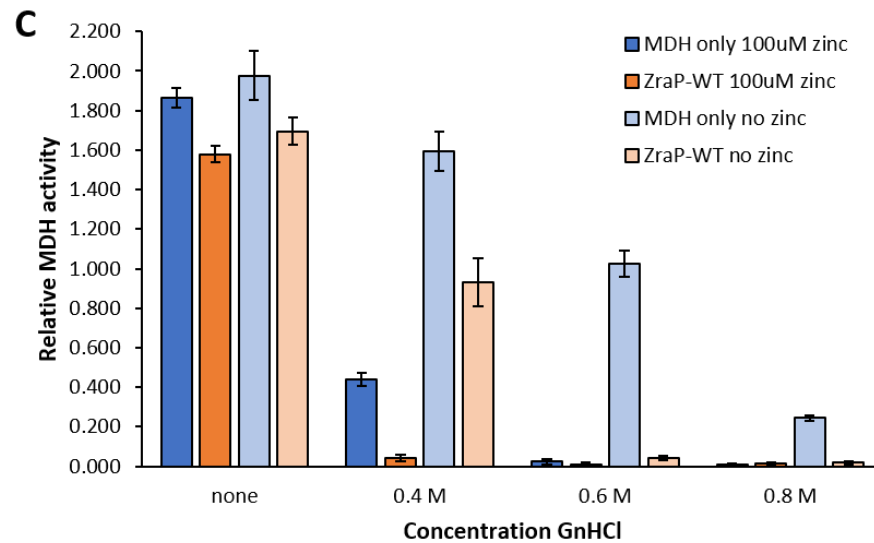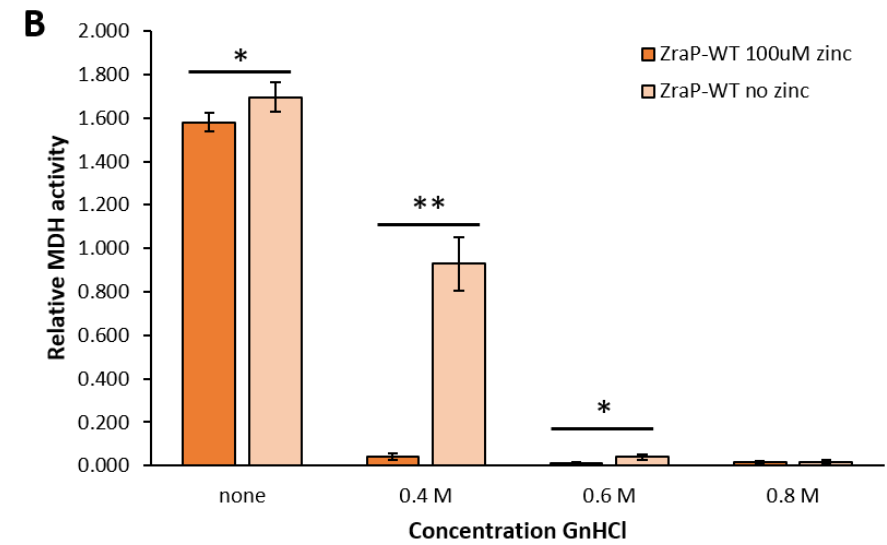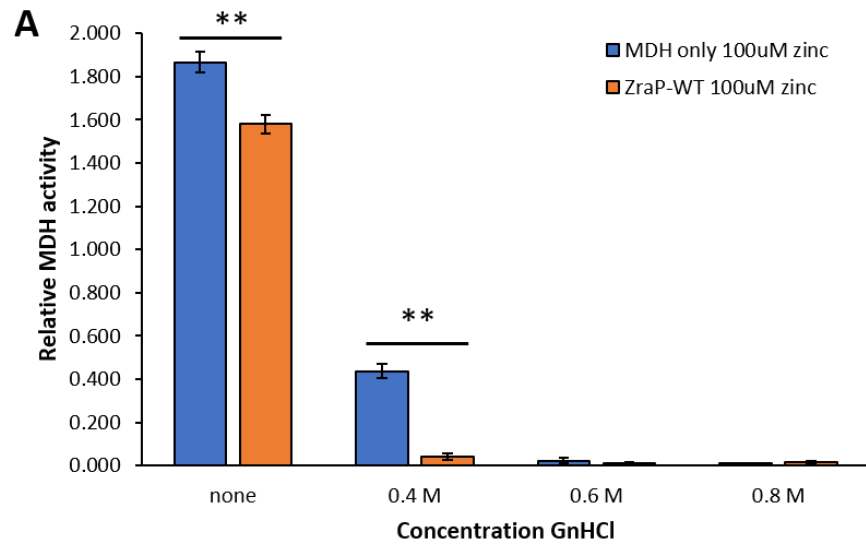
Figure 5.9 Chaperone activity of *Strep*-tagged ZraP-WT. MDH activity assays carried out in Tris buffer, presented as relative MDH activity. **A.** Incubation with ZraP-WT significantly reduces MDH activity. **B.** Zinc significantly reduces MDH activity when incubated with ZraP-WT. **C.** ZraP-WT is not able to preserve MDH activity during exposure to GnHCl. Both the presence of zinc and the presence of ZraP-WT have a significantly negative effect on the ability of MDH to convert oxaloacetate into L-malate. Significant differences between the conditions compared underneath the marker line are indicated by * (P < 0.05) and ** (P < 0.01), Student's t-test assuming equal variance, n = 3. Error bars indicate standard deviation.
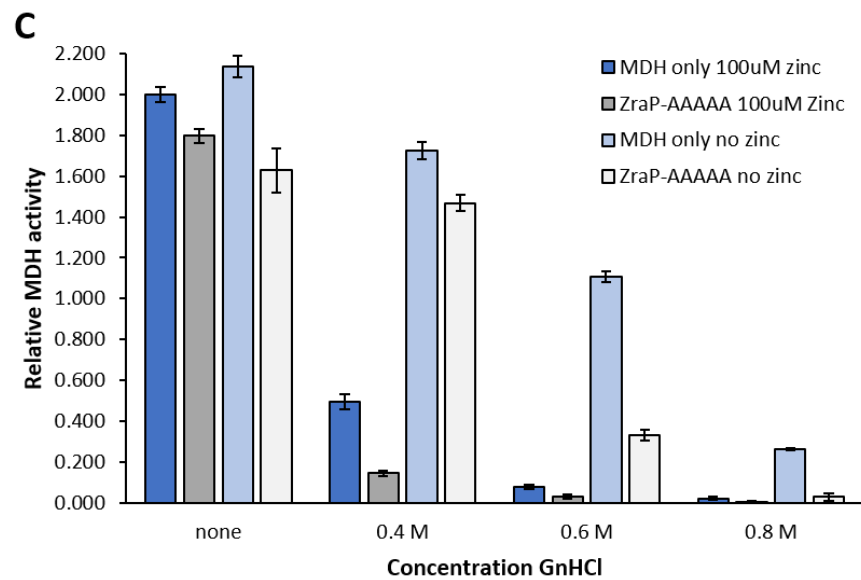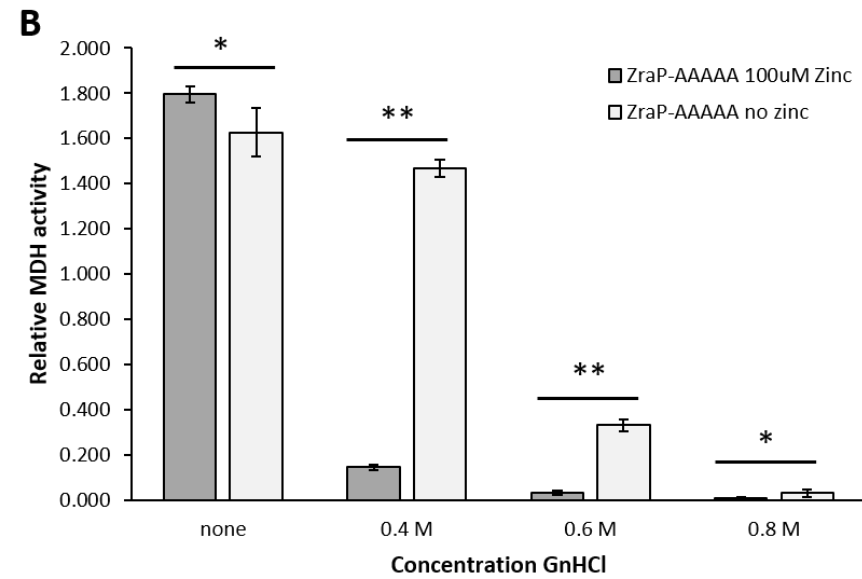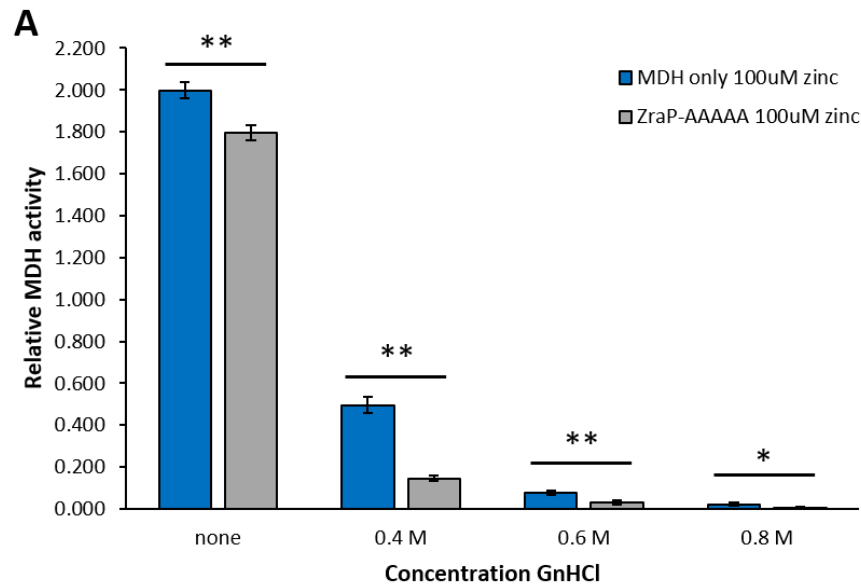
Figure 5.10 Chaperone activity of *Strep*-tagged ZraP-AAAAA. MDH activity assays carried out in Tris buffer, presented as relative MDH activity. **A.** Incubation with ZraP-AAAAA (^{44}AAAAA^{48}) significantly reduces MDH activity. **B.** Zinc significantly reduces MDH activity when incubated with ZraP-AAAAA. **C.** ZraP-AAAAA is not able to preserve MDH activity during exposure to GnHCl. Both the presence of zinc and the presence of ZraP-AAAAA have a significantly negative effect on the ability of MDH to convert oxaloacetate into L-malate. Significant differences between the conditions compared underneath the marker line are indicated by * (P < 0.05) and ** (P < 0.01), Student's t-test assuming equal variance, n = 3. Error bars indicate standard deviation.
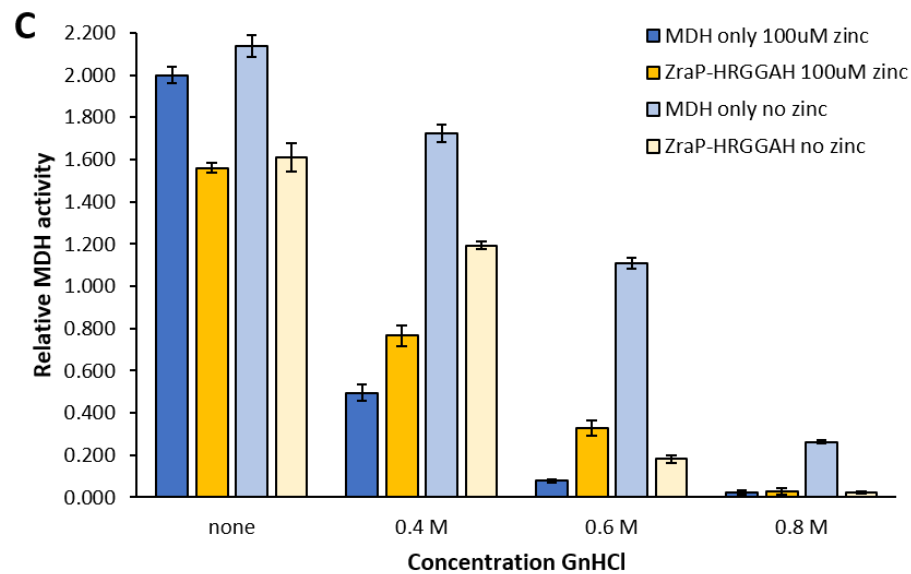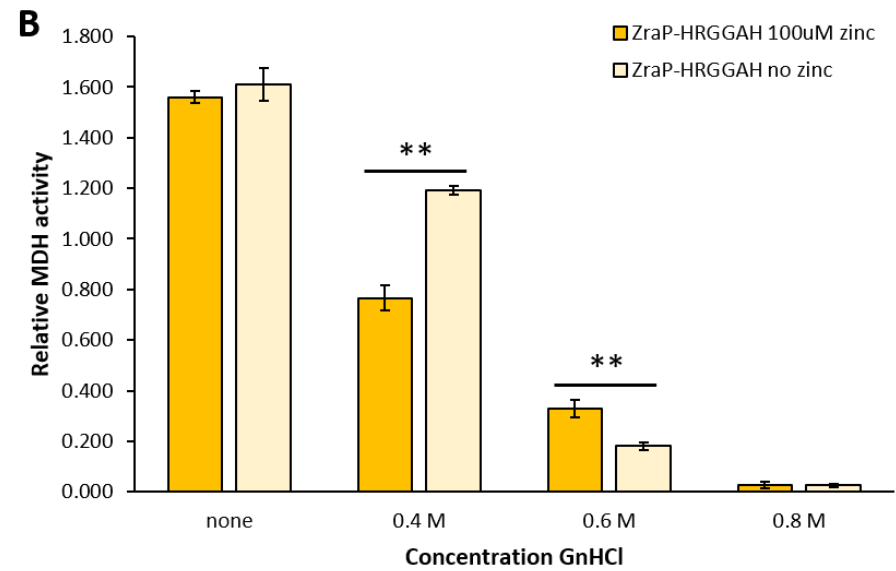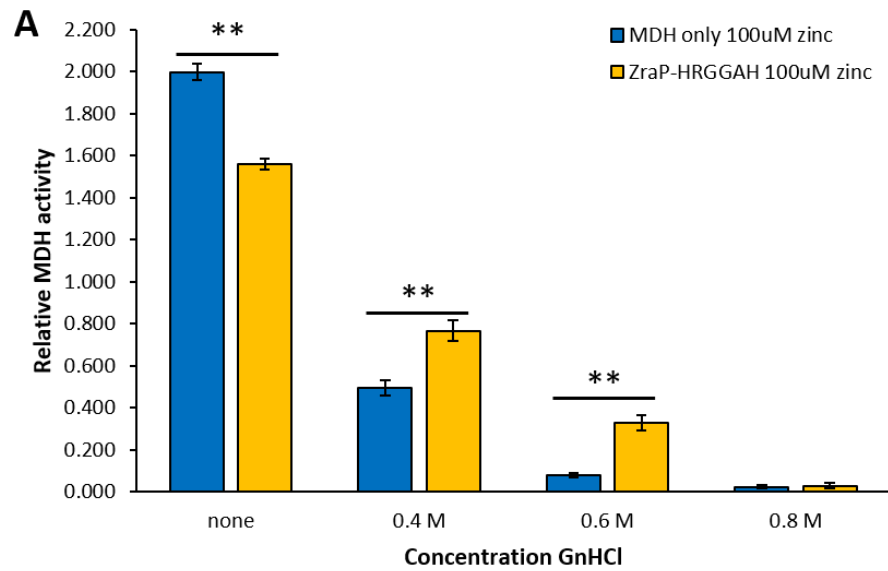
Figure 5.11 Chaperone activity of *Strep*-tagged ZraP-HRGGAH. MDH activity assays carried out in Tris buffer, presented as relative MDH activity. **A.** Incubation with ZraP-HRGGAH significantly reduces MDH activity in the absence of a denaturant. In the presence of 0.4-0.6 M GnHCl, ZraP-HRGGAH promotes MDH activity. **B.** In the presence of 0.4 GnHCl Zinc significantly promotes MDH activity when incubated with ZraP-HRGGAH, whereas at 0.4 GnHCl zinc significantly reduces activity. **C.** ZraP-HRGGAH can either promote or inhibit MDH activity depending on the conditions tested. Significant differences between the conditions compared underneath the marker line are indicated by * ($P < 0.05$) and ** ($P < 0.01$), Student's t-test assuming equal variance, n = 3. Error bars indicate standard deviation.
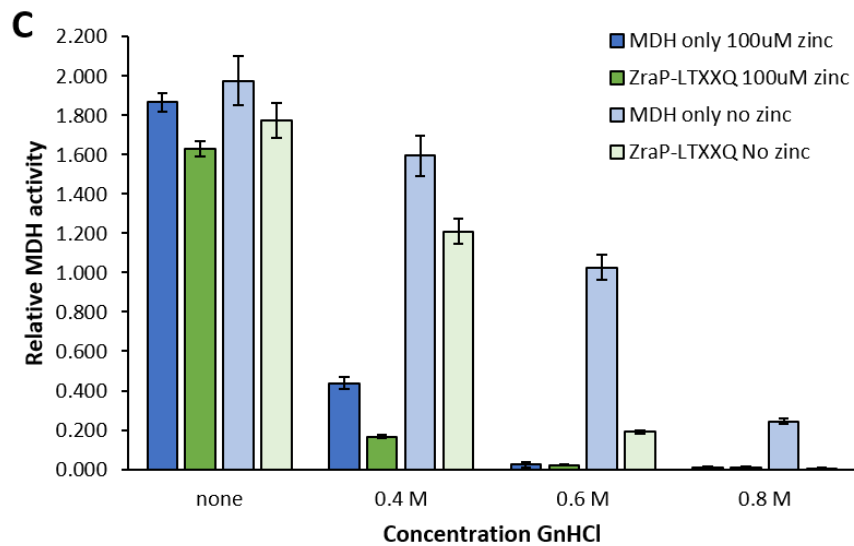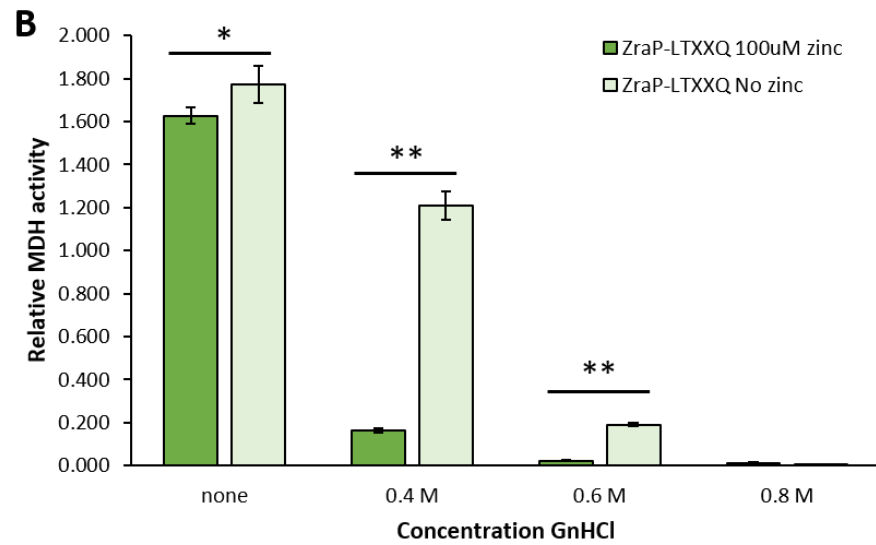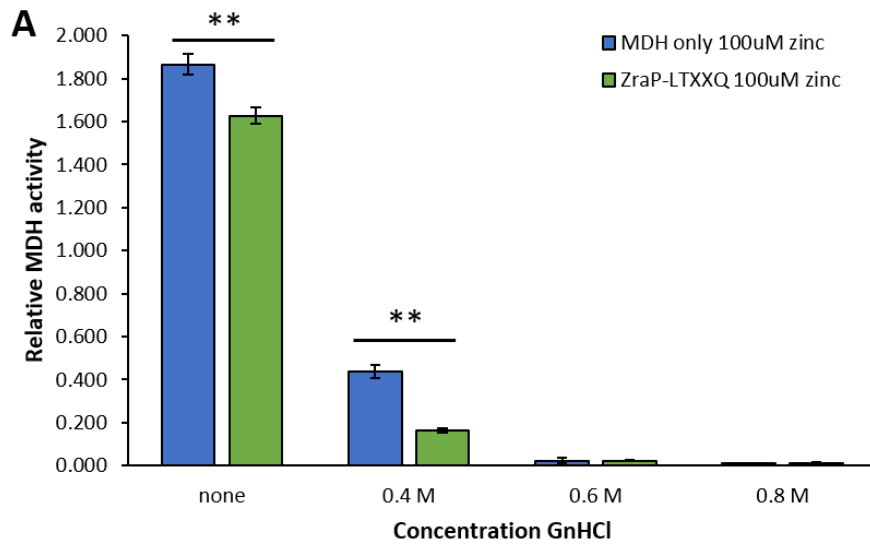
Figure 5.12 Chaperone activity of *Strep*-tagged ZraP-LTXXQ. MDH activity assays carried out in Tris buffer, presented as relative MDH activity. **A.** Incubation with ZraP-LTXXQ significantly reduces MDH activity. **B.** Zinc significantly reduces MDH activity when incubated with ZraP-LTXXQ. **C.** ZraP-LTXXQ is not able to preserve MDH activity during exposure to GnHCl. Both the presence of zinc and the presence of ZraP-LTXXQ have a significantly negative effect on the ability of MDH to convert oxaloacetate into L-malate. Significant differences between the conditions compared underneath the marker line are indicated by * ($P < 0.05$) and ** ($P < 0.01$), Student's t-test assuming equal variance, n = 3. Error bars indicate standard deviation.
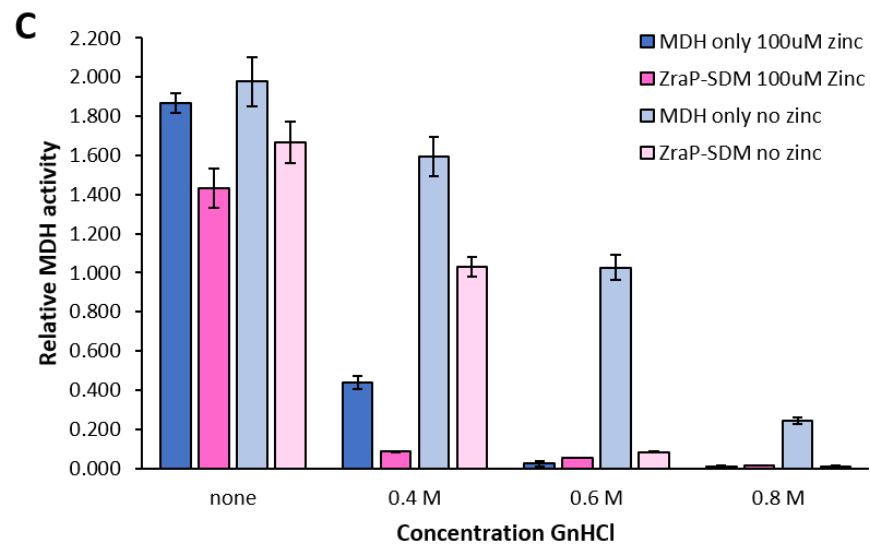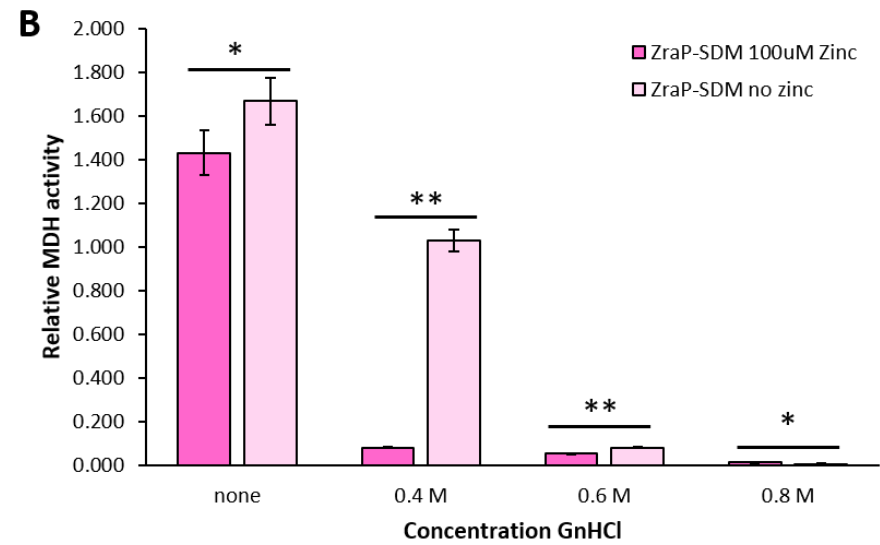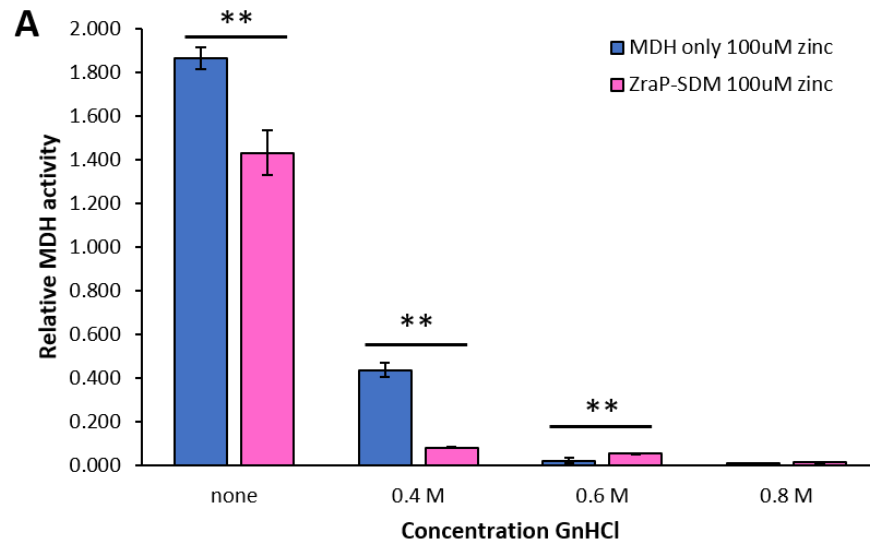
Figure 5.13 Chaperone activity of *Strep*-tagged ZraP-SDM. MDH activity assays carried out in Tris buffer, presented as relative MDH activity. **A.** Incubation with ZraP-SDM significantly reduces MDH activity. **B.** Zinc significantly reduces MDH activity when incubated with ZraP-SDM. **C.** ZraP-SDM is not able to preserve MDH activity during exposure to GnHCl. Both the presence of zinc and the presence of ZraP-SDM have a significantly negative effect on the ability of MDH to convert oxaloacetate into L-malate. Significant differences between the conditions compared underneath the marker line are indicated by * (P < 0.05) and ** (P < 0.01), Student's t-test assuming equal variance, n = 3. Error bars indicate standard deviation.
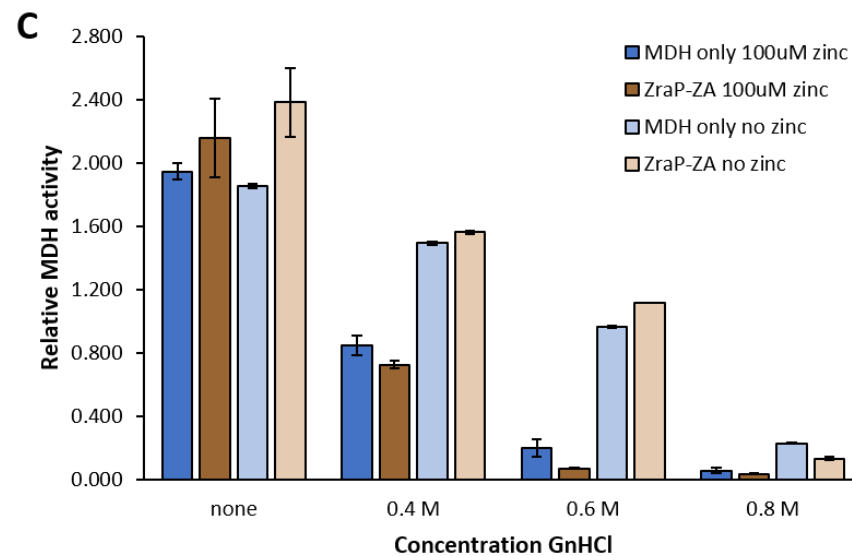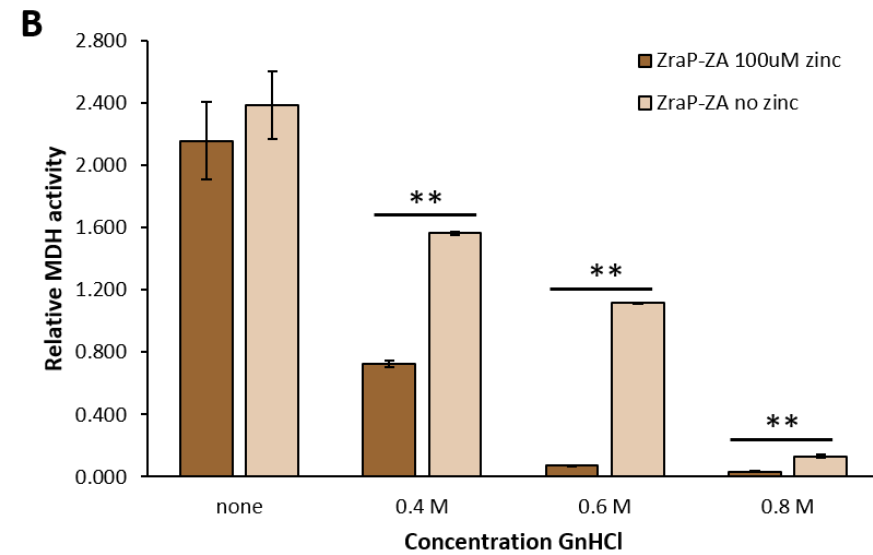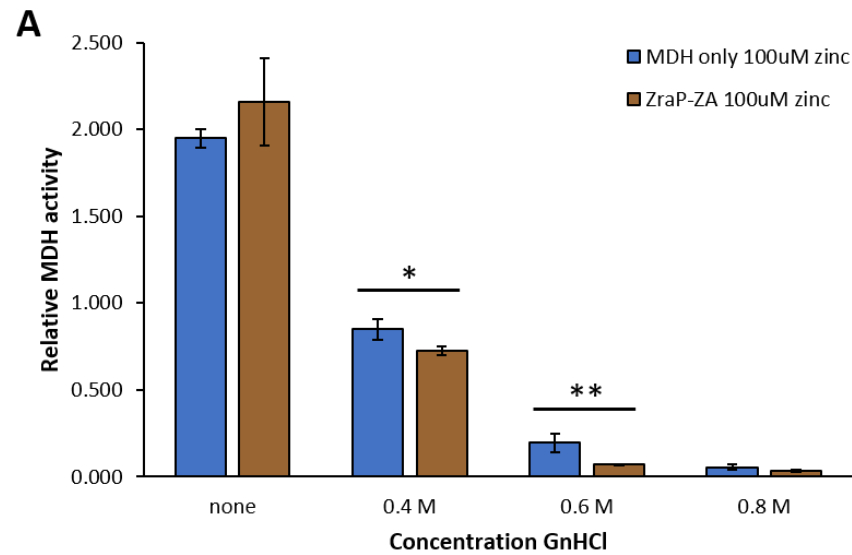
Figure 5.14 Chaperone activity of *Strep*-tagged ZraP-ZA. MDH activity assays carried out in Tris buffer, presented as relative MDH activity. **A.** Incubation with ZraP-ZA ([139]AAAAAA[144]) significantly reduces MDH activity. It should be noted that this inhibition is not as severe as the inhibition observed for the ZraP-WT and ZraP-AAAAA/LTXXQ/SDM mutants. **B.** Zinc significantly reduces MDH activity when incubated with ZraP-ZA. **C.** ZraP-ZA is not able to preserve MDH activity during exposure to GnHCl, however, it does not appear to affect MDH activity as negatively as other tested proteins either. Significant differences between the conditions compared underneath the marker line are indicated by * (P < 0.05) and ** (P < 0.01), Student's t-test assuming equal variance, n = 3. Error bars indicate standard deviation.

5.3.3 ZraP negatively affects DNA gyrase activity

DNA gyrase is a bacterial topoisomerase that is involved in the negative supercoiling of double stranded bacterial DNA. It is targeted by quinolones and aminocoumarins, as well as *seco*-cyclothialidines (Reece and Maxwell, 1991; Rudolph *et al.*, 2001). As DNA gyrase is an important antibiotic target, the protein is frequently used in screens for new antibiotic compounds. DNA gyrase activity can be investigated by ATPase assays and supercoiling assays (Inspiralis Limited, 2017). The former assay utilises spectrophotometry to analyse gyrase activity by measuring conversion of coloured NADH to colourless NAD^+, this conversion is linked to the hydrolysis of ATP, required for gyrase activity. The latter assay uses agarose gel electrophoresis to investigate the relaxed *versus* supercoiled state of substrate DNA (figure 5.15).
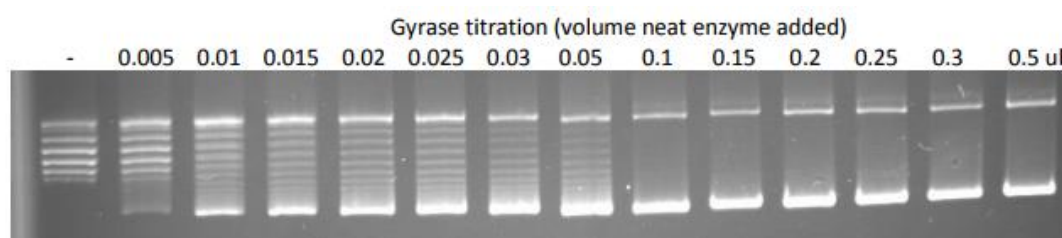
Figure 5.15 DNA gyrase supercoiling assay. This DNA gyrase supercoiling assay demonstrates the gradual supercoiling of the pBR322 substrate by DNA gyrase. As the gyrase concentration increases, so does the level of supercoiling, until all relaxed DNA is supercoiled (Inspiralis Limited, 2017).

DNA gyrase is a temperature sensitive enzyme, that rapidly loses activity when stored at sub-optimal conditions (-80°C). To investigate the potential of ATP-independent periplasmic chaperones to increase shelf time of biotechnologically relevant, temperature sensitive enzymes, the ability of ZraP to protect DNA gyrase was investigated in collaboration with Inspiralis Ltd. Assays were carried out testing the effect of zinc on DNA gyrase activity, and showed that gyrase activity is not inhibited in the presence of 100µM $ZnCl_2$ (figure 5.16). In the absence of excess zinc, ZraP did not inhibit DNA gyrase activity (data not shown). However, when incubated overnight with both ZraP-WT and 100µM $ZnCl_2$, DNA gyrase activity was significantly inhibited when stored both at -80°C and at -20°C (figure 5.16).
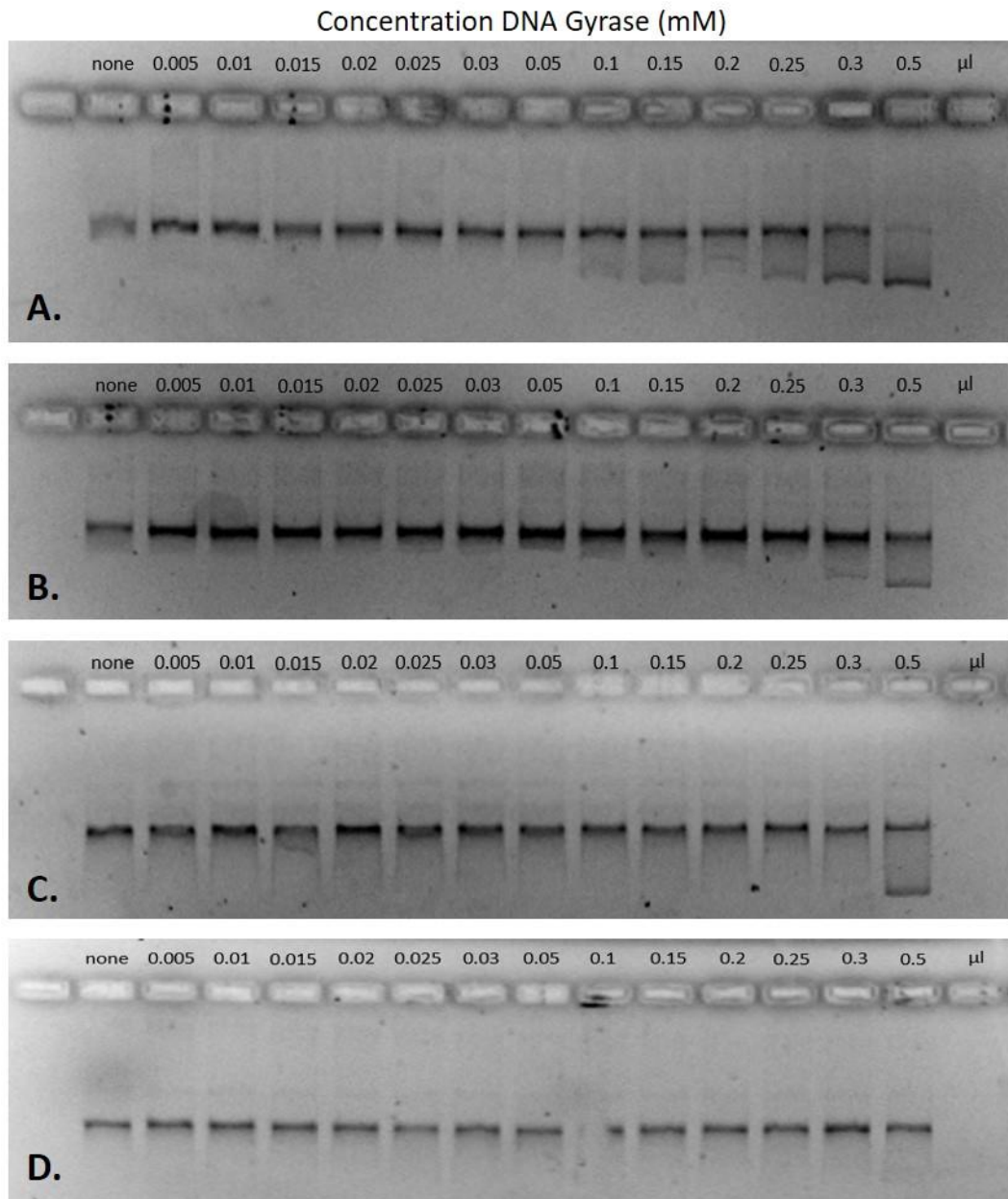
Figure 5.16 DNA gyrase supercoiling assays testing ZraP chaperone activity. The ability of ZraP to protect DNA gyrase activity during storage at higher temperatures was analysed using DNA gyrase supercoiling assays. The activity of DNA gyrase was analysed by investigating the relaxed state (left) *versus* supercoiled state (right) of the substrate DNA pBR322. **A.** Assay testing DNA gyrase stored overnight at -80°C, in the presence of 100µM $ZnCl_2$. Increasing levels of supercoiled substrate detected at higher DNA gyrase concentrations indicate zinc does not inhibit DNA gyrase activity. **B.** Assay testing DNA gyrase stored overnight at -20°C, in the presence of 100µM $ZnCl_2$. Increasing levels of supercoiled substrate detected at higher DNA gyrase concentrations indicate zinc does not inhibit DNA gyrase activity. **C.** Assay testing DNA gyrase stored overnight at -80°C, in the presence of ZraP-WT and 100µM $ZnCl_2$. The lack of substrate supercoiling suggests that the presence of ZraP-WT and 100µM $ZnCl_2$ inhibits DNA gyrase activity. **D.** Assay testing DNA gyrase stored overnight at -20°C, in the presence of ZraP-WT and 100µM $ZnCl_2$. The lack of substrate supercoiling suggests that the presence of ZraP-WT and 100µM $ZnCl_2$ inhibits DNA gyrase activity.

5.3.4 Identification of natural ZraP targets using protein pull-down assays.

Despite its conserved nature, little is known about the protective role of ZraP, and the envelope stress signals that activate the ZraSRP system. Identification of natural ZraP targets could provide information about the protective nature of the ZraSRP system, as well as provide information about environmental activation signals.

In an attempt to identify natural ZraP targets, pull-down assays were carried out using *myc*-His-tagged ZraP-WT. Studies carried out by Wells (2015) suggested that ZraP may be activated in response to heat stress. To identify potential ZraP targets, STM SL1344 Δ*zraP* was exposed to 55°C for 15 minutes before cell lysate was collected and used in the pull-down assay. A study conducted by Appia-Ayme *et al*. (2011) indicated that in tungstate exposed STM SL1344 Δ*baeR*, ZraP is upregulated. To identify potential ZraP targets, STM SL1344 Δ*baeR* was grown in the presence of 20mM sodium tungstate, before cell lysate was collected and used in the pull-down assay. Analysis of the pull-down assay eludates (figure 5.17) reveals clear bands for ZraP monomers at the 15kDa marker. The eludate for the heat exposed lysate demonstrates another band at approximately 35kDa. However, this band is frequently found when analysing high concentrations ZraP using SDS-PAGE, and represents ZraP oligomers. No further bands of interest were found in the heat-challenge. The eludate for the tungstate challenged lysate also demonstrates a clear band for ZraP monomers. Another relatively clear band can be found at approximately 12kDa. This band is a very common band found in SDS-PAGE analysis of *Salmonella* full-cell lysates (figures 4.7-4.12). Considering these bands are usually very profound, whereas here they show only faintly, it is likely that these bands are the result of an incomplete wash. If this protein is indeed a natural target of ZraP, a much clearer band would have been expected, considering the band size of ZraP. Overall, the pull-down assays conducted in this study failed to identify potential natural ZraP targets.
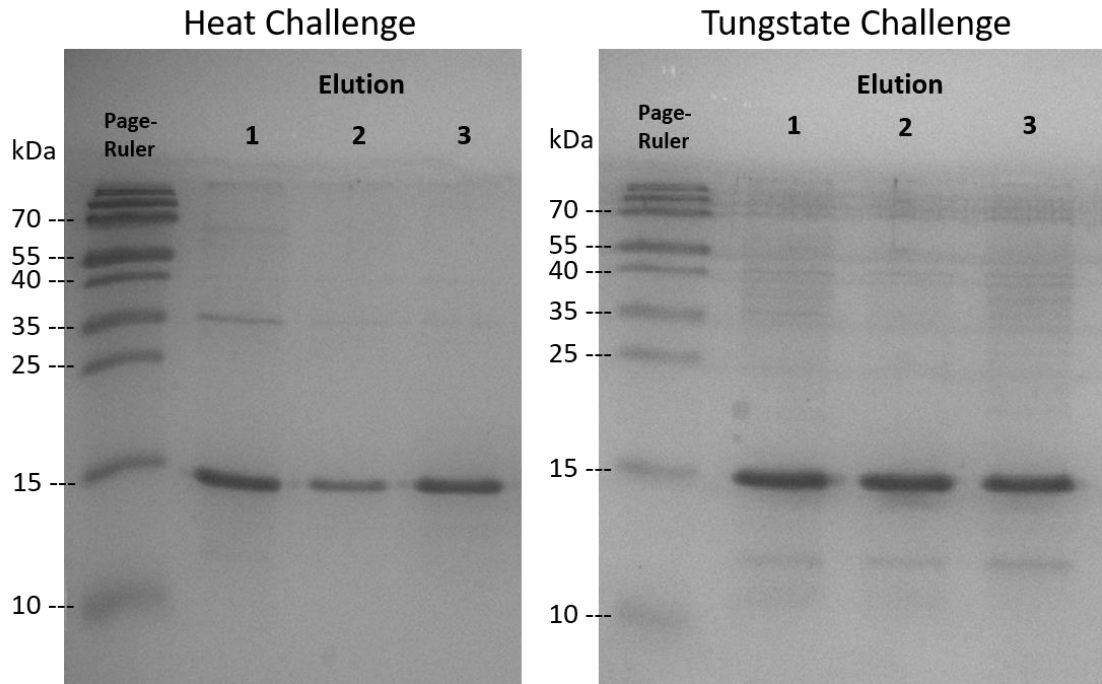
Figure 5.17 ZraP Pull-down assays following heat challenge and tungstate challenge. The SDS-PAGE profile of the pull-down assay eludates reveals some clear bands. The thick bands found at the 15kDa marker in the eludates of both heat-challenged and tungstate challenged cells represent monomeric ZraP. The band found in the first eludate of the lysate of the heat-challenged cells, likely represents ZraP in oligomeric state. The bands found at approximately 12kDa in the tungstate challenge are also found as thick bands on SDS-PAGE gels analysing full cell lysates. Considering the bands found on this gel are faint, these bands are more likely to be the result of full lysate contamination.

5.4 Discussion and future work

5.4.1 Further optimisation of the malate dehydrogenase activity assays should include mechanism of inhibition assays.

The ability of ZraP to protect aggregation of thermally challenged MDH was initially demonstrated by Appia-Ayme (2012) and has since been confirmed by Petit-Härtlein (2015) and Wells (2015). Although the ability of ZraP to protect proteins from aggregation has been demonstrated, it is not known if ZraP is also capable of protecting enzyme activity during stress. To gain better understanding of the cellular function of ZraP (e.g. Preventing aggregation or protecting protein function), MDH activity assays were carried out analysing the ability of ZraP to protect the activity of chemically denatured MDH. Prior to comparing the chaperoning of differently mutated ZraP, the MDH activity assays were optimised. Following the apparent lack of MDH activity in HEPES buffer, the switch to PBS buffer was made. The use of PBS was recommended in protocols describing MDH assays (Worthington

Biochemical Corporation., 2015), and the activity of MDH in PBS was confirmed in published studies (Han *et al.*, 2014; Karuppanan *et al.*, 2017). Furthermore, ZraP assays investigating aggregation of thermally denatured MDH have also been carried out in PBS (Appia-Ayme *et al.*, 2012; Petit-Hartlein *et al.*, 2015; Wells, 2015). The initial switch in the use of PBS buffer to Tris buffer for the conduction of MDH activity assays was the result of an accidental mix-up of bottles. However, the significant increase in MDH activity when conducting assays in Tris buffer was immediately apparent. Considering the near three-fold increase in relative MDH activity and the significant improvement in repeatability, Tris buffer replaced PBS for MDH activity testing. However, the use of Tris buffer revealed a complication to the MDH activity assays that had not been observed during testing in PBS; the presence of zinc negatively influences the ability of MDH to convert oxaloacetate into L-malate. Investigations into why this zinc-induced inhibition had not been observed before in assays conducted in PBS, pointed out an issue with the use of PBS buffer that had not been considered when choosing the buffer. Phosphate buffers, including PBS, sequester divalent cations and deposit them as phosphate salts which makes them unsuitable for assays investigating divalent zinc.(Cold Spring Harbor Protocols, 2006; EMBL, 2017). The inhibiting effect of zinc on MDH activity was unexpected, considering the material data sheets provided with the MDH protein (ROCHE) indicate that zinc acts as activator. However, this manual refers to the reverse reaction in which MDH reduces NAD^+ to NADH to convert L-malate into oxaloacetate. It is interesting that zinc acts as an inhibitor in the reverse reaction. The active site MDH contains a charge-relay pair formed of a histidine and an aspartate residue (Nicholls *et al.*, 1992; Goward and Nicholls, 1994), and both residues are known to be capable of binding zinc (McCall, Huang and Fierke, 2000). However, if this active site would bind zinc, then an inhibitory effect would be expected for MDH activity in both directions. Considering zinc also has an inhibiting effect on the oxaloacetate-interacting enzyme oxaloacetate decarboxylase, it is also possible that zinc interacts with oxaloacetate, reducing the amount of available substrate and thus reducing the reaction rate (Sender *et al.*, 2004). To further optimise the MDH assays for ZraP chaperone activity screens, the type of inhibition performed by ZraP and zinc on MDH activity should be determined by conducting a mechanism of inhibition assay. Enzyme kinetics assays study the rate of a reaction by following the creation of a product as a function of time. During enzymatic assays, the substrate concentration decreases as the product concentration increases until an equilibrium has been reached, and there is no net change in the concentrations of either substrate (S) or product. Most reactions slow down over time, so the rate of reaction (V0) is often measured just after the

start of the reaction. Using the Michaelis-Menten equation (V0 = Vmax * ([S]/[S]*Km)), a Lineweaver-Burk plot can be drawn. This double-reciprocal plot displays 1/V0 against 1/[S], and yields a straight line that intercepts the y-axis at 1/Vmax and intercepts the x-axis at -1/KM. The slope of this line represents KM/Vmax. The type of enzyme inhibition can be determined when comparing the Lineweaver-Burk plot of the enzyme with and without inhibitor (figure 5.18) (Berg, Tymoczko and Stryer, 2006). To determine the type of inhibition exhibited on MDH by zinc as well as by ZraP, MDH activity assays should be carried out at a range of oxaloacetate concentrations, both in the presence and in the absence of either inhibitor.
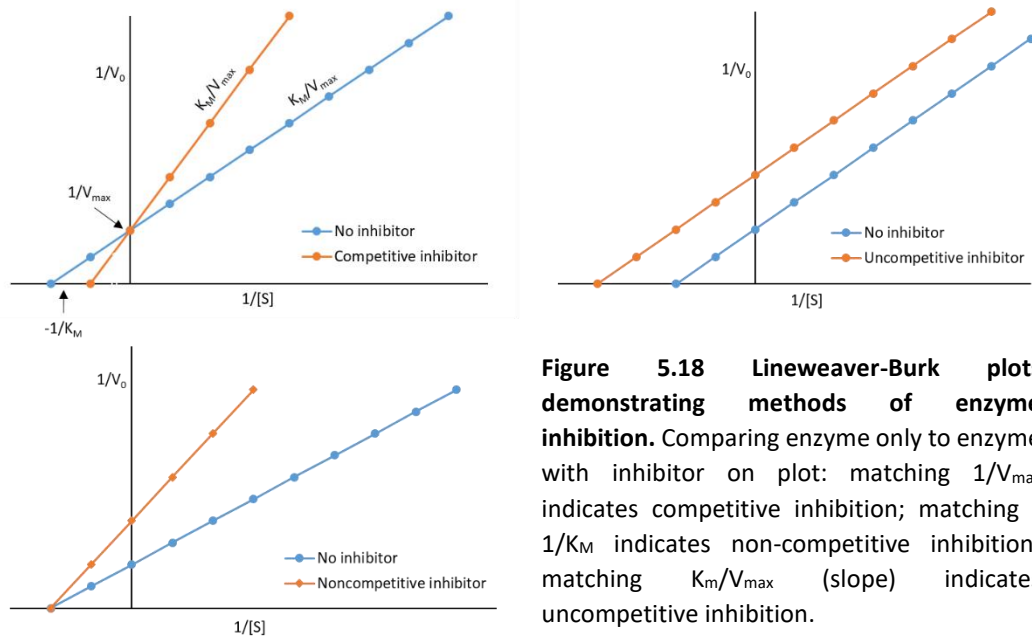
Figure 5.18 Lineweaver-Burk plots demonstrating methods of enzyme inhibition. Comparing enzyme only to enzyme with inhibitor on plot: matching $1/V_{max}$ indicates competitive inhibition; matching $-1/K_M$ indicates non-competitive inhibition; matching K_m/V_{max} (slope) indicates uncompetitive inhibition.

5.4.2. The N-terminal [139]HRGGGH[144] region of ZraP may be involved in the ZraP-induced inhibition of MDH activity.

MDH activity assays testing chaperone activity were carried out for ZraP-WT and five ZraP mutants in the presence and absence of zinc. The agent used to chemically denature MDH is the strong organic base guanidine hydrochloride, which primarily exists as guanidium ions at pH 8.0 (Martindale, 1993). Although previous reports by Wells (2015) suggested that ZraP-WT was capable of protecting MDH activity in the presence of GnHCl concentrations up to 1.2 M, the data presented in this study do not confirm those findings. It should be noted that the former study used HEPES buffer during the MDH activity assays. The assays conducted in this study using Tris buffer suggest that ZraP is not able to protect MDH activity against chemical denaturation by GnHCl at any of the concentrations tested. That is not to say there is no interaction between ZraP and MDH. The significant inhibition of MDH activity when incubated with ZraP suggests that the interaction between ZraP and MDH either occurs at the MDH active site, or that ZraP binds an allosteric site, resulting in reduced MDH activity. The enzyme activity of the dimeric mitochondrial MDH used is allosterically regulated, as the NADH/NAD$^+$ cofactors bind at a different location than the oxaloacetate/L-malate substrate (Harada and Wolfe, 1968; Mullinax et $al.$, 1982). If interaction of ZraP with MDH interferes with the availability of either of these binding sites, enzyme activity will be affected. Incubation with ZraP does not protect MDH activity during exposure to GnHCl. Although the exact mechanism of denaturation by GnHCl is unclear, it is thought that the dipolar electric field created by the Gn$^+$ and Cl$^-$ ions causes the charged residues of α-helices to stretch, resulting in an unfolding of the helix (Camilloni et $al.$, 2008). Considering dimer formation is critical for MDH activity (Harada and Wolfe, 1968), and crystallography studies have demonstrated that the dimer interface of MDH consists mainly of interacting α-helices (Breiter, Resnik and Banaszak, 1994), GnHCl was the preferred method of denaturation. However, it should be noted that the structure of ZraP also consists primarily of α-helices, and therefore the chaperone itself is at risk of denaturation in the presence of GnHCl. It may be worth considering the use of urea as a denaturing agent for future MDH activity assays. Whereas GnHCl primarily targets α-helices, urea destabilises β-sheets first (Camilloni et $al.$, 2008). The conserved NAD$^+$-binding domain of MDH contains four β-sheets arranged in parallel structures, and ZraP does not contain any β-sheets, urea may be a more suitable denaturing agent when investigating ZraP chaperone activity (Hall, Levitt and Banaszak, 1992). However, potential denaturation of ZraP in the presence of GnHCl does not fully explain the lack of protection of activity by the chaperone. After all, even in the presence of

GnHCl, the MDH samples incubated with ZraP were significantly less active than the samples incubated without a chaperone. This suggests that ZraP also interacts with MDH in the presence of GnHCl. Although it is clear that ZraP is not capable of protecting MDH activity during chemical exposure, it would be interesting to see if ZraP can still protect against GnHCl induced protein aggregation. This would require a repeat of the published MDH aggregation assays, replacing thermal denaturation of MDH with chemical denaturants (Appia-Ayme *et al.*, 2012; Petit-Hartlein *et al.*, 2015; Wells, 2015). Alternatively, thermal denaturation could be considered as a method of MDH denaturation. Experiments conducted by Appia-Ayme (2012), Petit-Härtlein (2015), and Wells (2015), have demonstrated that MDH is prone to high-temperature induced aggregation, and that this aggregation can be relieved in the presence of ZraP.

Unlike WT ZraP, proteins mutated in the [139]HRGGGH[144] region (ZraP-HRGGAH and ZraP-ZA), did not inhibit MDH activity as strongly as either the WT or the other mutant strains. ZraP-HRGGAH may actually protect MDH activity in the presence of 0.4 M and 0.6 M GnHCl. Considering the significant difference in the activity between MDH incubated with and without mutated protein, it is unlikely that the reduction in inhibition is the result of a lack of interaction between the mutated chaperones and MDH. However, it is possible that ZraP mutated in the [139]HRGGGH[144] region binds MDH less strongly than ZraP-WT, resulting in a lesser inhibition of substrate and/or cofactor interaction. It is also possible that the mutations in this region cause a shift in ZraP binding specificity, resulting in a differently interacting MDH-ZraP complex that allows for more substrate and/or cofactor binding. Alternatively, there is the possibility that mutations in the [139]HRGGGH[144] region result in a greater flexibility within the ZraP structure, which in turn may allow for more flexibility in the interacting proteins. MDH activity involves conformational changes of the active sites (Bell *et al.*, 2001). If the binding of ZraP locks these sites into one conformation, it effectively inhibits MDH activity. An increased flexibility in ZraP may allow conformational changes of the variable sites, resulting in increased MDH activity. Further investigation into the interaction between ZraP-WT and MDH, as well as ZraP-HRGGAH/ZA and MDH is required. It would be interesting to study the SAXS envelope of these mutants, to investigate any potential differences in overall chaperone shape or flexibility of the mutants compared to ZraP-WT. Furthermore, *in silico* experiments may be able to create a model of the interaction between ZraP and MDH. This would provide more information about the possible nature of ZraP-induced enzyme inhibition. However, it should be noted that although MDH is a ubiquitous protein, and the structural similarity between eukaryotic MDH and *E. coli* MDH is

approximately 58%, MDH is not a periplasmic protein and therefore unlikely to be a natural target of ZraP (Minárik *et al.*, 2002). The identification of a natural ZraP target would benefit studies into the chaperone activity of ZraP.

5.4.3. ZraP interaction with *E. coli* DNA gyrase inhibits gyrase activity

Similar to the MDH activity assays, DNA gyrase supercoiling experiments investigating the protective potential of ZraP, demonstrated inhibition of the target protein after inhibition with ZraP. The ZraP-induced inhibition of DNA gyrase was only apparent in the presence of zinc, whereas activity of DNA gyrase incubated with EDTA treated ZraP-WT did not appear to be negatively affected. The presence of excess zinc, without chaperone, did not affect Gyrase activity either. In comparison, MDH activity was negatively affected by ZraP in the absence of zinc as well as by zinc in the absence of ZraP. These data suggest that the inhibition of DNA gyrase requires the presence of both zinc and ZraP. Chaperone activity of thermally denatured MDH by ZraP is significantly increased in the presence of zinc. It is possible that chaperoning of DNA gyrase by ZraP is also boosted by zinc. The initial aim of the supercoiling experiments conducted in this study was to determine if ZraP would be able to protect the function of DNA gyrase at higher storage temperatures. The experiments presented in this study suggest that, as opposed to provide protection, the interaction between ZraP and DNA Gyrase further reduces gyrase activity. As such, ZraP does not appear to be a good candidate for the protection of enzymatic function of commercially available enzymes. However, colourimetric DNA gyrase assays involving the conversion of NADH to NAD+ may provide an alternative option to MDH activity assays in the study for ZraP chaperone function. The data presented in this study suggest that zinc does not affect DNA gyrase activity, whereas zinc does significantly inhibit MDH activity. Furthermore, the reduction in DNA gyrase activity when incubated with ZraP and zinc suggests that the chaperone can interact with DNA gyrase.

5.4.4 Further optimisation of ZraP pull-down assays is required.

The assays conducted to investigate ZraP chaperone function use either cytoplasmic or eukaryotic protein substrates that are very unlikely to be natural targets of ZraP. Considering the limited knowledge of the nature of the ZraSRP system, the environmental stresses it protects against, the role of zinc in its activation and the importance of its natural function, further investigations into this chaperone and this envelope stress response as a whole would greatly benefit from the identification of natural targets of ZraP. Pull-down assays were conducted using myc-His-tagged ZraP-WT as prey protein to bait potential targets from

either heat-challenged cell lysates or tungsten challenged cell lysates. This study failed to identify natural targets of ZraP from either lysate. However, the experiment may be optimised by using only periplasmic lysates of stressed cells, as well as by extending the range of stresses tested. Furthermore, the assays could be carried out in different buffers, as well as in the presence of excess zinc. However, as ZraSRP is an envelope stress responsive system, it should be considered that the natural targets of ZraP are likely to involve misfolded membrane proteins. The hydrophobic nature of these proteins means they are not particularly soluble, and often end up in the cell pellet after centrifugation. These proteins would not be present in the lysate used for the pull-down assays, and therefore the natural targets of ZraP may not be baited if they are indeed membrane proteins. Addition of detergents to the buffer during lysate collection will allow these hydrophobic proteins to become soluble in aqueous solutions, and may aid in the identification of natural targets of ZraP (Lin and Guidotti, 2009).

Chapter 6. General discussion

Each chapter in this thesis has been discussed individually. As a result, the general discussion will be highlighting the major research outcomes of this study, and their wider context.

6.1 Context

The global impact of *Salmonella* infections is significant, and its treatment and prevention are proving to be both a medical as well as a social-economical challenge. Systemic *Salmonella* infections are mostly restricted to middle- and low-income countries, where sanitation and disease-control measures are insufficient (Gilchrist, MacLennan and Hill, 2015). Reports of antibiotic resistant *Salmonella* infections are on the rise (Das and Bhattacharya, 2000; Dutta *et al.*, 2001; Gupta, Swarnkar and Choudhary, 2001; Neopane *et al.*, 2008; Kariuki *et al.*, 2015), and available *Salmonella* vaccines offer short-term protection only (Galen *et al.*, 2016). Furthermore, non-systemic Salmonellosis is among the leading causes of foodborne diarrhoeal infections worldwide (Majowicz *et al.*, 2010; Havelaar *et al.*, 2015), and presents a significant economic burden to developing and developed countries alike (Ailes *et al.*, 2013; Suijkerbuijk *et al.*, 2016).

The ability to adapt to changing environments is a major contributor to the pathogenicity of *Salmonella*. This adaptability does not only allow *Salmonella* to survive in water, soil, and industrial food-processing plants, but it also contributes to *Salmonella*'s endurance against its host's native and adapted immune responses, and it allows *Salmonella* to compete with the natural flora found in the gut of the host (Griffin and McSorley, 2011; Condell *et al.*, 2012; Dubois-Brissonnet, 2012; Aviles *et al.*, 2013). The Gram-negative cell envelope plays an important role in the natural resistance of *Salmonella* against a range of antimicrobial agents, and it helps protect *Salmonella* against the immediate effects of changing environments. The cell envelope presents itself as a double membrane, separated by a periplasmic space. The latter acts as a buffer against immediate threats to the intracellular space. Because the periplasm is more sensitive to changes in the extra-cellular environment than the cytoplasm, envelope stress response systems have evolved that allow for the sensing of membrane stress indicative of environmental changes, and the activation of suitable stress-response pathways required for *Salmonella*'s adaptability and survival (Raivio, 2005; Rowley *et al.*, 2006; Runkel, Wells and Rowley, 2013).

6.2 Why are periplasmic chaperones being studied?

Periplasmic chaperones play a vital role in the biogenesis, maintenance and repair of the outer membrane. Outer membrane proteins (OMPs) are synthesised in the cytoplasm, and

transported across the inner membrane and the periplasm, before they can be inserted into the outer membrane (Noinaj, Gumbart and Buchanan, 2017). OMPs are largely hydrophobic molecules, and to prevent aggregation of the unfolded OMPs, periplasmic chaperones such as Skp, SurA and FkpA assist in their transport across the periplasm (Sklar *et al.*, 2007). Disruptions in the expression of periplasmic chaperones result in major defects in the outer membrane. Other periplasmic chaperones such as CpxP and Spy, are involved in the scavenging of misfolded OMPs to protect against the accumulation of toxic aggregates (Quan *et al.*, 2011; Thede *et al.*, 2011). These chaperones deliver misfolded and aggregated OMPs to the periplasmic protease HtrA for degradation (Isaac *et al.*, 2005). Some periplasmic chaperones, such as CpxP and ZraP, are part of envelope stress-sensing two-component systems. The current model of their functioning suggests that these chaperones interact with the sensor domain of their associated response system during times of non-stress. However, aggregated OMPs titrate these chaperones away, which allows for the activation of their associated stress response systems (DiGiuseppe and Silhavy, 2003; Appia-Ayme *et al.*, 2012). As a result of their protective functions and their indirect regulation of envelope stress response systems, periplasmic chaperones are a major contributor to the overall adaptability and pathogenicity of *Salmonella*.

Current knowledge regarding the cellular function of periplasmic chaperones originates primarily from studies conducted on laboratory *E. coli* strains and pathogenic EPEC and EHEC strains. However, studies conducted in other Gram-negative organisms, such as *Klebsiella, Salmonella*, and *Yersinia,* have demonstrated that there can be distinct differences in the function and importance between chaperone homologs of various species. This study aimed to investigate the involvement of several periplasmic chaperones in the protection against environmental stress encountered by *Salmonella*.

The results presented in this study suggest that, similarly to *E. coli*, Skp, SurA, and to a lesser extend FkpA, play a major role in the protection of outer membrane integrity. In *E. coli,* SurA is considered the most essential of the three aforementioned chaperones (Sklar *et al.*, 2007), whereas in *Neisseria meningitidis,* Skp is considered the primary chaperone involved in OMP transport (Volokhina *et al.*, 2011). The data presented in this study demonstrate that in *Salmonella*, both Δ*skp* and Δ*surA* mutants demonstrate significantly increased sensitivity to the majority of the conditions tested. These results suggest that in Skp is a greater contributor to overall outer membrane integrity in *Salmonella* than in *E. coli.* Furthermore, investigation into two separate STM SL1344 Δ*skp* strains demonstrating various levels of susceptibility to antimicrobial agents (data not included), suggest that *skp* mutations in

Salmonella may result in suppressor mutations. The potential presence of suppressor mutations in *Salmonella* Δ*skp* would imply Skp plays an important role in overall outer membrane integrity, and is something that would be worth investigating further.

An interesting observation was the apparent involvement of ZraP in the protection against penicillin G. *Salmonella* carries a natural resistance to penicillins because the outer membrane prevents them from interacting with the peptidoglycan subunits. The observation of penicillin G susceptibility in several Δ*zraP* strains, suggests that the deletion of this chaperone may increase membrane permeability to the level that penicillin G is able to cross the outer membrane.

Another party interested in the investigation of periplasmic chaperones is the biotechnological industry. Their innate ability to perform a chaperoning function in the absence of ATP, has encouraged investigations into their interactions with commercially available products. Many enzymes used in biotechnological and biomedical research have a limited shelf-life time, or need to be stored at sub-zero temperatures. The addition of periplasmic chaperones to these protein samples could potentially improve their shelf-life time and storage conditions. Results presented in the current study suggest that the periplasmic chaperone ZraP is capable of interacting with storage temperature-sensitive *E. coli* DNA gyrase. However, the interaction appears to be inhibiting rather than enhancing in nature, and results in the loss of gyrase activity. Whether this inhibition is due to ZraP binding to an active site, or whether the interaction between DNA gyrase and ZraP forces the gyrase into a single conformation is unclear and requires further investigation.

6.3 Understanding the structural properties of periplasmic chaperones

The structures of periplasmic chaperones have been investigated to gain a better understanding of their chaperoning mechanisms. Published crystal structures of FkpA and SurA demonstrated these chaperones form flexible dimeric structures that can adopt different conformational orientations. The flexibility of these proteins suggest that these chaperones are likely to be involved in the folding of their native OMP substrates, and provides further support for their suggested PPIase activity (Bitto and McKay, 2002; Saul *et al.*, 2004). The investigation into the structure of the periplasmic protease HtrA demonstrated that the resting state of the protein is an inactive, collapsed hexamer, in which the protease active sites are occluded. However, during envelope stress, HtrA assembles into

large oligomers that allows access to its functional proteolytic sites (Jiang *et al.*, 2008; Krojer *et al.*, 2008; Hansen and Hilgenfeld, 2013).

The CpxP family of bacterial chaperones includes CpxP, Spy and ZraP. Previous studies have demonstrated that, similarly to CpxP, ZraP is involved in the regulation of its associated two-component system ZraSR. Furthermore, MDH aggregation assays have demonstrated that ZraP is capable of protecting thermally denatured MDH against aggregation in a more effective manner than Spy (Appia-Ayme *et al.*, 2012). The crystal structures of CpxP and Spy show that these two chaperones form cradle-shaped homodimers with hydrophobic patches on the concave surface of the structure. It has been suggested that this concave site interacts with hydrophobic regions of OMPs, the cradle-like dimers flexing around the substrate to prevent aggregation (Kwon *et al.*, 2010; Quan *et al.*, 2011; Thede *et al.*, 2011). Unlike the other two chaperones of this family, the published crystal structure of ZraP presents a decameric, ring-shaped protein. However, over 40% of the protein structure is missing from the model, suggesting they form highly flexible structures. Experiments carried out in the Rowley lab, preceding the current study, suggested that mutations of the C-terminal [128]GGCGGY[133] region of *Salmonella* ZraP interfere with the chaperone's ability to adopt higher oligomeric structures in the absence of zinc (Wells, 2015). This study investigated the supposed difference between the wild type ZraP (ZraP-WT) and the ZraP construct mutated in the [128]GGCGGY[133] region (ZraP-SDM) with X-ray crystallography and Small-angle X-ray scattering (SAXS) experiments. The results, presented in detail in chapter 4, demonstrated that ZraP-WT and ZraP-SDM both form decameric ring-structures when in crystal formation. However, it was postulated that the decameric crystal structure of the ZraP-SDM mutant may have been an artefact of the extreme conditions required for crystal formation. To investigate the envelope structure of ZraP, SAXS experiments were conducted comparing the shapes if ZraP-WT and ZraP-SDM. The SAXS-derived data confirmed the data previously obtained, suggesting both ZraP-WT and ZraP-SDM form proteins of higher oligomeric order. However, unlike the ring-shaped decamer presented by the X-ray crystallography model, SAXS analysis suggests that ZraP-WT forms a slightly elongated globular protein, and the ZraP-SDM mutant is more spherical in shape compared to the WT protein. Investigations comparing ZraP proteins carrying a *myc*-HIS C-terminal epitope to ZraP proteins carrying a *strepII* C-terminal epitope suggest a potential explanation for the differences in the ZraP-oligomerisation reported by Wells (2015), and the observations for the oligomeric state reported in this study. Examination of the SAXS data retrieved for *myc*-His-tagged ZraP and *strepII*-tagged ZraP, revealed that the *myc*-His epitope interferes with the formation of larger

ZraP-SDM oligomers in the absence of zinc. Whereas *strepII*-tagged ZraP-SDM forms spherical proteins of higher oligomeric structure, the *myc*-His-tagged ZraP-SDM has a significantly smaller volume in solution. This difference in oligomeric state was not observed between the *myc*-His-tagged and *strepII*-tagged ZraP-WT, suggesting that the previous observations of the inability of ZraP-SDM to form proteins of higher oligomeric order is an artefact of the *myc*-His epitope. Furthermore, SAXS experiments carried out on ZraP samples exposed to different zinc concentrations suggest that zinc does not influence protein structure significantly, nor is the presence of zinc required for the formation of higher oligomeric structures of either ZraP-WT or ZraP-SDM.

The low resolution of the X-ray data collected during this study did not allow for an improved model of the current ZraP crystal structure. The collected SAXS data suggested that the protein is more likely to be cylindrical or spherical in structure. DAMMIF and DAMMIN model data solved using the SAXS data-sets experimentally collected from ZraP samples (models not included in this thesis), seem to suggest the presence of a disc-shaped protein core. Although the models created were often a poor fit to the experimental data provided, the rig-shaped model obtained by X-ray crystallography always fit in the core of the models solved by DAMMIF. Combined, these data suggest that the ZraP is likely to form a globular protein with a rigid core and highly flexible N- and C- terminal regions that fill the core of the protein and extend outwardly to form the cylindrical shape presented in figure 4.26.

Due to the low resolution of the SAXS-data, and the incompleteness of the ZraP crystal model, it is difficult to predict how ZraP may be interacting with its substrates. In order to gain a better understanding of the chaperoning mechanism of ZraP, small-angle scattering analysis can be carried out on samples containing both the chaperone and a substrate. However, considering ZraP substrates are proteins themselves, SAXS experiments would now allow for the differentiation between data collected for the chaperone and the data collected for the substrate. However, small-angle scattering analysis using neutron scattering (SANS) can be used to investigate protein interactions (Yan *et al.*, 2010; Chaudhuri, 2015; Ibrahim *et al.*, 2017). SANS data of samples containing a mixture of deuterated and non-deuterated peptides can be separated, allowing for the identification of different protein samples in the same solution. In preparation for potential SANS experiments, attempts were made to isolate and identify natural ZraP substrates. Unfortunately, the experiments to isolate ZraP substrates were unsuccessful and the natural substrates of ZraP remain enigmatic.

6.4 Understanding the functional mechanisms of periplasmic chaperones

Molecular chaperones are found in prokaryotes and eukaryotes alike. They play an important role in the folding of precursor proteins into their tertiary structure, and in the protection of proteins during transport across the cell (Cooper and Hausman, 2007). The overall mechanisms of cellular chaperones are well understood, and they generally rely on the hydrolysis of ATP to provide energy for their folding activities (Beissinger and Buchner, 1998; Hartl, Bracher and Hayer-Hartl, 2011). However, the mechanism by which periplasmic chaperones interact with and fold their substrates are less well understood. The periplasm is devoid of ATP, and as such the mechanisms by which cytoplasmic chaperones fold their substrates do not apply. Evidence suggests that periplasmic chaperones are involved in the folding of OMPs to some extent (Schafer, Beck and Muller, 1999; Bulieris *et al.*, 2003; Patel *et al.*, 2009; Schwalm *et al.*, 2013), but it is unclear how they fold and/or release their substrates.

The expression of ZraP is upregulated in response to increased levels of zinc (Leonhartsberger *et al.*, 2001; Appia-Ayme *et al.*, 2012; Wells, 2015). The lack of a *Salmonella* Δ*zraPSR* phenotype in high zinc conditions ruled out involvement in the protection against zinc toxicity (data not included in this thesis). SAXS data presented in chapter 4 demonstrated that zinc is not required for the oligomerisation of ZraP, nor does the presence of zinc appear to elicit significant changes in overall protein shape. However, studies into the chaperone function of ZraP have indicated that the chaperone activity of ZraP is enhanced in the presence of zinc, and is reduced in the presence of the zinc-chelating agent EDTA (Appia-Ayme *et al.*, 2012; Wells, 2015). Whereas previous studies investigated the ability of ZraP to protect against substrate aggregation, this study attempted to investigate if ZraP is capable of protecting substrate function during environmental stress. The data presented in chapter 5 demonstrate that ZraP is capable of interacting with MDH. However, this interaction appears to reduce MDH activity significantly. A similar result was observed in the DNA gyrase experiments, investigating the ability of ZraP to protect DNA gyrase against thermal denaturation. The results obtained in this study suggest that interactions with ZraP render the tested substrate less active or inactive. The mechanism by which ZraP inactivates its substrates is unclear, but it is possible that ZraP either binds to an active site, or perhaps the interaction between ZraP and substrate lock MDH and DNA gyrase into a single

conformation, rendering them inactive. Due to the inhibiting effect of zinc on MDH, future investigations in the ability of ZraP to protect substrate function would benefit from an alternative substrate.

Investigation into the chaperone function of mutated ZraP constructs suggested that ZraP-ZA and ZraP-HRGGAH (both mutated in the C-terminal ^{139}HRGGAH^{144} region) do not inhibit MDH activity as severely as the other tested mutant. To determine if this phenomenon is the result of a decreased level of chaperone-substrate binding, it would be worth to subject these mutants to the inhibition of aggregation assays carried out by Appia-Ayme (2012) and Wells (2015).

6.5 Concluding remarks

The research described in this thesis can be separated into two distinct parts. The first part aimed to clarify the role of periplasmic chaperones in the protection of *Salmonella* against environmental challenges. The obtained results and suggestions for future work are discussed in chapter three. The second part of this thesis investigated the structural and functional characteristics of ZraP. The obtained results and suggestions for future work are discussed in chapter four and five respectively.

Investigation into the periplasmic chaperones of Gram-negative bacteria could provide new targets for treatment strategies, including the development of new antibiotic treatments and the presentation of new vaccine targets against *Salmonella* infections. The results presented in this study demonstrate that defects in the expression of certain periplasmic chaperones such as Skp and SurA lead to alterations of the outer membrane. These alterations render the cell susceptible to antimicrobials and extracellular stresses that the wild type *Salmonella* strain would otherwise be naturally resistant to. Targeting periplasmic chaperones may increase the susceptibility of *Salmonella* antibiotics it is currently resistant to. Furthermore, periplasmic mutations that render *Salmonella* more sensitive to environmental stresses such as heat and oxidative stress, may be suitable targets for the development of new *Salmonella* vaccines.

Although the investigation into the functional characteristics of ZraP failed to identify the function of zinc in ZraP chaperone activity, it did confirm that ZraP is capable of binding to various substrates. Furthermore, the research presented in this study suggest that ZraP may be an unsuitable for use in the biotechnological industry, as it renders the tested substrates inactive. However, there are other periplasmic chaperones that show ability to interact with

non-native proteins, which may be tested for their ability to protect enzyme function. Finally, the investigation into the structural characteristics of ZraP has provided some clarification regarding the missing fragments in the protein structure of ZraP. Data presented in this study suggest that ZraP does not form a ring-shaped protein as is suggested by the data obtained using X-ray crystallography data, but rather it forms a cylindrical or spherical globular oligomer. This shape is distinctly different from the other members of the CpxP-family of periplasmic chaperones, and requires further investigation to unravel the chaperoning mechanisms employed by this protein.

Although this study has contributed to the overall knowledge of periplasmic chaperone function in *Salmonella*, in particular for the periplasmic chaperone ZraP, there are still a lot of questions regarding periplasmic chaperone function and contribution to the overall protection of the cell. Further investigations into the functioning of these chaperones would contribute to our understanding of the mechanisms by which *Salmonella* adapts to changing and hostile environments, and would allow us to fight this pathogen more effectively.

Chapter 7 References

Acosta, N., Pukatzki, S. and Raivio, T. L. (2015) 'The Vibrio cholerae Cpx envelope stress response senses and mediates adaptation to low iron.', *Journal of Bacteriology*, pp. 262–276.

Ahuja, N., Korkin, D., Chaba, R., Cezairliyan, B. O., Sauer, R. T., Kim, K. K. and Gross, C. A. (2009) 'Analyzing the interaction of RseA and RseB, the two negative regulators of the sigmaE envelope stress response, using a combined bioinformatic and experimental strategy.', *The Journal of biological chemistry*, 284(8), pp. 5403–5413.

Ailes, E., Budge, P., Shankar, M., Collier, S., Brinton, W., Cronquist, A., Chen, M., Thornton, A., Beach, M. J. and Brunkard, J. M. (2013) 'Economic and health impacts associated with a Salmonella Typhimurium drinking water outbreak–Alamosa, CO, 2008.', *PLoS ONE*. doi: 10.1371/journal.pone.0057439.

Akiyama, H., Fujii, K., Yamasaki, O., Oono, T. and Iwatsuki, K. (2001) 'Antibacterial action of several tannins against Staphylococcus aureus.', *The Journal of antimicrobial chemotherapy*, 48(4), pp. 487–491.

Alba, B. M., Leeds, J. A., Onufryk, C., Lu, C. Z. and Gross, C. A. (2002) 'DegS and YaeL participate sequentially in the cleavage of RseA to activate the sigma(E)-dependent extracytoplasmic stress response.', *Genes & development*, 16(16), pp. 2156–2168. doi: 10.1101/gad.1008902.

Alberts, I. L., Nadassy, K. and Wodak, S. J. (1998) 'Analysis of zinc binding sites in protein crystal structures.', *Protein science: a publication of the Protein Society*, 7(8), pp. 1700–1716. doi: 10.1002/pro.5560070805.

Aldred, K. J., Kerns, R. J. and Osheroff, N. (2014) 'Mechanism of quinolone action and resistance.', *Biochemistry*, 53(10), pp. 1565–1574. doi: 10.1021/bi5000564.

Aleksic, S., Heinzerling, F. and Bockemuhl, J. (1996) 'Human infection caused by Salmonellae of subspecies II to VI in Germany, 1977-1992.', *Zentralblatt fur Bakteriologie : international journal of medical microbiology*, 283(3), pp. 391–398.

Altier, C. (2005) 'Genetic and environmental control of Salmonella invasion.', *Journal of microbiology (Seoul, Korea)*, 43, pp. 85–92.

Ammendola, S., Pasquali, P., Pistoia, C., Petrucci, P., Petrarca, P., Rotilio, G. and Battistoni, A. (2007) 'High-affinity Zn2+ uptake system ZnuABC is required for bacterial zinc homeostasis in intracellular environments and contributes to the virulence of Salmonella

enterica.', *Infection and immunity*, 75(12), pp. 5867–5876. doi: 10.1128/IAI.00559-07.

Amy, M., Velge, P., Senocq, D., Bottreau, E., Mompart, F. and Virlogeux-Payant, I. (2004) 'Identification of a new Salmonella enterica serovar Enteritidis locus involved in cell invasion and in the colonisation of chicks.', *Research in microbiology*, 155(7), pp. 543–552. doi: 10.1016/j.resmic.2004.03.005.

Andreini, C., Banci, L., Bertini, I. and Rosato, A. (2006) 'Zinc through the three domains of life.', *Journal of proteome research*, 5(11), pp. 3173–3178. doi: 10.1021/pr0603699.

Antonoaea, R., Furst, M., Nishiyama, K.-I. and Muller, M. (2008) 'The periplasmic chaperone PpiD interacts with secretory proteins exiting from the SecYEG translocon.', *Biochemistry*, 47(20), pp. 5649–5656. doi: 10.1021/bi800233w.

Ao, T. T., Feasey, N. A., Gordon, M. A., Keddy, K. H., Angulo, F. J. and Crump, J. A. (2015) 'Global burden of invasive nontyphoidal Salmonella disease, 2010.', *Emerging Infectious Diseases*, 21(6), pp. 941–949.

Appia-Ayme, C., Hall, A., Patrick, E., Rajadurai, S., Clarke, T. A. and Rowley, G. (2012) 'ZraP is a periplasmic molecular chaperone and a repressor of the zinc-responsive two-component regulator ZraSR.', *The Biochemical journal*, 442(1), pp. 85–93. doi: 10.1042/BJ20111639.

Appia-Ayme, C., Patrick, E., Sullivan, M. J., Alston, M. J., Field, S. J., AbuOun, M., Anjum, M. F. and Rowley, G. (2011) 'Novel Inducers of the Envelope Stress Response BaeSR in Salmonella Typhimurium: BaeR is critically required for Tungstate waste disposal.', *PloS one*, 6(8).

Arie, J. P., Sassoon, N. and Betton, J. M. (2001) 'Chaperone function of FkpA, a heat shock prolyl isomerase, in the periplasm of Escherichia coli.', *Molecular microbiology*, 39(1), pp. 199–210.

Arnold, K., Hong, C. S., Nelwan, R., Zavala-Trujillo, I., Kadio, A., Barros, M. A. and de Garis, S. (1993) 'Randomized comparative study of fleroxacin and chloramphenicol in typhoid fever.', *The American journal of medicine*, 94(3A), p. 195S–200S.

Aviles, B., Klotz, C., Eifert, J., Williams, R. and Ponder, M. (2013) 'Biofilms promote survival and virulence of Salmonella enterica sv. Tennessee during prolonged dry storage and after passage through an in vitro digestion system.', *International journal of food microbiology*, 162(3), pp. 252–259. doi: 10.1016/j.ijfoodmicro.2013.01.026.

Bader, M. W., Navarre, W. W., Shiau, W., Nikaido, H., Frye, J. G., McClelland, M., Fang, F. C.

and Miller, S. I. (2003) 'Regulation of Salmonella Typhimurium virulence gene expression by cationic antimicrobial peptides.', *Molecular microbiology*, 50(1), pp. 219–230.

Bang, I. S., Audia, J. P., Park, Y. K. and Foster, J. W. (2002) 'Autoinduction of the ompR response regulator by acid shock and control of the Salmonella enterica acid tolerance response.', *Molecular microbiology*, 44(5), pp. 1235–1250.

Baranova, N. and Nikaido, H. (2002) 'The baeSR two-component regulatory system activates transcription of the yegMNOB (mdtABCD) transporter gene cluster in Escherichia coli and increases its resistance to novobiocin and deoxycholate.', *Journal of bacteriology*, 184(15), pp. 4168–4176.

Barchinger, S. E. and Ades, S. E. (2013) 'Regulated proteolysis: control of the Escherichia coli sigma(E)-dependent cell envelope stress response.', *Sub-cellular biochemistry*, 66, pp. 129–160. doi: 10.1007/978-94-007-5940-4_6.

Barna, J. C. and Williams, D. H. (1984) 'The structure and mode of action of glycopeptide antibiotics of the vancomycin group.', *Annual review of microbiology*, 38, pp. 339–357. doi: 10.1146/annurev.mi.38.100184.002011.

Barrow, K. and Kwon, D. H. (2009) 'Alterations in two-component regulatory systems of phoPQ and pmrAB are associated with polymyxin B resistance in clinical isolates of Pseudomonas aeruginosa.', *Antimicrobial agents and chemotherapy*, 53(12), pp. 5150–5154. doi: 10.1128/AAC.00893-09.

Battesti, A., Majdalani, N. and Gottesman, S. (2011) 'The RpoS-mediated general stress response in Escherichia coli.', *Annual review of microbiology*, 65, pp. 189–213. doi: 10.1146/annurev-micro-090110-102946.

Battye, T. G. G., Kontogiannis, L., Johnson, O., Powell, H. R. and Leslie, A. G. W. (2011) 'iMOSFLM: a new graphical interface for diffraction-image processing with MOSFLM.', *Acta crystallographica. Section D, Biological crystallography*, 67(Pt 4), pp. 271–281. doi: 10.1107/S0907444910048675.

Bäumler, A. J., Kusters, J. G., Stojiljkovic, I. and Heffron, F. (1994) 'Salmonella Typhimurium loci involved in survival within macrophages.', *Infection and Immunity*, pp. 1623–1630.

Baumler, A. J., Tsolis, R. M., Ficht, T. A. and Adams, L. G. (1998) 'Evolution of host adaptation in Salmonella enterica.', *Infection and immunity*, 66(10), pp. 4579–4587.

Bearson, B. L., Wilson, L. and Foster, J. W. (1998) 'A low pH-inducible, PhoPQ-dependent

acid tolerance response protects Salmonella Typhimurium against inorganic acid stress.', *Journal of bacteriology*, 180(9), pp. 2409–2417.

Behrens-Kneip, S. (2010) 'The role of SurA factor in outer membrane protein transport and virulence.', *International journal of medical microbiology : IJMM*, 300(7), pp. 421–428. doi: 10.1016/j.ijmm.2010.04.012.

Behrens, S., Maier, R., de Cock, H., Schmid, F. X. and Gross, C. A. (2001) 'The SurA periplasmic PPIase lacking its parvulin domains functions in vivo and has chaperone activity.', *The EMBO Journal*, pp. 285–294. doi: 10.1093/emboj/20.1.285.

Beissinger, M. and Buchner, J. (1998) 'How chaperones fold proteins.', *Biological chemistry*, 379(3), pp. 245–259.

Bell, J. K., Yennawar, H. P., Wright, S. K., Thompson, J. R., Viola, R. E. and Banaszak, L. J. (2001) 'Structural analyses of a malate dehydrogenase with a variable active site.', *The Journal of biological chemistry*, 276(33), pp. 31156–31162. doi: 10.1074/jbc.M100902200.

Bennion, D., Charlson, E. S., Coon, E. and Misra, R. (2010) 'Dissection of β-barrel outer membrane protein assembly pathways through characterizing BamA POTRA 1 mutants of Escherichia coli.', *Molecular microbiology*, pp. 1153–1171. doi: 10.1111/j.1365-2958.2010.07280.x.

Berg, J. M., Tymoczko, J. L. and Stryer, L. (2006) 'Chapter 8. Enzymes: basic concepts and kinetics.', in *Biochemistry*. 6th edn. New York: W. H. Freeman and Company, pp. 216–228.

Bergal, H. T., Hopkins, A. H., Metzner, S. I. and Sousa, M. C. (2016) 'The structure of a BamA-BamD fusion illuminates the architecture of the beta-barrel assembly machine core.', *Structure (London, England : 1993)*, 24(2), pp. 243–251. doi: 10.1016/j.str.2015.10.030.

Bergler, H., Abraham, D., Aschauer, H. and Turnowsky, F. (1994) 'Inhibition of lipid biosynthesis induces the expression of the pspA gene.', *Microbiology (Reading, England)*, 140 (Pt 8, pp. 1937–1944. doi: 10.1099/13500872-140-8-1937.

Bijapur, G. A. M., Kakkeri, S. R., Raysa, N. P. and Usman, S. M. (2014) 'A study to determine significant titre-values of widal test in the diagnosis of enteric fever for a population of north Kerala, India.', *Al Ameen Journal of Medical Sciences*, 7(1), pp. 72–77.

BioSAXS (2017) *Small Angle X-Ray Scattering*. Available at: http://biosaxs.com/technique.html.

Bitto, E. and McKay, D. B. (2002) 'Crystallographic structure of SurA, a molecular chaperone that facilitates folding of outer membrane porins.', *Structure (London, England : 1993)*, 10(11), pp. 1489–1498.

Blindauer, C. A. (2015) 'Advances in the molecular understanding of biological zinc transport.', *Chemical communications (Cambridge, England)*, 51(22), pp. 4544–4563. doi: 10.1039/c4cc10174j.

Blondel, C. J., Jimenez, J. C., Contreras, I. and Santiviago, C. A. (2009) 'Comparative genomic analysis uncovers 3 novel loci encoding type six secretion systems differentially distributed in Salmonella serotypes.', *BMC genomics*, 10, p. 354. doi: 10.1186/1471-2164-10-354.

Bochner, B. R. (1984) 'Curing bacterial cells of lysogenic viruses by using ucb indicator plates.', *Biotechniques*, 2(4), pp. 234–240.

Botos, I., Majdalani, N., Mayclin, S. J., McCarthy, J. G., Lundquist, K., Wojtowicz, D., Barnard, T. J., Gumbart, J. C. and Buchanan, S. K. (2016) 'Structural and functional characterization of the LPS transporter LptDE from Gram-negative pathogens.', *Structure*, 24(6), pp. 965–976. doi: 10.1016/j.str.2016.03.026.

Bougdour, A., Cunning, C., Baptiste, P. J., Elliott, T. and Gottesman, S. (2008) 'Multiple pathways for regulation of sigmaS (RpoS) stability in Escherichia coli via the action of multiple anti-adaptors.', *Molecular microbiology*, 68(2), pp. 298–313.

Bougdour, A. and Gottesman, S. (2007) 'PpGpp regulation of RpoS degradation via anti-adaptor protein IraP.', *Proceedings of the National Academy of Sciences of the United States of America*, 104(31), pp. 12896–12901. doi: 10.1073/pnas.0705561104.

Brandi, G., Salvaggio, L., Cattabeni, F. and Cantoni, O. (1991) 'Cytocidal and filamentous response of Escherichia coli cells exposed to low concentrations of hydrogen peroxide and hydroxyl radical scavengers.', *Environmental and molecular mutagenesis*, 18(1), pp. 22–27.

Breiman, R. F., Cosmas, L., Njuguna, H., Audi, A., Olack, B., Ochieng, J. B., Wamola, N., Bigogo, G. M., Awiti, G., Tabu, C. W., Burke, H., Williamson, J., Oundo, J. O., Mintz, E. D. and Feikin, D. R. (2012) 'Population-based incidence of typhoid fever in an urban informal settlement and a rural area in Kenya: implications for typhoid vaccine use in Africa.', *PloS one*, 7(1). doi: 10.1371/journal.pone.0029119.

Breiter, D. R., Resnik, E. and Banaszak, L. J. (1994) 'Engineering the quaternary structure of an enzyme: construction and analysis of a monomeric form of malate dehydrogenase from

Escherichia coli.', *Protein science : a publication of the Protein Society*, 3(11), pp. 2023–2032. doi: 10.1002/pro.5560031115.

Brenner, F. W., Villar, R. G., Angulo, F. J., Tauxe, R. and Swaminathan, B. (2000) 'Salmonella nomenclature.', *Journal of clinical microbiology*, 38(7), pp. 2465–2467.

Bringer, M.-A., Barnich, N., Glasser, A.-L., Bardot, O. and Darfeuille-Michaud, A. (2005) 'HtrA stress protein is involved in intramacrophagic replication of adherent and invasive Escherichia coli strain LF82 isolated from a patient with Crohn's disease.', *Infection and immunity*, 73(2), pp. 712–721. doi: 10.1128/IAI.73.2.712-721.2005.

Brissette, J. L., Russel, M., Weiner, L. and Model, P. (1990) 'Phage shock protein, a stress protein of Escherichia coli.', *Proceedings of the National Academy of Sciences of the United States of America*, 87(3), pp. 862–866.

Brissette, J. L., Weiner, L., Ripmaster, T. L. and Model, P. (1991) 'Characterization and sequence of the Escherichia coli stress-induced psp operon.', *Journal of molecular biology*, 220(1), pp. 35–48.

Brown, L. and Elliott, T. (1997) 'Mutations that increase expression of the rpoS gene and decrease its dependence on hfq function in Salmonella Typhimurium.', *Journal of bacteriology*, 179(3), pp. 656–662.

Buckle, G. C., Walker, C. L. F. and Black, R. E. (2012) 'Typhoid fever and paratyphoid fever: Systematic review to estimate global morbidity and mortality for 2010', *Journal of Global Health*. doi: 10.7189/jogh.02.010401.

Buelow, D. R. and Raivio, T. L. (2005) 'Cpx signal transduction is influenced by a conserved N-terminal domain in the novel inhibitor CpxP and the periplasmic protease DegP.', *Journal of bacteriology*, 187(19), pp. 6622–6630. doi: 10.1128/JB.187.19.6622-6630.2005.

Bulieris, P. V, Behrens, S., Holst, O. and Kleinschmidt, J. H. (2003) 'Folding and insertion of the outer membrane protein OmpA is assisted by the chaperone Skp and by lipopolysaccharide.', *The Journal of biological chemistry*, 278(11), pp. 9092–9099. doi: 10.1074/jbc.M211177200.

Burgess, N. K., Dao, T. P., Stanley, A. M. and Fleming, K. G. (2008) 'Beta-barrel proteins that reside in the Escherichia coli outer membrane in vivo demonstrate varied folding behavior in vitro.', *The Journal of biological chemistry*, 283(39), pp. 26748–26758. doi: 10.1074/jbc.M802754200.

Burmann, B. M., Wang, C. and Hiller, S. (2013) 'Conformation and dynamics of the periplasmic membrane-protein-chaperone complexes OmpX-Skp and tOmpA-Skp.', *Nature structural & molecular biology*, 20(11), pp. 1265–1272. doi: 10.1038/nsmb.2677.

Bury-Mone, S., Nomane, Y., Reymond, N., Barbet, R., Jacquet, E., Imbeaud, S., Jacq, A. and Bouloc, P. (2009) 'Global analysis of extracytoplasmic stress signaling in Escherichia coli.', *PLoS genetics*, 5(9). doi: 10.1371/journal.pgen.1000651.

Cajal, Y., Rogers, J., Berg, O. G. and Jain, M. K. (1996) 'Intermembrane molecular contacts by polymyxin B mediate exchange of phospholipids.', *Biochemistry*, 35(1), pp. 299–308. doi: 10.1021/bi9512408.

Camilloni, C., Rocco, A. G., Eberini, I., Gianazza, E., Broglia, R. A. and Tiana, G. (2008) 'Urea and guanidinium chloride denature protein L in different ways in molecular dynamics simulations.', *Biophysical journal*, 94(12), pp. 4654–4661. doi: 10.1529/biophysj.107.125799.

Campbell, E. A., Tupy, J. L., Gruber, T. M., Wang, S., Sharp, M. M., Gross, C. A. and Darst, S. A. (2003) 'Crystal structure of Escherichia coli sigmaE with the cytoplasmic domain of its anti-sigma RseA.', *Molecular cell*, 11(4), pp. 1067–1078.

Campoy, S., Jara, M., Busquets, N., Perez De Rozas, A. M., Badiola, I. and Barbe, J. (2002) 'Role of the high-affinity zinc uptake znuABC system in Salmonella enterica serovar Typhimurium virulence.', *Infection and immunity*, 70(8), pp. 4721–4725.

Capdevila, D., Wang, J. and Giedroc, D. P. (2016) 'Bacterial strategies to maintain zinc metallostasis at the host-pathogen interface.', *The Journal of biological chemistry*, 291(40), pp. 20858–20868.

Capra, E. J. and Laub, M. T. (2012) 'Evolution of two-component signal transduction systems.', *Annual review of microbiology*, 66, pp. 325–347. doi: 10.1146/annurev-micro-092611-150039.

Carlsson, K. E., Liu, J., Edqvist, P. J. and Francis, M. S. (2007) 'Extracytoplasmic-stress-responsive pathways modulate type III secretion in Yersinia pseudotuberculosis.', *Infection and immunity*, 75(8), pp. 3913–3924. doi: 10.1128/IAI.01346-06.

Castanie-Cornet, M.-P., Cam, K., Bastiat, B., Cros, A., Bordes, P. and Gutierrez, C. (2010) 'Acid stress response in Escherichia coli: mechanism of regulation of gadA transcription by RcsB and GadE.', *Nucleic acids research*, 38(11), pp. 3546–3554. doi: 10.1093/nar/gkq097.

CastilloKeller, M. and Misra, R. (2003) 'Protease-deficient DegP suppresses lethal effects of a mutant OmpC protein by its capture.', *Journal of bacteriology*, 185(1), pp. 148–154.

CCP4 (1994) 'The CCP4 suite: programs for protein crystallography.', *Acta crystallographica. Section D, Biological crystallography*, 50(Pt 5), pp. 760–763. doi: 10.1107/S0907444994003112.

Cerasi, M., Liu, J. Z., Ammendola, S., Poe, A. J., Petrarca, P., Pesciaroli, M., Pasquali, P., Raffatellu, M. and Battistoni, A. (2014) 'The ZupT transporter plays an important role in zinc homeostasis and contributes to Salmonella enterica virulence.', *Metallomics : integrated biometal science*, 6(4), pp. 845–853. doi: 10.1039/c3mt00352c.

Cezairliyan, B. O. and Sauer, R. T. (2007) 'Inhibition of regulated proteolysis by RseB.', *Proceedings of the National Academy of Sciences of the United States of America*, 104(10), pp. 3771–3776. doi: 10.1073/pnas.0611567104.

Chang, Z. (2016) 'The function of the DegP (HtrA) protein: protease versus chaperone.', *IUBMB life*, 68(11), pp. 904–907. doi: 10.1002/iub.1561.

Charbit, A., Wang, J., Michel, V. and Hofnung, M. (1998) 'A cluster of charged and aromatic residues in the C-terminal portion of maltoporin participates in sugar binding and uptake.', *Molecular & general genetics : MGG*, 260(2–3), pp. 185–192.

Charlson, E. S., Werner, J. N. and Misra, R. (2006) 'Differential effects of yfgL mutation on Escherichia coli outer membrane proteins and lipopolysaccharide', *Journal of Bacteriology*, pp. 7186–7194. doi: 10.1128/JB.00571-06.

Chatterjee, M., Chakraborty, B., Chatterjee, S. S., Bose, M., Mukherjee, K., Basu, A., Das, S., Banerjee, M. and Ghosh, U. (2012) 'Enteric fever in an HIV/AIDS patient: atypical manifestations', *Iranian Journal of Microbiology*, pp. 150–152.

Chaudhuri, B. N. (2015) 'Emerging applications of small angle solution scattering in structural biology.', *Protein Science : A Publication of the Protein Society*, pp. 267–276. doi: 10.1002/pro.2624.

Chen, R. and Henning, U. (1996) 'A periplasmic protein (Skp) of Escherichia coli selectively binds a class of outer membrane proteins.', *Molecular microbiology*, 19(6), pp. 1287–1294.

Chen, Y. H., Chen, T. P., Lu, P. L., Su, Y. C., Hwang, K. P., Tsai, J. J., Cheng, H. H. and Peng, C. F. (1999) 'Salmonella choleraesuis bacteremia in southern Taiwan.', *The Kaohsiung journal of medical sciences*, 15(4), pp. 202–208.

Chen, Z., Zhan, L. H., Hou, H. F., Gao, Z. Q., Xu, J. H., Dong, C. and Dong, Y. H. (2016) 'Structural basis for the interaction of BamB with the POTRA3-4 domains of BamA.', *Acta Crystallographia. Section D, Structural Biology*, 72(2), pp. 236–244.

Chinh, N. T., Parry, C. M., Ly, N. T., Ha, H. D., Thong, M. X., Diep, T. S., Wain, J., White, N. J. and Farrar, J. J. (2000) 'A randomized controlled comparison of azithromycin and ofloxacin for treatment of multidrug-resistant or nalidixic acid-resistant enteric fever.', *Antimicrobial agents and chemotherapy*, 44(7), pp. 1855–1859.

Chiu, C.-H., Su, L.-H. and Chu, C. (2004) 'Salmonella enterica serotype Choleraesuis: epidemiology, pathogenesis, clinical disease, and treatment.', *Clinical microbiology reviews*, 17(2), pp. 311–322.

Chiu, C. H., Lin, T. Y. and Ou, J. T. (1999) 'Predictors for extraintestinal infection of non-typhoidal Salmonella in patients without AIDS.', *International journal of clinical practice*, 53(3), pp. 161–164.

Chiu, C. H., Lin, T. Y. and Ou, J. T. (2000) 'Age-related differences of nontyphoid Salmonella bacteremia in clinical presentation and outcome: association with specific serovars but not necessarily with the virulence plasmids.', *Clinical infectious diseases : an official publication of the Infectious Diseases Society of America*, pp. 239–241. doi: 10.1086/313624.

Chng, S.-S., Gronenberg, L. S. and Kahne, D. (2010) 'Proteins required for lipopolysaccharide assembly in Escherichia coli form a transenvelope complex.', *Biochemistry*, 49(22), pp. 4565–4567. doi: 10.1021/bi100493e.

Chng, S.-S., Ruiz, N., Chimalakonda, G., Silhavy, T. J. and Kahne, D. (2010) 'Characterization of the two-protein complex in Escherichia coli responsible for lipopolysaccharide assembly at the outer membrane.', *Proceedings of the National Academy of Sciences of the United States of America*, 107(12), pp. 5363–5368. doi: 10.1073/pnas.0912872107.

Cho, S.-H., Szewczyk, J., Pesavento, C., Zietek, M., Banzhaf, M., Roszczenko, P., Asmar, A., Laloux, G., Hov, A.-K., Leverrier, P., Van der Henst, C., Vertommen, D., Typas, A. and Collet, J.-F. (2014) 'Detecting envelope stress by monitoring beta-barrel assembly.', *Cell*, 159(7), pp. 1652–1664. doi: 10.1016/j.cell.2014.11.045.

Clarke, D. J., Holland, I. B. and Jacq, A. (1997) 'Point mutations in the transmembrane domain of DjlA, a membrane-linked DnaJ-like protein, abolish its function in promoting colanic acid production via the Rcs signal transduction pathway.', *Molecular microbiology*,

25(5), pp. 933–944.

Clarke, E. J. and Voigt, C. A. (2011) 'Characterization of combinatorial patterns generated by multiple two-component sensors in E. coli that respond to many stimuli.', *Biotechnology and bioengineering*, 108(3), pp. 666–675. doi: 10.1002/bit.22966.

Clausell, A., Garcia-Subirats, M., Pujol, M., Busquets, M. A., Rabanal, F. and Cajal, Y. (2007) 'Gram-negative outer and inner membrane models: insertion of cyclic cationic lipopeptides.', *The journal of physical chemistry. B*, 111(3), pp. 551–563. doi: 10.1021/jp064757+.

Clausell, A., Rabanal, F., Garcia-Subirats, M., Asuncion Alsina, M. and Cajal, Y. (2006) 'Membrane association and contact formation by a synthetic analogue of polymyxin B and its fluorescent derivatives.', *The journal of physical chemistry. B*, 110(9), pp. 4465–4471. doi: 10.1021/jp0551972.

Clifton, L. A., Skoda, M. W. A., Le Brun, A. P., Ciesielski, F., Kuzmenko, I., Holt, S. A. and Lakey, J. H. (2015) 'Effect of divalent cation removal on the structure of gram-negative bacterial outer membrane models.', *Langmuir : the ACS journal of surfaces and colloids*, 31(1), pp. 404–412. doi: 10.1021/la504407v.

De Cock, H., Schafer, U., Potgeter, M., Demel, R., Muller, M. and Tommassen, J. (1999) 'Affinity of the periplasmic chaperone Skp of Escherichia coli for phospholipids, lipopolysaccharides and non-native outer membrane proteins. Role of Skp in the biogenesis of outer membrane protein.', *European journal of biochemistry*, 259(1–2), pp. 96–103.

Cohen, J. I., Bartlett, J. A. and Corey, G. R. (1987) 'Extra-intestinal manifestations of Salmonella infections.', *Medicine*, 66(5), pp. 349–388.

Cold Spring Harbor Protocols (2006) 'Phosphate buffer.', p. doi:10.1101/pdb.rec8543.

Cole, J. L., Lary, J. W., Moody, T. and Laue, T. M. (2008) 'Analytical ultracentrifugation: sedimentation velocity and sedimentation equilibrium.', *Methods in cell biology*, pp. 143–179. doi: 10.1016/S0091-679X(07)84006-4.

Compton, L. A., Davis, J. M., Macdonald, J. R. and Bachinger, H. P. (1992) 'Structural and functional characterization of Escherichia coli peptidyl-prolyl cis-trans isomerases.', *European journal of biochemistry*, 206(3), pp. 927–934.

Condell, O., Iversen, C., Cooney, S., Power, K. A., Walsh, C., Burgess, C. and Fanning, S. (2012) 'Efficacy of biocides used in the modern food industry to control Salmonella

enterica, and links between biocide tolerance and resistance to clinically relevant antimicrobial compounds.', *Applied and Environmental Microbiology*, pp. 3087–3097. doi: 10.1128/AEM.07534-11.

Cooper, G. M. and Hausman, R. E. (2007) 'Protein synthesis, processing, and regulation.', in *The cell: A molecular approach*, pp. 309–354.

Cordeiro, R. P., Krause, D. O., Doria, J. H. and Holley, R. A. (2014) 'Role of the BaeSR two-component regulatory system in resistance of Escherichia coli O157:H7 to allyl isothiocyanate.', *Food microbiology*, 42, pp. 136–141. doi: 10.1016/j.fm.2014.03.011.

Cortes, G., de Astorza, B., Benedi, V. J. and Alberti, S. (2002) 'Role of the htrA gene in Klebsiella pneumoniae virulence.', *Infection and immunity*, 70(9), pp. 4772–4776.

Cristiano, P., Imparato, L., Carpinelli, C., Lauria, F., Iovene, M. R., Corrado, M. F., Maio, P. and Imperatore, C. (1995) 'Pefloxacin versus chloramphenicol in the therapy of typhoid fever.', *Infection*, 23(2), pp. 103–106.

Crosa, J. H., Brenner, D. J., Ewing, W. H. and Falkow, S. (1973) 'Molecular relationships among the Salmonelleae.', *Journal of bacteriology*, 115(1), pp. 307–315.

Crump, J. A., Luby, S. P. and Mintz, E. D. (2004) 'The global burden of typhoid fever.', *Bulletin of the World Health Organization*, 82(5), pp. 346–353.

Crump, J. A. and Mintz, E. D. (2010) 'Global trends in typhoid and paratyphoid fever', *Clinical infectious diseases : an official publication of the Infectious Diseases Society of America*, pp. 241–246. doi: 10.1086/649541.

Danese, P. N., Oliver, G. R., Barr, K., Bowman, G. D., Rick, P. D. and Silhavy, T. J. (1998) 'Accumulation of the enterobacterial common antigen lipid II biosynthetic intermediate stimulates degP transcription in Escherichia coli.', *Journal of bacteriology*, 180(22), pp. 5875–5884.

Danese, P. N. and Silhavy, T. J. (1998) 'CpxP, a stress-combative member of the Cpx regulon.', *Journal of bacteriology*, 180(4), pp. 831–839.

Daniel, A. G. and Farrell, N. P. (2014) 'The dynamics of zinc sites in proteins: electronic basis for coordination sphere expansion at structural sites.', *Metallomics : integrated biometal science*, 6(12), pp. 2230–2241. doi: 10.1039/c4mt00213j.

Dartigalongue, C., Missiakas, D. and Raina, S. (2001) 'Characterization of the Escherichia coli

sigma E regulon.', *The Journal of biological chemistry*, 276(24), pp. 20866–20875. doi: 10.1074/jbc.M100464200.

Dartigalongue, C. and Raina, S. (1998) 'A new heat-shock gene, ppiD, encodes a peptidyl-prolyl isomerase required for folding of outer membrane proteins in Escherichia coli.', *The EMBO journal*, 17(14), pp. 3968–3980. doi: 10.1093/emboj/17.14.3968.

Darwin, K. H. and Miller, V. L. (1999) 'Molecular basis of the interaction of Salmonella with the intestinal mucosa.', *Clinical microbiology reviews*, 12(3), pp. 405–428.

Das, U. and Bhattacharya, S. S. (2000) 'Multidrug resistant Salmonella Typhi in Rourkela, Orissa.', *Indian journal of pathology & microbiology*, 43(2), pp. 135–138.

Datsenko, K. A. and Wanner, B. L. (2000) 'One-step inactivation of chromosomal genes in Escherichia coli K-12 using PCR products.', *Proceedings of the National Academy of Sciences of the United States of America*, 97(12), pp. 6640–6645. doi: 10.1073/pnas.120163297.

Davies, B. W., Kohansko, M. A., Simmons, L. A., Winkler, J. A., Collins, J. J. and Walker, G. C. (2009) 'Hydroxyurea induces hydroxyl radical-mediated cell death in Escherichia coli.', *Molecular cell*, 36(5), pp. 845–860. doi: 10.1016/j.molcel.2009.11.024.

Davis, B. D. (1987) 'Mechanism of bactericidal action of aminoglycosides.', *Microbiological Reviews*, pp. 341–350.

Debnath, I., Norton, J. P., Barber, A. E., Ott, E. M., Dhakal, B. K., Kulesus, R. R. and Mulvey, M. A. (2013) 'The Cpx stress response system potentiates the fitness and virulence of uropathogenic Escherichia coli.', *Infection and immunity*, 81(5), pp. 1450–9. doi: 10.1128/IAI.01213-12.

Delgado, M. A., Mouslim, C. and Groisman, E. A. (2006) 'The PmrA/PmrB and RcsC/YojN/RcsB systems control expression of the Salmonella O-antigen chain length determinant.', *Molecular microbiology*, 60(1), pp. 39–50. doi: 10.1111/j.1365-2958.2006.05069.x.

Demelar, B. (2005) 'UltraScan - A Comprehensive Data Analysis Software Package for Analytical Ultracentrifugation Experiments.', in SCOTT, D. J., HARDING, S. E., and ROWE, A. J. (eds) *Analytical Ultracentrifugation: Techniques and Methods.* The Royal Society of Chemistry, pp. 210–230.

DeRoeck, D., Ochiai, R. L., Yang, J., Anh, D. D., Alag, V. and Clemens, J. D. (2008) 'Typhoid vaccination: the Asian experience.', *Expert review of vaccines*, 7(5), pp. 547–560. doi:

10.1586/14760584.7.5.547.

Desvaux, M., Parham, N. J. and Henderson, I. R. (2004) 'The autotransporter secretion system.', *Research in microbiology*, 155(2), pp. 53–60. doi: 10.1016/j.resmic.2003.10.002.

Diamond Light Source (2017) *Diamond Light Source*. Available at: http://www.diamond.ac.uk/Home.html.

DiGiuseppe, P. A. and Silhavy, T. J. (2003) 'Signal detection and target gene induction by the CpxRA two-component system.', *Journal of bacteriology*, 185(8), pp. 2432–2440.

Djoko, K. Y., Ong, C. Y., Walker, M. J. and McEwan, A. G. (2015) 'The Role of Copper and Zinc Toxicity in Innate Immune Defense against Bacterial Pathogens.', *The Journal of biological chemistry*, 290(31), pp. 18954–18961. doi: 10.1074/jbc.R115.647099.

Dong, C., Hou, H. F., Yang, X., Shen, Y. Q. and Dong, Y. H. (2012) 'Structure of Escherichia coli BamD and its functional implications in outer membrane protein assembly.', *Acta crystallographica. Section D, Biological crystallography*, 68(Pt 2), pp. 95–101. doi: 10.1107/S0907444911051031.

Dong, H., Xiang, Q., Gu, Y., Wang, Z., Paterson, N. G., Stansfeld, P. J., He, C., Zhang, Y., Wang, W. and Dong, C. (2014) 'Structural basis for outer membrane lipopolysaccharide insertion.', *Nature*, 511(7507), pp. 52–56. doi: 10.1038/nature13464.

Doolittle, R. F., Feng, D. F., Tsang, S., Cho, G. and Little, E. (1996) 'Determining divergence times of the major kingdoms of living organisms with a protein clock.', *Science (New York, N.Y.)*, 271(5248), pp. 470–477.

Dorel, C., Lejeune, P. and Rodrigue, A. (2006) 'The Cpx system of Escherichia coli, a strategic signaling pathway for confronting adverse conditions and for settling biofilm communities?', *Research in microbiology*, 157(4), pp. 306–314. doi: 10.1016/j.resmic.2005.12.003.

Dorel, C., Vidal, O., Prigent-Combaret, C., Vallet, I. and Lejeune, P. (1999) 'Involvement of the Cpx signal transduction pathway of E. coli in biofilm formation.', *FEMS microbiology letters*, 178(1), pp. 169–175.

Dubois-Brissonnet, F. (2012) 'Adaptation of Salmonella to antimicrobials in food-processing environments', in Annous, B. A. and Gurtler, J. B. (eds) *Salmonella: distribution, adaptation, control measures and molecular technologies, Chapter: Adaptation of Salmonella to antimicrobials in food-processing environments*. Intech, pp. 123–146. doi: 10.5772/29612.

Dundas, C. M., Demonte, D. and Park, S. (2013) 'Streptavidin-biotin technology: improvements and innovations in chemical and biological applications.', *Applied microbiology and biotechnology*. Germany, 97(21), pp. 9343–9353. doi: 10.1007/s00253-013-5232-z.

Dutta, P., Mitra, U., Dutta, S., De, A., Chatterjee, M. K. and Bhattacharya, S. K. (2001) 'Ceftriaxone therapy in ciprofloxacin treatment failure typhoid fever in children.', *The Indian journal of medical research*, 113, pp. 210–213.

El-Kazzaz, W., Morita, T., Tagami, H., Inada, T. and Aiba, H. (2004) 'Metabolic block at early stages of the glycolytic pathway activates the Rcs phosphorelay system via increased synthesis of dTDP-glucose in Escherichia coli.', *Molecular microbiology*, 51(4), pp. 1117–1128.

Ellermeier, C. D. and Slauch, J. M. (2006) 'The genus Salmonella.', in Dworkin, M., Falkow, S., Rosenberg, E., Schleiffer, K. H., and Stackebrandt, E. (eds) *The Prokaryotes*. New York: Springer New York, pp. 123–158.

Ellis, R. J. and van der Vies, S. M. (1991) 'Molecular chaperones.', *Annual review of biochemistry*, 60, pp. 321–347. doi: 10.1146/annurev.bi.60.070191.001541.

EMBL (2017) 'Protein Purification, choice of lysis buffer and additives.'

Emsley, P. and Cowtan, K. (2004) 'Coot: model-building tools for molecular graphics.', *Acta crystallographica. Section D, Biological crystallography*, 60(Pt 12 Pt 1), pp. 2126–2132. doi: 10.1107/S0907444904019158.

Engl, C., Jovanovic, G., Lloyd, L. J., Murray, H., Spitaler, M., Ying, L., Errington, J. and Buck, M. (2009) 'In vivo localizations of membrane stress controllers PspA and PspG in Escherichia coli.', *Molecular microbiology*, 73(3), pp. 382–396. doi: 10.1111/j.1365-2958.2009.06776.x.

Eschenfeldt, W. H., Maltseva, N., Stols, L., Donnelly, M. I., Gu, M., Nocek, B., Tan, K., Kim, Y. and Joachimiak, A. (2010) 'Cleavable C-terminal His-tag vectors for structure determination.', *Journal of structural and functional genomics*, pp. 31–39. doi: 10.1007/s10969-010-9082-y.

Evans, M. L., Schmidt, J. C., Ilbert, M., Doyle, S. M., Quan, S., Bardwell, J. C. A., Jakob, U., Wickner, S. and Chapman, M. R. (2011) 'E. coli chaperones DnaK, Hsp33 and Spy inhibit bacterial functional amyloid assembly.', *Prion*, 5(4), pp. 323–334. doi: 10.4161/pri.18555.

Evans, P. (2006) 'Scaling and assessment of data quality.', *Acta crystallographica. Section D, Biological crystallography*, 62(Pt 1), pp. 72–82. doi: 10.1107/S0907444905036693.

Evans, P. R. and Murshudov, G. N. (2013) 'How good are my data and what is the resolution?', *Acta crystallographica. Section D, Biological crystallography*, 69(Pt 7), pp. 1204–1214. doi: 10.1107/S0907444913000061.

Fang, F. C., Libby, S. J., Buchmeier, N. A., Loewen, P. C., Switala, J., Harwood, J. and Guiney, D. G. (1992) 'The alternative sigma factor katF (rpoS) regulates Salmonella virulence.', *Proceedings of the National Academy of Sciences of the United States of America*, 89(24), pp. 11978–11982.

Fang, F. C., Libby, S. J., Castor, M. E. and Fung, A. M. (2005) 'Isocitrate lyase (AceA) is required for Salmonella persistence but not for acute lethal infection in mice.', *Infection and immunity*, 73(4), pp. 2547–2549. doi: 10.1128/IAI.73.4.2547-2549.2005.

Fardini, Y., Chettab, K., Grépinet, O., Rochereau, S., Trotereau, J., Harvey, P., Amy, M., Bottreau, E., Bumstead, N., Barrow, P. A. and Virlogeux-Payant, I. (2007) 'The YfgL lipoprotein is essential for type III secretion system expression and virulence of Salmonella enterica serovar Enteritidis.', *Infection and Immunity*, pp. 358–370. doi: 10.1128/IAI.00716-06.

Fardini, Y., Trotereau, J., Bottreau, E., Souchard, C., Velge, P. and Virlogeux-Payant, I. (2009) 'Investigation of the role of the BAM complex and SurA chaperone in outer-membrane protein biogenesis and type III secretion system expression in Salmonella.', *Microbiology (Reading, England)*, 155(Pt 5), pp. 1613–1622. doi: 10.1099/mic.0.025155-0.

Farooqui, B. J., Khurshid, M., Ashfaq, M. K. and Khan, M. A. (1991) 'Comparative yield of Salmonella Typhi from blood and bone marrow cultures in patients with fever of unknown origin.', *Journal of clinical pathology*, 44(3), pp. 258–259.

Farris, C., Sanowar, S., Bader, M. W., Pfuetzner, R. and Miller, S. I. (2010) 'Antimicrobial peptides activate the Rcs regulon through the outer membrane lipoprotein RcsF.', *Journal of bacteriology*, 192(19), pp. 4894–4903. doi: 10.1128/JB.00505-10.

Feasey, N. A., Dougan, G., Kingsley, R. A., Heyderman, R. S. and Gordon, M. A. (2012) 'Invasive non-typhoidal Salmonella disease: an emerging and neglected tropical disease in Africa.', *Lancet*, pp. 2489–2499. doi: 10.1016/S0140-6736(11)61752-2.

Feasey, N. A., Hadfield, J., Keddy, K. H., Dallman, T. J., Jacobs, J., Deng, X., Wigley, P.,

Barquist, L., Langridge, G. C., Feltwell, T., Harris, S. R., Mather, A. E., Fookes, M., Aslett, M., Msefula, C., Kariuki, S., Maclennan, C. A., Onsare, R. S., Weill, F.-X., Le Hello, S., Smith, A. M., McClelland, M., Desai, P., Parry, C. M., Cheesbrough, J., French, N., Campos, J., Chabalgoity, J. A., Betancor, L., Hopkins, K. L., Nair, S., Humphrey, T. J., Lunguya, O., Cogan, T. A., Tapia, M. D., Sow, S. O., Tennant, S. M., Bornstein, K., Levine, M. M., Lacharme-Lora, L., Everett, D. B., Kingsley, R. A., Parkhill, J., Heyderman, R. S., Dougan, G., Gordon, M. A. and Thomson, N. R. (2016) 'Distinct Salmonella Enteritidis lineages associated with enterocolitis in high-income settings and invasive disease in low-income settings', *Nat Genet*, 48(10), pp. 1211–1217. Available at: http://dx.doi.org/10.1038/ng.3644.

Fehlner-Gardiner, C. C. and Valvano, M. A. (2002) 'Cloning and characterization of the Burkholderia vietnamiensis norM gene encoding a multi-drug efflux protein.', *FEMS microbiology letters*, 215(2), pp. 279–283.

Ferrieres, L. and Clarke, D. J. (2003) 'The RcsC sensor kinase is required for normal biofilm formation in Escherichia coli K-12 and controls the expression of a regulon in response to growth on a solid surface.', *Molecular microbiology*, 50(5), pp. 1665–1682.

Figueira, R. and Holden, D. W. (2012) 'Functions of the Salmonella pathogenicity island 2 (SPI-2) type III secretion system effectors.', *Microbiology (Reading, England)*, 158(Pt 5), pp. 1147–1161. doi: 10.1099/mic.0.058115-0.

Figueira, R., Watson, K. G., Holden, D. W. and Helaine, S. (2013) 'Identification of Salmonella pathogenicity island-2 type III secretion system effectors involved in intramacrophage replication of S. enterica serovar Typhimurium: implications for rational vaccine design.', *mBio*, 4(2), p. e00065. doi: 10.1128/mBio.00065-13.

Flores-Kim, J. and Darwin, A. J. (2012) 'Phage shock protein C (PspC) of Yersinia enterocolitica is a polytopic membrane protein with implications for regulation of the Psp stress response.', *Journal of bacteriology*, 194(23), pp. 6548–6559. doi: 10.1128/JB.01250-12.

Flores-Kim, J. and Darwin, A. J. (2015) 'Activity of a bacterial cell envelope stress response is controlled by the interaction of a protein binding domain with different partners.', *The Journal of biological chemistry*, 290(18), pp. 11417–11430. doi: 10.1074/jbc.M114.614107.

Flores-Kim, J. and Darwin, A. J. (2016) 'The phage shock protein response.', *Annual review of microbiology*, 70, pp. 83–101. doi: 10.1146/annurev-micro-102215-095359.

Flynn, J. M., Levchenko, I., Sauer, R. T. and Baker, T. A. (2004) 'Modulating substrate choice: the SspB adaptor delivers a regulator of the extracytoplasmic-stress response to the AAA+ protease ClpXP for degradation.', *Genes & development*, 18(18), pp. 2292–2301. doi: 10.1101/gad.1240104.

Fookes, M., Schroeder, G. N., Langridge, G. C., Blondel, C. J., Mammina, C., Connor, T. R., Seth-Smith, H., Vernikos, G. S., Robinson, K. S., Sanders, M., Petty, N. K., Kingsley, R. A., Baumler, A. J., Nuccio, S.-P., Contreras, I., Santiviago, C. A., Maskell, D., Barrow, P., Humphrey, T., Nastasi, A., Roberts, M., Frankel, G., Parkhill, J., Dougan, G. and Thomson, N. R. (2011) 'Salmonella bongori provides insights into the evolution of the Salmonellae.', *PLoS pathogens*, 7(8), p. e1002191. doi: 10.1371/journal.ppat.1002191.

Foster, J. W. (1991) 'Salmonella acid shock proteins are required for the adaptive acid tolerance response.', *Journal of bacteriology*, 173(21), pp. 6896–6902.

Francez-Charlot, A., Castanié-Cornet, M.-P., Gutierrez, C. and Cam, K. (2005) 'Osmotic regulation of the Escherichia coli bdm (biofilm-dependent modulation) gene by the RcsCDB His-Asp phosphorelay.', *Journal of Bacteriology*, pp. 3873–3877. doi: 10.1128/JB.187.11.3873-3877.2005.

Francez-Charlot, A., Laugel, B., Van Gemert, A., Dubarry, N., Wiorowski, F., Castanie-Cornet, M.-P., Gutierrez, C. and Cam, K. (2003) 'RcsCDB His-Asp phosphorelay system negatively regulates the flhDC operon in Escherichia coli.', *Molecular microbiology*, 49(3), pp. 823–832.

Franke, D. and Svergun, D. I. (2009) 'DAMMIF, a program for rapid ab-initio shape determination in small-angle scattering.', *Journal of applied crystallography*, 42(Pt 2), pp. 342–346. doi: 10.1107/S0021889809000338.

Freinkman, E., Chng, S.-S. and Kahne, D. (2011) 'The complex that inserts lipopolysaccharide into the bacterial outer membrane forms a two-protein plug-and-barrel.', *Proceedings of the National Academy of Sciences of the United States of America*, 108(6), pp. 2486–2491. doi: 10.1073/pnas.1015617108.

Freinkman, E., Okuda, S., Ruiz, N. and Kahne, D. (2012) 'Regulated assembly of the transenvelope protein complex required for lipopolysaccharide export.', *Biochemistry*, 51(24), pp. 4800–4806. doi: 10.1021/bi300592c.

Fu, Y. and Galan, J. E. (1999) 'A Salmonella protein antagonizes Rac-1 and Cdc42 to mediate

host-cell recovery after bacterial invasion.', *Nature*, 401(6750), pp. 293–297. doi: 10.1038/45829.

Fung, D. K. C., Chan, E. W. C., Chin, M. L. and Chan, R. C. Y. (2010) 'Delineation of a bacterial starvation stress response network which can mediate antibiotic tolerance development', *Antimicrobial Agents and Chemotherapy*, pp. 1082–1093. doi: 10.1128/AAC.01218-09.

Galen, J. E., Buskirk, A. D., Tennant, S. M. and Pasetti, M. F. (2016) 'Live attenuated human Salmonella vaccine candidates: tracking the pathogen in natural infection and stimulation of host immunity.', *EcoSal Plus*. doi: 10.1128/ecosalplus.ESP-0010-2016.

Gammoh, N. Z. and Rink, L. (2017) 'Zinc in infection and inflammation.', *Nutrients*. doi: 10.3390/nu9060624.

Gan, L., Chen, S. and Jensen, G. J. (2008) 'Molecular organization of Gram-negative peptidoglycan.', *Proceedings of the National Academy of Sciences of the United States of America*, 105(48), pp. 18953–18957. doi: 10.1073/pnas.0808035105.

Garcia-del Portillo, F., Zwick, M. B., Leung, K. Y. and Finlay, B. B. (1993) 'Salmonella induces the formation of filamentous structures containing lysosomal membrane glycoproteins in epithelial cells.', *Proceedings of the National Academy of Sciences of the United States of America*, 90(22), pp. 10544–10548.

Ge, X., Lyu, Z.-X., Liu, Y., Wang, R., Zhao, X. S., Fu, X. and Chang, Z. (2014) 'Identification of FkpA as a key quality control factor for the biogenesis of outer membrane proteins under heat shock conditions.', *Journal of bacteriology*, 196(3), pp. 672–680. doi: 10.1128/JB.01069-13.

Ge, X., Wang, R., Ma, J., Liu, Y., Ezemaduka, A. N., Chen, P. R., Fu, X. and Chang, Z. (2014) 'DegP primarily functions as a protease for the biogenesis of beta-barrel outer membrane proteins in the Gram-negative bacterium Escherichia coli.', *The FEBS journal*, 281(4), pp. 1226–1240. doi: 10.1111/febs.12701.

Gemma, S., Molteni, M. and Rossetti, C. (2016) 'Lipopolysaccharides in Cyanobacteria: a brief overview.', *Advances in Microbiology*, 6(5), pp. 391–397.

Geyer, R., Galanos, C., Westphal, O. and Golecki, J. R. (1979) 'A lipopolysaccharide-binding cell-surface protein from Salmonella minnesota. Isolation, partial characterization and occurrence in different Enterobacteriaceae.', *European journal of biochemistry*, 98(1), pp. 27–38.

Ghosh, P. (2004) 'Process of protein transport by the type III secretion system.', *Microbiology and molecular biology reviews : MMBR*, 68(4), pp. 771–795. doi: 10.1128/MMBR.68.4.771-795.2004.

Giammanco, G. M., Pignato, S., Mammina, C., Grimont, F., Grimont, P. A. D., Nastasi, A. and Giammanco, G. (2002) 'Persistent endemicity of Salmonella bongori 48:z(35):– in southern Italy: molecular characterization of human, animal, and environmental isolates', *Journal of Clinical Microbiology*, pp. 3502–3505. doi: 10.1128/JCM.40.9.3502-3505.2002.

Gilchrist, J. J., MacLennan, C. A. and Hill, A. V. S. (2015) 'Genetic susceptibility to invasive Salmonella disease.', *Nature reviews. Immunology*, 15(7), pp. 452–463. doi: 10.1038/nri3858.

Giles, N. M., Watts, A. B., Giles, G. I., Fry, F. H., Littlechild, J. A. and Jacob, C. (2003) 'Metal and redox modulation of cysteine protein function.', *Chemistry & biology*, 10(8), pp. 677–693.

Gilston, B. A., Wang, S., Marcus, M. D., Canalizo-Hernandez, M. A., Swindell, E. P., Xue, Y., Mondragon, A. and O'Halloran, T. V (2014) 'Structural and mechanistic basis of zinc regulation across the E. coli Zur regulon.', *PLoS biology*, 12(11), p. e1001987. doi: 10.1371/journal.pbio.1001987.

Golynskiy, M. V, Gunderson, W. A., Hendrich, M. P. and Cohen, S. M. (2006) 'Metal binding studies and EPR spectroscopy of the manganese transport regulator MntR.', *Biochemistry*, pp. 15359–15372. doi: 10.1021/bi0607406.

Gonzalez-Escobedo, G., Marshall, J. M. and Gunn, J. S. (2011) 'Chronic and acute infection of the gall bladder by Salmonella Typhi: understanding the carrier state.', *Nature reviews. Microbiology*, 9(1), pp. 9–14. doi: 10.1038/nrmicro2490.

Gottesman, S., Trisler, P. and Torres-Cabassa, A. (1985) 'Regulation of capsular polysaccharide synthesis in Escherichia coli K-12: characterization of three regulatory genes.', *Journal of Bacteriology*, pp. 1111–1119.

Goward, C. R. and Nicholls, D. J. (1994) 'Malate dehydrogenase: a model for structure, evolution, and catalysis.', *Protein science : a publication of the Protein Society*, 3(10), pp. 1883–1888. doi: 10.1002/pro.5560031027.

Grabowicz, M., Koren, D. and Silhavy, T. J. (2016) 'The CpxQ sRNA negatively regulates Skp to prevent mistargeting of beta-barrel outer membrane proteins into the cytoplasmic

membrane.', *mBio*, 7(2), pp. e00312-16. doi: 10.1128/mBio.00312-16.

Graham, A. I., Hunt, S., Stokes, S. L., Bramall, N., Bunch, J., Cox, A. G., McLeod, C. W. and Poole, R. K. (2009) 'Severe zinc depletion of Escherichia coli: roles for high affinity zinc binding by ZinT, zinc transport and zinc-independent proteins.', *The Journal of biological chemistry*, 284(27), pp. 18377–18389. doi: 10.1074/jbc.M109.001503.

Graham, A. I., Sanguinetti, G., Bramall, N., McLeod, C. W. and Poole, R. K. (2012) 'Dynamics of a starvation-to-surfeit shift: a transcriptomic and modelling analysis of the bacterial response to zinc reveals transient behaviour of the Fur and SoxS regulators.', *Microbiology (Reading, England)*, 158(Pt 1), pp. 284–292. doi: 10.1099/mic.0.053843-0.

Grant, T. (2014) 'SAXS Part I: Introduction to biological small angle scattering.', in.

Grass, G., Otto, M., Fricke, B., Haney, C. J., Rensing, C., Nies, D. H. and Munkelt, D. (2005) 'FieF (YiiP) from Escherichia coli mediates decreased cellular accumulation of iron and relieves iron stress.', *Archives of microbiology*, 183(1), pp. 9–18. doi: 10.1007/s00203-004-0739-4.

Greenfield, L. K. and Whitfield, C. (2012) 'Synthesis of lipopolysaccharide O-antigens by ABC transporter-dependent pathways.', *Carbohydrate research*, 356, pp. 12–24. doi: 10.1016/j.carres.2012.02.027.

Griffin, A. J. and McSorley, S. J. (2011) 'Development of protective immunity to Salmonella, a mucosal pathogen with a systemic agenda.', *Mucosal immunology*, 4(4), pp. 371–382. doi: 10.1038/mi.2011.2.

Grimont, P. A. D. and Weill, F. X. (2007) 'Antigentic formulae of the Salmonella serovars, 9th edition', *W.H.O. Collaborating Centre for Reference and Research on Salmonella*. .

Gu, Y., Stansfeld, P. J., Zeng, Y., Dong, H., Wang, W. and Dong, C. (2015) 'Lipopolysaccharide is inserted into the outer membrane through an intramembrane hole, a lumen gate, and the lateral opening of LptD.', *Structure*, 23(3), pp. 496–504. doi: 10.1016/j.str.2015.01.001.

Gueguen, E., Savitzky, D. C. and Darwin, A. J. (2009) 'Analysis of the Yersinia enterocolitica PspBC proteins defines functional domains, essential amino acids and new roles within the phage-shock-protein response.', *Molecular microbiology*, 74(3), pp. 619–633. doi: 10.1111/j.1365-2958.2009.06885.x.

Guerrero, P., Collao, B., Alvarez, R., Salinas, H., Morales, E. H., Calderon, I. L., Saavedra, C. P. and Gil, F. (2013) 'Salmonella enterica serovar Typhimurium BaeSR two-component system

positively regulates sodA in response to ciprofloxacin.', *Microbiology (Reading, England)*, 159(Pt 10), pp. 2049–2057. doi: 10.1099/mic.0.066787-0.

Guo, M. S., Updegrove, T. B., Gogol, E. B., Shabalina, S. A., Gross, C. A. and Storz, G. (2014) 'MicL, a new sigmaE-dependent sRNA, combats envelope stress by repressing synthesis of Lpp, the major outer membrane lipoprotein.', *Genes & development*, 28(14), pp. 1620–1634. doi: 10.1101/gad.243485.114.

Guo, X.-P., Ren, G.-X., Zhu, H., Mao, X.-J. and Sun, Y.-C. (2015) 'Differential regulation of the hmsCDE operon in Yersinia pestis and Yersinia pseudotuberculosis by the Rcs phosphorelay system.', *Scientific Reports*. doi: 10.1038/srep08412.

Gupta, A., Swarnkar, N. K. and Choudhary, S. P. (2001) 'Changing antibiotic sensitivity in enteric fever.', *Journal of tropical pediatrics*, 47(6), pp. 369–371.

Hagenmaier, S., Stierhof, Y. D. and Henning, U. (1997) 'A new periplasmic protein of Escherichia coli which is synthesized in spheroplasts but not in intact cells.', *Journal of bacteriology*, 179(6), pp. 2073–2076.

Hagiwara, D., Sugiura, M., Oshima, T., Mori, H., Aiba, H., Yamashino, T. and Mizuno, T. (2003) 'Genome-wide analyses revealing a signaling network of the RcsC-YojN-RcsB phosphorelay system in Escherichia coli.', *Journal of bacteriology*, 185(19), pp. 5735–5746.

Hall, M. D., Levitt, D. G. and Banaszak, L. J. (1992) 'Crystal structure of Escherichia coli malate dehydrogenase. A complex of the apoenzyme and citrate at 1.87 A resolution.', *Journal of molecular biology*, 226(3), pp. 867–882.

Han, W., Wu, B., Li, L., Zhao, G., Woodward, R., Pettit, N., Cai, L., Thon, V. and Wang, P. G. (2012) 'Defining function of lipopolysaccharide O-antigen ligase WaaL using chemoenzymatically synthesized substrates.', *The Journal of biological chemistry*, 287(8), pp. 5357–5365. doi: 10.1074/jbc.M111.308486.

Han, X., Tong, Y., Tian, M., Zhang, Y., Sun, X., Wang, S., Qiu, X., Ding, C. and Yu, S. (2014) 'Enzymatic activity analysis and catalytic essential residues identification of Brucella abortus malate dehydrogenase.', *The Scientific World Journal*, p. 8.

Hansen-Wester, I. and Hensel, M. (2001) 'Salmonella pathogenicity islands encoding type III secretion systems.', *Microbes and infection*, 3(7), pp. 549–559.

Hansen, G. and Hilgenfeld, R. (2013) 'Architecture and regulation of HtrA-family proteins involved in protein quality control and stress response.', *Cellular and molecular life*

sciences : CMLS, 70(5), pp. 761–775. doi: 10.1007/s00018-012-1076-4.

Harada, K. and Wolfe, R. G. (1968) 'Malic dehydrogenase. VII. The catalytic mechanism and possible role of identical protein subunits.', *The Journal of biological chemistry*, 243(15), pp. 4131–4137.

Haraga, A., Ohlson, M. B. and Miller, S. I. (2008) 'Salmonellae interplay with host cells.', *Nature reviews. Microbiology*, 6(1), pp. 53–66. doi: 10.1038/nrmicro1788.

Harel, Y. M., Bailone, A. and Bibi, E. (1999) 'Resistance to bacitracin as modulated by an Escherichia coli homologue of the bacitracin ABC transporter BcrC subunit from Bacillus licheniformis.', *Journal of bacteriology*, 181(19), pp. 6176–6178.

Hartl, F. U., Bracher, A. and Hayer-Hartl, M. (2011) 'Molecular chaperones in protein folding and proteostasis.', *Nature*, 475(7356), pp. 324–332. doi: 10.1038/nature10317.

Havelaar, A. H., Kirk, M. D., Torgerson, P. R., Gibb, H. J., Hald, T., Lake, R. J., Praet, N., Bellinger, D. C., de Silva, N. R., Gargouri, N., Speybroeck, N., Cawthorne, A., Mathers, C., Stein, C., Angulo, F. J. and Devleesschauwer, B. (2015) 'World health organization global estimates and regional comparisons of the burden of foodborne disease in 2010.', *PLoS medicine*, 12(12), p. e1001923. doi: 10.1371/journal.pmed.1001923.

Healy, V. L., Lessard, I. A., Roper, D. I., Knox, J. R. and Walsh, C. T. (2000) 'Vancomycin resistance in enterococci: reprogramming of the D-ala-D-Ala ligases in bacterial peptidoglycan biosynthesis.', *Chemistry & biology*, 7(5), pp. R109-19.

Hedstrom, L. (2002) 'Serine protease mechanism and specificity.', *Chemical Reviews*, 102, pp. 4501–4523.

Heidary, S., Rahim, R. A., Eissazadeh, S., Moeini, H., Chor, A. L. T. and Abdullah, M. P. (2014) 'Proteome analysis of Escherichia coli periplasmic proteins in response to over-expression of recombinant human interferon alpha2b.', *Biotechnology letters*, 36(7), pp. 1479–1484. doi: 10.1007/s10529-014-1504-7.

Henderson, C. A., Vincent, H. A., Casamento, A., Stone, C. M., Phillips, J. O., Cary, P. D., Sobott, F., Gowers, D. M., Taylor, J. E. and Callaghan, A. J. (2013) 'Hfq binding changes the structure of Escherichia coli small noncoding RNAs OxyS and RprA, which are involved in the riboregulation of rpoS.', *RNA (New York, N.Y.)*, 19(8), pp. 1089–1104. doi: 10.1261/rna.034595.112.

Hersh, D., Monack, D. M., Smith, M. R., Ghori, N., Falkow, S. and Zychlinsky, A. (1999) 'The

Salmonella invasin SipB induces macrophage apoptosis by binding to caspase-1.',
Proceedings of the National Academy of Sciences of the United States of America, 96(5), pp.
2396–2401.

Heuck, A., Schleiffer, A. and Clausen, T. (2011) 'Augmenting beta-augmentation: structural
basis of how BamB binds BamA and may support folding of outer membrane proteins.',
Journal of molecular biology, 406(5), pp. 659–666. doi: 10.1016/j.jmb.2011.01.002.

Hirakawa, H., Nishino, K., Hirata, T. and Yamaguchi, A. (2003) 'Comprehensive studies of
drug resistance mediated by overexpression of response regulators of two-component
signal transduction systems in Escherichia coli.', *Journal of bacteriology*, 185(6), pp. 1851–
1856.

Hirakawa, H., Nishino, K., Yamada, J., Hirata, T. and Yamaguchi, A. (2003) 'Beta-lactam
resistance modulated by the overexpression of response regulators of two-component
signal transduction systems in Escherichia coli.', *The Journal of antimicrobial chemotherapy*,
52(4), pp. 576–582. doi: 10.1093/jac/dkg406.

Hiratsu, K., Amemura, M., Nashimoto, H., Shinagawa, H. and Makino, K. (1995) 'The rpoE
gene of Escherichia coli, which encodes sigma E, is essential for bacterial growth at high
temperature.', *Journal of bacteriology*, 177(10), pp. 2918–2922.

Hirsch, M. and Elliott, T. (2002) 'Role of ppGpp in rpoS stationary-phase regulation in
Escherichia coli.', *Journal of Bacteriology*, pp. 5077–5087. doi: 10.1128/JB.184.18.5077-
5087.2002.

Hirsch, M. and Elliott, T. (2005) 'Fis regulates transcriptional induction of RpoS in
Salmonella enterica.', *Journal of bacteriology*, 187(5), pp. 1568–1580. doi:
10.1128/JB.187.5.1568-1580.2005.

Hohmann, A. W., Schmidt, G. and Rowley, D. (1978) 'Intestinal colonization and virulence of
Salmonella in mice.', *Infection and immunity*, 22(3), pp. 763–770.

Holst, O. (2007) 'The structures of core regions from enterobacterial lipopolysaccharides -
an update.', *FEMS microbiology letters*, 271(1), pp. 3–11. doi: 10.1111/j.1574-
6968.2007.00708.x.

Hood, M. I. and Skaar, E. P. (2012) 'Nutritional immunity: transition metals at the pathogen-
host interface.', *Nature reviews. Microbiology*, 10(8), pp. 525–537. doi:
10.1038/nrmicro2836.

Horowitz, S., Salmon, L., Koldewey, P., Ahlstrom, L. S., Martin, R., Quan, S., Afonine, P. V, van den Bedem, H., Wang, L., Xu, Q., Trievel, R. C., Brooks, C. L. and Bardwell, J. C. A. (2016) 'Visualizing chaperone-assisted protein folding.', *Nature structural & molecular biology*, pp. 691–697. doi: 10.1038/nsmb.3237.

Horwich, A. L., Low, K. B., Fenton, W. A., Hirshfield, I. N. and Furtak, K. (1993) 'Folding in vivo of bacterial cytoplasmic proteins: role of GroEL.', *Cell*, 74(5), pp. 909–917.

Hryckowian, A. J., Battesti, A., Lemke, J. J., Meyer, Z. C. and Welch, R. A. (2014) 'IraL is an RssB anti-adaptor that stabilizes RpoS during logarithmic phase growth in Escherichia coli and Shigella.', *mBio*, 5(3), pp. e01043-14. doi: 10.1128/mBio.01043-14.

Humphreys, S., Rowley, G., Stevenson, A., Anjum, M. F., Woodward, M. J., Gilbert, S., Kormanec, J. and Roberts, M. (2004) 'Role of the two-component regulator CpxAR in the virulence of Salmonella enterica serotype Typhimurium.', *Infection and Immunity*, pp. 4654–4661. doi: 10.1128/IAI.72.8.4654-4661.2004.

Humphreys, S., Stevenson, A., Bacon, A., Weinhardt, A. B. and Roberts, M. (1999) 'The alternative sigma factor, sigmaE, is critically important for the virulence of Salmonella Typhimurium.', *Infection and immunity*, 67(4), pp. 1560–1568.

Huvet, M., Toni, T., Sheng, X., Thorne, T., Jovanovic, G., Engl, C., Buck, M., Pinney, J. W. and Stumpf, M. P. H. (2011) 'The evolution of the phage shock protein response system: interplay between protein function, genomic organization, and system function.', *Molecular biology and evolution*, 28(3), pp. 1141–1155. doi: 10.1093/molbev/msq301.

Ibrahim, Z., Martel, A., Moulin, M., Kim, H. S., Härtlein, M., Franzetti, B. and Gabel, F. (2017) 'Time-resolved neutron scattering provides new insight into protein substrate processing by a AAA+ unfoldase.', *Scientific Reports*. doi: 10.1038/srep40948.

Inspiralis Limited (2017) *Inspiralis, supporting drug discovery.*, *Technical/Protocols/Gyrase*.

Ipinza, F., Collao, B., Monsalva, D., Bustamante, V. H., Luraschi, R., Alegria-Arcos, M., Almonacid, D. E., Aguayo, D., Calderon, I. L., Gil, F., Santiviago, C. A., Morales, E. H., Calva, E. and Saavedra, C. P. (2014) 'Participation of the Salmonella OmpD porin in the infection of RAW264.7 macrophages and BALB/c mice.', *PloS one*, 9(10), p. e111062. doi: 10.1371/journal.pone.0111062.

Isaac, D. D., Pinkner, J. S., Hultgren, S. J. and Silhavy, T. J. (2005) 'The extracytoplasmic adaptor protein CpxP is degraded with substrate by DegP.', *Proceedings of the National*

Academy of Sciences of the United States of America, 102(49), pp. 17775–17779. doi: 10.1073/pnas.0508936102.

Island, M. D., Wei, B. Y. and Kadner, R. J. (1992) 'Structure and function of the uhp genes for the sugar phosphate transport system in Escherichia coli and Salmonella Typhimurium.', *Journal of bacteriology*, 174(9), pp. 2754–2762.

Itou, A., Matsumoto, K. and Hara, H. (2012) 'Activation of the Cpx phosphorelay signal transduction system in acidic phospholipid-deficient pgsA mutant cells of Escherichia coli.', *Biochemical and biophysical research communications*, 421(2), pp. 296–300. doi: 10.1016/j.bbrc.2012.04.003.

Jabado, N., Jankowski, A., Dougaparsad, S., Picard, V., Grinstein, S. and Gros, P. (2000) 'Natural resistance to intracellular infections: natural resistance-associated macrophage protein 1 (Nramp1) functions as a pH-dependent manganese transporter at the phagosomal membrane.', *The Journal of experimental medicine*, 192(9), pp. 1237–1248.

Jacob-Dubuisson, F., Locht, C. and Antoine, R. (2001) 'Two-partner secretion in Gram-negative bacteria: a thrifty, specific pathway for large virulence proteins.', *Molecular microbiology*, 40(2), pp. 306–313.

Jansen, K. B., Baker, S. L. and Sousa, M. C. (2015) 'Crystal structure of BamB bound to a periplasmic domain fragment of BamA, the central component of the β-Barrel assembly machine', *The Journal of Biological Chemistry*, pp. 2126–2136. doi: 10.1074/jbc.M114.584524.

Jarvelainen, H. A., Galmiche, A. and Zychlinsky, A. (2003) 'Caspase-1 activation by Salmonella.', *Trends in cell biology*, 13(4), pp. 204–209.

Jiang, J., Zhang, X., Chen, Y., Wu, Y., Zhou, Z. H., Chang, Z. and Sui, S.-F. (2008) 'Activation of DegP chaperone-protease via formation of large cage-like oligomers upon binding to substrate proteins.', *Proceedings of the National Academy of Sciences of the United States of America*, pp. 11939–11944. doi: 10.1073/pnas.0805464105.

Jiang, X., Rossanese, O. W., Brown, N. F., Kujat-Choy, S., Galan, J. E., Finlay, B. B. and Brumell, J. H. (2004) 'The related effector proteins SopD and SopD2 from Salmonella enterica serovar Typhimurium contribute to virulence during systemic infection of mice.', *Molecular microbiology*, 54(5), pp. 1186–1198. doi: 10.1111/j.1365-2958.2004.04344.x.

Jin, Y. (2008) 'Enteric fever in south China: Guangxi province.', *Journal of infection in*

developing countries, 2(4), pp. 283–288.

Jones, T. F., Ingram, L. A., Cieslak, P. R., Vugia, D. J., Tobin-D'Angelo, M., Hurd, S., Medus, C., Cronquist, A. and Angulo, F. J. (2008) 'Salmonellosis outcomes differ substantially by serotype.', *The Journal of infectious diseases*, 198(1), pp. 109–114. doi: 10.1086/588823.

Jovanovic, G., Engl, C. and Buck, M. (2009) 'Physical, functional and conditional interactions between ArcAB and phage shock proteins upon secretin-induced stress in Escherichia coli.', *Molecular microbiology*, 74(1), pp. 16–28. doi: 10.1111/j.1365-2958.2009.06809.x.

Jovanovic, G., Engl, C., Mayhew, A. J., Burrows, P. C. and Buck, M. (2010) 'Properties of the phage-shock-protein (Psp) regulatory complex that govern signal transduction and induction of the Psp response in Escherichia coli.', *Microbiology (Reading, England)*, 156(Pt 10), pp. 2920–2932. doi: 10.1099/mic.0.040055-0.

Jovanovic, G., Weiner, L. and Model, P. (1996) 'Identification, nucleotide sequence, and characterization of PspF, the transcriptional activator of the Escherichia coli stress-induced psp operon.', *Journal of bacteriology*, 178(7), pp. 1936–1945.

Jubelin, G., Vianney, A., Beloin, C., Ghigo, J.-M., Lazzaroni, J.-C., Lejeune, P. and Dorel, C. (2005) 'CpxR/OmpR interplay regulates curli gene expression in response to osmolarity in Escherichia coli.', *Journal of bacteriology*, 187(6), pp. 2038–2049. doi: 10.1128/JB.187.6.2038-2049.2005.

Justice, S. S., Hunstad, D. A., Harper, J. R., Duguay, A. R., Pinkner, J. S., Bann, J., Frieden, C., Silhavy, T. J. and Hultgren, S. J. (2005) 'Periplasmic peptidyl prolyl cis-trans isomerases are not essential for viability, but SurA is required for pilus biogenesis in Escherichia coli.', *Journal of bacteriology*, 187(22), pp. 7680–7686. doi: 10.1128/JB.187.22.7680-7686.2005.

Justice, S. S., Lauer, S. R., Hultgren, S. J. and Hunstad, D. A. (2006) 'Maturation of intracellular Escherichia coli communities requires SurA', *Infection and Immunity*, pp. 4793–4800. doi: 10.1128/IAI.00355-06.

Kachala, M., Valentini, E. and Svergun, D. I. (2015) 'Application of SAXS for the Structural Characterization of IDPs', in Felli, I. C. and Pierattelli, R. (eds) *Intrinsically Disordered Proteins Studied by NMR Spectroscopy*. Springer, pp. 261–289.

Kanehara, K., Ito, K. and Akiyama, Y. (2002) 'YaeL (EcfE) activates the sigma(E) pathway of stress response through a site-2 cleavage of anti-sigma(E), RseA.', *Genes & development*, 16(16), pp. 2147–2155. doi: 10.1101/gad.1002302.

Kariuki, S., Gordon, M. A., Feasey, N. and Parry, C. M. (2015) 'Antimicrobial resistance and management of invasive Salmonella disease', *Vaccine*, pp. C21-9. doi: 10.1016/j.vaccine.2015.03.102.

Karlinsey, J. E., Maguire, M. E., Becker, L. A., Crouch, M.-L. V and Fang, F. C. (2010) 'The phage shock protein PspA facilitates divalent metal transport and is required for virulence of Salmonella enterica sv. Typhimurium.', *Molecular microbiology*, pp. 669–685. doi: 10.1111/j.1365-2958.2010.07357.x.

Karuppanan, K., Duhra-Gill, S., Kailemia, M. J., Phu, M. L., Lebrilla, C. B., Dandekar, A. M., Rodriguez, R. L., Nandi, S. and McDonald, K. A. (2017) 'Expression, purification, and biophysical characterization of a secreted anthrax decoy fusion protein in Nicotiana benthamiana.', *International journal of molecular sciences*, 18(1). doi: 10.3390/ijms18010089.

Kashyap, D. R., Wang, M., Liu, L.-H., Boons, G.-J., Gupta, D. and Dziarski, R. (2011) 'Peptidoglycan recognition proteins kill bacteria by activating protein-sensing two-component systems.', *Nature medicine*, 17(6), pp. 676–683. doi: 10.1038/nm.2357.

Kaur, J. and Jain, S. K. (2012) 'Role of antigens and virulence factors of Salmonella enterica serovar Typhi in its pathogenesis.', *Microbiological research*, 167(4), pp. 199–210. doi: 10.1016/j.micres.2011.08.001.

Keegan, R. M. and Winn, M. D. (2007) 'Automated search-model discovery and preparation for structure solution by molecular replacement.', *Acta Crystallographica Section D*, 63(4), pp. 447–457. doi: 10.1107/S0907444907002661.

Kelly, B. G., Vespermann, A. and Bolton, D. J. (2009) 'The role of horizontal gene transfer in the evolution of selected foodborne bacterial pathogens.', *Food and chemical toxicology : an international journal published for the British Industrial Biological Research Association*, 47(5), pp. 951–968. doi: 10.1016/j.fct.2008.02.006.

Kenyon, W. J., Humphreys, S., Roberts, M. and Spector, M. P. (2010) 'Periplasmic peptidyl-prolyl isomerases SurA and FkpA play an important role in the starvation-stress response (SSR) of Salmonella enterica serovar Typhimurium.', *Antonie van Leeuwenhoek*, pp. 51–63. doi: 10.1007/s10482-010-9428-2.

Kenyon, W. J., Sayers, D. G., Humphreys, S., Roberts, M. and Spector, M. P. (2002) 'The starvation-stress response of Salmonella enterica serovar Typhimurium requires sigma(E)-,

but not CpxR-regulated extracytoplasmic functions.', *Microbiology (Reading, England)*, 148(Pt 1), pp. 113–122. doi: 10.1099/00221287-148-1-113.

Kidgell, C., Reichard, U., Wain, J., Linz, B., Torpdahl, M., Dougan, G. and Achtman, M. (2002) 'Salmonella Typhi, the causative agent of typhoid fever, is approximately 50,000 years old.', *Infection, genetics and evolution : journal of molecular epidemiology and evolutionary genetics in infectious diseases*, 2(1), pp. 39–45.

Kihara, A., Akiyama, Y. and Ito, K. (1995) 'FtsH is required for proteolytic elimination of uncomplexed forms of SecY, an essential protein translocase subunit.', *Proceedings of the National Academy of Sciences of the United States of America*, 92(10), pp. 4532–4536.

Kihara, A., Akiyama, Y. and Ito, K. (1998) 'Different pathways for protein degradation by the FtsH/HflKC membrane-embedded protease complex: an implication from the interference by a mutant form of a new substrate protein, YccA.', *Journal of molecular biology*, 279(1), pp. 175–188. doi: 10.1006/jmbi.1998.1781.

Kim, D. Y., Jin, K. S., Kwon, E., Ree, M. and Kim, K. K. (2007) 'Crystal structure of RseB and a model of its binding mode to RseA.', *Proceedings of the National Academy of Sciences of the United States of America*, 104(21), pp. 8779–8784. doi: 10.1073/pnas.0703117104.

Kim, K.-H., Jung, E. J., Im, H., Lelie, D. Van Der and Kim, E. E. (2008) 'Expression, purification, and crystallization and preliminary X-ray crystallographic analysis of CnrX from Cupriavidus metallidurans CH34.', *Journal of microbiology and biotechnology*, 18(1), pp. 43–47.

Kim, K. H., Aulakh, S. and Paetzel, M. (2011) 'Crystal structure of β-barrel assembly machinery BamCD protein complex.', *The Journal of Biological Chemistry*, pp. 39116–39121. doi: 10.1074/jbc.M111.298166.

Kim, K. H., Aulakh, S. and Paetzel, M. (2012) 'The bacterial outer membrane β-barrel assembly machinery.', *Protein Science : A Publication of the Protein Society*, pp. 751–768. doi: 10.1002/pro.2069.

Kim, K. H., Aulakh, S., Tan, W. and Paetzel, M. (2011) 'Crystallographic analysis of the C-terminal domain of the Escherichia coli lipoprotein BamC.', *Acta crystallographica. Section F, Structural biology and crystallization communications*, 67(Pt 11), pp. 1350–1358. doi: 10.1107/S174430911103363X.

Kim, K. H. and Paetzel, M. (2011) 'Crystal structure of Escherichia coli BamB, a lipoprotein component of the beta-barrel assembly machinery complex.', *Journal of molecular biology*,

406(5), pp. 667–678. doi: 10.1016/j.jmb.2010.12.020.

Kim, K. I., Park, S. C., Kang, S. H., Cheong, G. W. and Chung, C. H. (1999) 'Selective degradation of unfolded proteins by the self-compartmentalizing HtrA protease, a periplasmic heat shock protein in Escherichia coli.', *Journal of molecular biology*, 294(5), pp. 1363–1374. doi: 10.1006/jmbi.1999.3320.

Kim, S., Grant, R. A. and Sauer, R. T. (2011) 'Covalent linkage of distinct substrate degrons controls assembly and disassembly of DegP proteolytic cages.', *Cell*, 145(1), pp. 67–78. doi: 10.1016/j.cell.2011.02.024.

Kimple, M. E., Brill, A. L. and Pasker, R. L. (2013) 'Overview of affinity tags for protein purification.', *Current protocols in protein science*, p. Unit-9.9. doi: 10.1002/0471140864.ps0909s73.

Kirk, M. D., Pires, S. M., Black, R. E., Caipo, M., Crump, J. A., Devleesschauwer, B., Döpfer, D., Fazil, A., Fischer-Walker, C. L., Hald, T., Hall, A. J., Keddy, K. H., Lake, R. J., Lanata, C. F., Torgerson, P. R., Havelaar, A. H. and Angulo, F. J. (2015) 'World Health Organization estimates of the global and regional disease burden of 22 foodborne bacterial, protozoal, and viral diseases, 2010: A data synthesis.', *PLoS Medicine*. doi: 10.1371/journal.pmed.1001921.

Klebba, P. E., Hofnung, M. and Charbit, A. (1994) 'A model of maltodextrin transport through the sugar-specific porin, LamB, based on deletion analysis.', *The EMBO journal*, 13(19), pp. 4670–4675.

Kleerebezem, M., Heutink, M. and Tommassen, J. (1995) 'Characterization of an Escherichia coli rotA mutant, affected in periplasmic peptidyl-prolyl cis/trans isomerase.', *Molecular microbiology*, 18(2), pp. 313–320.

Klein, G., Lindner, B., Brade, H. and Raina, S. (2011) 'Molecular basis of lipopolysaccharide heterogeneity in Escherichia coli: envelope stress-responsive regulators control the incorporation of glycoforms with a third 3-deoxy-alpha-D-manno-oct-2-ulosonic acid and rhamnose.', *The Journal of biological chemistry*, 286(50), pp. 42787–42807. doi: 10.1074/jbc.M111.291799.

Klein, G. and Raina, S. (2015) 'Regulated control of the assembly and diversity of LPS by noncoding sRNAs.', *BioMed research international*, 2015, p. 153561. doi: 10.1155/2015/153561.

Knodler, L. A. and Steele-Mortimer, O. (2005) 'The Salmonella effector PipB2 affects late endosome/lysosome distribution to mediate Sif extension.', *Molecular biology of the cell*, 16(9), pp. 4108–4123. doi: 10.1091/mbc.E05-04-0367.

Knowles, T. J., Browning, D. F., Jeeves, M., Maderbocus, R., Rajesh, S., Sridhar, P., Manoli, E., Emery, D., Sommer, U., Spencer, A., Leyton, D. L., Squire, D., Chaudhuri, R. R., Viant, M. R., Cunningham, A. F., Henderson, I. R. and Overduin, M. (2011) 'Structure and function of BamE within the outer membrane and the β-barrel assembly machine.', *EMBO Reports*, pp. 123–128. doi: 10.1038/embor.2010.202.

Kobayashi, H., Yamamoto, M. and Aono, R. (1998) 'Appearance of a stress-response protein, phage-shock protein A, in Escherichia coli exposed to hydrophobic organic solvents.', *Microbiology (Reading, England)*, 144 (Pt 2, pp. 353–359. doi: 10.1099/00221287-144-2-353.

Kobayashi, R., Suzuki, T. and Yoshida, M. (2007) 'Escherichia coli phage-shock protein A (PspA) binds to membrane phospholipids and repairs proton leakage of the damaged membranes.', *Molecular microbiology*, 66(1), pp. 100–109. doi: 10.1111/j.1365-2958.2007.05893.x.

Koldewey, P., Stull, F., Horowitz, S., Martin, R. and Bardwell, J. C. A. (2016) 'Forces driving chaperone action.', *Cell*, 166(2), pp. 369–379. doi: 10.1016/j.cell.2016.05.054.

Konovalova, A., Mitchell, A. M. and Silhavy, T. J. (2016) 'A lipoprotein/β-barrel complex monitors lipopolysaccharide integrity transducing information across the outer membrane.', *eLife*. doi: 10.7554/eLife.15276.

Konovalova, A., Perlman, D. H., Cowles, C. E. and Silhavy, T. J. (2014) 'Transmembrane domain of surface-exposed outer membrane lipoprotein RcsF is threaded through the lumen of beta-barrel proteins.', *Proceedings of the National Academy of Sciences of the United States of America*, 111(41), pp. E4350-8. doi: 10.1073/pnas.1417138111.

Kowarz, L., Coynault, C., Robbe-Saule, V. and Norel, F. (1994) 'The Salmonella typhimurium katF (rpoS) gene: cloning, nucleotide sequence, and regulation of spvR and spvABCD virulence plasmid genes.', *Journal of Bacteriology*, pp. 6852–6860.

Krojer, T., Garrido-Franco, M., Huber, R., Ehrmann, M. and Clausen, T. (2002) 'Crystal structure of DegP (HtrA) reveals a new protease-chaperone machine.', *Nature*, 416(6879), pp. 455–459. doi: 10.1038/416455a.

Krojer, T., Sawa, J., Schafer, E., Saibil, H. R., Ehrmann, M. and Clausen, T. (2008) 'Structural basis for the regulated protease and chaperone function of DegP.', *Nature*, 453(7197), pp. 885–890. doi: 10.1038/nature07004.

Kwoh, D. Y. and Kemper, J. (1978) 'Bacteriophage P22-mediated specialized transduction in Salmonella Typhimurium: high frequency of aberrant prophage excision.', *Journal of Virology*, pp. 519–534.

Kwon, D. H. and Lu, C.-D. (2006) 'Polyamines increase antibiotic susceptibility in Pseudomonas aeruginosa.', *Antimicrobial Agents and Chemotherapy*, pp. 1623–1627. doi: 10.1128/AAC.50.5.1623-1627.2006.

Kwon, E., Kim, D. Y., Gross, C. A., Gross, J. D. and Kim, K. K. (2010) 'The crystal structure Escherichia coli Spy.', *Protein science : a publication of the Protein Society*, 19(11), pp. 2252–2259. doi: 10.1002/pro.489.

Kwon, E., Kim, D. Y., Ngo, T. D., Gross, C. A., Gross, J. D. and Kim, K. K. (2012) 'The crystal structure of the periplasmic domain of Vibrio parahaemolyticus CpxA.', *Protein science : a publication of the Protein Society*, 21(9), pp. 1334–1343. doi: 10.1002/pro.2120.

Labandeira-Rey, M., Brautigam, C. A. and Hansen, E. J. (2010) 'Characterization of the CpxRA regulon in Haemophilus ducreyi.', *Infection and immunity*, 78(11), pp. 4779–4791. doi: 10.1128/IAI.00678-10.

De Las Penas, A., Connolly, L. and Gross, C. A. (1997) 'The sigmaE-mediated response to extracytoplasmic stress in Escherichia coli is transduced by RseA and RseB, two negative regulators of sigmaE.', *Molecular microbiology*, 24(2), pp. 373–385.

Laubacher, M. E. and Ades, S. E. (2008) 'The Rcs phosphorelay is a cell envelope stress response activated by peptidoglycan stress and contributes to intrinsic antibiotic resistance.', *Journal of bacteriology*, 190(6), pp. 2065–2074. doi: 10.1128/JB.01740-07.

Lazar, S. W., Almiron, M., Tormo, A. and Kolter, R. (1998) 'Role of the Escherichia coli SurA protein in stationary-phase survival.', *Journal of bacteriology*, 180(21), pp. 5704–5711.

Lazar, S. W. and Kolter, R. (1996) 'SurA assists the folding of Escherichia coli outer membrane proteins.', *Journal of bacteriology*, 178(6), pp. 1770–1773.

Leblanc, S. K. D., Oates, C. W. and Raivio, T. L. (2011) 'Characterization of the induction and cellular role of the BaeSR two-component envelope stress response of Escherichia coli.', *Journal of bacteriology*, 193(13), pp. 3367–3375. doi: 10.1128/JB.01534-10.

Lee, H.-J., Park, S.-J., Choi, S. H. and Lee, K.-H. (2008) 'Vibrio vulnificus rpoS expression is repressed by direct binding of cAMP-cAMP receptor protein complex to its two promoter regions.', *The Journal of Biological Chemistry*, pp. 30438–30450. doi: 10.1074/jbc.M802219200.

Lee, L. J., Barrett, J. A. and Poole, R. K. (2005) 'Genome-wide transcriptional response of chemostat-cultured Escherichia coli to zinc.', *Journal of Bacteriology*, pp. 1124–1134. doi: 10.1128/JB.187.3.1124-1134.2005.

Leive, L. (1965) 'Release of lipopolysaccharide by EDTA treatment of E. coli.', *Biochemical and Biophysical Research Communications*, 21(4), pp. 290–296. doi: http://dx.doi.org/10.1016/0006-291X(65)90191-9.

Leonhartsberger, S., Huber, A., Lottspeich, F. and Bock, A. (2001) 'The hydH/G Genes from Escherichia coli code for a zinc and lead responsive two-component regulatory system.', *Journal of molecular biology*, 307(1), pp. 93–105. doi: 10.1006/jmbi.2000.4451.

Levine, M. M., Black, R. E. and Lanata, C. (1982) 'Precise estimation of the numbers of chronic carriers of Salmonella Typhi in Santiago, Chile, an endemic area.', *The Journal of infectious diseases*, 146(6), pp. 724–726.

Lewis, C., Skovierova, H., Rowley, G., Rezuchova, B., Homerova, D., Stevenson, A., Spencer, J., Farn, J., Kormanec, J., Roberts, M. and Roberts, M. (2009) 'Salmonella enterica Serovar Typhimurium HtrA : regulation of expression and role of the chaperone and protease activities during infection', *Microbiology*, 155(3), pp. 873–881. doi: 10.1099/mic.0.023754-0.

Leyton, D. L., Rossiter, A. E. and Henderson, I. R. (2012) 'From self sufficiency to dependence: mechanisms and factors important for autotransporter biogenesis.', *Nature Reviews Microbiology*, 10, pp. 213–225.

Li, X., Gu, Y., Dong, H., Wang, W. and Dong, C. (2015) 'Trapped lipopolysaccharide and LptD intermediates reveal lipopolysaccharide translocation steps across the Escherichia coli outer membrane.', *Scientific reports*, 5, p. 11883. doi: 10.1038/srep11883.

Lima, S., Guo, M. S., Chaba, R., Gross, C. A. and Sauer, R. T. (2013) 'Dual molecular signals mediate the bacterial response to outer-membrane stress.', *Science (New York, N.Y.)*, 340(6134), pp. 837–841. doi: 10.1126/science.1235358.

Lin, M.-F., Lin, Y.-Y. and Lan, C.-Y. (2015) 'The role of the two-component system BaeSR in

disposing chemicals through regulating transporter systems in Acinetobacter baumannii.', *PloS one*, 10(7), p. e0132843. doi: 10.1371/journal.pone.0132843.

Lin, M.-F., Lin, Y.-Y., Yeh, H.-W. and Lan, C.-Y. (2014) 'Role of the BaeSR two-component system in the regulation of Acinetobacter baumannii adeAB genes and its correlation with tigecycline susceptibility.', *BMC microbiology*, 14, p. 119. doi: 10.1186/1471-2180-14-119.

Lin, S. and Guidotti, G. (2009) 'Chapter 35: Purification of Membrane Proteins', in Burgess, R. R. and Deutscher, M. P. (eds) *Methods in enzymology*. 2nd edn. Elsevier, pp. 619–629.

Linley, E., Denyer, S. P., McDonnell, G., Simons, C. and Maillard, J.-Y. (2012) 'Use of hydrogen peroxide as a biocide: new consideration of its mechanisms of biocidal action.', *Journal of Antimicrobial Chemotherapy*, 67(7), pp. 1589–1596.

Lipinska, B., Fayet, O., Baird, L. and Georgopoulos, C. (1989) 'Identification, characterization, and mapping of the Escherichia coli htrA gene, whose product is essential for bacterial growth only at elevated temperatures.', *Journal of bacteriology*, 171(3), pp. 1574–1584.

Lipinska, B., Zylicz, M. and Georgopoulos, C. (1990) 'The HtrA (DegP) protein, essential for Escherichia coli survival at high temperatures, is an endopeptidase.', *Journal of Bacteriology*, pp. 1791–1797.

Liu, H. and Zwart, P. H. (2012) 'Determining pair distance distribution function from SAXS data using parametric functionals.', *Journal of structural biology*, 180(1), pp. 226–234. doi: 10.1016/j.jsb.2012.05.011.

Liu, J. and Walsh, C. T. (1990) 'Peptidyl-prolyl cis-trans-isomerase from Escherichia coli: a periplasmic homolog of cyclophilin that is not inhibited by cyclosporin A.', *Proceedings of the National Academy of Sciences of the United States of America*, 87(11), pp. 4028–4032.

Liu, J. Z., Jellbauer, S., Poe, A. J., Ton, V., Pesciaroli, M., Kehl-Fie, T. E., Restrepo, N. A., Hosking, M. P., Edwards, R. A., Battistoni, A., Pasquali, P., Lane, T. E., Chazin, W. J., Vogl, T., Roth, J., Skaar, E. P. and Raffatellu, M. (2012) 'Zinc sequestration by the neutrophil protein calprotectin enhances Salmonella growth in the inflamed gut.', *Cell host & microbe*, 11(3), pp. 227–239. doi: 10.1016/j.chom.2012.01.017.

Liu, Y., Fu, X., Shen, J., Zhang, H., Hong, W. and Chang, Z. (2004) 'Periplasmic proteins of Escherichia coli are highly resistant to aggregation: reappraisal for roles of molecular chaperones in periplasm.', *Biochemical and biophysical research communications*, 316(3),

pp. 795–801. doi: 10.1016/j.bbrc.2004.02.125.

Lloyd, L. J., Jones, S. E., Jovanovic, G., Gyaneshwar, P., Rolfe, M. D., Thompson, A., Hinton, J. C. and Buck, M. (2004) 'Identification of a new member of the phage shock protein response in Escherichia coli, the phage shock protein G (PspG).', *The Journal of biological chemistry*, 279(53), pp. 55707–55714. doi: 10.1074/jbc.M408994200.

Ma, Z., Jacobsen, F. E. and Giedroc, D. P. (2009) 'Coordination chemistry of bacterial metal transport and sensing.', *Chemical reviews*, 109(10), pp. 4644–4681. doi: 10.1021/cr900077w.

MacLennan, C. A., Martin, L. B. and Micoli, F. (2014) 'Vaccines against invasive Salmonella disease: current status and future directions.', *Human vaccines & immunotherapeutics*, 10(6), pp. 1478–1493. doi: 10.4161/hv.29054.

Mahoney, T. F. and Silhavy, T. J. (2013) 'The Cpx stress response confers resistance to some, but not all, bactericidal antibiotics.', *Journal of bacteriology*, 195(9), pp. 1869–1874. doi: 10.1128/JB.02197-12.

Majdalani, N., Chen, S., Murrow, J., St John, K. and Gottesman, S. (2001) 'Regulation of RpoS by a novel small RNA: the characterization of RprA.', *Molecular microbiology*, 39(5), pp. 1382–1394.

Majdalani, N., Cunning, C., Sledjeski, D., Elliott, T. and Gottesman, S. (1998) 'DsrA RNA regulates translation of RpoS message by an anti-antisense mechanism, independent of its action as an antisilencer of transcription.', *Proceedings of the National Academy of Sciences of the United States of America*, 95(21), pp. 12462–12467.

Majdalani, N. and Gottesman, S. (2005) 'The Rcs phosphorelay: a complex signal transduction system.', *Annual review of microbiology*, 59, pp. 379–405. doi: 10.1146/annurev.micro.59.050405.101230.

Majowicz, S. E., Musto, J., Scallan, E., Angulo, F. J., Kirk, M., O'Brien, S. J., Jones, T. F., Fazil, A. and Hoekstra, R. M. (2010) 'The global burden of nontyphoidal Salmonella gastroenteritis.', *Clinical infectious diseases : an official publication of the Infectious Diseases Society of America*, 50(6), pp. 882–889. doi: 10.1086/650733.

Malojčić, G., Andres, D., Grabowicz, M., George, A. H., Ruiz, N., Silhavy, T. J. and Kahne, D. (2014) 'LptE binds to and alters the physical state of LPS to catalyze its assembly at the cell surface.', *Proceedings of the National Academy of Sciences of the United States of America*,

pp. 9467–9472. doi: 10.1073/pnas.1402746111.

Mandin, P. and Gottesman, S. (2010) 'Integrating anaerobic/aerobic sensing and the general stress response through the ArcZ small RNA.', *The EMBO journal*, 29(18), pp. 3094–3107. doi: 10.1038/emboj.2010.179.

Martindale, W. (1993) *Martindale: The Extra Pharmacopoeia.* 30th edn. Edited by J. E. F. Reynolds. London: Pharmaceutical Press.

Martorana, A. M., Sperandeo, P., Polissi, A. and Deho, G. (2011) 'Complex transcriptional organization regulates an Escherichia coli locus implicated in lipopolysaccharide biogenesis.', *Research in microbiology*, 162(5), pp. 470–482. doi: 10.1016/j.resmic.2011.03.007.

Matern, Y., Barion, B. and Behrens-Kneip, S. (2010) 'PpiD is a player in the network of periplasmic chaperones in Escherichia coli.', *BMC microbiology*, 10, p. 251. doi: 10.1186/1471-2180-10-251.

McCall, K. A., Huang, C. and Fierke, C. A. (2000) 'Function and mechanism of zinc metalloenzymes.', *The Journal of nutrition*, 130(5S Suppl), p. 1437S–46S.

McClelland, M., Florea, L., Sanderson, K., Clifton, S. W., Parkhill, J., Churcher, C., Dougan, G., Wilson, R. K. and Miller, W. (2000) 'Comparison of the Escherichia coli K-12 genome with sampled genomes of a Klebsiella pneumoniae and three Salmonella enterica serovars, Typhimurium, Typhi and Paratyphi', *Nucleic Acids Research*, pp. 4974–4986.

McClelland, M., Sanderson, K. E., Clifton, S. W., Latreille, P., Porwollik, S., Sabo, A., Meyer, R., Bieri, T., Ozersky, P., McLellan, M., Harkins, C. R., Wang, C., Nguyen, C., Berghoff, A., Elliott, G., Kohlberg, S., Strong, C., Du, F., Carter, J., Kremizki, C., Layman, D., Leonard, S., Sun, H., Fulton, L., Nash, W., Miner, T., Minx, P., Delehaunty, K., Fronick, C., Magrini, V., Nhan, M., Warren, W., Florea, L., Spieth, J. and Wilson, R. K. (2004) 'Comparison of genome degradation in Paratyphi A and Typhi, human-restricted serovars of Salmonella enterica that cause typhoid.', *Nature genetics*, 36(12), pp. 1268–1274. doi: 10.1038/ng1470.

McClelland, M., Sanderson, K. E., Spieth, J., Clifton, S. W., Latreille, P., Courtney, L., Porwollik, S., Ali, J., Dante, M., Du, F., Hou, S., Layman, D., Leonard, S., Nguyen, C., Scott, K., Holmes, A., Grewal, N., Mulvaney, E., Ryan, E., Sun, H., Florea, L., Miller, W., Stoneking, T., Nhan, M., Waterston, R. and Wilson, R. K. (2001) 'Complete genome sequence of Salmonella enterica serovar Typhimurium LT2.', *Nature*, 413(6858), pp. 852–856. doi:

10.1038/35101614.

McCoy, A. J., Grosse-Kunstleve, R. W., Adams, P. D., Winn, M. D., Storoni, L. C. and Read, R. J. (2007) 'Phaser crystallographic software.', *Journal of applied crystallography*, 40(Pt 4), pp. 658–674. doi: 10.1107/S0021889807021206.

McDonald, C., Jovanovic, G., Ces, O. and Buck, M. (2015) 'Membrane stored curvature elastic stress modulates recruitment of maintenance proteins PspA and Vipp1.', *mBio*, 6(5), pp. e01188-15. doi: 10.1128/mBio.01188-15.

McEwen, J. and Silverman, P. (1980) 'Chromosomal mutations of Escherichia coli that alter expression of conjugative plasmid functions.', *Proceedings of the National Academy of Sciences of the United States of America*, 77(1), pp. 513–517.

McGhie, E. J., Hayward, R. D. and Koronakis, V. (2001) 'Cooperation between actin-binding proteins of invasive Salmonella: SipA potentiates SipC nucleation and bundling of actin.', *The EMBO journal*, 20(9), pp. 2131–2139. doi: 10.1093/emboj/20.9.2131.

MERSELIS, J. G. J., KAYE, D., CONNOLLY, C. S. and HOOK, E. W. (1964) 'Quantative bacteriology of the typhoid carrier state.', *The American journal of tropical medicine and hygiene*, 13, pp. 425–429.

Mertens, H. D. T. and Svergun, D. I. (2010) 'Structural characterization of proteins and complexes using small-angle X-ray solution scattering.', *Journal of structural biology*, 172(1), pp. 128–141. doi: 10.1016/j.jsb.2010.06.012.

Michalopoulos, A. S., Livaditis, I. G. and Gougoutas, V. (2011) 'The revival of fosfomycin.', *International journal of infectious diseases : IJID : official publication of the International Society for Infectious Diseases*, 15(11), pp. e732-9. doi: 10.1016/j.ijid.2011.07.007.

Mika, F. and Hengge, R. (2005) 'A two-component phosphotransfer network involving ArcB, ArcA, and RssB coordinates synthesis and proteolysis of sigmaS (RpoS) in E. coli.', *Genes & development*, 19(22), pp. 2770–2781. doi: 10.1101/gad.353705.

Minárik, P., Tomásková, N., Kollárová, M. and Antalík, M. (2002) 'Malate dehydrogenases - structure and function.', *General Physiology and Biophysics.*, 21(3), pp. 257–265.

Misra, R. (2012) 'Assembly of the β-barrel outer membrane proteins in Gram-negative bacteria, mitochondria, and chloroplasts.', *ISRN Molecular Biology*, pp. 1–15.

Misra, R., CastilloKeller, M. and Deng, M. (2000) 'Overexpression of protease-deficient

DegP(S210A) rescues the lethal phenotype of Escherichia coli OmpF assembly mutants in a degP background.', *Journal of bacteriology*, 182(17), pp. 4882–4888.

Missiakas, D., Betton, J. M. and Raina, S. (1996) 'New components of protein folding in extracytoplasmic compartments of Escherichia coli SurA, FkpA and Skp/OmpH.', *Molecular microbiology*, 21(4), pp. 871–884.

Missiakas, D., Mayer, M. P., Lemaire, M., Georgopoulos, C. and Raina, S. (1997) 'Modulation of the Escherichia coli sigmaE (RpoE) heat-shock transcription-factor activity by the RseA, RseB and RseC proteins.', *Molecular microbiology*, 24(2), pp. 355–371.

Miticka, H., Rowley, G., Rezuchova, B., Homerova, D., Humphreys, S., Farn, J., Roberts, M. and Kormanec, J. (2003) 'Transcriptional analysis of the rpoE gene encoding extracytoplasmic stress response sigma factor sigmaE in Salmonella enterica serovar Typhimurium.', *FEMS microbiology letters*, 226(2), pp. 307–314.

Mo, E., Peters, S. E., Willers, C., Maskell, D. J. and Charles, I. G. (2006) 'Single, double and triple mutants of Salmonella enterica serovar Typhimurium degP (htrA), degQ (hhoA) and degS (hhoB) have diverse phenotypes on exposure to elevated temperature and their growth in vivo is attenuated to different extents.', *Microbial pathogenesis*, 41(4–5), pp. 174–182. doi: 10.1016/j.micpath.2006.07.004.

Moffatt, J. H., Harper, M., Harrison, P., Hale, J. D. F., Vinogradov, E., Seemann, T., Henry, R., Crane, B., St Michael, F., Cox, A. D., Adler, B., Nation, R. L., Li, J. and Boyce, J. D. (2010) 'Colistin resistance in Acinetobacter baumannii is mediated by complete loss of lipopolysaccharide production.', *Antimicrobial agents and chemotherapy*, 54(12), pp. 4971–4977. doi: 10.1128/AAC.00834-10.

Mogasale, V., Maskery, B., Ochiai, R. L., Lee, J. S., Mogasale, V. V, Ramani, E., Kim, Y. E., Park, J. K. and Wierzba, T. F. (2014) 'Burden of typhoid fever in low-income and middle-income countries: a systematic, literature-based update with risk-factor adjustment.', *The Lancet Global Health*, 2(10), pp. e570–e580. doi: 10.1016/S2214-109X(14)70301-8.

Molenkamp, G. C. and Veerkamp, J. H. (1976) 'Effects of antibiotics on metabolism of peptidoglycan, protein, and lipids in Bifidobacterium bifidum subsp. pennsylvanicus.', *Antimicrobial agents and chemotherapy*, 10(5), pp. 786–794.

Monack, D. M., Bouley, D. M. and Falkow, S. (2004) 'Salmonella Typhimurium persists within macrophages in the mesenteric lymph nodes of chronically infected Nramp1+/+

mice and can be reactivated by IFNgamma neutralization.', *The Journal of experimental medicine*, 199(2), pp. 231–241. doi: 10.1084/jem.20031319.

Moreau, P. L. (2014) 'Protective role of the RpoE (sigmaE) and Cpx envelope stress responses against gentamicin killing of nongrowing Escherichia coli incubated under aerobic, phosphate starvation conditions.', *FEMS microbiology letters*, pp. 151–156. doi: 10.1111/1574-6968.12534.

Mouslim, C. and Groisman, E. A. (2003) 'Control of the Salmonella ugd gene by three two-component regulatory systems.', *Molecular microbiology*, 47(2), pp. 335–344.

Mullinax, T. R., Mock, J. N., McEvily, A. J. and Harrison, J. H. (1982) 'Regulation of mitochondrial malate dehydrogenase. Evidence for an allosteric citrate-binding site.', *The Journal of biological chemistry*, 257(22), pp. 13233–13239.

Munita, J. M. and Arias, C. A. (2016) 'Mechanisms of antibiotic resistance.', *Microbiology spectrum*. doi: 10.1128/microbiolspec.VMBF-0016-2015.

Murphy, K. C. (1998) 'Use of bacteriophage λ recombination functions to promote gene replacement in Escherichia coli.', *Journal of Bacteriology*, 180(8), pp. 2063–2071.

Murshudov, G. N., Skubak, P., Lebedev, A. A., Pannu, N. S., Steiner, R. A., Nicholls, R. A., Winn, M. D., Long, F. and Vagin, A. A. (2011) 'REFMAC5 for the refinement of macromolecular crystal structures.', *Acta crystallographica. Section D, Biological crystallography*, 67(Pt 4), pp. 355–367. doi: 10.1107/S0907444911001314.

Narita, S., Masui, C., Suzuki, T., Dohmae, N. and Akiyama, Y. (2013) 'Protease homolog BepA (YfgC) promotes assembly and degradation of β-barrel membrane proteins in Escherichia coli.', *Proceedings of the National Academy of Sciences of the United States of America*, pp. E3612-21. doi: 10.1073/pnas.1312012110.

Nemčovičová, I. and Kutá-Smatanova, I. (2012) 'Alternative Protein Crystallization Technique: Cross-Influence Procedure (CIP)', in Borisenko, E. (ed.) *Crystallization and Materials Science of Modern Artificial and Natural Crystals*. InTech, pp. 249–276. doi: 10.5772/30461.

Neopane, A., Singh, S. B., Bhatta, R., Dhital, B. and Karki, D. B. (2008) 'Changing spectrum of antibiotic sensitivity in enteric fever.', *Kathmandu University medical journal*, 6(1), pp. 12–15.

Nevesinjac, A. Z. and Raivio, T. L. (2005) 'The Cpx envelope stress response affects

expression of the type IV bundle-forming pili of enteropathogenic Escherichia coli.', *Journal of bacteriology*, 187(2), pp. 672–686. doi: 10.1128/JB.187.2.672-686.2005.

Ni, D., Wang, Y., Yang, X., Zhou, H., Hou, X., Cao, B., Lu, Z., Zhao, X., Yang, K. and Huang, Y. (2014) 'Structural and functional analysis of the β-barrel domain of BamA from Escherichia coli.', *The FASEB Journal*, 28(6), pp. 2677–2685.

Nicholls, D. J., Miller, J., Scawen, M. D., Clarke, A. R., Holbrook, J. J., Atkinson, T. and Goward, C. R. (1992) 'The importance of arginine 102 for the substrate specificity of Escherichia coli malate dehydrogenase.', *Biochemical and biophysical research communications*, 189(2), pp. 1057–1062.

Nickerson, C. A. and Curtiss, R. (1997) 'Role of sigma factor RpoS in initial stages of Salmonella Typhimurium infection.', *Infection and Immunity*, pp. 1814–1823.

Nielsen, H. (2017) 'Predicting secretory proteins with SignalP.', *Methods in molecular biology*, 1611, pp. 59–73. doi: 10.1007/978-1-4939-7015-5_6.

Nikaido, E., Giraud, E., Baucheron, S., Yamasaki, S., Wiedemann, A., Okamoto, K., Takagi, T., Yamaguchi, A., Cloeckaert, A. and Nishino, K. (2012) 'Effects of indole on drug resistance and virulence of Salmonella enterica serovar Typhimurium revealed by genome-wide analyses.', *Gut Pathogens*, p. 5. doi: 10.1186/1757-4749-4-5.

Nikaido, H. (1992) 'Porins and specific channels of bacterial outer membranes.', *Molecular microbiology*, 6(4), pp. 435–442.

Nikaido, H. (2003) 'Molecular basis of bacterial outer membrane permeability revisited.', *Microbiology and molecular biology reviews : MMBR*, 67(4), pp. 593–656.

Noinaj, N., Gumbart, J. C. and Buchanan, S. K. (2017) 'The [beta]-barrel assembly machinery in motion', *Nat Rev Micro*. Nature Publishing Group, a division of Macmillan Publishers Limited. All Rights Reserved., 15(4), pp. 197–204.

Noll, M., Petrukhin, K. and Lutsenko, S. (1998) 'Identification of a novel transcription regulator from Proteus mirabilis, PMTR, revealed a possible role of YJAI protein in balancing zinc in Escherichia coli.', *The Journal of biological chemistry*, 273(33), pp. 21393–21401.

Nuccio, S.-P. and Baumler, A. J. (2015) 'Reconstructing pathogen evolution from the ruins.', *Proceedings of the National Academy of Sciences of the United States of America*, 112(3), pp. 647–648. doi: 10.1073/pnas.1423499112.

O'Neal, C. R., Gabriel, W. M., Turk, A. K., Libby, S. J., Fang, F. C. and Spector, M. P. (1994) 'RpoS is necessary for both the positive and negative regulation of starvation survival genes during phosphate, carbon, and nitrogen starvation in Salmonella Typhimurium.', *Journal of bacteriology*, 176(15), pp. 4610–4616.

Okuda, S., Freinkman, E. and Kahne, D. (2012) 'Cytoplasmic ATP hydrolysis powers transport of lipopolysaccharide across the periplasm in E. coli.', *Science (New York, N.Y.)*, 338(6111), pp. 1214–1217. doi: 10.1126/science.1228984.

Okuda, S., Sherman, D. J., Silhavy, T. J., Ruiz, N. and Kahne, D. (2016) 'Lipopolysaccharide transport and assembly at the outer membrane: the PEZ model.', *Nature reviews. Microbiology*, pp. 337–345. doi: 10.1038/nrmicro.2016.25.

Old, D. C. (1992) 'Nomenclature of Salmonella.', *Journal of medical microbiology*, pp. 361–363. doi: 10.1099/00222615-37-6-361.

Onufryk, C., Crouch, M.-L., Fang, F. C. and Gross, C. A. (2005) 'Characterization of six lipoproteins in the sigmaE regulon.', *Journal of bacteriology*, 187(13), pp. 4552–4561. doi: 10.1128/JB.187.13.4552-4561.2005.

Oropeza, R., Salgado-Bravo, R. and Calva, E. (2015) 'Deletion analysis of RcsC reveals a novel signalling pathway controlling poly-N-acetylglucosamine synthesis and biofilm formation in Escherichia coli.', *Microbiology (Reading, England)*, 161(Pt 4), pp. 903–913. doi: 10.1099/mic.0.000050.

Osadnik, H., Schopfel, M., Heidrich, E., Mehner, D., Lilie, H., Parthier, C., Risselada, H. J., Grubmuller, H., Stubbs, M. T. and Bruser, T. (2015) 'PspF-binding domain PspA1-144 and the PspA.F complex: New insights into the coiled-coil-dependent regulation of AAA+ proteins.', *Molecular microbiology*, 98(4), pp. 743–759. doi: 10.1111/mmi.13154.

Otto, K. and Silhavy, T. J. (2002) 'Surface sensing and adhesion of Escherichia coli controlled by the Cpx-signaling pathway.', *Proceedings of the National Academy of Sciences of the United States of America*, 99(4), pp. 2287–2292. doi: 10.1073/pnas.042521699.

Outten, C. E. and O'Halloran, T. V (2001) 'Femtomolar sensitivity of metalloregulatory proteins controlling zinc homeostasis.', *Science (New York, N.Y.)*, 292(5526), pp. 2488–2492. doi: 10.1126/science.1060331.

Padilla, E., Llobet, E., Domenech-Sanchez, A., Martinez-Martinez, L., Bengoechea, J. A. and Alberti, S. (2010) 'Klebsiella pneumoniae AcrAB efflux pump contributes to antimicrobial

resistance and virulence.', *Antimicrobial agents and chemotherapy*, 54(1), pp. 177–183. doi: 10.1128/AAC.00715-09.

Pakkanen, S. H., Kantele, J. M., Savolainen, L. E., Rombo, L. and Kantele, A. (2015) 'Specific and cross-reactive immune response to oral Salmonella Typhi Ty21a and parenteral Vi capsular polysaccharide typhoid vaccines administered concomitantly.', *Vaccine*, 33(3), pp. 451–458. doi: 10.1016/j.vaccine.2014.11.030.

Pamp, S. J., Gjermansen, M., Johansen, H. K. and Tolker-Nielsen, T. (2008) 'Tolerance to the antimicrobial peptide colistin in Pseudomonas aeruginosa biofilms is linked to metabolically active cells, and depends on the pmr and mexAB-oprM genes.', *Molecular microbiology*, 68(1), pp. 223–240. doi: 10.1111/j.1365-2958.2008.06152.x.

Panina, E. M., Mironov, A. A. and Gelfand, M. S. (2003) 'Comparative genomics of bacterial zinc regulons: enhanced ion transport, pathogenesis, and rearrangement of ribosomal proteins.', *Proceedings of the National Academy of Sciences of the United States of America*, 100(17), pp. 9912–9917. doi: 10.1073/pnas.1733691100.

Pannen, D., Fabisch, M., Gausling, L. and Schnetz, K. (2016) 'Interaction of the RcsB response regulator with auxiliary transcription regulators in Escherichia coli.', *The Journal of biological chemistry*, 291(5), pp. 2357–2370. doi: 10.1074/jbc.M115.696815.

Panosa, A., Roca, I. and Gibert, I. (2010) 'Ribonucleotide reductases of Salmonella Typhimurium: transcriptional regulation and differential role in pathogenesis.', *PloS one*, 5(6), p. e11328. doi: 10.1371/journal.pone.0011328.

Papenfort, K., Pfeiffer, V., Mika, F., Lucchini, S., Hinton, J. C. D. and Vogel, J. (2006) 'SigmaE-dependent small RNAs of Salmonella respond to membrane stress by accelerating global omp mRNA decay.', *Molecular microbiology*, 62(6), pp. 1674–1688.

Parkhill, J., Dougan, G., James, K. D., Thomson, N. R., Pickard, D., Wain, J., Churcher, C., Mungall, K. L., Bentley, S. D., Holden, M. T., Sebaihia, M., Baker, S., Basham, D., Brooks, K., Chillingworth, T., Connerton, P., Cronin, A., Davis, P., Davies, R. M., Dowd, L., White, N., Farrar, J., Feltwell, T., Hamlin, N., Haque, A., Hien, T. T., Holroyd, S., Jagels, K., Krogh, A., Larsen, T. S., Leather, S., Moule, S., O'Gaora, P., Parry, C., Quail, M., Rutherford, K., Simmonds, M., Skelton, J., Stevens, K., Whitehead, S. and Barrell, B. G. (2001) 'Complete genome sequence of a multiple drug resistant Salmonella enterica serovar Typhi CT18.', *Nature*, 413(6858), pp. 848–852. doi: 10.1038/35101607.

Patel, G. J., Behrens-Kneip, S., Holst, O. and Kleinschmidt, J. H. (2009) 'The periplasmic chaperone Skp facilitates targeting, insertion, and folding of OmpA into lipid membranes with a negative membrane surface potential.', *Biochemistry*, 48(43), pp. 10235–10245. doi: 10.1021/bi901403c.

Patel, K., Kumar, A. and Durani, S. (2007) 'Analysis of the structural consensus of the zinc coordination centers of metalloprotein structures.', *Biochimica et biophysica acta*, 1774(10), pp. 1247–1253. doi: 10.1016/j.bbapap.2007.07.010.

Pedersen, L. L., Radulic, M., Doric, M. and Abu Kwaik, Y. (2001) 'HtrA homologue of Legionella pneumophila: an indispensable element for intracellular infection of mammalian but not protozoan cells.', *Infection and immunity*, 69(4), pp. 2569–2579. doi: 10.1128/IAI.69.4.2569-2579.2001.

Penner, J. L. (1988) 'International Committee on Systematic Bacteriology Taxonomic Subcommittee on Enterobacteriaceae', *International Journal of Systematic and Evolutionary Microbiology*, 38(2), pp. 223–224.

Pernestig, A.-K., Georgellis, D., Romeo, T., Suzuki, K., Tomenius, H., Normark, S. and Melefors, O. (2003) 'The Escherichia coli BarA-UvrY two-component system is needed for efficient switching between glycolytic and gluconeogenic carbon sources.', *Journal of bacteriology*, 185(3), pp. 843–853.

Perry, R. D., Craig, S. K., Abney, J., Bobrov, A. G., Kirillina, O., Mier, I. J., Truszczynska, H. and Fetherston, J. D. (2012) 'Manganese transporters Yfe and MntH are Fur-regulated and important for the virulence of Yersinia pestis.', *Microbiology (Reading, England)*, 158(Pt 3), pp. 804–815. doi: 10.1099/mic.0.053710-0.

Pescaretti, M. de L. M., Lopez, F. E., Morero, R. D. and Delgado, M. A. (2010) 'Transcriptional autoregulation of the RcsCDB phosphorelay system in Salmonella enterica serovar Typhimurium.', *Microbiology (Reading, England)*, 156(Pt 12), pp. 3513–3521. doi: 10.1099/mic.0.041319-0.

Pescaretti, M. de L. M., Lopez, F. E., Morero, R. D. and Delgado, M. A. (2011) 'The PmrA/PmrB regulatory system controls the expression of the wzzfepE gene involved in the O-antigen synthesis of Salmonella enterica serovar Typhimurium.', *Microbiology (Reading, England)*, 157(Pt 9), pp. 2515–2521. doi: 10.1099/mic.0.050088-0.

Petit-Hartlein, I., Rome, K., de Rosny, E., Molton, F., Duboc, C., Gueguen, E., Rodrigue, A.

and Coves, J. (2015) 'Biophysical and physiological characterization of ZraP from Escherichia coli, the periplasmic accessory protein of the atypical ZraSR two-component system.', *The Biochemical journal*, 472(2), pp. 205–216. doi: 10.1042/BJ20150827.

Petrarca, P., Ammendola, S., Pasquali, P. and Battistoni, A. (2010) 'The Zur-regulated ZinT protein is an auxiliary component of the high-affinity ZnuABC zinc transporter that facilitates metal recruitment during severe zinc shortage.', *Journal of bacteriology*, 192(6), pp. 1553–1564. doi: 10.1128/JB.01310-09.

Pontel, L. B., Pezza, A. and Soncini, F. C. (2010) 'Copper stress targets the rcs system to induce multiaggregative behavior in a copper-sensitive Salmonella strain.', *Journal of bacteriology*, 192(23), pp. 6287–6290. doi: 10.1128/JB.00781-10.

Porcheron, G., Garenaux, A., Proulx, J., Sabri, M. and Dozois, C. M. (2013) 'Iron, copper, zinc, and manganese transport and regulation in pathogenic Enterobacteria: correlations between strains, site of infection and the relative importance of the different metal transport systems for virulence.', *Frontiers in cellular and infection microbiology*, 3, p. 90. doi: 10.3389/fcimb.2013.00090.

Porwollik, S., Boyd, E. F., Choy, C., Cheng, P., Florea, L., Proctor, E. and McClelland, M. (2004) 'Characterization of Salmonella enterica subspecies I genovars by use of microarrays', *Journal of Bacteriology*, pp. 5883–5898. doi: 10.1128/JB.186.17.5883-5898.2004.

Poteete, A. R. and Fenton, A. C. (1984) 'λ red-dependent growth and recombination of phage P22.', *Virology*, 134(1), pp. 161–167.

Prigent-Combaret, C., Brombacher, E., Vidal, O., Ambert, A., Lejeune, P., Landini, P. and Dorel, C. (2001) 'Complex regulatory network controls initial adhesion and biofilm formation in Escherichia coli via regulation of the csgD gene.', *Journal of bacteriology*, 183(24), pp. 7213–7223. doi: 10.1128/JB.183.24.7213-7223.2001.

Pullinger, G. D., van Diemen, P. M., Dziva, F. and Stevens, M. P. (2010) 'Role of two-component sensory systems of Salmonella enterica serovar Dublin in the pathogenesis of systemic salmonellosis in cattle.', *Microbiology (Reading, England)*, 156(Pt 10), pp. 3108–3122. doi: 10.1099/mic.0.041830-0.

Purdy, G. E., Fisher, C. R. and Payne, S. M. (2007) 'IcsA surface presentation in Shigella flexneri requires the periplasmic chaperones DegP, Skp, and SurA.', *Journal of Bacteriology*,

pp. 5566–5573. doi: 10.1128/JB.00483-07.

Qiao, S., Luo, Q., Zhao, Y., Zhang, X. C. and Huang, Y. (2014) 'Structural basis for lipopolysaccharide insertion in the bacterial outer membrane.', *Nature*, 511(7507), pp. 108–111. doi: 10.1038/nature13484.

Quan, S., Koldewey, P., Tapley, T., Kirsch, N., Ruane, K. M., Pfizenmaier, J., Shi, R., Hofmann, S., Foit, L., Ren, G., Jakob, U., Xu, Z., Cygler, M. and Bardwell, J. C. A. (2011) 'Genetic selection designed to stabilize proteins uncovers a chaperone called Spy.', *Nature structural & molecular biology*, 18(3), pp. 262–269. doi: 10.1038/nsmb.2016.

Rabsch, W., Tschape, H. and Baumler, A. J. (2001) 'Non-typhoidal salmonellosis: emerging problems.', *Microbes and infection*, 3(3), pp. 237–247.

R Core Team (2013) 'R: A language and environment for statistical computing.' R Foundation for Statistical Computing. Available at: http://www.r-project.org/.

Raetz, C. R. H. and Whitfield, C. (2002) 'Lipopolysaccharide endotoxins.', *Annual review of biochemistry*, 71, pp. 635–700. doi: 10.1146/annurev.biochem.71.110601.135414.

Raffa, R. G. and Raivio, T. L. (2002) 'A third envelope stress signal transduction pathway in Escherichia coli.', *Molecular microbiology*, 45(6), pp. 1599–1611.

Raivio, T. L. (2005) 'Envelope stress responses and Gram-negative bacterial pathogenesis.', *Molecular microbiology*, 56(5), pp. 1119–1128. doi: 10.1111/j.1365-2958.2005.04625.x.

Raivio, T. L. (2014) 'Everything old is new again: an update on current research on the Cpx envelope stress response.', *Biochimica et biophysica acta*, 1843(8), pp. 1529–1541. doi: 10.1016/j.bbamcr.2013.10.018.

Raivio, T. L., Laird, M. W., Joly, J. C. and Silhavy, T. J. (2000) 'Tethering of CpxP to the inner membrane prevents spheroplast induction of the cpx envelope stress response.', *Molecular microbiology*, 37(5), pp. 1186–1197.

Raivio, T. L., Leblanc, S. K. D. and Price, N. L. (2013) 'The Escherichia coli Cpx envelope stress response regulates genes of diverse function that impact antibiotic resistance and membrane integrity.', *Journal of bacteriology*, 195(12), pp. 2755–2767. doi: 10.1128/JB.00105-13.

Raivio, T. L., Popkin, D. L. and Silhavy, T. J. (1999) 'The Cpx envelope stress response is controlled by amplification and feedback inhibition.', *Journal of bacteriology*, 181(17), pp.

5263–5272.

Rasmussen, A. A., Eriksen, M., Gilany, K., Udesen, C., Franch, T., Petersen, C. and Valentin-Hansen, P. (2005) 'Regulation of ompA mRNA stability: the role of a small regulatory RNA in growth phase-dependent control.', *Molecular microbiology*, 58(5), pp. 1421–1429. doi: 10.1111/j.1365-2958.2005.04911.x.

Ravikumar, S., Yoo, I., Lee, S. Y. and Hong, S. H. (2011) 'A study on the dynamics of the zraP gene expression profile and its application to the construction of zinc adsorption bacteria.', *Bioprocess and biosystems engineering*, 34(9), pp. 1119–1126. doi: 10.1007/s00449-011-0562-7.

Reece, R. J. and Maxwell, A. (1991) 'DNA gyrase: structure and function.', *Critical reviews in biochemistry and molecular biology*, 26(3–4), pp. 335–375. doi: 10.3109/10409239109114072.

Ribera, A., Ruiz, J., Jiminez de Anta, M. T. and Vila, J. (2002) 'Effect of an efflux pump inhibitor on the MIC of nalidixic acid for Acinetobacter baumannii and Stenotrophomonas maltophilia clinical isolates.', *The Journal of antimicrobial chemotherapy*, pp. 697–698.

Rinker, S. D., Trombley, M. P., Gu, X., Fortney, K. R. and Bauer, M. E. (2011) 'Deletion of mtrC in Haemophilus ducreyi increases sensitivity to human antimicrobial peptides and activates the CpxRA regulon.', *Infection and immunity*, 79(6), pp. 2324–2334. doi: 10.1128/IAI.01316-10.

Rosen, R. and Ron, E. Z. (2002) 'Proteome analysis in the study of the bacterial heat-shock response.', *Mass spectrometry reviews*, 21(4), pp. 244–265. doi: 10.1002/mas.10031.

Rouviere, P. E. and Gross, C. A. (1996) 'SurA, a periplasmic protein with peptidyl-prolyl isomerase activity, participates in the assembly of outer membrane porins.', *Genes & development*, 10(24), pp. 3170–3182.

Rowley, G., Skovierova, H., Stevenson, A., Rezuchova, B., Homerova, D., Lewis, C., Sherry, A., Kormanec, J. and Roberts, M. (2011) 'The periplasmic chaperone Skp is required for successful Salmonella Typhimurium infection in a murine typhoid model.', *Microbiology (Reading, England)*, 157(Pt 3), pp. 848–858. doi: 10.1099/mic.0.046011-0.

Rowley, G., Spector, M., Kormanec, J. and Roberts, M. (2006) 'Pushing the envelope: extracytoplasmic stress responses in bacterial pathogens.', *Nature reviews. Microbiology*, 4(5), pp. 383–394. doi: 10.1038/nrmicro1394.

Rudolph, J., Theis, H., Hanke, R., Endermann, R., Johannsen, L. and Geschke, F. (2001) 'Seco-Cyclothialidines: new concise synthesis, inhibitory activity toward bacterial and human DNA topoisomerases, and antibacterial properties.', *Journal of medicinal chemistry*, 44(4), pp. 619–626.

Ruiz, N., Chng, S.-S., Hiniker, A., Kahne, D. and Silhavy, T. J. (2010) 'Nonconsecutive disulfide bond formation in an essential integral outer membrane protein.', *Proceedings of the National Academy of Sciences of the United States of America*, 107(27), pp. 12245–12250. doi: 10.1073/pnas.1007319107.

Ruiz, N., Gronenberg, L. S., Kahne, D. and Silhavy, T. J. (2008) 'Identification of two inner-membrane proteins required for the transport of lipopolysaccharide to the outer membrane of Escherichia coli.', *Proceedings of the National Academy of Sciences of the United States of America*, 105(14), pp. 5537–5542. doi: 10.1073/pnas.0801196105.

Runkel, S., Wells, H. C. and Rowley, G. (2013) 'Living with stress: A lesson from the enteric pathogen Salmonella enterica.', in Sariaslani, S. and Gadd, G. M. (eds) *Advances in Applied Microbiology volume 83*. Elsevier, pp. 87–144.

Runyen-Janecky, L., Dazenski, E., Hawkins, S. and Warner, L. (2006) 'Role and regulation of the Shigella flexneri sit and MntH systems.', *Infection and immunity*, 74(8), pp. 4666–4672. doi: 10.1128/IAI.00562-06.

Rupp, B. (2009) *Biomolecular Crystallography: Principles, Practise and Application to Stuctural Biology.* New York: Garland Science.

Sabbagh, S. C., Forest, C. G., Lepage, C., Leclerc, J.-M. and Daigle, F. (2010) 'So similar, yet so different: uncovering distinctive features in the genomes of Salmonella enterica serovars Typhimurium and Typhi.', *FEMS microbiology letters*, 305(1), pp. 1–13. doi: 10.1111/j.1574-6968.2010.01904.x.

Sahu, S. N., Acharya, S., Tuminaro, H., Patel, I., Dudley, K., LeClerc, J. E., Cebula, T. A. and Mukhopadhyay, S. (2003) 'The bacterial adaptive response gene, barA, encodes a novel conserved histidine kinase regulatory switch for adaptation and modulation of metabolism in Escherichia coli.', *Molecular and cellular biochemistry*, 253(1–2), pp. 167–177.

Salscheider, S. L., Jahn, A. and Schnetz, K. (2014) 'Transcriptional regulation by BglJ-RcsB, a pleiotropic heteromeric activator in Escherichia coli.', *Nucleic acids research*, 42(5), pp. 2999–3008. doi: 10.1093/nar/gkt1298.

Sampson, T. R., Liu, X., Schroeder, M. R., Kraft, C. S., Burd, E. M. and Weiss, D. S. (2012) 'Rapid killing of Acinetobacter baumannii by polymyxins is mediated by a hydroxyl radical death pathway.', *Antimicrobial agents and chemotherapy*, 56(11), pp. 5642–5649. doi: 10.1128/AAC.00756-12.

Samuels, D. J., Frye, J. G., Porwollik, S., McClelland, M., Mrazek, J., Hoover, T. R. and Karls, A. C. (2013) 'Use of a promiscuous, constitutively-active bacterial enhancer-binding protein to define the sigma(5)(4) (RpoN) regulon of Salmonella Typhimurium LT2.', *BMC genomics*, 14, p. 602. doi: 10.1186/1471-2164-14-602.

Sandoval, C. M., Baker, S. L., Jansen, K., Metzner, S. I. and Sousa, M. C. (2011) 'Crystal structure of BamD: an essential component of the beta-Barrel assembly machinery of gram-negative bacteria.', *Journal of molecular biology*, 409(3), pp. 348–357. doi: 10.1016/j.jmb.2011.03.035.

Santos, R. L., Zhang, S., Tsolis, R. M., Kingsley, R. A., Adams, L. G. and Baumler, A. J. (2001) 'Animal models of Salmonella infections: enteritis versus typhoid fever.', *Microbes and infection*, 3(14–15), pp. 1335–1344.

Saul, F. A., Arie, J.-P., Vulliez-le Normand, B., Kahn, R., Betton, J.-M. and Bentley, G. A. (2004) 'Structural and functional studies of FkpA from Escherichia coli, a cis/trans peptidyl-prolyl isomerase with chaperone activity.', *Journal of molecular biology*, 335(2), pp. 595–608.

Schafer, U., Beck, K. and Muller, M. (1999) 'Skp, a molecular chaperone of gram-negative bacteria, is required for the formation of soluble periplasmic intermediates of outer membrane proteins.', *The Journal of biological chemistry*, 274(35), pp. 24567–24574.

Schleiff, E. and Soll, J. (2005) 'Membrane protein insertion: mixing eukaryotic and prokaryotic concepts.', *EMBO Reports*, pp. 1023–1027. doi: 10.1038/sj.embor.7400563.

Schnablegger, H. and Singh, Y. (2013) *The SAXS Guide: Getting acquinted with the principles.*

Schonbrunner, E. R., Mayer, S., Tropschug, M., Fischer, G., Takahashi, N. and Schmid, F. X. (1991) 'Catalysis of protein folding by cyclophilins from different species.', *The Journal of biological chemistry*, 266(6), pp. 3630–3635.

Schroder, H., Langer, T., Hartl, F. U. and Bukau, B. (1993) 'DnaK, DnaJ and GrpE form a cellular chaperone machinery capable of repairing heat-induced protein damage.', *The*

EMBO journal, 12(11), pp. 4137–4144.

Schrödinger, L. (2015) 'The PyMOL Molecular Graphics System'.

Schwalm, J., Mahoney, T. F., Soltes, G. R. and Silhavy, T. J. (2013) 'Role for Skp in LptD assembly in Escherichia coli.', *Journal of bacteriology*, 195(16), pp. 3734–42. doi: 10.1128/JB.00431-13.

Selander, R. K., Beltran, P., Smith, N. H., Helmuth, R., Rubin, F. A., Kopecko, D. J., Ferris, K., Tall, B. D., Cravioto, A. and Musser, J. M. (1990) 'Evolutionary genetic relationships of clones of Salmonella serovars that cause human typhoid and other enteric fevers.', *Infection and immunity*, 58(7), pp. 2262–2275.

Sender, P. D., Martin, M. G., Peiru, S. and Magni, C. (2004) 'Characterization of an oxaloacetate decarboxylase that belongs to the malic enzyme family.', *FEBS letters*, 570(1–3), pp. 217–222. doi: 10.1016/j.febslet.2004.06.038.

Seo, J., Savitzky, D. C., Ford, E. and Darwin, A. J. (2007) 'Global analysis of tolerance to secretin-induced stress in Yersinia enterocolitica suggests that the phage-shock-protein system may be a remarkably self-contained stress response.', *Molecular microbiology*, 65(3), pp. 714–727. doi: 10.1111/j.1365-2958.2007.05821.x.

Sevcenco, A.-M., Pinkse, M. W. H., Wolterbeek, H. T., Verhaert, P. D. E. M., Hagen, W. R. and Hagedoorn, P.-L. (2011) 'Exploring the microbial metalloproteome using MIRAGE.', *Metallomics : integrated biometal science*, 3(12), pp. 1324–1330. doi: 10.1039/c1mt00154j.

Seymour, R. L., Mishra, P. V, Khan, M. A. and Spector, M. P. (1996) 'Essential roles of core starvation-stress response loci in carbon-starvation-inducible cross-resistance and hydrogen peroxide-inducible adaptive resistance to oxidative challenge in Salmonella Typhimurium.', *Molecular microbiology*, 20(3), pp. 497–505.

Shah, D. H., Lee, M., Park, J., Lee, J., Eo, S., Kwon, J. and Chae, J. (2005) 'Identification of Salmonella Gallinarum virulence genes in a chicken infection model using PCR-based signature-tagged mutagenesis.', *Microbiology (Reading, England)*, 151(Pt 12), pp. 3957–3968. doi: 10.1099/mic.0.28126-0.

Shin, S. and Park, C. (1995) 'Modulation of flagellar expression in Escherichia coli by acetyl phosphate and the osmoregulator OmpR.', *Journal of bacteriology*, 177(16), pp. 4696–4702.

Shpargel, J. S., Berardi, R. S. and Lenz, D. (1985) 'Salmonella Typhi carrier state 52 years

after illness with typhoid fever: a case study.', *American journal of infection control*, 13(3), pp. 122–123.

Sinha, N. K. and Snustad, D. P. (1972) 'Mechanism of inhibition of deoxyribonucleic acid synthesis in Escherichia coli by hydroxyurea.', *Journal of Bacteriology*, pp. 1321–1334.

Sinnott, C. R. and Teall, A. J. (1987) 'Persistent gallbladder carriage of Salmonella Typhi.', *Lancet (London, England)*, p. 976.

Skerra, A. and Schmidt, T. G. (2000) 'Use of the Strep-Tag and streptavidin for detection and purification of recombinant proteins.', *Methods in enzymology*, 326, pp. 271–304.

Sklar, J. G., Wu, T., Kahne, D. and Silhavy, T. J. (2007) 'Defining the roles of the periplasmic chaperones SurA, Skp, and DegP in Escherichia coli.', *Genes & development*, 21(19), pp. 2473–2484. doi: 10.1101/gad.1581007.

Song, T., Mika, F., Lindmark, B., Liu, Z., Schild, S., Bishop, A., Zhu, J., Camilli, A., Johansson, J., Vogel, J. and Wai, S. N. (2008) 'A new Vibrio cholerae sRNA modulates colonization and affects release of outer membrane vesicles.', *Molecular microbiology*, 70(1), pp. 100–111. doi: 10.1111/j.1365-2958.2008.06392.x.

Spector, M. P. (1998) 'The starvation-stress response (SSR) of Salmonella.', *Advances in microbial physiology*, 40, pp. 233–279.

Spector, M. P. and Cubitt, C. L. (1992) 'Starvation-inducible loci of Salmonella Typhimurium: regulation and roles in starvation-survival.', *Molecular microbiology*, 6(11), pp. 1467–1476.

Spector, M. P., Garcia del Portillo, F., Bearson, S. M., Mahmud, A., Magut, M., Finlay, B. B., Dougan, G., Foster, J. W. and Pallen, M. J. (1999) 'The rpoS-dependent starvation-stress response locus stiA encodes a nitrate reductase (narZYWV) required for carbon-starvation-inducible thermotolerance and acid tolerance in Salmonella Typhimurium.', *Microbiology (Reading, England)*, 145 (Pt 1, pp. 3035–3045. doi: 10.1099/00221287-145-11-3035.

Spector, M. P. and Kenyon, W. J. (2012) 'Resistance and survival strategies of Salmonella enterica to environmental stresses', *Food Research International*, 45(2), pp. 455–481. doi: http://dx.doi.org/10.1016/j.foodres.2011.06.056.

Sperandeo, P., Lau, F. K., Carpentieri, A., De Castro, C., Molinaro, A., Deho, G., Silhavy, T. J. and Polissi, A. (2008) 'Functional analysis of the protein machinery required for transport of lipopolysaccharide to the outer membrane of Escherichia coli.', *Journal of bacteriology*, 190(13), pp. 4460–4469. doi: 10.1128/JB.00270-08.

Sperandeo, P., Martorana, A. M. and Polissi, A. (2016) 'Lipopolysaccharide biogenesis and transport at the outer membrane of Gram-negative bacteria.', *Biochimica et biophysica acta*. doi: 10.1016/j.bbalip.2016.10.006.

Spiess, C., Beil, A. and Ehrmann, M. (1999) 'A temperature-dependent switch from chaperone to protease in a widely conserved heat shock protein.', *Cell*, 97(3), pp. 339–347.

Srinivasan, V. B., Vaidyanathan, V., Mondal, A. and Rajamohan, G. (2012) 'Role of the two component signal transduction system CpxAR in conferring cefepime and chloramphenicol resistance in Klebsiella pneumoniae NTUH-K2044.', *PloS one*, 7(4), p. e33777. doi: 10.1371/journal.pone.0033777.

Stafford, S. L., Bokil, N. J., Achard, M. E. S., Kapetanovic, R., Schembri, M. A., McEwan, A. G. and Sweet, M. J. (2013) 'Metal ions in macrophage antimicrobial pathways: emerging roles for zinc and copper.', *Bioscience reports*, 33(4). doi: 10.1042/BSR20130014.

Standar, K., Mehner, D., Osadnik, H., Berthelmann, F., Hause, G., Lunsdorf, H. and Bruser, T. (2008) 'PspA can form large scaffolds in Escherichia coli.', *FEBS letters*, 582(25–26), pp. 3585–3589. doi: 10.1016/j.febslet.2008.09.002.

Stein, M. A., Leung, K. Y., Zwick, M., Garcia-del Portillo, F. and Finlay, B. B. (1996) 'Identification of a Salmonella virulence gene required for formation of filamentous structures containing lysosomal membrane glycoproteins within epithelial cells.', *Molecular microbiology*, 20(1), pp. 151–164.

van Stelten, J., Silva, F., Belin, D. and Silhavy, T. J. (2009) 'Effects of antibiotics and a proto-oncogene homolog on destruction of protein translocator SecY.', *Science (New York, N.Y.)*, 325(5941), pp. 753–756. doi: 10.1126/science.1172221.

Stoker, K., Reijnders, W. N., Oltmann, L. F. and Stouthamer, A. H. (1989) 'Initial cloning and sequencing of hydHG, an operon homologous to ntrBC and regulating the labile hydrogenase activity in Escherichia coli K-12.', *Journal of bacteriology*, 171(8), pp. 4448–4456.

Stork, M., Grijpstra, J., Bos, M. P., Manas Torres, C., Devos, N., Poolman, J. T., Chazin, W. J. and Tommassen, J. (2013) 'Zinc piracy as a mechanism of Neisseria meningitidis for evasion of nutritional immunity.', *PLoS pathogens*, 9(10), p. e1003733. doi: 10.1371/journal.ppat.1003733.

Stout, V., Torres-Cabassa, A., Maurizi, M. R., Gutnick, D. and Gottesman, S. (1991) 'RcsA, an

unstable positive regulator of capsular polysaccharide synthesis.', *Journal of bacteriology*, 173(5), pp. 1738–1747.

Stratmann, T., Pul, U., Wurm, R., Wagner, R. and Schnetz, K. (2012) 'RcsB-BglJ activates the Escherichia coli leuO gene, encoding an H-NS antagonist and pleiotropic regulator of virulence determinants.', *Molecular microbiology*, 83(6), pp. 1109–1123. doi: 10.1111/j.1365-2958.2012.07993.x.

Strauch, K. L., Johnson, K. and Beckwith, J. (1989) 'Characterization of degP, a gene required for proteolysis in the cell envelope and essential for growth of Escherichia coli at high temperature.', *Journal of bacteriology*, 171(5), pp. 2689–2696.

Stull, F., Koldewey, P., Humes, J. R., Radford, S. E. and Bardwell, J. C. A. (2016) 'Protein folding occurs while bound to the ATP-independent chaperone Spy.', *Nature structural & molecular biology*, pp. 53–58. doi: 10.1038/nsmb.3133.

Suar, M., Jantsch, J., Hapfelmeier, S., Kremer, M., Stallmach, T., Barrow, P. A. and Hardt, W.-D. (2006) 'Virulence of broad- and narrow-host-range Salmonella enterica serovars in the streptomycin-pretreated mouse model.', *Infection and immunity*, 74(1), pp. 632–644. doi: 10.1128/IAI.74.1.632-644.2006.

Suar, M. and Ryan, D. (2015) 'Small RNA in the acid tolerance response of Salmonella and their role in virulence.', *Virulence*, pp. 105–106. doi: 10.4161/21505594.2014.988543.

Subashchandrabose, S., Hazen, T. H., Brumbaugh, A. R., Himpsl, S. D., Smith, S. N., Ernst, R. D., Rasko, D. A. and Mobley, H. L. T. (2014) 'Host-specific induction of Escherichia coli fitness genes during human urinary tract infection', *Proceedings of the National Academy of Sciences of the United States of America*, pp. 18327–18332. doi: 10.1073/pnas.1415959112.

Suijkerbuijk, A. W. M., Bouwknegt, M., Mangen, M.-J. J., de Wit, G. A., van Pelt, W., Bijkerk, P. and Friesema, I. H. M. (2016) 'The economic burden of a Salmonella Thompson outbreak caused by smoked salmon in the Netherlands, 2012-2013.', *European journal of public health*. doi: 10.1093/eurpub/ckw205.

Svergun, D. I. (1992) 'Determination of the regulatization parameter in indirect-transform methods using perceptual criteria.', *Journal of applied crystallography*, 25, pp. 495–503.

Svergun, D. I. (1999) 'Restoring low resolution structure of biological macromolecules from solution scattering using simulated annealing.', *Biophysical journal*, 76(6), pp. 2879–2886.

doi: 10.1016/S0006-3495(99)77443-6.

Svergun, D. I., Barberato, C. and Koch, M. H. J. (1995) 'CRYSOL - a program to evaluate X-ray solution scattering of biological macromolecules from atomic coordinates.', *Journal of applied crystallography*, 28, pp. 768–773.

Svergun, D. I. and Koch, M. H. (2003) 'Small-angle scattering studies of biological macromolecules in solution.', *Reports on Progress in Physics*, 66, pp. 1735–1782.

Svergun, D. I., Petoukhov, M. V and Koch, M. H. (2001) 'Determination of domain structure of proteins from X-ray solution scattering.', *Biophysical Journal*, pp. 2946–2953.

Sydenham, M., Douce, G., Bowe, F., Ahmed, S., Chatfield, S. and Dougan, G. (2000) 'Salmonella enterica serovar Typhimurium surA mutants are attenuated and effective live oral vaccines.', *Infection and immunity*, 68(3), pp. 1109–1115.

Tainer, J. A., Roberts, V. A. and Getzoff, E. D. (1991) 'Metal-binding sites in proteins.', *Current opinion in biotechnology*, 2(4), pp. 582–591.

Takeda, S., Fujisawa, Y., Matsubara, M., Aiba, H. and Mizuno, T. (2001) 'A novel feature of the multistep phosphorelay in Escherichia coli: a revised model of the RcsC --> YojN --> RcsB signalling pathway implicated in capsular synthesis and swarming behaviour.', *Molecular microbiology*, 40(2), pp. 440–450.

Tam, C. and Missiakas, D. (2005) 'Changes in lipopolysaccharide structure induce the sigma(E)-dependent response of Escherichia coli.', *Molecular microbiology*, 55(5), pp. 1403–1412. doi: 10.1111/j.1365-2958.2005.04497.x.

Tam, M. A., Rydstrom, A., Sundquist, M. and Wick, M. J. (2008) 'Early cellular responses to Salmonella infection: dendritic cells, monocytes, and more.', *Immunological reviews*, 225, pp. 140–162. doi: 10.1111/j.1600-065X.2008.00679.x.

Tamayo, R., Ryan, S. S., McCoy, A. J. and Gunn, J. S. (2002) 'Identification and genetic characterization of PmrA-regulated genes and genes involved in polymyxin B resistance in Salmonella enterica serovar Typhimurium.', *Infection and immunity*, 70(12), pp. 6770–6778.

Tamm, L. K., Arora, A. and Kleinschmidt, J. H. (2001) 'Structure and assembly of beta-barrel membrane proteins.', *The Journal of biological chemistry*, 276(35), pp. 32399–32402. doi: 10.1074/jbc.R100021200.

Taylor, D. E. and Eves, G. E. (1969) 'An unusual type of Salmonella causing enteric fever.',

Pathology, 1(3), pp. 221–224.

Tennant, S. M. and Levine, M. M. (2015) 'Live attenuated vaccines for invasive Salmonella infections.', *Vaccine*, 33 Suppl 3, pp. C36-41. doi: 10.1016/j.vaccine.2015.04.029.

Tennant, S. M., MacLennan, C. A., Simon, R., Martin, L. B. and Khan, M. I. (2016) 'Nontyphoidal salmonella disease: Current status of vaccine research and development.', *Vaccine*, 34(26), pp. 2907–2910. doi: 10.1016/j.vaccine.2016.03.072.

Terwilliger, T. C. (2000) 'Maximum-likelihood density modification.', *Acta crystallographica. Section D, Biological crystallography*, 56(Pt 8), pp. 965–972.

Terwilliger, T. C., Grosse-Kunstleve, R. W., Afonine, P. V, Moriarty, N. W., Zwart, P. H., Hung, L. W., Read, R. J. and Adams, P. D. (2008) 'Iterative model building, structure refinement and density modification with the PHENIX AutoBuild wizard.', *Acta crystallographica. Section D, Biological crystallography*, 64(Pt 1), pp. 61–69. doi: 10.1107/S090744490705024X.

Thede, G. L., Arthur, D. C., Edwards, R. A., Buelow, D. R., Wong, J. L., Raivio, T. L. and Glover, J. N. M. (2011) 'Structure of the periplasmic stress response protein CpxP.', *Journal of bacteriology*, 193(9), pp. 2149–2157. doi: 10.1128/JB.01296-10.

Thorbjarnardottir, S. H., Magnusdottir, R. A. and Eggertsson, G. (1978) 'Mutations determining generalized resistance to aminoglycoside antibiotics in Escherichia coli.', *Molecular & general genetics : MGG*, 161(1), pp. 89–98.

Tormo, A., Almiron, M. and Kolter, R. (1990) 'surA, an Escherichia coli gene essential for survival in stationary phase.', *Journal of bacteriology*, 172(8), pp. 4339–4347.

Tracz, D. M., Tabor, H., Jerome, M., Ng, L.-K. and Gilmour, M. W. (2006) 'Genetic determinants and polymorphisms specific for human-adapted serovars of Salmonella enterica that cause enteric fever.', *Journal of clinical microbiology*, 44(6), pp. 2007–2018. doi: 10.1128/JCM.02630-05.

Trepreau, J., Grosse, C., Mouesca, J.-M., Sarret, G., Girard, E., Petit-Haertlein, I., Kuennemann, S., Desbourdes, C., de Rosny, E., Maillard, A. P., Nies, D. H. and Coves, J. (2014) 'Metal sensing and signal transduction by CnrX from Cupriavidus metallidurans CH34: role of the only methionine assessed by a functional, spectroscopic, and theoretical study.', *Metallomics : integrated biometal science*, 6(2), pp. 263–273. doi: 10.1039/c3mt00248a.

Tschauner, K., Hörnschemeyer, P., Müller, V. S. and Hunke, S. (2014) 'Dynamic interaction between the CpxA sensor kinase and the periplasmic accessory protein CpxP mediates signal recognition in E. coli.', *PloS one*, 9(9), p. e107383. doi: 10.1371/journal.pone.0107383.

Ureta, A. R., Endres, R. G., Wingreen, N. S. and Silhavy, T. J. (2007) 'Kinetic analysis of the assembly of the outer membrane protein LamB in Escherichia coli mutants each lacking a secretion or targeting factor in a different cellular compartment.', *Journal of Bacteriology*, pp. 446–454. doi: 10.1128/JB.01103-06.

Uzzau, S., Brown, D. J., Wallis, T., Rubino, S., Leori, G., Bernard, S., Casadesús, J., Platt, D. J. and Olsen, J. E. (2000) 'Host adapted serotypes of Salmonella enterica.', *Epidemiology and Infection*, pp. 229–255.

Vaara, M. (1992) 'Agents that increase the permeability of the outer membrane.', *Microbiological Reviews*, pp. 395–411.

Vainberg, I. E., Lewis, S. A., Rommelaere, H., Ampe, C., Vandekerckhove, J., Klein, H. L. and Cowan, N. J. (1998) 'Prefoldin, a chaperone that delivers unfolded proteins to cytosolic chaperonin.', *Cell*, 93(5), pp. 863–873.

Vallee, B. L. and Auld, D. S. (1993) 'New perspective on zinc biochemistry: cocatalytic sites in multi-zinc enzymes.', *Biochemistry*, 32(26), pp. 6493–6500.

Vallenas, C., Hernandez, H., Kay, B., Black, R. and Gotuzzo, E. (1985) 'Efficacy of bone marrow, blood, stool and duodenal contents cultures for bacteriologic confirmation of typhoid fever in children.', *Pediatric infectious disease*, 4(5), pp. 496–498.

Velkov, T., Roberts, K. D., Nation, R. L., Thompson, P. E. and Li, J. (2013) 'Pharmacology of polymyxins: new insights into an "old" class of antibiotics.', *Future microbiology*, 8(6). doi: 10.2217/fmb.13.39.

Velkov, T., Thompson, P. E., Nation, R. L. and Li, J. (2010) 'Structure—activity relationships of polymyxin antibiotics.', *Journal of medicinal chemistry*, pp. 1898–1916. doi: 10.1021/jm900999h.

Venkatesh, G. R., Kembou Koungni, F. C., Paukner, A., Stratmann, T., Blissenbach, B. and Schnetz, K. (2010) 'BglJ-RcsB heterodimers relieve repression of the Escherichia coli bgl operon by H-NS.', *Journal of bacteriology*, 192(24), pp. 6456–6464. doi: 10.1128/JB.00807-10.

Verma, N. K., Quigley, N. B. and Reeves, P. R. (1988) 'O-antigen variation in Salmonella spp.: rfb gene clusters of three strains.', *Journal of Bacteriology*, pp. 103–107.

Vertommen, D., Ruiz, N., Leverrier, P., Silhavy, T. J. and Collet, J.-F. (2009) 'Characterization of the role of the Escherichia coli periplasmic chaperone SurA using differential proteomics.', *Proteomics*, 9(9), pp. 2432–2443. doi: 10.1002/pmic.200800794.

Volokhina, E. B., Grijpstra, J., Stork, M., Schilders, I., Tommassen, J. and Bos, M. P. (2011) 'Role of the periplasmic chaperones Skp, SurA, and DegQ in outer membrane protein biogenesis in Neisseria meningitidis.', *Journal of bacteriology*, 193(7), pp. 1612–21. doi: 10.1128/JB.00532-10.

Voulhoux, R., Bos, M. P., Geurtsen, J., Mols, M. and Tommassen, J. (2003) 'Role of a highly conserved bacterial protein in outer membrane protein assembly.', *Science (New York, N.Y.)*, 299(5604), pp. 262–265. doi: 10.1126/science.1078973.

Wallrodt, I., Jelsbak, L., Thomsen, L. E., Brix, L., Lemire, S., Gautier, L., Nielsen, D. S., Jovanovic, G., Buck, M. and Olsen, J. E. (2014) 'Removal of the phage-shock protein PspB causes reduction of virulence in Salmonella enterica serovar Typhimurium independently of NRAMP1.', *Journal of medical microbiology*. England, 63(Pt 6), pp. 788–795. doi: 10.1099/jmm.0.072223-0.

Walsh, N. P., Alba, B. M., Bose, B., Gross, C. A. and Sauer, R. T. (2003) 'OMP peptide signals initiate the envelope-stress response by activating DegS protease via relief of inhibition mediated by its PDZ domain.', *Cell*, 113(1), pp. 61–71.

Walther, D. M., Rapaport, D. and Tommassen, J. (2009) 'Biogenesis of beta-barrel membrane proteins in bacteria and eukaryotes: evolutionary conservation and divergence.', *Cellular and molecular life sciences : CMLS*, 66(17), pp. 2789–2804. doi: 10.1007/s00018-009-0029-z.

Walton, T. A., Sandoval, C. M., Fowler, C. A., Pardi, A. and Sousa, M. C. (2009) 'The cavity-chaperone Skp protects its substrate from aggregation but allows independent folding of substrate domains.', *Proceedings of the National Academy of Sciences of the United States of America*, 106(6), pp. 1772–1777. doi: 10.1073/pnas.0809275106.

Walton, T. A. and Sousa, M. C. (2004) 'Crystal structure of Skp, a prefoldin-like chaperone that protects soluble and membrane proteins from aggregation.', *Molecular cell*, 15(3), pp. 367–374. doi: 10.1016/j.molcel.2004.07.023.

Wang, L., Wang, Q. and Reeves, P. R. (2010) 'The variation of O antigens in Gram-negative bacteria.', *Sub-cellular biochemistry*, 53, pp. 123–152. doi: 10.1007/978-90-481-9078-2_6.

Wang, P., Kuhn, A. and Dalbey, R. E. (2010) 'Global change of gene expression and cell physiology in YidC-depleted Escherichia coli.', *Journal of bacteriology*, 192(8), pp. 2193–2209. doi: 10.1128/JB.00484-09.

Wang, Y. (2002) 'The function of OmpA in Escherichia coli.', *Biochemical and biophysical research communications*, 292(2), pp. 396–401. doi: 10.1006/bbrc.2002.6657.

Warner, D. M. and Levy, S. B. (2010) 'Different effects of transcriptional regulators MarA, SoxS and Rob on susceptibility of Escherichia coli to cationic antimicrobial peptides (CAMPs): Rob-dependent CAMP induction of the marRAB operon.', *Microbiology (Reading, England)*, 156(Pt 2), pp. 570–578. doi: 10.1099/mic.0.033415-0.

Weatherspoon-Griffin, N., Zhao, G., Kong, W., Kong, Y., Morigen, Andrews-Polymenis, H., McClelland, M. and Shi, Y. (2011) 'The CpxR/CpxA two-component system up-regulates two Tat-dependent peptidoglycan amidases to confer bacterial resistance to antimicrobial peptide.', *The Journal of biological chemistry*, 286(7), pp. 5529–5539. doi: 10.1074/jbc.M110.200352.

Webb, C. T., Selkrig, J., Perry, A. J., Noinaj, N., Buchanan, S. K. and Lithgow, T. (2012) 'Dynamic association of BAM complex modules includes surface exposure of the lipoprotein BamC.', *Journal of molecular biology*, 422(4), pp. 545–555. doi: 10.1016/j.jmb.2012.05.035.

Wei, Y. and Fu, D. (2006) 'Binding and transport of metal ions at the dimer interface of the Escherichia coli metal transporter YiiP.', *The Journal of biological chemistry*, 281(33), pp. 23492–23502. doi: 10.1074/jbc.M602254200.

Weiner, L., Brissette, J. L. and Model, P. (1991) 'Stress-induced expression of the Escherichia coli phage shock protein operon is dependent on sigma 54 and modulated by positive and negative feedback mechanisms.', *Genes & development*, 5(10), pp. 1912–1923.

Weiner, L. and Model, P. (1994) 'Role of an Escherichia coli stress-response operon in stationary-phase survival.', *Proceedings of the National Academy of Sciences of the United States of America*, 91(6), pp. 2191–2195.

Weininger, U., Jakob, R. P., Kovermann, M., Balbach, J. and Schmid, F. X. (2010) 'The prolyl isomerase domain of PpiD from Escherichia coli shows a parvulin fold but is devoid of

catalytic activity.', *Protein science : a publication of the Protein Society*, 19(1), pp. 6–18. doi: 10.1002/pro.277.

Wells, H. C. (2015) *Further characterisation of the envelope stress response of Salmonella Typhimurium.* University of East Anglia.

Wilken, C., Kitzing, K., Kurzbauer, R., Ehrmann, M. and Clausen, T. (2004) 'Crystal structure of the DegS stress sensor: How a PDZ domain recognizes misfolded protein and activates a protease.', *Cell*, 117(4), pp. 483–494.

Willey, J. M., Sherwood, L. M. and Woolverton, C. J. (2008) *Prescott, Harley, and Klein's Microbiology.* 7th Editio. New York: McGraw-Hill International.

Williams, K., Oyston, P. C., Dorrell, N., Li, S., Titball, R. W. and Wren, B. W. (2000) 'Investigation into the role of the serine protease HtrA in Yersinia pestis pathogenesis.', *FEMS microbiology letters*, 186(2), pp. 281–286.

Wilson, R. P., Raffatellu, M., Chessa, D., Winter, S. E., Tukel, C. and Baumler, A. J. (2008) 'The Vi-capsule prevents Toll-like receptor 4 recognition of Salmonella.', *Cellular microbiology*, 10(4), pp. 876–890. doi: 10.1111/j.1462-5822.2007.01090.x.

Winter, G. and Waterman, D. (2012) *The xia2 manual*.

Woodward, D. L., Khakhria, R. and Johnson, W. M. (1997) 'Human salmonellosis associated with exotic pets.', *Journal of clinical microbiology*, 35(11), pp. 2786–2790.

World Health Organisation (2011) *Guidelines for the management of Typhoid fever.*

World Health Organisation Department of Vaccines andBiologicals. (2003) *Background document: the diagnosis, prevention and treatment of Typhoid fever.* Geneva.

Worthington Biochemical Corporation. (2015) 'Malate Dehydrogenase Assay'.

Wu, S., Ge, X., Lv, Z., Zhi, Z., Chang, Z. and Zhao, X. S. (2011) 'Interaction between bacterial outer membrane proteins and periplasmic quality control factors: a kinetic partitioning mechanism.', *The Biochemical journal*, 438(3), pp. 505–511. doi: 10.1042/BJ20110264.

De Wulf, P., McGuire, A. M., Liu, X. and Lin, E. C. C. (2002) 'Genome-wide profiling of promoter recognition by the two-component response regulator CpxR-P in Escherichia coli.', *The Journal of biological chemistry*, 277(29), pp. 26652–26661. doi: 10.1074/jbc.M203487200.

Xu, X., Wang, S., Hu, Y.-X. and McKay, D. B. (2007) 'The periplasmic bacterial molecular chaperone SurA adapts its structure to bind peptides in different conformations to assert a sequence preference for aromatic residues.', *Journal of molecular biology*, pp. 367–381. doi: 10.1016/j.jmb.2007.07.069.

Yamaguchi, S., Reid, D. A., Rothenberg, E. and Darwin, A. J. (2013) 'Changes in Psp protein binding partners, localization and behaviour upon activation of the Yersinia enterocolitica phage shock protein response.', *Molecular microbiology*, 87(3), pp. 656–671. doi: 10.1111/mmi.12122.

Yamamoto, K., Hirao, K., Oshima, T., Aiba, H., Utsumi, R. and Ishihama, A. (2005) 'Functional characterization in vitro of all two-component signal transduction systems from Escherichia coli.', *The Journal of biological chemistry*, 280(2), pp. 1448–1456. doi: 10.1074/jbc.M410104200.

Yamamoto, K. and Ishihama, A. (2006) 'Characterization of copper-inducible promoters regulated by CpxA/CpxR in Escherichia coli.', *Bioscience, biotechnology, and biochemistry*, 70(7), pp. 1688–1695. doi: 10.1271/bbb.60024.

Yan, J., Pan, L., Chen, X., Wu, L. and Zhang, M. (2010) 'The structure of the harmonin/sans complex reveals an unexpected interaction mode of the two Usher syndrome proteins.', *Proceedings of the National Academy of Sciences of the United States of America*, 107(9), pp. 4040–4045. doi: 10.1073/pnas.0911385107.

Yang, H. H., Wu, C. G., Xie, G. Z., Gu, Q. W., Wang, B. R., Wang, L. Y., Wang, H. F., Ding, Z. S., Yang, Y., Tan, W. S., Wang, W. Y., Wang, X. C., Qin, M., Wang, J. H., Tang, H. A., Jiang, X. M., Li, Y. H., Wang, M. L., Zhang, S. L. and Li, G. L. (2001) 'Efficacy trial of Vi polysaccharide vaccine against typhoid fever in south-western China.', *Bulletin of the World Health Organization*, 79(7), pp. 625–631.

Yang, J., Dong, B. Q., Wang, M. L., Tang, Z. Z., Gong, J., Li, C. Y., Zeng, J. and Yang, H. H. (2004) 'Analysis of prevalent status of Paratyphus A and typhus in Guangxi Autonomous Region in 1994-2002.', *China Tropical Medicine*, 4, pp. 177–180.

Yitzhaki, S., Rostron, J. E., Xu, Y., Rideout, M. C., Authement, R. N., Barlow, S. B. and Segall, A. M. (2012) 'Similarities between exogenously- and endogenously-induced envelope stress: the effects of a new antibacterial molecule, TPI1609-10.', *PloS one*, 7(10), p. e44896. doi: 10.1371/journal.pone.0044896.

Yocum, R. R., Rasmussen, J. R. and Strominger, J. L. (1980) 'The mechanism of action of penicillin. Penicillin acylates the active site of Bacillus stearothermophilus D-alanine carboxypeptidase.', *The Journal of biological chemistry*, 255(9), pp. 3977–3986.

Yu, Z., Qin, W., Lin, J., Fang, S. and Qiu, J. (2015) 'Antibacterial mechanisms of polymyxin and bacterial resistance.', *BioMed Research International*. doi: 10.1155/2015/679109.

Zaharik, M. L., Cullen, V. L., Fung, A. M., Libby, S. J., Kujat Choy, S. L., Coburn, B., Kehres, D. G., Maguire, M. E., Fang, F. C. and Finlay, B. B. (2004) 'The Salmonella enterica serovar Typhimurium divalent cation transport systems MntH and SitABCD are essential for virulence in an Nramp1G169 murine typhoid model.', *Infection and immunity*, 72(9), pp. 5522–5525. doi: 10.1128/IAI.72.9.5522-5525.2004.

Zahrl, D., Wagner, M., Bischof, K. and Koraimann, G. (2006) 'Expression and assembly of a functional type IV secretion system elicit extracytoplasmic and cytoplasmic stress responses in Escherichia coli.', *Journal of bacteriology*, 188(18), pp. 6611–6621. doi: 10.1128/JB.00632-06.

Zgurskaya, H. I., Krishnamoorthy, G., Ntreh, A. and Lu, S. (2011) 'Mechanism and function of the outer membrane channel TolC in multidrug resistance and physiology of Enterobacteria.', *Frontiers in Microbiology*. doi: 10.3389/fmicb.2011.00189.

Zhang, J., Van Lanen, S. G., Ju, J., Liu, W., Dorrestein, P. C., Li, W., Kelleher, N. L. and Shen, B. (2008) 'A phosphopantetheinylating polyketide synthase producing a linear polyene to initiate enediyne antitumor antibiotic biosynthesis.', *Proceedings of the National Academy of Sciences of the United States of America*, 105(5), pp. 1460–1465. doi: 10.1073/pnas.0711625105.

Zhao, W., Xu, M., Liang, Z., Ding, B., Niu, L., Liu, H. and Teng, M. (2011) 'Structure-based de novo prediction of zinc-binding sites in proteins of unknown function.', *Bioinformatics (Oxford, England)*, 27(9), pp. 1262–1268. doi: 10.1093/bioinformatics/btr133.

Zhou, X., Keller, R., Volkmer, R., Krauss, N., Scheerer, P. and Hunke, S. (2011) 'Structural basis for two-component system inhibition and pilus sensing by the auxiliary CpxP protein.', *The Journal of biological chemistry*, 286(11), pp. 9805–9814. doi: 10.1074/jbc.M110.194092.

Zhou, Y., Gottesman, S., Hoskins, J. R., Maurizi, M. R. and Wickner, S. (2001) 'The RssB response regulator directly targets sigma(S) for degradation by ClpXP.', *Genes &*

development, 15(5), pp. 627–637. doi: 10.1101/gad.864401.

Zhou, Z., McCann, A., Weill, F.-X., Blin, C., Nair, S., Wain, J., Dougan, G. and Achtman, M. (2014) 'Transient Darwinian selection in Salmonella enterica serovar Paratyphi A during 450 years of global spread of enteric fever.', *Proceedings of the National Academy of Sciences of the United States of America*, 111(33), pp. 12199–12204. doi: 10.1073/pnas.1411012111.

Zhou, Z., White, K. A., Polissi, A., Georgopoulos, C. and Raetz, C. R. (1998) 'Function of Escherichia coli MsbA, an essential ABC family transporter, in lipid A and phospholipid biosynthesis.', *The Journal of biological chemistry*, 273(20), pp. 12466–12475.

Zoetendal, E. G., Smith, A. H., Sundset, M. A. and Mackie, R. I. (2008) 'The BaeSR two-component regulatory system mediates resistance to condensed tannins in Escherichia coli.', *Applied and environmental microbiology*, 74(2), pp. 535–539. doi: 10.1128/AEM.02271-07.

8. Appendices

Appendix A. Media, supplements and antibiotics.

Table A1. Media composition

Media	Components	Description
Luria-Bertani (LB) broth (litre)	10 g Sodium chloride 10 g Triptone 5 g Yeast extract	(Bertani, 1951) Components dissolved in 800mL dH2O. Solution topped up to 1000mL and autoclaved to sterilise.
Luria-Bertani (LB) agar (litre)	10 g Sodium chloride 10 g Triptone 5 g Yeast extract 1.5% (w/v) agar	LB broth prepared as described. Broth aliquoted into 200mL volumes, 3 g agar added to each flask. Autoclaved to sterilise
LB Top agar (litre)	10 g Sodium chloride 10 g Triptone 5 g Yeast extract 0.75% agarose	LB broth prepared as described. Broth aliquoted into 50mL volumes, 375mg agarose added to each flask. Autoclaved to sterilise
Lennox Broth (LB-half salt)	5 g Sodium chloride 10 g Triptone 5 g Yeast extract	modified from Bertani (1951) Components dissolved in 800mL dH2O. Solution topped up to 1000mL and autoclaved to sterilise.
LBO agar (LB without salt)	10 g Triptone 5 g Yeast extract 1.5% (w/v) agar	modified from Bertani (1951) LB broth minus salt prepared as described. Broth aliquoted into 200mL volumes, 3 g agar added to each flask. Autoclaved to sterilise
MOPS defined media High Carbon	50mL 10X MOPS* 2.5mL 0.132M K2HPO4 25μL 1 mg/mL Thiamine 250μL 40 mg/mL Histidine 4% glucose	(Neidhardt et al., 1974) Top op solution to 500mL using dH2O and filter sterilise.

Table A1. Media composition - continued

Media	Components	Description
MOPS defined mediaLow Carbon	50mL 10X MOPS* 2.5mL 0.132M K2HPO4 25µL 1 mg/mL Thiamine 250µL 40 mg/mL Histidine 4% glucose	(Neidhardt et al., 1974) Top op solution to 500mL using dH2O and filter sterilise.
UCB Indicator Plates (Green Plates)	8 Tryptone 1 Yeast extract 5 Sodium chloride 1.5% Agar Indicator supplements*	Modified from Bochner (1984) Triptone, yease and NaCl dissolved in 800mL dH2O and topped up to 950mL. Aliqoted into volumes of 190mL, 3 g of agar added to each aliquot, and autoclaved to sterilise. Indicator supplements added to media cooled to 60ºC, prior to pouring plates.

Appendix B. Buffers and solutions

Table B1. Electrophoresis and Western blotting buffers

Buffer	Conc.	Components	Description
Blocking buffer	1X	1X TBST buffer 5% (w/v) fat-free skimmed milk powder	Fat-free skimmed milk (2.5 g) dissolved in 1X TBST (50mL) and kept at 4°C
Chemoluminescent buffer A	1X	10mL 100mM Tris buffer pH 8.5 45µL courmanic acid 100µl luminol	Freshly made before use. Courmanic acid and luminol added to the Tris buffer. Luminol is light sensitive, so solution was wrapped in aluminium foil until use.
Chemoluminescent buffer B	1X	10mL 100mM Tris buffer pH 8.5 6µL 30% hydrogen peroxide	Freshly made before use. H2O2 dissolved in tris buffer.
Ponceau Strain	1X	2% (w/v) Ponceau S 30% trichloracetic acid 30% sulphosalicyclic acid	Components were dissolved in dH2O and stored at room temperature
SDS-loading buffer	1x	50 mM Tris-Cl (pH 6.8) 10% (v/v) Glycerol 2% (w/v) SDS 0.1% (w/v) Bromophenol blue 5% (v/v) β-mercaptoethanol	SDS-loading buffer minus β-mercaptoethanol was prepared in stocks of 20mL and stored at RT until further use. When used for SDS-PAGE analysis, 1mL aliquots were taken from stock and β-mercaptoethanol was added 1:19
TAE buffer	50X	242 g Tris free base 18.61 g Disodiumn EDTA 57.1 ml Glacial Acetic Acid	Tris and EDTA dissolved in 800mL dH2O. Glacial Acetic acid added. Final volume adjusted to 1 L.
TBE buffer	10x	108 g Tris base 55 g Boric acid 20 mL 0.5M EDTA (pH 8.0)	components dissolved in 950mL dH2O. Adjust pH to 8.3 and topped up to 1 L. 1X working solution created by diluting 1:9 in dH2O.
TBS	10X	60.5 g Tris 87.6 g Sodium chloride	Components dissolved in 800mL dH2O, pH adjusted to 7.5 using concentrated HCl, and volume adjusted to 1 L. Stored at 4°C 1X working solution created by diluting 1:9 in dH2O.

Table B2. Protein purification and storage buffers -continued

Buffer	Conc.	Components	Description
TBST	1X	1X TBS buffer 0.1% (v/v) TWEEN-20	TBS buffer diluted to 1X buffer by dissolving in dH2O 0.1% TWEEN-20 (1mL per L) added Stored at 4°C
TGS buffer	10x	30.2 g Tris-base 144 g Glycine 20 g SDS	Components dissolved in 800mL dH2O, and volume adjusted to 1 L. 1X working solution created by diluting 1:9 in dH2O.
Transfer buffer	1X	1x TGS buffer 20% (v/v) methanol	1X TGS buffer prepared by diluting 10X TGS buffer in dH2O and add methanol 1:4 ratio with buffer.
Hepes elution buffer	1X	100mM HEPES buffer 300mM imidazole	300mM imidazole dissolved in HEPES buffer and filter sterilised into autoclaved bottles
HEPES storage buffer	1X	100mM HEPES	HEPES dissolved in dH2O and pH adjusted to 7.5 using HCl. Filter steriled into autoclaved bottles.
StrepII elution buffer	1X	1X StrepII storage buffer 2.5mM desthiobiotin	Desthiobiotin dissolved in StrepII storage buffer prior to elution of protein samples. Kept at 4°C.
StrepII storage buffer	1X	100mM Tris-HCl 150mM sodium chloride 1mM EDTA	Buffer prepared using acid-washed glass ware. Components dissolved in 800mL Sigma water, pH adjusted to pH 8. Filter sterilised into autoclaved, acid washed bottle.
StrepII storage buffer (EDTA free)	1X	100mM Tris-HCl 150mM sodium chloride	Prepared as StrepII buffer minus EDTA.
DNA gyrase assay buffer	5X	35mM Tris·HCl (pH 7.5) 24mM Potassium chloride 4 mM Magnesium chloride 2 mM DTT (Dithiothreitol) 1.8 mM spermidine, 1 mM ATP 6.5 % (w/v) glycerol 0.1 mg/ml albumin	Buffer supplied by Inspiralis Ltd. Stored at -20°C.

Table B2. Protein purification and storage buffers -continued

Buffer	Conc.	Components	Description
DNA gyrase dilution buffer	1X	50mM Tris·HCl (pH 7.5) 100mM Potassium chloride 2mM DTT (Dithiothreitol) 1mM EDTA 50% (w/v) glycerol	Buffer supplied by Inspiralis Ltd. Stored at -20°C.
M9 minimal salts buffer	5X	64 Sodium phosphate dibasic heptahydrate 15 Monopotassium phosphate 2.5 Sodium chloride 5 Ammonium chloride	Modified from (Maniatis, 1982) Components dissolved in 800mL dH2O, adjust to 1 L and sterilise by autoclaving. 1X salts buffer produced by diluting 1:4 in dH2O.
MIB buffer	10X	4.15 g of sodium malonate dibasic monohydr 2.55 g imidazole 2.32 g boric acid.	Components dissolved in 80mL dH2O, pH adjusted according to required buffer using HCl and NaOH. Final volume adjusted to 100mL. Filter sterilised.
PBS buffer	1X	8 g sodium chloride 0.2 g potassium chloride 1.44 g sodium phosphate dibasic 0.24 g potassium phosphate monobasic	Components dissolved in 800mL dH2O, pH adjusted to 7.5 using HCl. Final volume adjusted to 1 L. Autoclaved to sterilise.
Qiagen N3	1X	4.2 M Guanidine hydrochloride 0.9 M Potassium acetate	Components dissolved in dH2O, pH adjusted to 4.8. Stored at room teperature.
Qiagen P1	1X	50mM Tris-HCl 10mM EDTA 100μg/mL RNase A	Tris base and EDTA dissolved in dH2O, pH adjusted to 8.0 using HCl. Autoclaved to sterilise. Stored at 4°C after addition of RNase A
Qiagen P2	1X	200mM NaOH 1% SDS (w/v)	Components dissolved in dH2O, and autoclaved to sterilise. Stored at room temperature.
SPG buffer	10X	1.48 g succinic acid 6.04 g sodium dihydrogen phosphate mono 3.28 g glycine	Components dissolved in 80mL dH2O, pH adjusted according to required buffer using HCl and NaOH. Final volume adjusted to 100mL. Filter sterilised.
STEB	1X	40 % (w/v) sucrose 100 mM Tris-HCl (pH 8.0) 10 mM EDTA 0.5 mg/ml Bromophenol Blue	Solution supplied by Inspiralis Ltd. Stored at 4°C.

Appendix C. Crystallography optimisation tray

	1	2	3	4	5	6
A	0.1 M Tris pH 8.5 0.1 M Lithium sulphate 20% PEG 3350	0.1 M Tris pH 8.5 0.1 M Lithium sulphate 22.5% PEG 3350	0.1 M Tris pH 8.5 0.1 M Lithium sulphate 25% PEG 3350	0.1 M Tris pH 8.5 0.1 M Lithium sulphate 27.5% PEG 3350	0.1 M Tris pH 8.5 0.1 M Lithium sulphate 30% PEG 3350	0.1 M Tris pH 8.5 0.1 M Lithium sulphate 32.5% PEG 3350
B	0.1 M Tris pH 8.5 0.2M Lithium sulphate 20% PEG 3350	0.1 M Tris pH 8.5 0.2M Lithium sulphate 22.5% PEG 3350	0.1 M Tris pH 8.5 0.2M Lithium sulphate 25% PEG 3350	0.1 M Tris pH 8.5 0.2M Lithium sulphate 27.5% PEG 3350	0.1 M Tris pH 8.5 0.2M Lithium sulphate 30% PEG 3350	0.1 M Tris pH 8.5 0.2M Lithium sulphate 32.5% PEG 3350
C	0.1 M Tris pH 8.5 0.3 M Lithium sulphate 20% PEG 3350	0.1 M Tris pH 8.5 0.3 M Lithium sulphate 22.5% PEG 3350	0.1 M Tris pH 8.5 0.3 M Lithium sulphate 25% PEG 3350	0.1 M Tris pH 8.5 0.3 M Lithium sulphate 27.5% PEG 3350	0.1 M Tris pH 8.5 0.3 M Lithium sulphate 30% PEG 3350	0.1 M Tris pH 8.5 0.3 M Lithium sulphate 32.5% PEG 3350
D	0.1 M Tris pH 8.5 0.4M Lithium sulphate 20% PEG 3350	0.1 M Tris pH 8.5 0.4M Lithium sulphate 22.5% PEG 3350	0.1 M Tris pH 8.5 0.4M Lithium sulphate 25% PEG 3350	0.1 M Tris pH 8.5 0.4M Lithium sulphate 27.5% PEG 3350	0.1 M Tris pH 8.5 0.4M Lithium sulphate 30% PEG 3350	0.1 M Tris pH 8.5 0.4M Lithium sulphate 32.5% PEG 3350
E	0.1 M MIB buffer pH 4.5 17.5% PEG 1500	0.1 M MIB buffer pH 4.5 20% PEG 1500	0.1 M MIB buffer pH 4.5 22.5% PEG 1500	0.1 M MIB buffer pH 4.5 25% PEG 1500	0.1 M MIB buffer pH 4.5 27.5% PEG 1500	0.1 M MIB buffer pH 4.5 30% PEG 1500
F	0.1 M MIB buffer pH 5.0 17.5% PEG 1500	0.1 M MIB buffer pH 5.0 20% PEG 1500	0.1 M MIB buffer pH 5.0 22.5% PEG 1500	0.1 M MIB buffer pH 5.0 25% PEG 1500	0.1 M MIB buffer pH 5.0 27.5% PEG 1500	0.1 M MIB buffer pH 5.0 30% PEG 1500
G	0.1 M MIB buffer pH 5.5 17.5% PEG 1500	0.1 M MIB buffer pH 5.5 20% PEG 1500	0.1 M MIB buffer pH 5.5 22.5% PEG 1500	0.1 M MIB buffer pH 5.5 25% PEG 1500	0.1 M MIB buffer pH 5.5 27.5% PEG 1500	0.1 M MIB buffer pH 5.5 30% PEG 1500
H	0.1 M MIB buffer pH 6.0 17.5% PEG 1500	0.1 M MIB buffer pH 6.0 20% PEG 1500	0.1 M MIB buffer pH 6.0 22.5% PEG 1500	0.1 M MIB buffer pH 6.0 25% PEG 1500	0.1 M MIB buffer pH 6.0 27.5% PEG 1500	0.1 M MIB buffer pH 6.0 30% PEG 1500

	7	8	9	10	11	12
A	0.1 M Tris pH 9.0 1.0 M Potassium phosphate	0.1 M Tris pH 9.0 1.25 M Potassium phosphate	0.1 M Tris pH 9.0 1.5 M Potassium phosphate	0.1 M Tris pH 9.0 1.75 M Potassium phosphate	0.1 M Tris pH 9.0 2.0 M Potassium phosphate	0.1 M Tris pH 9.0 2.25 M Potassium phosphate
B	0.1 M Tris pH 8.5 1.0 M Potassium phosphate	0.1 M Tris pH 8.5 1.25 M Potassium phosphate	0.1 M Tris pH 8.5 1.5 M Potassium phosphate	0.1 M Tris pH 8.5 1.75 M Potassium phosphate	0.1 M Tris pH 8.5 2.0 M Potassium phosphate	0.1 M Tris pH 8.5 2.25 M Potassium phosphate
C	0.1 M Tris pH 8.0 1.0 M Potassium phosphate	0.1 M Tris pH 8.0 1.25 M Potassium phosphate	0.1 M Tris pH 8.0 1.5 M Potassium phosphate	0.1 M Tris pH 8.0 1.75 M Potassium phosphate	0.1 M Tris pH 8.0 2.0 M Potassium phosphate	0.1 M Tris pH 8.0 2.25 M Potassium phosphate
D	0.1 M Tris pH 7.5 1.0 M Potassium phosphate	0.1 M Tris pH 7.5 1.25 M Potassium phosphate	0.1 M Tris pH 7.5 1.5 M Potassium phosphate	0.1 M Tris pH 7.5 1.75 M Potassium phosphate	0.1 M Tris pH 7.5 2.0 M Potassium phosphate	0.1 M Tris pH 7.5 2.25 M Potassium phosphate
E	0.1 M SPG buffer pH 9.0 17.5% PEG 1500	0.1 M SPG buffer pH 9.0 20% PEG 1500	0.1 M SPG buffer pH 9.0 22.5% PEG 1500	0.1 M SPG buffer pH 9.0 25% PEG 1500	0.1 M SPG buffer pH 9.0 27.5% PEG 1500	0.1 M SPG buffer pH 9.0 30% PEG 1500
F	0.1 M SPG buffer pH 8.5 17.5% PEG 1500	0.1 M SPG buffer pH 8.5 20% PEG 1500	0.1 M SPG buffer pH 8.5 22.5% PEG 1500	0.1 M SPG buffer pH 8.5 25% PEG 1500	0.1 M SPG buffer pH 8.5 27.5% PEG 1500	0.1 M SPG buffer pH 8.5 30% PEG 1500
G	0.1 M SPG buffer pH 8.0 17.5% PEG 1500	0.1 M SPG buffer pH 8.0 20% PEG 1500	0.1 M SPG buffer pH 8.0 22.5% PEG 1500	0.1 M SPG buffer pH 8.0 25% PEG 1500	0.1 M SPG buffer pH 8.0 27.5% PEG 1500	0.1 M SPG buffer pH 8.0 30% PEG 1500
H	0.1 M SPG buffer pH 7.5 17.5% PEG 1500	0.1 M SPG buffer pH 7.5 20% PEG 1500	0.1 M SPG buffer pH 7.5 22.5% PEG 1500	0.1 M SPG buffer pH 7.5 25% PEG 1500	0.1 M SPG buffer pH 7.5 27.5% PEG 1500	0.1 M SPG buffer pH 7.5 30% PEG 1500

Appendix D – Sequencing results of strepII-tagged pBAD ZraP constructs

Sequence alignment ZraP-AAAAA with STM SL1444 – ZraP retrieved from coliBASE.

Sequencing results *versus zraP* genetic sequence:

```
ZraPAAAAA    CTAAGGAGGATTAACCATGGTGAAACGGAACAATAAATCAGCTATCGCGCTAATTGCCCT
ZraP         -----------------ATGAAACGGAACAATAAATCAGCTATCGCGCTAATTGCCCT
                              ************************************

ZraPAAAAA    CTCTCTTTTGGCCCTGAGCTCCGGCGCCGCCTTCGCCGGGCATCACTGGGGCAACAATGA
ZraP         CTCTCTTTTGGCCCTGAGCTCCGGCGCCGCCTTCGCCGGGCATCACTGGGGCAACAATGA
             ************************************************************

ZraPAAAAA    CGGTATGTGGCAACAGGGAGGTAGCCCGGCAGCTGCGGCAGCGCAGGCGACGGCGCAGAA
ZraP         CGGTATGTGGCAACAGGGAGGTAGCCCGTTAACTACGGAACAGCAGGCGACGGCGCAGAA
              ***************************  *  **  ***  *  *****************

ZraPAAAAA    GATTTATGATGATTACTATACGCAGACCAGCGCGCTGCGCCAGCAACTGATATCCAAACG
ZraP         GATTTATGATGATTACTATACGCAGACCAGCGCGCTGCGCCAGCAACTGATATCCAAACG
             ************************************************************

ZraPAAAAA    TTATGAATACAACGCGCTACTGACCGCCAGTTCGCCGGATACTGCGAAAATTAACGCGGT
ZraP         TTATGAATACAACGCGCTACTGACCGCCAGTTCGCCGGATACTGCGAAAATTAACGCGGT
             ************************************************************

ZraPAAAAA    TGCCAAAGAGATGGAGTCATTAGGCCAGAAGTTAGATGAGCAACGCGTGAAACGGGATGT
ZraP         TGCCAAAGAGATGGAGTCATTAGGCCAGAAGTTAGATGAGCAACGCGTGAAACGGGATGT
             ************************************************************

ZraPAAAAA    CGCGATGGCGCAGGCTGGCATACCACGCGGCGCAGGAATGGGCTATGGCGGTTGCGGCGG
ZraP         CGCGATGGCGCAGGCTGGCATACCACGCGGCGCAGGAATGGGCTATGGCGGTTGCGGCGG
             ************************************************************

ZraPAAAAA    CTATGGCGGCGGTTATCATCGCGGCGGCGGTCACATGGGTATGGGAAACTGGTGGAGCCA
ZraP         CTATGGCGGCGGTTATCATCGCGGCGGCGGTCACATGGGTATGGGAAACTGGT------
             ****************************************************

ZraPAAAAA    TCCACAATTTGAAAAATGAGTTTAAACGGTCTCCAGCTTGGCTGTTTTGGCGGATGAGAG
ZraP         ------------------------------------------------------------
```

ExPASy translated results for ZraP-AAAAA *versus* ZraP protein sequence

```
ZraP-AAAAA   MVKRNNKSAIALIALSLLALSSGAAFAGHHWGNNDGMWQQGGSPAAAAAQATAQKIYDDY
ZraP          MKRNNKSAIALIALSLLALSSGAAFAGHHWGNNDGMWQQGGSPLTTEQQATAQKIYDDY
             :******************************************* :: **********

ZraP-AAAAA   YTQTSALRQQLISKRYEYNALLTASSPDTAKINAVAKEMESLGQKLDEQRVKRDVAMAQA
ZraP         YTQTSALRQQLISKRYEYNALLTASSPDTAKINAVAKEMESLGQKLDEQRVKRDVAMAQA
             ************************************************************

ZraP-AAAAA    GIPRGAGMGYGGCGGYGGGYHRGGGHMGMGNWWSHPQFEK
ZraP          GIPRGAGMGYGGCGGYGGGYHRGGGHMGMGNW--------
              *******************************
```

Sequence alignment ZraP-HRGGAH with STM SL1444 – ZraP retrieved from coliBASE.

Sequencing results *versus zraP* genetic sequence:

```
ZraPHRGGAH    ACGGAGGAATTAACCATGGTGAAACGGAACAATAAATCAGCTATCGCGCTAATTGCCCTC
ZraP          ----------------ATGAAACGGAACAATAAATCAGCTATCGCGCTAATTGCCCTC
                              ******************************************

ZraPHRGGAH    TCTCTTTTGGCCCTGAGCTCCGGCGCCGCCTTCGCCGGGCATCACTGGGGCAACAATGAC
ZraP          TCTCTTTTGGCCCTGAGCTCCGGCGCCGCCTTCGCCGGGCATCACTGGGGCAACAATGAC
              ************************************************************

ZraPHRGGAH    GGTATGTGGCAACAGGGAGGTAGCCCGTTAACTACGGAACAGCAGGCGACGGCGCAGAAG
ZraP          GGTATGTGGCAACAGGGAGGTAGCCCGTTAACTACGGAACAGCAGGCGACGGCGCAGAAG
              ************************************************************

ZraPHRGGAH    ATTTATGATGATTACTATACGCAGACCAGCGCGCTGCGCCAGCAACTGATATCCAAACGT
ZraP          ATTTATGATGATTACTATACGCAGACCAGCGCGCTGCGCCAGCAACTGATATCCAAACGT
              ************************************************************

ZraPHRGGAH    TATGAATACAACGCGCTACTGACCGCCAGTTCGCCGGATACTGCGAAAATTAACGCGGTT
ZraP          TATGAATACAACGCGCTACTGACCGCCAGTTCGCCGGATACTGCGAAAATTAACGCGGTT
              ************************************************************

ZraPHRGGAH    GCCAAAGAGATGGAGTCATTAGGCCAGAAGTTAGATGAGCAACGCGTGAAACGGGATGTC
ZraP          GCCAAAGAGATGGAGTCATTAGGCCAGAAGTTAGATGAGCAACGCGTGAAACGGGATGTC
              ************************************************************

ZraPHRGGAH    GCGATGGCGCAGGCTGGCATACCACGCGGCGCAGGAATGGGCTATGGCGGTTGCGGCGGC
ZraP          GCGATGGCGCAGGCTGGCATACCACGCGGCGCAGGAATGGGCTATGGCGGTTGCGGCGGC
              ************************************************************

ZraPHRGGAH    TATGGCGGCGGTTATCATCGCGGCGGCGCTCACATGGGTATGGGAAACTGGTGGAGCCAT
ZraP          TATGGCGGCGGTTATCATCGCGGCGGCGGTCACATGGGTATGGGAAACTGGTAA-----
              ************************** *********************

ZraPHRGGAH    CCACAATTTGAAAAATGAGTTTAAACGGTCTCCAGCTTGGCTGTTTTGGCGGATGAGAGA
ZraP          ------------------------------------------------------------
```

ExPASy translated results for ZraP-HRGGAH *versus* ZraP protein sequence

```
ZraP-HRGGAH   MVKRNNKSAIALIALSLLALSSGAAFAGHHWGNNDGMWQQGGSPLTTEQQATAQKIYDDY
ZraP           MKRNNKSAIALIALSLLALSSGAAFAGHHWGNNDGMWQQGGSPLTTEQQATAQKIYDDY
              :*********************************************************

ZraP-HRGGAH   YTQTSALRQQLISKRYEYNALLTASSPDTAKINAVAKEMESLGQKLDEQRVKRDVAMAQA
ZraP          YTQTSALRQQLISKRYEYNALLTASSPDTAKINAVAKEMESLGQKLDEQRVKRDVAMAQA
              ************************************************************

ZraP-HRGGAH    GIPRGAGMGYGGCGGYGGGYHRGGAHMGMGNWWSHPQFEK
ZraP           GIPRGAGMGYGGCGGYGGGYHRGGHMGMGNW--------
              ************************.*******
```

Sequence alignment ZraP-LTxxQ with STM SL1444 – ZraP retrieved from coliBASE.

Sequencing results *versus zraP* genetic sequence:

```
ZraPLTXXQ    GCTACGGAGGATTAACCATGGTGAAACGGAACAATAAATCAGCTATCGCGCTAATTGCCC
ZraP         ------------------ATGAAACGGAACAATAAATCAGCTATCGCGCTAATTGCCC
                               ************************************

ZraPLTXXQ    TCTCTCTTTTGGCCCTGAGCTCCGGCGCCGCCTTCGCCGGGCATCACTGGGGCAACAATG
ZraP         TCTCTCTTTTGGCCCTGAGCTCCGGCGCCGCCTTCGCCGGGCATCACTGGGGCAACAATG
             ************************************************************

ZraPLTXXQ    ACGGTATGTGGCAACAGGGAGGTAGCCCGTTAACTACGGAAGCGCAGGCGACGGCGCAGA
ZraP         ACGGTATGTGGCAACAGGGAGGTAGCCCGTTAACTACGGAACAGCAGGCGACGGCGCAGA
             *****************************************   ****************

ZraPLTXXQ    AGATTTATGATGATTACTATACGCAGACCAGCGCGCTGCGCCAGCAACTGATATCCAAAC
ZraP         AGATTTATGATGATTACTATACGCAGACCAGCGCGCTGCGCCAGCAACTGATATCCAAAC
             ************************************************************

ZraPLTXXQ    GTTATGAATACAACGCGCTACTGACCGCCAGTTCGCCGGATACTGCGAAAATTAACGCGG
ZraP         GTTATGAATACAACGCGCTACTGACCGCCAGTTCGCCGGATACTGCGAAAATTAACGCGG
             ************************************************************

ZraPLTXXQ    TTGCCAAAGAGATGGAGTCATTAGGCCAGAAGTTAGATGAGCAACGCGTGAAACGGGATG
ZraP         TTGCCAAAGAGATGGAGTCATTAGGCCAGAAGTTAGATGAGCAACGCGTGAAACGGGATG
             ************************************************************

ZraPLTXXQ    TCGCGATGGCGCAGGCTGGCATACCACGCGGCGCAGGAATGGGCTATGGCGGTTGCGGCG
ZraP         TCGCGATGGCGCAGGCTGGCATACCACGCGGCGCAGGAATGGGCTATGGCGGTTGCGGCG
             ************************************************************

ZraPLTXXQ    GCTATGGCGGCGGTTATCATCGCGGCGGCGGTCACATGGGTATGGGAAACTGGTGGAGCC
ZraP         GCTATGGCGGCGGTTATCATCGCGGCGGCGGTCACATGGGTATGGGAAACTGGTAA----
             *****************************************************

ZraPLTXXQ    ATCCACAATTTGAAAAATGAGTTTAAACGGTCTCCAGCTTGGCTGTTTTGGCGGATGAGA
ZraP         ------------------------------------------------------------
```

ExPASy translated results for ZraP-LTxxQ *versus* ZraP protein sequence

```
ZraPLTXXQ    MVKRNNKSAIALIALSLLALSSGAAFAGHHWGNNDGMWQQGGSPLTTEAQATAQKIYDDY
ZraP         -MKRNNKSAIALIALSLLALSSGAAFAGHHWGNNDGMWQQGGSPLTTEQQATAQKIYDDY
              :***********************************************  **********

ZraPLTXXQ    YTQTSALRQQLISKRYEYNALLTASSPDTAKINAVAKEMESLGQKLDEQRVKRDVAMAQA
ZraP         YTQTSALRQQLISKRYEYNALLTASSPDTAKINAVAKEMESLGQKLDEQRVKRDVAMAQA
             ************************************************************

ZraPLTXXQ    GIPRGAGMGYGGCGGYGGGYHRGGGHMGMGNWWSHPQFEK
ZraP         GIPRGAGMGYGGCGGYGGGYHRGGGHMGMGNW--------
             *******************************
```

Sequence alignment ZraP-SDM with STM SL1444 – ZraP retrieved from coliBASE.

Sequencing results *versus zraP* genetic sequence:

```
ZraPSDM     AAGGAGGATTAACCATGGTGAAACGGAACAATAAATCAGCTATCGCGCTAATTGCCCTCT
ZraP        ----------------ATGAAACGGAACAATAAATCAGCTATCGCGCTAATTGCCCTCT
                            ******************************************

ZraPSDM     CTCTTTTGGCCCTGAGCTCCGGCGCCGCCTTCGCCGGGCATCACTGGGGCAACAATGACG
ZraP        CTCTTTTGGCCCTGAGCTCCGGCGCCGCCTTCGCCGGGCATCACTGGGGCAACAATGACG
            ************************************************************

ZraPSDM     GTATGTGGCAACAGGGAGGTAGCCCGTTAACTACGGAACAGCAGGCGACGGCGCAGAAGA
ZraP        GTATGTGGCAACAGGGAGGTAGCCCGTTAACTACGGAACAGCAGGCGACGGCGCAGAAGA
            ************************************************************

ZraPSDM     TTTATGATGATTACTATACGCAGACCAGCGCGCTGCGCCAGCAACTGATATCCAAACGTT
ZraP        TTTATGATGATTACTATACGCAGACCAGCGCGCTGCGCCAGCAACTGATATCCAAACGTT
            ************************************************************

ZraPSDM     ATGAATACAACGCGCTACTGACCGCCAGTTCGCCGGATACTGCGAAAATTAACGCGGTTG
ZraP        ATGAATACAACGCGCTACTGACCGCCAGTTCGCCGGATACTGCGAAAATTAACGCGGTTG
            ************************************************************

ZraPSDM     CCAAAGAGATGGAGTCATTAGGCCAGAAGTTAGATGAGCAACGCGTGAAACGGGATGTCG
ZraP        CCAAAGAGATGGAGTCATTAGGCCAGAAGTTAGATGAGCAACGCGTGAAACGGGATGTCG
            ************************************************************

ZraPSDM     CGATGGCGCAGGCTGGCATACCACGCGGCGCAGGAATGGGCTATGCCGCTGCCGCCGCCG
ZraP        CGATGGCGCAGGCTGGCATACCACGCGGCGCAGGAATGGGCTATGGCGGTTGCGGCGGCT
             ***********************************************  **  *   **  ** *

ZraPSDM     CTGGCGGCGGTTATCATCGCGGCGGCGGTCACATGGGTATGGGAAACTGGTGGAGCCATC
ZraP        ATGGCGGCGGTTATCATCGCGGCGGCGGTCACATGGGTATGGGAAACTGGTAA-------
            **************************************************

ZraPSDM     CACAATTTGAAAAATGAGTTTAAACGGTCTCCAGCTTGGCTGTTTTGGCGGATGAGAGAA
ZraP        ------------------------------------------------------------
```

ExPASy translated results for ZraP-SDM *versus* ZraP protein sequence

```
ZraPSDM     MVKRNNKSAIALIALSLLALSSGAAFAGHHWGNNDGMWQQGGSPLTTEQQATAQKIYDDY
ZraP        -MKRNNKSAIALIALSLLALSSGAAFAGHHWGNNDGMWQQGGSPLTTEQQATAQKIYDDY
             :**********************************************************

ZraPSDM     YTQTSALRQQLISKRYEYNALLTASSPDTAKINAVAKEMESLGQKLDEQRVKRDVAMAQA
ZraP        YTQTSALRQQLISKRYEYNALLTASSPDTAKINAVAKEMESLGQKLDEQRVKRDVAMAQA
            ************************************************************

ZraPSDM     GIPRGAGMGYAAAAAAGGGYHRGGGHMGMGNWWSHPQFEK
ZraP        GIPRGAGMGYGGCGGYGGGYHRGGGHMGMGNW--------
            **********.....  ***************
```

Sequence alignment ZraP-WT with STM SL1444 – ZraP retrieved from coliBASE.

Sequencing results *versus zraP* genetic sequence:

```
ZraPWT      GTACGGAGGATTAACCATGGTGAAACGGAACAATAAATCAGCTATCGCGCTAATTGCCCT
ZraP        ------------------ATGAAACGGAACAATAAATCAGCTATCGCGCTAATTGCCCT
                              *************************************

ZraPWT      CTCTCTTTTGGCCCTGAGCTCCGGCGCCGCCTTCGCCGGGCATCACTGGGGCAACAATGA
ZraP        CTCTCTTTTGGCCCTGAGCTCCGGCGCCGCCTTCGCCGGGCATCACTGGGGCAACAATGA
            ************************************************************

ZraPWT      CGGTATGTGGCAACAGGGAGGTAGCCCGTTAACTACGGAACAGCAGGCGACGGCGCAGAA
ZraP        CGGTATGTGGCAACAGGGAGGTAGCCCGTTAACTACGGAACAGCAGGCGACGGCGCAGAA
            ************************************************************

ZraPWT      GATTTATGATGATTACTATACGCAGACCAGCGCGCTGCGCCAGCAACTGATATCCAAACG
ZraP        GATTTATGATGATTACTATACGCAGACCAGCGCGCTGCGCCAGCAACTGATATCCAAACG
            ************************************************************

ZraPWT      TTATGAATACAACGCGCTACTGACCGCCAGTTCGCCGGATACTGCGAAAATTAACGCGGT
ZraP        TTATGAATACAACGCGCTACTGACCGCCAGTTCGCCGGATACTGCGAAAATTAACGCGGT
            ************************************************************

ZraPWT      TGCCAAAGAGATGGAGTCATTAGGCCAGAAGTTAGATGAGCAACGCGTGAAACGGGATGT
ZraP        TGCCAAAGAGATGGAGTCATTAGGCCAGAAGTTAGATGAGCAACGCGTGAAACGGGATGT
            ************************************************************

ZraPWT      CGCGATGGCGCAGGCTGGCATACCACGCGGCGCAGGAATGGGCTATGGCGGTTGCGGCGG
ZraP        CGCGATGGCGCAGGCTGGCATACCACGCGGCGCAGGAATGGGCTATGGCGGTTGCGGCGG
            ************************************************************

ZraPWT      CTATGGCGGCGGTTATCATCGCGGCGGCGGTCACATGGGTATGGGAAACTGG==TGGAGCCA==
ZraP        CTATGGCGGCGGTTATCATCGCGGCGGCGGTCACATGGGTATGGGAAACTGGTAA-----
            ***************************************************

ZraPWT      ==TCCACAATTTGAAAAA==TGAGTTTAAACGG
ZraP        ---------------------------
```

ExPASy translated results for ZraP-SDM *versus* ZraP protein sequence

```
ZraPWT      MVKRNNKSAIALIALSLLALSSGAAFAGHHWGNNDGMWQQGGSPLTTEQQATAQKIYDDY
ZraP        -MKRNNKSAIALIALSLLALSSGAAFAGHHWGNNDGMWQQGGSPLTTEQQATAQKIYDDY
             :*********************************************************

ZraPWT      YTQTSALRQQLISKRYEYNALLTASSPDTAKINAVAKEMESLGQKLDEQRVKRDVAMAQA
ZraP        YTQTSALRQQLISKRYEYNALLTASSPDTAKINAVAKEMESLGQKLDEQRVKRDVAMAQA
            ************************************************************

ZraPWT      GIPRGAGMGYGGCGGYGGGYHRGGGHMGMGNW==WSHPQFEK==
ZraP        GIPRGAGMGYGGCGGYGGGYHRGGGHMGMGNW--------
            *******************************
```

Sequence alignment ZraP-ZA with STM SL1444 – ZraP retrieved from coliBASE.

Sequencing results *versus zraP* genetic sequence:

```
ZraPZA      TACGGAGGAATTAACCATGGTCAAACGGAACAATAAATCAGCTATCGCGCTAATTGCCCT
ZraP        ------------------ATGAAACGGAACAATAAATCAGCTATCGCGCTAATTGCCCT
                          *  ***********************************

ZraPZA      CTCTCTTTTGGCCCTGAGCTCCGGCGCCGCCTTCGCCGGGCATCACTGGGGCAACAATGA
ZraP        CTCTCTTTTGGCCCTGAGCTCCGGCGCCGCCTTCGCCGGGCATCACTGGGGCAACAATGA
            ************************************************************

ZraPZA      CGGTATGTGGCAACAGGGAGGTAGCCCGTTAACTACGGAACAGCAGGCGACGGCGCAGAA
ZraP        CGGTATGTGGCAACAGGGAGGTAGCCCGTTAACTACGGAACAGCAGGCGACGGCGCAGAA
            ************************************************************

ZraPZA      GATTTATGATGATTACTATACGCAGACCAGCGCGCTGCGCCAGCAACTGATATCCAAACG
ZraP        GATTTATGATGATTACTATACGCAGACCAGCGCGCTGCGCCAGCAACTGATATCCAAACG
            ************************************************************

ZraPZA      TTATGAATACAACGCGCTACTGACCGCCAGTTCGCCGGATACTGCGAAAATTAACGCGGT
ZraP        TTATGAATACAACGCGCTACTGACCGCCAGTTCGCCGGATACTGCGAAAATTAACGCGGT
            ************************************************************

ZraPZA      TGCCAAAGAGATGGAGTCATTAGGCCAGAAGTTAGATGAGCAACGCGTGAAACGGGATGT
ZraP        TGCCAAAGAGATGGAGTCATTAGGCCAGAAGTTAGATGAGCAACGCGTGAAACGGGATGT
            ************************************************************

ZraPZA      CGCGATGGCGCAGGCTGGCATACCACGCGGCGCAGGAATGGGCTATGGCGGTTGCGGCGG
ZraP        CGCGATGGCGCAGGCTGGCATACCACGCGGCGCAGGAATGGGCTATGGCGGTTGCGGCGG
            ************************************************************

ZraPZA      CTATGGCGGCGGTTAT<mark style="background:cyan">GCTGCCGCCGCCGCTGCT</mark>ATGGGTATGGGAAACTGG<mark style="background:yellow">TGGAGCCA</mark>
ZraP        CTATGGCGGCGGTTAT<mark style="background:cyan">CATCGCGGCGGCGGTCAC</mark>ATGGGTATGGGAAACTGGTAA-----
            ****************   *   ** ** ** *     *****************

ZraPZA      <mark style="background:yellow">TCCACAATTTGAAAAA</mark>TGAGTTTAAACGGTCTCCAGCTTGGCTGTTTTGGCGGATGAGAG
ZraP        ------------------------------------------------------------
```

ExPASy translated results for ZraP-ZA *versus* ZraP protein sequence

```
ZraPZA      MVKRNNKSAIALIALSLLALSSGAAFAGHHWGNNDGMWQQGGSPLTTEQQATAQKIYDDY
ZraP        -MKRNNKSAIALIALSLLALSSGAAFAGHHWGNNDGMWQQGGSPLTTEQQATAQKIYDDY
             :*********************************************************

ZraPZA      YTQTSALRQQLISKRYEYNALLTASSPDTAKINAVAKEMESLGQKLDEQRVKRDVAMAQA
ZraP        YTQTSALRQQLISKRYEYNALLTASSPDTAKINAVAKEMESLGQKLDEQRVKRDVAMAQA
            ************************************************************

ZraPZA      GIPRGAGMGYGGCGGYGGGY<mark style="background:cyan">AAAAAA</mark>MGMGNW<mark style="background:yellow">WSHPQFEK</mark>
ZraP        GIPRGAGMGYGGCGGYGGGY<mark style="background:cyan">HRGGGH</mark>MGMGNW--------
            *******************   ...  ******
```

Appendix E. Overview of all susceptibility test results

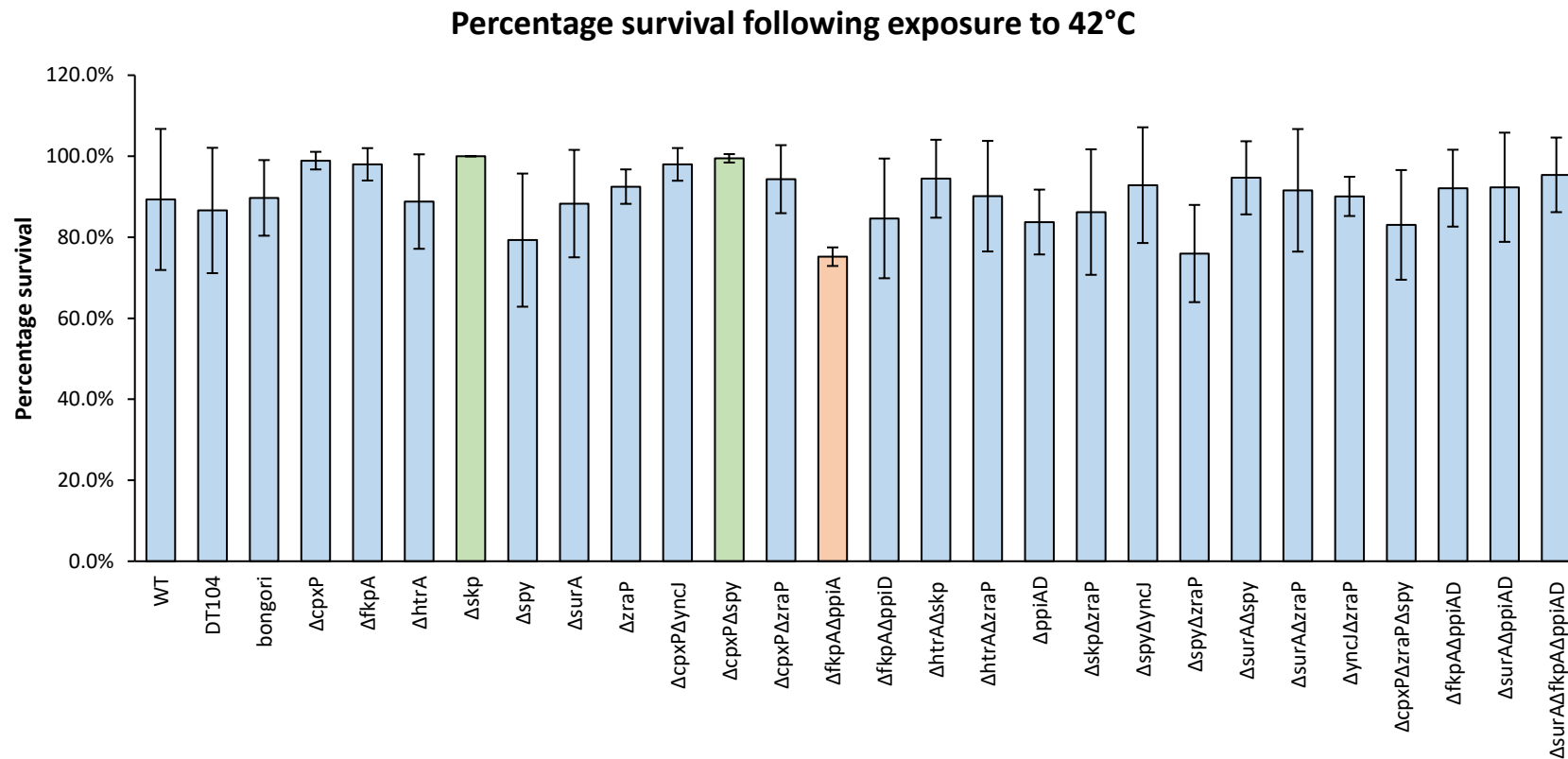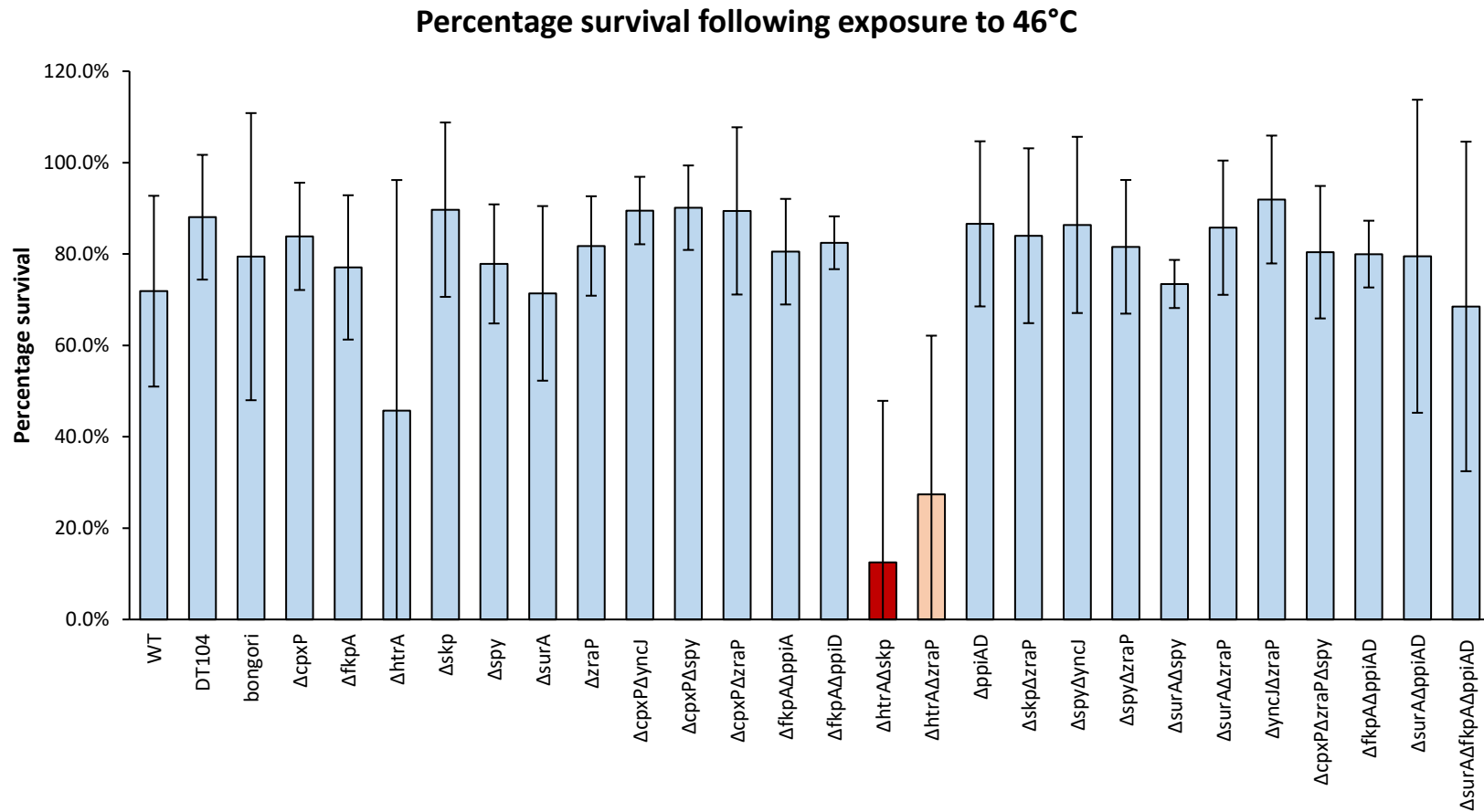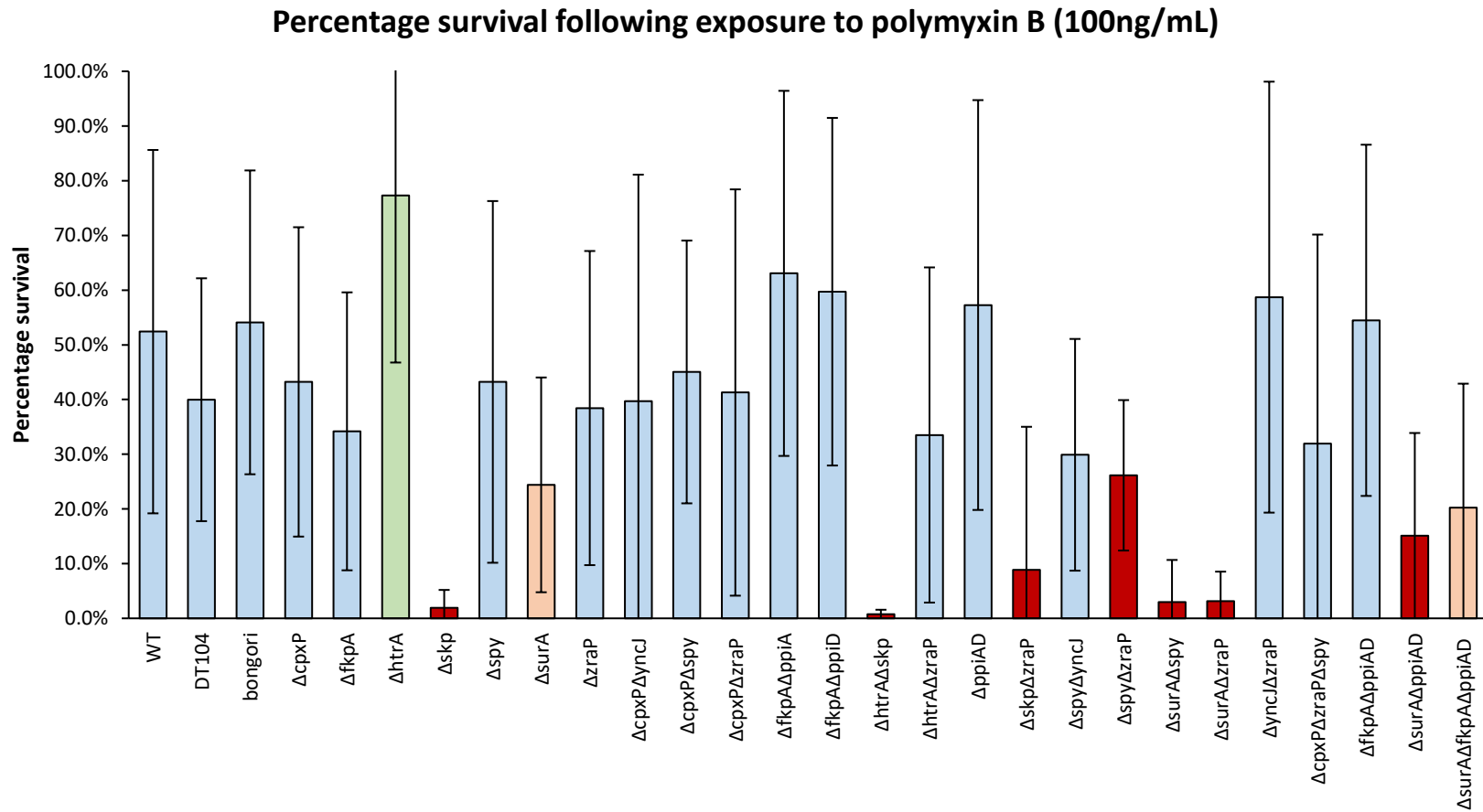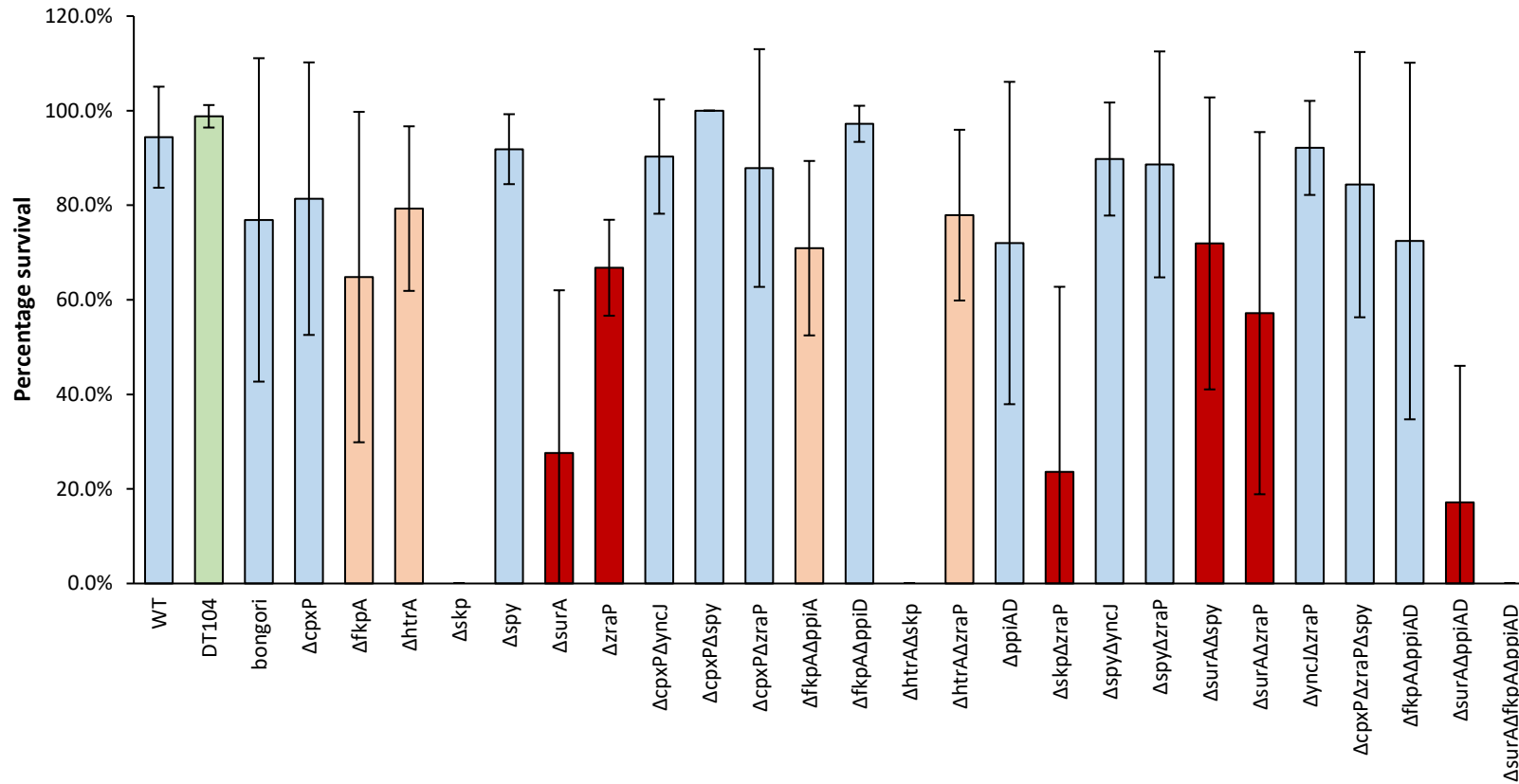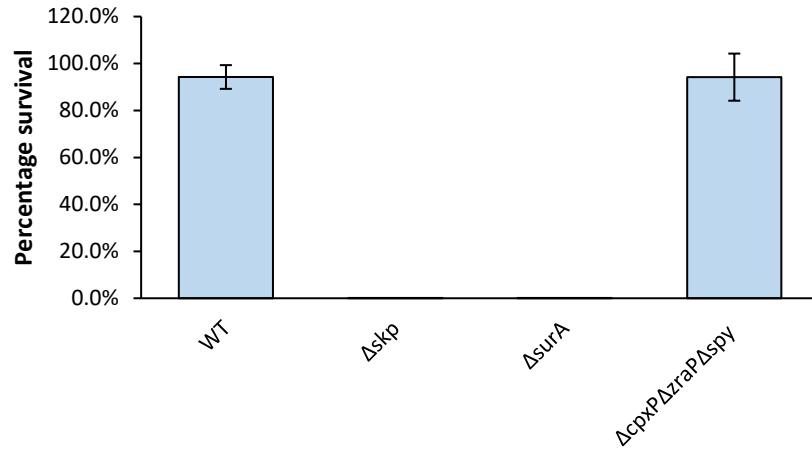## Percentage survival following exposure to 42°C

Figure E1. Percentage survival of *Salmonella* strains grown at 42°C for 36 hours. Summary of all spot-plate strains tested in this condition. Error bars represent standard deviation. Student T-tests statistics displayed in colour: light blue = no statistical difference, light green = significantly better survival ($P < 0.05$), light red = significantly worse survival ($P < 0.05$).

Figure E2. Percentage survival of *Salmonella* strains grown at 46°C for 48 hours. Summary of all spot-plate strains tested in this condition. Error bars represent standard deviation. Student T-tests statistics displayed in colour: light blue = no statistical difference, light red = significantly worse survival (P < 0.05), **dark red** = significant worse survival (P<0.01).

Figure E3. Percentage survival of *Salmonella* strains grown in 100ng/mL polymyxin B. Summary of all spot-plate strains tested in this condition. Error bars represent standard deviation. Student T-tests statistics displayed in colour: light blue = no statistical difference, light green = significantly better survival (P < 0.05), light red = significantly worse survival (P < 0.05), dark red = significant worse survival (P<0.01).

Figure E4. Percentage survival of *Salmonella* strains grown in 65µg/mL vancomycin. Summary of all spot-plate strains tested in this condition. Error bars represent standard deviation. Student T-tests statistics displayed in colour: light blue = no statistical difference, light green = significantly better survival (P < 0.05), light red = significantly worse survival (P < 0.05), **dark red** = significant worse survival (P<0.01).

Figure E5. Percentage survival of *Salmonella* strains grown in 1µg/mL nalidixic acid and 50ng/mL phosphomycin. Summary of all spot-plate strains tested in this condition. Error bars represent standard deviation. Student T-tests statistics displayed in colour: light blue = no statistical difference, light red = significantly worse survival (P < 0.05), dark red = significant worse survival (P<0.01).
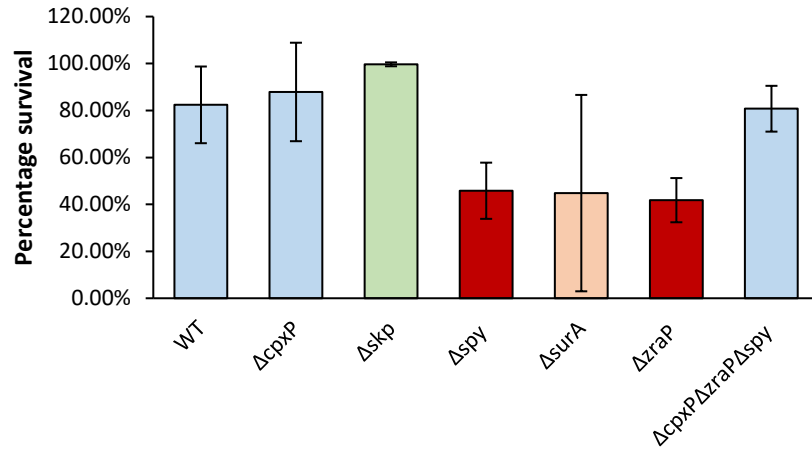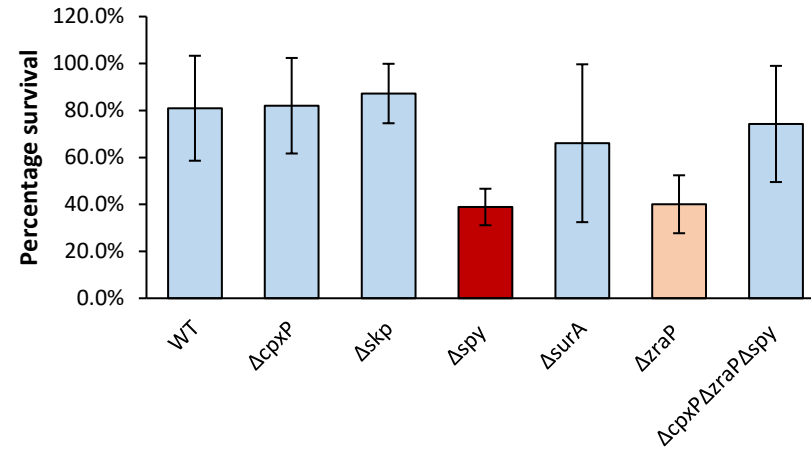
Figure E6. Percentage survival of *Salmonella* strains grown in 2mM indole and 6mM spermidine. Summary of all spot-plate strains tested in this condition. Error bars represent standard deviation. Student T-tests statistics displayed in colour: light blue = no statistical difference, light green = significantly better survival (P < 0.05), light red = significantly worse survival (P < 0.05), dark red = significant worse survival (P<0.01).
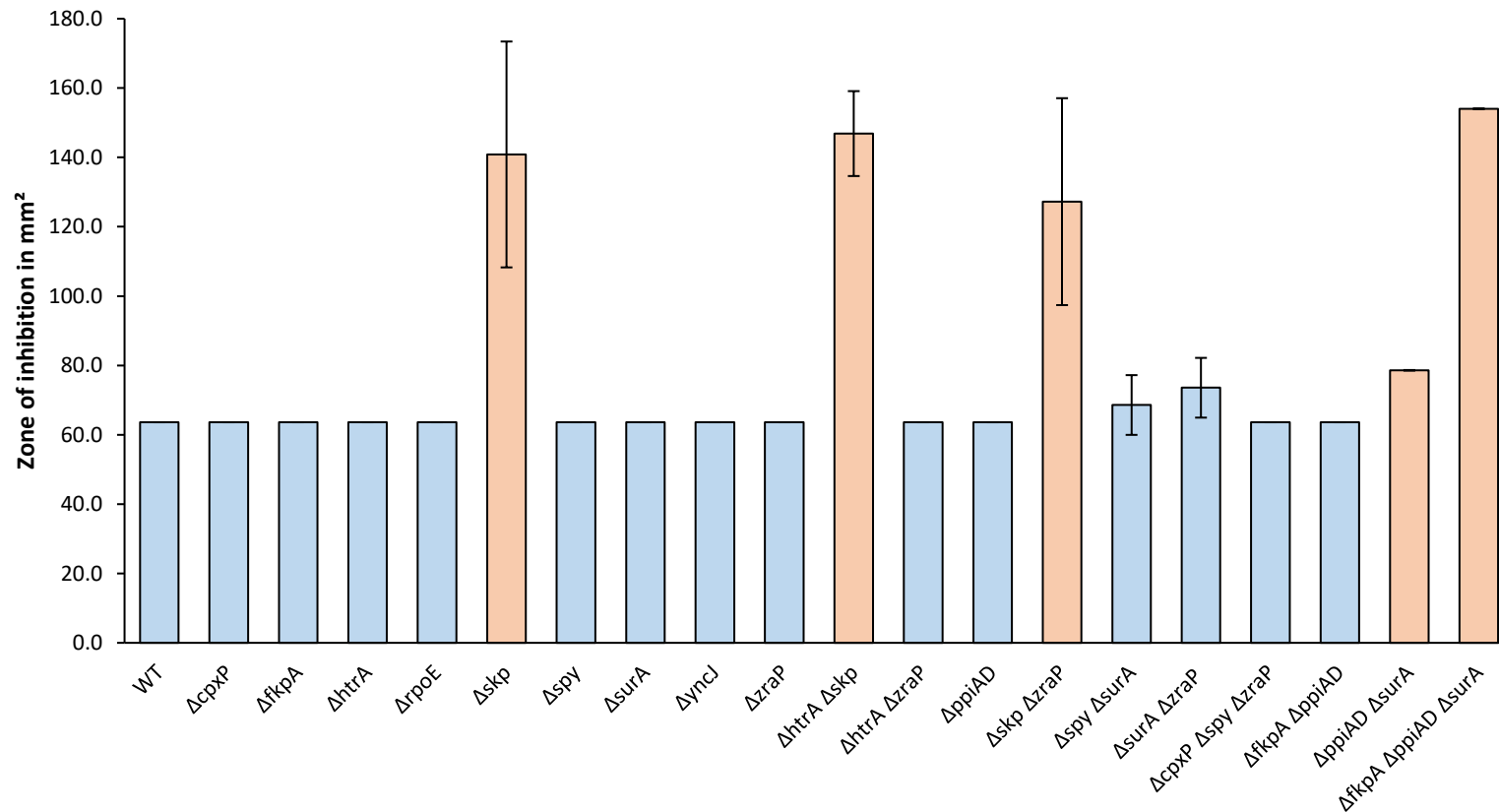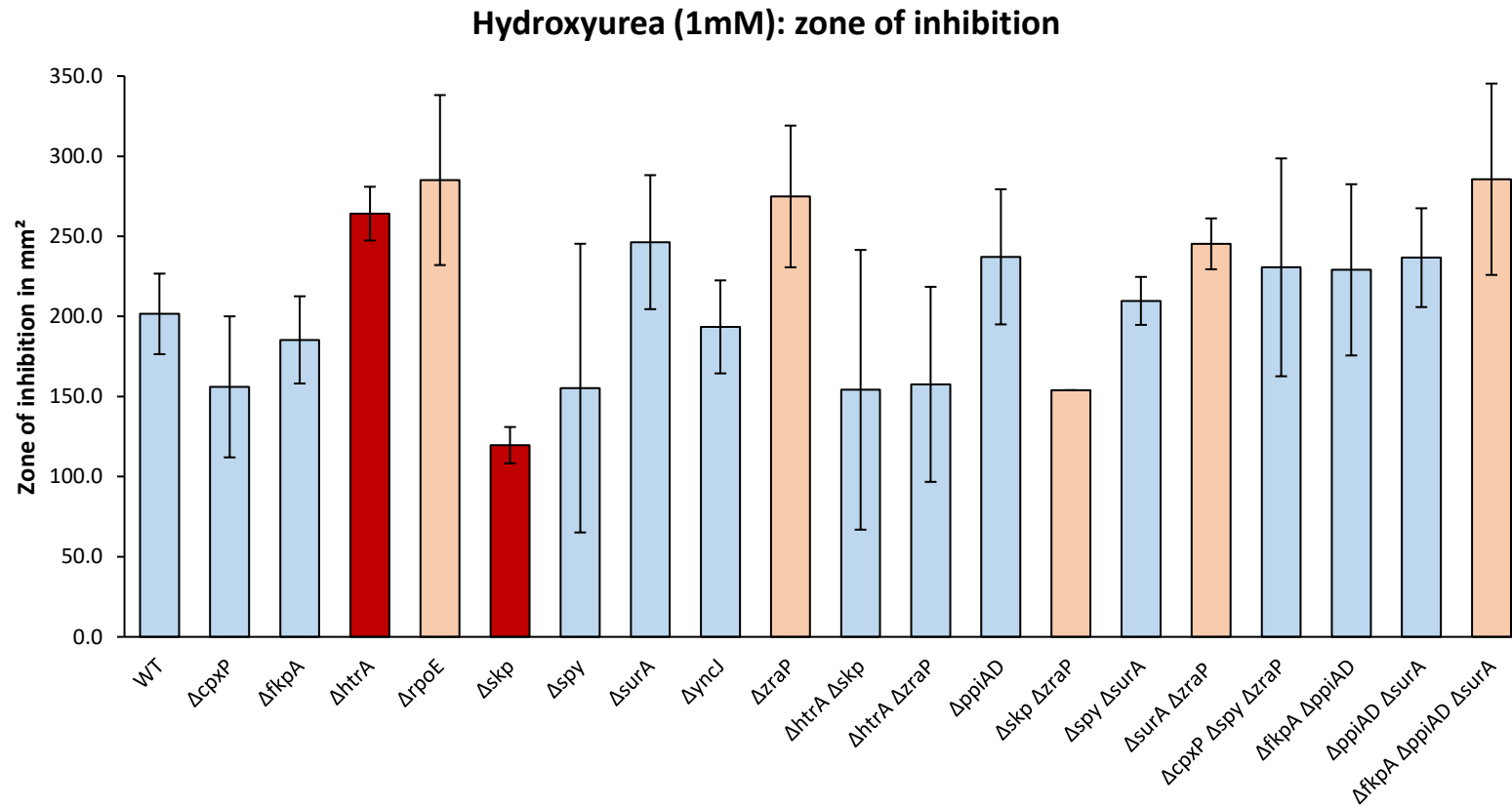
Figure E7. Zone of inhibition of *Salmonella* strains on disc diffusion plates containing 10mM Bacitracin. Summary of all spot-plate strains tested in this condition. Error bars represent standard deviation. Student T-tests statistics displayed in colour: light blue = no statistical difference, light red = significantly more susceptible ($P < 0.05$).
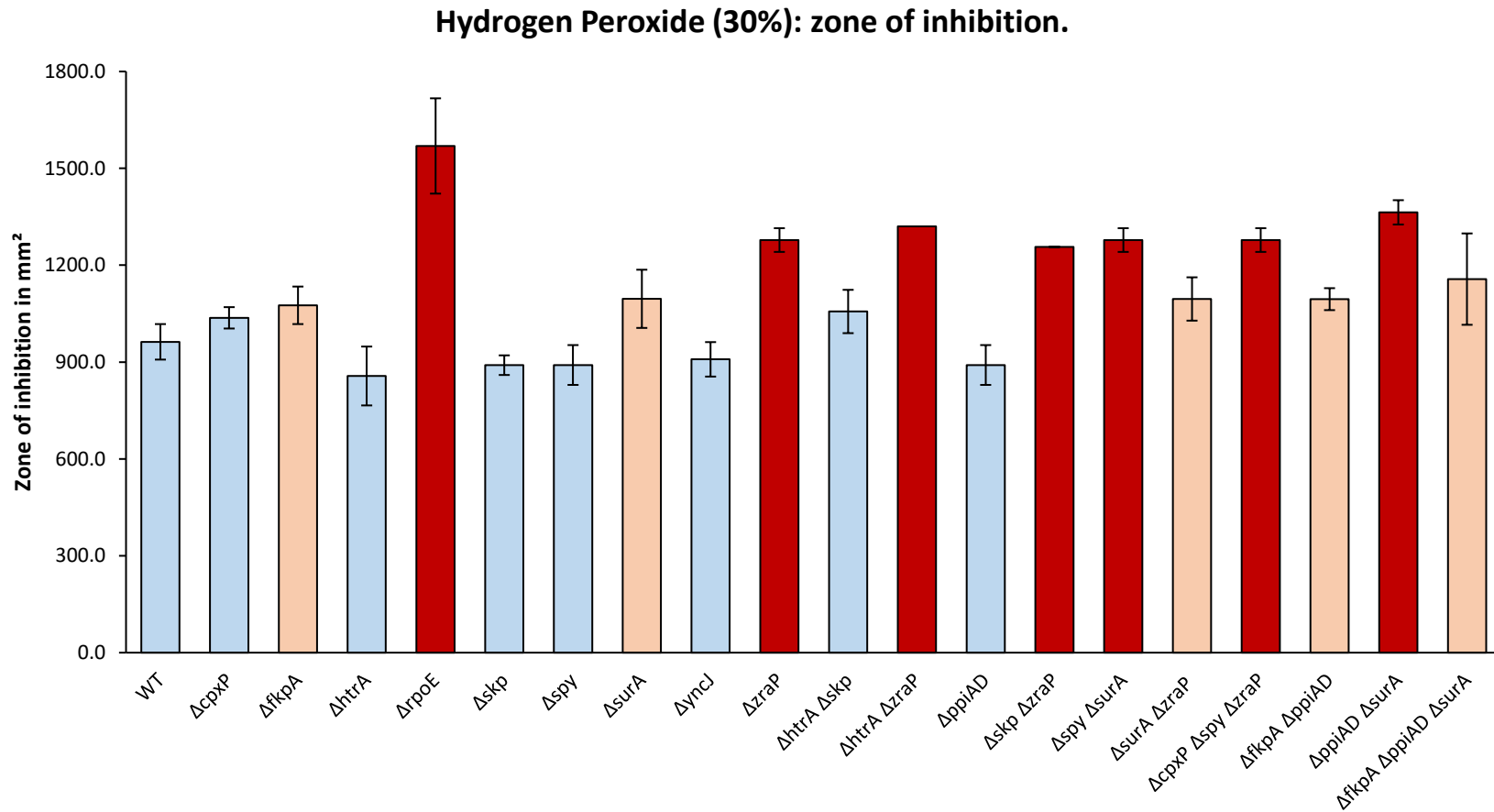
Figure E8. Zone of inhibition of *Salmonella* strains on disc diffusion plates containing 30% hydrogen peroxide. Summary of all spot-plate strains tested in this condition. Error bars represent standard deviation. Student T-tests statistics displayed in colour: light blue = no statistical difference, light red = significantly more susceptible (P < 0.05), **dark red** = significantly more susceptible (P < 0.01).
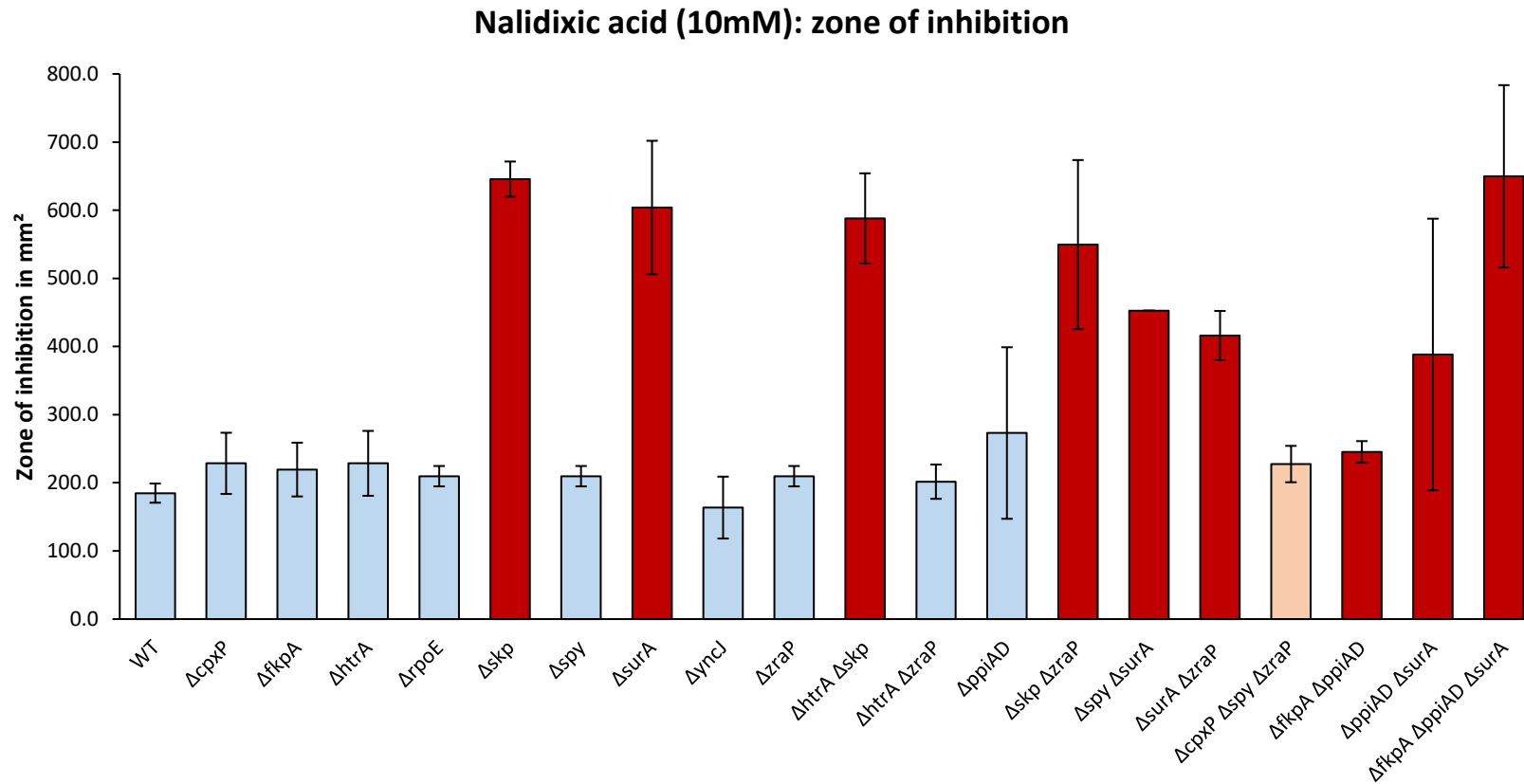
Figure E9. Zone of inhibition of *Salmonella* strains on disc diffusion plates containing 1mM hydroxyurea. Summary of all spot-plate strains tested in this condition. Error bars represent standard deviation. Student T-tests statistics displayed in colour: light blue = no statistical difference, light red = significantly more susceptible (P < 0.05), **dark red** = significantly more susceptible (P < 0.01).
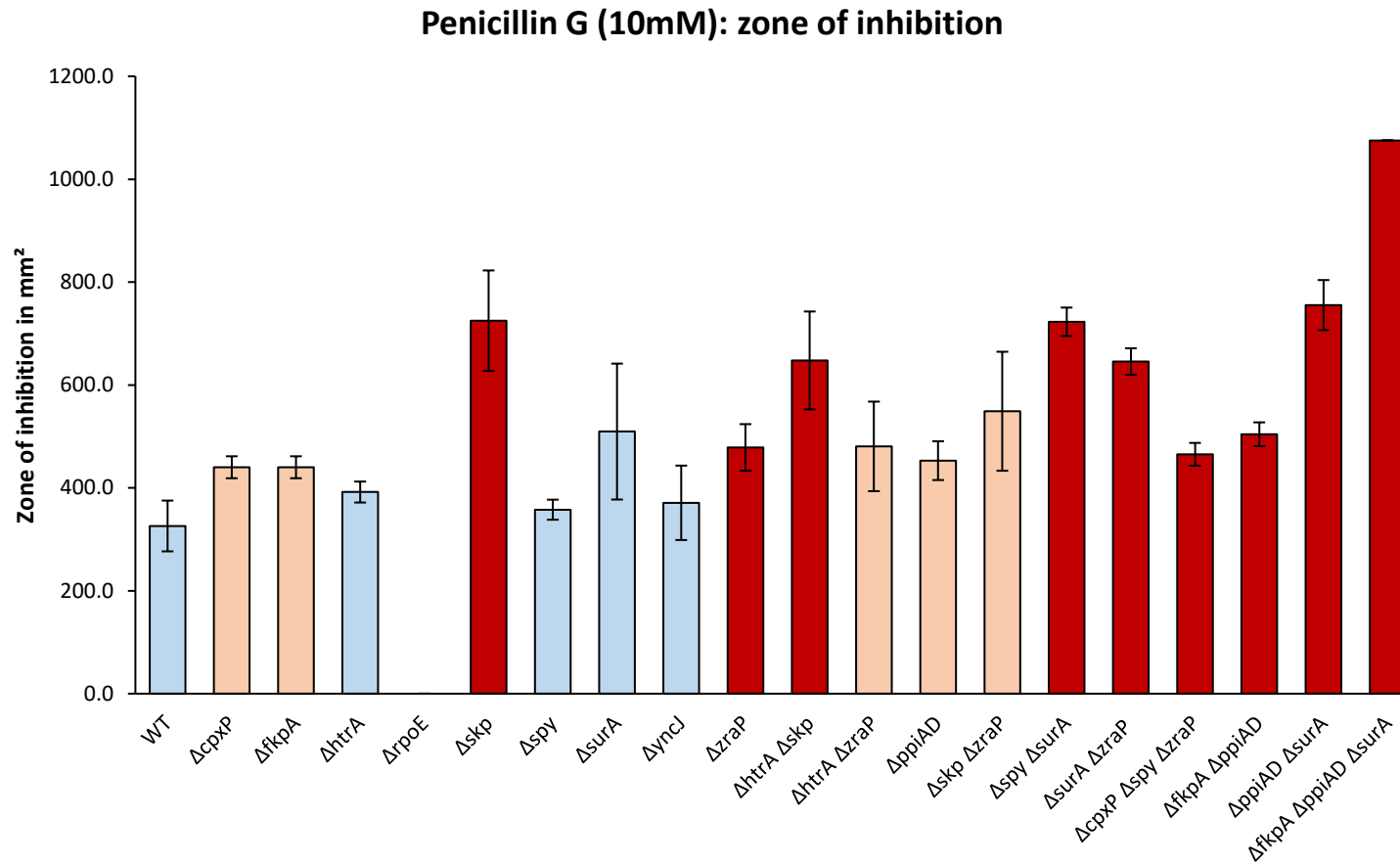
Figure E10. Zone of inhibition of *Salmonella* strains on disc diffusion plates containing 10mM nalidixic acid. Summary of all spot-plate strains tested in this condition. Error bars represent standard deviation. Student T-tests statistics displayed in colour: light blue = no statistical difference, light red = significantly more susceptible (P < 0.05), dark red = significantly more susceptible (P < 0.01).
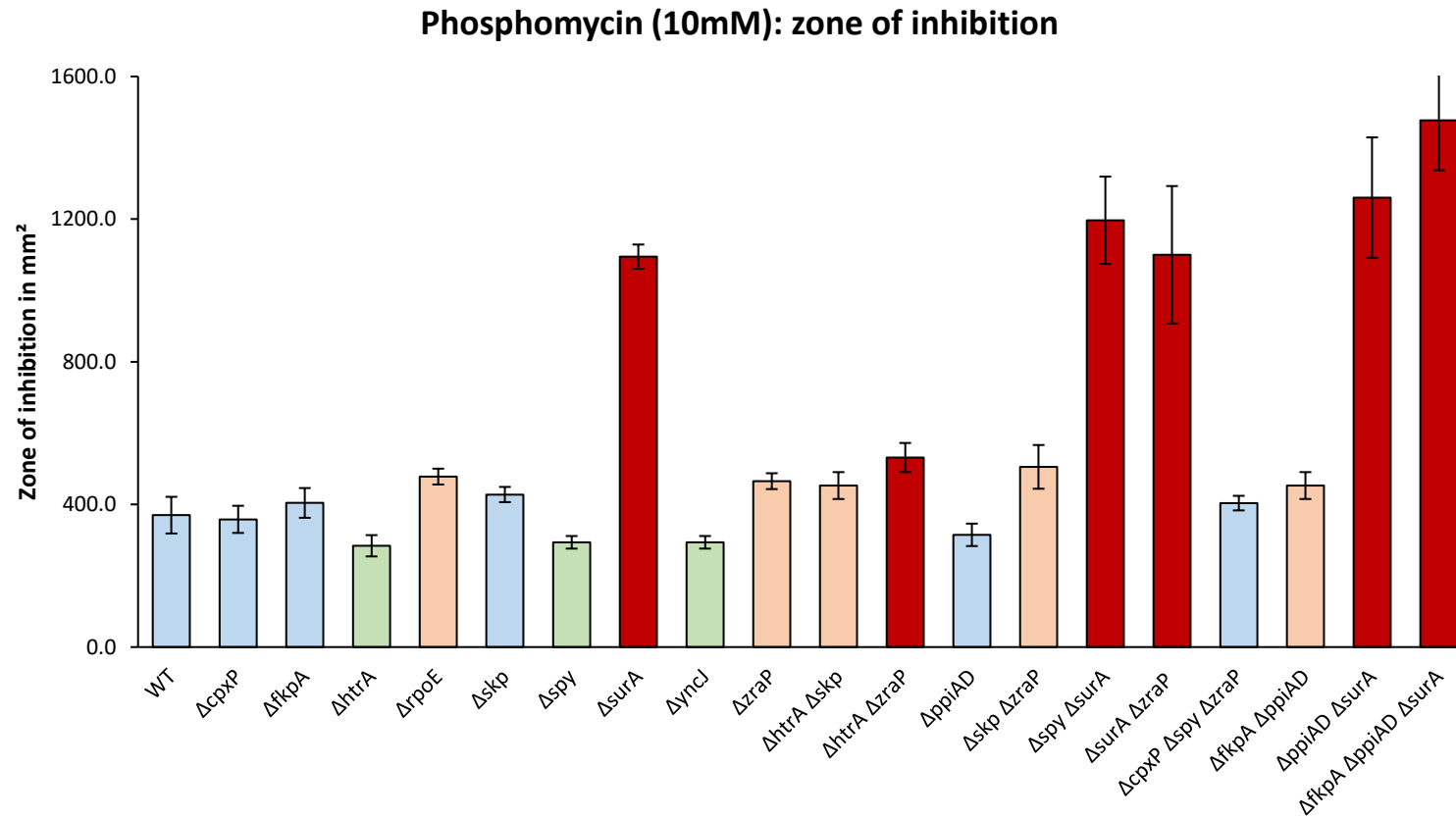
Figure E11. Zone of inhibition of *Salmonella* strains on disc diffusion plates containing 10mM penicillin G. Summary of all spot-plate strains tested in this condition. Error bars represent standard deviation. Student T-tests statistics displayed in colour: light blue = no statistical difference, light red = significantly more susceptible (P < 0.05), **dark red** = significantly more susceptible (P < 0.01).

Figure E12. Zone of inhibition of *Salmonella* strains on disc diffusion plates containing 10mM phosphomycin. Summary of all spot-plate strains tested in this condition. Error bars represent standard deviation. Student T-tests statistics displayed in colour: light blue = no statistical difference, light green = significantly less susceptible, (P < 0.05), light red = significantly more susceptible (P < 0.05), dark red = significantly more susceptible (P < 0.01).

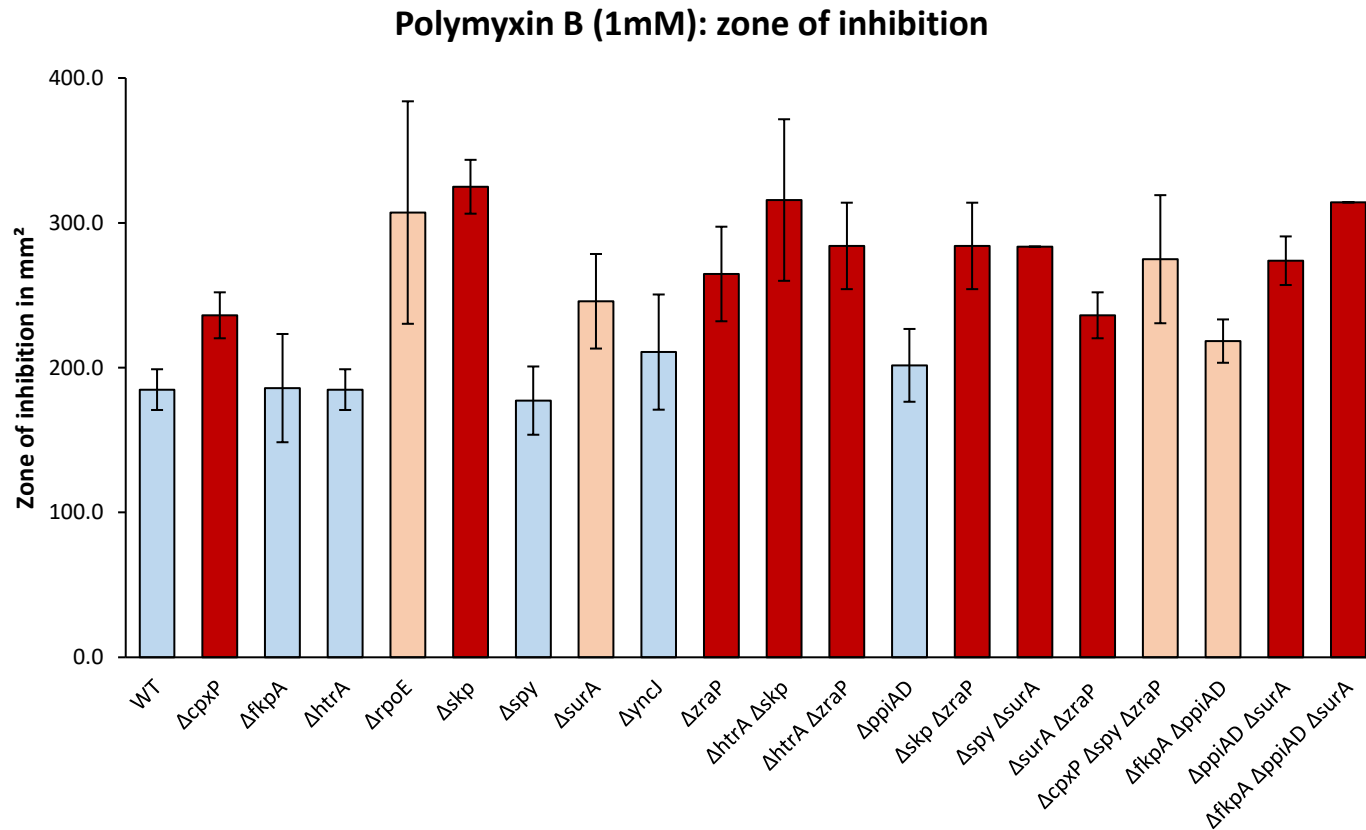**Polymyxin B (1mM): zone of inhibition**

Figure E13. Zone of inhibition of *Salmonella* strains on disc diffusion plates containing 1mM polymyxin B. Summary of all spot-plate strains tested in this condition. Error bars represent standard deviation. Student T-tests statistics displayed in colour: light blue = no statistical difference, light red = significantly more susceptible (P < 0.05), dark red = significantly more susceptible (P < 0.01).
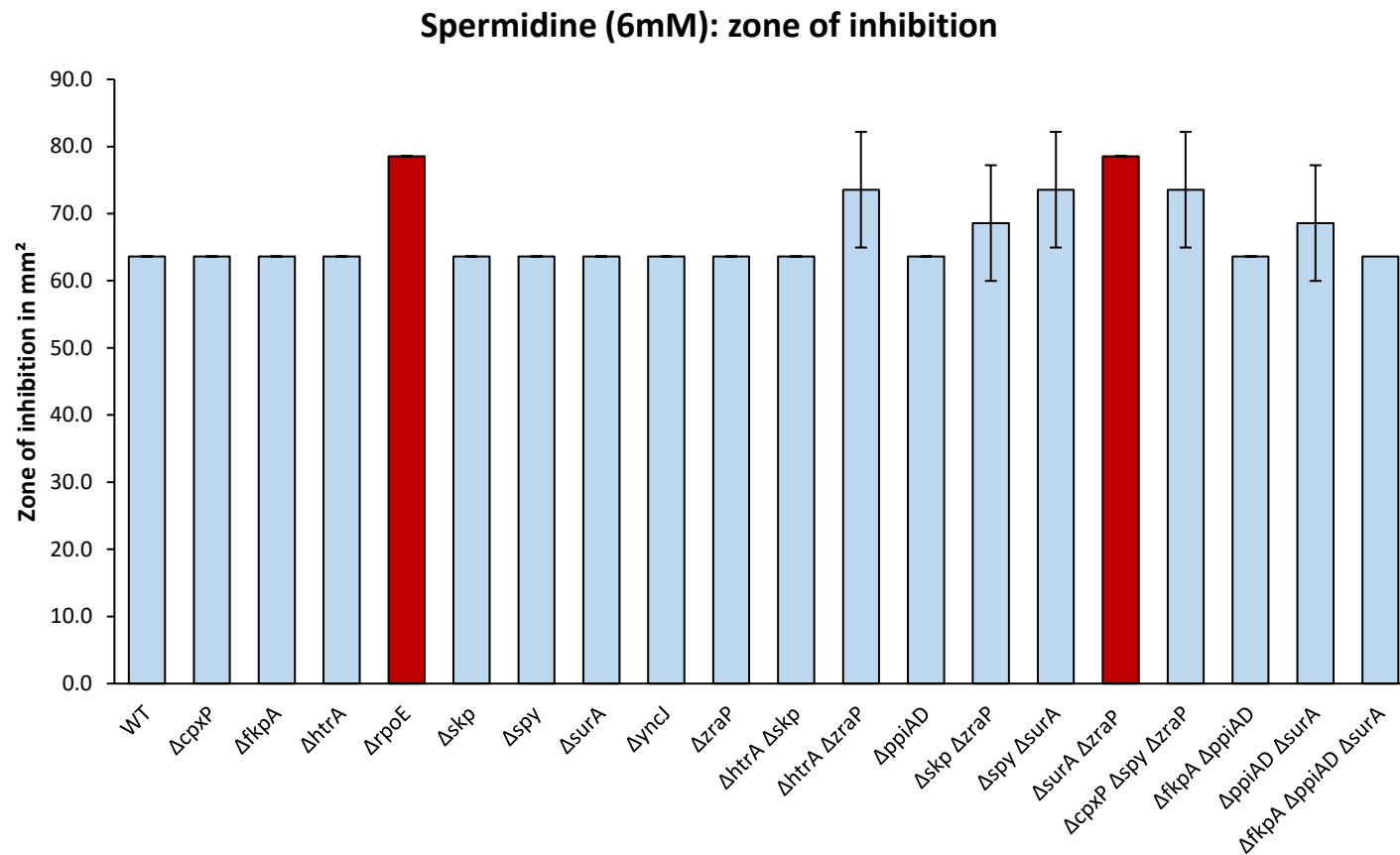
Figure E14. Zone of inhibition of *Salmonella* strains on disc diffusion plates containing 6mM spermidine. Summary of all spot-plate strains tested in this condition. Error bars represent standard deviation. Student T-tests statistics displayed in colour: light blue = no statistical difference, **dark red** = significantly more susceptible (P < 0.01).
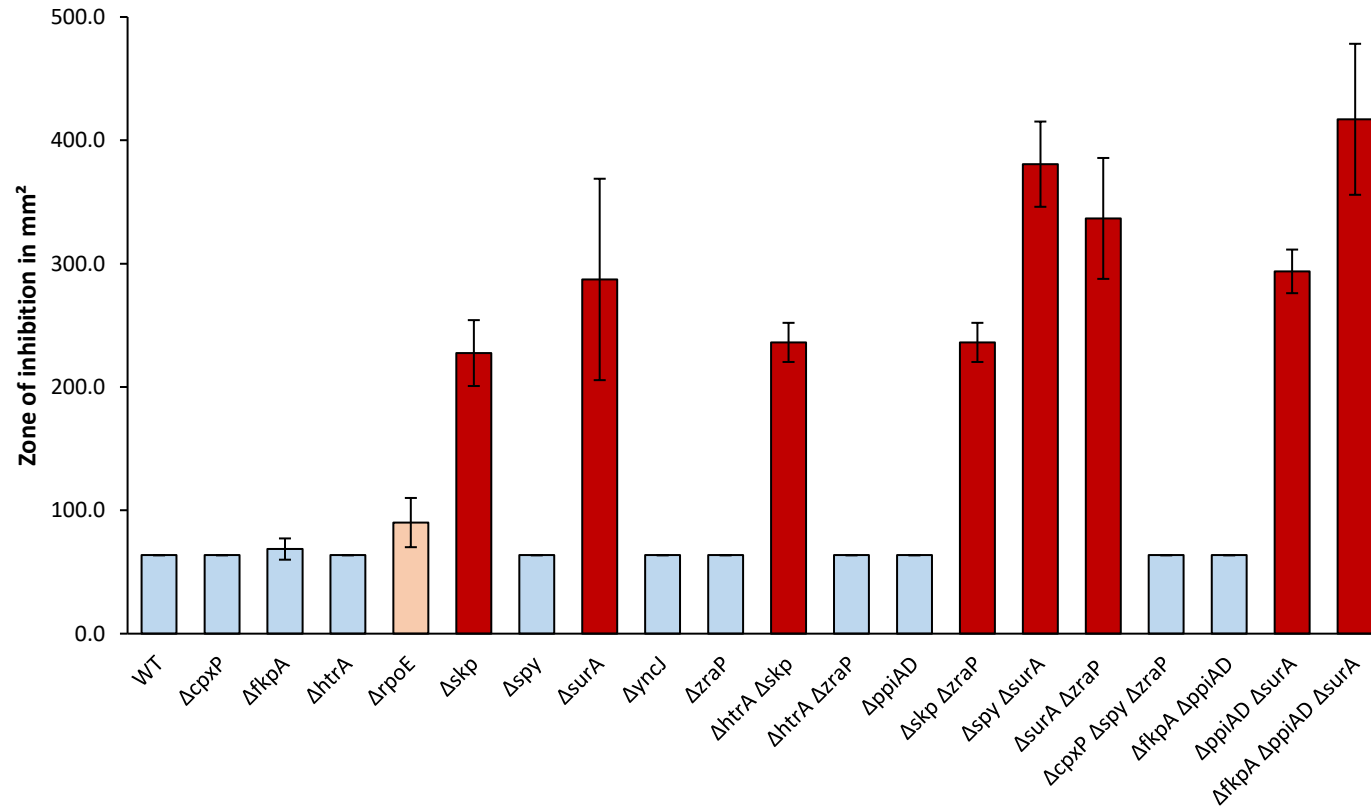
Figure E15. Zone of inhibition of *Salmonella* strains on disc diffusion plates containing 65µg/mL vancomycin. Summary of all spot-plate strains tested in this condition. Error bars represent standard deviation. Student T-tests statistics displayed in colour: light blue = no statistical difference, **dark red** = significantly more susceptible (P < 0.01).